Power Electronic Control in Electrical Systems

NEWNES POWER ENGINEERING SERIES

Series editors
Professor TJE Miller, University of Glasgow, UK
Associate Professor Duane Hanselman, University of Maine, USA
Professor Thomas M Jahns, University of Wisconsin-Madison, USA
Professor Jim McDonald, University of Strathclyde, UK

Newnes Power Engineering Series is a new series of advanced reference texts covering the core areas of modern electrical power engineering, encompassing transmission and distribution, machines and drives, power electronics, and related areas of electricity generation, distribution and utilization. The series is designed for a wide audience of engineers, academics, and postgraduate students, and its focus is international, which is reflected in the editorial team. The titles in the series offer concise but rigorous coverage of essential topics within power engineering, with a special focus on areas undergoing rapid development.

The series complements the long-established range of Newnes titles in power engineering, which includes the *Electrical Engineer's Reference Book*, first published by Newnes in 1945, and the classic *J&P Transformer Book*, as well as a wide selection of recent titles for professionals, students and engineers at all levels.

Further information on the **Newnes Power Engineering Series** is available from bhmarketing@repp.co.uk
www.newnespress.com

Please send book proposals to Matthew Deans, Newnes Publisher
matthew.deans@repp.co.uk

Other titles in the Newnes Power Engineering Series
Miller   Electronic Control of Switched Reluctance Machines   0-7506-5073-7
Agrawal   Industrial Power Engineering and Applications Handbook   0-7506-7351-6

Power Electronic Control in Electrical Systems

E. Acha
V.G. Agelidis
O. Anaya-Lara
T.J.E. Miller

Newnes

Preface

Although the basic concepts of reactive power control in power systems remain unchanged, state-of-the-art developments associated with power electronics equipment are dictating new ways in which such control may be achieved not only in high-voltage transmission systems but also in low-voltage distribution systems. The book addresses, therefore, not only the fundamental concepts associated with the topic of reactive power control but also presents the latest equipment and devices together with new application areas and associated computer-assisted studies.

The book offers a solid theoretical foundation for the electronic control of active and reactive power. The material gives an overview of the composition of electrical power networks; a basic description of the most popular power systems studies and indicates, within the context of the power system, where the Flexible Alternating Current Transmission Systems (FACTS) and Custom Power equipment belong.

FACTS relies on state-of-the-art power electronic devices and methods applied on the high-voltage side of the power network to make it electronically controllable. From the operational point of view, it is concerned with the ability to control the path of power flows throughout the network in an adaptive fashion. This equipment has the ability to control the line impedance and the nodal voltage magnitudes and angles at both the sending and receiving ends of key transmission corridors while enhancing the security of the system.

Custom Power focuses on low-voltage distribution systems. This technology is a response to reports of poor power quality and reliability of supply to factories, offices and homes. Today's automated equipment and production lines require reliable and high quality power, and cannot tolerate voltage sags, swells, harmonic distortions, impulses or interruptions.

Chapter 1 gives an overview of electrical power networks. The main plant components of the power network are described, together with the new generation of power network controllers, which use state-of-the-art power electronics technology to give the power network utmost operational flexibility and an almost instantaneous speed of response. The chapter also describes the main computer assisted studies used by power systems engineers in the planning, management and operation of the network.

Chapter 2 provides a broad review of the basic theoretical principles of power engineering, with relevant examples of AC circuit analysis, per-unit systems, three-phase systems, transformer connections, power measurement and other topics. It covers the basic precepts of power and frequency control, voltage control and load balancing, and provides a basic understanding of the reactive compensation of loads.

Chapter 3 reviews the principles of transmission system compensation including shunt and series compensation and the behaviour of long transmission lines and cables.

Chapter 4 addresses the mathematical modelling of the electrical power network suitable for steady state analysis. Emphasis is placed on the modelling of plant components used to control active and reactive power flows, voltage magnitude and network impedance in high-voltage transmission. The model of the power network is the classical non-linear model, based on voltage-dependent nodal power equations and solved by iteration using the Newton–Raphson method. The basic method is then expanded to encompass the models of the new generation of power systems controllers. The new models are simple and yet comprehensive.

Chapter 5 introduces the power semiconductor devices and their characteristics as part of a power electronic system. It discusses the desired characteristics to be found in an ideal switch and provides information on components, power semiconductor device protection, hardware issues of converters and future trends.

Chapter 6 covers in detail the thyristor-based power electronic equipment used in power systems for reactive power control. It provides essential background theory to understand its principle of operation and basic analytical expression for assessing its switching behaviour. It then presents basic power electronic equipment built with voltage-source converters. These include single-phase and three-phase circuits along with square wave and pulse-width modulation control. It discusses the basic concepts of multilevel converters, which are used in high power electronic equipment. Energy storage systems based on superconducting material and uninterruptible power supplies are also presented. Towards the end of the chapter, conventional HVDC systems along with VSC-based HVDC and active filtering equipment are also presented.

Chapter 7 deals with the all-important topic of power systems harmonics. To a greater or lesser extent all power electronic controllers generate harmonic currents, but from the operator's perspective, and the end-user, these are parasitic or nuisance effects. The book addresses the issue of power systems harmonics with emphasis on electronic compensation.

Chapter 8 provides basic information on how the industry standard software package PSCAD/EMTDC can be used to simulate and study not only the periodic steady state response of power electronic equipment but also their transient response. Specifically, detailed simulation examples are presented of the Static Var compensator, thyristor controlled series compensator, STATCOM, solid-state transfer switch, DVR and shunt-connected active filters based on the VSC concept.

<div align="right">

Enrique Acha
Vassilios G. Agelidis
Olimpo Anaya-Lara
Tim Miller

</div>

1

Electrical power systems – an overview

1.1 Introduction

The main elements of an electrical power system are generators, transformers, transmission lines, loads and protection and control equipment. These elements are interconnected so as to enable the generation of electricity in the most suitable locations and in sufficient quantity to satisfy the customers' demand, to transmit it to the load centres and to deliver good-quality electric energy at competitive prices.

The quality of the electricity supply may be measured in terms of:

- constant voltage magnitude, e.g. no voltage sags
- constant frequency
- constant power factor
- balanced phases
- sinusoidal waveforms, e.g. no harmonic content
- lack of interruptions
- ability to withstand faults and to recover quickly.

1.2 Background

The last quarter of the nineteenth century saw the development of the electricity supply industry as a new, promising and fast-growing activity. Since that time electrical power networks have undergone immense transformations (Hingorani and Gyugyi, 2000; Kundur, 1994). Owing to the relative 'safety' and 'cleanliness' of electricity, it quickly became established as a means of delivering light, heat and motive power. Nowadays it is closely linked to primary activities such as industrial production, transport, communications and agriculture. Population growth, technological innovations and higher capital gains are just a few of the factors that have maintained the momentum of the power industry.

Clearly it has not been easy for the power industry to reach its present status. Throughout its development innumerable technical and economic problems have been overcome, enabling the supply industry to meet the ever increasing demand for energy with electricity at competitive prices. The generator, the incandescent lamp and the industrial motor were the basis for the success of the earliest schemes. Soon the transformer provided a means for improved efficiency of distribution so that generation and transmission of alternating current over considerable distances provided a major source of power in industry and also in domestic applications.

For many decades the trend in electric power production has been towards an inter-connected network of transmission lines linking generators and loads into large integrated systems, some of which span entire continents. The main motivation has been to take advantage of load diversity, enabling a better utilization of primary energy resources. It may be argued that interconnection provides an alternative to a limited amount of generation thus enhancing the security of supply (Anderson and Fouad, 1977).

Interconnection was further enhanced, in no small measure, by early break-throughs in high-current, high-power semiconductor valve technology. Thyristor-based high voltage direct current (HVDC) converter installations provided a means for interconnecting power systems with different operating frequencies, e.g. 50/60 Hz, for interconnecting power systems separated by the sea, e.g. the cross-Channel link between England and France, and for interconnecting weak and strong power systems (Hingorani, 1996). The rectifier and inverter may be housed within the same converter station (back-to-back) or they may be located several hundred kilometres apart, for bulk-power, extra-long-distance transmission. The most recent development in HVDC technology is the HVDC system based on solid state voltage source converters (VSCs), which enables independent, fast control of active and reactive powers (McMurray, 1987). This equipment uses insulated gate bipolar transistors (IGBTs) or gate turn-off thyristors (GTOs) 'valves' and pulse width modulation (PWM) control techniques (Mohan et al., 1995). It should be pointed out that this technology was first developed for applications in industrial drive systems for improved motor speed control. In power transmission applications this technology has been termed HVDC Light (Asplund et al., 1998) to differentiate it from the well-established HVDC links based on thyristors and phase control (Arrillaga, 1999). Throughout this book, the terms HVDC Light and HVDC based on VSCs are used interchangeably.

Based on current and projected installations, a pattern is emerging as to where this equipment will find widespread application: deregulated market applications in primary distribution networks, e.g. the 138 kV link at Eagle Pass, interconnecting the Mexican and Texas networks (Asplund, 2000). The 180 MVA Directlink in Australia, interconnecting the Queensland and New South Wales networks, is another example.

Power electronics technology has affected every aspect of electrical power networks; not just HVDC transmission but also generation, AC transmission, distribution and utilization. At the generation level, thyristor-based automatic voltage regulators (AVRs) have been introduced to enable large synchronous generators to respond quickly and accurately to the demands of interconnected environments. Power system stabilizers (PSSs) have been introduced to prevent power oscillations from building up as a result of sympathetic interactions between generators. For instance, several of the large generators in Scotland are fitted with

PSSs to ensure trouble-free operation between the Scottish power system and its larger neighbour, the English power system (Fairnley et al., 1982). Deregulated markets are imposing further demands on generating plant, increasing their wear and tear and the likelihood of generator instabilities of various kinds, e.g. transient, dynamic, sub-synchronous resonance (SSR) and sub-synchronous torsional interactions (SSTI). New power electronic controllers are being developed to help generators operate reliably in the new market place. The thyristor-controlled series compensator (TCSC) is being used to mitigate SSR, SSTI and to damp power systems' oscillations (Larsen et al., 1992). Examples of where TCSCs have been used to mitigate SSR are the TCSCs installed in the 500 kV Boneville Power Administration's Slatt substation and in the 400 kV Swedish power network. However, it should be noted that the primary function of the TCSC, like that of its mechanically controlled counterpart, the series capacitor bank, is to reduce the electrical length of the compensated transmission line. The aim is still to increase power transfers significantly, but with increased transient stability margins.

A welcome result of deregulation of the electricity supply industry and open access markets for electricity worldwide, is the opportunity for incorporating all forms of renewable generation into the electrical power network. The signatories of the Kyoto agreement in 1997 set themselves a target to lower emission levels by 20% by 2010. As a result of this, legislation has been enacted and, in many cases, tax incentives have been provided to enable the connection of micro-hydro, wind, photovoltaic, wave, tidal, biomass and fuel cell generators. The power generated by some of these sources of electricity is suitable for direct input, via a step-up transformer, into the AC distribution system. This is the case with micro-hydro and biomass generators. Other sources generate electricity in DC form or in AC form but with large, random variations which prevent direct connection to the grid; for example fuel cells and asynchronous wind generators. In both cases, power electronic converters such as VSCs provide a suitable means for connection to the grid.

In theory, the thyristor-based static var compensator (SVC) (Miller, 1982) could be used to perform the functions of the PSS, while providing fast-acting voltage support at the generating substation. In practice, owing to the effectiveness of the PSS and its relative low cost, this has not happened. Instead, the high speed of response of the SVC and its low maintenance cost have made it the preferred choice to provide reactive power support at key points of the transmission system, far away from the generators. For most practical purposes they have made the rotating synchronous compensator redundant, except where an increase in the short-circuit level is required along with fast-acting reactive power support. Even this niche application of rotating synchronous compensators may soon disappear since a thyristor-controlled series reactor (TCSR) could perform the role of providing adaptive short-circuit compensation and, alongside, an SVC could provide the necessary reactive power support. Another possibility is the displacement of not just the rotating synchronous compensator but also the SVC by a new breed of static compensators (STATCOMs) based on the use of VSCs. The STATCOM provides all the functions that the SVC can provide but at a higher speed and, when the technology reaches full maturity, its cost will be lower. It is more compact and requires only a fraction of the land required by an SVC installation. The VSC is the basic building block of the new generation of power controllers emerging from flexible alternating current transmission

systems (FACTS) and Custom Power research (Hingorani and Gyugyi, 2000). In high-voltage transmission, the most promising equipment is: the STATCOM, the unified power flow controller (UPFC) and the HVDC Light. At the low-voltage distribution level, the VSC provides the basis for the distribution STATCOM (D-STATCOM), the dynamic voltage restorer (DVR), the power factor corrector (PFC) and active filters.

1.3   General composition of the power network

For most practical purposes, the electrical power network may be divided into four parts, namely generation, transmission, distribution and utilization. The four parts are illustrated in Figure 1.1.

This figure gives the one-line diagram of a power network where two transmission levels are observed, namely 400 kV and 132 kV. An expanded view of one of the generators feeding into the high-voltage transmission network is used to indicate that the generating plant consists of three-phase synchronous generators driven by either hydro or steam turbines. Similarly, an expanded view of one of the load points is used to indicate the composition of the distribution system, where voltage levels are shown, i.e. 33 kV, 11 kV, 415 V and 240 V. Within the context of this illustration, industrial consumers would be supplied with three-phase electricity at 11 kV and domestic users with single-phase electricity at 240 V.

Figure 1.1 also gives examples of power electronics-based plant components and where they might be installed in the electrical power network. In high-voltage transmission systems, a TCSC may be used to reduce the electrical length of long transmission lines, increasing power transfers and stability margins. An HVDC link may be used for the purpose of long distance, bulk power transmission. An SVC or a STATCOM may be used to provide reactive power support at a network location far away from synchronous generators. At the distribution level, e.g. 33 kV and 11 kV, a D-STATCOM may be used to provide voltage magnitude support, power factor improvement and harmonic cancellation. The interfacing of embedded DC generators, such as fuel cells, with the AC distribution system would require a thyristor-based converter or a VSC.

Also, a distinction should be drawn between conventional, large generators, e.g. hydro, nuclear and coal, feeding directly into the high-voltage transmission, and the small size generators, e.g. wind, biomass, micro-gas, micro-hydro, fuel cells and photovoltaics, embedded into the distribution system. In general, embedded generation is seen as an environmentally sound way of generating electricity, with some generators using free, renewable energy from nature as a primary energy resource, e.g. wind, solar, micro-hydro and wave. Other embedded generators use non-renewable resources, but still environmentally benign, primary energy such as oxygen and gas. Diesel generators are an example of non-renewable, non-environmentally friendly embedded generation.
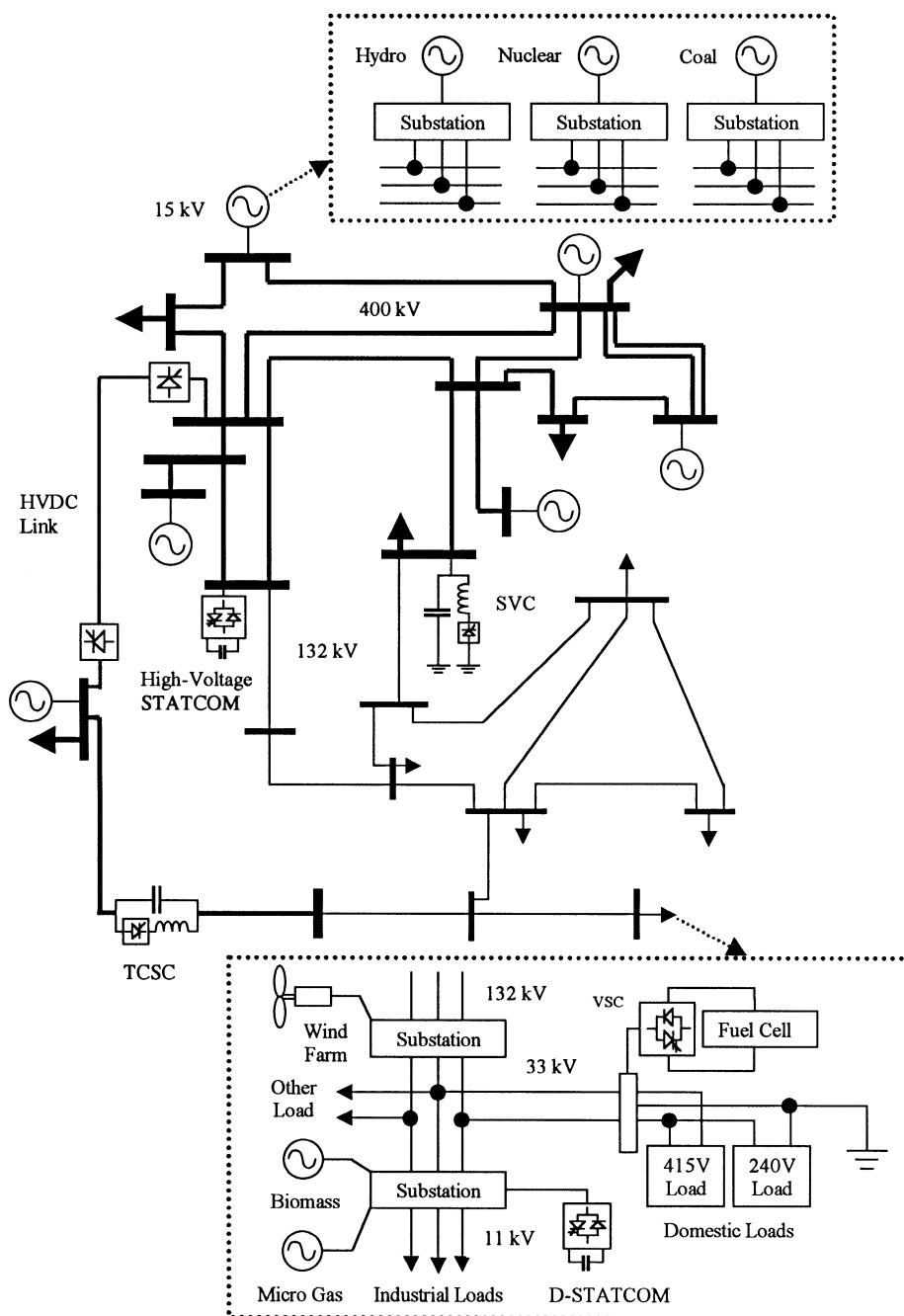
Fig. 1.1 Power network.

1.3.1   Generation

The large demand for electrical energy coupled with its continuous varying nature and our inability to store electrical energy in significant quantities calls for a diversity of generating sources in the power network. The traditional view is that the use of different primary energy resources helps with continuity of supply and a more stable pricing mechanism.

Most of the electricity consumed worldwide is produced by three-phase synchronous generators (Kundur, 1994). However, three-phase induction generators will increase their production share when wind generation (Heier, 1998) becomes more widely available. Similarly, three-phase and single-phase static generators in the form of fuel cells and photovoltaic arrays should contribute significantly to global electricity production in the future.

For system analysis purposes the synchronous machine can be seen as consisting of a stationary part, i.e. armature or stator, and a moving part, the rotor, which under steady state conditions rotates at synchronous speed.

Synchronous machines are grouped into two main types, according to their rotor structure (Fitzgerald et al., 1983):

1. salient pole machines
2. round rotor machines.

Steam turbine driven generators (turbo-generators) work at high speed and have round rotors. The rotor carries a DC excited field winding. Hydro units work at low speed and have salient pole rotors. They normally have damper windings in addition to the field winding. Damper windings consist of bars placed in slots on the pole faces and connected together at both ends. In general, steam turbines contain no damper windings but the solid steel of the rotor offers a path for eddy currents, which have similar damping effects. For simulation purposes, the currents circulating in the solid steel or in the damping windings can be treated as currents circulating in two closed circuits (Kundur, 1994). Accordingly, a three-phase synchronous machine may be assumed to have three stator windings and three rotor windings. All six windings will be magnetically coupled.

Figure 1.2 shows the schematic diagram of the machine while Figure 1.3 shows the coupled circuits. The relative position of the rotor with respect to the stator is given by the angle between the rotor's direct axis and the axis of the phase A winding in the stator. In the rotor, the direct axis (d-axis) is magnetically centred in the north pole. A second axis located 90 electrical degrees behind the direct axis is called the quadrature axis (q-axis).

In general, three main control systems directly affect the turbine-generator set:

1. the boiler's firing control
2. the governor control
3. the excitation system control.

Figure 1.4 shows the interaction of these controls and the turbine-generator set.

The excitation system control consists of an exciter and the AVR. The latter regulates the generator terminal voltage by controlling the amount of current supplied to the field winding by the exciter. The measured terminal voltage and the
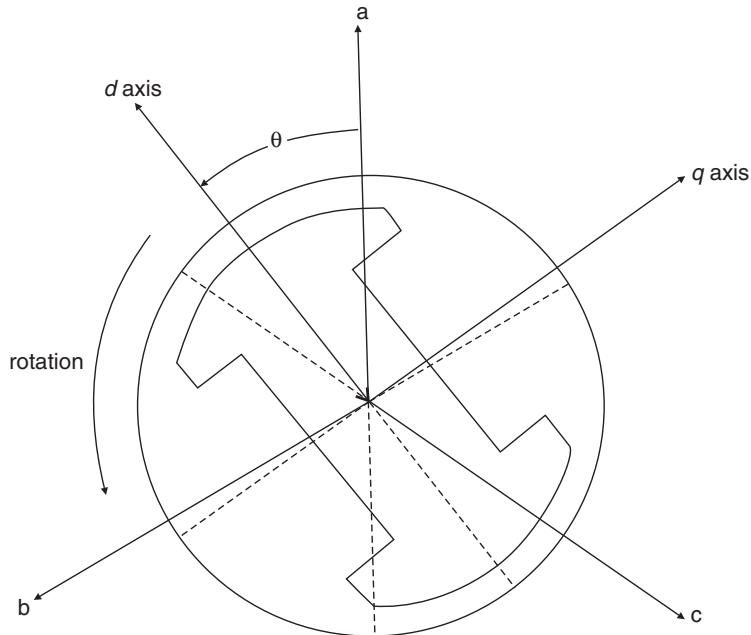
**Fig. 1.2** Schematic diagram of a synchronous machine.
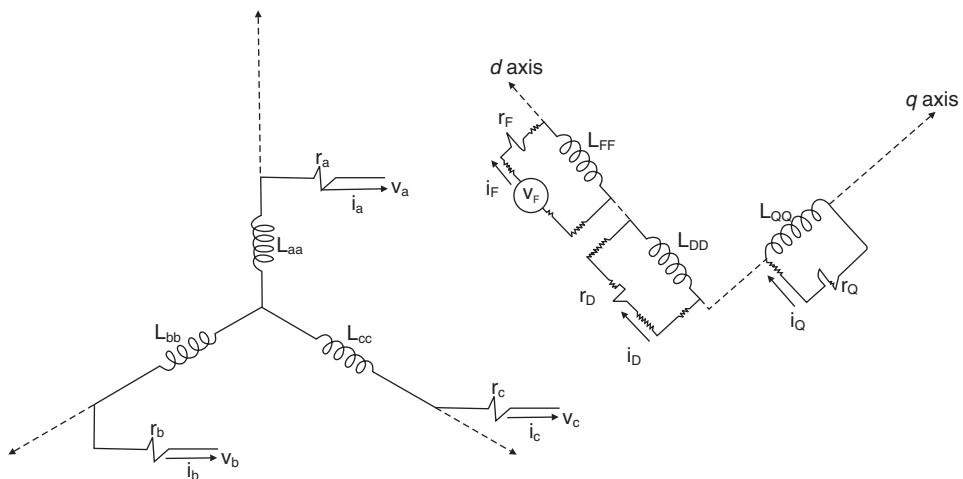
Fig. 1.3 Coupled windings of a synchronous machine.

desired reference voltage are compared to produce a voltage error which is used to alter the exciter output. Generally speaking, exciters can be of two types: (1) rotating; or (2) static. Nowadays, static exciters are the preferred choice owing to their higher
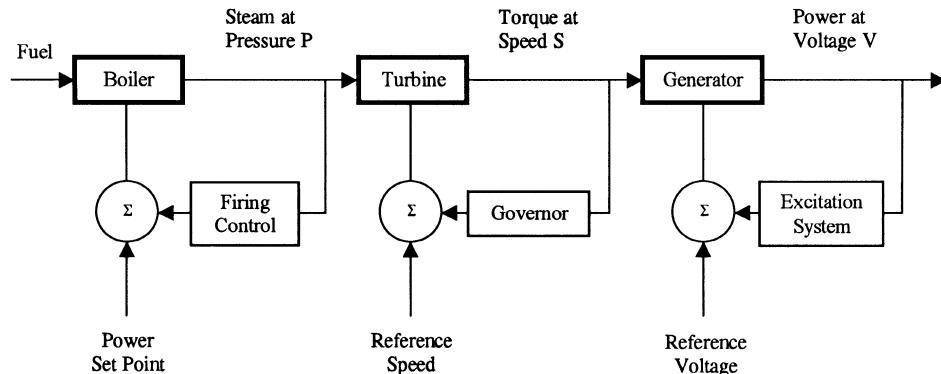
Fig. 1.4 Main controls of a generating unit.

speed of response and smaller size. They use thyristor rectifiers to adjust the field current (Aree, 2000).

1.3.2   Transmission

Transmission networks operate at high voltage levels such as 400 kV and 275 kV, because the transmission of large blocks of energy is more efficient at high voltages (Weedy, 1987). Step-up transformers in generating substations are responsible for increasing the voltage up to transmission levels and step-down transformers located in distribution substations are responsible for decreasing the voltage to more manageable levels such as 66 kV or 11 kV.

High-voltage transmission is carried by means of AC overhead transmission lines and DC overhead transmission lines and cables. Ancillary equipment such as switchgear, protective equipment and reactive power support equipment is needed for the correct functioning of the transmission system.

High-voltage transmission networks are usually 'meshed' to provide redundant paths for reliability. Figure 1.5 shows a simple power network.

Under certain operating conditions, redundant paths may give rise to circulating power and extra losses. Flexible alternating current transmission systems controllers are able to prevent circulating currents in meshed networks (IEEE/CIGRE, 1995).

Overhead transmission lines are used in high-voltage transmission and in distribution applications. They are built in double circuit, three-phase configuration in the same tower, as shown in Figure 1.6.

They are also built in single circuit, three-phase configurations, as shown in Figure 1.7.

Single and double circuit transmission lines may form busy transmission corridors. In some cases as many as six three-phase circuits may be carried on just one tower.

In high-voltage transmission lines, each phase consists of two or four conductors per phase, depending on their rated voltage, in order to reduce the total series impedance of the line and to increase transmission capacity. One or two sky wires are used for protection purposes against lightning strikes.

Underground cables are used in populated areas where overhead transmission lines are impractical. Cables are manufactured in a variety of forms to serve different
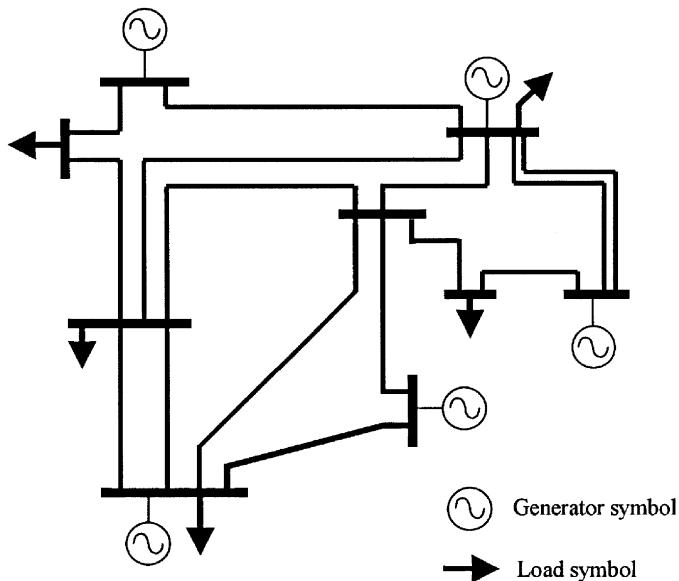
Fig. 1.5 Meshed transmission network.
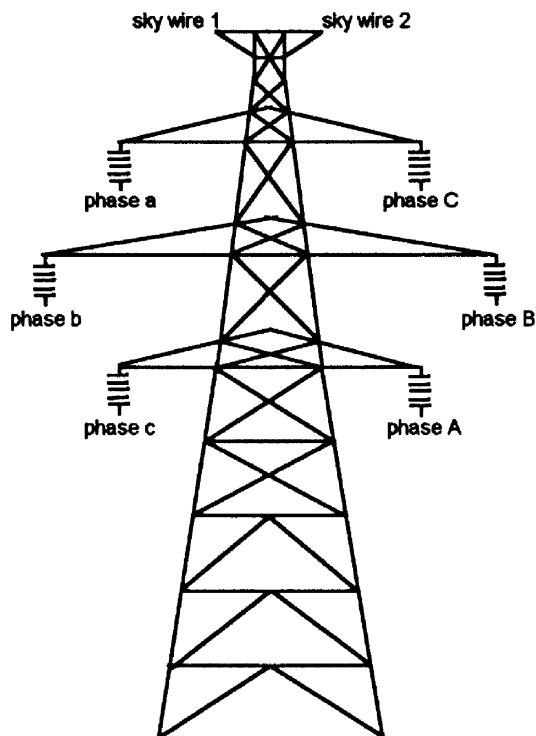
Fig. 1.6 Double circuit transmission line.
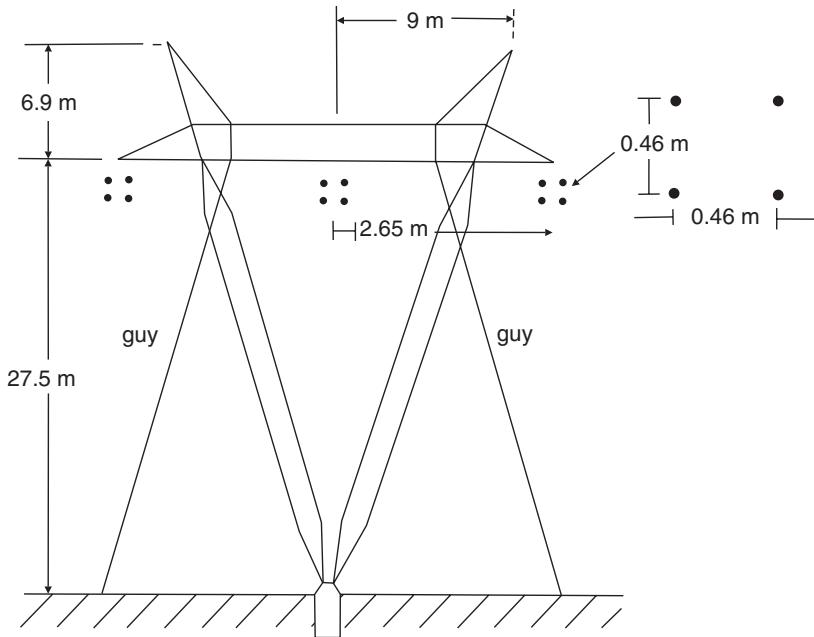
Fig. 1.7 Single circuit transmission line.
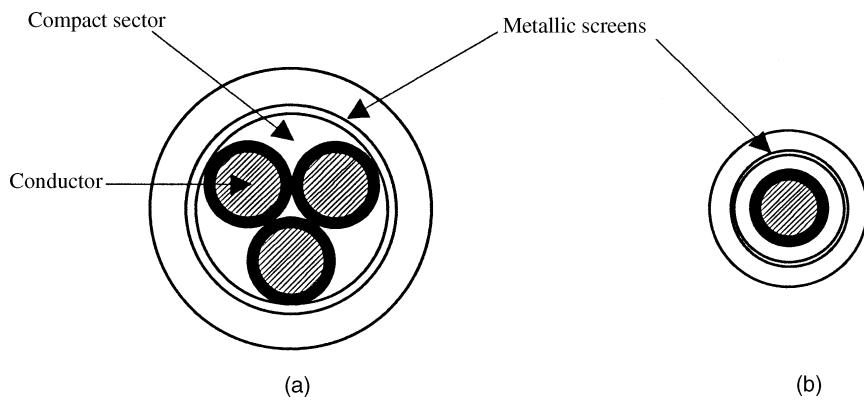
Fig. 1.8 (a) Three-conductor, shielded, compact sector; and (b) one-conductor, shielded.

applications. Figure 1.8 shows shielded, three-phase and single-phase cables; both have a metallic screen to help confine the electromagnetic fields.

Belted cables are generally used for three-phase, low-voltage operation up to approximately 5 kV, whilst three-conductor, shielded, compact sector cables are most commonly used in three-phase applications at the 5–46 kV voltage range. At higher voltages either gas or oil filled cables are used.

Power transformers are used in many different ways. Some of the most obvious applications are:

- as step-up transformers to increase the operating voltage from generating levels to transmission levels;
- as step-down transformers to decrease the operating voltage from transmission levels to utilization levels;
- as control devices to redirect power flows and to modulate voltage magnitude at a specific point of the network;
- as 'interfaces' between power electronics equipment and the transmission network.

For most practical purposes, power transformers may be seen as consisting of one or more iron cores and two or three copper windings per phase. The three-phase windings may be connected in a number of ways, e.g. star–star, star–delta and delta–delta.

Modern three-phase power transformers use one of the following magnetic core types: three single-phase units, a three-phase unit with three legs or a three-phase unit with five legs.

Reactive power equipment is an essential component of the transmission system (Miller, 1982). It is used for voltage regulation, stability enhancement and for increasing power transfers. These functions are normally carried out with mechanically controlled shunt and series banks of capacitors and non-linear reactors. However, when there is an economic and technical justification, the reactive power support is provided by electronic means as opposed to mechanical means, enabling near instantaneous control of reactive power, voltage magnitude and transmission line impedance at the point of compensation.

The well-established SVC and the STATCOM, a more recent development, is the equipment used to provide reactive power compensation (Hingorani and Gyugyi, 2000). Figure 1.9 shows a three-phase, delta connected, thyristor-controlled reactor (TCR) connected to the secondary side of a two-winding, three-legged transformer. Figure 1.10 shows a similar arrangement but for a three-phase STATCOM using GTO switches. In lower power applications, IGBT switches may be used instead.

Although the end function of series capacitors is to provide reactive power to the compensated transmission line, its role in power system compensation is better understood as that of a series reactance compensator, which reduces the electrical length of the line. Figure 1.11(a) illustrates one phase of a mechanically controlled, series bank of capacitors whereas Figure 1.11(b) illustrates its electronically controlled counterpart (Kinney et al., 1994). It should be pointed out that the latter has the ability to exert instantaneous active power flow control.

Several other power electronic controllers have been built to provide adaptive control to key parameters of the power system besides voltage magnitude, reactive power and transmission line impedance. For instance, the electronic phase shifter is used to enable instantaneous active power flow control. Nowadays, a single piece of equipment is capable of controlling voltage magnitude and active and reactive power. This is the UPFC, the most sophisticated power controller ever built (Gyugyi, 1992). In its simplest form, the UPFC comprises two back-to-back VSCs, sharing a DC capacitor. As illustrated in Figure 1.12, one VSC of the UPFC is connected in shunt and the second VSC is connected in series with the power network.
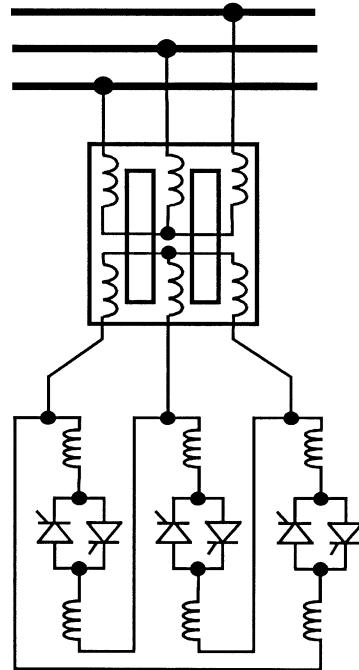
**Fig. 1.9** Three-phase thyristor-controlled reactor connected in delta.
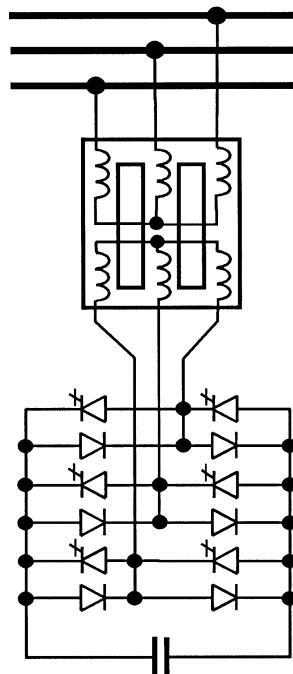
**Fig. 1.10** Three-phase GTO-based STATCOM.

(a)

(b)
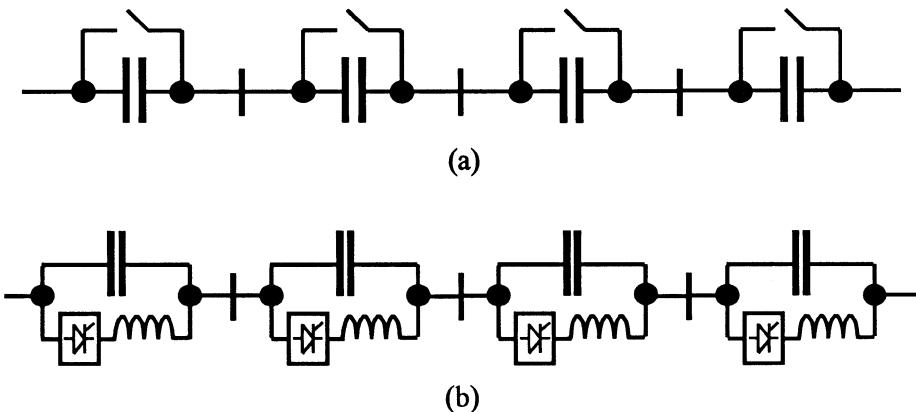
Fig. 1.11 One phase of a series capacitor. (a) mechanically controlled; and (b) electronically controlled.

HVDC Light is a very recent development in electric power transmission. It has many technical and economical characteristics, which make it an ideal candidate for a variety of transmission applications where conventional HVDC is unable to compete. For instance, it can be used to supply passive loads, to provide reactive power support and to improve the quality of supply in AC networks. The installation contributes no short-circuit current and may be operated with no transformers. It is said that it has brought down the economical power range of HVDC transmission to only a few megawatts (Asplund et al., 1998). The HVDC Light at Hellsjön is reputed to be the world's first installation and is rated at 3 MW and ±10 kV DC. At present, the technology enables power ratings of up to 200 MW. In its simplest form, it comprises two STATCOMs linked by a DC cable, as illustrated in Figure 1.13.

1.3.3   Distribution

Distribution networks may be classified as either meshed or radial. However, it is customary to operate meshed networks in radial fashion with the help of mechanically operated switches (Gönen, 1986). It is well understood that radial networks are less reliable than interconnected networks but distribution engineers have preferred them because they use simple, inexpensive protection schemes, e.g. over-current protection. Distribution engineers have traditionally argued that in meshed distribution networks operated in radial fashion, most consumers are brought back on supply a short time after the occurrence of a fault by moving the network's open points. Open-point movements are carried out by reswitching operations.

Traditional construction and operation practices served the electricity distribution industry well for nearly a century. However, the last decade has seen a marked increase in loads that are sensitive to poor quality electricity supply. Some large industrial users are critically dependent on uninterrupted electricity supply and suffer large financial losses as a result of even minor lapses in the quality of electricity supply (Hingorani, 1995).
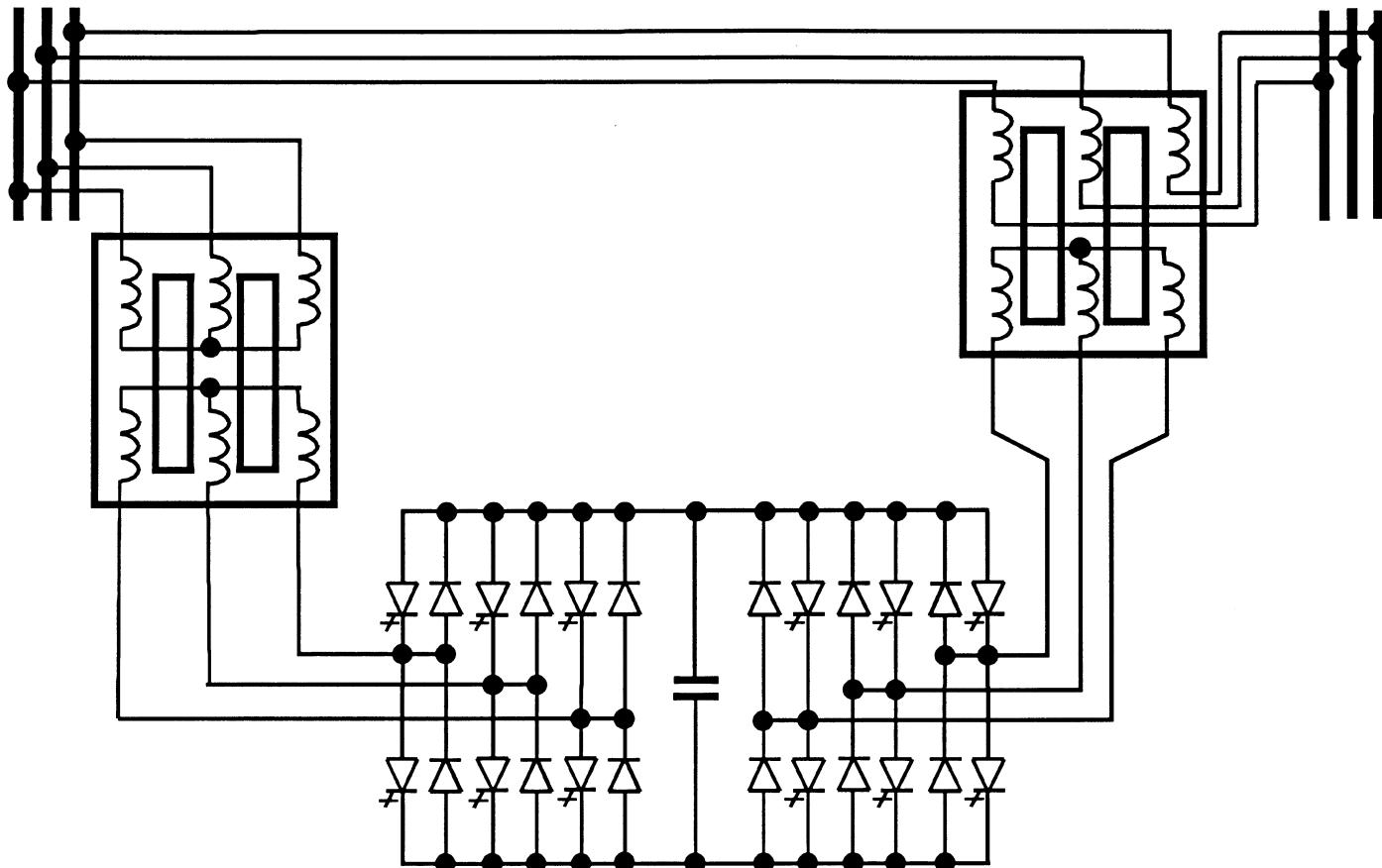
Fig. 1.12 Three-phase unified power flow controller.

Cable Impedance

Rectifier Station

Inverter Station
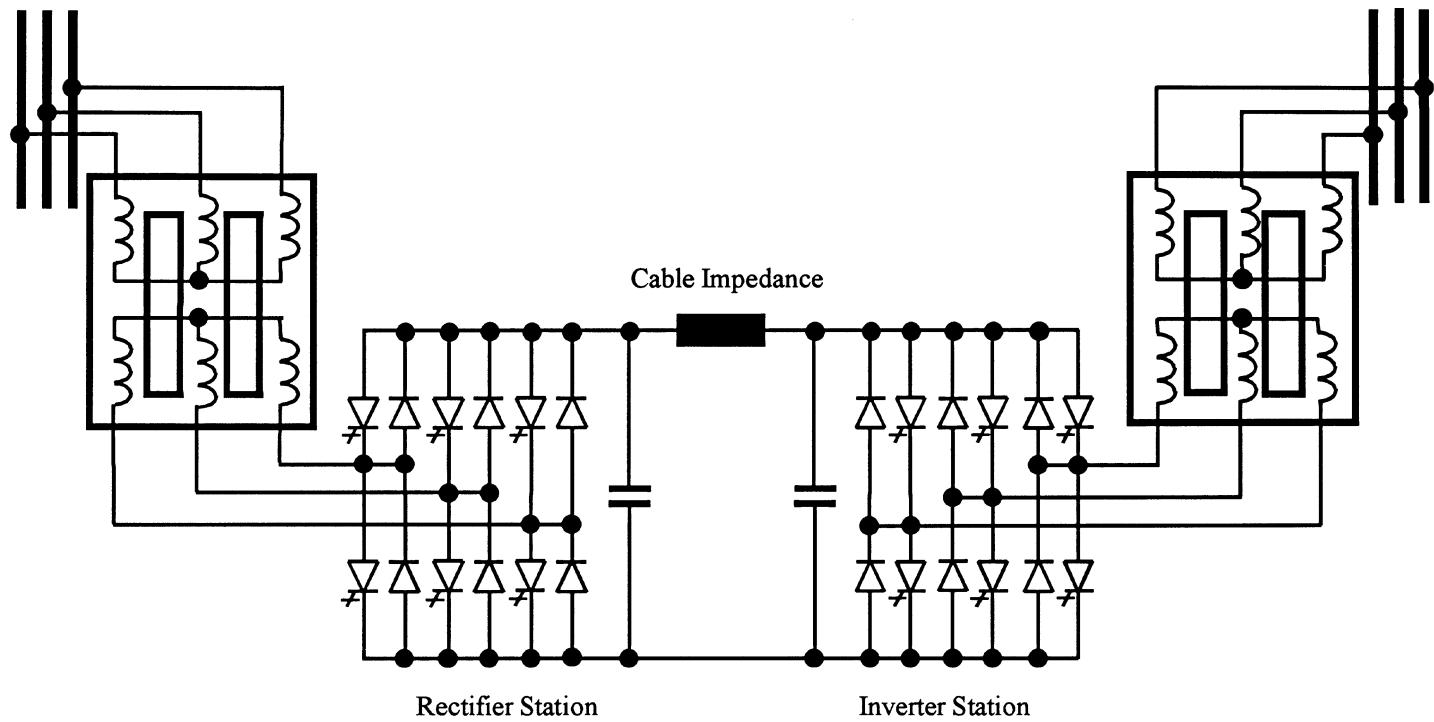
Fig. 1.13 HVDC Light systems using VSCs.

These factors coupled with the ongoing deregulation and open access electricity markets, where large consumers may shop around for competitively priced, high-quality electricity, have propelled the distribution industry into unprecedented change. On the technical front, one major development is the incorporation of power electronics controllers in the distribution system to supply electricity with high quality to selected customers. The generic, systematic solution being considered by the utility to counter the problem of interruptions and low power quality at the end-user level is known as Custom Power. This is the low voltage counterpart of the more widely known FACTS technology.

Although FACTS and custom power initiatives share the same technological base, they have different technical and economic objectives (Hingorani and Gyugyi, 2000). Flexible alternating current transmission systems controllers are aimed at the transmission level whereas Custom Power controllers are aimed at the distribution level, in particular, at the point of connection of the electricity distribution company with clients with sensitive loads and independent generators. Custom Power focuses primarily on the reliability and quality of power flows. However, voltage regulation, voltage balancing and harmonic cancellation may also benefit from this technology.

The STATCOM, the DVR and the solid state switch (SSS) are the best known Custom Power equipment. The STATCOM and the DVR both use VSCs, but the former is a shunt connected device which may include the functions of voltage control, active filtering and reactive power control. The latter is a series connected device which precisely compensates for waveform distortion and disturbances in the neighbourhood of one or more sensitive loads. Figure 1.10 shows the schematic representation of a three-phase STATCOM. Figure 1.14 shows that of a DVR and Figure 1.15 shows one phase of a three-phase thyristor-based SSS.

The STATCOM used in Custom Power applications uses PWM switching control as opposed to the fundamental frequency switching strategy preferred in FACTS applications. PWM switching is practical in Custom Power because this is a relatively low power application.

On the sustainable development front, environmentally aware consumers and government organizations are providing electricity distribution companies with a good business opportunity to supply electricity from renewable sources at a premium. The problem yet to be resolved in an interconnected system with a generation mix is how to comply with the end-user's desire for electricity from a renewable source. Clearly, a market for renewable generation has yet to be realized.

1.3.4   Utilization

The customers of electricity vendors may be classified as industrial, commercial and domestic (Weedy, 1987). In industrialized societies, the first group may account for as much as two fifths of total demand. Traditionally, induction motors have formed the dominant component in the vast array of electric equipment found in industry, both in terms of energy consumption and operational complexity. However, computer-assisted controllers and power electronics-based equipment, essential features in modern manufacturing processes, present the current challenge in terms of ensuring their trouble-free operation. This equipment requires to be supplied with high quality electricity.
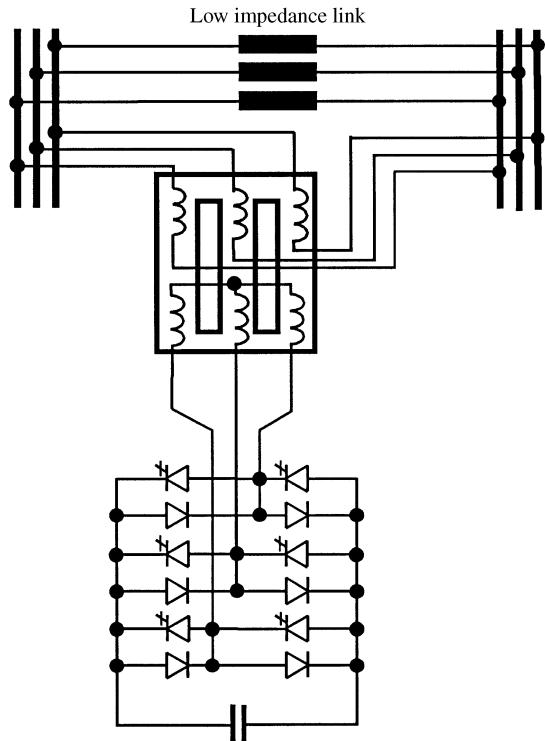
**Fig. 1.14** Three-phase dynamic voltage restorer.
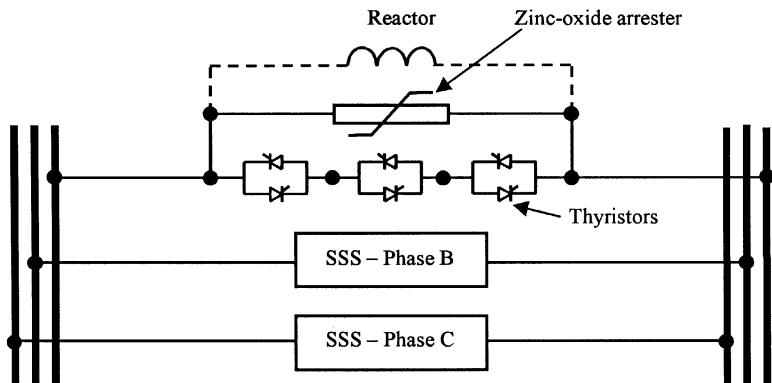
Fig. 1.15 Thyristor-based solid state switch.

Some loads draw constant current from the power system and their operation may be affected by supply voltage and frequency variations. Examples of these loads are:

- induction motors
- synchronous motors
- DC motors.

Other types of loads are less susceptible to voltage and frequency variations and exhibit a constant resistance characteristic:

● incandescent lighting
● heating.

Large clusters of end user loads based on power electronics technology are capable of injecting significant harmonic currents back into the network. Examples of these are:

● colour TV sets
● microwave ovens
● energy saving lamps
● computer equipment
● industrial variable speed motor drives
● battery recharging stations.

Electric energy storage is an area of great research activity, which over the last decade has experienced some very significant breakthroughs, particularly with the use of superconductivity and hydrogen related technologies. Nevertheless, for the purpose of industrial applications it is reasonable to say that, apart from pumped hydro storage, there is very little energy storage in the system. Thus, at any time the following basic relation must be met:

$$Generation = Demand + Transmission\ Losses$$

Power engineers have no direct control over the electricity demand. Load shedding may be used as a last resort but this is not applicable to normal system control. It is normally carried out only under extreme pressure when serious faults or overloads persist.

1.4   An overview of the dynamic response of electrical power networks

Electrical power systems aim to provide a reliable service to all consumers and should be designed to cope with a wide range of normal, i.e. expected, operating conditions, such as:

● connection and disconnection of both large and small loads in any part of the network
● connection and disconnection of generating units to meet system demand
● scheduled topology changes in the transmission system.

They must also cope with a range of abnormal operating conditions resulting from faulty connections in the network, such as sudden loss of generation, phase conductors falling to the ground and phase conductors coming into direct contact with each other.

    The ensuing transient phenomena that follow both planned and unplanned events bring the network into dynamic operation. In practice, the system load and the generation are changing continuously and the electrical network is never in a truly steady state condition, but in a perpetual dynamic state. The dynamic performance of

the network exhibits a very different behaviour within different time frames because of the diversity of its components (de Mello, 1975):

- rotating machinery
- transmission lines and cables
- power transformers
- power electronics based controllers
- protective equipment
- special controls.

The various plant components respond differently to the same stimulus. Accordingly, it is necessary to simplify, as much as is practicable, the representation of the plant components which are not relevant to the phenomena under study and to represent in sufficient detail the plant components which are essential to the study being taken. A general formulation and analysis of the electrical power network is complex because electrical, mechanical and thermal effects are interrelated.

For dynamic analysis purposes the power network has traditionally been sub-divided as follows (Anderson and Fouad, 1977):

- synchronous generator and excitation system
- turbine-governor and automatic generation control
- boiler control
- transmission network
- loads.

The importance of the study, the time scales for which the study is intended and the time constants of the plant components are some of the factors which influence model selection (de Mello, 1975). Figure 1.16 gives a classification of power systems' dynamic phenomena.
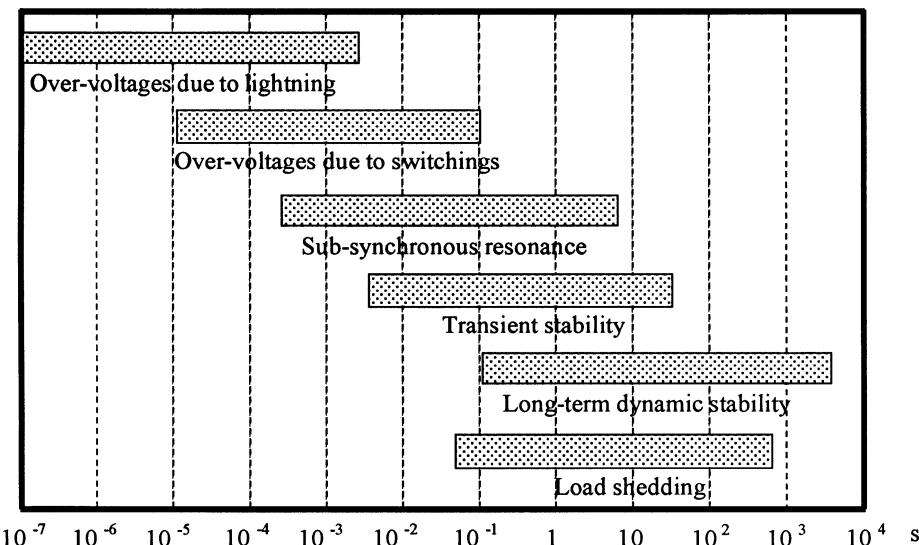

Fig. 1.16 Classification of power systems' dynamic studies.

Studies involving over-voltages due to lightning and switching operations require a detailed representation of the transmission system and the electrical properties of the generators, with particular attention paid to the capacitive effects of transmission lines, cables, generators and transformers. Over very short time scales the mechanical parameters of the generators and most controls can be ignored because they have no time to react to these very fast events, which take place in the time scale $10^{-7}\,\text{s} \leq t \leq 10^{-2}\,\text{s}$.

On the other hand, the long term dynamics associated with load frequency control and load shedding involve the dynamic response of the boiler and turbine-governor set and do not require a detailed representation of the transmission system because at the time scales $10^{-1}\,\text{s} \leq t \leq 10^{3}\,\text{s}$, the electrical transient has already died out. However, a thorough representation of the turbine governor and boiler controls is essential if meaningful conclusions are to be obtained. The mechanical behaviour of the generators has to be represented in some detail because mechanical transients take much longer to die out than electrical transients.

1.4.1 Transient stability

Sub-synchronous resonance and transient stability studies are used to assess power systems' dynamic phenomena that lie somewhere in the middle, between electromagnetic transients due to switching operations and long-term dynamics associated with load frequency control. In power systems transient stability, the boiler controls and the electrical transients of the transmission network are neglected but a detailed representation is needed for the AVR and the mechanical and electrical circuits of the generator. The controls of the turbine governor are represented in some detail. In sub-synchronous resonance studies, a detailed representation of the train shaft system is mandatory (Bremner, 1996).

Arguably, transient stability studies are the most popular dynamic studies. Their main objective is to determine the synchronous generator's ability to remain stable after the occurrence of a fault or following a major change in the network such as the loss of an important generator or a large load (Stagg and El-Abiad, 1968).

Faults need to be cleared as soon as practicable. Transient stability studies provide valuable information about the critical clearance times before one or more synchronous generators in the network become unstable. The internal angles of the generator give reasonably good information about critical clearance times.

Figure 1.17 shows a five-node power system, containing two generators, seven transmission lines and four load points.

A three-phase to ground fault occurs at the terminals of Generator two, located at node two, and the transient stability study shows that both generators are stable with a fault lasting 0.1 s, whilst Generator two is unstable with a fault lasting 0.2 s. Figure 1.18 shows the internal voltage angles of the two generators and their ratio of actual to rated speed. Figures 1.18(a) and (b) show the results of the fault lasting 0.1 s and (c) and (d) the results of the fault lasting 0.2 s (Stagg and El-Abiad, 1968).

Transient stability studies are time-based studies and involve solving the differential equations of the generators and their controls, together with the algebraic equations representing the transmission power network. The differential equations

are discretized using the trapezoidal rule of integration and then combined with the network's equations using nodal analysis. The solution procedure is carried out step-by-step (Arrillaga and Watson, 2001).
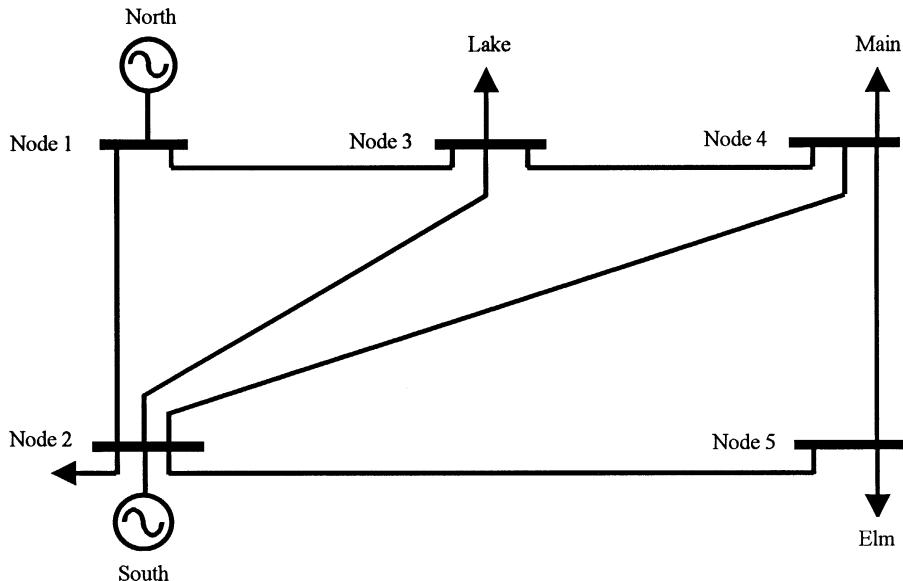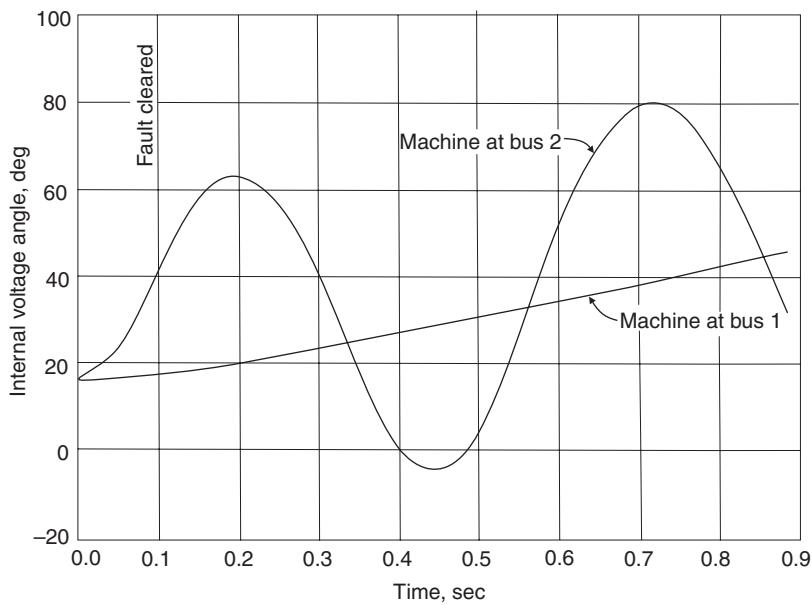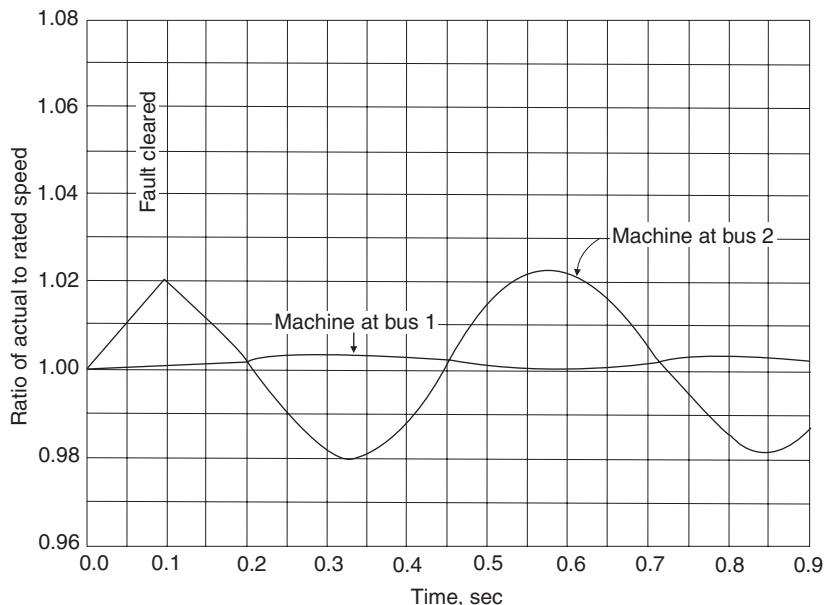
Fig. 1.17 A five-node power network with two generators, seven transmission lines and four loads.

(a)
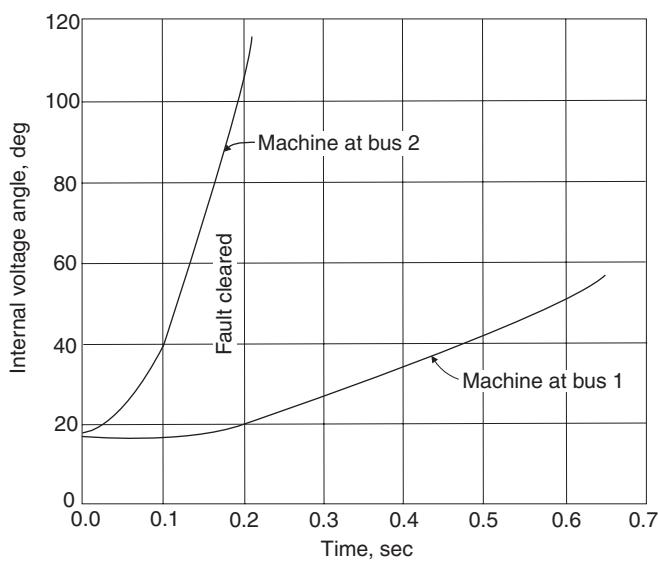
Fig 1.18 (*continued*)

(b)

(c)
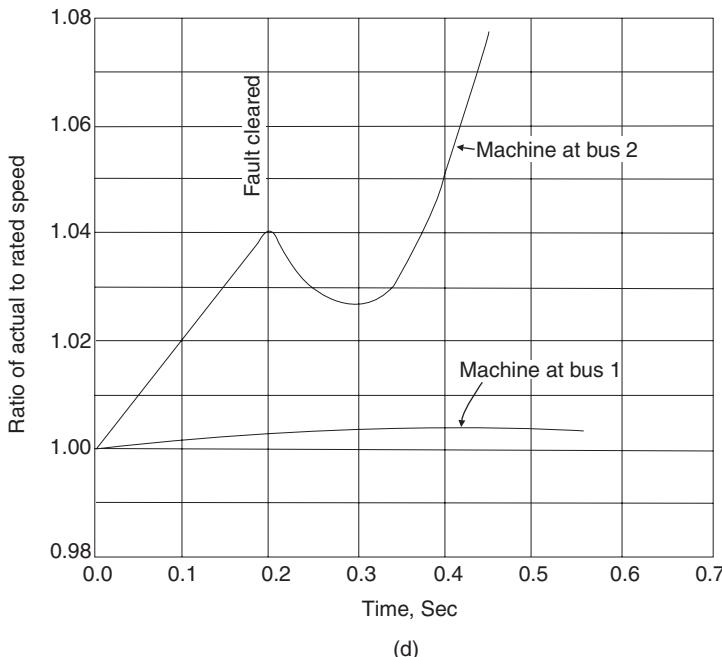
Fig. 1.18 Internal voltage angles of the generators in a five-node system with two generators: (i) fault duration of 0.1 s: (a) internal voltage angles in degrees; (b) ratio of actual to rated speed; (ii) fault duration of 0.2 s: (c) internal voltage angles in degrees; and (d) ratio of actual to rated speed (1) (© 1968 McGraw-Hill).

Flexible alternating current transmission systems equipment responds with little delay to most power systems' disturbances occurring in their vicinity. They modify one or more key network parameters and their control objectives are: (i) to aid the system to remain stable following the occurrence of a fault by damping power oscillations; (ii) to prevent voltage collapse following a steep change in load; and (iii) to damp torsional vibration modes of turbine generator units (IEEE/CIGRE, 1995). Power system transient stability packages have been upgraded or are in the process of being upgraded to include suitable representation of FACTS controllers (Edris, 2000).

1.5   Snapshot-like power network studies

1.5.1   Power flow studies

Although in reality the power network is in a continuous dynamic state, it is useful to assume that at one point the transient produced by the last switching operation or topology change has died out and that the network has reached a state of equilibrium, i.e. steady state. This is the limiting case of long-term dynamics and the time frame of such steady state operation would be located at the far right-hand side of Figure 1.16. The analysis tool used to assess the steady state operation of the power

system is known as Load Flow or Power Flow (Arrillaga and Watson, 2001), and in its most basic form has the following objectives:

- to determine the nodal voltage magnitudes and angles throughout the network;
- to determine the active and reactive power flows in all branches of the network;
- to determine the active and reactive power contributed by each generator;
- to determine active and reactive power losses in each component of the network.

In steady state operation, the plant components of the network are described by their impedances and loads are normally recorded in MW and MVAr. Ohm's law and Kirchhoff's laws are used to model the power network as a single entity where the nodal voltage magnitude and angle are the state variables. The power flow is a non-linear problem because, at a given node, the power injection is related to the load impedance by the square of the nodal voltage, which itself is not known at the beginning of the study. Thus, the solution has to be reached by iteration. The solution of the non-linear set of algebraic equations representing the power flow problem is achieved efficiently using the Newton–Raphson method. The generators are represented as nodal power injections because in the steady state the prime mover is assumed to drive the generator at a constant speed and the AVR is assumed to keep the nodal voltage magnitude at a specified value.

Flexible alternating current transmission systems equipment provides adaptive regulation of one or more network parameters at key locations. In general, these controllers are able to regulate either nodal voltage magnitude or active power within their design limits. The most advanced controller, i.e. the UPFC, is able to exert simultaneous control of nodal voltage magnitude, active power and reactive power. Comprehensive models of FACTS controllers suitable for efficient, large-scale power flow solutions have been developed recently (Fuerte-Esquivel, 1997).

1.5.2 Optimal power flow studies

An optimal power flow is an advanced form of power flow algorithm. Optimal power flow studies are also used to determine the steady state operating conditions of power networks but they incorporate an objective function which is optimized without violating system operational constraints. The choice of the objective function depends on the operating philosophy of each utility company. However, active power generation cost is a widely used objective function. Traditionally, the constraint equations include the network equations, active and reactive power consumed at the load points, limits on active and reactive power generation, stability and thermal limits on transmission lines and transformers. Optimal power flow studies provide an effective tool for reactive power management and for assessing the effectiveness of FACTS equipment from the point of view of steady state operation. Comprehensive models of FACTS controllers suitable for efficient, large-scale optimal power flow solutions have been developed recently (Ambriz-Perez, 1998).

1.5.3 Fault studies

If it is assumed that the power network is operating in steady state and that a sudden change takes place due to a faulty condition, then the network will enter a dynamic state. Faults have a variable impact over time, with the highest values of current
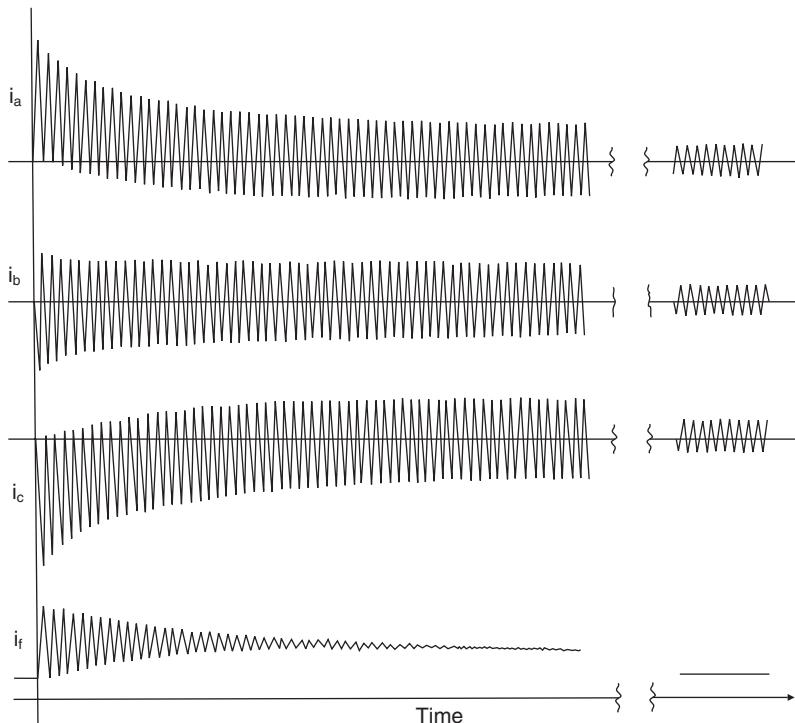
Fig. 1.19 Short-circuit currents of a synchronous generator (© 1995 IEEE).

being present during the first few cycles after the disturbance has occurred. This can be appreciated from Figure 1.19, where a three-phase, short-circuit at the terminals of a synchronous generator give rise to currents that clearly show the transient and steady (sustained) states. The figure shows the currents in phases *a*, *b* and *c*, as well as the field current. The source of this oscillogram is (Kimbark, 1995).

Faults are unpredictable events that may occur anywhere in the power network. Given that faults are unforeseen events, strategies for dealing with them must be decided well in advance (Anderson, 1973). Faults can be divided into those involving a single (nodal) point in the network, i.e. shunt faults, and those involving two points in one or more phases in a given plant component, i.e. series faults. Simultaneous faults involve any combination of the above two kinds of faults in one or more locations in the network. The following are examples of shunt faults:

- three-phase-to-ground short-circuit
- one-phase-to-ground short-circuit
- two-phase short-circuit
- two-phase-to-ground short-circuit.

The following are examples of series faults:

- one-phase conductor open
- two-phase conductors open
- three-phase conductors open.

In addition to the large currents flowing from the generators to the point in fault following the occurrence of a three-phase short-circuit, the voltage drops to extremely low values for the duration of the fault. The greatest voltage drop takes place at the point in fault, i.e. zero, but neighbouring locations will also be affected to varying degrees. In general, the reduction in root mean square (rms) voltage is determined by the electrical distance to the short-circuit, the type of short-circuit and its duration.

The reduction in rms voltage is termed voltage sag or voltage dip. Incidents of this are quite widespread in power networks and are caused by short-circuit faults, large motors starting and fast circuit breaker reclosures. Voltage sags are responsible for spurious tripping of variable speed motor drives, process control systems and computers. It is reported that large production plants have been brought to a halt by sags of 100 ms duration or less, leading to losses of hundreds of thousands of pounds (McHattie, 1998). These kinds of problems provided the motivation for the development of Custom Power equipment (Hingorani, 1995).

1.5.4   Random nature of system load

The system load varies continuously with time in a random fashion. Significant changes occur from hour to hour, day to day, month to month and year to year (Gross and Galiana, 1987). Figure 1.20 shows a typical load measured in a distribution substation for a period of four days.

The random nature of system load may be included in power flow studies and this finds useful applications in planning studies and in the growing 'energy stock market'. Some possible approaches for modelling random loads within a power flow study are:

● modelling the load as a distribution function, e.g. normal distribution;
● future load is forecast by means of time series analysis based on historic values, then normal power flow studies are performed for each forecast point;
● the same procedure as in two but load forecasting is achieved using Neural Networks.
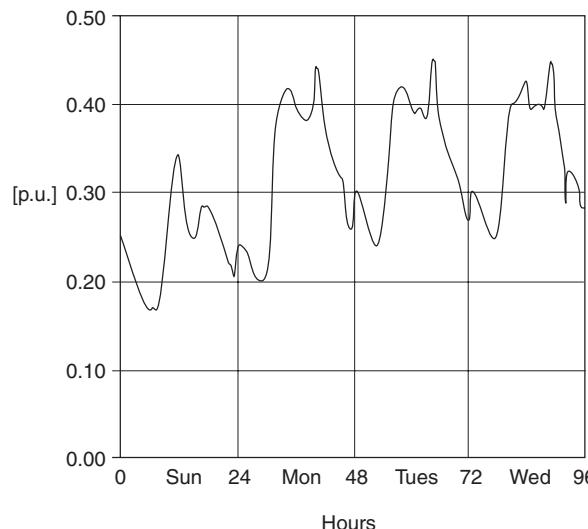
Fig. 1.20 A typical load measured at a distribution substation.

1.5.5 Non-linear loads

Many power plant components have the ability to draw non-sinusoidal currents and, under certain conditions, they distort the sinusoidal voltage waveform in the power network. In general, if a plant component is excited with sinusoidal input and produces non-sinusoidal output, then such a component is termed non-linear, otherwise, it is termed linear (Acha and Madrigal, 2001). Among the non-linear power plant components we have:

- power electronics equipment
- electric arc furnaces
- large concentration of energy saving lamps
- saturated transformers
- rotating machinery.

Some of the more common adverse effects caused by non-linear equipment are:

- the breakdown of sensitive industrial processes
- permanent damage to utility and consumer equipment
- additional expenditure in compensating and filtering equipment
- loss of utility revenue
- additional losses in the network
- overheating of rotating machinery
- electromagnetic compatibility problems in consumer installations
- interference in neighbouring communication circuits
- spurious tripping of protective devices.

1.6 The role of computers in the monitoring, control and planning of power networks

Computers play a key role in the operation, management and planning of electrical power networks. Their use is on the increase due to the complexity of today's interconnected electrical networks operating under free market principles.

1.6.1 Energy control centres

Energy control centres have the objective to monitor and control the electrical network in real-time so that secure and economic operation is achieved round the clock, with a minimum of operator intervention. They include:

- 'smart' monitoring equipment
- fast communications
- power systems application software
- an efficient database
- mainframe computers.
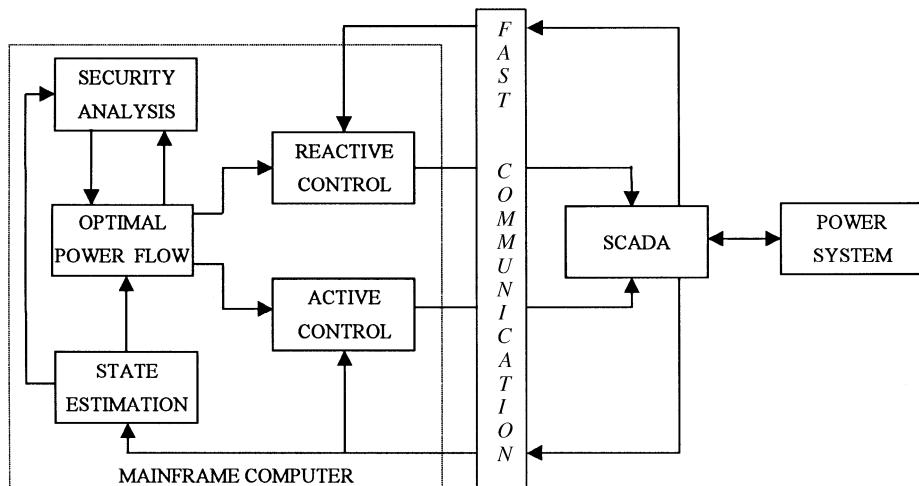
Fig. 1.21 Real-time environment.

The main power systems software used for the real-time control of the network is (Wood and Wollenberg, 1984):

- state estimation
- security analysis
- optimal power flows.

These applications provide the real-time means of controlling and operating power systems securely. In order to achieve such an objective they execute sequentially. Firstly, they validate the condition of the power system using the state estimator and then they develop control actions, which may be based on economic considerations while avoiding actual or potential security violations.

Figure 1.21 shows the real-time environment where the supervisory control and data acquisition (SCADA) and the active and reactive controls interact with the real-time application programmes.

1.6.2 Distribution networks

Most distribution networks do not have real-time control owing to its expense and specialized nature, but SCADA systems are used to gather load data information. Data is a valuable resource that allows better planning and, in general, better management of the distribution network (Gönen, 1986). The sources of data typically found in UK distribution systems are illustrated in Figure 1.22. These range from half hourly telemetered measurements of voltage, current and power flow at the grid supply point down to the pole mounted transformer supplying residential loads, where the only information available is the transformer rating. Most distribution substations have the instrumentation needed to measure and store current information every half hour, and some of them also have provision to measure and store voltage information. Large industrial customers may have SCADA systems of their
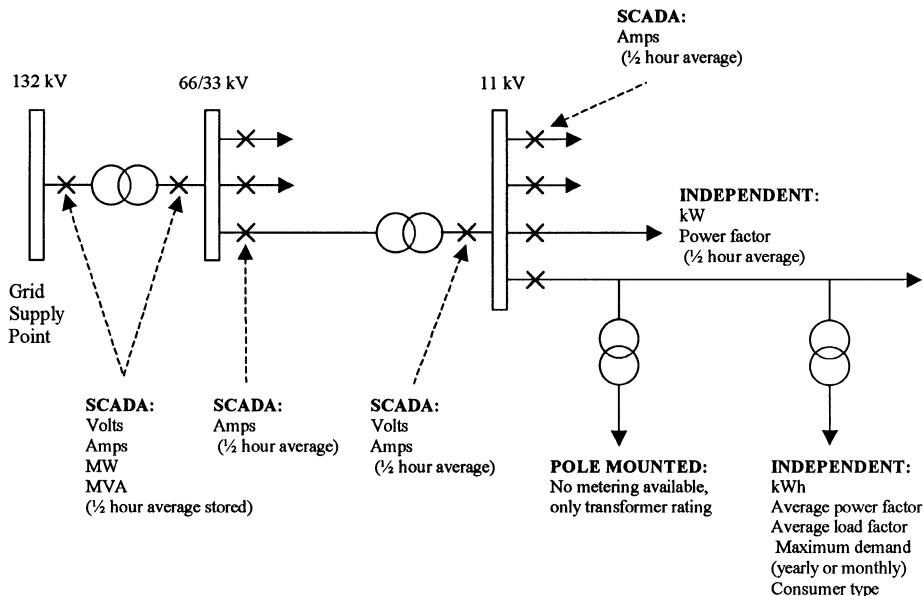
Fig. 1.22 Distribution system data sources.

own and are able to measure electricity consumption, power factor and average load factor.

1.6.3   Planning

At the planning level, increasingly powerful computer resources are dedicated to hosting the extensive power systems analysis tools already available (Stoll, 1989). At present, the emphasis is on corporate databases, geographic information systems and interactive graphics to develop efficient interfaces which blend seamlessly with legacy power systems software. The current trend is towards web applications and e-business which should help companies to cope with the very severe demands imposed on them by market forces.

1.7   Conclusion

This chapter has presented an overview of the composition of electrical power networks and the computer assisted studies that are used for their planning, operation and management.

The main plant components used in modern power networks are described, and the growing ascendancy of power electronics-based equipment in power network control is emphasized. This equipment is classified into equipment used in high voltage transmission and equipment used in low voltage distribution. The former belongs to the family of plant components known as FACTS equipment and the latter belongs to the family of Custom Power equipment. A generic power system

network has been used to give examples of FACTS and Custom Power plant equipment and in which locations of the network they may be deployed.

The random nature of the power system load, the ability of a certain class of loads to generate harmonic distortion, and our limited capacity to store electrical energy in significant quantities are issues used to exemplify some of the challenges involved in the planning and operation of electrical power networks. This is in addition to the fact that power networks span entire continents and they are never in a steady state condition but rather in a perpetual dynamic state. This is part of the complex background which since the late 1950s has continuously called for the use of state-of-the-art computers and advanced algorithms to enable their reliable and economic operation. The main computer-based studies used in today's power systems are outlined in this introductory chapter.

2

Power systems engineering – fundamental concepts

2.1 Reactive power control

In an ideal AC power system the voltage and frequency at every supply point would be constant and free from harmonics, and the power factor would be unity. In particular these parameters would be independent of the size and characteristics of consumers' loads. In an ideal system, each load could be designed for optimum performance at the given supply voltage, rather than for merely adequate performance over an unpredictable range of voltage. Moreover, there could be no interference between different loads as a result of variations in the current taken by each one (Miller, 1982).

In three-phase systems, the phase currents and voltages must also be balanced.[1] The *stability* of the system against oscillations and faults must also be assured. All these criteria add up to a notion of *power quality*. A single numerical definition of power quality does not exist, but it is helpful to use quantities such as the maximum fluctuation in rms supply voltage averaged over a stated period of time, or the total harmonic distortion (THD), or the 'availability' (i.e. the percentage of time, averaged over a period of, say, a year, for which the supply is uninterrupted).

The maintenance of constant frequency requires an exact balance between the overall power supplied by generators and the overall power absorbed by loads, irrespective of the voltage. However, the voltage plays an important role in maintaining the stability of power transmission, as we shall see. Voltage levels are very sensitive to the flow of reactive power and therefore the control of reactive power is

---

[1] Unbalance causes negative-sequence current which produces a backward-rotating field in rotating AC machines, causing torque fluctuations and power loss with potential overheating.

important. This is the subject of *reactive compensation*. Where the focus is on individual loads, we speak of *load compensation*, and this is the main subject of this chapter along with several related fundamental topics of power systems engineering. Chapter 3 deals with reactive power control on long-distance high-voltage transmission systems, that is, *transmission system compensation*.

Load compensation is the management of reactive power to improve the quality of supply at a particular load or group of loads. Compensating equipment – such as power-factor correction equipment – is usually installed on or near to the consumer's premises. In load compensation there are three main objectives:

1. power-factor correction
2. improvement of voltage regulation[2]
3. load balancing.

Power-factor correction and *load balancing* are desirable even when the supply voltage is 'stiff': that is, even when there is no requirement to improve the voltage regulation. Ideally the reactive power requirements of a load should be provided locally, rather than drawing the reactive component of current from a remote power station. Most industrial loads have lagging power factors; that is, they absorb reactive power. The load current therefore tends to be larger than is required to supply the real power alone. Only the real power is ultimately useful in energy conversion and the excess load current represents a waste to the consumer, who has to pay not only for the excess cable capacity to carry it, but also for the excess Joule loss in the supply cables. When load power factors are low, generators and distribution networks cannot be used at full efficiency or full capacity, and the control of voltage throughout the network can become more difficult. Supply tariffs to industrial customers usually penalize low power-factor loads, encouraging the use of power-factor correction equipment.

In *voltage regulation* the supply utilities are usually bound by statute to maintain the voltage within defined limits, typically of the order of $\pm 5\%$ at low voltage, averaged over a period of a few minutes or hours. Much more stringent constraints are imposed where large, rapidly varying loads could cause voltage dips hazardous to the operation of protective equipment, or flicker annoying to the eye.

The most obvious way to improve voltage regulation would be to 'strengthen' the power system by increasing the size and number of generating units and by making the network more densely interconnected. This approach is costly and severely constrained by environmental planning factors. It also raises the fault level and the required switchgear ratings. It is better to size the transmission and distribution system according to the maximum demand for *real* power and basic security of supply, and to manage the reactive power by means of compensators and other equipment which can be deployed more flexibly than generating units, without increasing the fault level.

Similar considerations apply in *load balancing*. Most AC power systems are three-phase, and are designed for balanced operation. Unbalanced operation gives rise to components of current in the wrong phase-sequence (i.e. negative- and zero-sequence

---

[2] 'Regulation' is an old-fashioned term used to denote the variation of voltage when current is drawn from the system.

components). Such components can have undesirable effects, including additional losses in motors and generating units, oscillating torque in AC machines, increased ripple in rectifiers, malfunction of several types of equipment, saturation of transformers, and excessive triplen harmonics and neutral currents.[3]

The harmonic content in the voltage supply waveform is another important measure in the quality of supply. Harmonics above the fundamental power frequency are usually eliminated by filters. Nevertheless, harmonic problems often arise together with compensation problems and some types of compensator even generate harmonics which must be suppressed internally or filtered.

The ideal compensator would

(a) supply the exact reactive power requirement of the load;
(b) present a constant-voltage characteristic at its terminals; and
(c) be capable of operating independently in the three phases.

In practice, one of the most important factors in the choice of compensating equipment is the underlying rate of change in the load current, power factor, or impedance. For example, with an induction motor running 24 hours/day driving a constant mechanical load (such as a pump), it will often suffice to have a fixed power-factor correction capacitor. On the other hand, a drive such as a mine hoist has an intermittent load which will vary according to the burden and direction of the car, but will remain constant for periods of one or two minutes during the travel. In such a case, power-factor correction capacitors could be switched in and out as required. An example of a load with extremely rapid variation is an electric arc furnace, where the reactive power requirement varies even within one cycle and, for a short time at the beginning of the melt, it is erratic and unbalanced. In this case a dynamic compensator is required, such as a TCR or a saturated-reactor compensator, to provide sufficiently rapid dynamic response.

Steady-state power-factor correction equipment should be deployed according to economic factors including the supply tariff, the size of the load, and its uncompensated power factor. For loads which cause fluctuations in the supply voltage, the degree of variation is assessed at the 'point of common coupling' (PCC), which is usually the point in the network where the customer's and the supplier's areas of responsibility meet: this might be, for example, the high-voltage side of the distribution transformer supplying a particular factory.

Loads that require compensation include arc furnaces, induction furnaces, arc welders, induction welders, steel rolling mills, mine winders, large motors (particularly those which start and stop frequently), excavators, chip mills, and several others. Non-linear loads such as rectifiers also generate harmonics and may require harmonic filters, most commonly for the 5th and 7th but sometimes for higher orders as well. Triplen harmonics are usually not filtered but eliminated by balancing the load and by trapping them in delta-connected transformer windings.

The power-factor and the voltage regulation can both be improved if some of the drives in a plant are synchronous motors instead of induction motors, because the synchronous motor can be controlled to supply (or absorb) an adjustable amount of reactive power and therefore it can be used as a compensator. Voltage dips caused by

---

[3] *Triplen* (literally *triple-n*) means harmonics of order 3n, where n is an integer. See §2.12.

Table 2.1 Typical voltage fluctuation standards

Load	Limits of voltage fluctuation
Large motor starts	1–3% depending on frequency
Mine winders, excavators, large motor drives	1–3% at distribution voltage level
	$\frac{1}{2}$–$1\frac{1}{2}$% at transmission voltage level
Welding plant	$\frac{1}{4}$–2% depending on frequency
Induction furnaces	Up to 1%
Arc furnaces	$<\frac{1}{2}$%

Table 2.2 Factors to consider in specifying compensating equipment

1. Continuous and short-time reactive power requirements.
2. Rated voltage and limits of voltage variation.
3. Accuracy of voltage regulation required.
4. Response time of the compensator for a specified disturbance.
5. Maximum harmonic distortion with compensator in service.
6. Performance with unbalanced supply voltages and/or with unbalanced load.
7. Environmental factors: noise level; indoor/outdoor installation; temperature, humidity, pollution, wind and seismic factors; leakage from transformers, capacitors, cooling systems.
8. Cabling requirements and layout; access, enclosure, grounding; provision for future expansion; redundancy and maintenance provisions.
9. Protection arrangements for the compensator and coordination with other protection systems, including reactive power limits if necessary.
10. Energization procedure and precautions.

motor starts can also be avoided by using a 'soft starter', that is, a phase-controlled thyristor switch in series with the motor, which gradually ramps the motor voltage from a reduced level instead of connecting suddenly at full voltage.

Standards for the quality of supply. One very noticeable effect of supply voltage variations is flicker especially in tungsten filament lamps. Slow variations of up to 3% may be tolerable, but rapid variations within the range of maximal visual sensitivity (between 1 and 25 Hz) must be limited to 0.25% or less. A serious consequence of undervoltage is the overcurrent that results from the fact that AC motors run at a speed which is essentially determined by the frequency, and if the voltage is low the current must increase in order to maintain the power. On the other hand, overvoltage is damaging to insulation systems.

Table 2.1 gives an idea of the appropriate standards which might be applied in different circumstances, but local statutes and conditions should be studied in each individual case.

Specification of a load compensator. Some of the factors which need to be considered when specifying a load compensator are summarized in Table 2.2.

2.2 Conventions used in power engineering

In power engineering it is helpful to have a set of conventions for symbols. Unfortunately many people disregard conventions, and this causes confusion. There is no universal standard, but the simple conventions given in Table 2.3 are widely used, practical, and consistent with most classic textbooks.

Table 2.3 Font and symbol conventions

Type	What is meant	Examples
Lower-case italic	*instantaneous* values	υ, i
Upper-case italic	RMS values or DC values	V, I
	Resistance, reactance, and impedance magnitude	R, X Z
	Inductance and capacitance	L, C
Upper-case boldface roman	Phasors	**V**, **I**
	Impedance	**Z**
	In handwritten work, you can't really use boldface, so use a bar or arrow or tilde – preferably *over* the symbol, e.g. $\vec{V}$, $\overline{V}$, $\tilde{V}$.	

Subscripts can be roman or italic; it is a matter of style

In three-phase systems, various conventions are used for the subscripts used to denote the three phases. In Europe (particularly Germany): U, V, W. In the UK: R, Y, B (for red, yellow, blue), or a, b, c. In the United States: a, b, c or A, B, C. You will also see 1, 2, 3 used: this seems an obvious choice, but if you are working with symmetrical components these subscripts can be confused with the positive, negative, and zero-sequence subscripts 1, 2, 0 (sometimes $+$, $-$, 0). The best advice is to be very careful! Never confuse **phasor** values with *scalar* values!

<div align="center">Examples</div>

Typeset	Comment
$V = RI$	RMS AC; or DC
$\mathbf{V} = jX\mathbf{I}$	**V** and **I** are phasors
	X is a scalar (reactance)
	$j\mathbf{X}$ is an impedance (complex)
$\mathbf{Z} = R + jX$	**Z** is complex (impedance)
	R is scalar (resistance)
	X is scalar (reactance)
$\upsilon = V_m \cos \omega t$	υ is an instantaneous value
	V_m is a fixed scalar value

2.3   Basic source/load relationships

2.3.1   Fault level and circuit-breaker ratings

The *fault level* (sometimes called *short-circuit level*) is a term used to describe the 'strength' of a power supply: that is, its ability to provide *both* current and voltage. It is defined as:

<div align="center">Fault level = Open-circuit voltage × Short-circuit current [VA/phase]</div>

The fault level provides a single number that can be used to select the size of circuit-breaker needed at a particular point in a power system. Circuit-breakers must interrupt fault currents (i.e. the current that flows if there is a short-circuit fault). When the contacts of the circuit-breaker are separating, there is an arc which must be extinguished (for example, by a blast of compressed air). The difficulty of extinguishing the arc depends on both the current and the system voltage. So it is convenient to take the product of these as a measure of the size or 'power' of the circuit-breaker that is needed. The fault level is used for this. The rating of a circuit-breaker should
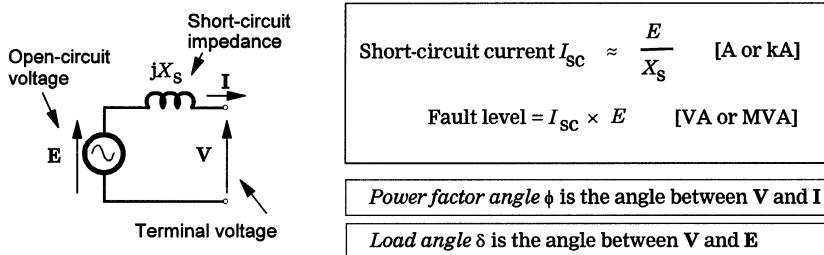
Fig. 2.1 Thévenin equivalent circuit of one phase of a supply system (neglecting resistance).

always exceed the fault level at the point where the circuit-breaker is connected – otherwise the circuit-breaker might not be capable of interrupting the fault current. This would be very dangerous: high-voltage circuit-breakers are often the final means of protection, and if they fail to isolate faults the damage can be extreme – *it would be like having a lightning strike that did not switch itself off.*

2.3.2   Thévenin equivalent circuit model of a power system

At any point where a load is connected to a power system, the power system can be represented by a Thévenin equivalent circuit[4] having an open-circuit voltage **E** and an internal impedance $\mathbf{Z}_s = R_s + jX_s$ (see Figure 2.1). Usually X_s is much bigger than R_s and $\mathbf{Z}_s$ is approximately equal to jX_s (as in the diagrams). The short-circuit current is $I_{sc} \approx E/X_s$ and the short-circuit level is $EI_{sc} = E^2/X_s$ in each phase. The short-circuit level is measured in volt-amperes, VA (or kVA or MVA), because **E** and $\mathbf{I}_{sc}$ are almost in phase quadrature.

2.3.3   Loads and phasor diagrams

A *resistive load R* on an AC power system draws power and produces a phase angle shift δ between the terminal voltage **V** and the open-circuit voltage **E**. δ is called the *load angle* (see Figure 2.2). The voltage drop across the Thévenin equivalent

(a) Resistive load   (b) Phasor diagram
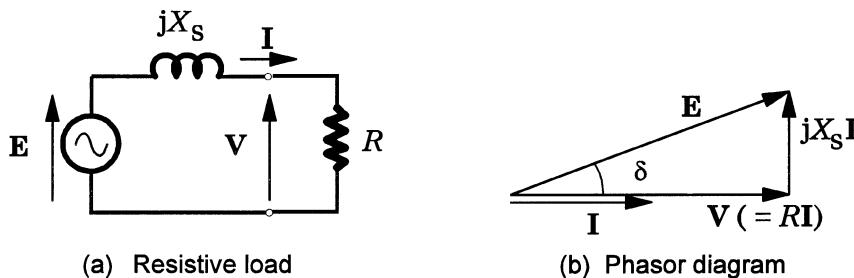
Fig. 2.2 Resistive load. (a) circuit diagram; and (b) phasor diagram.

---

[4] The Thévenin equivalent circuit is a series equivalent circuit, in which the source is a voltage source and it is in series with the internal impedance. In the *Norton* equivalent circuit, the source is a current source in parallel with the internal impedance.

(a) Shunt reactor reduces the voltage: $V < E$ (b) Phasor diagram
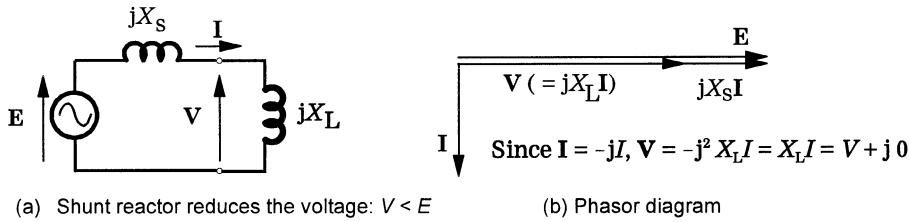
Fig. 2.3 Purely inductive load. (a) circuit diagram; and (b) phasor diagram.

(a) Shunt capacitor raises the voltage: $V > E$ (b) Phasor diagram
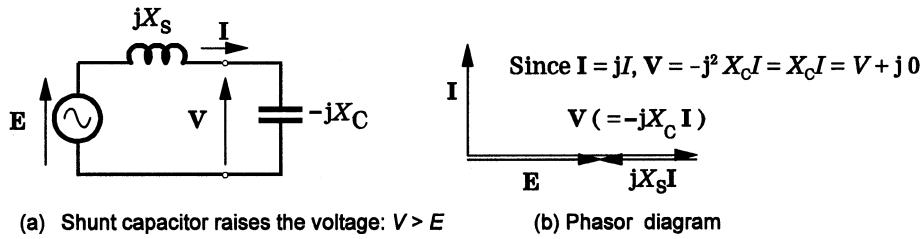
Fig. 2.4 Purely capacitive load. (a) circuit diagram; and (b) phasor diagram.

impedance is $jX_s\mathbf{I}$, which is orthogonal to the terminal voltage $\mathbf{V}(= RI)$. Because of the orthogonality, V does not fall very much below E, even though X_sI might be a sizeable fraction of E. Note that the *power factor angle* ϕ is zero for resistive loads; ϕ is the angle between $\mathbf{V}$ and $\mathbf{I}$.[5]

A *purely inductive load* draws no power and produces no phase-angle shift between $\mathbf{V}$ and $\mathbf{E}$: i.e. $\delta = 0$ (see Figure 2.3). The terminal voltage V is quite sensitive to the inductive load current because the volt-drop $jX_s\mathbf{I}$ is directly in phase with both $\mathbf{E}$ and $\mathbf{V}$. You might ask, 'what is the use of a load that draws no power?' One example is that *shunt reactors* are often used to limit the voltage on transmission and distribution systems, especially in locations remote from tap-changing transformers or generating stations. Because of the shunt capacitance of the line, the voltage tends to rise when the load is light (e.g. at night). By connecting an inductive load (shunt reactor), the voltage can be brought down to its correct value. Since the reactor is not drawing any real power (but only reactive power), there is no energy cost apart from a small amount due to losses in the windings and core.

A *purely capacitive load* also draws no power and produces no phase-angle shift between $\mathbf{V}$ and $\mathbf{E}$: i.e. $\delta = 0$. The system volt-drop $jX_s\mathbf{I}$ is directly in *anti-phase* with $\mathbf{E}$ and $\mathbf{V}$, and this causes the terminal voltage V to *rise* above E. Again you might ask 'what is the use of a load that draws no power?' An example is that *shunt capacitors* are often used to raise the voltage on transmission and distribution systems, especially in locations remote from tap-changing transformers or generating stations. Because of the series inductance of the line, the voltage tends to fall when the load is heavy (e.g. mid-morning), and this is when shunt capacitors would be connected.

---

[5] It is assumed that the AC voltage and current are sinewaves at fundamental frequency, so ϕ is the phase angle at this frequency.

(a) Symmetrical system
—the simplest 'interconnected' power system

(b) Phasor diagram
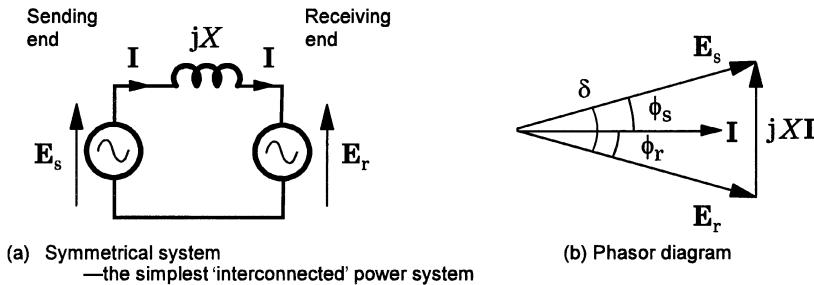
Fig. 2.5 Symmetrical system.

Shunt reactors and capacitors are sometimes thyristor-controlled, to provide rapid response. This is sometimes necessary near rapidly-changing loads such as electric arc furnaces or mine hoists. Of course the use of thyristors causes the current to contain harmonics, and these must usually be filtered.

2.3.4 The symmetrical system

The *symmetrical system* is an important example – indeed the simplest example – of an interconnected power system, Figure 2.5. It comprises two synchronous machines coupled by a transmission line. It might be used, for example, as a simple model of a power system in which the main generating stations are at two locations, separated by a transmission line that is modelled by a simple inductive impedance jX. The loads (induction motors, lighting and heating systems, etc., are connected in parallel with the generators, but in the simplest model they are not even shown, because the power transmission system engineer is mostly concerned with the power flow along the line, and this is controlled by the prime-movers at the generating stations (i.e. the steam turbines, water turbines, gas turbines, wind turbines etc.).

Although the circuit diagram of a symmetrical system just looks like two generators connected by an inductive impedance, power can flow in *either direction*. The symmetrical system can be used to derive the *power flow equation*, which is one of the most important basic equations in power system operation; see §2.8. If E_s and E_r are the open-circuit voltages at the two generators, then

$$P = \frac{E_s E_r}{X} \sin \delta \tag{2.1}$$

where δ is the phase angle between the phasors $\mathbf{E}_s$ and $\mathbf{E}_r$. Note that in Figure 2.5 there are two power factor angles: ϕ_s between $\mathbf{E}_s$ and $\mathbf{I}$ at the sending end, and ϕ_r between $\mathbf{E}_r$ and $\mathbf{I}$ at the receiving end.

2.4 Complex power, apparent power, real and reactive power

Consider a simple load $R + jX$ with a current $\mathbf{I}$ and voltage $\mathbf{V}$, Figure 2.6. The *complex power* $\mathbf{S}$ is defined as

$$\mathbf{S} = \mathbf{VI}^* = P + jQ \tag{2.2}$$

(a) AC load   (b) Phasor diagram   (c) Power triangle
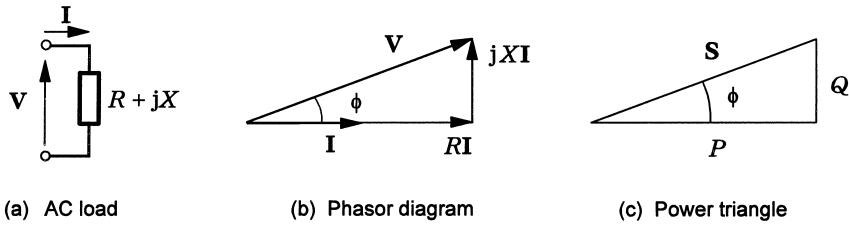
Fig. 2.6 Development of the complex power triangle.

$\mathbf{S}$ can be expressed graphically as the complex number $P + jQ$, as shown in Figure 2.6, where

P is the real power in W, kW or MW, averaged over one cycle

Q is the reactive power in VAr, kVAr, or MVAr, also averaged over one cycle[6]

$S = |\mathbf{S}|$ is the apparent power or 'volt–amperes', in VA, kVA or MVA[7]

Let $\mathbf{V}$ be the reference phasor, and suppose that the load is inductive. Then

$$\mathbf{I} = I\mathrm{e}^{-j\phi} = I\cos\phi - jI\sin\phi \qquad (2.3)$$

where $\phi = \tan^{-1}(X/R) = \tan^{-1}(Q/P)$. The negative phase rotation $-j\phi$ means that the current lags behind the voltage. When we take the conjugate $\mathbf{I}^*$ and multiply by $\mathbf{V}$ we get

$$P = VI\cos\phi \quad \text{and} \quad Q = VI\sin\phi \qquad (2.4)$$

Evidently P is positive and so is Q. A load that has positive reactive power is said to 'absorb' VArs. Inductive loads absorb VArs. Conversely, a capacitive load would have

$$\mathbf{I} = I\mathrm{e}^{+j\phi} = I\cos\phi + jI\sin\phi \qquad (2.5)$$

In this case the current leads the voltage. P is still positive, but when we take the conjugate $\mathbf{I}^*$ we get negative Q. We say that a capacitive load *generates* or *supplies* VArs.

There is a distinction between the receiving end and the sending end. The expression '$VI\cos\phi$' is correctly interpreted as *power absorbed by the load* at the receiving end. But at the sending end the generated power P is supplied *to* the system, not absorbed *from* it. The distinction is that the sending end is a source of power, while the receiving end is a sink. In Figure 2.5, for example, both $P_{\mathrm{s}} = E_{\mathrm{s}}I\cos\phi_{\mathrm{s}}$ and

---

[6] VAr = 'volt–amperes, reactive'

[7] Although $\mathbf{S}$ is a complex number, it is not a phasor quantity. The power triangle merely represents the relationship between P, Q, ϕ, and the apparent power S. Note that P, Q, and S are all *average* quantities (averaged over one cycle); they are not rms quantities. On the other hand V and I are rms quantities.

Table 2.4 Generating and absorbing reactive power: sink and source conventions

	Lagging PF ($\mathbf{I}$ lags $\mathbf{V}$)	Leading PF ($\mathbf{I}$ leads $\mathbf{V}$)
Load (sink)	$Q_r > 0$ Absorbing VArs	$Q_r < 0$ Generating VArs
Generator (source)	$Q_s > 0$ Generating VArs	$Q_s < 0$ Absorbing VArs

$P_r = E_r I \cos \phi_r$ are positive, supplied *to* the system at the sending end and taken *from* it at the receiving end.[8]

A similar distinction arises with reactive power. The receiving end in Figure 2.5 evidently has a lagging power factor and is absorbing VArs. The sending end has a leading power factor and is *absorbing* VArs. In Figure 2.9, the power factor is lagging at both the generator and the load, but the load is absorbing VArs while the generator is generating VARs. These conventions and interpretations are summarized in Table 2.4.

Note that

$$\tan \phi = \frac{Q}{P} \quad \text{and} \quad \cos \phi = \frac{P}{\sqrt{P^2 + Q^2}} \tag{2.6}$$

where $\cos \phi$ is the power factor.

Remember that phasors apply only when the voltage and currents are purely sinusoidal, and this expression for power factor is meaningless if either the voltage or current waveform is non-sinusoidal. A more general expression for power factor with non-sinusoidal current and waveforms is

$$PF = \frac{\text{Average Power}}{\text{RMS volts} \times \text{RMS amps}} \tag{2.7}$$

2.5   Leading and lagging loads

Figure 2.7 shows a circuit with a supply system whose open-circuit voltage is $\mathbf{E}$ and short-circuit impedance is $\mathbf{Z}_s = 0 + jX_s$, where $X_s = 0.1 \, \Omega$. The load impedance is
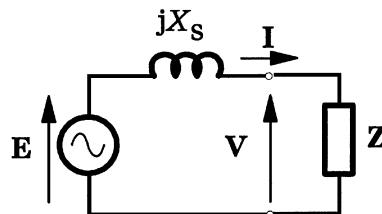

Fig. 2.7 AC supply and load circuit.

---

[8] For a source, the arrows representing positive voltage and current are in the same direction. For a sink, they are in opposite directions. This convention is not universal: for example, in German literature the opposite convention is used.
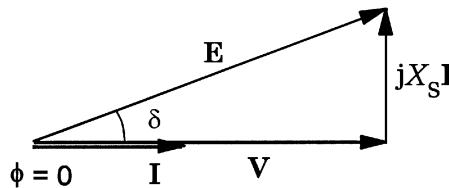
**Fig. 2.8** Phasor diagram, resistive load.
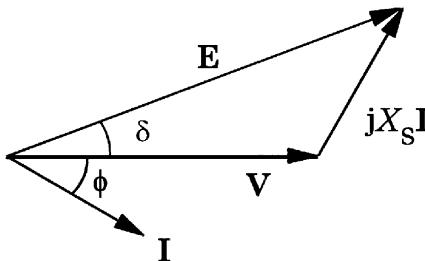
Fig. 2.9 Phasor diagram, inductive load.

$Z = 1\,\Omega$ but the power factor can be unity, 0.8 lagging, or 0.8 leading. For each of these three cases, the supply voltage E can be adjusted to keep the terminal voltage $V = 100$ V. For each case we will determine the value of E, the power-factor angle ϕ, the load angle δ, the power P, the reactive power Q, and the volt–amperes S.

Unity power factor. In Figure 2.8, we have $E\cos\delta = V = 100$ and $E\sin\delta = X_s I = 0.1 \times 100/1 = 10$ V. Therefore $\mathbf{E} = 100 + \mathrm{j}10 = 100.5\mathrm{e}^{\mathrm{j}5.71°}$ V. The power-factor angle is $\phi = \cos^{-1}(1) = 0$, $\delta = 5.71°$, and $\mathbf{S} = P + \mathrm{j}Q = \mathbf{VI}^* = 100 \times 100\mathrm{e}^{\mathrm{j}0} = 10$ kVA, with $P = 10$ kW and $Q = 0$.

Lagging power factor. In Figure 2.9, the current is rotated negatively (i.e. clockwise) to a phase angle of $\phi = \cos^{-1}(0.8) = -36.87°$. Although $I = 100$ A and $X_s I$ is still 10 V, its new orientation 'stretches' the phasor $\mathbf{E}$ to a larger magnitude: $\mathbf{E} = \mathbf{V} + \mathrm{j}X_s\mathbf{I} = (100 + \mathrm{j}0) + \mathrm{j}0.1 \times 100\mathrm{e}^{-\mathrm{j}36.87°} = 106.3\mathrm{e}^{\mathrm{j}4.32°}$ V. When the power-factor is lagging a higher supply voltage E is needed for the same load voltage. The load angle is $\delta = 4.32°$ and $\mathbf{S} = \mathbf{VI}^* = 100 \times 100\mathrm{e}^{+\mathrm{j}36.87} = 8000 + \mathrm{j}6000$ VA. Thus $S = 10$ kVA, $P = 8$ kW and $Q = +6$ kVAr (absorbed).

Leading power factor. The leading power factor angle causes a reduction in the value of E required to keep V constant: $\mathbf{E} = 100 + \mathrm{j}0.1 \times 100\mathrm{e}^{+\mathrm{j}36.87°} = 94.3\mathrm{e}^{\mathrm{j}4.86°}$ V. The load angle is $\delta = 4.86°$, and $\mathbf{S} = 10000\mathrm{e}^{-\mathrm{j}36.87°} = 8000 - \mathrm{j}6000$; i.e. $P = 8$ kW and $Q = 6$ kVAr (generated).

We have seen that when the load power and current are kept the same, the inductive load with its lagging power factor requires a higher source voltage E, and the capacitive load with its leading power factor requires a lower source voltage. Conversely, if the source voltage E were kept constant, then the inductive load would have a lower terminal voltage V and the capacitive load would have a higher terminal voltage. As an exercise, repeat the calculations for $E = 100$ V and determine V in each case, assuming that $Z = 1\,\Omega$ with each of the three different power factors.
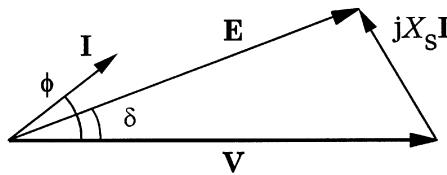
Fig. 2.10 Phasor diagram, capacitive load.

We can see from this that power-factor correction capacitors (connected in parallel with an inductive load) will not only raise the power factor but will also increase the voltage. On the other hand, if the voltage is too high, it can be reduced by connecting inductors in parallel. In modern high-voltage power systems it is possible to control the voltage by varying the amount of inductive or capacitive current drawn from the system at the point where the voltage needs to be adjusted. This is called *reactive compensation* or *static VAR control*. In small, isolated power systems (such as an automotive or aircraft power system supplied from one or two generators) this is not generally necessary because the open-circuit voltage of the generator E can be varied by field control, using a *voltage regulator*.

2.6   Power factor correction

The load in Figure 2.7 can be expressed as an admittance $\mathbf{Y} = G + jB$ supplied from a voltage $\mathbf{V}$, where $\mathbf{Y} = 1/\mathbf{Z}$. G is the *conductance*, i.e. the real part of the admittance $\mathbf{Y}$, and B is the *susceptance*, i.e. the reactive or imaginary part of the admittance $\mathbf{Y}$. The load current is $\mathbf{I}$ and for an inductive load the reactive component is negative (equation (2.3)) so we can write

$$\mathbf{I} = I_R - jI_X = \mathbf{V}(G - jB) = VG - jVB \tag{2.8}$$

Both $\mathbf{V}$ and $\mathbf{I}$ are phasors, and equation (2.8) is represented in the phasor diagram (Figure 2.11) in which $\mathbf{V}$ is the reference phasor. The voltage $\mathbf{V}$ and current $\mathbf{I}$ are in common with Figure 2.9, but Figure 2.11 shows the components of the current $\mathbf{I}$ and omits $\mathbf{E}$ and the voltage drop across the supply impedance. The load current has a 'resistive' or 'real' component I_R in phase with $\mathbf{V}$, and a 'reactive' or 'imaginary' component, $I_X = VB$ in quadrature with $\mathbf{V}$. The angle between $\mathbf{V}$ and $\mathbf{I}$ is ϕ, the power-factor angle. The apparent power supplied to the load is given by equation. (2.2) with $P = V^2G$ and $Q = V^2B$. For a capacitive load I_X is positive and $Q = V^2B$, which is negative.

The real power P is usefully converted into heat, mechanical work, light, or other forms of energy. The reactive volt–amperes Q cannot be converted into useful forms of energy but is nevertheless an inherent requirement of the load. For example, in AC induction motors it is associated with production of flux and is often called the 'magnetizing reactive power'.

The supply current exceeds the real component by the factor $1/\cos\phi$, where $\cos\phi$ is the power factor: that is, the ratio between the real power P and the apparent power S. The power factor is that fraction of the apparent power which can be
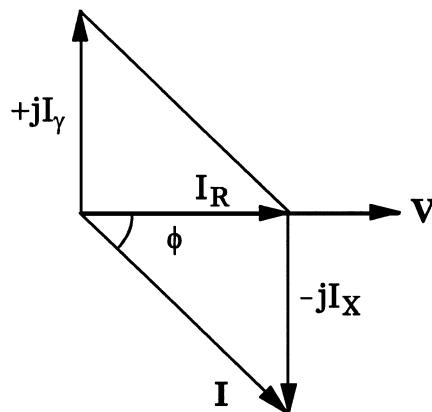
Fig. 2.11 Phasor diagram for power factor correction.

usefully converted into other forms of energy. The Joule losses in the supply cables are increased by the factor $1/\cos^2 \phi$. Cable ratings must be increased accordingly, and the losses must be paid for by the consumer.

The principle of power-factor correction is to compensate for the reactive power; that is, to provide it locally by connecting in parallel with the load a compensator having a purely reactive admittance of opposite sign to that of the reactive component of the load admittance. An inductive load is compensated by a capacitive admittance $+jB_\gamma$ and a capacitive load by an inductive admittance $-jB_\gamma$. If the compensating admittance is equal to the reactive part of the load admittance, then for an inductive load the supply current becomes

$$\mathbf{I}_s = \mathbf{I} + \mathbf{I}_\gamma = \mathbf{V}(G - jB) + \mathbf{V}(jB) = VG = I_R \qquad (2.9)$$

which is in phase with $\mathbf{V}$, making the *overall* power-factor unity. Figure 2.11 shows the phasor diagram.

With 100% compensation the supply current $\mathbf{I}_s$ now has the smallest value capable of supplying full power P at the voltage V, and all the reactive power required by the load is supplied locally by the compensator. The reactive power rating of the compensator is related to the rated *power P* of the load by $Q_\gamma = P \tan \phi$. The compensator current Q_γ/V equals the reactive current of the load at rated voltage. Relieved of the reactive requirements of the load, the supply now has excess capacity which is available for supplying other loads. The load may also be partially compensated (i.e. $|Q_\gamma| < |Q|$).

A fixed-admittance compensator cannot follow variations in the reactive power requirement of the load. In practice a compensator such as a bank of capacitors can be divided into parallel sections, each switched separately, so that discrete changes in the compensating reactive power may be made, according to the requirements of the load. More sophisticated compensators (e.g. synchronous condensers or static compensators) are capable of continuous variation of their reactive power.

The foregoing analysis has taken no account of the effect of supply voltage variations on the effectiveness of the compensator in maintaining an overall power

factor of unity. In general the reactive power of a fixed-reactance compensator will not vary in sympathy with that of the load as the supply voltage varies, and a compensation 'error' will arise. In Section 2.7 the effects of voltage variations are examined, and we will find out what extra features the ideal compensator must have to perform satisfactorily when both the load and the supply system parameters can vary.

2.7   Compensation and voltage control

Figure 2.12 shows a one-line diagram of an AC power system, which could represent either a single-phase system, or one phase of a three-phase system. Figure 2.13 shows the phasor diagram for an inductive load.

When the load draws current from the supply, the terminal voltage V falls below the open-circuit value E. The relationship between V and the load current I is called the *system load line*, Figure 2.14.
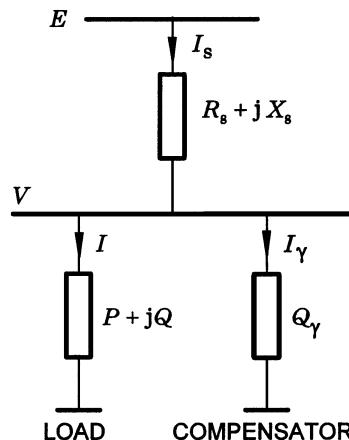

**Fig. 2.12** Equivalent circuit of supply and load.
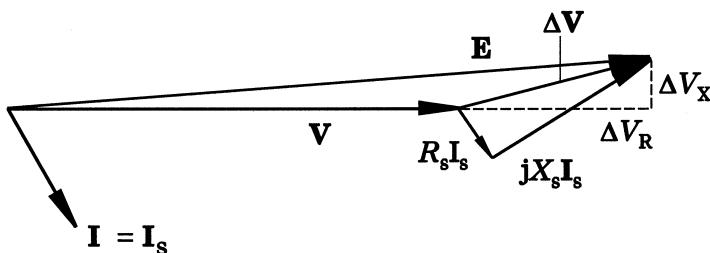
**Fig. 2.13** Phasor diagram (uncompensated).
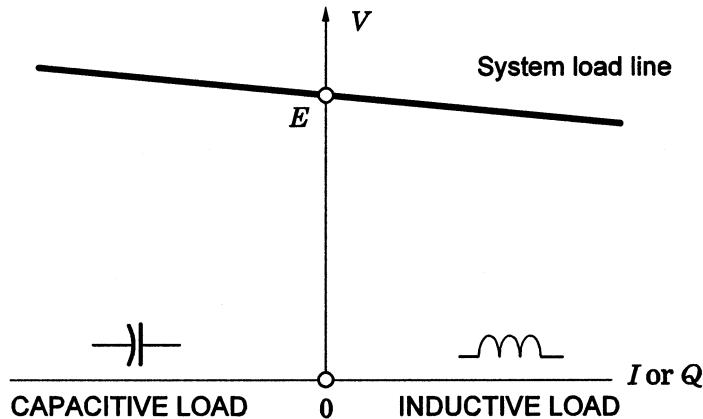
Fig. 2.14 System load line.

The 'load' can be measured by its current I, but in power systems parlance it is the reactive volt-amperes Q of the load that is held chiefly responsible for the voltage drop. From Figures 2.12 and 2.13,

$$\Delta \mathbf{V} = \mathbf{E} - \mathbf{V} = \mathbf{Z}_s \mathbf{I} \tag{2.10}$$

where $\mathbf{I}$ is the load current. The complex power of the load (per phase) is defined by equation (2.2), so

$$\mathbf{I} = \frac{P - jQ}{\mathbf{V}} \tag{2.11}$$

and if $\mathbf{V} = V + j0$ is taken as the reference phasor we can write

$$\Delta \mathbf{V} = (R_s + jX_s)\left(\frac{P - jQ}{V}\right) = \frac{R_s P + X_s Q}{V} + j\frac{X_s P - R_s Q}{V} = \Delta V_R + j\Delta V_X \tag{2.12}$$

The voltage drop $\Delta \mathbf{V}$ has a component ΔV_R in phase with $\mathbf{V}$ and a component ΔV_X in quadrature with $\mathbf{V}$; Figure 2.13. Both the magnitude and phase of $\mathbf{V}$, relative to the open-circuit voltage E, are functions of the magnitude and phase of the load current, and of the supply impedance $R_s + jX_s$. Thus $\Delta \mathbf{V}$ depends on both the real and reactive power of the load.

By adding a compensating impedance or 'compensator' in parallel with the load, it is possible to maintain $|\mathbf{V}| = |\mathbf{E}|$. In Figure 2.15 this is accomplished with a purely reactive compensator. The load reactive power is replaced by the sum $Q_s = Q + Q_\gamma$, and Q_γ (the compensator reactive power) is adjusted in such a way as to rotate the phasor $\Delta \mathbf{V}$ until $|\mathbf{V}| = |\mathbf{E}|$. From equations (2.10) and (2.12),

$$|\mathbf{E}|^2 = \left[V + \frac{R_s P + X_s Q_s}{V}\right]^2 + \left[\frac{X_s P - R_s Q_s}{V}\right]^2 \tag{2.13}$$

The value of Q_γ required to achieve this 'constant voltage' condition is found by solving equation (2.13) for Q_s with $V = |\mathbf{E}|$; then $Q_\gamma = Q_s - Q$. In practice the value can be determined automatically by a closed-loop control that maintains constant
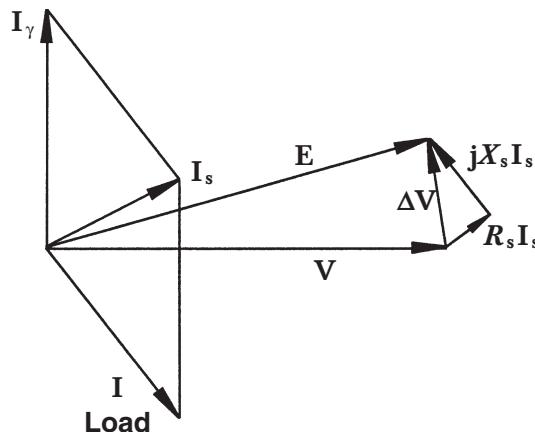
Fig. 2.15 Phasor diagram, compensated for constant voltage.

voltage V. Equation (2.13) always has a solution for Q_s, implying that: *A purely reactive compensator can eliminate voltage variations caused by changes in both the real and the reactive power of the load.*

Provided that the reactive power of the compensator Q_γ can be controlled smoothly over a sufficiently wide range (both lagging and leading), and at an adequate rate, the compensator can perform as an *ideal voltage regulator*.

We have seen that a compensator can be used for power-factor correction. For example, if the power factor is corrected to unity, $Q_s = 0$ and $Q_\gamma = Q$. Then

$$\Delta \mathbf{V} = (R_s + jX_s)\frac{P}{V} \tag{2.14}$$

which is independent of Q and therefore not under the control of the compensator. Thus: *A purely reactive compensator cannot maintain both constant voltage and unity power factor at the same time.*

The only exception is when $P = 0$, but this is not of practical interest.

2.7.1 System load line

In high-voltage power systems R_s is often much smaller than X_s and is ignored. Instead of using the system *impedance*, it is more usual to talk about the system *short-circuit level* $S = E^2/X_s$. Moreover, when voltage-drop is being considered, ΔV_X is ignored because it tends to produce only a phase change between $\mathbf{V}$ and $\mathbf{E}$. Then

$$\Delta \mathbf{V} = \Delta V_R \quad \text{and} \quad \frac{\Delta V}{V} = \frac{X_s Q}{V^2} \approx \frac{Q}{S} \tag{2.15}$$

and

$$V \approx E\left(1 - \frac{Q}{S}\right) \tag{2.16}$$

This relationship is a straight line, as shown in Figure 2.14. It is called the *system load line*.

2.8   Control of power and frequency

In power systems it is essential to keep the *frequency* and the *voltage* close to their rated values. The frequency is controlled by controlling the balance between the power supplied to the system and the power taken from it. Figure 2.16 shows a transmission system with a prime mover driving a generator, and a motor driving a mechanical load. Table 2.5 gives examples of prime movers and loads.

The power P_{in} supplied *to* the system is determined by the prime mover(s). In a steam-turbine generator, the steam valves are the main means of control. Of course, if the valves are opened wide, the boiler must be able to provide sufficient steam (at the correct pressure and temperature) to develop the required power. This means that the boiler control must be coordinated with the steam valves. Similarly, in a wind turbine the power transmitted to the generator is determined by the wind speed and the blade pitch, which can be varied to control the power to the required level.

The power P_{out} taken *from* the system is determined by the mechanical and electrical loads. For example, consider a direct-connected induction motor driving a pump. The motor rotates at a speed determined by the intersection of its torque/speed characteristic with the pump's torque/speed characteristic. Since the motor torque/speed characteristic is very steep near synchronous speed, the motor tends to run near synchronous speed and the torque is then determined by the requirements of the pump (depending on the pressure head and the flow rate). So the power is jointly determined by the pump and the motor. With passive electrical loads (such as lighting and heating), the power supplied to the load depends on the voltage and the load impedance.
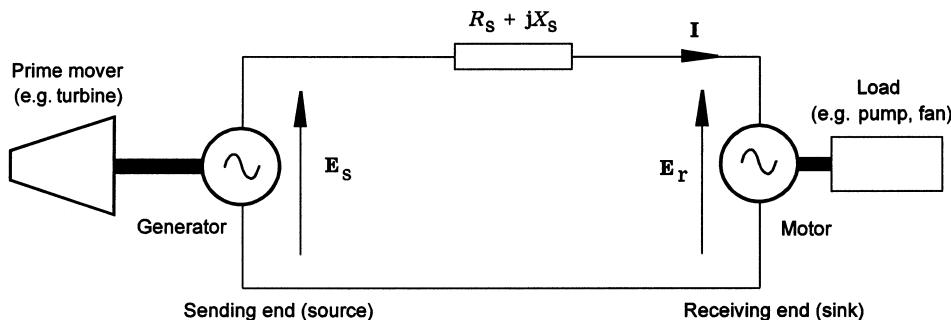

Fig. 2.16 Transmission system with prime mover, generator, motor and load. The voltages at both ends of the transmission system are assumed to be controlled, so the symbol **E** is used instead of **V**. At the sending end, the voltage is E_s; at the receiving end, E_r.

Table 2.5 Examples of prime movers and mechanical loads

Examples of prime movers	Examples of mechanical loads
Steam turbine-generator (coil, oil, gas, nuclear, etc. – i.e. 'thermal')	Pumps (water, sewage, process fluids, foods, etc.)
Hydro-electric turbine generator	Fans and blowers (air-moving)
Wind turbine generator	Compressors
Diesel engine	Machinery, hoists, conveyors, elevators

It is evident that P_{in} and P_{out} are determined quite independently. Yet in the steady state they must be essentially equal, otherwise energy would be accumulating somewhere in the transmission system.[9] The power system operator can control P_{in} but s/he has no control over P_{out}, since customers can connect and disconnect loads at will. The power system operator does not even have any practical means of measuring P_{out} for the entire system, and in any case, even if this parameter was available, there may be several generating stations in the system, so it appears to be somewhat arbitrary as to what contributions should be supplied by the individual generating stations at any instant.

In the short term (i.e. over a period of a fraction of a second), it is the *frequency control* that ensures that $P_{in} = P_{out}$, and this control is effected by maintaining the speed of the generators extremely close to the nominal value. Suppose the power system is in a steady state and $P_{in} = P_{out}$. Suppose that the load increases so that more power is taken from the system, tending to make $P_{out} > P_{in}$. The prime mover and the generator will tend to slow down. Therefore the prime mover has a *governor* (i.e. a valve controller) that increases P_{in} when the frequency is below the rated value, and decreases P_{in} when the frequency is above the rated value.

In an isolated power system with only one generator, the governor has a relatively simple job to do, to maintain the speed of the generator at the correct synchronous speed to hold the frequency constant. But what happens in a power system with multiple generators? In this case usually there is a mixture of power stations. The large ones which produce the most economical power are usually best operated at constant power for long periods, without varying their contribution to P_{in}. Apart from the economics, one reason for this is that if the power is varied, the temperature distribution in the turbine, boiler, and generator will be affected, and 'thermal cycling' is considered undesirable in these very large machines. So these generators have a relatively steep or insensitive governor characteristic, such that the frequency would have to change by quite a large amount to change the contribution to P_{in} ('Quite a large amount' might mean only a fraction of 1 Hz). Elsewhere in the power system, or sometimes in the same power station, there are special generators assigned to the task of frequency control. These generators have very flat governor characteristics such that a tiny change in frequency will cause a large swing in power. They are usually gas turbine powered, up to 20 MW or so, but very large rapid-response generators are sometimes built into hydro-electric pumped-storage schemes. For example, the Dinorwic power station in North Wales has a rating of 1800 MW and can change from zero to maximum power in a few tens of seconds.

The rapid-response generators in a large interconnected power system (such as the United Kingdom system) are used for frequency control in the short term (over a few minutes or hours). They provide a time buffer to allow the larger power stations to vary their contribution. As the total system load changes during the day, the frequency is maintained almost constant, within 0.1 Hz. Averaged over 24 hours, the frequency is kept virtually dead accurate .

---

[9] Losses in the transmission system are assumed to be negligible for the purposes of this discussion.

[10] In fossil-fuel power stations two-pole generators predominate, and the speed is 3000 rev/min in a 50-Hz system or 3600 rev/min in a 60-Hz system. In nuclear power stations, four-pole generators are more common, running at 1500 rev/min (1800 rev/min at 60 Hz). In hydro plants, the generators have larger numbers of poles with speeds in the range 100–1000 rev/min.

Some of the generators in a large system may be operated at light load in a state of readiness or 'spinning reserve', in case the system load increases suddenly by a large amount. This can happen, for example, at the end of television transmissions when the number of viewers is exceptionally high.

2.8.1 Relationships between power, reactive power, voltage levels and load angle

The phasor diagram for the system in Figure 2.16 is shown in Figure 2.17, assuming that the load has a lagging power factor angle ϕ. The line or cable is represented by its impedance $R_s + jX_s$, and R_s is again neglected (being usually much smaller than X_s). The voltage drop across the transmission line is $jX_s\mathbf{I}$, which leads the phasor $\mathbf{I}$ by 90°. The angle between $\mathbf{E}_s$ and $\mathbf{E}_r$ is the *load angle*, δ and

$$E_s \cos \delta = E_r + X_s I \sin \phi \quad \text{and} \quad E_s \sin \delta = X_s I \cos \phi \qquad (2.17)$$

Also

$$P + jQ = \mathbf{E}_r \mathbf{I}^* = E_r I \cos \phi + jE_r I \sin \phi \qquad (2.18)$$

From this we get the power flow equation

$$P = \frac{E_s E_r}{X_s} \sin \delta \qquad (2.19)$$

and the reactive power equation for the receiving end

$$Q_r = E_r \frac{E_s \cos \delta - E_r}{X_s} \qquad (2.20)$$

Evidently $P = P_s = P_r$ as long as the transmission losses are negligible. At the sending end,

$$P_s + jQ_s = E_s I \cos(\phi + \delta) + jE_s I \sin(\phi + \delta) \qquad (2.21)$$
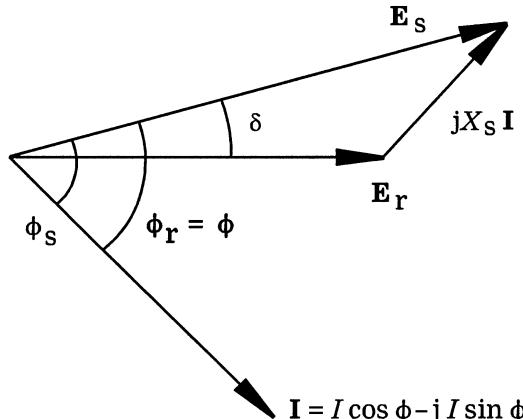
Fig. 2.17 Phasor diagram for Figure 2.16.

from which it can be shown that

$$Q_s = E_s I(\sin\delta\cos\phi + \cos\delta\sin\phi)$$

$$= E_s\sin\delta\frac{E_s\sin\delta}{X_s} + E_s\cos\delta\frac{E_s\cos\delta - E_r}{X_s} \qquad (2.22)$$

$$= E_s\frac{E_s - E_r\cos\delta}{X_s}$$

Note the symmetry between this expression and the one for Q_r in equation (2.20).

Example 1
Suppose $E_s = E_r = 1.0$ p.u. and $P = 1.0$ p.u.[11] The transmission system has $X_s = 0.1$ p.u. and R_s is negligible. We have $\sin\delta = PX_s/E_sE_r = 1 \times 0.1/1 \times 1 = 0.1$ so $\delta = 5.739°$ and $\cos\delta = 0.995$. Then $Q_s = 1.0\,(1.0 - 1.0 \times 0.995)/0.1 = +0.050$ p.u. and $Q_r = 1.0\,(1.0 \times 0.995 - 1.0)/0.1 = -0.050$ p.u. Thus the receiving end is generating reactive power and so is the sending end. The power factor is lagging at the sending end and leading at the receiving end. The phasor diagram is shown in Figure 2.5b (not to scale).

Example 2
Suppose $E_s = 1.0$ p.u. while the receiving-end voltage is reduced to $E_r = 0.95$ p.u., with $P = 1.0$ p.u. and $X_s = 0.1$ p.u. Now $\sin\delta = 1.0 \times 0.1/1.0 \times 0.95 = 0.105$ and $\delta = 6.042°$, slightly larger than in example 1 because E_r is reduced by 5%. Also $Q_s = 1.0\,(1.0 - 0.95\cos 6.042°)/0.1 = 0.553$ p.u. and $Q_r = 0.95\,(1.0\cos 6.042° - 1.0)/0.1 = 0.422$ p.u. Since Q_s is positive, the sending-end generator is generating VArs. Q_r is also positive, meaning that the receiving-end load is absorbing VArs. The phasor diagram is similar to that shown in Figure 2.17 (but not to the same scale).

Notice that a 5% reduction in voltage at one end of the line causes a *massive* change in the reactive power flow. Conversely, a change in the power factor at either end tends to cause a change in the voltage. A 5% voltage swing is, of course, a very large one. Changes in the *power* tend to produce much smaller changes in voltage; instead, the load angle δ changes almost in proportion to the power as long as δ is fairly small (then $\sin\delta \approx \delta$).

The transmission system has an inductive impedance and therefore we would expect it to absorb VArs. If we regard jX_s as another impedance in series with the load impedance, we can treat it the same way. The current is obtained from $I\sin\phi = (E_s\cos\delta - E_r)/X_s = 0.444$ p.u., and $I\cos\phi = E_s\sin\delta/X_s = 1.053$ p.u. Therefore $\mathbf{I} = 0.444 + j1.053$ p.u. $= 1.143e^{j22.891°}$ p.u. (with $\mathbf{E}_r$ as reference phasor). The voltage drop across X_s is $jX_s\mathbf{I}$ and the reactive power is $I^2X_s = 1.143^2 \times 0.1 = 0.131$ p.u. Note that this equals the difference between Q_s and Q_r.

We could have made a similar calculation in example 1, where $I^2X_s = 0.1$. Again this is $Q_s - Q_r$. In Example 1 also $|Q_s| = |Q_r|$, which means that each end of the line is supplying half the reactive VArs absorbed in X_s.

---

[11] The per-unit system is explained in Section 2.13. If you aren't familiar with it, try to read these examples as practice in the use of normalized (per-unit) values. In effect, they make it possible to forget about the units of volts, amps, etc.

2.9   Three-phase systems

Most power systems (from 415 V upwards) are three-phase systems. When the phases are balanced, the phasor diagrams and equations of one phase represent all three phases.

Why three-phase? The main reasons for having more than one phase are as follows:

(a) better utilization of materials such as copper, iron, and insulation in lines, cables, transformers, generators and motors
(b) constant power flow
(c) diversity and security of supply and
(d) 'natural rotation', permitting the widespread use of AC induction motors.

2.9.1   Development of three-phase systems

To achieve 'diversity' – that is, the ability to supply different loads from different circuits so that a failure in one circuit would not affect the others – we can use separate circuits or 'phases' as shown in Figure 2.18.

The power in each phase is $V_{ph}I_{ph} \cos \phi$ where V_{ph} and I_{ph} are the RMS voltage and current as shown in Figure 2.18. The total power is $3 V_{ph}I_{ph} \cos \phi$. Assuming that the cable works at a certain current-density determined by its allowable temperature rise, the total cross-section area of conductor is 6 A.

Suppose that the three phase currents are shifted in time phase by 120° from one another as shown in Figure 2.19. The RMS currents are unchanged, as is the power in each phase and the total power. The sum of the three currents is zero, and we can express this in terms of instantaneous or phasor values

$$i_a + i_b + i_c = 0 \quad \text{and} \quad \mathbf{I}_a + \mathbf{I}_b + \mathbf{I}_c = 0 \tag{2.23}$$
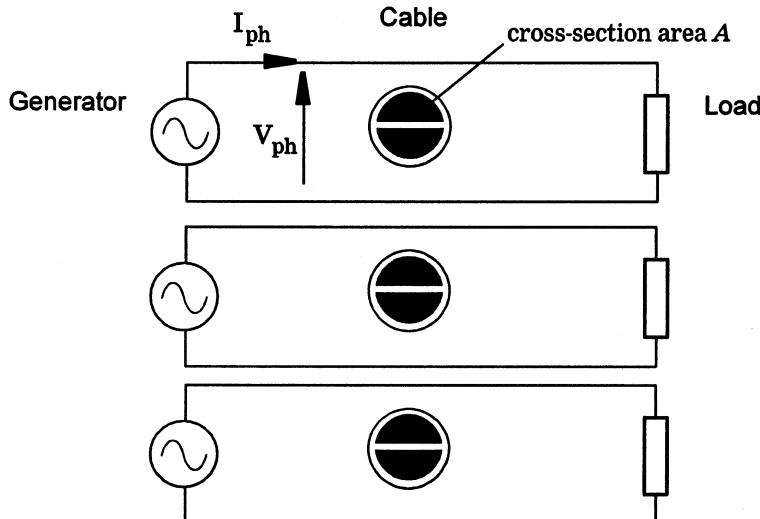
**Fig. 2.18** Three single-phase cables.
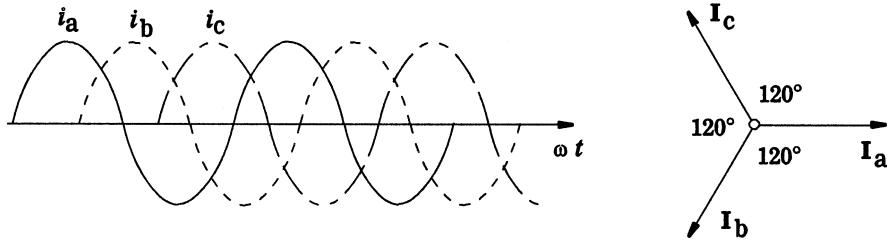
Fig. 2.19 Three-phase instantaneous and phasor currents.

This suggests that the circuit could be equally well served by the *three-phase* connection shown in Figure 2.20, which has only half the number of conductors compared with Figure 2.18. Figure 2.20 also shows the cross-section of a three-phase cable capable of carrying the required current. The total cross-section of conductor is 3 A, that is a saving of 50%.

In the voltage phasor diagram in Figure 20, the voltage across each phase of the load remains the same as in Figure 2.20, but the voltage between lines is increased: evidently from the geometry of the triangles

$$\mathbf{V}_{ab} = \mathbf{V}_a - \mathbf{V}_b = \sqrt{3}\mathbf{V}e^{j30°}$$
$$\mathbf{V}_{bc} = \mathbf{V}_b - \mathbf{V}_c = \sqrt{3}\mathbf{V}e^{-j90°} \qquad (2.24)$$
$$\mathbf{V}_{ca} = \mathbf{V}_c - \mathbf{V}_a = \sqrt{3}\mathbf{V}e^{j150°}$$

where $\mathbf{V}$ is the reference phase voltage taken as $\mathbf{V}_a$, measured between line A and the 'star point' of the load or the 'neutral point' of the supply. Likewise the phase voltage $\mathbf{V}_b$ is measured between line B and the star-point of the load, and $\mathbf{V}_c$ between line C and the star point. The line–line voltages are $\sqrt{3}$ times the phase voltages. In Figure 2.20 both the load and the generator are 'wye connected' and in terms of the RMS values only, we have

$$V_{LL} = \sqrt{3}V_{ph} \quad \text{and} \quad I_L = I_{ph} \qquad (2.25)$$
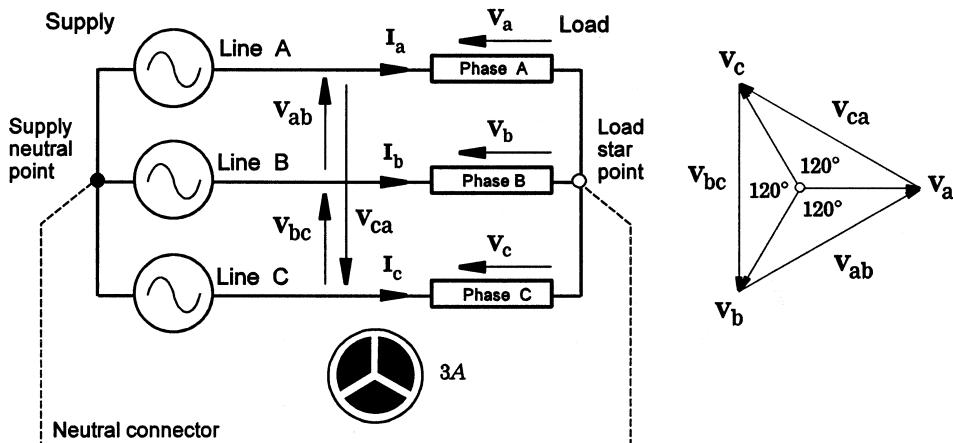
Fig. 2.20 Three-phase connection with wye-connected load and phasor diagram.

where I_L is the line current and I_{ph} is the phase current. With wye connection they are one and the same current. The dotted line in Figure 2.20 shows the possibility of a connection between the neutral point of the supply and the star point of the load. This connection may be used to stabilize the potential of the star point where there is an excess of triplen harmonics in the current or voltage waveforms of the load.

The current and voltage in Figures 2.19 and 2.20 are displaced in phase by the power factor angle ϕ. Figure 2.21 shows a complete phasor diagram for a balanced wye-connected load with a lagging power factor.

An alternative connection of the three phases is the delta connection shown in Figure 2.22 together with the construction of the phasor diagram under balanced conditions with a lagging power factor.

For the delta connection,

$$V_{LL} = V_{ph} \quad \text{and} \quad I_L = \sqrt{3}I_{ph} \tag{2.26}$$

The delta connection is used to provide a path for triplen harmonic currents. For example, when transformers operate at higher than normal voltage the magnetizing
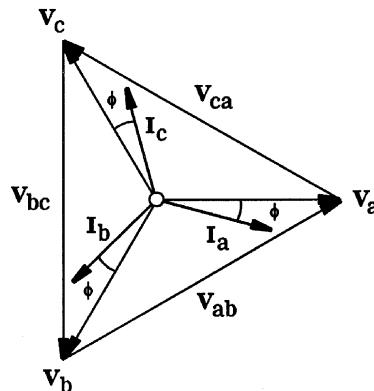

**Fig. 2.21** Phasor diagram for balanced wye-connected load.
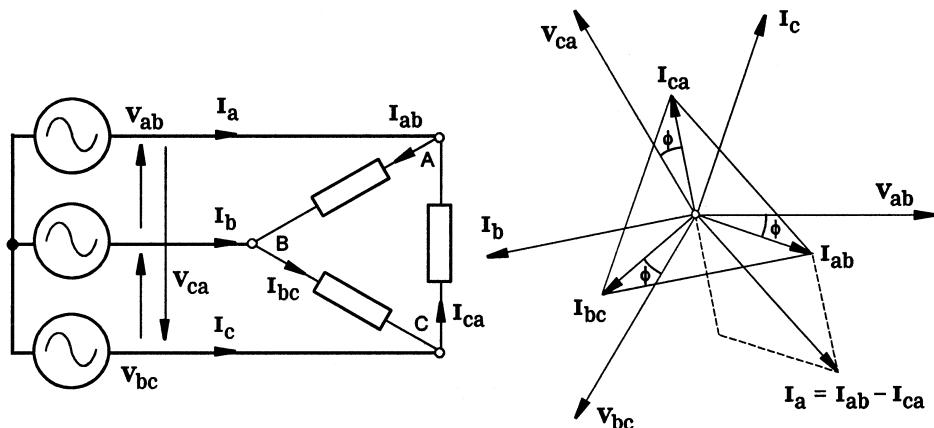
Fig. 2.22 Three-phase connection with delta-connected load and phasor diagram.
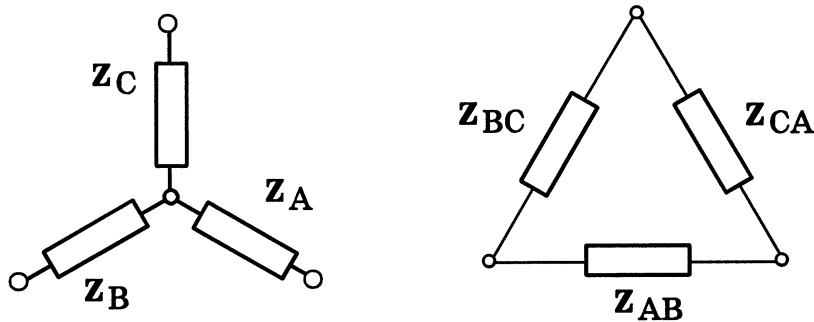
Fig. 2.23 Wye–delta transformation.

current in each phase tends to become distorted, and the triplen harmonics are allowed to flow locally in a delta-connected winding without entering the external circuit. In electric motors a delta winding permits the use of a larger number of turns of smaller-gauge wire, because the phase voltage is increased while the phase current is decreased, compared with the wye connection.

2.9.2 The wye–delta transformation

A wye-connected load can be represented by a virtual load connected in delta, and vice-versa, Figure 2.23. To transform the delta connection into a wye connection,

$$\mathbf{Z}_A = \frac{\mathbf{Z}_{AB}\mathbf{Z}_{CA}}{\mathbf{Z}_\Delta}; \quad \mathbf{Z}_B = \frac{\mathbf{Z}_{BC}\mathbf{Z}_{AB}}{\mathbf{Z}_\Delta}; \quad \mathbf{Z}_C = \frac{\mathbf{Z}_{CA}\mathbf{Z}_{BC}}{\mathbf{Z}_\Delta} \tag{2.27}$$

where $\mathbf{Z}_\Delta = \mathbf{Z}_{AB} + \mathbf{Z}_{BC} + \mathbf{Z}_{CA}$. To transform the wye connection into a delta connection,

$$\mathbf{Y}_{AB} = \frac{\mathbf{Y}_A\mathbf{Y}_B}{\mathbf{Y}_Y}; \quad \mathbf{Y}_{BC} = \frac{\mathbf{Y}_B\mathbf{Y}_C}{\mathbf{Y}_Y}; \quad \mathbf{Y}_{CA} = \frac{\mathbf{Y}_C\mathbf{Y}_A}{\mathbf{Y}_Y} \tag{2.28}$$

where $\mathbf{Y}_Y = \mathbf{Y}_A + \mathbf{Y}_B + \mathbf{Y}_C$

2.9.3 Balancing an unbalanced load

It can be shown by means of a series of diagrams, that an unbalanced linear ungrounded three-phase load can be transformed into a balanced, real three-phase load without changing the power exchange between source and load, by connecting an ideal reactive compensating network in parallel with it. Assume that the load is delta-connected with admittances $\mathbf{Y}_{ab} = G_{ab} + jB_{ab}$, $\mathbf{Y}_{bc} = G_{bc} + jB_{bc}$, $\mathbf{Y}_{ca} = G_{ca} + jB_{ca}$, as shown in Figure 2.24.

The power factor of each phase can be corrected to unity by connecting compensating admittances in parallel, as shown, where $jB_{\gamma ab} = -jB_{ab}$, $jB_{\gamma bc} = -jB_{bc}$, and $jB_{\gamma ca} = -jB_{ca}$. The resulting network is real, Figure 2.25.
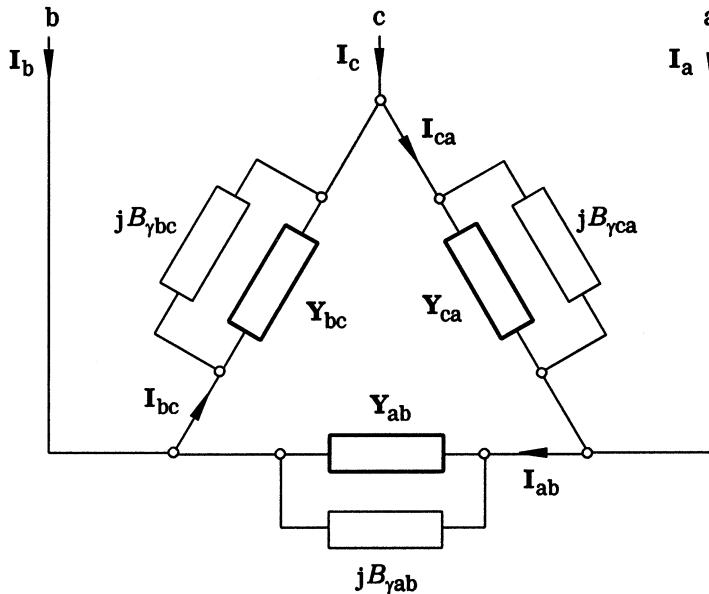
Fig. 2.24 Unbalanced delta-connected load with power-factor correction admittances.
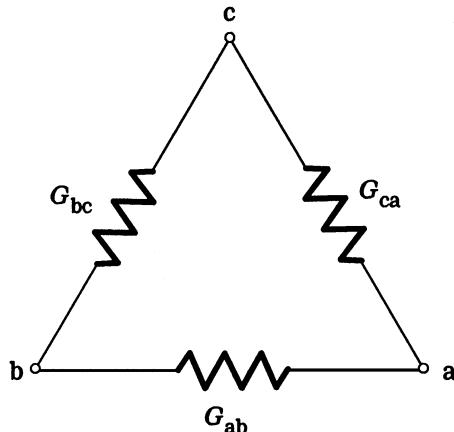
Fig. 2.25 Unbalanced load corrected with unity power factor in each phase.

If we now take one of the resistive admittances, G_{ab}, we can connect this in a so-called Steinmetz network with an inductor and a capacitor to produce balanced line currents as shown in Figure 2.26. The phasor diagram in Figure 2.27 shows how the balanced line currents are achieved, and the resulting equivalent circuit in Figure 2.28 is real, balanced, and wye-connected.
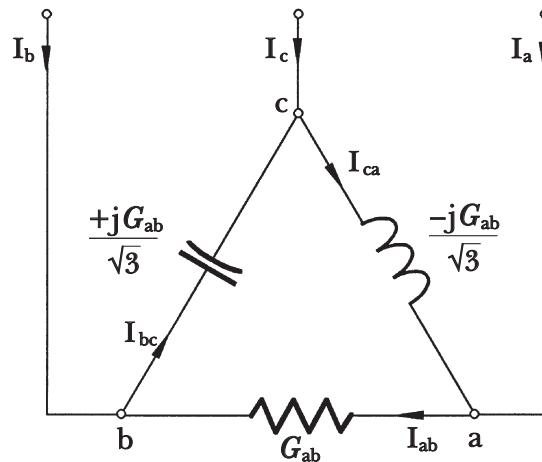
**Fig. 2.26** Steinmetz network with balanced line currents.
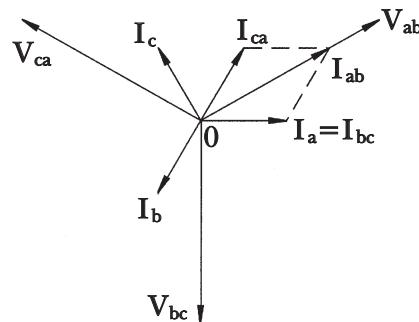
Fig. 2.27 Phasor diagram for Steinmetz network.
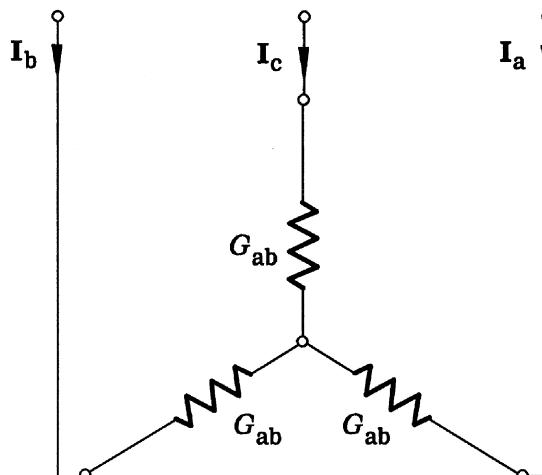

Fig. 2.28 Balanced network resulting from compensation of G_{ab} with the Steinmetz network.

The resulting compensating admittances are given in equation (2.29).

$$jB_{\gamma ab} = -jB_{ab} + j(G_{ca} - G_{bc})/\sqrt{3}$$
$$jB_{\gamma bc} = -jB_{bc} + j(G_{ab} - G_{ca})/\sqrt{3} \qquad (2.29)$$
$$jB_{\gamma ca} = -jB_{ca} + j(G_{bc} - G_{ab})/\sqrt{3}$$

2.10 Power flow and measurement

2.10.1 Single-phase

Suppose we have a single-phase load as in Figure 2.7 supplied with a sinusoidal voltage whose instantaneous value is $\upsilon = V_m \cos \omega t$. The RMS value is $V = V_m/\sqrt{2}$ and the phasor value is $\mathbf{V}$. If the load is linear (i.e. its impedance is constant and does not depend on the current or voltage), the current will be sinusoidal too. It leads or lags the voltage by a phase angle ϕ, depending on whether the load is capacitive or inductive. With a lagging (inductive) load, $i = I_m \cos(\omega t - \phi)$; see Figure 2.29.
The instantaneous power is given by $p = \upsilon i$, so

$$p = V_m I_m \cos \omega t \cos(\omega t - \phi) = \frac{V_m I_m}{2}[\cos \phi + \cos(2\omega t - \phi)] \qquad (2.30)$$

This expression has a constant term and a second term that oscillates at double frequency. The constant term represents the *average* power P: we can write this as

$$P = \frac{V_m}{\sqrt{2}} \times \frac{I_m}{\sqrt{2}} \cos \phi = VI \cos \phi \qquad (2.31)$$

P is equal to the product of the rms voltage $V = V_m/\sqrt{2}$, the RMS current $I = I_m/\sqrt{2}$, and the power factor $\cos \phi$. The amplitude of the oscillatory term is fixed: i.e. it does not depend on the power factor. It shows that the instantaneous power p varies from 0 to $V_m I_m$ to $-V_m I_m$ and back to 0 twice every cycle. Since the
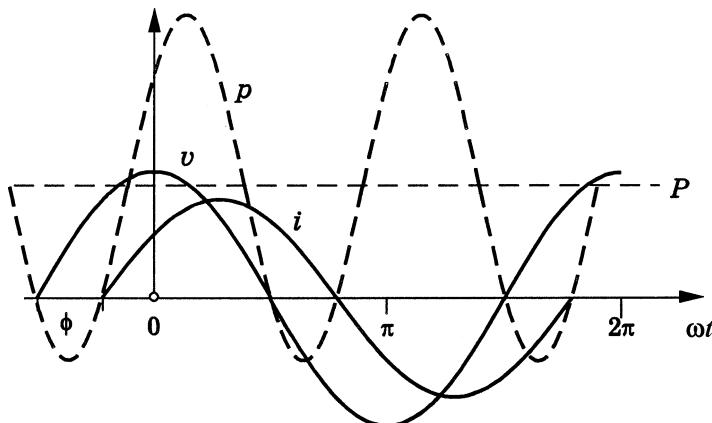

Fig. 2.29 Instantaneous current, voltage and power in a single-phase AC circuit.

average power is $V_m I_m/2$, this represents a peak–peak fluctuation 200% of the mean power, at double frequency. The oscillation of power in single-phase circuits contributes to lamp flicker and causes vibration in motors and transformers, producing undesirable acoustic noise.

2.10.2 Two-phase

Suppose we have a two-phase load with phases a and b, with $\upsilon_a = V_m \cos \omega t$, $i_a = I_m \cos(\omega t - \phi)$ and $\upsilon_b = V_m \sin \omega t$, $i_b = I_m \sin(\omega t - \phi)$. This system is said to be *balanced*, because the voltages and currents have the same RMS (and peak) values in both phases, *and* their phase angles are orthogonal. The total instantaneous power is now given by

$$
\begin{aligned}
p &= \upsilon_a i_a + \upsilon_b i_b \\
&= V_m I_m [\cos(\omega t)\cos(\omega t - \phi) + \sin(\omega t)\sin(\omega t - \phi)] \\
&= V_m I_m \cos \phi \\
&= 2VI \cos \phi
\end{aligned}
\tag{2.32}
$$

The oscillatory term has vanished altogether, which means that the power flow is constant, with no fluctuation, and the average power P is therefore equal to the instantaneous power p. Note that if the phases become unbalanced, an oscillatory term reappears.

2.10.3 Three-phase

Suppose we have a three-phase load as in Figures 2.20 and 2.22, with phases a, b and c, with

$$
\begin{array}{ll}
\upsilon_a = V_m \cos \omega t & i_a = I_m \cos(\omega t - \phi) \\
\upsilon_b = V_m \cos(\omega t - 2\pi/3) & i_b = I_m \cos(\omega t - 2\pi/3 - \phi) \\
\upsilon_c = V_m \cos(\omega t + 2\pi/3) & i_c = I_m \cos(\omega t + 2\pi/3 - \phi)
\end{array}
\tag{2.33}
$$

This system is said to be *balanced*, because the voltages and currents have the same RMS (and peak) values in all three phases, and their phase angles are equi-spaced (i.e. with a 120° symmetrical phase displacement). The total instantaneous power is now given by

$$
\begin{aligned}
p &= \upsilon_a i_a + \upsilon_b i_b + \upsilon_c i_c \\
&= V_m I_m [\cos(\omega t)\cos(\omega t - \phi) + \cos(\omega t - 2\pi/3)\cos(\omega t - 2\pi/3 - \phi) \\
&\quad + \cos(\omega t + 2\pi/3)\cos(\omega t + 2\pi/3 - \phi)] \\
&= \frac{3}{2} V_m I_m \cos \phi \\
&= 3VI \cos \phi
\end{aligned}
\tag{2.34}
$$

As in the two-phase system, the oscillatory term has vanished. The power flow is constant, with no fluctuation, and the average power P is equal to the instantaneous power p. If the phases become unbalanced, an oscillatory term reappears.

The voltages and currents in equation (2.34) are *phase* quantities. In terms of *line* quantities, for a wye connection we have $V_L = \sqrt{3}V_{ph}$ and $I_L = I_{ph}$, whereas for a delta connection we have $I_L = \sqrt{3}I_{ph}$ and $V_{LL} = V_{ph}$. In both cases, therefore,

$$P = \sqrt{3}V_{LL}I_L \cos \phi \tag{2.35}$$

where ϕ is the angle between the phasors $\mathbf{V}_{ph}$ and $\mathbf{I}_{ph}$.

2.10.4   Power measurement

Classical electro-dynamometer wattmeter or 'Wattmeter'

The classical wattmeter circuit symbol (Figure 2.30) is derived from the classical wattmeter (Figure 2.31), which is still widely used. Accuracy is typically 0.5% in calibrated instruments. The readings of these instruments are usually reliable if the voltage and current waveforms are sinusoidal with fairly high power factor. They are generally not suitable with distorted waveforms, but special versions have been manufactured for use at low power factor.
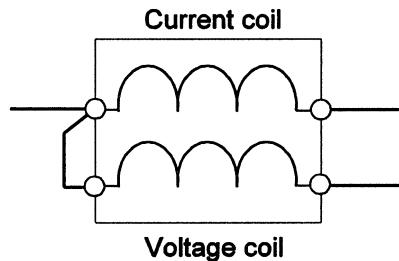

Fig. 2.30 Wattmeter symbol.
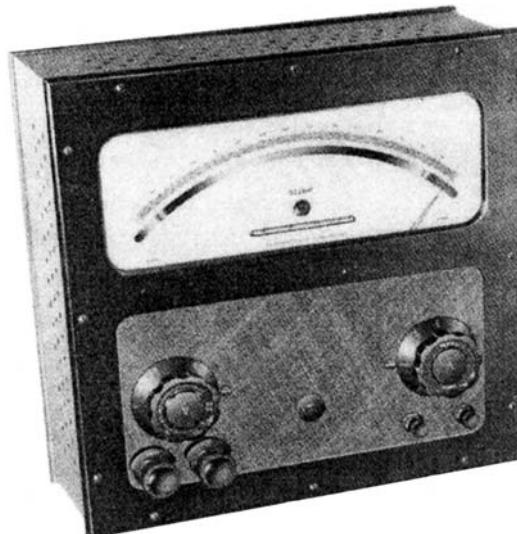
Fig. 2.31 Classical electro-dynamometer wattmeter.

Electronic wattmeter

These instruments multiply the instantaneous voltage and current together and take the average. Both digital and analog models are available. They are designed to be used with CTs and VTs, (current transformers and voltage transformers) and they come in single-phase and three-phase versions. Single-phase instruments have bandwidths up to several hundred kHz, so they give effective readings with distorted waveforms such as are caused by rectifiers and inverters, provided the harmonic content is not too great. See Figure 2.32.

Processing of sampled waveforms

The most exacting power measurements are in circuits with high-frequency switching (as in power electronics with PWM [pulse-width modulation]), especially if the power factor is low. In these cases the technique is to sample the voltage and current at high frequency and then digitally compute the power from the voltage and current samples: $\upsilon [1, 2, \ldots k \ldots N]$ and $i [1, 2, \ldots k \ldots N]$. The *average* power over time T is computed from:

$$P_{\mathrm{avg}} = \frac{1}{T} \sum_{k=1}^{N} p[k]\Delta t = \frac{1}{T} \sum_{k=1}^{N} \upsilon[k]i[k]\,\Delta t, \quad \text{where} \quad T = (N-1)\Delta t \qquad (2.36)$$

Some digital processing oscilloscopes can perform this function, but there are specialist data acquisition systems with fast sampling and analog/digital conversion, and they may include software for processing the equation (2.36).

The sampling process is illustrated in Figure 2.33. The double samples at the steep edges in the voltage waveform show the ambiguity (uncertainty) that arises when the sampling rate is too low relative to the frequency content of the sampled waveform. This is a particular problem in power electronics, where the voltage may switch from 0–100% in the order of 1 μs. If we use a sampling frequency of 10 MHz to give 10 samples on each voltage switching, then if the fundamental frequency is 50 Hz we will need $1/50 \times 10^7 = 200\,000$ samples for just one cycle. This illustrates the tradeoff between sample length and sampling frequency. The tradeoff is more difficult if a high resolution is required (for example, 12-bit A/D conversion, a resolution of 1 part in 4096).

Wattmeter connections

Figure 2.34 shows the connection of three wattmeters to measure the total power in three phases. The voltage coils of the wattmeters are returned to a common point which effectively forms a false neutral point 0. This is convenient because the star point of the load may not be available for connection (particularly if the load is an induction motor). The instantaneous power is

$$p = \upsilon_{\mathrm{as}}i_{\mathrm{a}} + \upsilon_{\mathrm{bs}}i_{\mathrm{b}} + \upsilon_{\mathrm{cs}}i_{\mathrm{c}} \qquad (2.37)$$

where i_{a} is the instantaneous current in phase A and υ_{as} is the instantaneous voltage across phase A, etc. In a three-wire connection, however,

$$i_{\mathrm{a}} + i_{\mathrm{b}} + i_{\mathrm{c}} = 0 \qquad (2.38)$$

and if we use this to eliminate i_{c} from equation (2.37) we get

$$\begin{aligned}
p &= (\upsilon_{\mathrm{as}} - \upsilon_{\mathrm{cs}})i_{\mathrm{a}} + (\upsilon_{\mathrm{bs}} - \upsilon_{\mathrm{cs}})i_{\mathrm{b}} \\
&= \upsilon_{\mathrm{ac}}i_{\mathrm{a}} + \upsilon_{\mathrm{bc}}i_{\mathrm{b}}
\end{aligned} \qquad (2.39)$$
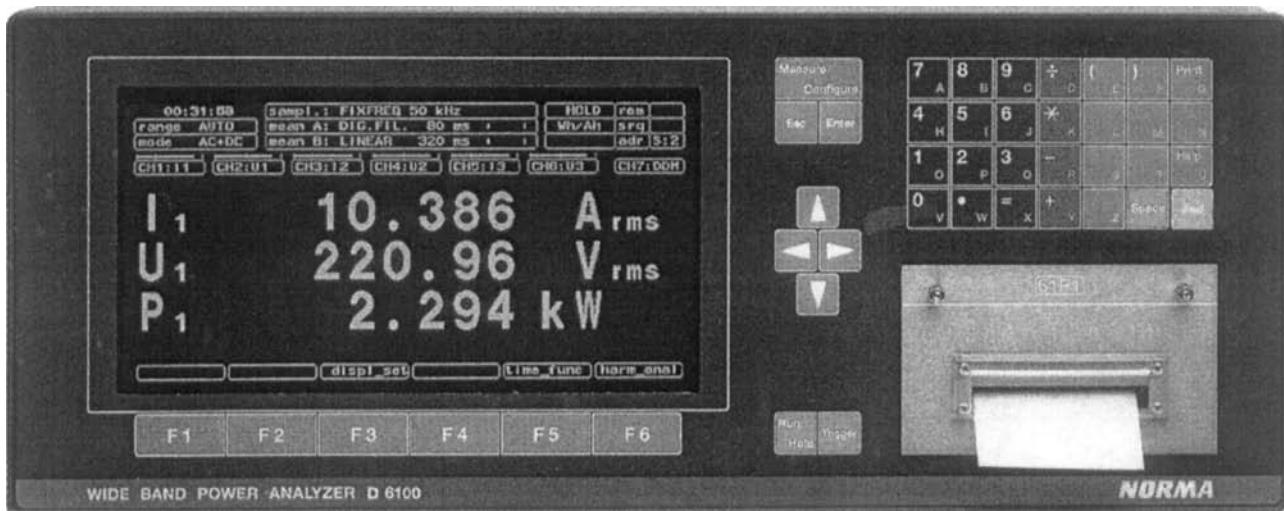
Fig. 2.32 Electronic wattmeter (Norma).
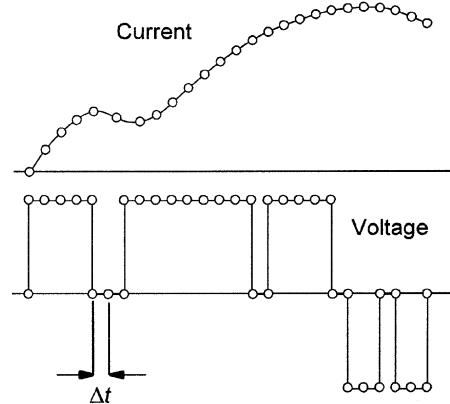
Fig. 2.33 Sampled voltage and current waveforms.
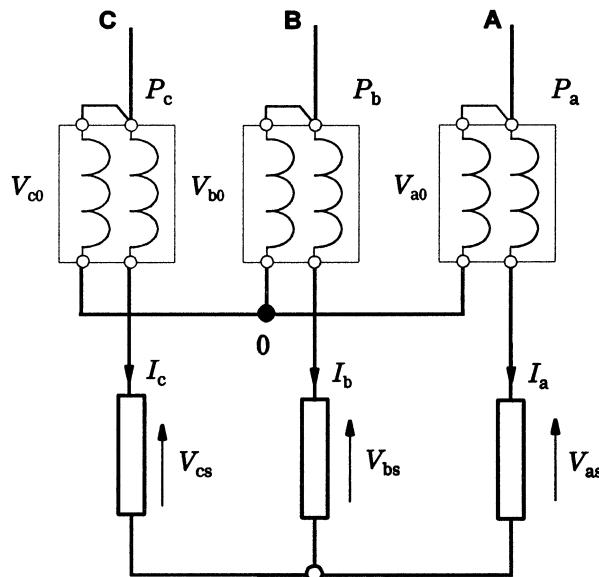
Fig. 2.34 Three-wattmeter connection.

which indicates that only two wattmeters are required, connected as shown in Figure 2.35. Since this is valid for instantaneous power, it is also valid for average power. It is valid irrespective of the waveforms of voltage and current, requiring only that the connection is three-wire.

Under sinusoidal AC conditions the two-wattmeter connection can be described by the equations

$$
\begin{aligned}
P_1 &= \langle v_{ac} i_a \rangle = \mathrm{Re}\{\mathbf{V}_{ac}\mathbf{I}_a^*\} = V_{ac} I_a \cos \phi_1 \\
P_2 &= \langle v_{bc} i_b \rangle = \mathrm{Re}\{\mathbf{V}_{bc}\mathbf{I}_b^*\} = V_{bc} I_b \cos \phi_2
\end{aligned}
\tag{2.40}
$$
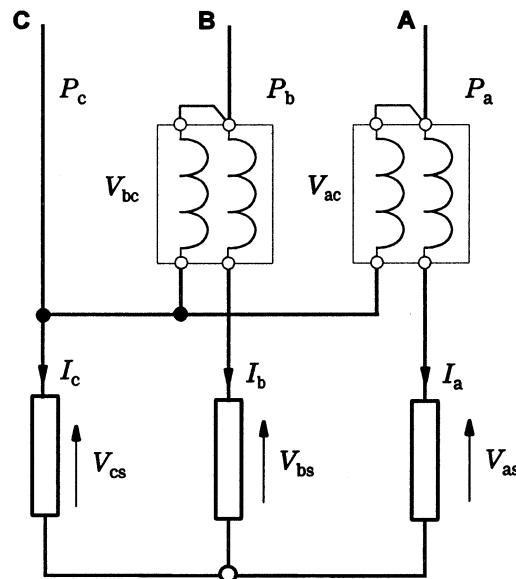
Fig. 2.35 Two-wattmeter connection.
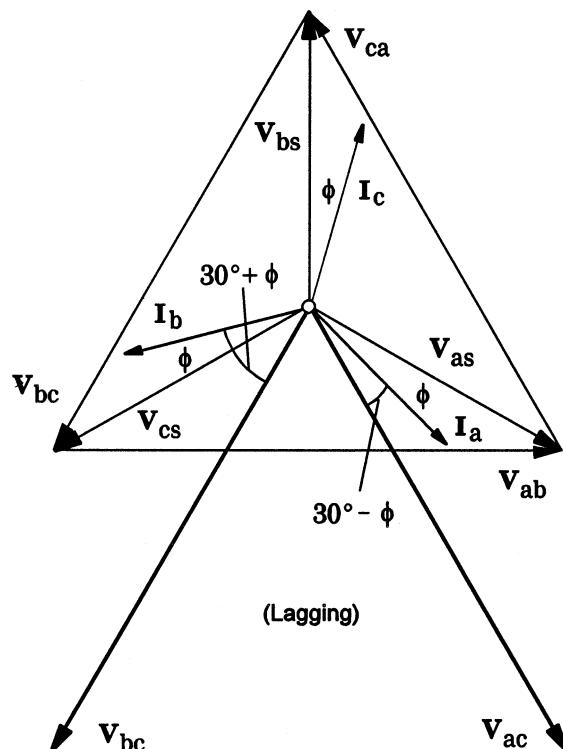
Fig. 2.36 Phasor diagram for two-wattmeter connection.

where the $\langle \rangle$ symbols mean 'time average' over one cycle, ϕ_1 is the phase angle between $\mathbf{V}_{ac}$ and $\mathbf{I}_a$, and ϕ_2 is the phase angle between $\mathbf{V}_{bc}$ and $\mathbf{I}_b$. These relationships are further illustrated in Figure 2.36, and under balanced conditions

$$\begin{aligned} P_1 &= V_{LL}I_L \cos(30° - \phi) \\ P_2 &= V_{LL}I_L \cos(30° + \phi) \end{aligned} \tag{2.41}$$

from which it follows that

$$\tan \phi = \sqrt{3}\frac{P_1 - P_2}{P_1 + P_2} \tag{2.42}$$

The wattmeter readings can be used in this equation to determine the power factor.

2.11   Polyphase transformers

2.11.1   Definition

A transformer is a set of 1, 2 or more magnetically coupled windings, usually wound on a common laminated magnetic iron core, Figure 2.37.

In an ideal transformer the voltages and currents on the primary and secondary sides are related by

$$\frac{\mathbf{V}_1}{\mathbf{V}_2} = \frac{N_1}{N_2} \quad \text{and} \quad \frac{\mathbf{I}_1}{\mathbf{I}_2} = \frac{N_2}{N_1} \tag{2.43}$$

where N_1/N_2 is the primary/secondary turns ratio. Equation (2.43) is valid not only for phasor values but also for instantaneous values. It follows from equation (2.43) that

$$\mathbf{V}_1\mathbf{I}_1^* = \mathbf{V}_2\mathbf{I}_2^* \tag{2.44}$$

so that the real and reactive power are both transmitted unaltered through an ideal transformer. The same is true for the instantaneous power. The ideal transformer has no losses and no reactive power requirement of its own. Of course, real transformers depart from the ideal, in that they have resistance, imperfect coupling, magnetizing
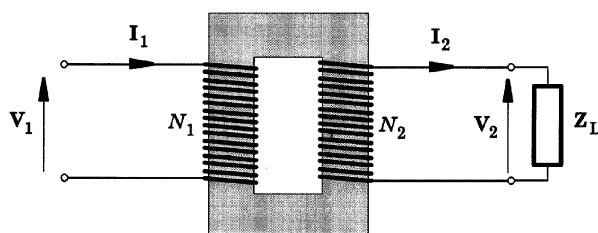

Fig. 2.37 Basic transformer.

current, and core losses; but these can be neglected when considering many of the main functions of transformers.[12]

The impedance 'looking into' the transformer at the primary terminals is the ratio V_1/I_1, and from equation (2.43) this is equal to $(N_1/N_2)^2 Z_L$, where Z_L is the load impedance connected on the secondary side. This is called the 'referred' impedance, Z_L'. If the primary side has a higher voltage than the secondary side, i.e. $N_1/N_2 > 1$, then Z_L' will be larger than Z_L. For example, in an $11\,kV/415\,V$ transformer the impedance ratio is $(11\,000/415)^2 = 702.5$.

2.11.2 Functions

Transformers have several functions in power transmission and distribution, for example:

(a) transform voltage level for optimum transmission
(b) isolate coupled circuits
(c) impedance matching
(d) introduce series impedance (to limit fault current)
(e) create a neutral point (e.g. ground connection remote from power station)
(f) suppress harmonics (especially triplen harmonics)
(g) provide tappings for loads along a tranmission line
(h) produce phase shift or multiple phases (e.g. for multiple-pulse converters)
(i) frequency-multiplication (saturated core)
(j) constant-voltage reactive compensation (saturated core).

Three-phase transformers are often wound on common cores such as the one shown in Figure 2.38. The windings on both sides may be connected in wye or delta, giving
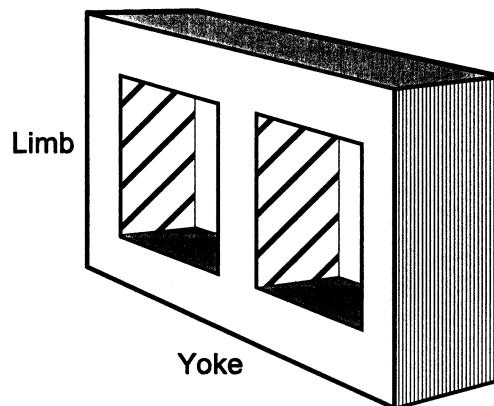
Fig. 2.38 Unwound 3-limb transformer core.

---

[12] These 'imperfections' can usually be included in calculations by means of additional parasitic impedances added to the equivalent circuit of Figure 2.37. One of the most important of these impedances is the leakage reactance which represents the imperfect magnetic coupling between the primary and secondary windings and appears as a series reactance either in the primary or secondary circuit, or shared between them.
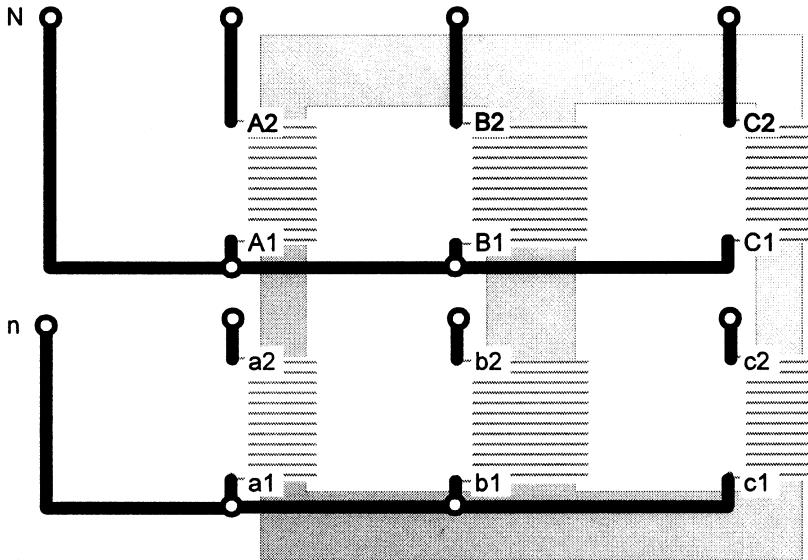
Fig. 2.39 Electrical connections of a Yyo transformer.

rise to a range of useful operational features. The simplest case is that of a Yy0 transformer shown in Figure 2.39. in which both sets of windings are wye-connected, and corresponding voltages are in phase. The windings are labelled A, B, C on the high-voltage side and a, b, c on the low-voltage side, with terminal two at higher potential than terminal one. The polarities are such that current flowing into terminal A2 would produce flux in the same direction as current flowing into terminal a2. From these considerations it is a straightforward matter to construct the voltage phasor diagram, as shown at top left in Figure 2.40. With no phase shift between corresponding primary and secondary windings, the Yy transformer is designated Yy0. In Figure 2.40 there are two other transformer connections with this property, the Dd0 and the Dz0,[13] and together these transformers are collectively known as 'Group 1' transformers.[14]

Figure 2.41 shows a Yd1 transformer in which the low-voltage winding is delta-connected, producing a 30° phase shift such that any voltage on the low-voltage side is retarded 30° in phase relative to the corresponding voltage on the high-voltage side: for example V_{AB} leads V_{ab} by 30° (see Figure 2.40). The phase shift of −30° is denoted by a '1' in the designation Yd1, and it refers to the clock position of a low-voltage phasor, when the corresponding high-voltage phasor is at 12 o'clock. In some cases the connection does not have a high-voltage winding with a voltage that sits at 12 o'clock without rotating the phasor diagram, so to preserve the orientation and symmetry in Figure 2.40 it is usual in these cases to construct an imaginary neutral which provides the required phasor: an example is the Dy1 transformer in Group III.

---

[13] 'Z' stands for 'zig-zag' which is a composite winding in which half the turns of each phase are on different limbs and their voltages are phase-shifted by 120°.
[14] These conventions are consistent with B.S. 171 or IEC 76/I.
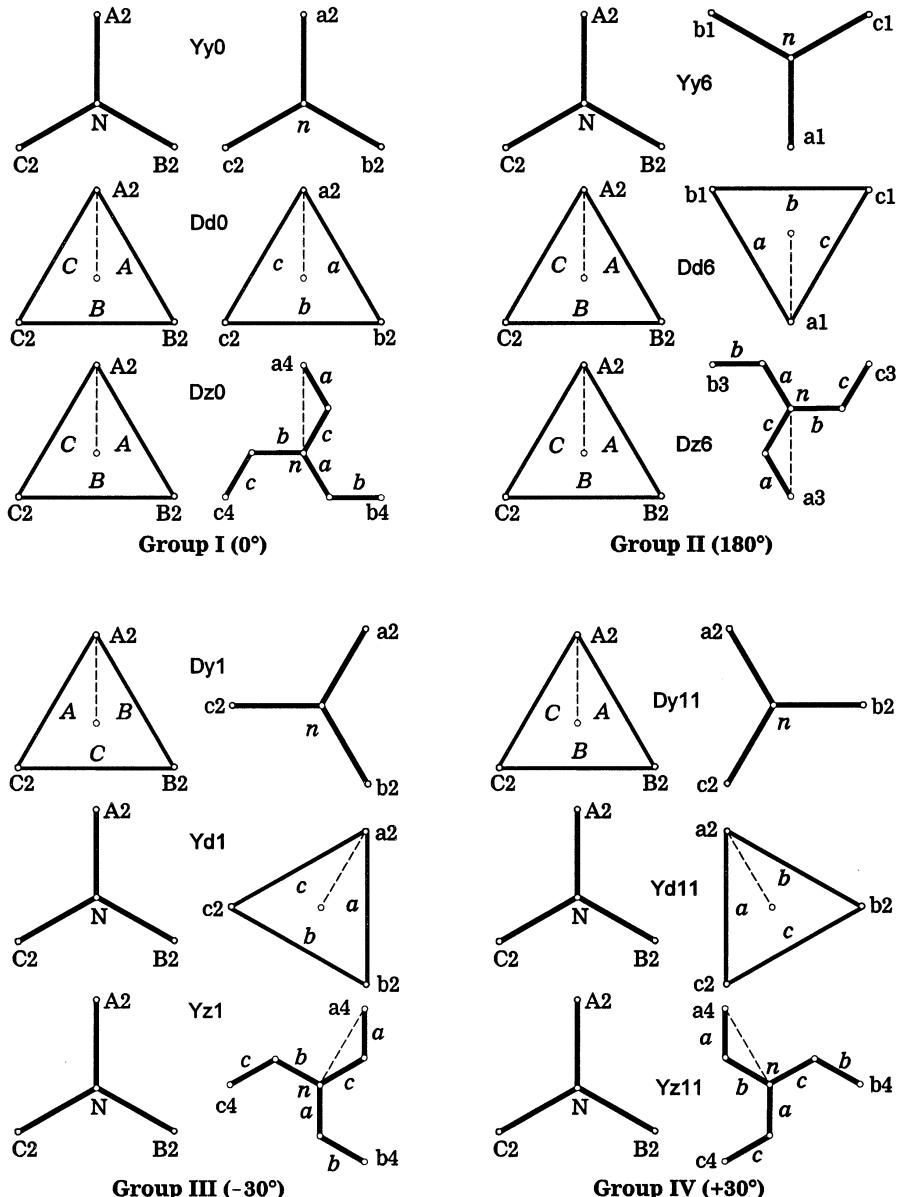
Fig. 2.40 Voltage phasor diagrams of polyphase transformers.

Note that the voltage and current ratios are affected by the connection. For example in a Yd1 transformer with N_1 turns per phase on the high-voltage winding and N_2 turns per phase on the low-voltage winding, the ratio between phase voltages is N_1/N_2, but the ratio between line–line voltages is $\sqrt{3} \times N_1/N_2$, while the ratio between line currents is $(N_1/N_2)/\sqrt{3}$. The impedance referral ratio is therefore $3(N_1/N_2)^2$.
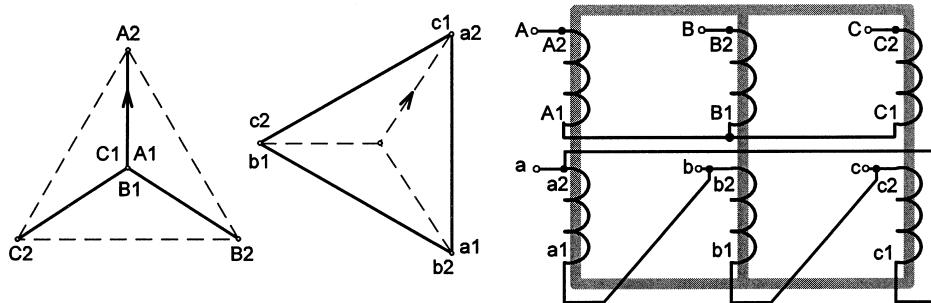
Fig. 2.41 Yd1 transformer.

2.11.3   Parallel operation

For connection in parallel, transformers must be designed for the same frequency and the same primary and secondary voltages, and they must be connected with the correct polarities. (That's why the labelling of transformer terminals is so important.)

The way in which parallel transformers share the load is important. To introduce the analysis it might be helpful to consider the simpler case of two DC batteries supplying a common load, Figure 2.42. By virtue of the parallel connection we have

$$V = E_1 - R_1 I_1 = E_2 - R_2 I_2 \tag{2.45}$$

Suppose we require battery one to supply a fraction x of the load current, and battery two to supply fraction $(1 - x)$. Then $I_1 = xI$ and $I_2 = (1 - x)I$. Substituting in equation (45) and rearranging, we get

$$E_1 - E_2 = [xR_1 - (1 - x)R_2]I \tag{2.46}$$

For this to be true for all values of the load current $I = I_1 + I_2$, we require the coefficient of I to be zero, which implies at least that $E_1 = E_2$. It further implies that the load is shared according to the values of R_1 and R_2, since $x = R_2/(R_1 + R_2)$ and $(1 - x) = R_1/(R_1 + R_2)$. Only when $R_1 = R_2$ is the load shared equally ($x = 0.5$). From this it is clear that the internal impedance of a supply is important in determining its contribution to the load when it is connected in parallel with other supplies.
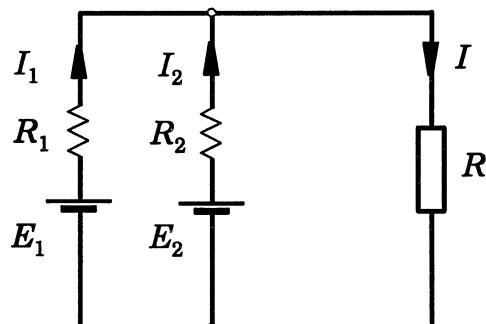
Fig. 2.42 Parallel batteries supplying a DC load.
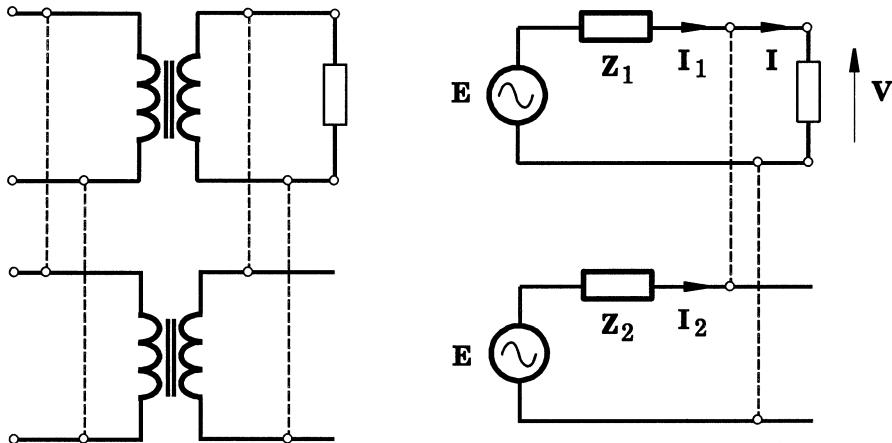
Fig. 2.43 Parallel transformers.

This theory can be extended to the parallel operation of transformers by representing them by their Thévenin equivalent circuits, in which the series impedance is approximately the leakage reactance. In general they are not required to share the load equally, but in proportion to their ratings. For this we shall see that their per-unit impedances must be equal, when evaluated on their own respective MVA bases and a common voltage base.

Working with Figure 2.43, the load current is

$$\mathbf{I} = \mathbf{I}_1 + \mathbf{I}_2 = \frac{\mathbf{E} - \mathbf{V}}{\mathbf{Z}_1} + \frac{\mathbf{E} - \mathbf{V}}{\mathbf{Z}_2} = (\mathbf{E} - \mathbf{V})\left[\frac{1}{\mathbf{Z}_1} + \frac{1}{\mathbf{Z}_2}\right] \tag{2.47}$$

and the respective transformer contributions are

$$\mathbf{I}_1 = \frac{1/\mathbf{Z}_1}{1/\mathbf{Z}_1 + 1/\mathbf{Z}_2}\mathbf{I} = \frac{\mathbf{Y}_1}{\mathbf{Y}_1 + \mathbf{Y}_2}\mathbf{I} = \frac{\mathbf{Z}_2}{\mathbf{Z}_1 + \mathbf{Z}_2}\mathbf{I} \tag{2.48}$$

and

$$\mathbf{I}_2 = \frac{1/\mathbf{Z}_2}{1/\mathbf{Z}_1 + 1/\mathbf{Z}_2}\mathbf{I} = \frac{\mathbf{Y}_2}{\mathbf{Y}_1 + \mathbf{Y}_2}\mathbf{I} = \frac{\mathbf{Z}_1}{\mathbf{Z}_1 + \mathbf{Z}_2}\mathbf{I} \tag{2.49}$$

Taking the ratio of equations (2.48) and (2.49),

$$\frac{\mathbf{I}_1}{\mathbf{I}_2} = \frac{\mathbf{Y}_1}{\mathbf{Y}_2} = \frac{\mathbf{Z}_2}{\mathbf{Z}_1} \tag{2.50}$$

i.e. the currents are in inverse proportion to the ohmic impedances.

Now calculate the complex powers through the two transformers, as fractions of the total complex power $\mathbf{S} = \mathbf{V}\mathbf{I}^*$:

$$\mathbf{S}_1 = \mathbf{V}\mathbf{I}_1^* = \left[\frac{\mathbf{Y}_1}{\mathbf{Y}_1 + \mathbf{Y}_2}\right]^*\mathbf{S} \quad \text{and} \quad \mathbf{S}_2 = \mathbf{V}\mathbf{I}_2^* = \left[\frac{\mathbf{Y}_2}{\mathbf{Y}_1 + \mathbf{Y}_2}\right]^*\mathbf{S} \tag{2.51}$$

Dividing these two equations,

$$\frac{\mathbf{S}_1}{\mathbf{S}_2} = \frac{\mathbf{Y}_1^*}{\mathbf{Y}_2^*} = \frac{\mathbf{Z}_2^*}{\mathbf{Z}_1^*} \tag{2.52}$$

Now define the per-unit complex powers $\mathbf{s}_1 = \mathbf{S}_1/S_{1b}$ and $\mathbf{s}_2 = \mathbf{S}_2/S_{2b}$ where 'b' means the 'base' MVA for each transformer.[15] Also, the per-unit impedances are defined as

$$\mathbf{z}_1 = \frac{\mathbf{Z}_1}{Z_{1b}} = \mathbf{Z}_1 \times \frac{S_{1b}}{V_{1b}^2} \quad \text{and} \quad \mathbf{z}_2 = \frac{\mathbf{Z}_2}{Z_{2b}} = \mathbf{Z}_2 \times \frac{S_{2b}}{V_{2b}^2} \tag{2.53}$$

so that

$$\frac{\mathbf{s}_1}{\mathbf{s}_2} = \frac{\mathbf{S}_1/S_{1b}}{\mathbf{S}_2/S_{2b}} = \frac{\mathbf{Z}_2^*}{\mathbf{Z}_1^*} \times \frac{S_{2b}}{S_{1b}} = \frac{\mathbf{z}_2^*}{\mathbf{z}_1^*} \times \frac{V_{2b}^2}{V_{1b}^2} \tag{2.54}$$

If V_{1b} is chosen to be equal to V_{2b}, then

$$\frac{\mathbf{s}_1}{\mathbf{s}_2} = \frac{\mathbf{z}_2^*}{\mathbf{z}_1^*} \tag{2.55}$$

If the transformers are to be loaded in proportion to their ratings, then $\mathbf{s}_1 = \mathbf{s}_2$, which requires that $\mathbf{z}_1 = \mathbf{z}_2$. That is, the per-unit impedances of the transformers must be equal, when evaluated on their own respective MVA bases and a common voltage base.

When three-phase transformers are connected in parallel, the requirement for 'correct polarity' is slightly more complicated. The phase shift between corresponding primary and secondary voltages must be the same in both transformers. This means that both transformers must belong to the same *group*. For example, a Yy0 transformer can be paralleled with a Dd0 transformer, because the phase shift is zero through both of them. But a Yd1 cannot be paralleled with a Yy0, because the Yd1 has a phase shift of $-30°$.

2.11.4 Zero-sequence effects in three-phase transformers

In normal operation of a three-phase system, the voltages and currents are balanced and

$$\mathbf{I}_a + \mathbf{I}_b + \mathbf{I}_c = 0 \tag{2.56}$$

This equation is satisfied not only by the line currents, but also by the line-neutral voltages and the line–line voltages in balanced operation.

In a transformer core the voltages establish fluxes in the core. If each phase winding has the same number of turns on each limb of the core, then the limb fluxes will also be balanced: i.e.,

$$\mathbf{\Phi}_a + \mathbf{\Phi}_b + \mathbf{\Phi}_c = 0 \tag{2.57}$$

In balanced operation, the flux through any limb at any instant is returning through the other two limbs, so there is no tendency for flux to leak outside the three limbs. (Figure 2.44).

If the operation is unbalanced there may be a 'residual' current, $\mathbf{I}_0 = \mathbf{I}_a + \mathbf{I}_b + \mathbf{I}_c$, and/or a residual voltage $\mathbf{V}_0 = \mathbf{V}_a + \mathbf{V}_b + \mathbf{V}_c$, and a residual flux $\mathbf{\Phi}_0 = \mathbf{\Phi}_a + \mathbf{\Phi}_b + \mathbf{\Phi}_c$. These residual quantities are also called 'zero-sequence' quantities.[16] Zero-sequence components are all in phase with each other. Unlike positive/negative-sequence

---

[15] See §2.13.
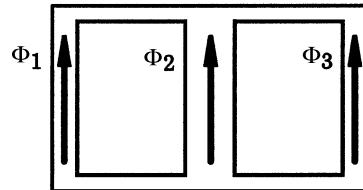
Fig. 2.44 Fluxes in 3-limb core.
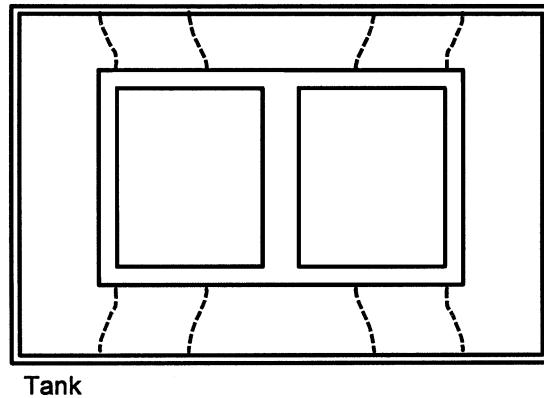
Fig. 2.45 Residual fluxes in 3-limb core and tank.

quantities, they do not sum to zero. The residual flux Φ_0 can be visualized as flux that is flowing in all three limbs at the same time. It must find a return path *outside the three main limbs*. In Figure 2.45 the return path is through the space surrounding the core and into the tank. Since the tank is not laminated it is liable to carry induced eddy-currents which can cause it to overheat. The flux path for the residual flux has a high reluctance and therefore a low inductance, because the flux must travel a long way through the gap between the core and the tank. Consequently the zero-sequence inductance is low, and the zero-sequence currents (which flow in the neutral wire) can be large. If there is no neutral, the potential of the neutral point will oscillate (see Figure 2.48).

In a five-limb core the return path is provided through two extra unwound limbs at the ends of the transformer core. The reluctance of the zero-sequence or residual flux-path is now low, so the zero-sequence inductance is high. This tends to limit the zero-sequence current in the neutral connection to a low value. The residual flux does not leak outside the core and there is therefore no risk of overheating the tank by eddy-currents.

---

[16] The term 'zero-sequence' comes from the theory of *symmetrical components*, which is the mathematical basis for analysis of unbalanced three-phase systems.

2.11.5 Providing a path for zero-sequence currents

It is generally essential in three-phase transformers to provide a path for zero-sequence current. A delta winding is used for this purpose. Zero-sequence currents can flow in the delta without magnetically short-circuiting the entire core.

The delta winding can be either the primary or the secondary, or it can be a *tertiary* winding provided specially for the purpose of mopping up residual current (especially when the primary and secondary are wye-connected). Tertiary windings have other uses: for example, they may be used to connect local loads, power factor correction capacitors, or static compensators. The tertiary winding must be designed for the full fault level at that point in the transmission system, but its continuous thermal rating is usually less than those of the primary and secondary.

2.12 Harmonics

Ideally the voltage and current in an AC power system are purely sinusoidal. When the waveform is distorted, it can be analysed (by Fourier's theorem) into components at the fundamental frequency and multiples thereof. Frequency components other than the fundamental are called *harmonics*. The main origins of harmonics are as follows:

(a) non-linear magnetic elements, such as saturated transformer cores
(b) non-sinusoidal airgap flux distribution in rotating AC machines and
(c) switched circuit elements, such as rectifiers, triacs, and other power-electronic converters.

The main undesirable effects can be summarized as follows:

(i)   additional heating of cables, transformers, motors etc.
(ii) interference to communications and other electrical/electronic circuits
(iii) electrical resonance, resulting in potentially dangerous voltages and currents and
(iv) electromechanical resonance, producing vibration, noise, and fatigue failure of mechanical components.

Fourier's theorem provides the mathematical tool for resolving a periodic waveform of virtually any shape into a sum of harmonic components: thus an arbitrary periodic voltage waveform $\upsilon(t)$ is written

$$\upsilon(t) = \upsilon_0 + \sum_{m=1}^{\infty} \sqrt{2} V_m \cos(m\omega t + \phi_m)$$
$$= \upsilon_0 + \sum_{m=1}^{\infty} [a_m \cos(m\omega t) + b_m \sin(m\omega t)]$$

(2.58)

where υ_0 is the average (DC) component. The first form expresses each harmonic in terms of its RMS value V_m and its phase ϕ_m. Each harmonic is itself sinusoidal and can be considered as a phasor, except that it rotates at m times the fundamental frequency. The second form expresses each harmonic in terms of cosine and sine coefficients a_m and b_m respectively. The main limitation is that the waveform $\upsilon(t)$ must be periodic, that is, it must repeat after a time $T = 1/f = 2\pi/\omega$, where f is the

fundamental frequency in Hz and $\omega = 2\pi f$. According to Fourier the coefficients a_m and b_m can be determined from the original waveform by the integrations

$$a_m = \frac{2}{2\pi} \int_0^{2\pi} \upsilon(\omega t) \cos(m\omega t) \, d(\omega t)$$

$$b_m = \frac{2}{2\pi} \int_0^{2\pi} \upsilon(\omega t) \sin(m\omega t) \, d(\omega t)$$

(2.59)

and the DC value from the integral

$$\upsilon_0 = \frac{1}{2\pi} \int_0^{2\pi} \upsilon(\omega t) \, d(\omega t)$$

(2.60)

2.12.1 Harmonic power

In general $p = \upsilon i$ so

$$
\begin{aligned}
P_{avg} &= \frac{1}{2\pi} \int_0^{2\pi} p(\omega t) \, d(\omega t) \\
&= \frac{1}{2\pi} \int_0^{2\pi} \sum_{\substack{m=0 \\ n=0}}^{\infty} \sqrt{2} V_m \cos(m\omega t) \cdot \sqrt{2} I_n \, \cos(n\omega t + \phi_n) \, d(\omega t) \\
&= \sum_{\substack{m=0 \\ n=0}}^{\infty} \frac{1}{2\pi} \int_0^{2\pi} V_m I_n \{\cos[(m+n)\omega t + \phi_n] + \cos[(m-n)\omega t - \phi_n]\} \\
&= \sum_{m=0}^{\infty} V_m I_m \cos \phi_m \\
&= V_0 I_0 + V_1 I_1 \cos \phi_1 + V_2 I_2 \cos \phi_2 + \ldots
\end{aligned}
$$

(2.61)

Products of the mth voltage harmonic and the nth current harmonic integrate to zero over one period, if $m \neq n$, leaving only the products of harmonics of the same order. The power associated with each harmonic can be determined individually with an equation of the form $VI \cos \phi$, where V and I are the rms voltage and current of that harmonic and ϕ is the phase angle between them.

2.12.2 RMS values in the presence of harmonics

If the current flows through a resistor R, $V_m = RI_m$ and the average power dissipation is

$$P_{avg} = \sum_{m=0}^{\infty} I_m^2 R = I^2 R \quad \text{where} \quad I = \sqrt{\sum_{m=0}^{\infty} I_m^2}$$

(2.62)

I is the rms current and equation (2.62) is consistent with the definition of rms current

$$I_{rms} = \sqrt{\frac{1}{T} \int_0^T i^2(t) dt}$$

(2.63)

Similar considerations apply to the voltage, such that

$$V_{\text{rms}} = \sqrt{\sum_{m=0}^{\infty} V_m^2} \qquad (2.64)$$

2.12.3 Phase sequence of harmonics in balanced three-phase systems

The three phase voltages can be expanded in terms of their harmonic components

$$\begin{aligned}
\upsilon_{\text{an}} &= V_1 \cos(\omega t) + V_3 \cos(3\omega t) + V_5 \cos(5\omega t) + \ldots \\
\upsilon_{\text{bn}} &= V_1 \cos(\omega t - 2\pi/3) + V_3 \cos 3(\omega t - 2\pi/3) + V_5 \cos 5(\omega t - 2\pi/3) + \ldots \\
\upsilon_{\text{cn}} &= V_1 \cos(\omega t + 2\pi/3) + V_3 \cos 3(\omega t + 2\pi/3) + V_5 \cos 5(\omega t + 2\pi/3) + \ldots
\end{aligned} \qquad (2.65)$$

that is

$$\begin{aligned}
\upsilon_{\text{an}} &= V_1 \cos(\omega t) + V_3 \cos(3\omega t) + V_5 \cos(5\omega t) + \ldots \\
\upsilon_{\text{bn}} &= V_1 \cos(\omega t - 2\pi/3) + V_3 \cos(3\omega t) + V_5 \cos(5\omega t + 2\pi/3) + \ldots \\
\upsilon_{\text{cn}} &= V_1 \cos(\omega t + 2\pi/3) + V_3 \cos(3\omega t) + V_5 \cos(5\omega t - 2\pi/3) + \ldots
\end{aligned} \qquad (2.66)$$

The three fundamental components form a balanced three-phase set of phasors rotating at the fundamental electrical angular velocity ω rad/s with *positive sequence abc*. Likewise the fifth harmonic phasors form a balanced set rotating at 5ω rad/s, but with *negative sequence acb*. The third harmonic components rotate at 3ω radians/s but they are all in phase with one another and are said to have *zero phase sequence*. They do not form a balanced set. The phasors are illustrated in Figure 2.46.

Positive sequence harmonics include those of orders 1, 7, 13, 19, 25, 31, 37, . . .; negative sequence those of orders 5, 11, 17, 23, 29, 35, . . .; and zero-sequence harmonics all the triplen harmonic orders 3, 9, 15, 21, 27. Note that $\mathbf{V}_{\text{a1}} + \mathbf{V}_{\text{b1}} + \mathbf{V}_{\text{c1}} = 0$, $\mathbf{V}_{\text{a3}} + \mathbf{V}_{\text{b3}} + \mathbf{V}_{\text{c3}} = 3\mathbf{V}_{\text{a3}} \neq 0$, and $\mathbf{V}_{\text{a5}} + \mathbf{V}_{\text{b5}} + \mathbf{V}_{\text{c5}} = 0$.

Positive sequence   Zero sequence   Negative sequence
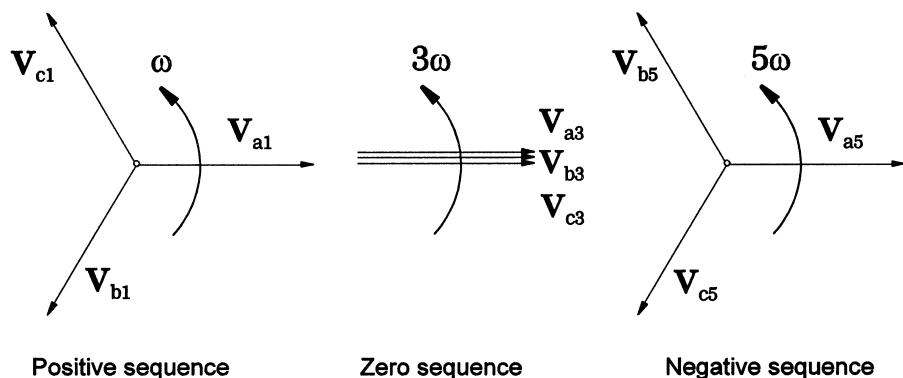
Fig. 2.46 Harmonic phasors.

2.12.4 Harmonics in balanced networks

In a wye connection we can observe that the actual instantaneous line–line voltage obeys the equation $\upsilon_{ab} = \upsilon_{an} - \upsilon_{bn}$, and so does its fundamental component: $\upsilon_{ab1} = \upsilon_{an1} - \upsilon_{bn1}$. However, the third harmonic component is $\upsilon_{ab3} = \upsilon_{an3} - \upsilon_{bn3} = 0$, which means that no triplen harmonic voltage can appear between two lines in a balanced system.

If there is no neutral, $i_a + i_b + i_c = 0$. Since $i_{a3} = i_{b3} = i_{c3}$, they must all be zero. In a three-wire balanced system, no triplen harmonic currents can flow in the lines. This is true for wye-connected and delta-connected loads. However, triplen harmonic currents can circulate around a delta without appearing in the lines. This property is used to provide the third-harmonic component of magnetizing current in saturated transformers. If the neutral (4th wire) is connected, the neutral current is

$$i_N = i_a + i_b + i_c = +3(i_3 + i_9 + \dots) \tag{2.67}$$

The neutral connection helps to prevent oscillation of the neutral voltage.

A non-linear load can draw non-sinusoidal currents in each phase, including 3rd harmonics. If such a load is connected in delta, the triplen harmonics can flow in the delta without appearing in the lines. The equivalent circuit of such a load must include a fictitious voltage source for each triplen harmonic, in series with the non-linear load impedance. In a delta connection, the sum of the triplen source voltage and the triplen harmonic voltage drop across the non-linear load impedance will be zero, so that no triplen harmonic voltage component appears between the lines. This is illustrated in Figure 2.47, with

$$\mathbf{E}_3 + \mathbf{Z}_3\mathbf{I}_3 = 0 \tag{2.68}$$
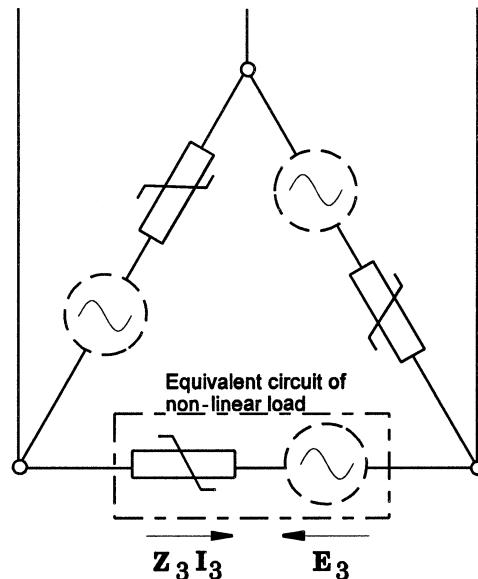
**Fig. 2.47** Equivalent circuit of non-linear load.
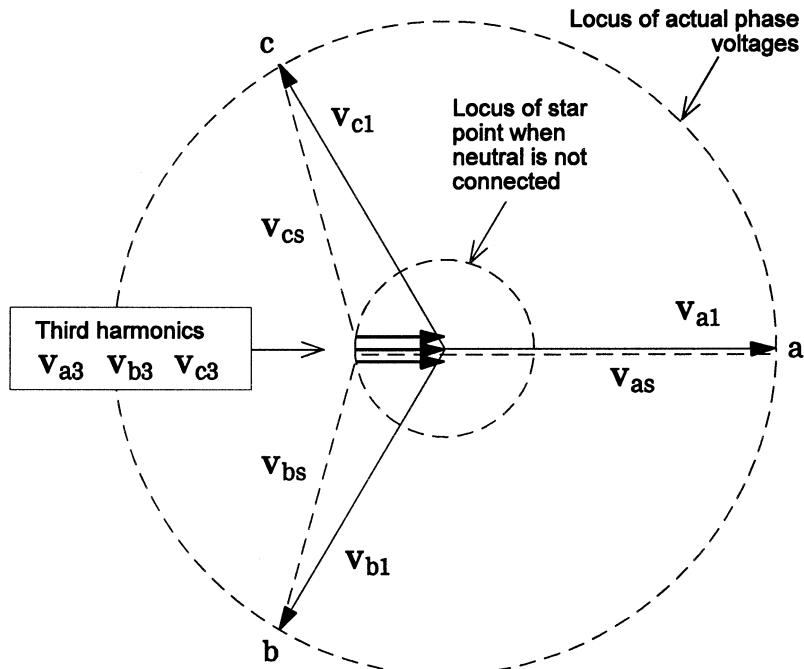
Fig. 2.48 Third-harmonic oscillation of the star-point potential.

in each phase. If the same load is reconnected in wye, the equivalent circuit does not change, but with a three-wire connection the zero-sequence triplen-harmonic currents are prevented from flowing, and therefore the load cannot operate normally. On the other hand, the triplen-harmonic voltage sources may still be active, and in this case, in order to eliminate the triplen-harmonic voltage components from the line–line voltages, the potential of the start point will oscillate, as shown in Figure 2.48.

2.12.5   AC line harmonics of three-phase rectifier

As an example of a harmonic-generating load, Figure 2.49 shows the circuit of a three-phase rectifier supplying a DC load. If the DC current has negligible ripple (i.e. the DC load has enough inductance to keep the current essentially constant through a 120° period), and if the commutation is perfect (i.e. the current passes from one SCR to the next at the instant when the voltage on the incoming phase exceeds the voltage on the outgoing phase), then the AC line current waveform is a 120° squarewave, Figure 2.50. By Fourier's theorem, using 1/4-cycle symmetry,

$$I_h = \frac{2}{2\pi} \times 4 \int_0^{\pi/2} I \cos(h\theta) d\theta = \frac{4}{h\pi} \sin\left(\frac{h\pi}{3}\right) \qquad (2.69)$$

If $h = 1$, $\sin \pi/3 = \sqrt{3}/2$ and $I_1/I = 4\sqrt{3}/2\pi = 2\sqrt{3}/\pi = 1.103$. If $h = 3$, $\sin 3\pi/3 = 0$ and $I_3/I = 0$. If $h = 5$, $\sin 5\pi/3 = -\sqrt{3}/2$ and $|I_5| = I_1/5$. If $h = 7$, $\sin 7\pi/3 = -\sqrt{3}/2$
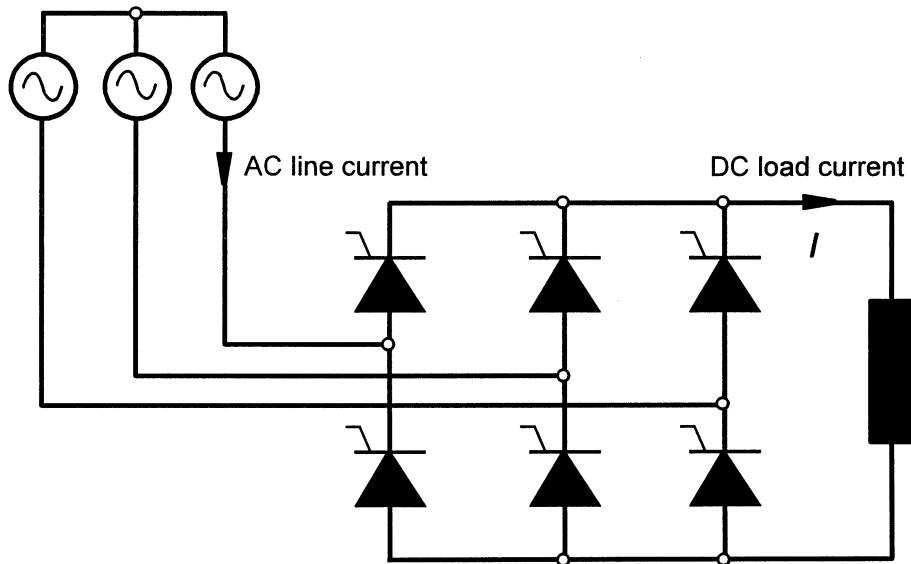
Fig. 2.49 Three-phase rectifier circuit.
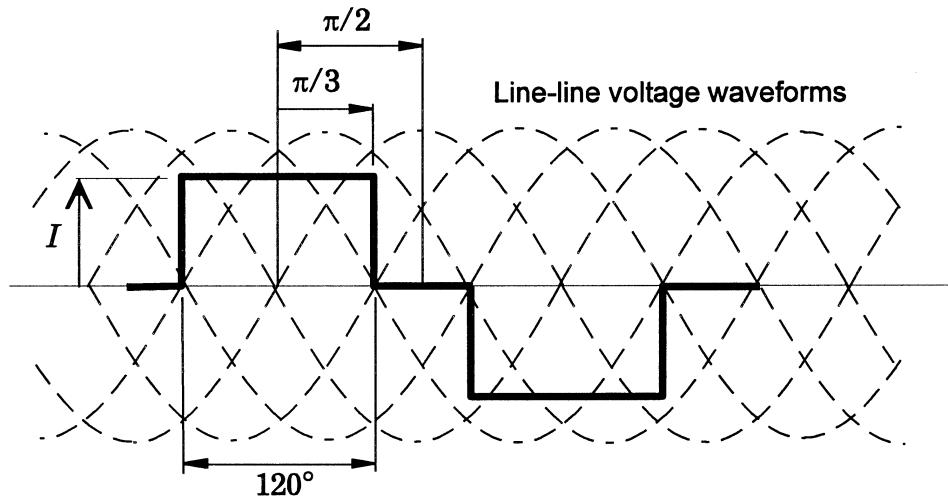
Fig. 2.50 Three-phase rectifier waveforms.

and $|I_7| = I_1/7$. Thus in general if h is an odd non-triplen integer, $|I_h| = I_1/h$. The harmonic orders present in the ideal three-phase rectifier are $h = kq \pm 1$, where k is any positive integer and q is the pulse number of the rectifier circuit. The circuit shown in Figure 2.49 is a six-pulse rectifier. Higher pulse numbers (e.g. 12, 24) are obtained by supplying two parallel rectifiers from phase-shifted secondaries of a three-phase transformer. For example, a 12-pulse rectifier uses one wye-connected secondary and one delta-connected secondary. The 30° phase shift between these secondaries eliminates harmonics of orders 5 and 7, so that the

lowest-order harmonics appearing in the line current are of order $1 \times 12 \pm 1 = 11$ and 13.

The harmonics of orders $kq \pm 1$ are called *characteristic harmonics*. In practice the commutation is imperfect (it takes time to transfer current from one SCR to the next), and the DC load current may not be perfectly smooth. Also, the supply voltages may not be perfectly balanced. These factors give rise to the appearance of *non-characteristic* harmonics. For example, a 5th or 7th harmonic in a 12-pulse rectifier is a non-characteristic harmonic: it would not appear under ideal conditions. Also, if the SCR firing is phase-shifted, additional harmonics are generated.

2.13 Per-unit quantities

Per-unit quantities are quantities that have been *normalized* to a *base* quantity. For example, consider a 5 kW motor operating at 3 kW. The actual power is 3 kW. The base power is 5 kW. The per-unit power is therefore $3/5 = 0.6$ p.u. As another example, a cable might be rated at 150 A. If it is carrying 89 A, and if we take the base current to be the same as the rated current, then the per-unit current is $89/150 = 0.593$ p.u.

In general,[17]

$$\mathbf{x} = \frac{X}{X_b} \text{ p.u.} \tag{2.70}$$

where $\mathbf{x}$ is a per-unit value, X is an actual value, and X_b is the base value. X and X_b are expressed in ordinary units, such as volts, amps, watts, Nm, etc. Per-unit quantities have no dimensions but it is normal practice to express them 'in p.u.', for example, 1.05 p.u.

Per-unit quantities express *relative* values – that is, relative to the base value. The choice of base value is important. In the simple example quoted above, the most natural choice of base was the rated value, which is the value associated with 'normal full-load operation'. However, base values may be freely chosen, as the next example shows.

Imagine two motors in parallel, one of 5 kW rating, the other of 50 kW rating, connected to a supply that is rated at 150 A. Suppose that the smaller motor draws its rated current of 7.5 A from the supply, while the larger one draws 75 A. If we consider each motor individually we could say that each one is working at 1 p.u. or 100% of its own rating. But if we choose 150 A as the common base current, then the first motor is drawing $7.5/150 = 0.05$ p.u. while the second one draws $75/150 = 0.5$ p.u. The total current is 0.55 p.u., or 82.5 A. This clearly expresses the fact that the smaller motor is taking 5% of the supply current while the larger one is taking 50%. The supply is working at only 55% of its capacity. Evidently we could add motors and almost double the load.

Per-unit systems are especially useful when we have a more complicated network with transformers, in which there may be several different voltage and current levels.

---

[17] Boldface lowercase letters denote per-unit values. Italic letters denote values in ordinary units.

When quantities are expressed in per-unit, most voltages are close to one under normal operation; higher values indicate overvoltage and lower values may indicate overload. This helps the engineer in scanning the results of a load-flow analysis or fault study, because abnormal conditions are immediately recognizable: for example, currents outside the 0–1 range, or voltages that deviate more than a few per cent from one. Under transient conditions, larger voltage and current swings may be encountered.

Engineering formulas often contain 'funny' coefficients such as $2\pi/\sqrt{2}$ or even constants such as 1.358, and it is often far from obvious where these came from.[18] In a well-chosen per-unit system, factors that are common to both the actual and the base values cancel out, and this gets rid of many of the spurious coefficients. Per-unit expressions are therefore less cluttered and express the essential physical nature of the system economically.

An example of this is the normalization of power in a three-phase system: in ordinary units

$$P = \sqrt{3}V_{LL}I_L \cos \phi \quad [W] \tag{2.71}$$

The bases P_b, V_b and I_b must be related by the same equation: thus

$$P_b = \sqrt{3}V_b I_b (\cos \phi)_b \quad [W] \tag{2.72}$$

Normalizing means dividing equation (2.71) by equation (2.72). Taking the base value of the power factor to be $(\cos \phi)_b = 1$, we get

$$\mathbf{p} = \mathbf{vi} \cos \phi \tag{2.73}$$

The factor $\sqrt{3}$ cancels out: this not only simplifies computation, but also expresses the power equation in a fundamental general form that is independent of the number of phases or whether the load is connected in wye or delta.

2.13.1   Standard formulas for three-phase systems

A three-phase system is rated according to its MVA capacity, S. Let the base value for volt-amperes be S_b MVA. If the base line–line voltage is V_b and the base line current is I_b, then

$$S_b = \sqrt{3}V_b I_b \tag{2.74}$$

Usually, V_b is expressed in kV and I_b is in kA. By convention the base impedance Z_b is the line-neutral impedance

$$Z_b = \frac{V_b/\sqrt{3}}{I_b} \ \Omega \tag{2.75}$$

---

[18] They usually arise in the theoretical derivation of the formula but they may arise because of the particular units used for parameters in the equation. A simple example is the equation $y = 25.4x$ to represent a length y in mm that is equal to another length x in inches. The equation expresses the essential equality of the dimensions y and x, but the 25.4 factor appears in the equation because of the difference in measurement units and makes y and x look as though they are unequal!

Combining equations (2.74) and (2.75), we get

$$Z_b = \frac{V_b^2}{S_b} \ \Omega \tag{2.76}$$

If V_b is expressed in kV and S_b in MVA, we can express equation (2.76) in the form that is widely used by power engineers

$$Z_b = \frac{(kV_{base})^2}{MVA_{base}} \ \Omega \tag{2.77}$$

2.13.2 Changing base

Sometimes the parameters for two elements in the same circuit are quoted in per-unit on different bases. For example, we might have a cable whose series impedance is quoted as $0.1 + j0.3$ p.u. on a base of 100 MVA and 33 kV. Suppose this cable is connected to a load whose impedance is given as $1.0 + j0.2$ p.u. on a base of 150 MVA and 22 kV. What is the combined series impedance? To proceed we must choose a single set of base quantities and convert all per-unit impedances to that set. Let us choose the cable's base values as the common base values: 100 MVA and 33 kV. We can convert the load impedance to this base set by ratioing, using equation (2.77)

$$\mathbf{Z}_{new} = \mathbf{Z}_{old} \times \frac{(kV_{b \ old})^2}{(kV_{b \ new})^2} \times \frac{MVA_{b \ new}}{MVA_{b \ old}} \tag{2.78}$$

The per-unit load impedance on the new (cable) base is therefore

$$(1.0 + j0.2) \times \frac{22^2}{33^2} \times \frac{100}{150} = 0.2963 + j0.0593 \ \text{p.u.} \tag{2.79}$$

With both impedances on the same base, we can now add them together to get $0.3963 + j0.3593$ p.u. (on a base of 100 MVA and 33 kV).

It is clear that 'p.u.' is not an absolute unit, since the same impedance can have different values, depending on the base. *A per-unit value is incomplete unless the base is stated.*

Per-unit quantities are used widely in power engineering. They are useful for expressing characteristics that are common to different devices. For example, in power stations the series impedance of most large 'unit transformers' (the ones that step up the generator voltage to 400 kV) is almost always about 0.10–0.15 p.u. The ohmic values differ widely according to the ratings and the actual voltages. Similarly, the magnetizing current of small induction motors is typically in the range 0.2–0.5 p.u. The ampere values vary over a wide range, depending on the ratings and the voltages, and therefore they obscure the essential uniformity of this design characteristic. Often a per-unit calculation can give insight that is not apparent when working in ordinary units.

2.13.3 Transformers in per-unit systems

One of the most useful simplifications of working in per-unit is in dealing with transformers. The ratio of base voltages between the primary and secondary can logically be taken to be the turns ratio, n. Then the ratio of base currents must be the

inverse of the turns ratio, $1/n$. Therefore the ratio of base impedances must be the square of the turns ratio, n^2. But this is precisely the ratio by which an impedance is referred from the secondary to the primary. Therefore, if we normalize an impedance to the base on one side of the transformer, and then refer this per-unit impedance to the other side, the per-unit value comes out exactly the same. This means that in a consistent per-unit system, ideal transformers simply disappear. Mathematically, this can be expressed as follows

$$Z_{b1} = n^2 Z_{b2} \tag{2.80}$$

On the secondary base, a load impedance Z (ohms) on the secondary side has the per-unit value

$$\mathbf{z} = \frac{Z}{Z_{b2}} \, \text{p.u.} \tag{2.81}$$

If we refer Z to the primary it becomes $Z' = n^2 Z$. The per-unit value of this on the primary base, is

$$\mathbf{z}' = \frac{Z'}{Z_{b1}} = \frac{n^2 Z}{n^2 Z_{b2}} = \mathbf{z} \tag{2.82}$$

This says that the per-unit value of an impedance is the same on both sides of the transformer. In other words, in per-unit the turns ratio of the transformer is unity and it can be removed from the circuit. This is only true if the primary and secondary base impedances are in the ratio n^2.

These comments apply to ideal transformers only. But real transformers can be modelled by an ideal transformer together with parasitic impedances (resistances, leakage reactances etc.) that can be lumped together with the other circuit impedances on either side. The equivalent circuit of a transformer in per-unit is just a series impedance equal to $\mathbf{r} + j\mathbf{x}$, where $\mathbf{r}$ is the sum of the per-unit primary and secondary resistances and $\mathbf{x}$ is the sum of the per-unit primary and secondary leakage reactances. The magnetizing branch appears as a shunt impedance. Wye/delta transformers have a more complex representation but still the ideal transformer disappears from the equivalent circuit. Similarly, tap-changing transformers can be represented by a simple network.

2.14   Conclusion

This chapter has laid the basic technical foundation for the study of reactive power control in power systems, with most of the analytical theory required for calculation of simple AC circuits including three-phase circuits and circuits with reactive compensators. Power-factor correction and the adjustment of voltage by means of reactive power control have been explained using phasor diagrams and associated circuit equations. The basic theory of transformers, harmonics, and per-unit systems has also been covered.

In the next chapter the simple analytical theory of reactive power control is extended to transmission systems which are long enough to be considered as distributed-parameter circuits.

3

Transmission system compensation

3.1 Introduction

It has always been desirable to transmit as much power as possible through transmission lines and cables, consistent with the requirements of stability and security of supply. Power transmission is limited mainly by thermal factors in cables, short transmission lines, transformers and generators; but in long lines and cables the variation of voltage and the maintenance of stability also constrain the power transmission. The voltage 'profile' and the stability of a transmission line or cable can be improved using 'reactive compensation'. In the early days reactive compensation took the form of fixed-value reactors and capacitors, usually controlled by mechanical switchgear. Synchronous condensers and large generators were used in cases where it was necessary to vary the reactive power continuously. Since the 1970s power-electronic equipment has been developed and applied to extend the range of control, with a variety of methods and products.

Bulk AC transmission of electrical power has two fundamental requirements:

1. *Synchronism*. The basis of AC transmission is a network of synchronous machines connected by transmission links. The voltage and frequency are defined by this network, even before any loads are contemplated. All the synchronous machines must remain constantly in synchronism: i.e. they must all rotate at exactly the same speed, and even the phase angles between them must not vary appreciably. By definition, the *stability* of the system is its tendency to recover from disturbances such as faults or changes of load.

The power transmitted between two synchronous machines can be slowly increased only up to a certain level called the *steady-state stability limit*. Beyond this level the synchronous machines fall out of step, i.e. lose synchronism. The steady-state stability limit can be considerably modified by the excitation level of the synchronous machines (and therefore the line voltage); by the number and connections of transmission lines; and by the pattern of real and reactive power flows in the system, which can be modulated by reactive compensation equipment.

A transmission system cannot be operated too close to the steady-state stability limit, because there must be a margin to allow for disturbances. In determining an appropriate margin, the concepts of *transient* and *dynamic stability* are useful. Dynamic stability is concerned with the ability to recover normal operation following a specified *minor* disturbance. Transient stability is concerned with the ability to recover normal operation following a specified *major* disturbance.

2. *Voltage profile*. It is obvious that the correct voltage level must be maintained within narrow limits at all levels in the network. Undervoltage degrades the performance of loads and causes overcurrent. Overvoltage is dangerous because of the risks of flashover, insulation breakdown, and saturation of transformers. Most voltage variations are caused by load changes, and particularly by the reactive components of current flowing in the reactive components of the network impedances. If generators are close by, excitation levels can be used to keep the voltage constant; but over long links the voltage variations are harder to control and may require reactive compensation equipment.

Different techniques are used for controlling the voltage according to the underlying rate of change of voltage. Cyclic, diurnal load variation is gradual enough to be compensated by excitation control or the timely switching in and out of capacitors and reactors. But sudden overvoltages – such as those resulting from disconnection of loads, line switching operations, faults, and lightning – require immediate suppression by means of surge arrestors or spark gaps. Between these extremes there are many possibilities for controlled reactive compensation equipment operating over time scales ranging from a few milliseconds to a few hours.

Table 3.1 is a matrix of methods for stability and voltage control, including a range of reactive power compensators. Some of the compensator devices can serve several functions, which makes the subject somewhat complicated. Table 3.2 lists some of the main advantages and disadvantages of the different compensators.

3.2 Uncompensated lines

3.2.1 Voltage and current equations of a long, lossless transmission line

Figure 3.1 shows one phase of a transmission line or cable with distributed inductance l H/m and capacitance c F/m. The voltage and current phasors $\mathbf{V}(x)$ and $\mathbf{I}(x)$ both obey the transmission line equation

$$\frac{d^2\mathbf{V}}{dx^2} = \Gamma^2\mathbf{V} \quad \text{where} \quad \Gamma = \sqrt{(r + j\omega l)(g + j\omega c)} \tag{3.1}$$

and x is distance along the line. r is the resistance per unit length [ohm/m] in series with l and g is the 'shunt' conductance per unit length [S/m] in parallel with c. ω is the radian frequency $2\pi f$. If r and g are both small, then $\Gamma = j\beta$ where $\beta = \omega\sqrt{(lc)}$ is the *wavenumber*. The propagation velocity $u = 1/\sqrt{(lc)}$ is rather lower than the speed of light (3×10^5 km/s) and $\beta = 2\pi f/u = 2\pi/\lambda$ where $\lambda = u/f$ is the wavelength. For example, at 50 Hz $\lambda = 3 \times 10^5/50 = 6000$ km and $\beta = 1.047 \times 10^{-3}$ rad/km $= 6.0°/100$ km.

Table 3.1 Methods for stability and voltage control

		Increase transmission voltage	Increase no. of lines in parallel	Transformer Tapchanging	Slow AVR control	Fast AVR control	Fast turbine valving	Rapid line-switching operations. Reclosing of circuit-breakers	Braking resistors	Shunt reactor (Switched/unswitched, linear/non-linear)	Shunt capacitor	Series reactor	Series capacitor	Synchronous condenser	Polyphase saturated reactor	Thyristor controlled reactor	Thyristor switched capacitor	Short-circuit limiting coupling (or fault current limiter)
1. Maintain synchronism	Improve steady-state stability	●	●		●	●				●	●		●	●	●	●	●	
	Improve dynamic stability					●								●		●	●	
	Improve transient stability	●				●	●	●	●	●				●	●	●	●	
2. Maintain voltage profile	Limit rapid voltage change					●		●		●				●	●	●	●	
	Limit slow voltage change			●	●					●				●	●	●	●	
	Limit overvoltages due to lightning, switching etc.									●				●	●	●		
Other requirements	Reactive power support at DC converter terminals													●	●	●	●	
	Increase short-circuit level											●		●				
	Decrease short-circuit level											●						●

Table 3.2 Advantages and disadvantages of different types of compensating equipment for transmission systems

| Compensating equipment	Advantages	Disadvantages
Switched shunt reactor	Simple	Fixed value
Switched shunt capacitor	Simple	Fixed value
		Switching transients
Series capacitor	Simple	Requires over-voltage protection and subharmonic filters
		Limited overload capability
Synchronous condenser	Has useful overload capability	High maintenance requirement
	Fully controllable	Slow response
	Low harmonics	Heavy
Polyphase-saturated reactor (TCR)	Rugged construction	Fixed value
	Large overload capability	Noisy
	Low harmonics	
Thyristor-controlled reactor (TCR)	Fast response	Requires shunt capacitors/filters
	Fully controllable	Generates harmonics
	No effect on fault level	
Thyristor-switched capacitor (TSC)	No harmonics	No inherent absorbing capability to limit over-voltages
		Complex buswork
		Low frequency resonances with system
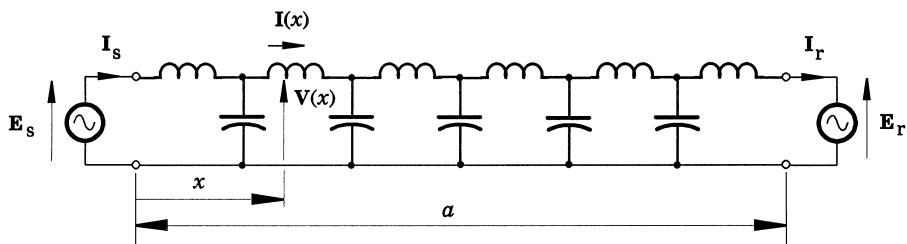
Fig. 3.1 Transmission line with distributed series inductance and shunt capacitance.

If a is the length of the line, $\theta = \beta a$ is the *electrical length*; for example, if $a = 100$ km, $\theta = 6.0°$.

The solution to equation (3.1) for a lossless line is

$$\mathbf{V}(x) = \mathbf{V}_r \cos \beta(a - x) + \mathrm{j}Z_0 \mathbf{I}_r \sin \beta(a - x)$$
$$\mathbf{I}(x) = \mathrm{j}\frac{\mathbf{V}_r}{Z_0} \sin \beta(a - x) + \mathbf{I}_r \cos \beta(a - x) \tag{3.2}$$

where $Z_0 = \sqrt{(l/c)}$ is the *surge impedance* [ohm]. A typical value of Z_0 for a high-voltage line is $250\,\Omega$, but cables have lower values because of their higher capacitance. Note that if $x_L = \omega l$ is the series inductive reactance [ohm/m] and $x_C = 1/\omega c$ is the shunt capacitive reactance [also ohm/m] then we can write $Z_0 = \sqrt{(x_L x_C)}$ and $\beta = \sqrt{(x_L/x_C)}$.

3.2.2   Surge impedance and natural loading of a transmission line

The surge impedance is the driving-point impedance of an infinitely long line, or a line which is terminated in a load impedance Z_0 such that $\mathbf{V}_r = Z_0 \mathbf{I}_r$. In either case, at a point x along the line, the ratio between the voltage $\mathbf{V}(x)$ and the current $\mathbf{I}(x)$ is given by equations (3.2) as

$$Z(x) = \frac{\mathbf{V}(x)}{\mathbf{I}(x)} = \frac{Z_0 \mathbf{I}_r[\cos \beta(a-x) + j\sin \beta(a-x)]}{\mathbf{I}_r[\cos \beta(a-x) + j\sin \beta(a-x)]} = Z_0 \tag{3.3}$$

which is not only independent of x but is real and equal to Z_0. This means that $\mathbf{V}$ and $\mathbf{I}$ are in phase at all points along the line. However, the phase angles of both phasors vary linearly along the line since

$$\mathbf{V}(x) = \mathbf{V}_r e^{j\beta(a-x)} \quad \text{and} \quad \mathbf{I}(x) = \mathbf{I}_r e^{j\beta(a-x)} \tag{3.4}$$

The phasor diagram of a line terminated in Z_0 is shown in Figure 3.2. The power transmitted along such a line is

$$P_0 = \frac{V^2}{Z_0} \tag{3.5}$$

If V is the line-neutral voltage this is the power per phase. If V is the line–line voltage it is the total power. The reactive power is zero at both ends of the line, since $\mathbf{V}$ and $\mathbf{I}$ are in phase at all points. If we equate the reactive power absorbed per unit length in the series inductance with the reactive power generated per unit length in the shunt capacitance, we get $V^2 \omega c = I^2 \omega l$, so that $V/I = \sqrt{(l/c)} = Z_0$.

A transmission line in this condition is said to be naturally loaded and P_0 is the *natural load* or *surge impedance load* (SIL). The voltage profile of a naturally loaded line is flat, since $|\mathbf{V}| = V$ is constant along the line. Note that P_0 is proportional to V^2, so that if we upgrade a 275 kV line with $Z_0 = 250\,\Omega$ to 400 kV, the SIL increases from $275^2/250 = 302.5$ MW to $400^2/250 = 640$ MW.

The surge impedance load is not a limit: it is merely the load at which the voltage profile is flat and the line requires no reactive power. Lines can be operated above or below the SIL. If the actual load is less than the SIL, the voltage tends to rise along the line; and if the load is less than the SIL, it tends to fall: see Figure 3.3. The SIL is
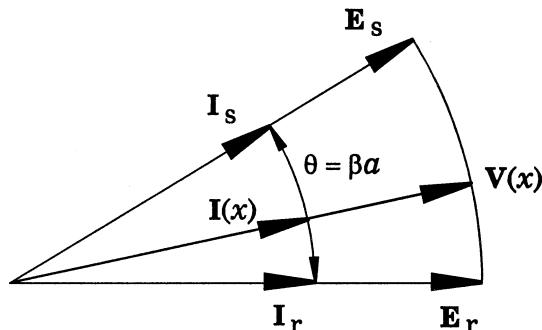

**Fig. 3.2** Phasor diagram of line terminated in Z_0.
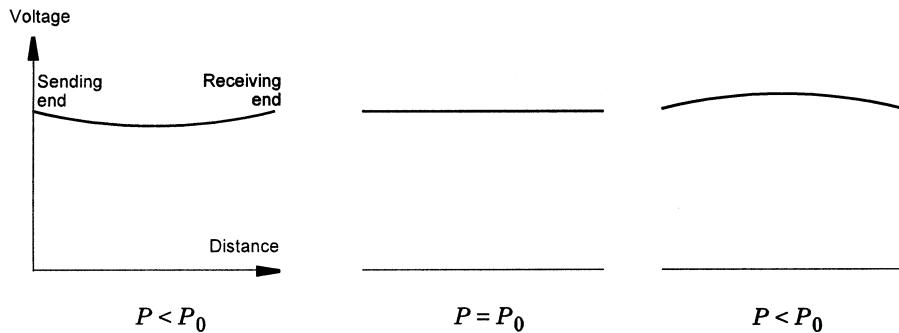
Fig. 3.3 Voltage profiles along a long, lossless symmetrical transmission line.

important with very long lines when there are no intermediate substations at which the voltage level can be controlled. Evidently it is desirable to operate such lines as close as possible to the SIL, to maintain a flat voltage profile. Shorter lines (typically those less than 50–100 km) do not have such a problem with the variation of the voltage profile with load, and the power transmission through them is more likely to be limited by other factors, such as the fault level or the current-carrying capacity of the conductors (which is thermally limited).

3.2.3   The uncompensated line on open-circuit

A lossless line that is energized by generators at the sending end and is open-circuited at the receiving end is described by equation (3.2) with $\mathbf{I}_r = 0$, so that

$$\mathbf{V}(x) = \mathbf{V}_r \cos \beta(a - x) \tag{3.6}$$

and

$$\mathbf{I}(x) = j\left[\frac{\mathbf{V}_r}{Z_0}\right] \sin \beta(a - x) \tag{3.7}$$

The voltage and current at the sending end are given by these equations with $x = 0$.

$$\mathbf{E}_s = \mathbf{V}_r \cos \theta \tag{3.8}$$

$$\mathbf{I}_s = j\left[\frac{\mathbf{V}_r}{Z_0}\right] \sin \theta = j\left[\frac{\mathbf{E}_s}{Z_0}\right] \tan \theta \tag{3.9}$$

$\mathbf{E}_s$ and $\mathbf{V}_r$ are in phase, which is consistent with the fact that there is no power transfer. The phasor diagram is shown in Figure 3.4.

The voltage and current profiles in equations (3.6) and (3.7) are more conveniently expressed in terms of $\mathbf{E}_s$:

$$\mathbf{V}(x) = \mathbf{E}_s \frac{\cos \beta(a - x)}{\cos \theta} \tag{3.10}$$

$$\mathbf{I}(x) = j\frac{\mathbf{E}_s}{Z_0} \frac{\sin \beta(a - x)}{\cos \theta} \tag{3.11}$$

**Fig. 3.4** Phasor diagram of uncompensated line on open-circuit.
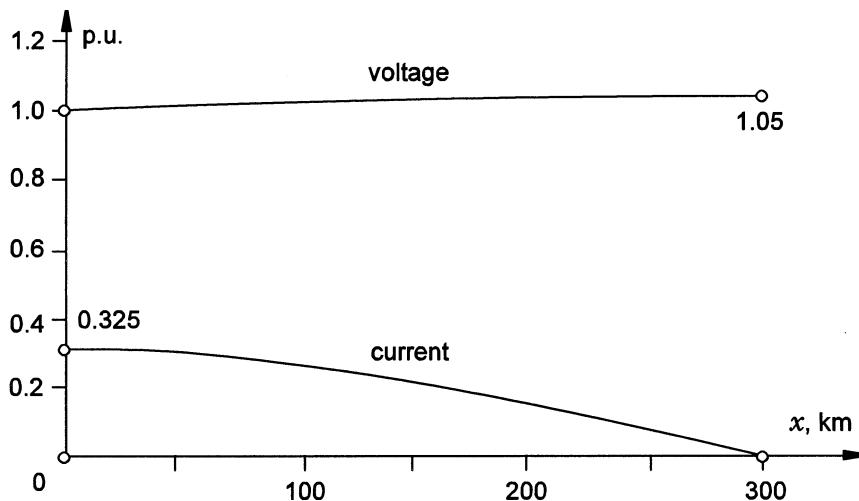
Fig. 3.5 Voltage and current profiles for a 300-km line at no load (open-circuit).

The general forms of these profiles are shown in Figure 3.5. For a line 300 km in length at 50 Hz, $\beta = 360° \times f/3 \times 10^5 = 6°$ per 100 km, so $\theta = 6 \times 3 = 18°$. Then $V_r = E_s/\cos \theta = 1.05 E_s$ and $I_s = (E_s/Z_0) \tan \theta = 0.329$ p.u. based on the SIL. The voltage rise on open-circuit is called the *Ferranti effect*.

Although the voltage rise of 5% seems small, the 'charging' current is appreciable and in such a line it must all be supplied by the generator, which is forced to run at leading power factor, for which it must be underexcited.[1] Note that a line for which $\theta = \beta a = \pi/2$ has a length of $\lambda/4$ (one quarter-wavelength, i.e. 1500 km at 50 Hz), producing an infinite voltage rise. Operation of any line approaching this length is completely impractical without some means of compensation.

In practice the open-circuit voltage rise will be greater than is indicated by equation (3.10), which assumes that the sending-end voltage is fixed. Following a

---

[1] The extent to which generators can absorb reactive power is limited by stability and core-end heating. Operation of generators in the absorbing mode, with a leading power factor, is called 'under-excited' because the field current and open-circuit emf are reduced below their normal rated-load values.

sudden open-circuiting of the line at the receiving end, the sending-end voltage tends to rise immediately to the *open-circuit voltage* of the sending-end generators, which exceeds the terminal voltage by approximately the voltage drop due to the prior current flowing in their short-circuit reactances.

3.3 Uncompensated lines under load

3.3.1 Radial line with fixed sending-end voltage

A load $P + jQ$ at the receiving end of a transmission line or cable (Figure 3.6) draws the current

$$\mathbf{I}_r = \frac{P - jQ}{\mathbf{V}_r^*} \qquad (3.12)$$

The sending- and receiving-end voltages are related by

$$\mathbf{E}_s = \mathbf{V}_r \cos \theta + jZ_0 \frac{P - jQ}{\mathbf{V}_r^*} \sin \theta \qquad (3.13)$$

If $\mathbf{E}_s$ is fixed, this quadratic equation can be solved for $\mathbf{V}_r$. The solution shows how $\mathbf{V}_r$ varies with the load and its power factor, and with the line length. A typical result is shown in Figure 3.7.

For each load power factor there is a maximum transmissible power, P_{max}, the *steady-state stability limit*. For any value of $P < P_{max}$, there are two possible solutions for $\mathbf{V}_r$, since equation (3.13) is quadratic. Normal operation is always at the upper value, within narrow limits around 1.0 p.u. Note that when $P = P_0$ and $Q = 0$, $V_r = E_s$.

The load power factor has a strong influence on the receiving-end voltage. Loads with lagging power factor tend to reduce V_r, while loads with leading power factor tend to increase it.
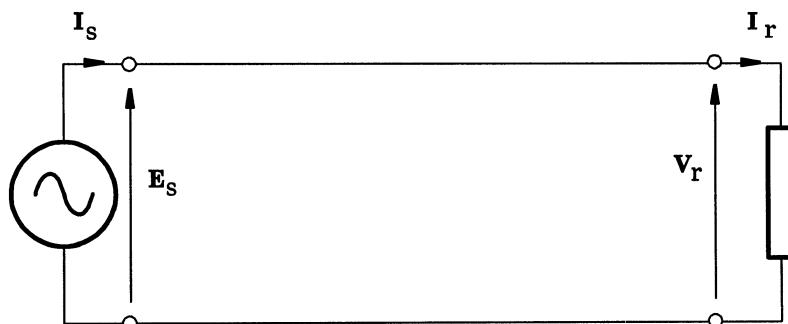

Fig. 3.6 Radial line or cable with load $P + jQ$.
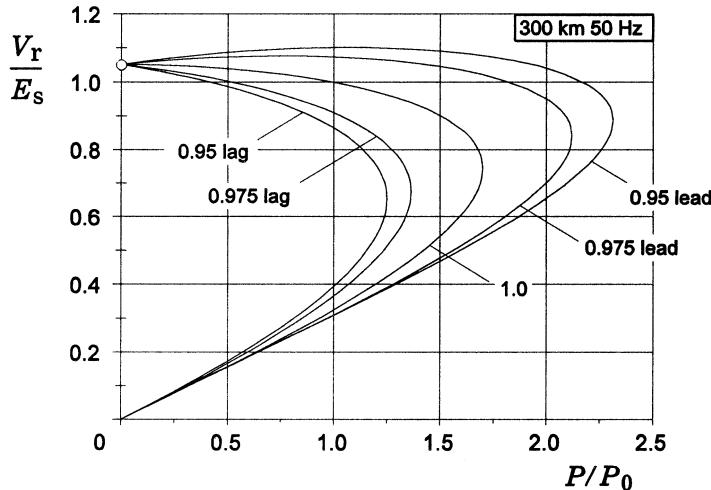
Fig. 3.7 Receiving-end voltage magnitude $|\mathbf{V}_r|$ as a function of load P/P_0 for a 300-km lossless radial line, at different power factors.

3.3.2   Uncompensated symmetrical line: variation of voltage and reactive power with load

The symmetrical line in Figure 3.8 has equal voltages at the sending and receiving ends, and the mid-point voltage and current are $\mathbf{V}_m$ and $\mathbf{I}_m$ respectively. The phasor diagram is shown in Figure 3.9. The equations for the sending-end half of the line are

$$\mathbf{E}_s = \mathbf{V}_m \cos\frac{\theta}{2} + jZ_0\mathbf{I}_m \sin\frac{\theta}{2}$$
$$\mathbf{I}_s = j\frac{\mathbf{V}_m}{Z_0}\sin\frac{\theta}{2} + \mathbf{I}_m \cos\frac{\theta}{2} \tag{3.14}$$

At the mid-point,

$$P_m + jQ_m = \mathbf{V}_m\mathbf{I}_m^* = P \tag{3.15}$$
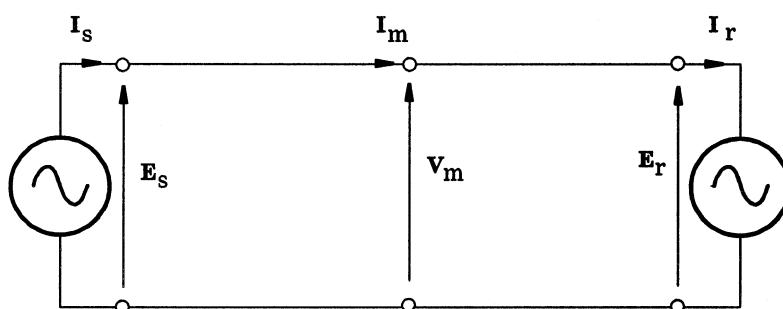

Fig. 3.8 Symmetrical line.
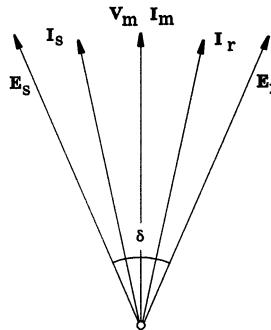
Fig. 3.9 Phasor diagram of symmetrical line.

where P is the transmitted power. Note that $Q_m = 0$, that is, no reactive power flows past the mid-point. The real and reactive power at the sending end are

$$P_s + jQ_s = \mathbf{E}_s\mathbf{I}_s^* \tag{3.16}$$

Substituting for $\mathbf{E}_s$ and $\mathbf{I}_s$ from equation (3.14) and treating $\mathbf{V}_m$ as reference phasor, $P_m = V_m I_m$ and

$$P_s + jQ_s = P + j\left[Z_0 I_m^2 - \frac{V_m^2}{Z_0}\right]\frac{\sin\theta}{2} \tag{3.17}$$

Since the line is assumed lossless, the result $P = P_s = P_r$ is expected. The expression for Q_s can be arranged as follows, making use of the relations $P_0 = V_0^2/Z_0$ and $P_m = V_m I_m$: thus

$$Q_s = P_0\left[\frac{P^2}{P_0^2}\frac{V_0^2}{V_m^2} - \frac{V_m^2}{V_0^2}\right]\frac{\sin\theta}{2} \tag{3.18}$$

This equation shows how the reactive power requirements of the symmetrical line are related to the mid-point voltage. By symmetry, equation (3.18) applies to both ends of the line, and each end supplies half the total reactive power. Because of the sign convention for $\mathbf{I}_s$ and $\mathbf{I}_r$ in Figure 3.8, this is written $Q_s = -Q_r$.

When $P = P_0$ (the natural load), if $V_m = 1.0$ then $Q_s = Q_r = 0$, and $E_s = E_r = V_m = V_0 = 1.0\,\text{p.u.}$ On the other hand, at no-load $P = 0$, and if the voltages are adjusted so that $E_s = E_r = V_0 = 1.0\,\text{p.u.}$, then $I_m = 0$ and

$$Q_s = -P_0\tan\frac{\theta}{2} = -Q_r \tag{3.19}$$

i.e. each end supplies the line-charging reactive power for half the line. If the terminal voltages are adjusted so that the mid-point voltage V_m is equal to $1.0\,\text{p.u.}$ at all levels of power transmission, then from equation (3.18)

$$Q_s = P_0\left[\frac{P^2}{P_0^2} - 1\right]\frac{\sin\theta}{2} = -Q_r \tag{3.20}$$

Table 3.3 Effect of power transmitted on voltage profile and reactive power requirements

$P < P_0$	$V_m > E_s, E_r$. There is an excess of line-charging reactive power, which is absorbed at the ends: $Q_s < 0$ and $Q_r > 0$.
$P > P_0$	$V_m < E_s, E_r$. There is a deficit of line-charging reactive power, which is supplied at the ends: $Q_s > 0$ and $Q_r < 0$.
$P = P_0$	$V_m = V_0 = E_s = E_r$. The voltage profile is flat. The line requires no reactive power and $Q_s = Q_r = 0$.

Moreover, from equations (3.12) and (3.13) it can be shown that if $V_m = V_0$,

$$E_s = E_r = V_0 \sqrt{1 - \left[1 - \frac{P^2}{P_0^2}\right] \sin^2 \frac{\theta}{2}} \tag{3.21}$$

Equations (3.20) and (3.21) illustrate the general behaviour of the symmetrical line. Note that the reactive power requirement is determined by the *square* of the transmitted power. According to equation (3.20) the line can be said to have a deficit or an excess of reactive power, depending on the ratio P/P_0, as summarized in Table 3.3.

Example: consider a line or cable with $\theta = 18°$ operating with $P = 1.5P_0$. Then $\sin \theta = 0.309$. From equation (3.20), $Q_s = -Q_r = 0.193P_0$. For every megawatt of power transmitted, a total reactive power of $2 \times 0.193/1.5 = 0.258$ MVAr has to be supplied from the ends. This represents a power factor of 0.968 at each end.

3.3.3 Maximum power and steady-state stability

Equation (3.13) is valid for synchronous and non-synchronous loads alike. If we consider the receiving end to be an equivalent synchronous machine, E_r is written instead of V_r and if this is taken as reference phasor, E_s can be written as

$$\mathbf{E}_s = E_s e^{j\delta} = E_s(\cos \delta + j \sin \delta) \tag{3.22}$$

where δ is the phase angle between $\mathbf{E}_s$ and $\mathbf{V}_r$ (Figure 3.9). δ is called the *load angle* or *transmission angle*. Equating the real and imaginary parts of equations (3.13) and (3.22)

$$E_s \cos \delta = E_r \cos \theta + Z_0 \frac{Q}{E_r} \sin \theta$$
$$E_s \sin \delta = Z_0 \frac{P}{E_r} \sin \theta \tag{3.23}$$

The second of these equations can be rearranged as

$$P = \frac{E_s E_r}{Z_0 \sin \theta} \sin \delta \tag{3.24}$$

A more familiar form of this equation is obtained for short lines, for which $\sin \theta \simeq \theta = \beta a = \omega a \sqrt{(lc)}$. Then $Z_0 \theta = \omega a \sqrt{(lc)} \times \sqrt{(l/c)} = \omega a l = X_L$, the series inductive reactance of the line. So

$$P = \frac{E_s E_r}{X_L} \sin \delta \qquad (3.25)$$

This equation is important because of its simplicity and wide-ranging validity. If E_s and E_r are held constant (as is normally the case), the power transmission is a function of only one variable, δ. As noted earlier, there is a maximum transmissible power,

$$P_{max} = \frac{E_s E_r}{X_L} = \frac{P_0}{\sin \theta} \qquad (3.26)$$

This is shown in Figure 3.10, which is usually plotted with δ as the independent variable; but in fact P is generally the independent variable and the power transmission has to be controlled to keep δ within safe limits below P_{max}. Typically δ is kept below 30°, giving a safety margin of 100% since $\sin 30° = 0.5$.

The reactive power required at the ends of the line can also be determined from equation (3.23): thus

$$Q_r = \frac{E_r(E_s \cos \delta - E_r \cos \theta)}{Z_0 \sin \theta}$$
$$Q_s = -\frac{E_s(E_r \cos \delta - E_s \cos \theta)}{Z_0 \sin \theta} \qquad (3.27)$$

If $E_s = E_r$ then

$$Q_s = -\frac{E_s^2(\cos \delta - \cos \theta)}{Z_0 \sin \theta} = -Q_r \qquad (3.28)$$

If $P < P_0$ and $E_s = 1.0$ p.u., then $\delta < \theta$, $\cos \delta > \cos \theta$, and $Q_s < 0$ and $Q_r > 0$. This means that there is an excess of line charging current and reactive power is being absorbed at both ends of the line. If $P > P_0$, reactive power is generated at both ends. If $P = 0$, $\cos \delta = 1$ and equation (3.28) reduces to equation (3.19).
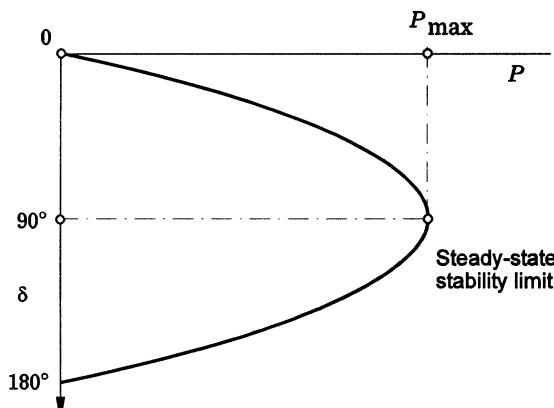

Fig. 3.10 Power vs. transmission angle.

For an electrically short line, $\cos\theta \to 1$ and $Z_0 \sin\theta \to X_L$, so that with $E_s = E_r$ equation (3.28) reduces to

$$Q_s = \frac{E_s^2(1 - \cos\delta)}{X_L} = -Q_r \tag{3.29}$$

3.4   Compensated transmission lines

Reactive compensation means the application of reactive devices

(a) to produce a substantially flat voltage profile at all levels of power transmission;
(b) to improve stability by increasing the maximum transmissible power; and/or
(c) to supply the reactive power requirements in the most economical way.

Ideally the compensation would modify the surge impedance by modifying the capacitive and/or inductive reactances of the line, so as to produce a virtual surge-impedance loading P_0' that was always equal to the actual power being transmitted. According to equation (3.4), this would ensure a flat voltage profile at all power levels. However, this is not sufficient by itself to ensure the *stability* of transmission, which depends also on the electrical line length θ; see equation (3.26). The electrical length can itself be modified by compensation to have a virtual value θ' shorter than the uncompensated value, resulting in an increase in the steady-state stability limit P_{max}.

These considerations suggest two broad classifications of compensation scheme, *surge-impedance compensation* and *line-length compensation*. Line-length compensation in particular is associated with series capacitors used in long-distance transmission. A third classification is *compensation by sectioning*, which is achieved by connecting constant-voltage compensators at intervals along the line. The maximum transmissible power is that of the weakest section, but since this is necessarily shorter than the whole line, an increase in maximum power and, therefore, in stability can be expected.

3.4.1   Passive and active compensators

Passive compensators include shunt reactors and capacitors and series capacitors. They modify the inductance and capacitance of the line. Apart from switching, they are uncontrolled and incapable of continuous variation. For example, shunt reactors are used to compensate the line capacitance to limit voltage rise at light load. They increase the virtual surge impedance and reduce the virtual natural load P_0'. Shunt capacitors may be used to augment the capacitance of the line under heavy loading. They generate reactive power which tends to boost the voltage. They reduce the virtual surge impedance and increase P_0'. Series capacitors are used for line-length compensation. A measure of surge-impedance compensation may be necessary in conjunction with series capacitors, and this may be provided by shunt reactors or by a dynamic compensator.

Active compensators are usually shunt-connected devices which have the property of tending to maintain a substantially constant voltage at their terminals. They do this by generating or absorbing precisely the required amount of corrective reactive

Table 3.4 Classification of compensators by function and type

Function	Passive	Active
Surge-impedance compensation	Shunt reactors (linear or non-linear)	Synchronous machines
		Synchronous condensers
	Shunt capacitors	Saturated-reactor compensators
		Thyristor-switched capacitors
		Thyristor-controlled reactors
Line-length compensation	Series capacitors	–
Compensation by sectioning	–	Synchronous condensers
		Saturated-reactor compensators
		Thyristor-switched capacitors
		Thyristor-controlled reactors

power in response to any small variation of voltage at their point of connection. They are usually capable of continuous (i.e. stepless) variation and rapid response. Control may be inherent, as in the saturated-reactor compensator; or by means of a control system, as in the synchronous condenser and thyristor-controlled compensators.

Active compensators may be applied either for surge-impedance compensation or for compensation by sectioning. In Z_0-compensation they are capable of all the functions performed by fixed shunt reactors and capacitors and have the additional advantage of continuous variability with rapid response. Compensation by sectioning is fundamentally different in that it is possible *only* with active compensators, which must be capable of virtually immediate response to the smallest variation in power transmission or voltage. Table 3.4 summarizes the classification of the main types of compensator according to their usual functions.

The automatic voltage regulators used to control the excitation of synchronous machines also have an important compensating effect in a power system. By dynamically maintaining constant voltage at the generator terminals they remove the Thévenin equivalent source impedance of the generator (i.e. the synchronous reactance) from the equivalent circuit of the transmission system.[2]

Compensating equipment is often an economical way to meet the reactive power requirements for transmission. An obvious example is where the power can be safely increased without the need for an additional line or cable. But compensators bring other benefits such as management of reactive power flows; damping of power oscillations; and the provision of reactive power at conventional HVDC converter terminals. Both passive and active compensators are in growing use, as are all the compensation strategies: virtual surge-impedance, line-length compensation and compensation by sectioning.

3.5 Static shunt compensation

Shunt reactors are used to limit the voltage rise at light load. On long lines they may be distributed at intermediate substations as shown in Figure 3.11, typically at intervals of the order of 50–100 km.

---

[2] During transients, however, the source impedance reappears with a value approaching the transient reactance x'_d.
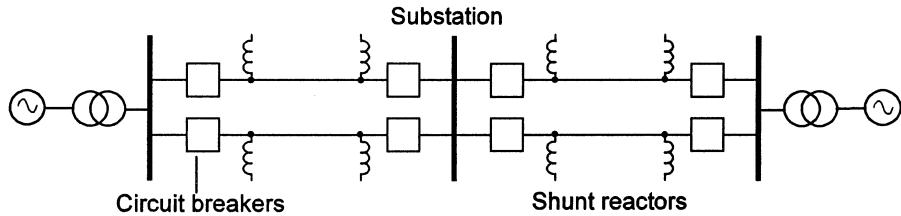
Fig. 3.11 Shunt reactors distributed along a high-voltage AC line.
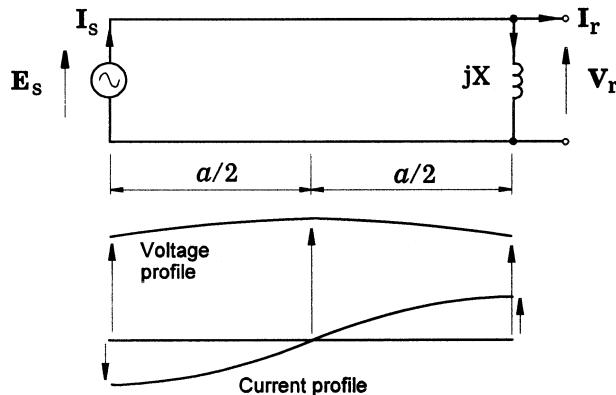

Fig. 3.12 Voltage and current profiles of a shunt-compensated system at no-load.

Consider the simple circuit in Figure 3.12, which has a single shunt reactor of reactance X at the receiving end and a pure voltage source $\mathbf{E}_s$ at the sending end. The receiving-end voltage is given by

$$\mathbf{V}_r = jX\mathbf{I}_r \tag{3.30}$$

From equation (3.2), $\mathbf{E}_s(x = 0)$ is given by

$$\mathbf{E}_s = \mathbf{V}_r \cos \beta a + jZ_0\mathbf{I}_r \sin \beta a = \mathbf{V}_r\left[\cos \theta + \frac{Z_0}{X}\sin \theta\right] \tag{3.31}$$

which shows that $\mathbf{E}_s$ and $\mathbf{V}_r$ are in phase, in keeping with the fact that the real power is zero. For the receiving-end voltage to be equal to the sending-end voltage, $V_r = E_s$, X must be given by

$$X = Z_0 \frac{\sin \theta}{1 - \cos \theta} \tag{3.32}$$

The sending-end current is given by equation (3.2) as

$$\mathbf{I}_s = j\frac{\mathbf{E}_s}{Z_0}\sin \theta + \mathbf{I}_r \cos \theta \tag{3.33}$$

Making use of equations (3.30–3.32), this can be arranged to give

$$\mathbf{I}_s = j\frac{\mathbf{E}_s}{Z_0}\frac{1 - \cos \theta}{\sin \theta} = j\frac{\mathbf{E}_s}{X} = -\mathbf{I}_r \tag{3.34}$$

since $\mathbf{E}_s = \mathbf{V}_r$. This means that the generator at the sending end behaves exactly like the shunt reactor at the receiving end in that both absorb the same amount of reactive power:

$$Q_s = -Q_r = \frac{E_s^2}{X} = \frac{E_s^2}{Z_0}\left[\frac{1 - \cos\theta}{\sin\theta}\right] \tag{3.35}$$

The charging current divides equally between the two halves of the line. The voltage profile is symmetrical about the mid-point, and is shown in Figure 3.12 together with the line-current profile. In the left half of the line the charging current is negative; at the mid-point it is zero; and in the right half it is positive. The maximum voltage occurs at the mid-point and is given by equation (3.2) with $x = a/2$

$$\mathbf{V}_m = \mathbf{V}_r\left[\cos\frac{\theta}{2} + \frac{Z_0}{X}\sin\frac{\theta}{2}\right] = \frac{\mathbf{E}_s}{\cos(\theta/2)} \tag{3.36}$$

Note that $\mathbf{V}_m$ is in phase with $\mathbf{E}_s$ and $\mathbf{V}_r$, as is the voltage at all points along the line. For a 300 km line at 50 Hz, $\theta = 18°$ and with $E_s = V_0 = 1.0$ p.u., the mid-point voltage is 1.0125 p.u. and the reactive power absorbed at each end is 0.158 P_0. These values should be compared with the receiving-end voltage of 1.05 p.u. and the sending-end reactive-power absorption of $Q_s = 0.329 P_0$ in the absence of the reactor. For continuous duty at no-load with a line–line voltage of 500 kV, the rating of the shunt reactor would be 53 MVAr per phase, if $Z_0 = 250\,\Omega$.

Equation (3.36) shows that at no-load the line behaves like a symmetrical line as though it were two separate open-circuited lines connected back-to-back and joined at the mid-point. The open-circuit voltage rise on each half is given by equation (3.36) which is consistent with equation (3.21) when $P = 0$.

3.5.1   Multiple shunt reactors along a long line

The analysis of Figure 3.12 can be generalized to deal with a line divided into n sections by $n - 1$ shunt reactors spaced at equal intervals, with a shunt reactor at each end. The voltage and current profiles in Figure 3.12 could be reproduced in every section if it were of length a and the terminal conditions were the same. The terminal voltages at the ends of the section shown in Figure 3.12 are equal in magnitude and phase. The currents are equal but opposite in phase. The correct conditions could, therefore, be achieved by connecting shunt reactors of half the reactance given by equation (3.32) at every junction between two sections, as shown in Figure 3.13. The shunt reactors at the ends of the line are each of twice the reactance of the inter-mediate ones. If a is the total length of the composite line, replacing a by a/n in equation (3.32) gives the required reactance of each intermediate reactor

$$X = \frac{Z_0}{2}\left[\frac{\sin(\theta/n)}{1 - \cos(\theta/n)}\right] \tag{3.37}$$

In Figure 3.13, the sending-end generator supplies no reactive current. In practice it would supply, to a first approximation, only the losses. If the sending-end reactor was removed, the generator would have to absorb the reactive current from the nearest half of the leftmost section. Each intermediate reactor absorbs the line-charging
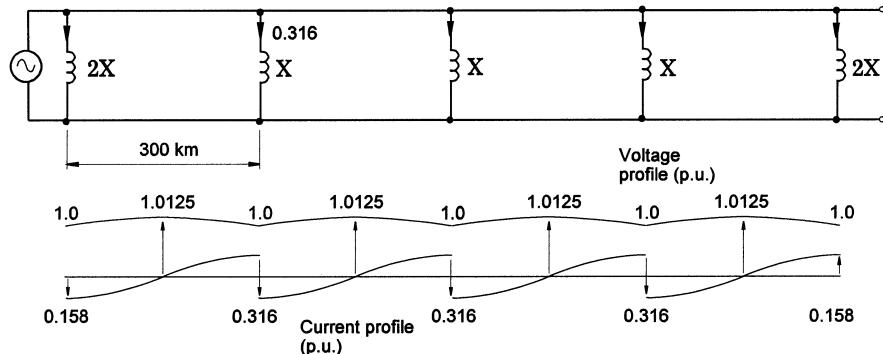
Fig. 3.13 Multiple shunt reactors along a long line.

current and reactive power from two half-sections of line, each of length $a/2n$ on either side of it, whereas the reactors at each end absorb the reactive power from the half-section on one side only. This again explains why the intermediate reactors have half the reactance.

3.5.2   Voltage control by means of switched shunt compensation

Figure 3.14 shows the principle of voltage control by means of switched shunt reactors. Voltage curves are shown for a line such as the one in Figure 3.12. Curve L applies when the shunt reactor is connected, and curve C applies when the shunt capacitor is connected. The receiving-end voltage can be kept within a narrow band as the load varies, by switching the reactor and the capacitor in and out.
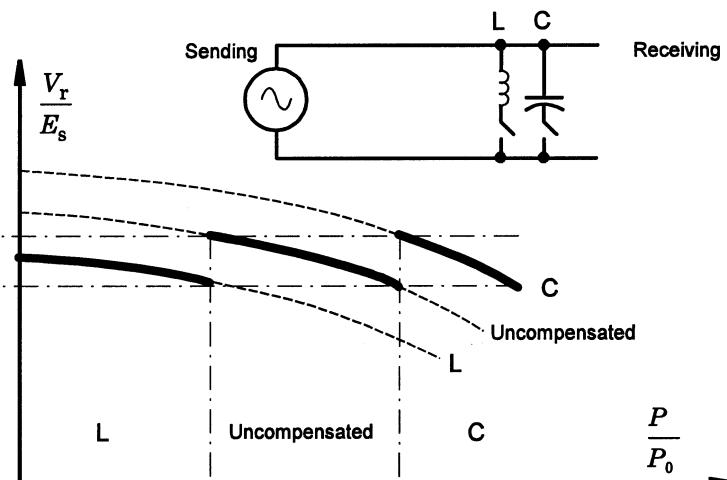
Fig. 3.14 Switched shunt compensation.

3.5.3 The mid-point shunt compensator

Figure 3.15 shows a symmetrical line with a mid-point shunt compensator of admittance jB_γ. Each half of the line is represented by a π-equivalent circuit. The synchronous machines at the ends are assumed to supply or absorb the reactive power for the leftmost and rightmost half-sections, leaving the compensator to supply or absorb only the reactive power for the central half of the line.

If the compensator can vary its admittance continuously in such a way as to maintain $V_m = E$, then in the steady state the line is sectioned into two independent halves with a power transmission characteristic given by

$$P = \frac{2E^2}{X_L} \sin \frac{\delta}{2} \tag{3.38}$$

The maximum transmissible power is $2E^2/X_L$, twice the steady-state limit of the uncompensated line. It is reached when $\delta/2 = \pi/2$, that is, with a transmission angle δ of 90° across each half of the line, and a total transmission angle of 180° across the whole line, Figure 3.16.
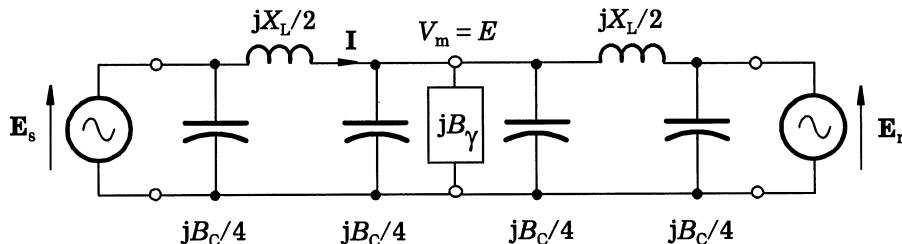

Fig. 3.15 Mid-point shunt compensator.
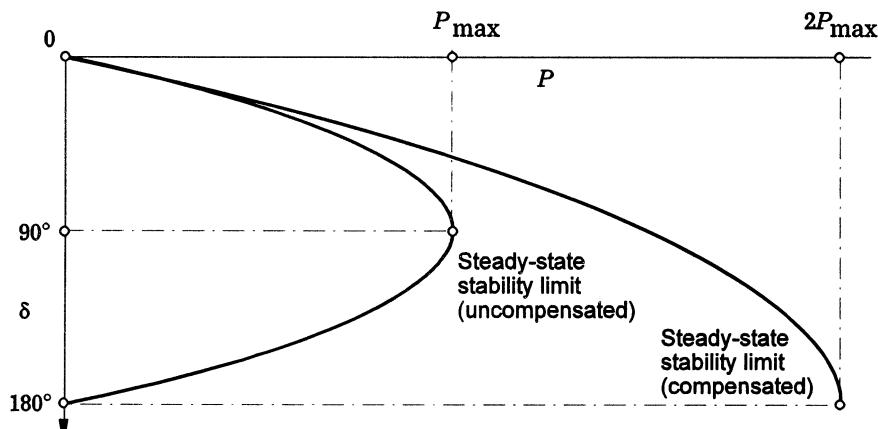
**Fig. 3.16** Power transmission characteristic with dynamic shunt compensation.
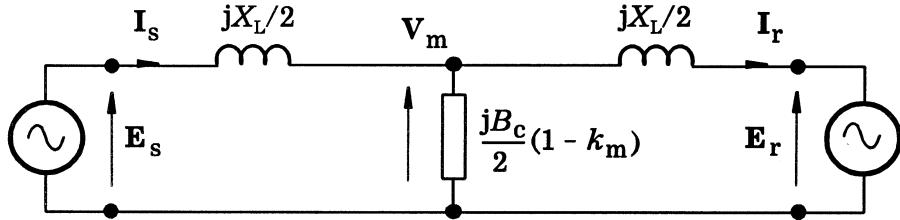
**Fig. 3.17** Mid-point shunt compensator.
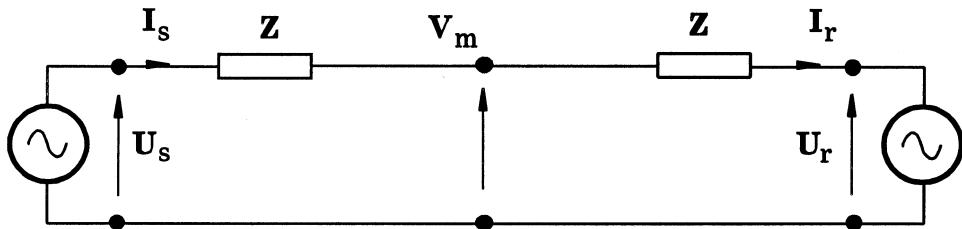
Fig. 3.18 Thévenin equivalent circuit of line with mid-point shunt compensation.

The equivalent circuit can be simplified to the one shown in Figure 3.17. The compensating admittance is expressed in terms of the 'degree of compensation' k_m, which is positive if the compensator is inductive and negative if it is capacitive

$$\mathrm{j}B_\gamma = -k_m \times \frac{\mathrm{j}B_c}{2} \tag{3.39}$$

The total shunt admittance in the centre is equal to

$$2 \times \frac{\mathrm{j}B_c}{4} + \mathrm{j}B_\gamma = 2 \times \frac{\mathrm{j}B_c}{4} - k_m \times \frac{\mathrm{j}B_c}{2} = \frac{\mathrm{j}B_c}{2} \times (1 - k_m) \tag{3.40}$$

The equivalent circuit can be simplified still further by splitting the central admittance into two equal parallel admittances and then reducing each half to its Thévenin equivalent, as in Figure 3.18. The Thévenin equivalent voltage at the sending end is

$$\mathbf{U}_s = \frac{\frac{1}{\mathrm{j}B_c(1-k_m)/4}}{\frac{1}{\mathrm{j}B_c(1-k_m)/4} + \frac{\mathrm{j}X_L}{2}} \mathbf{E}_s = \frac{\mathbf{E}_s}{1-s} \quad \text{where} \quad s = \frac{X_L}{2}\frac{B_c}{4}(1-k_m) \tag{3.41}$$

and

$$\mathbf{Z} = \frac{1}{\mathrm{j}B_c(1-k_m)/4 + \frac{1}{\mathrm{j}X_L/2}} = \frac{\mathrm{j}X_L/2}{1-s} \tag{3.42}$$

The parameter s is a potentiometer ratio determined by the relative values of X_L, B_c and k_m. If we assume that $E_s = E_r = E$, the phasor diagram is as shown in Figure 3.19 and the mid-point voltage is given by
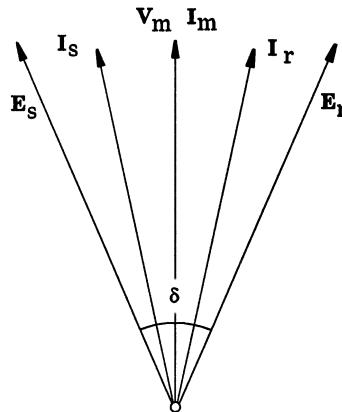
Fig. 3.19 Phasor diagram of symmetrical line.

$$V_{\mathrm{m}} = \frac{E \cos (\delta/2)}{1 - s} \tag{3.43}$$

If we now substitute for s in equation (3.43) we can determine the value of compensating susceptance B_γ required to maintain a given ratio V_{m}/E: thus

$$B_\gamma = -\frac{4}{X_{\mathrm{L}}} \left[1 - \frac{E}{V_{\mathrm{m}}} \cos \frac{\delta}{2} \right] + \frac{B_{\mathrm{c}}}{2} \tag{3.44}$$

This equation tells how B_γ must vary with the transmission angle δ in order to maintain a given value of mid-point voltage V_{m}. Naturally, through δ, B_γ varies with the power being transmitted. From Figure 3.19, using the analogy with the symmetrical line in Figure 3.8 and equation (3.25), the power transmission can be deduced to be controlled by the equation

$$P = \frac{E^2}{(1 - s)X_{\mathrm{L}}} \sin \delta = \frac{E_{\mathrm{m}}E}{X_{\mathrm{L}} \cos (\delta/2)} \sin \delta = 2 \frac{E_{\mathrm{m}}E}{X_{\mathrm{L}}} \sin \frac{\delta}{2} \tag{3.45}$$

This establishes equation (3.38) which was earlier written down by inspection of Figure 3.15.

3.6   Series compensation

A series capacitor can be used to cancel part of the reactance of the line. This increases the maximum power, reduces the transmission angle at a given level of power transfer, and increases the virtual natural load. Since the effective line reactance is reduced, it absorbs less of the line-charging reactive power, so shunt reactors may be needed as shown in Figure 3.20. Series capacitors are most often used in very long distance transmission, but they can also be used to adjust the power sharing between parallel lines. A line with 100% series compensation would have a resonant frequency equal to the power frequency, and since the damping in power systems is
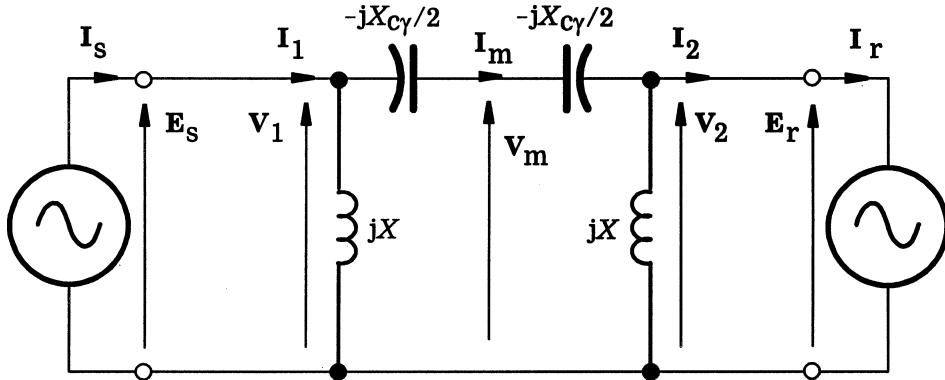
Fig. 3.20 Series compensated transmission line.

very low, such a system would be hypersensitive to small changes. For this reason the degree of series compensation is limited in practice to about 80%.

It is not practicable to distribute the capacitance in small units along the line, so in practice lumped capacitors are installed at a small number of locations (typically one or two) along the line. This makes for an uneven voltage profile.

The line in Figure 3.20 is assumed to be a lossless, symmetrical line with a mid-point series capacitor with equal shunt reactors connected on either side. To permit the line to be analysed in two halves, the capacitor is split into two equal series parts.

3.6.1   Power-transfer characteristics and maximum transmissible power

The general phasor diagram is shown in Figure 3.21. Note that $\mathbf{V}_2$ leads $\mathbf{V}_1$ in phase as a result of the voltage $\mathbf{V}_{C\gamma}$ inserted by the capacitor. Considering the sending-end half, the conditions at its two ends are related by equation (3.2)

$$\mathbf{E}_s = \mathbf{V}_1 \cos \frac{\theta}{2} + jZ_0 \mathbf{I}_1 \sin \frac{\theta}{2}$$
$$\mathbf{I}_s = j\frac{\mathbf{V}_1}{Z_0} \sin \frac{\theta}{2} = \mathbf{I}_1 \cos \frac{\theta}{2} \tag{3.46}$$

The receiving-end half behaves similarly. The capacitor reactance is $X_{C\gamma} = 1/\omega C_\gamma$ and the voltage across the capacitor is given by

$$\mathbf{V}_{C\gamma} = \mathbf{V}_1 - \mathbf{V}_2 = -j\mathbf{I}_m X_{C\gamma} \tag{3.47}$$

By symmetry, $P = V_m I_m$, $E = E_r$, and

$$\mathbf{V}_m = \mathbf{V}_1 - {}^1\!\!/_2\mathbf{V}_{C\gamma} = \mathbf{V}_2 + {}^1\!\!/_2\mathbf{V}_{C\gamma} \tag{3.48}$$

The currents $\mathbf{I}_1$ and $\mathbf{I}_2$ are given by

$$\mathbf{I}_m = \mathbf{I}_1 + \frac{j\mathbf{V}_1}{X} = \mathbf{I}_2 - j\frac{\mathbf{V}_2}{X} \tag{3.49}$$
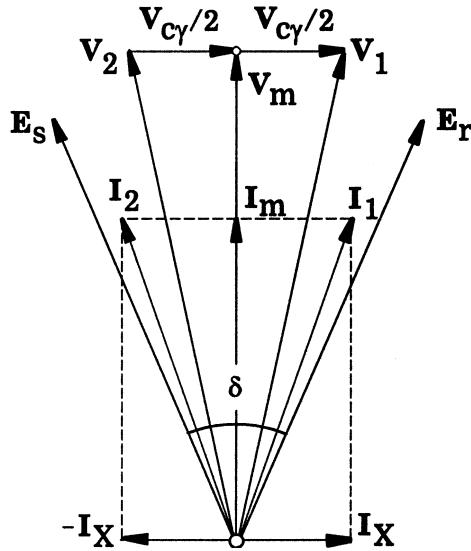
Fig. 3.21 Series compensated line: phasor diagram.

Using these relationships, and taking $\mathbf{V}_m$ as reference phasor, it is possible to derive the basic power-transfer characteristic as

$$P = \frac{E_s V_m}{Z_0 \sin \theta/2 - \frac{X_{C\gamma}}{2} \left[\cos \frac{\theta}{2} + \frac{Z_0}{X} \sin \frac{\theta}{2}\right]} \sin \frac{\delta}{2} \tag{3.50}$$

with

$$E_s \cos \frac{\delta}{2} = V_m \left[\cos \frac{\theta}{2} + \frac{Z_0}{X} \sin \frac{\theta}{2}\right] = E_r \cos \frac{\delta}{2} \tag{3.51}$$

If V_m is substituted from equation (3.51) into equation (3.50), the following result is obtained for the symmetrical line, if $E_s = E_r$:

$$P = \frac{E_s E_r}{\left[Z_0 \sin \theta - \frac{X_{C\gamma}}{2}(1 + \cos \theta)\mu\right]\mu} \sin \delta \tag{3.52}$$

where

$$\mu = 1 + \frac{Z_0}{X} \frac{\sin \theta}{1 + \cos \theta} = 1 + \frac{Z_0}{X} \tan \frac{\theta}{2} \tag{3.53}$$

With no shunt reactors, $\mu = 1$. With fixed terminal voltages, $E_s = E_r = E$, the transmission angle δ can be determined from equation (3.52) for any level of power transmission below the maximum. Once δ is known, V_m can be determined from equation (3.50). Then $\mathbf{V}_1$, $\mathbf{V}_2$, $\mathbf{V}_{C\gamma}$ and other quantities follow.

One simplification is to ignore the shunt capacitance of the line and remove the shunt reactors. Then $Z_0 \sin \theta$ is replaced by X_L and $\mu = 1$, so that with $E_s = E_r = E$,

$$P = \frac{E^2}{X_L - X_{C\gamma}} \sin \delta \tag{3.54}$$
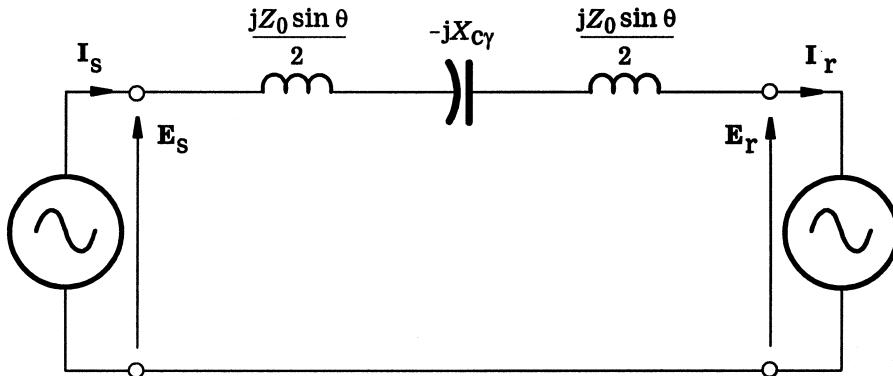
Fig. 3.22 Simplified equivalent circuit of series compensated line.

If the degree of series compensation k_{se} is defined by

$$k_{se} = \frac{X_{C\gamma}}{X_L} = \frac{X_{C\gamma}}{\omega a l} \tag{3.55}$$

then

$$P = \frac{E^2}{X_L(1 - k_{se})} \sin \delta \tag{3.56}$$

Another important special case arises when the shunt reactors are chosen to compensate the line capacitance perfectly as discussed in Section 3.4. Their reactances are then each

$$X = Z_0 \frac{\sin (\theta/2)}{1 - \cos (\theta/2)} \tag{3.57}$$

From equation (3.53) the shunt reactance factor μ reduces to $\sec(\theta/2)$ and the power-transfer characteristic becomes (with $E_s = E_r = E$)

$$P = \frac{E^2}{2Z_0 \sin \theta/2 - X_{C\gamma}} \sin \delta \tag{3.58}$$

Shunt compensation of the capacitance of each half of the line leaves only the series reactance in the equivalent circuit, Figure 3.22. This equivalent circuit does not take into account the fact that because the shunt-inductive compensation is concentrated, the line voltage profile is not perfectly flat, even at no-load.

3.7   Conclusion

This chapter has examined the behaviour of long-distance, high-voltage transmission lines with distributed parameters, in which the voltage and current tend to vary along the line. The same behaviour is obtained with cables of only moderate length

(upwards of 50 km). The theory covers the operation at all load levels and considers the reactive power requirements, the voltage profile, and the stability. Compensation methods are identified for improving the performance with respect to all three of these aspects, including both shunt and series compensating elements, and both passive (fixed-value) and active compensators.

4

Power flows in compensation and control studies

4.1 Introduction

The main objective of a power flow study is to determine the steady state operating condition of the electrical power network. The steady state may be determined by finding out the flow of active and reactive power throughout the network and the voltage magnitudes and phase angles at all nodes of the network.

The planning and daily operation of modern power systems call for numerous power flow studies. Such information is used to carry out security assessment analysis, where the nodal voltage magnitudes and active and reactive power flows in transmission lines and transformers are carefully observed to assess whether or not they are within prescribed operating limits. If the power flow study indicates that there are voltage magnitudes outside bounds at certain points in the network, then appropriate control actions become necessary in order to regulate the voltage magnitude. Similarly, if the study predicts that the power flow in a given transmission line is beyond the power carrying capacity of the line then control action will be taken.

Voltage magnitude regulation is achieved by controlling the amount of reactive power generated/absorbed at key points of the network as well as by controlling the flow of reactive power throughout the network (Miller, 1982). Voltage regulation is carried out locally and, traditionally, the following devices have been used for such a purpose:

1. Automatic voltage regulators, which control the generator's field excitation in order to maintain a specified voltage magnitude at the generator terminal.
2. Sources and sinks of reactive power, such as shunt capacitors, shunt reactors, rotating synchronous condensers and SVCs. Shunt capacitors and reactors are

only capable of providing passive compensation since their generation/absorption of reactive power depends on their rating, and the voltage level at the connection point. On the other hand, the reactive power generated/absorbed by synchronous condensers and SVCs is automatically adjusted in order to maintain fixed voltage magnitude at the connection points.

3. Load-tap changing transformers (LTCs), which are used to regulate voltage magnitude at the LTC terminals by adjusting its transformation ratio.

If no control action is taken, active and reactive power flows in AC transmission networks are determined by the topology of the network, the nodal voltage magnitudes and phase angles and the impedances of the various plant components making up the network. However, stable operation of the power network under a wide range of operating conditions requires good control of power flows network-wide. For instance, reactive power flows are minimized as much as possible in order to reduce network transmission losses and to maintain a uniform voltage profile. Reactive power flow control may be achieved by generating/absorbing reactive power at suitable locations in the network using one or more of the plant components mentioned above. On the other hand, the options for controlling the path of active power flows in AC transmission networks have been very limited, with on-load phase shifting transformers having provided the only practical option. These transformers are fitted with a tap changing mechanism, the purpose of which is to control the voltage phase angle difference across its terminals and, hence, to regulate the amount of active power that flows through the transformer.

4.2   FACTS equipment representation in power flows

Until very recently, with the exception of the SVC, all plant components used in high-voltage transmission to provide voltage and power flow control were equipment based on electro-mechanical technology, which severely impaired the effectiveness of the intended control actions, particularly during fast changing operating conditions (Ledu et al., 1992). This situation has begun to change; building on the operational experience afforded by the many SVC installations and breakthroughs in power electronics valves and their control, a vast array of new power electronics-based controllers has been developed. Controllers used in high-voltage transmission are grouped under the heading of FACTS (Hingorani, 1993) and those used in low-voltage distribution under the heading of Custom Power (Hingorani, 1995). The most prominent equipment and their main steady state characteristics relevant for power flow modelling are discussed below.

4.2.1   The SVC

From the operational point of view, the SVC behaves like a shunt-connected variable reactance, which either generates or absorbs reactive power in order to regulate the voltage magnitude at the point of connection to the AC network (Miller, 1982). In its simplest form, the SVC consists of a TCR in parallel with a bank of capacitors. The thyristor's firing angle control enables the SVC to have an almost instantaneous
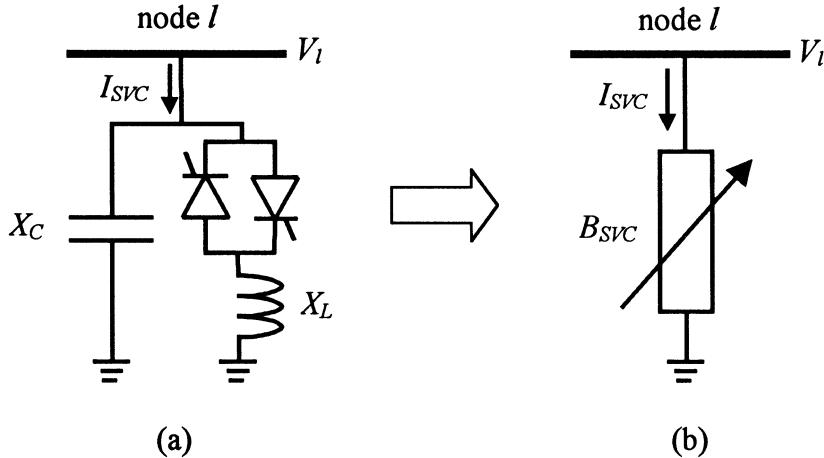
Fig. 4.1 SVC. (a) structure formed by fixed capacitor and TCR; and (b) variable susceptance representation.

speed of response. It is used extensively to provide fast reactive power and voltage regulation support. It is also known to increase system stability margin and to damp power system oscillations (Kundur, 1994).

In power flow studies the SVC is normally modelled as a synchronous generator with zero active power generation; upper and lower limits are given for reactive power generation. The generator representation of the SVC is changed to a constant admittance if the SVC reaches one of its limits (IEEE Special Stability Controls Working Group, 1995).

A more flexible and realistic SVC power flow model is presented in this chapter. It is based on the concept of a non-linear shunt reactance, which is adjusted using Newton's algorithm to satisfy a specified voltage magnitude at the terminal of the SVC (Ambriz-Perez et al., 2000). The schematic representation of the SVC and its equivalent circuit are shown in Figure 4.1, where a TCR is connected in parallel with a fixed bank of capacitors. A more detailed schematic representation of the TCR is shown in Figure 1.9.

An ideal variable shunt compensator is assumed to contain no resistive components, i.e. $G_{SVC} = 0$. Accordingly, it draws no active power from the network. On the other hand, its reactive power is a function of nodal voltage magnitude at the connection point, say node l, and the SVC equivalent susceptance, B_{SVC}

$$P_l = 0$$
$$Q_l = -|V_l|^2 B_{SVC} \tag{4.1}$$

4.2.2 The TCSC

The TCSC varies the electrical length of the compensated transmission line with little delay. Owing to this characteristic, it may be used to provide fast active power flow regulation. It also increases the stability margin of the system and has proved very effective in damping SSR and power oscillations (Larsen et al., 1992).

The TCSC power flow model presented in this chapter is based on the concept of a non-linear series reactance, which is adjusted using Newton's algorithm to satisfy a specified active power flow across the variable reactance representing the TCSC (Fuerte-Esquivel and Acha, 1997). The schematic representation of the TCSC and its equivalent circuit are shown in Figure 4.2. This schematic representation is a lumped equivalent of the TCSC shown in Figure 1.11(b).

The active power transfer P_{lm} across an impedance connected between nodes l and m is determined by the voltage magnitudes $|V_l|$ and $|V_m|$, the difference in voltage phase angles θ_l and θ_m and the transmission line resistance R_{lm} and reactance X_{lm}. In high-voltage transmission lines, the reactance is much larger than the resistance and the following approximate equation may be used to calculate the active power transfer P_{lm}

$$P_{lm} = \frac{|V_l||V_m|}{X_{lm}} \cdot \sin(\theta_l - \theta_m) \tag{4.2}$$

If the electrical branch is a TCSC controller as opposed to a transmission line then P_{lm} is calculated using the following expression

$$P_{lm}^{reg} = \frac{|V_l||V_m|}{X_{TCSC}} \cdot \sin(\theta_l - \theta_m) \tag{4.3}$$
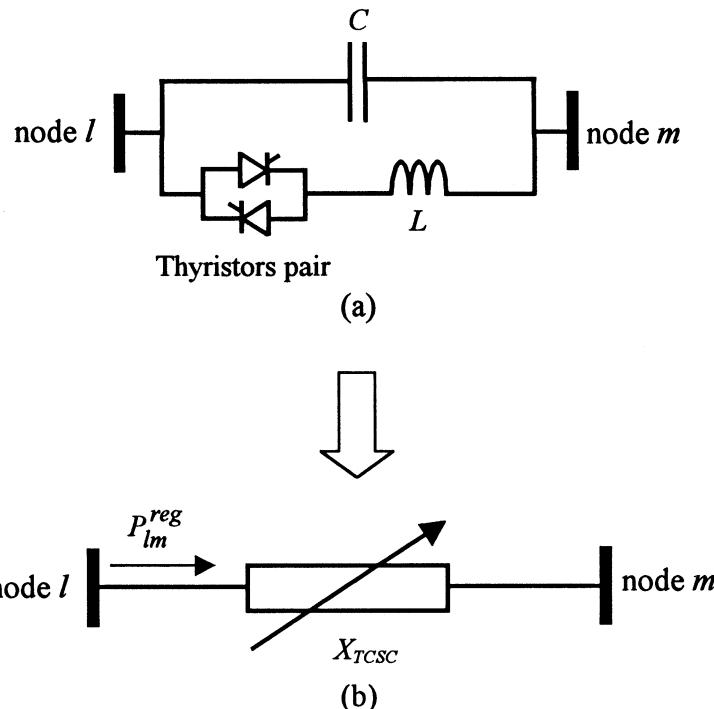
Fig. 4.2 TCSC. (a) structure formed by fixed capacitor and TCR; and (b) variable reactance representation.

where X_{TCSC} is the equivalent reactance of the TCSC controller which may be adjusted to regulate the transfer of active power across the TCSC, hence, P_{lm} becomes P_{lm}^{reg}.

4.2.3 The static phase shifter

The static phase shifter (SPS) varies the phase angles of the line end voltages with little delay. This is achieved by injecting a voltage in quadrature with the line end voltage at the sending end. This equipment may also be used to provide fast active power flow regulation (Hingorani and Gyugyi, 2000).

   The power flow model of the static phase shifter presented in this chapter is based on the concept of a lossless transformer with complex taps. The control variable is a phase angle, which is adjusted using Newton's algorithm to satisfy a specified active power flow across the lossless transformer representing the static phase shifter (Fuerte-Esquivel and Acha, 1997). The schematic representation of the SPS and its equivalent circuit are shown in Figure 4.3.
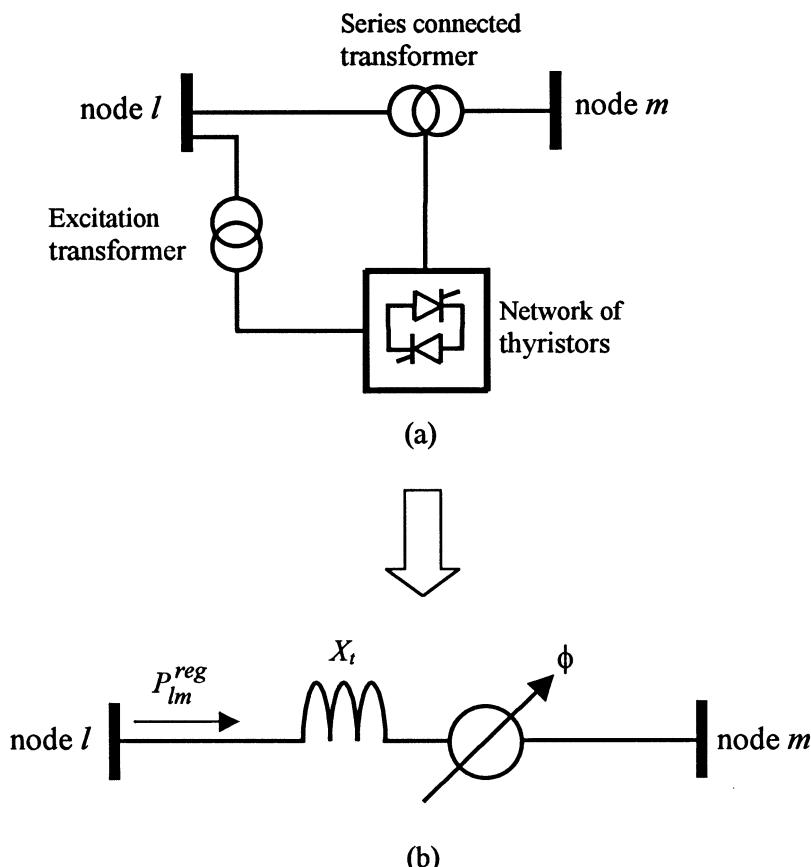
Fig. 4.3 SPS. (a) structure formed by a series transformer, an excitation transformer and a network of thyristors; and (b) variable phase angle representation.

A phase shifting controller with the complex phase angle relationships: $T_V = \cos\phi + \mathrm{j}\sin\phi$ and $T_I = \cos\phi - \mathrm{j}\sin\phi$ has the following transfer admittance matrix

$$\begin{bmatrix} I_l \\ I_m \end{bmatrix} = \frac{1}{X_t} \begin{bmatrix} 1 & -(\cos\phi + \mathrm{j}\sin\phi) \\ -(\cos\phi - \mathrm{j}\sin\phi) & 1 \end{bmatrix} \begin{bmatrix} V_l \\ V_m \end{bmatrix} \qquad (4.4)$$

where X_t is the leakage reactance of the series transformer and T_V and T_I are complex tap changing variables related to each other by the conjugate operation. Their magnitude is 1 and their phase angle is ϕ.

The active power transfer across the phase shifter P_{lm} is calculated using the following expression

$$P_{lm}^{\mathrm{reg}} = \frac{|V_l||V_m|}{X_t} \cdot \sin(\theta_l - \theta_m - \phi) \qquad (4.5)$$

Suitable adjustment of the phase angle ϕ enables regulation of active power P_{lm}^{reg} across the phase shifter. It should be remarked that the phase shifter achieves phase angle regulation at the expense of consuming reactive power from the network.

4.2.4   The STATCOM

The STATCOM is the static counterpart of the rotating synchronous condenser but it generates/absorbs reactive power at a faster rate because no moving parts are involved. In principle, it performs the same voltage regulation function as the SVC but in a more robust manner because unlike the SVC, its operation is not impaired by the presence of low voltages (IEEE/CIGRE, 1995). It goes on well with advanced energy storage facilities, which opens the door for a number of new applications, such as energy markets and network security (Dewinkel and Lamoree, 1993).

The schematic representation of the STATCOM and its equivalent circuit are shown in Figure 4.4. A fuller representation of the STATCOM is shown in Figure 1.10.

The STATCOM has the ability to either generate or absorb reactive power by suitable control of the inverted voltage $|V_{vR}|\angle\theta_{vR}$ with respect to the AC voltage on the high-voltage side of the STATCOM transformer, say node l, $|V_l|\angle\theta_l$.

In an ideal STATCOM, with no active power loss involved, the following reactive power equation yields useful insight into how the reactive power exchange with the AC system is achieved

$$Q_{vR} = \frac{|V_l|^2}{X_{vR}} - \frac{|V_l||V_{vR}|}{X_{vR}} \cdot \cos(\theta_l - \theta_{vR}) = \frac{|V_l|^2 - |V_l||V_{vR}|}{X_{vR}} \qquad (4.6)$$

where $\theta_{vR} = \theta_l$ for the case of a lossless STATCOM.

If $|V_l| > |V_{vR}|$ then Q_{vR} becomes positive and the STATCOM absorbs reactive power. On the other hand, Q_{vR} becomes negative if $|V_l| < |V_{vR}|$ and the STATCOM generates reactive power.

In power flow studies the STATCOM may be represented in the same way as a synchronous condenser (IEEE/CIGRE, 1995), which in most cases is the model
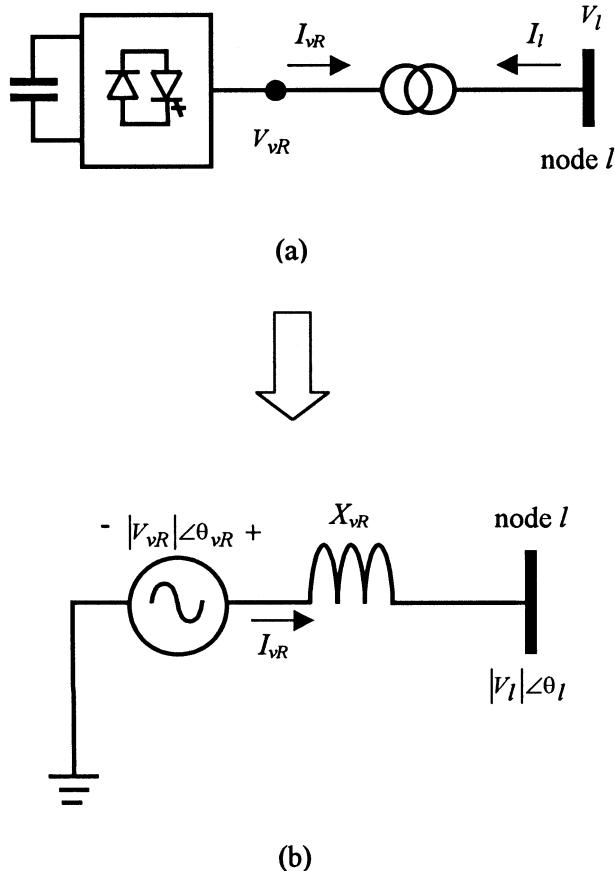
Fig. 4.4 STATCOM. (a) VSC connected to the AC network via a shunt transformer; and (b) shunt connected variable solid-state voltage source.

of a synchronous generator with zero active power generation. A more flexible STATCOM power flow model is presented in this chapter. It adjusts the voltage source magnitude and phase angle using Newton's algorithm to satisfy a specified voltage magnitude at the point of connection with the AC network

$$V_{vR} = |V_{vR}|(\cos\theta_{vR} + j\sin\theta_{vR}) \tag{4.7}$$

It should be pointed out that maximum and minimum limits will exist for $|V_{vR}|$ which are a function of the STATCOM capacitor rating. On the other hand, θ_{vR} can take any value between 0 and 2π radians but in practice it will keep close to θ_l.

4.2.5   The DVR

The DVR is a series connected VSC. The strength of this device is in low-voltage distribution applications where it is used to alleviate a range of dynamic power quality problems such as voltage sags and swells (Hingorani, 1995).
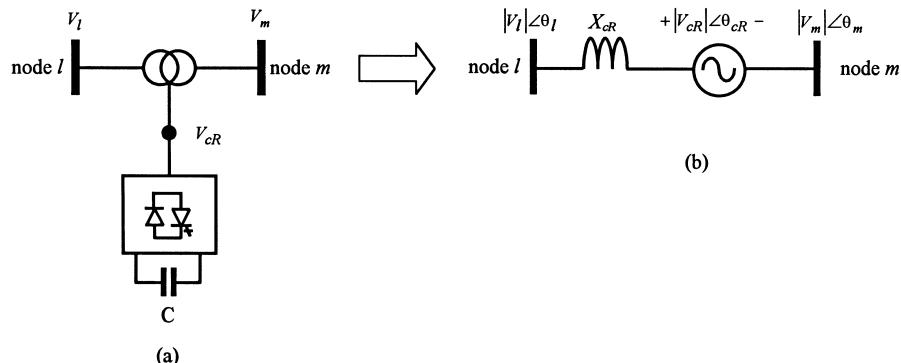
Fig. 4.5 DVR. (a) VSC connected to the AC network via a series transformer; and (b) series connected variable solid state voltage source.

For the purpose of steady state operation, the DVR performs a similar function to the SPS; it injects voltage in quadrature with one of the line end voltages in order to regulate active power flow. However, the DVR is a far more versatile controller because it does not draw reactive power from the AC system; it has its own reactive power provisions in the form of a DC capacitor. This characteristic makes the DVR capable of regulating both active and reactive power flow within the limits imposed by its rating. It may perform the role of a phase shifter and a variable series impedance compensator. The schematic representation of the DVR and its equivalent circuit are shown in Figure 4.5.

The DVR power flow model presented in this chapter is based on the concept of a series connected voltage source

$$V_{cR} = |V_{cR}|(\cos\theta_{cR} + j\sin\theta_{cR}) \tag{4.8}$$

The magnitude and phase angle of the DVR model are adjusted using Newton's algorithm to satisfy a specified active and reactive power flow across the DVR. Similarly to the STATCOM, maximum and minimum limits will exist for the voltage magnitude $|V_{cR}|$, which are a function of the DVR capacitor rating. On the other hand, the voltage phase angle θ_{cR} can take any value between 0 and 2π radians.

4.2.6 The UPFC

The UPFC may be seen to consist of one STATCOM and one DVR sharing a common capacitor on their DC side and a unified control system. The UPFC allows simultaneous control of active power flow, reactive power flow and voltage magnitude at the UPFC terminals. Alternatively, the controller may be set to control one or more of these parameters in any combination or to control none of them. A simpler schematic representation of the UPFC shown in Figure 1.12 is given in Figure 4.6 together with its equivalent circuit (Fuerte-Esquivel et al., 2000).

The active power demanded by the series converter is drawn by the shunt converter from the AC network and supplied via the DC link. The inverted voltage of the series converter is added to the nodal voltage, at say node l, to boost the nodal voltage at node m. The voltage magnitude of the inverted voltage $|V_{cR}|$ provides voltage
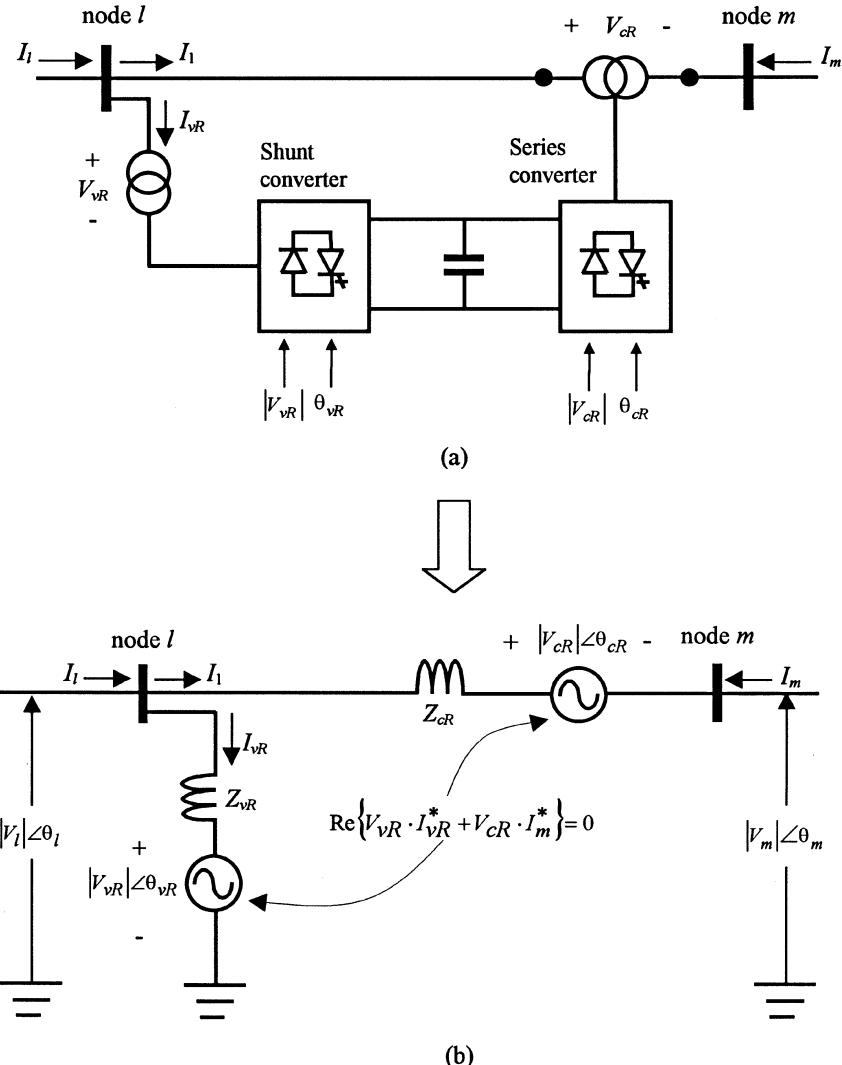
Fig. 4.6 UPFC. (a) back-to-back VSCs with one VSC connected to the AC network via a shunt transformer and a second VSC connected to the AC network via a series transformer; and (b) equivalent circuit based on solid-state voltage sources.

regulation and the phase angle θ_{cR} determines the mode of power flow control (Hingorani and Gyugyi, 2000):

1. If θ_{cR} is in phase with the voltage phase angle θ_l, it regulates no active power flow.
2. If θ_{cR} is in quadrature with the voltage phase angle θ_l, it controls active power flow performing as a phase shifter but drawing no reactive power from the AC network.

3. If θ_{cR} is in quadrature with the current angle then it controls active power flow performing as a variable series impedance compensator.
4. At any other value of θ_{cR}, it performs as a combination of a phase shifter and a variable series impedance compensator. This is in addition to being a voltage regulator by suitable control of $|V_{cR}|$.

In addition to providing a supporting role in the active power exchange that takes place between the series converter and the AC system, the shunt converter may also generate or absorb reactive power in order to provide independent voltage magnitude regulation at its point of connection with the AC system.

The UPFC power flow model presented in this chapter uses the equivalent circuit shown in Figure 4.6(b), which consists of a shunt connected voltage source, a series connected voltage source and an active power constraint equation which links the two voltage sources

$$V_{vR} = |V_{vR}|(\cos \theta_{vR} + j \sin \theta_{vR}) \tag{4.9}$$

$$V_{cR} = |V_{cR}|(\cos \theta_{cR} + j \sin \theta_{cR}) \tag{4.10}$$

$$\text{Re}\{-V_{vR}I_{vR}^* + V_{cR}I_m^*\} = 0 \tag{4.11}$$

These equations are adjusted in a coordinated fashion using Newton's algorithm to satisfy the specified control requirements. Similarly to the shunt and series voltage sources used to represent the STATCOM and the DVR, respectively, the voltage sources used in the UPFC application would also have limits. For the shunt converter the voltage magnitude and phase angle limits are: $V_{vR\,\text{min}} \leq V_{vR} \leq V_{vR\,\text{max}}$ and $0 \leq \theta_{vR} \leq 2\pi$. The corresponding limits for the series converter are: $V_{cR\,\text{min}} \leq V_{cR} \leq V_{cR\,\text{max}}$ and $0 \leq \theta_{cR} \leq 2\pi$.

4.2.7 The HVDC-Light

The HVDC-Light comprises two VSCs, one operating as a rectifier and the other as an inverter. The two converters are connected either back-to-back or joined together by a DC cable, depending on the application. Its main function is to transmit constant DC power from the rectifier to the inverter station, with high controllability. The schematic representation of the HVDC light and its equivalent circuit are shown in Figure 4.7. A fuller schematic representation is shown in Figure 1.13.

One VSC controls DC voltage and the other the transmission of active power through the DC link. Assuming lossless converters, the active power flow entering the DC system must equal the active power reaching the AC system at the inverter end minus the transmission losses in the DC cable. During normal operation, both converters have independent reactive power control.

The power flow model for the back-to-back HVDC light may be based on the use of one voltage source for the rectifier and one voltage source for the inverter linked together by a constrained power equation

$$V_{vR1} = |V_{vR1}|(\cos \theta_{vR1} + j \sin \theta_{vR1}) \tag{4.12}$$
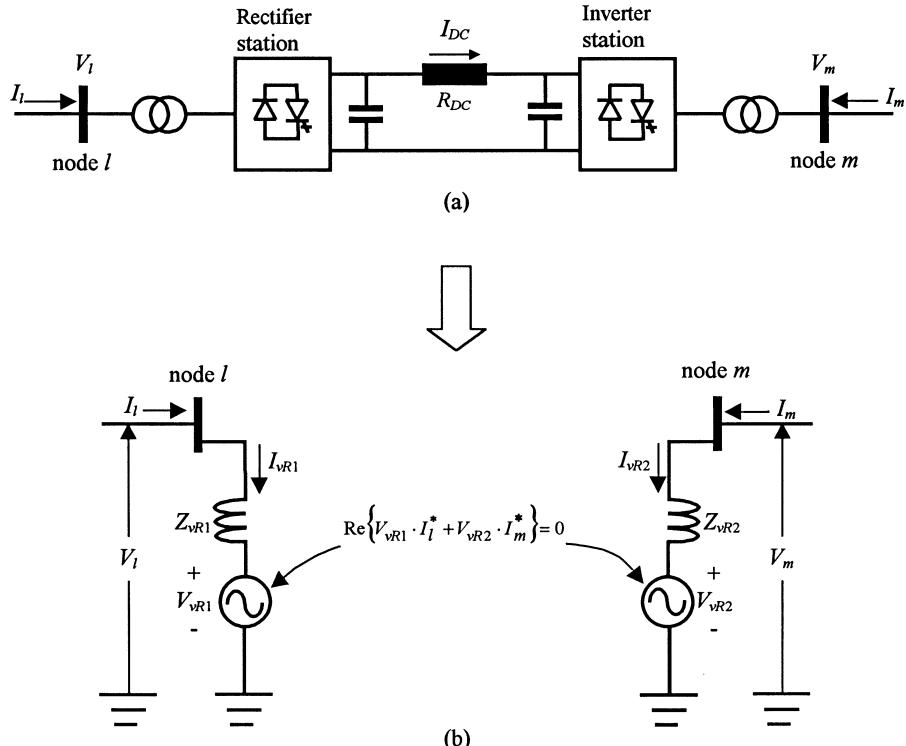
Fig. 4.7 HVDC Light. (a) the VSC at the sending end performs the role of rectifier and the VSC at the receiving end performs the role of inverter; and (b) equivalent circuit.

$$V_{vR2} = |V_{vR2}|(\cos\theta_{vR2} + j\sin\theta_{vR2}) \tag{4.13}$$

$$\mathrm{Re}\{-V_{vR1}I^* + V_{vR2}I_m^*\} = 0 \tag{4.14}$$

In this application the two shunt voltage sources used to represent the two converters have the following voltage magnitudes and phase angles limits: $V_{vR\min1} \leq V_{vR1} \leq V_{vR\max1}; 0 \leq \theta_{vR1} \leq 2\pi; V_{vR\min2} \leq V_{vR2} \leq V_{vR\max2}$ and $0 \leq \theta_{vR2} \leq 2\pi$.

4.3 Fundamental network equations

4.3.1 Nodal admittances

Nodal analysis is a tool of fundamental importance in power systems calculations. The nodal matrix equation of an AC electrical circuit may be determined by combining Ohm's law and Kirchhoff's current law.

The following relationships exist in an electrical branch of impedance Z_k connected between nodes l and m

$$V_l - V_m = Z_k I_k \qquad \Rightarrow \qquad I_k = \frac{V_l - V_m}{Z_k} = Y_k \Delta V \tag{4.15}$$

where $\Delta V = V_l - V_m$ and $Y_k = \frac{1}{Z_k}$.

The injected nodal current at node i may be expressed as a function of the currents entering and leaving the node through the q branches connected to the node

$$I_i = \sum_{k=1}^{q} I_k \tag{4.16}$$

where I_i is the nodal current at node i and branch k is connected to node i. Also, I_k is the current in branch k.

Combining equations (4.15) and (4.16) leads to the key equation used in nodal analysis

$$I_i = \sum_{k=1}^{q} Y_k(V_l - V_m) \tag{4.17}$$

which can also be expressed in matrix form for the case of n nodes

$$
\begin{bmatrix} I_1 \\ I_2 \\ I_3 \\ \vdots \\ I_n \end{bmatrix} =
\begin{bmatrix}
Y_{11} & Y_{12} & Y_{13} & \cdots & Y_{1n} \\
Y_{21} & Y_{22} & Y_{23} & \cdots & Y_{2n} \\
Y_{31} & Y_{32} & Y_{33} & \cdots & Y_{3n} \\
\vdots & \vdots & \vdots & \ddots & \vdots \\
Y_{n1} & Y_{n2} & Y_{n3} & \cdots & Y_{nn}
\end{bmatrix}
\begin{bmatrix} V_1 \\ V_2 \\ V_3 \\ \vdots \\ V_n \end{bmatrix}
\tag{4.18}
$$

where $i = 1, 2, 3, \cdots n$.

4.3.2   Numerical example 1

The theory presented above is used to determine the nodal matrix equation for the circuit in Figure 4.8. This circuit consists of six branches and four nodes. The branches are numbered 1 to 6 and the nodes are a, b, c and d. All branches have admittance values Y, with the values of the diagonal elements being negative.
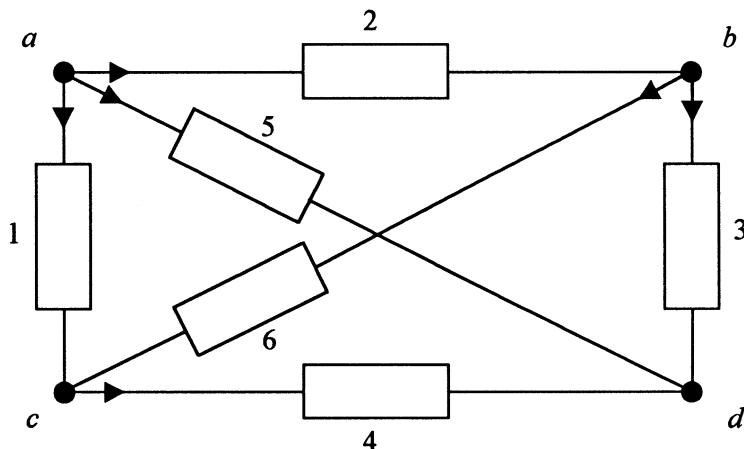

Fig. 4.8 Lattice circuit.

The arrows show the directions of the currents assumed for this example. It should be remarked that these currents serve the purpose of the nodal analysis and may not correspond to physical currents.

The following conventions are used in nodal analysis:

- currents leaving the node are taken to be positive
- currents entering the node are taken to be negative.

Using Ohm's law

$$
\begin{aligned}
I_1 &= Y(V_a - V_c) \\
I_2 &= Y(V_a - V_b) \\
I_3 &= Y(V_b - V_d) \\
I_4 &= Y(V_c - V_d) \\
I_5 &= -Y(V_a - V_d) \\
I_6 &= -Y(V_b - V_c)
\end{aligned}
\tag{4.19}
$$

and from Kirchhoff's current law

$$
\begin{aligned}
+I_2 + I_1 + I_5 &= I_a \\
-I_2 + I_6 + I_3 &= I_b \\
-I_1 - I_6 + I_4 &= I_c \\
-I_5 - I_3 - I_4 &= I_d
\end{aligned}
\tag{4.20}
$$

Substituting equations (4.19) into equations (4.20) gives

$$
\begin{aligned}
+YV_a - YV_b - YV_c + YV_d &= I_a \\
-YV_a + YV_b + YV_c - YV_d &= I_b \\
-YV_a + YV_b + YV_c - YV_d &= I_c \\
+YV_a - YV_b - YV_c + YV_d &= I_d
\end{aligned}
\tag{4.21}
$$

or, in matrix form

$$
\begin{bmatrix} I_a \\ I_b \\ I_c \\ I_d \end{bmatrix} =
\begin{bmatrix}
Y & -Y & -Y & Y \\
-Y & Y & Y & -Y \\
-Y & Y & Y & -Y \\
Y & -Y & -Y & Y
\end{bmatrix}
\begin{bmatrix} V_a \\ V_b \\ V_c \\ V_d \end{bmatrix}
\tag{4.22}
$$

4.3.3   Rules for building the nodal admittance matrix

In practice, nodal admittance matrices are easier to construct by applying a set of available empirical rules than by applying the procedure outlined above. The same result is obtained by using the following three simple rules:

1. Each diagonal element in the nodal admittance matrix, Y_{ii}, is the sum of the admittances of the branches terminating in node i.
2. Each off-diagonal element of the nodal admittance matrix, Y_{ij}, is the negative of the branch admittance connected between nodes i and j.

3. If no direct connection exists between nodes i and j then the corresponding off-diagonal element in the nodal admittance matrix will have a zero entry.

Applying this set of rules to form the nodal admittance matrix of the circuit of Figure 4.8 produces the following nodal admittance matrix

$$\mathbf{Y} = \begin{bmatrix} (Y+Y-Y) & -Y & -Y & Y \\ -Y & (Y+Y-Y) & Y & -Y \\ -Y & Y & (Y+Y-Y) & -Y \\ Y & -Y & -Y & (Y+Y-Y) \end{bmatrix} = \begin{bmatrix} Y & -Y & -Y & Y \\ -Y & Y & Y & -Y \\ -Y & Y & Y & -Y \\ Y & -Y & -Y & Y \end{bmatrix}$$

(4.23)

which is identical to the result generated in Example 1.

This result illustrates the simplicity and efficiency with which nodal admittance matrices can be generated. This is particularly useful in the study of large-scale systems.

It should be pointed out that the inverse of nodal admittance matrix equation (4.23) does not exist, i.e. the matrix is singular. The reason is that no reference node has been selected in the electrical circuit of Figure 4.8. In most practical cases a reference node exists and the nodal admittance matrix can be inverted. In electrical power networks, the reference node is the ground, which in power systems analysis is taken to be at zero potential.

4.3.4 Nodal impedances

If the nodal admittance matrix of the network can be inverted then the resulting matrix is known as the nodal impedance matrix. In an n-node network, the nodal impedance matrix equation takes the following form

$$\begin{bmatrix} V_1 \\ V_2 \\ V_3 \\ \vdots \\ V_n \end{bmatrix} = \begin{bmatrix} Z_{11} & Z_{12} & Z_{13} & \cdots & Z_{1n} \\ Z_{21} & Z_{22} & Z_{23} & \cdots & Z_{2n} \\ Z_{31} & Z_{32} & Z_{33} & \cdots & Z_{3n} \\ \vdots & \vdots & \vdots & \ddots & \vdots \\ Z_{n1} & Z_{n2} & Z_{n3} & \cdots & Z_{nn} \end{bmatrix} \begin{bmatrix} I_1 \\ I_2 \\ I_3 \\ \vdots \\ I_n \end{bmatrix}$$

(4.24)

There are several well-established ways to determine the nodal impedance matrix, some of which are mentioned below:

- By inverting the nodal admittance matrix (Shipley, 1976), i.e.

$$\begin{bmatrix} Y_{11} & Y_{12} & Y_{13} & \cdots & Y_{1n} \\ Y_{21} & Y_{22} & Y_{23} & \cdots & Y_{2n} \\ Y_{31} & Y_{32} & Y_{33} & \cdots & Y_{3n} \\ \vdots & \vdots & \vdots & \ddots & \vdots \\ Y_{n1} & Y_{n2} & Y_{n3} & \cdots & Y_{nn} \end{bmatrix}^{-1} = \begin{bmatrix} Z_{11} & Z_{12} & Z_{13} & \cdots & Z_{1n} \\ Z_{21} & Z_{22} & Z_{23} & \cdots & Z_{2n} \\ Z_{31} & Z_{32} & Z_{33} & \cdots & Z_{3n} \\ \vdots & \vdots & \vdots & \ddots & \vdots \\ Z_{n1} & Z_{n2} & Z_{n3} & \cdots & Z_{nn} \end{bmatrix}$$

(4.25)

In most practical situations, the resulting impedance matrix contains no zero elements regardless of the degree of sparsity of the admittance matrix, i.e. ratio of zero to non-zero elements. Therefore, this approach is only useful for small networks or

large networks which are fully interconnected and therefore have a low degree of sparsity. In such cases there is no advantage gained by using sparsity techniques.

- By factorizing the nodal admittance matrix using sparsity techniques (Zollenkopf, 1970). In this case, the nodal admittance matrix is not inverted explicitly and the resulting vector factors will contain almost the same degree of sparsity as the original matrix. Sparsity techniques allow the solution of very large-scale networks with minimum computational effort.
- By directly building up the impedance matrix (Brown, 1975). A set of rules exists to form the nodal impedance matrix but they are not as simple as the rules used to form the nodal admittance matrix. It outperforms the method of explicit inversion in terms of calculation speed but the resulting impedance matrix is also full. This approach is not competitive with respect to sparse factorization techniques.

4.3.5 Numerical example 2

The network impedance shown in Figure 4.9 is energized at node one with a current source of 1 p.u. The branch admittances all have values of 1 p.u. Let us determine the nodal voltages in the network.

The nodal admittance matrix for this circuit is formed using the empirical rules given above.

$$
\begin{bmatrix} I_1 \\ I_2 \\ I_3 \\ I_0 \end{bmatrix} = \begin{bmatrix} (1+1) & -1 & 0 & -1 \\ -1 & (1+1+1) & -1 & -1 \\ 0 & -1 & (1+1) & -1 \\ -1 & -1 & -1 & (1+1+1) \end{bmatrix} \begin{bmatrix} V_1 \\ V_2 \\ V_3 \\ V_0 \end{bmatrix} = \begin{bmatrix} 2 & -1 & 0 & -1 \\ -1 & 3 & -1 & -1 \\ 0 & -1 & 2 & -1 \\ -1 & -1 & -1 & 3 \end{bmatrix} \begin{bmatrix} V_1 \\ V_2 \\ V_3 \\ V_0 \end{bmatrix}
$$

(4.26)

The nodal admittance matrix is singular and, hence, the nodal impedance matrix does not exist. However, the singularity can be removed by choosing a reference node. In power systems analysis the ground node (node 0) is normally selected as the reference node because the voltage at this node has a value of zero. The row and column corresponding to node 0 are removed from the nodal matrix equation and in this example the solution for the nodal voltages is carried out via a matrix inversion operation.
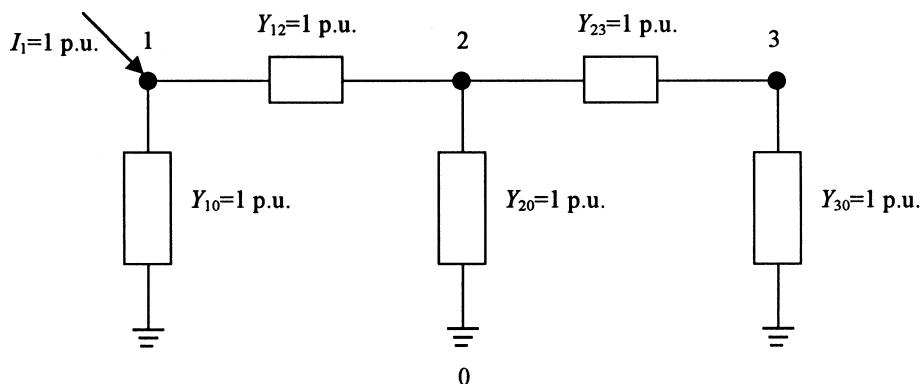

Fig. 4.9 Network of admittances.

$$
\begin{bmatrix} V_1 \\ V_2 \\ V_3 \end{bmatrix} = \begin{bmatrix} 2 & -1 & 0 \\ -1 & 3 & -1 \\ 0 & -1 & 2 \end{bmatrix}^{-1} \begin{bmatrix} 1 \\ 0 \\ 0 \end{bmatrix} = \frac{1}{8} \begin{bmatrix} 5 & 2 & 1 \\ 2 & 4 & 2 \\ 1 & 2 & 5 \end{bmatrix} \begin{bmatrix} 1 \\ 0 \\ 0 \end{bmatrix} = \frac{1}{8} \begin{bmatrix} 5 \\ 2 \\ 1 \end{bmatrix} \qquad (4.27)
$$

4.4   The power flow theory

4.4.1   Basic concepts

From the mathematical modelling point of view, the power flow exercise consists in solving the set of non-linear, algebraic equations which describe the power network under steady state conditions. Over the years, several approaches have been put forward for the solution of the power flow equations (Freris and Sasson, 1968; Stott, 1974). Early approaches were based on numerical techniques of the Gauss–Seidel type, which exhibit poor convergence characteristic when applied to the solution of networks of realistic size. They have been superseded by numerical techniques of the Newton–Raphson type, owing to their very strong convergence characteristic.

In conventional power flow studies, nodes can be of three different types:

1. *Voltage controlled node*. If sufficient reactive power is available at the node, the nodal voltage magnitude may be regulated and the node will be of the voltage controlled type. Synchronous generators and SVCs may be used to provide voltage regulation. In the case of generators the amount of active power which the generator has been scheduled to meet is specified whereas in the case of SVCs the active power is specified to be zero. The unknown variables are the nodal voltage phase angle and the net reactive power. These nodes are also known as PV type, where P relates to active power and V relates to voltage magnitude.
2. *Load node*. If no generation facilities exist at the node, this will be of the load type. For these kinds of nodes the net active and reactive powers are specified and the nodal voltage magnitude and phase angle are unknown variables. These nodes are also known as PQ type. In this case P and Q relate to active and reactive power, respectively. If neither generation nor demand exist in a particular node, it will be treated as a PQ type node with zero power injection. Practical design considerations impose limits in the amount of reactive power that a generator can either supply or absorb. If such limits are violated, the generator will be unable to regulate the nodal voltage magnitude. To represent this practical operational condition in the power flow algorithm, the node will change from PV to PQ type.
3. *Slack node*. The third kind of node in a power flow study is the Slack node. In conventional power flow studies one node is specified to be the Slack node. The need for a Slack node arises from the fact that both the active and reactive losses in the power network are not known prior to the power flow solution. The generator connected to the Slack node will generate enough power to meet the transmission losses and to pick up any demand surplus which the other generators in the network might not have been able to meet. To a certain extent the specification of the Slack node is arbitrary, as long as there is sufficient generation available in that node, or as long as such a node is a grid supply point. In this kind

of node the voltage magnitude and phase angle are known variables, whilst the active and reactive powers are the unknown variables.

4.4.2 Conventional power plant representation

Alternating current power transmission networks are designed and operated in a three-phase manner. However, for the purpose of conventional power flow studies, a perfect geometric balance between all three phases of the power network is assumed to exist. In most cases this is a reasonable assumption, and allows the analysis to be carried out on a per-phase basis, using only the positive sequence parameters of the power plant components. More realistic, though more time consuming solutions may be achieved by means of three-phase power flow studies.

The plant components of the electrical power network normally represented in power flow studies are generators, transformers, transmission lines, loads and passive shunt and series compensation. Substation busbars are represented as buses, i.e. nodal points in the power network. Nodal transfer admittance representations are used for transmission lines and transformers whereas generators and loads are represented by sources/sinks of active and reactive power.

A generic node, say node l, including generation, load, transmission lines and active and reactive power flows is shown in Figure 4.10. In this figure, the generator injects active and reactive powers into node l whereas the load draws active and reactive powers from the node. The figure also indicates that active and reactive powers flow from node l to node k, active and reactive powers flow from node n to node l, active power flows from node l to node m and reactive power flows from node m to node l.

The nominal π-circuit shown in Figure 4.11 is used to derive the transfer admittance matrix of the transmission line model used in fundamental frequency studies.

$$\begin{bmatrix} I_l \\ I_m \end{bmatrix} = \begin{bmatrix} \frac{1}{R+jX_l} + \frac{jB_c}{2} & -\frac{1}{R+jX_l} \\ -\frac{1}{R+jX_l} & \frac{1}{R+jX_l} + \frac{jB_c}{2} \end{bmatrix} \begin{bmatrix} V_l \\ V_m \end{bmatrix} \tag{4.28}$$
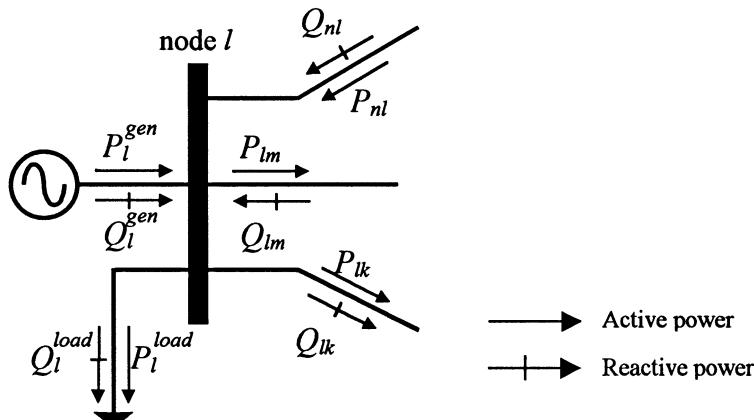

**Fig. 4.10** Generic node of the electrical power network.
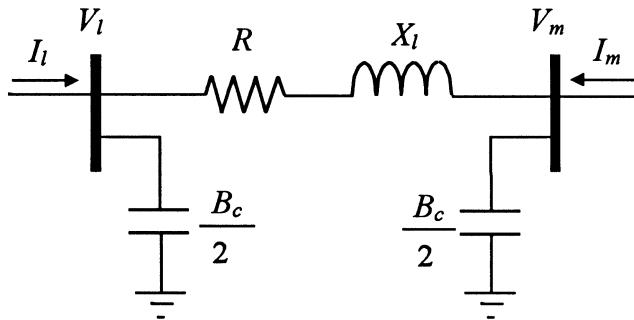
Fig. 4.11 Nominal π representation of the transmission line.
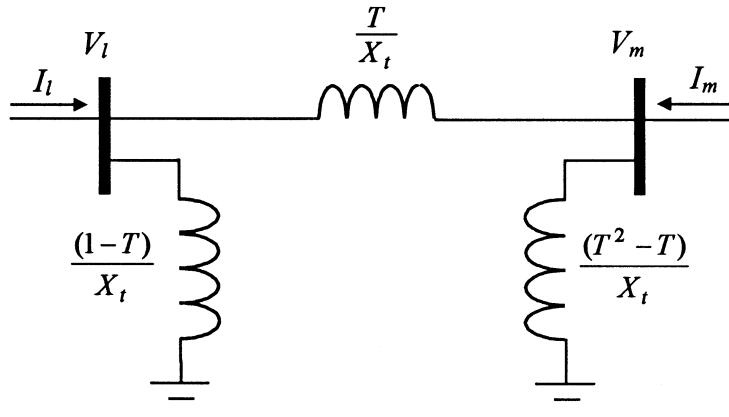

Fig. 4.12 Circuit representation of tap-changing transformer.

In power flow studies, the transformer is normally represented only by its leakage reactance X_t, i.e. the resistance is neglected. The π-circuit shown in Figure 4.12 is used to derive the transfer admittance of a transformer with off-nominal tap setting T:1.

$$\begin{bmatrix} I_l \\ I_m \end{bmatrix} = \begin{bmatrix} \frac{1}{jX_t} & -\frac{T}{jX_t} \\ -\frac{T}{jX_t} & \frac{T^2}{jX_t} \end{bmatrix} \begin{bmatrix} V_l \\ V_m \end{bmatrix} \tag{4.29}$$

Series compensation is represented by a capacitive reactance X_c connected between nodes l and m, as shown in Figure 4.13. The transfer admittance of the series capacitor is,

$$\begin{bmatrix} I_l \\ I_m \end{bmatrix} = \begin{bmatrix} -\frac{1}{jX_c} & \frac{1}{jX_c} \\ \frac{1}{jX_c} & -\frac{1}{jX_c} \end{bmatrix} \begin{bmatrix} V_l \\ V_m \end{bmatrix} \tag{4.30}$$

By way of example, the nodal admittance matrix of the three-node network shown in Figure 4.14 is given as

$$\begin{bmatrix} I_1 \\ I_2 \\ I_3 \end{bmatrix} = \begin{bmatrix} \frac{1}{jX_t} & -\frac{T}{jX_t} & 0 \\ -\frac{T}{jX_t} & \frac{T^2}{jX_t} + \frac{1}{R+jX_l} + \frac{jB_c}{2} & -\frac{1}{R+jX_l} \\ 0 & -\frac{1}{R+jX_l} & \frac{1}{R+jX_l} + \frac{jB_c}{2} - \frac{1}{jX_c} \end{bmatrix} \begin{bmatrix} V_1 \\ V_2 \\ V_3 \end{bmatrix} \tag{4.31}$$
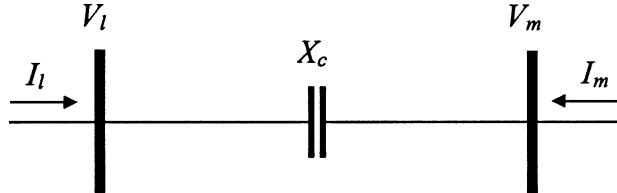
**Fig. 4.13** Representation of series capacitor.
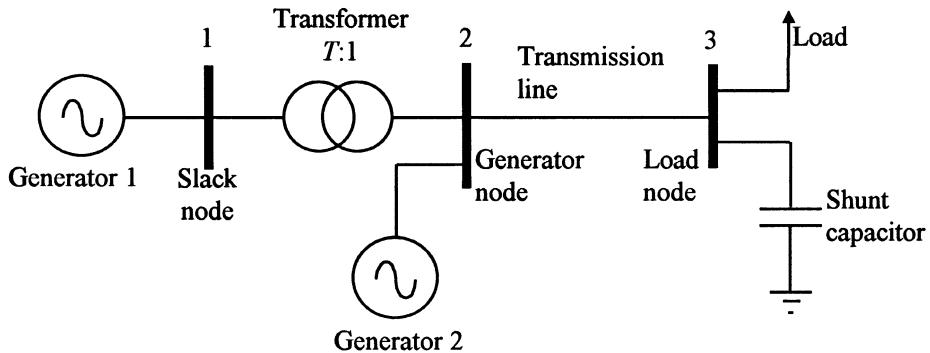
Fig. 4.14 A three-node test system.

It should be mentioned that in power flow studies the contribution of generators and loads is made through the vector of nodal currents as opposed to the nodal admittance matrix. In this example, the admittance elements in equation (4.29) were placed in locations $(1, 1)$, $(1, 2)$, $(2, 1)$ and $(2, 2)$ of the matrix in equation (4.31) since the transformer is connected between nodes one and two of the network. Similarly, the admittances in equation (4.28) were placed in locations $(2, 2)$, $(2, 3)$, $(3, 2)$ and $(3, 3)$ since the transmission line is connected between nodes 2 and 3. The contribution of the shunt capacitor is only in location $(3, 3)$. It should be noted that zero entries exist in locations $(1, 3)$ and $(3, 1)$ since there is no transmission element directly linking nodes one and three in this network.

4.4.3 Nodal impedance based power flow method

Power flow solutions may be achieved quite simply by using equation (4.18), which is the nodal admittance matrix equation of the network. The simplest case corresponds to a power network where only one generator exists in the system. By definition, this would be the Slack generator and the voltage magnitude and phase angle become known at its point of connection, say node one,

$$
\begin{bmatrix} I_1 \\ I_2 \\ I_3 \\ \vdots \\ I_n \end{bmatrix} = \begin{bmatrix} Y_{11} & Y_{12} & Y_{13} & \cdots & Y_{1n} \\ Y_{21} & Y_{22} & Y_{23} & \cdots & Y_{2n} \\ Y_{31} & Y_{32} & Y_{33} & \cdots & Y_{3n} \\ \vdots & \vdots & \vdots & \ddots & \vdots \\ Y_{n1} & Y_{n2} & Y_{n3} & \cdots & Y_{nn} \end{bmatrix} \begin{bmatrix} V_1 \\ V_2 \\ V_3 \\ \vdots \\ V_n \end{bmatrix} \tag{4.32}
$$

This equation may be partitioned as follows

$$[I_1] = [Y_{11}][V_1] + [Y_{12} \ Y_{13} \cdots Y_{1n}] \begin{bmatrix} V_2 \\ V_3 \\ \vdots \\ V_n \end{bmatrix} \tag{4.33}$$

$$\begin{bmatrix} I_2 \\ I_3 \\ \vdots \\ I_n \end{bmatrix} = \begin{bmatrix} Y_{21} \\ Y_{31} \\ \vdots \\ Y_{n1} \end{bmatrix} [V_1] + \begin{bmatrix} Y_{22} & Y_{23} & \cdots & Y_{2n} \\ Y_{32} & Y_{33} & \cdots & Y_{3n} \\ \vdots & \vdots & \ddots & \vdots \\ Y_{n2} & Y_{n3} & \cdots & Y_{nn} \end{bmatrix} \begin{bmatrix} V_2 \\ V_3 \\ \vdots \\ V_n \end{bmatrix} \tag{4.34}$$

Equation (4.34), in rearranged form, is used to find the solution for the unknown $n - 1$ nodal complex voltages by iteration

$$\begin{bmatrix} V_2 \\ V_3 \\ \vdots \\ V_n \end{bmatrix}^{(r+1)} = \begin{bmatrix} Z_{22} & Z_{23} & \cdots & Z_{2n} \\ Z_{32} & Z_{33} & \cdots & Z_{3n} \\ \vdots & \vdots & \ddots & \vdots \\ Z_{n2} & Z_{n3} & \cdots & Z_{nn} \end{bmatrix} \left\{ \begin{bmatrix} I_2 \\ I_3 \\ \vdots \\ I_n \end{bmatrix}^{(r)} - \begin{bmatrix} Y_{21} \\ Y_{31} \\ \vdots \\ Y_{n1} \end{bmatrix} [V_1] \right\} \tag{4.35}$$

where (r) is an iteration counter and V_1 is the complex voltage at the Slack node. The voltage phase angle at this node is normally specified to be 0 and provides a reference for the remaining $n - 1$ voltage phase angles in the network. The voltage magnitude is also specified at this node.

The vector of complex current injections is obtained from the active and reactive powers consumed by the $n - 1$ loads and voltage information calculated at the previous iteration

$$\begin{bmatrix} I_2 \\ I_3 \\ \vdots \\ I_n \end{bmatrix}^{(r)} = \begin{bmatrix} -(P_2^{\text{load}} - jQ_2^{\text{load}})/V_2^{*(r)} \\ -(P_3^{\text{load}} - jQ_3^{\text{load}})/V_3^{*(r)} \\ \vdots \\ -(P_n^{\text{load}} - jQ_n^{\text{load}})/V_n^{*(r)} \end{bmatrix} \tag{4.36}$$

The voltages $V_2, \ldots V_n$ are not known at the beginning and initial estimates are given to these nodes to start the iterative process. It should be noted that the current expressions in equation (4.36) are derived from the complex power equation, i.e. $S = VI^*$, and that the negative sign outside the parentheses is due to the fact that the loads consume power. The symbol $*$ is used to denote the conjugate complex operation.

The convergence characteristic of equation (4.35) is reasonably good for small and medium size systems. Although limited to networks containing only one generator, the method has found application in industrial systems where the Slack node is the electricity company's infeed point to the plant. Equation (4.35) may also be modified to include voltage-controlled nodes (Stagg and El-Abiad, 1968) but it has been found that its convergence characteristic deteriorates rapidly with the number of voltage-controlled nodes in the network. In spite of its simplicity and intuitive appeal, this has prevented its use in most practical applications. To overcome this limitation,

the Newton–Raphson algorithm and derived formulations have been used instead (Tinney and Hart, 1967; Peterson and Scott-Meyer, 1971).

The issue of convergence has become even more critical today, with the wide range of power systems controllers that need inclusion in power flow computer algorithms (Fuerte-Esquivel, 1997; Ambriz-Perez, 1998). As outlined in Section 4.2, the new controllers regulate not just voltage magnitude but also voltage phase angle, impedance magnitude and active and reactive power flow. It is unlikely that the nodal impedance based method would be able to cope with the very severe demands imposed by the models of the new controllers on the power flow algorithms. Intensive research work has shown the Newton–Raphson algorithm to be the most reliable vehicle for solving FACTS upgraded networks (Acha et al., 2000; Ambriz-Perez et al., 2000; Fuerte-Esquivel et al., 2000), with other formulations derived from the Newton–Raphson method becoming viable but less desirable alternatives (Acha, 1993; Noroozian and Andersson, 1993).

4.4.4 Newton–Raphson power flow method

The equation describing the complex power injection at node l is the starting point for deriving nodal active and reactive power flow equations suitable for the Newton–Raphson power flow Algorithm (Tinney and Hart, 1967)

$$S_l = P_l + jQ_l = V_l I_l^* \tag{4.37}$$

where S_l is the complex power injection at node l,
P_l is the active power injection at node l,
Q_l is the reactive power injection at node l,
V_l is the complex voltage at node l and
I_l is the complex current injection at node l.

The injected current I_l may be expressed as a function of the currents flowing in the n branches connected to node l,

$$I_l = \sum_{m=1}^{n} Y_{lm} V_m \tag{4.38}$$

where $Y_{lm} = G_{lm} + jB_{lm}$ and Y_{lm}, G_{lm} and B_{lm} are the admittance, conductance and susceptance of branch l–m, respectively.

Substitution of equation (4.38) into equation (4.37) gives the following intermediate result

$$P_l + jQ_l = V_l \sum_{m=1}^{n} Y_{lm}^* V_m^* \tag{4.39}$$

Expressions for the active and reactive powers are obtained by representing the complex voltages in polar form, $V_l = |V_l| e^{j\theta_l}$ and $V_m = |V_m| e^{j\theta_m}$

$$P_l + jQ_l = |V_l| \sum_{m=1}^{n} |V_m|(G_{lm} - jB_{lm}) e^{j(\theta_l - \theta_m)} \tag{4.40}$$

$$P_l + jQ_l = |V_l| \sum_{m=1}^{n} |V_m|(G_{lm} - jB_{lm})\{\cos(\theta_l - \theta_m) + j\sin(\theta_l - \theta_m)\} \tag{4.41}$$

$$P_l = |V_l| \sum_{m=1}^{n} |V_m| \{ G_{lm} \cos(\theta_l - \theta_m) + B_{lm} \sin(\theta_l - \theta_m) \tag{4.42}$$

$$Q_l = |V_l| \sum_{m=1}^{n} |V_m| \{ G_{lm} \sin(\theta_l - \theta_m) - B_{lm} \cos(\theta_l - \theta_m) \tag{4.43}$$

where $|V_l|$ and $|V_m|$ are the nodal voltage magnitudes at nodes l and m and θ_l and θ_m are the nodal voltage phase angles at nodes l and m.

These equations provide a convenient device for assessing the steady state behaviour of the power network. The equations are non-linear and their solution is reached by iteration. Two of the variables are specified while the remaining two variables are determined by calculation to a specified accuracy. In PQ type nodes two equations are required since the voltage magnitude and phase angle $|V_l|$ and θ_l are not known. The active and reactive powers P_l and Q_l are specified. In PV type nodes one equation is required since only the voltage phase angle θ_l is unknown. The active power P_l and voltage magnitude $|V_l|$ are specified. For the case of the Slack node both the voltage magnitude and phase angle $|V_l|$ and θ_l are specified, as opposed to being determined by iteration. Accordingly, no equations are required for this node during the iterative step.

Equations (4.42) and (4.43) can be solved efficiently using the Newton–Raphson method. It requires a set of linearized equations to be formed expressing the relationship between changes in active and reactive powers and changes in nodal voltage magnitudes and phase angles. Under the assumption that node one is the Slack node, the linearized relationship takes the following form for an n-node network

$$
\begin{bmatrix}
\Delta P_2 \\
\Delta P_3 \\
\vdots \\
\Delta P_n \\
\hline
\Delta Q_2 \\
\Delta Q_3 \\
\vdots \\
\Delta Q_n
\end{bmatrix}^{(r)}
=
\begin{bmatrix}
\frac{\partial P_2}{\partial \theta_2} & \frac{\partial P_2}{\partial \theta_3} & \cdots & \frac{\partial P_2}{\partial \theta_n} & \frac{\partial P_2}{\partial |V_2|} & \frac{\partial P_2}{\partial |V_3|} & \cdots & \frac{\partial P_2}{\partial |V_n|} \\
\frac{\partial P_3}{\partial \theta_2} & \frac{\partial P_3}{\partial \theta_3} & \cdots & \frac{\partial P_3}{\partial \theta_n} & \frac{\partial P_3}{\partial |V_2|} & \frac{\partial P_3}{\partial |V_3|} & \cdots & \frac{\partial P_3}{\partial |V_n|} \\
\vdots & \vdots & \ddots & \vdots & \vdots & \vdots & \ddots & \vdots \\
\frac{\partial P_n}{\partial \theta_2} & \frac{\partial P_n}{\partial \theta_3} & \cdots & \frac{\partial P_n}{\partial \theta_n} & \frac{\partial P_n}{\partial |V_2|} & \frac{\partial P_n}{\partial |V_3|} & \cdots & \frac{\partial P_n}{\partial |V_n|} \\
\hline
\frac{\partial Q_2}{\partial \theta_2} & \frac{\partial Q_2}{\partial \theta_3} & \cdots & \frac{\partial Q_2}{\partial \theta_n} & \frac{\partial Q_2}{\partial |V_2|} & \frac{\partial Q_2}{\partial |V_3|} & \cdots & \frac{\partial Q_2}{\partial |V_n|} \\
\frac{\partial Q_3}{\partial \theta_2} & \frac{\partial Q_3}{\partial \theta_3} & \cdots & \frac{\partial Q_3}{\partial \theta_n} & \frac{\partial Q_3}{\partial |V_2|} & \frac{\partial Q_3}{\partial |V_3|} & \cdots & \frac{\partial Q_3}{\partial |V_n|} \\
\vdots & \vdots & \ddots & \vdots & \vdots & \vdots & \ddots & \vdots \\
\frac{\partial Q_n}{\partial \theta_2} & \frac{\partial Q_n}{\partial \theta_3} & \cdots & \frac{\partial Q_n}{\partial \theta_n} & \frac{\partial Q_n}{\partial |V_2|} & \frac{\partial Q_n}{\partial |V_3|} & \cdots & \frac{\partial Q_n}{\partial |V_n|}
\end{bmatrix}^{(r)}
\begin{bmatrix}
\Delta \theta_2 \\
\Delta \theta_3 \\
\vdots \\
\Delta \theta_n \\
\hline
\Delta |V_2| \\
\Delta |V_3| \\
\vdots \\
\Delta |V_n|
\end{bmatrix}^{(r)}
\tag{4.44}
$$

where

$\Delta P_l = P_l^{\text{net}} - P_l^{\text{calc}}$ is the active power mismatch at node l,

$\Delta Q_l = Q_l^{\text{net}} - Q_l^{\text{calc}}$ is the reactive power mismatch at node l,

P_l^{calc} and Q_l^{calc} are the calculated active and reactive powers at node l,

$P_l^{\text{net}} = P_l^{\text{gen}} - P_l^{\text{load}}$ is the net scheduled active powers at node l,

$Q_l^{\text{net}} = Q_l^{\text{gen}} - Q_l^{\text{load}}$ is the net scheduled reactive powers at node l,

P_l^{gen} and Q_l^{gen} are the active and reactive powers generated at node l,

P_l^{load} and Q_l^{load} are the active and reactive powers consumed by the load at node l,

$\Delta\theta_l$ and $\Delta|V_l|$ are the incremental changes in nodal voltage magnitude and phase angle at node l,

(r) represents the r-th iterative step and $l = 2, 3, 4, \ldots n$.

The elements of the Jacobian matrix can be found by differentiating equations (4.42) and (4.43) with respect to θ_l, θ_m, $|V_l|$ and $|V_m|$.

For the case when $l = m$:

$$\frac{\partial P_l}{\partial \theta_l} = |V_l| \sum_{m=l}^{n} |V_m|\{-G_{lm}\sin(\theta_l - \theta_m) + B_{lm}\cos(\theta_l - \theta_m)\} - |V_l|^2 B_{ll} = -Q_l - |V_l|^2 B_{ll}$$

(4.45)

$$\frac{\partial P_l}{\partial |V_l|} = \sum_{m=l}^{n} |V_m|\{G_{lm}\cos(\theta_l - \theta_m) + B_{lm}\sin(\theta_l - \theta_m)\} + |V_l|G_{ll} = \frac{P_l}{|V_l|} + |V_l|G_{ll} \quad (4.46)$$

$$\frac{\partial Q_l}{\partial \theta_l} = |V_l| \sum_{m=l}^{n} |V_m|\{G_{lm}\cos(\theta_l - \theta_m) + B_{lm}\sin(\theta_l - \theta_m)\} - |V_l|^2 G_{ll} = P_l - |V_l|^2 G_{ll}$$

(4.47)

$$\frac{\partial Q_l}{\partial |V_l|} = \sum_{m=l}^{n} |V_m|\{G_{lm}\sin(\theta_l - \theta_m) - B_{lm}\cos(\theta_l - \theta_m)\} - |V_l|B_{ll} = \frac{Q_l}{|V_l|} - |V_l|B_{ll}$$

(4.48)

For the case when $l \neq m$

$$\frac{\partial P_l}{\partial \theta_m} = |V_l||V_m|\{G_{lm}\sin(\theta_l - \theta_m) - B_{lm}\cos(\theta_l - \theta_m)\} \quad (4.49)$$

$$\frac{\partial P_l}{\partial |V_m|} = |V_l|\{G_{lm}\cos(\theta_l - \theta_m) + B_{lm}\sin(\theta_l - \theta_m)\} = -\frac{1}{|V_m|}\frac{\partial Q_l}{\partial \theta_m} \quad (4.50)$$

$$\frac{\partial Q_l}{\partial \theta_m} = -|V_l||V_m|\{G_{lm}\cos(\theta_l - \theta_m) + B_{lm}\sin(\theta_l - \theta_m)\} \quad (4.51)$$

$$\frac{\partial Q_l}{\partial |V_m|} = |V_l|\{G_{lm}\sin(\theta_l - \theta_m) - B_{lm}\cos(\theta_l - \theta_m)\} = \frac{1}{|V_m|}\frac{\partial P_l}{\partial \theta_m} \quad (4.52)$$

To start the iterative solution, initial estimates of the nodal voltage magnitudes and phase angles at all the PQ nodes and voltage phase angles at all the PV nodes are given to calculate the active and reactive power injections using equations (4.42–4.43). Since it is unlikely that the initial estimated voltages will agree with the voltages at the solution point, the calculated power injections will not agree with the known specified powers.

The mismatch power vectors may be defined as

$$\Delta\mathbf{P}^{(r)} = (\mathbf{P}^{\text{gen}} - \mathbf{P}^{\text{load}}) - \mathbf{P}^{\text{calc},(r)} = \mathbf{P}^{\text{net}} - \mathbf{P}^{\text{calc},(r)} \quad (4.53)$$
$$\Delta\mathbf{Q}^{(r)} = (\mathbf{Q}^{\text{gen}} - \mathbf{Q}^{\text{load}}) - \mathbf{Q}^{\text{calc},(r)} = \mathbf{Q}^{\text{net}} - \mathbf{Q}^{\text{calc},(r)} \quad (4.54)$$

The Jacobian elements are then calculated and the linearized equation (4.44) is solved to obtain the vectors of voltage updates

$$\boldsymbol{\theta}^{(r+1)} = \boldsymbol{\theta}^{(r)} + \Delta\boldsymbol{\theta}^{(r)} \quad (4.55)$$
$$|\boldsymbol{V}|^{(r+1)} = |\boldsymbol{V}|^{(r)} + \Delta|\boldsymbol{V}|^{(r)} \quad (4.56)$$

The evaluation of equations (4.42)–(4.44) and (4.53)–(4.56) are repeated in sequence until the desired change in power injection (power mismatch) ΔP and ΔQ are within a small tolerance, e.g. $\varepsilon = 10^{-12}$

As the process approaches the solution, the linearized equation (4.44) becomes more and more accurate and convergence is very rapid. Figure 4.15 gives the overall flow diagram for the power flow Newton–Raphson method.
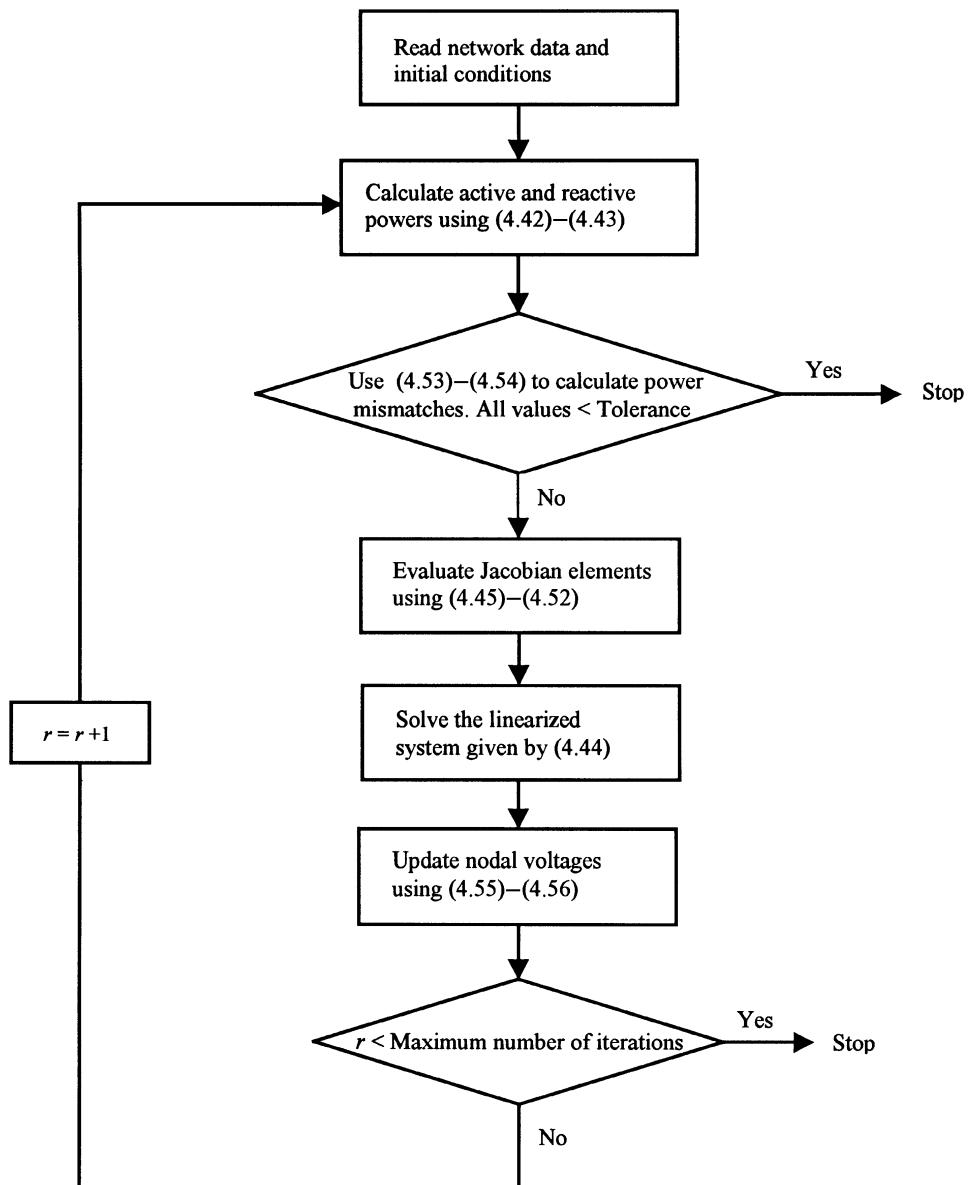

Fig. 4.15 Flow diagram for power flow Newton–Raphson method.

4.4.5 Numerical example 3

The power transmission circuit shown in Figure 4.16 consists of two nodes, one generator, one transmission line and one load. The load has a value of $1 + j0.5$ p.u. and the reactance of the transmission line is 0.1 p.u. The voltage magnitude and phase angle at the generator point (Slack node) are kept at 1 p.u. and 0 radians, respectively.

Using the Newton–Raphson power flow method, the nodal voltage magnitude and phase angle at node two will be determined using 1 p.u. voltage magnitude and zero phase angle at the load point as the initial condition.

Applying the theory presented in Section 4.3, the nodal admittance matrix is formed for this system

$$\mathbf{Y} = \mathbf{G} + j\mathbf{B} = \begin{bmatrix} -j10 & j10 \\ j10 & -j10 \end{bmatrix} \text{p.u.}$$

The net active and reactive powers are calculated

$$\mathbf{P}^{\text{net}} = \mathbf{P}^{\text{gen}} - \mathbf{P}^{\text{load}} = \begin{bmatrix} ? \\ -1 \end{bmatrix} \text{p.u.} \qquad \mathbf{Q}^{\text{net}} = \mathbf{Q}^{\text{gen}} - \mathbf{Q}^{\text{load}} = \begin{bmatrix} ? \\ -0.5 \end{bmatrix} \text{p.u.}$$

First iteration

Using the initial voltage values $|V_1| = |V_2| = 1$, $\theta_1 = \theta_2 = 0$ and the values in the nodal admittance matrix in equations (4.42) and (4.43), the following powers are calculated

$$
\begin{aligned}
P_2^{\text{calc}} &= |V_2||V_1|\{G_{21}\cos(\theta_2 - \theta_1) + B_{21}\sin(\theta_2 - \theta_1)\} \\
&\quad + |V_2||V_2|\{G_{22}\cos(\theta_2 - \theta_2) + B_{22}\sin(\theta_2 - \theta_2)\} = 0 \\
Q_2^{\text{calc}} &= |V_2||V_1|\{G_{21}\sin(\theta_2 - \theta_1) - B_{21}\cos(\theta_2 - \theta_1)\} \\
&\quad + |V_2||V_2|\{G_{22}\sin(\theta_2 - \theta_2) - B_{22}\cos(\theta_2 - \theta_2)\} = 0
\end{aligned}
\tag{4.57}
$$
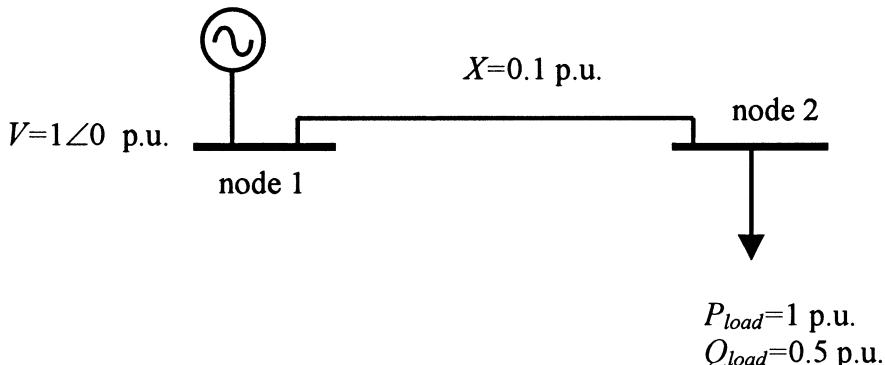
Fig. 4.16 A two-node system.

According to equations (4.53) and (4.54), the mismatch power equations are

$$\begin{bmatrix} \Delta P_1 \\ \Delta P_2 \end{bmatrix}^{(1)} = \begin{bmatrix} P_1^{net} \\ P_2^{net} \end{bmatrix} - \begin{bmatrix} P_1^{calc} \\ P_2^{calc} \end{bmatrix} = \begin{bmatrix} ? \\ -1 \end{bmatrix} \text{p.u.}$$

$$\begin{bmatrix} \Delta Q_1 \\ \Delta Q_2 \end{bmatrix}^{(1)} = \begin{bmatrix} Q_1^{net} \\ Q_2^{net} \end{bmatrix} - \begin{bmatrix} Q_1^{calc} \\ Q_2^{calc} \end{bmatrix} = \begin{bmatrix} ? \\ -0.5 \end{bmatrix} \text{p.u.}$$

(4.58)

The Slack node plays no role during the iterative solution. Using equations (4.45)–(4.52), and the numeric values $P_2^{calc} = 0$ and $Q_2^{calc} = 0$ calculated above, the Jacobian elements for node two are

$$\frac{\partial P_2}{\partial \theta_2} = 10 \qquad \frac{\partial P_2}{\partial |V_2|} = 0 \qquad \frac{\partial Q_2}{\partial \theta_2} = 0 \qquad \frac{\partial Q_2}{\partial |V_2|} = 10$$

The solution of the linearized system of equations is

$$\begin{bmatrix} \Delta P_2 \\ \Delta Q_2 \end{bmatrix}^{(1)} = \begin{bmatrix} 10 & 0 \\ 0 & 10 \end{bmatrix} \begin{bmatrix} \Delta \theta_2 \\ \Delta |V_2| \end{bmatrix}^{(1)} \Rightarrow \begin{bmatrix} \Delta \theta_2 \\ \Delta |V_2| \end{bmatrix}^{(1)} = \begin{bmatrix} 0.1 & 0 \\ 0 & 0.1 \end{bmatrix} \begin{bmatrix} -1 \\ -0.5 \end{bmatrix} = \begin{bmatrix} -0.1 \\ -0.05 \end{bmatrix} \quad (4.59)$$

Using equations (4.55) and (4.56) the voltage magnitude and phase angle at the end of the first iteration are

$$\begin{bmatrix} \theta_2 \\ |V_2| \end{bmatrix}^{(1)} = \begin{bmatrix} 0 \\ 1 \end{bmatrix}^{(0)} + \begin{bmatrix} -0.1 \\ -0.05 \end{bmatrix}^{(1)} = \begin{bmatrix} -0.1 \\ 0.95 \end{bmatrix} \text{p.u.} \qquad (4.60)$$

It should be noted that the voltage magnitude is in p.u. and the phase angle is in radians.

Second iteration

Using updated voltage information, i.e. $|V_1| = 1$, $|V_2| = 0.95$, $\theta_1 = 0$ and $\theta_2 = -0.1$, in equations (4.42) and (4.43), new active and reactive powers are calculated, giving the following result

$$P_2^{calc} = -0.94841 \text{ p.u.}$$

$$Q_2^{calc} = -0.4275 \text{ p.u.}$$

The mismatch power equations are

$$\begin{bmatrix} \Delta P_1 \\ \Delta P_2 \end{bmatrix}^{(2)} = \begin{bmatrix} P_1^{net} \\ P_2^{net} \end{bmatrix} - \begin{bmatrix} P_1^{calc} \\ P_2^{calc} \end{bmatrix} = \begin{bmatrix} ? \\ -1 \end{bmatrix} - \begin{bmatrix} ? \\ -0.948417 \end{bmatrix} = \begin{bmatrix} ? \\ -0.051583 \end{bmatrix} \text{p.u.}$$

$$\begin{bmatrix} \Delta Q_1 \\ \Delta Q_2 \end{bmatrix}^{(2)} = \begin{bmatrix} Q_1^{net} \\ Q_2^{net} \end{bmatrix} - \begin{bmatrix} Q_1^{calc} \\ Q_2^{calc} \end{bmatrix} = \begin{bmatrix} ? \\ -0.5 \end{bmatrix} - \begin{bmatrix} ? \\ -0.42754 \end{bmatrix} = \begin{bmatrix} ? \\ -0.07246 \end{bmatrix} \text{p.u.}$$

(4.61)

It should be noted that the power mismatches have decreased by almost one order of magnitude compared to the mismatch values obtained during the first iteration.

The Jacobian elements for node two are:

$$\frac{\partial P_2}{\partial \theta_2} = 9.45254 \qquad \frac{\partial P_2}{\partial |V_2|} = -0.998334 \qquad \frac{\partial Q_2}{\partial \theta_2} = -0.948417 \qquad \frac{\partial Q_2}{\partial |V_2|} = 8.574958$$

The solution of the linearized system of equations is

$$\begin{bmatrix} \Delta P_2 \\ \Delta Q_2 \end{bmatrix}^{(2)} = \begin{bmatrix} 9.45254 & -0.998334 \\ -0.948417 & 8.574958 \end{bmatrix} \begin{bmatrix} \Delta \theta_2 \\ \Delta |V_2| \end{bmatrix}^{(2)}$$

$$\begin{bmatrix} \Delta \theta_2 \\ \Delta |V_2| \end{bmatrix}^{(2)} = \begin{bmatrix} 0.107042 & 0.012462 \\ 0.011839 & 0.117996 \end{bmatrix} \begin{bmatrix} -0.051583 \\ -0.07246 \end{bmatrix} = \begin{bmatrix} -0.006425 \\ -0.009161 \end{bmatrix} \tag{4.62}$$

The voltage magnitude and phase angle at node two at the end of the second iteration are

$$\begin{bmatrix} \theta_2 \\ |V_2| \end{bmatrix}^{(2)} = \begin{bmatrix} -0.1 \\ 0.95 \end{bmatrix}^{(1)} + \begin{bmatrix} -0.006425 \\ -0.009161 \end{bmatrix}^{(2)} = \begin{bmatrix} -0.106425 \\ 0.940839 \end{bmatrix} \tag{4.63}$$

At this stage, the complex voltages at nodes one and two are

$$\begin{bmatrix} V_1 \\ V_2 \end{bmatrix}^{(2)} = \begin{bmatrix} 1\angle 0 \\ 0.940839\angle -0.106425 \end{bmatrix} \text{p.u.} \tag{4.64}$$

These voltages are quite close to the actual solution. If the procedure is repeated for two more iterations then ΔP_2 and ΔQ_2 become smaller than 10^{-6}.

4.4.6 Numerical example 4

The test system shown in Figure 4.17 is used in this example (Stagg and El-Abiad, 1968). The original figure has been redrawn to accommodate the power flow results. In subsequent examples in this chapter, the system is used in modified form, to illustrate how the various FACTS controllers perform in network-wide applications.

The original test system is solved using a power flow computer program written in C + + using object-oriented programming (OOP) techniques (Fuerte-Esquivel, 1997). The power flow results are shown on Figure 4.17 and the nodal voltage magnitudes and phase angles are given in Table 4.1. The network parameters required for the power flow study are given in Tables 4.2–4.4. This power flow solution will be used as the base case against which all other solutions will be compared.

In conventional power flow calculations, generators are set to generate a pre-specified amount of active power, except the Slack generator which is left free, since it has to generate sufficient active power to meet any shortfall in system generation. It will also generate or absorb any reactive power excess in the system. In this example, the generator connected at the North node is selected to be the Slack generator, generating 131.12 MW and 90.81 MVAr. The voltage magnitude was kept at 1.06 p.u and the voltage phase angle at 0°. The generator connected at the South node was set to generate 40 MW and the power flow solution indicates that it absorbs 61.59 MVAr to keep the nodal voltage magnitude at the specified value of 1 p.u. The remaining three nodes contain no equipment to provide local reactive support and their nodal
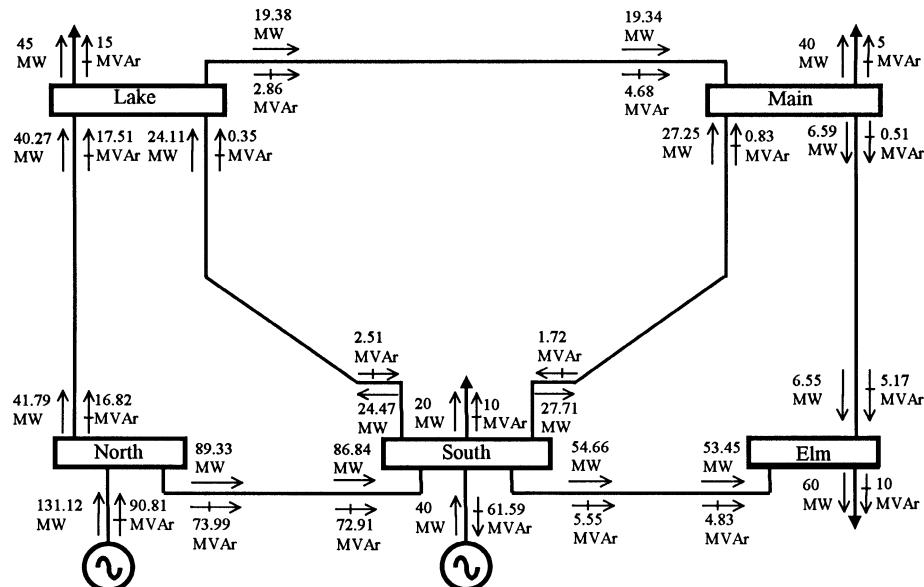
Fig. 4.17 Test network and power flow results for base case.

Table 4.1 Nodal complex voltages of original network

Voltage information	System nodes				
	North	South	Lake	Main	Elm
$|V|$ (p.u.)	1.06	1	0.987	0.984	0.972
θ (degrees)	0	-2.06	-4.64	-4.96	-5.77

Table 4.2 Network connectivity and transmission line parameters

Sending node	Receiving node	R (p.u.)	X (p.u.)	B (p.u.)
North	South	0.02	0.06	0.06
North	Lake	0.08	0.24	0.05
South	Lake	0.06	0.18	0.04
South	Main	0.06	0.18	0.04
South	Elm	0.04	0.12	0.03
Lake	Main	0.01	0.03	0.02
Main	Elm	0.08	0.24	0.05

Table 4.3 Generator parameters

Node	P_G(MW)	Q_{min}(MVAr)	Q_{max}(MVAr)	$|V|$(p.u.)
South	40	-300	300	1

Table 4.4 Load parameters

Node	P_{load}(MW)	Q_{load}(MVAr)
South	20	10
Lake	45	15
Main	40	5
Elm	60	10

voltage magnitudes drop below 1 p.u. However, they keep above 0.95 p.u., which is the minimum accepted value by most electricity companies. So, the power network does not seem to be in risk of undergoing voltage collapse at any point if an incremental load increase were to occur.

It should be noted that the maximum phase angle difference between any pair of adjacent nodes is smaller than 5°, which indicates that the power network is not over-stretched in terms of active power flows. The largest active power flow takes place in the transmission line connecting the North and South nodes: 89.33 MW leave the sending end of the transmission line and 86.84 MW reach the receiving end. The largest transmission active power loss also takes place in this transmission line, 2.49 MW. From the planning and operational point of view, this may be considered a good result. However, it should be pointed out that no attempt was made to optimize the performance of the operation. If an optimized solution is required, where generator fuel cost and transmission power loss are minimized then an optimal power flow algorithm (Ambriz-Perez, 1998) would be used as opposed to a conventional power flow algorithm (Fuerte-Esquivel, 1997).

4.5   Reactive power control

4.5.1   General aspects

In electric power systems, nodal voltages are significantly affected by load variations and by changes in transmission network topology. When the network is operating under heavy loading the voltage may drop considerably and even collapse. This will cause operation of under-voltage relays and other voltage sensitive controls, leading to extensive disconnection of loads, adversely affecting customers. On the other hand, when the level of load in the system is low, over-voltages may arise due to Ferranti effect in unloaded lines, leading to capacitive over-compensation and over-excitation of synchronous machines. Over-voltages cause equipment failures due to insulation breakdown and produce magnetic saturation in transformers, resulting in undesirable harmonic generation. Accordingly, voltage magnitudes throughout the network cannot deviate significantly from their nominal values if an efficient and reliable operation of the power system is to be achieved.

Traditionally, iron-cored inductors have been used to absorb reactive power, resulting in a reduction of the voltage level at the point of connection. Conversely, banks of capacitors have been used to supply reactive power resulting in a voltage level increase at the point of connection. When adaptive voltage regulation was required, synchronous condensers were employed. They generate and absorb reactive

power from the network depending on whether they are operated in an over-excited or in an under-excited mode, in a not dissimilar manner as synchronous generators do, except that they do not produce active power. Advances in power electronics together with sophisticated electronic control methods made possible the development of fast SVC equipment in the early 1970s, leading to a near displacement of the synchronous condenser (Miller, 1982). The most recent development in the area of electronically controlled shunt compensation is the STATCOM (Hingorani and Gyugyi, 2000). It is based on the VSC and combines the operational advantages of the rotating synchronous condenser and the SVC. For most practical purposes, it is expected to replace the SVC once the technology becomes more widely understood among practising engineers and prices drop.

4.5.2 SVC power flow modelling

There are several SVC models available in the open literature for power flow studies. In particular, the models recommended by Conférence Internationale des Grands Reseaux Électriques (CIGRE) (Erinmez, 1986; IEEE Special Stability Controls Working Group, 1995) are widely used. To a greater or lesser extent, these models are based on the premise that the SVC may be represented as a synchronous generator, i.e. synchronous condenser, behind an inductive reactance.

The simplest model represents the SVC as a generator with zero active power output and reactive power limits. The node at which the *generator* is connected is represented as a PV node. This assumption may be justified as long as the SVC operates within limits. However, gross errors may result if the SVC operates outside limits (Ambriz-Perez et al., 2000). An additional drawback of the SVC models based on the *generator* principle is that it assumes that the SVC draws constant reactive power in order to keep the voltage magnitude at the target value whereas, in practice, the SVC is an adjustable reactance, which is a function of voltage magnitude.

A simple and efficient way to model the SVC in a Newton–Raphson power flow algorithm is described in this section (Fuerte-Esquivel and Acha, 1997). It is based on the use of the variable susceptance concept, which it is adjusted automatically in order to achieve a specified voltage magnitude. The shunt susceptance represents the total SVC susceptance necessary to maintain the voltage magnitude at the specified value.

Its implementation in a Newton–Raphson power flow algorithm requires the introduction of an additional type of node, namely PVB (where P relates to active power, Q to reactive power and B to shunt susceptance). It is a controlled node where the nodal voltage magnitude and the nodal active and reactive powers are specified while the SVC's variable susceptance B_{SVC} is handled as state variable. If B_{SVC} is within limits, the specified voltage is attained and the controlled node remains PVB type. However, if B_{SVC} goes out of limits, B_{SVC} is fixed at the violated limit and the node becomes PQ type in the absence of any other regulating equipment connected to the node and capable of achieving voltage control.

As discussed in Section 4.2.1, the active and reactive powers drawn by a variable shunt compensator connected at node l are

$$P_l = 0$$
$$Q_l = -|V_l|^2 B_{\text{SVC}}$$

(4.65)

The linearized SVC equation is given below, where the variable susceptance B_{SVC} is taken to be the state variable

$$\begin{bmatrix} \Delta P_l \\ \Delta Q_l \end{bmatrix} = \begin{bmatrix} 0 & 0 \\ 0 & \frac{\partial Q_l}{\partial B_{SVC}} \end{bmatrix} \begin{bmatrix} \Delta \theta_l \\ \Delta B_{SVC} \end{bmatrix} \tag{4.66}$$

At the end of iteration (r), the variable shunt susceptance B_{SVC} is updated

$$B_{SVC}^{(r+1)} = B_{SVC}^{(r)} + \Delta B_{SVC}^{(r)} \tag{4.67}$$

4.5.3 Numerical example 5

The five-node network detailed in Section 4.4.6 is modified to include one SVC connected at node Lake to maintain the nodal voltage magnitude at 1 p.u. Convergence is obtained in four iterations to a power mismatch tolerance of $\varepsilon \leq 10^{-12}$ using an OOP Newton–Raphson power flow program (Fuerte-Esquivel et al., 1988). The power flow solution is shown in Figure 4.18 whereas the nodal voltage magnitudes and phase angles are given in Table 4.5.

The power flow result indicates that the SVC generates 20.5 MVAr in order to keep the voltage magnitude at 1 p.u. voltage magnitude at Lake node. The SVC installation results in an improved network voltage profile except in Elm, which is too far away from Lake node to benefit from the SVC influence.

The Slack generator reduces its reactive power generation by almost 6% compared to the base case and the reactive power exported from North to Lake reduces by more than 30%. The largest reactive power flow takes place in the transmission line connecting North and South, where 74.1 MVAr leaves North and 74 MVAr arrives at South. In general, more reactive power is available in the network than in the base case and the generator connected at South increases its share of reactive power
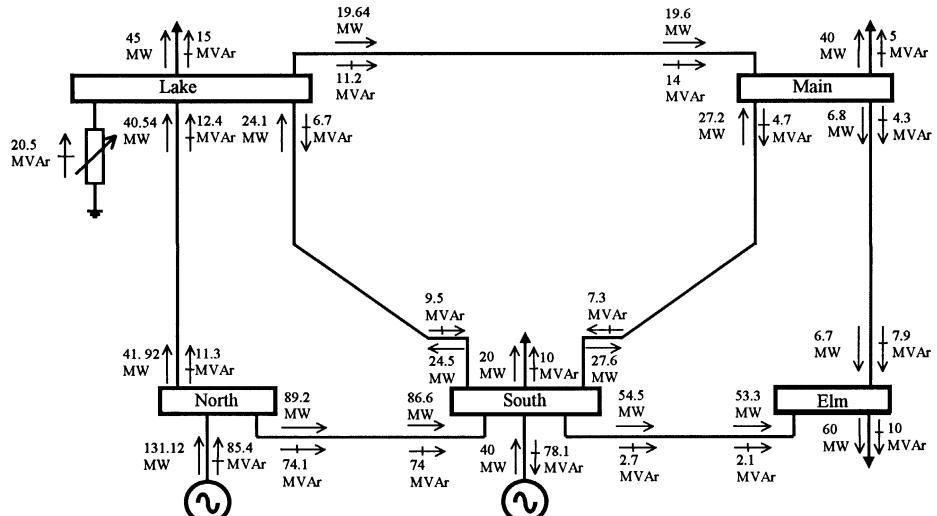
Fig. 4.18 SVC upgraded test network and power flow results.

Table 4.5 Nodal complex voltages of SVC upgraded network

Voltage information	System nodes				
	North	South	Lake	Main	Elm
$|V|$ (p.u.)	1.06	1	1	0.994	0.975
θ (degrees)	0	−2.05	−4.83	−5.11	−5.80

absorption compared to the base case. As expected, active power flows are only marginally affected by the SVC installation.

4.5.4 STATCOM power flow modelling

The STATCOM operational characteristic resembles that of an ideal synchronous machine that generates balanced, three-phase voltages with rapidly controllable amplitude and phase angle. Such a characteristic enables the STATCOM to be well represented in positive sequence power flow studies as a synchronous generator with zero active power generation and reactive power limits (IEEE/CIGRE, 1995).

The node at which the STATCOM is connected is represented as a PV node, which may change to a PQ node in the event of limits being violated. In such a case, the generated/absorbed reactive power would correspond to the violated limit. Contrary to the SVC, the STATCOM is represented as a voltage source for the full range of operation, enabling a more robust voltage support mechanism.

An alternative way to model the STATCOM in a Newton–Raphson power flow algorithm is described in this section. It is a simple and efficient model based on the use of a variable voltage source, which adjusts automatically in order to achieve a specified voltage magnitude. In this case, the node at which the STATCOM is connected is a controlled node where the nodal voltage magnitude and the nodal active and reactive powers are specified while the source voltage magnitude is handled as a state variable.

Based on the representation given in Figure 4.4, the following equation can be written

$$I_{vR} = Y_{vR}(V_{vR} - V_l) \tag{4.68}$$

where

$$Y_{vR} = \frac{1}{Z_{vR}} = G_{vR} + jB_{vR} \tag{4.69}$$

The active and reactive powers injected by the source may be derived using the complex power equation

$$S_{vR} = V_{vR}I_{vR}^* = V_{vR}Y_{vR}^*(V_{vR}^* - V_l^*) \tag{4.70}$$

Taking the variable voltage source to be $V_{vR} = |V_{vR}|(\cos\theta_{vR} + j\sin\theta_{vR})$, and after performing some complex operations, the following active and reactive power equations are obtained

$$P_{vR} = |V_{vR}|^2 G_{vR} - |V_{vR}||V_l|\{G_{vR}\cos(\theta_{vR} - \theta_l) + B_{vR}\sin(\theta_{vR} - \theta_l)\} \tag{4.71}$$

$$Q_{vR} = -|V_{vR}|^2 B_{vR} - |V_{vR}||V_l|\{G_{vR}\sin(\theta_{vR} - \theta_l) - B_{vR}\cos(\theta_{vR} - \theta_l)\} \tag{4.72}$$

If the STATCOM is connected at node l and it is assumed that its conductance is negligibly small and that there is no active power exchanged with the AC system, i.e. $G_{vR} = 0$ and $\theta_{vR} = \theta_l$

$$
\begin{aligned}
P_{vR} &= 0 \\
Q_{vR} &= -|V_{vR}|^2 B_{vR} + |V_{vR}||V_l|B_{vR}
\end{aligned}
\tag{4.73}
$$

Based on these equations, the linearized STATCOM equation is given below, where the variable voltage magnitude $|V_{vR}|$ is taken to be the state variable

$$
\begin{bmatrix} \Delta P_l \\ \Delta Q_{vR} \end{bmatrix} =
\begin{bmatrix} \frac{\partial P_l}{\partial \theta_l} & \frac{\partial P_l}{\partial |V_{vR}|} \\ \frac{\partial Q_{vR}}{\partial \theta_l} & \frac{\partial Q_{vR}}{\partial |V_{vR}|} \end{bmatrix}
\begin{bmatrix} \Delta \theta_l \\ \Delta |V_{vR}| \end{bmatrix}
\tag{4.74}
$$

At the end of iteration (r), the variable voltage magnitude $|V_{vR}|$ is updated

$$
|V_{vR}|^{(r+1)} = |V_{vR}|^{(r)} + \Delta |V_{vR}|^{(r)}
\tag{4.75}
$$

The SVC in the modified five-node network used in Example 5 was replaced with a STATCOM to maintain nodal voltage magnitude at Lake node at 1 p.u. In this case the power flow solution is identical to the case when the SVC is used. It should be remarked that this is a special case, which yields the same result whether the shunt controller is an SVC or a STATCOM. At regulated voltage magnitudes different from 1 p.u. the results will not coincide. This is better appreciated from Figure 4.19 where the performance of an ideal reactive power controller, e.g. STATCOM, is compared against the performance of an ideal variable susceptance controller, e.g. SVC.
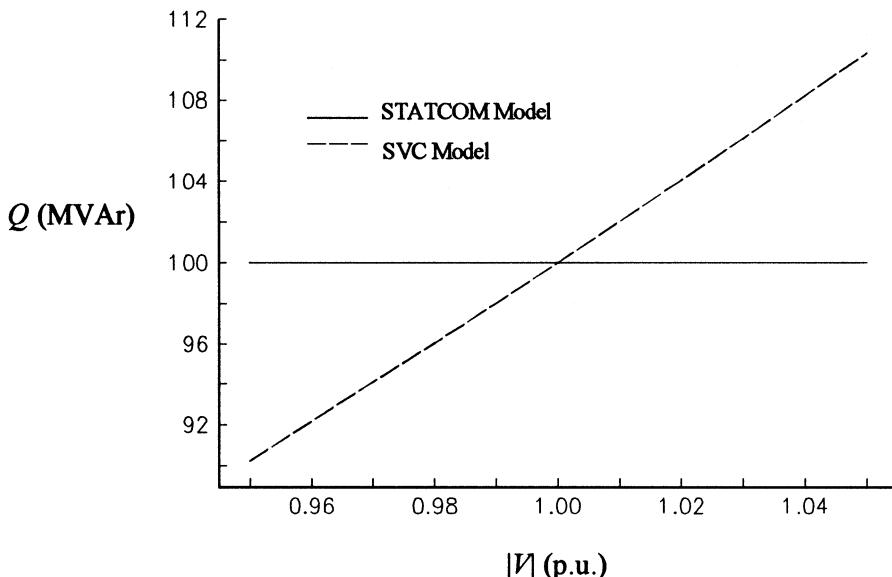
Fig. 4.19 Reactive powers injected by a STATCOM and an SVC as a function of voltage magnitude.

4.6   Active power control

4.6.1   General aspects

A well-established method to increase the transmission line capability is to install series compensation in order to reduce the transmission line's net series impedance. From the control point of view there is great incentive to provide compensation by electronic means. For instance, the TCSC enables effective active power flow regulation in the compensated transmission line. The TCSC has the ability to operate in both the inductive and the capacitive regions. TCSC operation in the inductive region will increase the electrical length of the line thereby reducing the line's ability to transfer power. Conversely, TCSC operation in the capacitive region will shorten the electrical length of the line, hence increasing power transfer margins.

The structure of a modern series compensator may consist of a large number of small inductive-capacitive parallel branches connected in tandem and each branch having independent control. Nevertheless, for the purpose of fundamental frequency, power flow studies, a variable series reactance provides a simple and very efficient way to model the TCSC. The changing reactance adjusts automatically to constrain the power flow across the branch to a specified value. The amount of reactance is determined efficiently by means of Newton's algorithm. The changing reactance X_{TCSC} represents the total equivalent reactance of all the TCSC modules connected in series.

Active power flow can also be controlled by adjusting the phase angle difference across a series connected impedance. As outlined in Section 4.2.3, this is the power transmission characteristic exploited by mechanically controlled phase shifting transformers and by electronic phase angle controllers. The latter has an almost instantaneous speed of response and it achieves its objective of controlling active power flow by inserting a variable quadrature voltage in series with the transmission line. The effectiveness of traditional phase shifters in performing this function has been well demonstrated in practice over many years (IEEE/CIGRE, 1995).

4.6.2   TCSC power flow modelling

For inductive operation the TCSC power equations at node l are

$$P_l = \frac{|V_l||V_m|}{X_{\text{TCSC}}} \cdot \sin(\theta_l - \theta_m) \tag{4.76}$$

$$Q_l = \frac{|V_l|^2}{X_{\text{TCSC}}} - \frac{|V_l||V_m|}{X_{\text{TCSC}}} \cdot \cos(\theta_l - \theta_m) \tag{4.77}$$

For capacitive operation, the signs of the equations are reversed. Also, for the power equations corresponding to node m the subscripts l and m are exchanged in equations (4.76)–(4.77).

For the case when the TCSC is controlling active power flowing from nodes l to m at a value P_{lm}^{reg} the set of linearized power flow equations are

$$
\begin{bmatrix} \Delta P_l \\ \Delta P_m \\ \Delta Q_l \\ \Delta Q_m \\ \Delta P_{lm} \end{bmatrix} = \begin{bmatrix} \frac{\partial P_l}{\partial \theta_l} & \frac{\partial P_l}{\partial \theta_m} & \frac{\partial P_l}{\partial |V_l|} & \frac{\partial P_l}{\partial |V_m|} & \frac{\partial P_l}{\partial X_{\text{TCSC}}} \\ \frac{\partial P_m}{\partial \theta_l} & \frac{\partial P_m}{\partial \theta_m} & \frac{\partial P_m}{\partial |V_l|} & \frac{\partial P_m}{\partial |V_m|} & \frac{\partial P_m}{\partial X_{\text{TCSC}}} \\ \frac{\partial Q_l}{\partial \theta_l} & \frac{\partial Q_l}{\partial \theta_m} & \frac{\partial Q_l}{\partial |V_l|} & \frac{\partial Q_l}{\partial |V_m|} & \frac{\partial Q_l}{\partial X_{\text{TCSC}}} \\ \frac{\partial Q_m}{\partial \theta_l} & \frac{\partial Q_m}{\partial \theta_m} & \frac{\partial Q_m}{\partial |V_l|} & \frac{\partial Q_m}{\partial |V_m|} & \frac{\partial Q_m}{\partial X_{\text{TCSC}}} \\ \frac{\partial P_{lm}}{\partial \theta_l} & \frac{\partial P_{lm}}{\partial \theta_m} & \frac{\partial P_{lm}}{\partial |V_l|} & \frac{\partial P_{lm}}{\partial |V_m|} & \frac{\partial P_{lm}}{\partial X_{\text{TCSC}}} \end{bmatrix} \begin{bmatrix} \Delta \theta_l \\ \Delta \theta_m \\ \Delta |V_l| \\ \Delta |V_m| \\ \Delta X_{\text{TCSC}} \end{bmatrix} \quad (4.78)
$$

The active power flow mismatch equation in the TCSC is,

$$
\Delta P_{lm} = P_{lm}^{\text{reg}} - P_{lm}^{\text{calc}} \quad (4.79)
$$

and the state variable X_{TCSC} of the series controller is updated at the end of iteration (r) using the following equation

$$
X_{\text{TCSC}}^{(r+1)} = X_{\text{TCSC}}^{(r)} + \Delta X_{\text{TCSC}}^{(r)} \quad (4.80)
$$

4.6.3 Numerical example 6

The original network has been modified to include one TCSC to compensate the transmission line connecting nodes Lake and Main. The TCSC is used to maintain active power flow towards Main at 21 MW. The initial condition of the TCSC is set at 50% of the transmission line inductive reactance given in Table 4.2, i.e. $X = 1.5\%$. Convergence was obtained in five iterations to a power mismatch tolerance of $\varepsilon \leq 10^{-12}$. The power flow results are shown on Figure 4.20 and the nodal voltage magnitudes and phase angles are given in Table 4.6.

Since the TCSC cannot generate active power, there is an increase in active power flowing towards Lake node, through the transmission lines connecting North to Lake and South to Lake, in order to meet the increase in active power specified at the sending end of the TCSC. In the transmission line South–Lake, the active power flow increases from 24.47 MW in the original network to 25.5 MW at the sending end of the line whereas in the transmission line North–Lake, the increase is from 41.79 MW to 42.43 MW.

It should be remarked that transmission line Lake–Main was series compensated to increase the active power flow from 19.38 MW to 21 MW, which is just under 8% active power increase. The nodal voltage magnitudes do not change compared to the base case but the voltage phase angles do change; particularly at Lake node where there is a negative increase of almost one degree to enable increases in active power flows.

4.6.4 SPS power flow modelling

The active and reactive powers injected at nodes l and m by the SPS shown in Figure 4.3 are

$$
P_l = |V_l|^2 G_{ll} + |V_l||V_m|(G_{lm} \cos(\theta_l - \theta_m) + B_{lm} \sin(\theta_l - \theta_m)) \quad (4.81)
$$

$$
Q_l = -|V_l|^2 B_{ll} - |V_l||V_m|(B_{lm} \cos(\theta_l - \theta_m) - G_{lm} \sin(\theta_l - \theta_m)) \quad (4.82)
$$
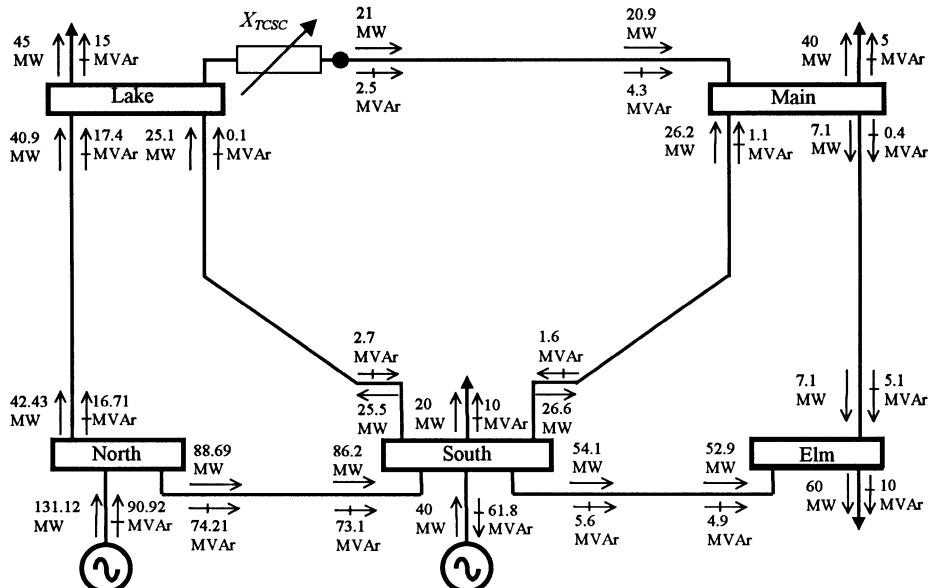
**Fig. 4.20** TCSC upgraded test network and power flow results.

Table 4.6 Nodal complex voltages of TCSC upgraded network

Voltage information	System nodes				
	North	South	Lake	Main	Elm
$|V|$ (p.u.)	1.06	1	0.987	0.984	0.972
θ (degrees)	0	−2.04	−4.73	−4.81	−5.7

For equations corresponding to node m the subscripts l and m are exchanged in equations (4.81)–(4.82).

For the case when the SPS is controlling active power flowing from nodes l to m at a value P_{lm}^{reg} the set of linearized power flow equations are

$$\begin{bmatrix} \Delta P_l \\ \Delta P_m \\ \Delta Q_l \\ \Delta Q_m \\ \Delta P_{lm} \end{bmatrix} = \begin{bmatrix} \frac{\partial P_l}{\partial \theta_l} & \frac{\partial P_l}{\partial \theta_m} & \frac{\partial P_l}{\partial |V_l|} & \frac{\partial P_l}{\partial |V_m|} & \frac{\partial P_l}{\partial \phi} \\ \frac{\partial P_m}{\partial \theta_l} & \frac{\partial P_m}{\partial \theta_m} & \frac{\partial P_m}{\partial |V_l|} & \frac{\partial P_m}{\partial |V_m|} & \frac{\partial P_m}{\partial \phi} \\ \frac{\partial Q_l}{\partial \theta_l} & \frac{\partial Q_l}{\partial \theta_m} & \frac{\partial Q_l}{\partial |V_l|} & \frac{\partial Q_l}{\partial |V_m|} & \frac{\partial Q_l}{\partial \phi} \\ \frac{\partial Q_m}{\partial \theta_l} & \frac{\partial Q_m}{\partial \theta_m} & \frac{\partial Q_m}{\partial |V_l|} & \frac{\partial Q_m}{\partial |V_m|} & \frac{\partial Q_m}{\partial \phi} \\ \frac{\partial P_{lm}}{\partial \theta_l} & \frac{\partial P_{lm}}{\partial \theta_m} & \frac{\partial P_{lm}}{\partial |V_l|} & \frac{\partial P_{lm}}{\partial |V_m|} & \frac{\partial P_{lm}}{\partial \phi} \end{bmatrix} \begin{bmatrix} \Delta \theta_l \\ \Delta \theta_m \\ \Delta |V_l| \\ \Delta |V_m| \\ \Delta \phi \end{bmatrix} \tag{4.83}$$

The active power flow mismatch equation in the SPS is,

$$\Delta P_{lm} = P_{lm}^{\text{reg}} - P_{lm}^{\text{calc}} \tag{4.84}$$

where equation (4.5) in Section 4.2.3 may be used for the purpose of calculating P_{lm}^{calc} and to derive the relevant Jacobian terms in equation (4.83).

It should be pointed out that the SPS in Figure 4.3(b) has the phase angle tapping in the primary winding and that its effect may be incorporated in the phase angle θ_m. Hence, the Jacobian terms corresponding to P_l, Q_l, P_m and Q_m are derived with respect to θ_m, as opposed to ϕ, using equations (4.81)–(4.82). For cases when the phase shifter angle is in the secondary winding the corresponding Jacobian terms are derived with respect to θ_l.

The state variable ϕ is updated at the end of iteration (r) using the following equation

$$\phi^{(r+1)} = \phi^{(r)} + \Delta\phi^{(r)} \tag{4.85}$$

4.6.5 Numerical example 7

The original network is modified to include one SPS to control active power flow in the transmission line connecting nodes Lake and Main. The SPS is used to maintain active power flow towards Main at 40 MW. The SPS reactance is 10% and the initial condition for the phase shifting angle is 0°. The actual phase shifting angle required to keep active power flow at 40 MW is −5.83°. Convergence is obtained in four iterations to a power mismatch tolerance of $\varepsilon \leq 10^{-12}$. The power flow results are shown on Figure 4.21 and the nodal voltage magnitudes and phase angles are given in Table 4.7.

Since the SPS cannot generate active power, there is a large increase in active power, compared to the base case, flowing towards Lake node through the transmission lines connecting North to Lake and South to Lake. In the transmission line North–Lake, the active power flow increases from 41.79 MW to 50.3 MW at the sending end of the line whereas in the transmission line South–Lake, the increase is from 24.47 MW to 37.6 MW.
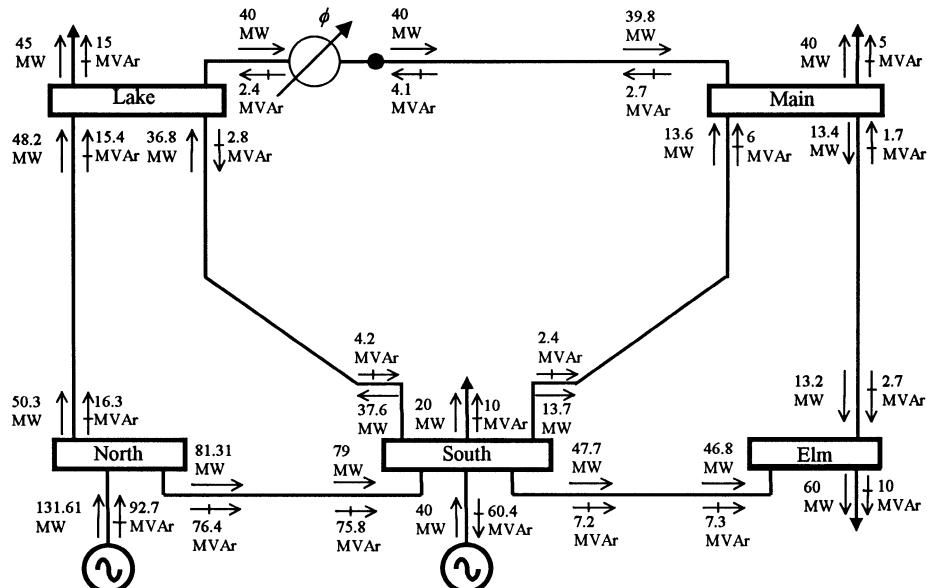
Fig. 4.21 SPS upgraded test network and power flow results.

Table 4.7 Nodal complex voltages of SPS upgraded network

Voltage information	System nodes				
	North	South	Lake	Main	Elm
$\lvert V \rvert$ (p.u.)	1.06	1	0.984	0.984	0.972
θ (degrees)	0	-1.77	-5.80	-3.06	-4.95

It should be noticed that the upgrade in transmission line Lake–Main has enabled very substantial increases in active power flow through this line, e.g. from 19.38 MW to 40 MW. The nodal voltage magnitudes do not change much compared to the base case but the phase angles do change; particularly at nodes Lake and Main where the absolute phase angle difference between the two nodes increases from $0.32°$ in the original case to $2.74°$ in the modified case of this example.

4.7 Combined active and reactive power control

4.7.1 General aspects

Simultaneous active and reactive power control is a new reality in high-voltage transmission and low-voltage distribution networks due to recent developments in power electronics technology and powerful digital control techniques. Such technological advances are embodied in the new generation of FACTS and Custom Power equipment, such as the UPFC, the DVR and the HVDC light. They are based on new power electronic converters using GTO and IGBT switches and PWM control techniques.

4.7.2 Simple UPFC power flow modelling

The UPFC can be modelled very simply by resorting to only conventional power flow concepts, namely the use of a PV type node and a PQ type node. Figure 4.22(a) shows the schematic representation of a UPFC connected between nodes l and m of a large power system. Figure 4.22(b) shows the equivalent circuit representation using the power flow terminology.

This simple way of modelling the UPFC was first reported by (Nabavi-Niaki and Iravani, 1996). This is an effective and elegant model but care should be exercised with its use because the model may lack control flexibility. For instance, the model only works if one wishes to exert simultaneous control of nodal voltage magnitude, active power flowing from nodes l to m and reactive power injected at node l. As illustrated in Figure 4.22, the UPFC is modelled by transforming node l into a PQ type node and node m into a PV type node. The UPFC active power flow is assigned to both the fictitious generator connected at node m and to the fictitious load connected at node l. The UPFC reactive power injected at node l is also assigned to the fictitious load. Furthermore, the UPFC voltage magnitude at node m is assigned to the newly created PV type node. It should be remarked that the implementation of this model in a computer program requires no modification of the code.
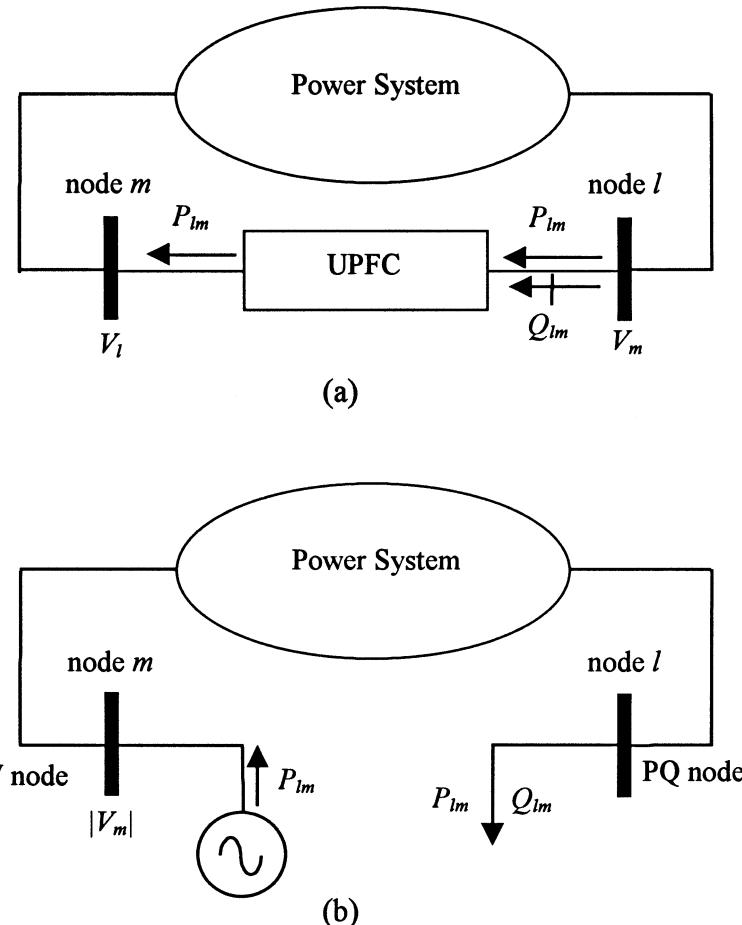
Fig. 4.22 UPFC model based on conventional power flow concepts.

4.7.3   Advanced UPFC power flow modelling

A more flexible UPFC power flow model is derived below starting from first principles. The UPFC model comes in the form of two coordinated voltage sources: one representing the fundamental component of the Fourier series of the switched voltage waveform at the AC terminals of the shunt connected converter, and the other representing a similar parameter at the AC terminals of the series connected converter. It should be noticed that the behaviour of these two voltage sources is not independent from each other but, rather, they satisfy a common active power exchange with the external power network. The equivalent circuit representation is shown in Figure 4.6(b).

As far as the power flow solution is concerned, the only restriction that this model may have is that the UPFC converter valves are taken to be lossless. However, active power losses in the converter valves are expected to be small and this is a reasonable assumption to make in power flow studies. In this situation, the active power

supplied to the shunt converter, $\mathrm{Re}\{V_{vR} \cdot I_{vR}^*\}$ satisfies the active power demanded by the series converter, $\mathrm{Re}\{V_{cR} \cdot I_m^*\}$. The impedance of the series and shunt transformers, Z_{cR} and Z_{vR}, are included explicitly in the model. The ideal voltage sources and the constraint power equation given in equations (4.9)–(4.11) are used to derive this UPFC model.

Based on the equivalent circuit shown in Figure 4.6(b), the following transfer admittance equation can be written

$$
\begin{bmatrix} I_l \\ I_m \end{bmatrix} = \begin{bmatrix} (Y_{cR} + Y_{vR}) & -Y_{cR} & -Y_{cR} & -Y_{vR} \\ -Y_{cR} & Y_{cR} & Y_{cR} & 0 \end{bmatrix} \begin{bmatrix} V_l \\ V_m \\ V_{cR} \\ V_{vR} \end{bmatrix} \tag{4.86}
$$

The injected active and reactive powers at nodes l and m may be derived using the complex power equation

$$
\begin{bmatrix} S_l \\ S_m \end{bmatrix} = \begin{bmatrix} V_l & 0 \\ 0 & V_m \end{bmatrix} \begin{bmatrix} I_l^* \\ I_m^* \end{bmatrix}
$$

$$
= \begin{bmatrix} V_l & 0 \\ 0 & V_m \end{bmatrix} \begin{bmatrix} (Y_{cR}^* + Y_{vR}^*) & -Y_{cR}^* & -Y_{cR}^* & -Y_{vR}^* \\ -Y_{cR}^* & Y_{cR}^* & Y_{cR}^* & 0 \end{bmatrix} \begin{bmatrix} V_l^* \\ V_m^* \\ V_{cR}^* \\ V_{vR}^* \end{bmatrix} \tag{4.87}
$$

$$
= \begin{bmatrix} V_l & 0 \\ 0 & V_m \end{bmatrix} \begin{bmatrix} G_{ll} - \mathrm{j}B_{ll} & G_{lm} - \mathrm{j}B_{lm} & G_{lm} - \mathrm{j}B_{lm} & G_{l0} - \mathrm{j}B_{l0} \\ G_{ml} - \mathrm{j}B_{ml} & G_{mm} - \mathrm{j}B_{mm} & G_{mm} - \mathrm{j}B_{mm} & 0 \end{bmatrix} \begin{bmatrix} V_l^* \\ V_m^* \\ V_{cR}^* \\ V_{vR}^* \end{bmatrix}
$$

After some straightforward but arduous algebra, the following active and reactive power equations are obtained

$$
\begin{aligned}
P_l = |V_l|^2 G_{ll} &+ |V_l||V_m|\{G_{lm}\cos(\theta_l - \theta_m) + B_{lm}\sin(\theta_l - \theta_m) \\
&+ |V_l||V_{cR}|\{G_{lm}\cos(\theta_l - \theta_{cR}) + B_{lm}\sin(\theta_l - \theta_{cR})\} \\
&+ |V_l||V_{vR}|\{G_{l0}\cos(\theta_l - \theta_{vR}) + B_{l0}\sin(\theta_l - \theta_{vR})\}
\end{aligned} \tag{4.88}
$$

$$
\begin{aligned}
Q_l = -|V_l|^2 B_{ll} &+ |V_l||V_m|\{G_{lm}\sin(\theta_l - \theta_m) - B_{lm}\cos(\theta_l - \theta_m)\} \\
&+ |V_l||V_{cR}|\{G_{lm}\sin(\theta_l - \theta_{cR}) - B_{lm}\cos(\theta_l - \theta_{cR})\} \\
&+ |V_l||V_{vR}|\{G_{l0}\sin(\theta_l - \theta_{vR}) - B_{l0}\cos(\theta_l - \theta_{vR})\}
\end{aligned} \tag{4.89}
$$

$$
\begin{aligned}
P_m = |V_m|^2 G_{mm} &+ |V_m||V_l|\{G_{ml}\cos(\theta_m - \theta_l) + B_{ml}\sin(\theta_m - \theta_l)\} \\
&+ |V_m||V_{cR}|\{G_{mm}\cos(\theta_m - \theta_{cR}) + B_{mm}\sin(\theta_m - \theta_{cR})\}
\end{aligned} \tag{4.90}
$$

$$
\begin{aligned}
Q_m = -|V_m|^2 B_{mm} &+ |V_m||V_l|\{G_{ml}\sin(\theta_m - \theta_l) - B_{ml}\cos(\theta_m - \theta_l)\} \\
&+ |V_m||V_{cR}|\{G_{mm}\sin(\theta_m - \theta_{cR}) - B_{mm}\cos(\theta_m - \theta_{cR})\}
\end{aligned} \tag{4.91}
$$

The active and reactive powers for the series converter are derived as follows:

$$S_{cR} = P_{cR} + \mathrm{j}Q_{cR} = V_{cR}I_m^* = V_{cR}\{Y_{ml}^*V_l^* + Y_{mm}^*V_m^* + Y_{mm}^*V_{cR}^*\} \tag{4.92}$$

$$P_{cR} = |V_{cR}|^2 G_{mm} + |V_{cR}||V_l|\{G_{ml}\cos(\theta_{cR} - \theta_l) + B_{ml}\sin(\theta_{cR} - \theta_l)\}$$
$$+ |V_{cR}||V_m|\{G_{mm}\cos(\theta_{cR} - \theta_m) + B_{mm}\sin(\theta_{cR} - \theta_m)\} \tag{4.93}$$

$$Q_{cR} = -|V_{cR}|^2 B_{mm} + |V_{cR}||V_l|\{G_{ml}\sin(\theta_{cR} - \theta_l) - B_{ml}\cos(\theta_{cR} - \theta_l)\}$$
$$+ |V_{cR}||V_m|\{G_{mm}\sin(\theta_{cR} - \theta_m) - B_{mm}\cos(\theta_{cR} - \theta_m)\} \tag{4.94}$$

The active and reactive powers for the shunt converter are derived as follows

$$S_{vR} = P_{vR} + \mathrm{j}Q_{vR} = V_{vR}I_{vR}^* = V_{vR}Y_{vR}^*\{V_{vR}^* - V_l^*\} \tag{4.95}$$

$$P_{vR} = -|V_{vR}|^2 G_{l0} + |V_{vR}||V_l|\{G_{l0}\cos(\theta_{vR} - \theta_l) + B_{l0}\sin(\theta_{vR} - \theta_l) \tag{4.96}$$

$$Q_{vR} = |V_{vR}|^2 B_{l0} + |V_{vR}||V_l|\{G_{l0}\sin(\theta_{vR} - \theta_l) - B_{l0}\cos(\theta_{vR} - \theta_l)\} \tag{4.97}$$

Assuming lossless converters, the UPFC neither absorbs nor injects active power with respect to the AC system. Hence, the following constraint equation must be satisfied

$$P_{vR} + P_{cR} = 0 \tag{4.98}$$

This is a complex model, which imposes severe demands on the numerical algorithms used for its solution. Since in power systems planning and operation reliability towards the convergence is the main concern, it is recommended that the Newton–Raphson algorithm be used for its solution (Fuerte-Esquivel et al., 2000). In this method the UPFC state variables are combined with the network nodal voltage magnitudes and phase angles in a single frame-of-reference for a unified, iterative solution. The UPFC state variables are adjusted automatically in order to satisfy specified power flows and voltage magnitudes.

Following the general principles laid out in Section 4.4.4, the relevant equations in (4.88)–(4.98) are derived with respect to the UPFC state variables. Equation (4.44) is suitably modified to incorporate the linearized equation representing the UPFC contribution. The UPFC is a very flexible controller and its linearized system of equations may take several possible forms. For instance, if nodes l and m are the nodes where the UPFC and the power network join together and the UPFC is set to control voltage magnitude at node l, active power flowing from node m to node l and reactive power injected at node m, then the following linearized equation shows the relevant portion of the overall system of equations

$$
\begin{bmatrix}
\Delta P_l \\
\Delta P_m \\
\Delta Q_l \\
\Delta Q_m \\
\Delta P_{ml} \\
\Delta Q_{ml} \\
\Delta P_{bb}
\end{bmatrix}
=
\begin{bmatrix}
\frac{\partial P_l}{\partial \theta_l} & \frac{\partial P_l}{\partial \theta_m} & \frac{\partial P_l}{\partial |V_{vR}|} & \frac{\partial P_l}{\partial |V_m|} & \frac{\partial P_l}{\partial \theta_{cR}} & \frac{\partial P_l}{\partial |V_{cR}|} & \frac{\partial P_l}{\partial \theta_{vR}} \\
\frac{\partial P_m}{\partial \theta_l} & \frac{\partial P_m}{\partial \theta_m} & 0 & \frac{\partial P_m}{\partial |V_m|} & \frac{\partial P_m}{\partial \theta_{cR}} & \frac{\partial P_m}{\partial |V_{cR}|} & 0 \\
\frac{\partial Q_l}{\partial \theta_l} & \frac{\partial Q_l}{\partial \theta_m} & \frac{\partial Q_l}{\partial |V_{vR}|} & \frac{\partial Q_l}{\partial |V_m|} & \frac{\partial Q_l}{\partial \theta_{cR}} & \frac{\partial Q_l}{\partial |V_{cR}|} & \frac{\partial Q_l}{\partial \theta_{vR}} \\
\frac{\partial Q_m}{\partial \theta_l} & \frac{\partial Q_m}{\partial \theta_m} & 0 & \frac{\partial Q_m}{\partial |V_m|} & \frac{\partial Q_m}{\partial \theta_{cR}} & \frac{\partial Q_m}{\partial |V_{cR}|} & 0 \\
\frac{\partial P_{ml}}{\partial \theta_l} & \frac{\partial P_{ml}}{\partial \theta_m} & 0 & \frac{\partial P_{ml}}{\partial |V_m|} & \frac{\partial P_{ml}}{\partial \theta_{cR}} & \frac{\partial P_{ml}}{\partial |V_{cR}|} & 0 \\
\frac{\partial Q_{ml}}{\partial \theta_l} & \frac{\partial Q_{ml}}{\partial \theta_m} & 0 & \frac{\partial Q_{ml}}{\partial |V_m|} & \frac{\partial Q_{ml}}{\partial \theta_{cR}} & \frac{\partial Q_{ml}}{\partial |V_{cR}|} & 0 \\
\frac{\partial P_{bb}}{\partial \theta_l} & \frac{\partial P_{bb}}{\partial \theta_m} & \frac{\partial P_{bb}}{\partial |V_{vR}|} & \frac{\partial P_{bb}}{\partial |V_m|} & \frac{\partial P_{bb}}{\partial \theta_{cR}} & \frac{\partial P_{bb}}{\partial |V_{cR}|} & \frac{\partial P_{bb}}{\partial \theta_{vR}}
\end{bmatrix}
\begin{bmatrix}
\Delta \theta_l \\
\Delta \theta_m \\
\Delta |V_{vR}| \\
\Delta |V_m| \\
\Delta \theta_{cR} \\
\Delta |V_{cR}| \\
\Delta \theta_{vR}
\end{bmatrix} \tag{4.99}
$$

where it is assumed that node m is PQ type. Also, ΔP_{bb} is the power mismatch given by equation (4.98).

Good starting conditions for all the UPFC state variables are mandatory to ensure a reliable iterative solution. It has been found that for the series voltage source such initial conditions may be obtained by assuming lossless coupling transformers together with null voltage phase angles in equations (4.88)–(4.91). For the shunt voltage source the exercise involves equations (4.93), (4.96) and (4.98) (Fuerte-Esquivel et al., 2000).

It should be remarked that the power flow equations for the DVR become readily available from the above equations by eliminating the contribution of the shunt voltage source from equations (4.88)–(4.94). Notice that equations (4.95)–(4.98) do not form part of the DVR power flow model. The linearized equation for the DVR has the voltage magnitudes and phase angles at nodes l and m and the series voltage source as state variables.

4.7.4 Numerical example 8

The five-node network is modified to include one UPFC to provide power and voltage control in the transmission line connected between nodes Lake and Main. The UPFC is used to maintain active and reactive powers leaving the UPFC towards Main at 40 MW and 2 MVAr, respectively. Moreover, the UPFC's shunt converter is set to regulate nodal voltage magnitude at Lake at 1 p.u.

The shunt and series voltage sources are taken to be limitless and to have the following reactance values: $X_{cR} = X_{vR} = 0.1$ p.u. The initial conditions of the voltage sources, as calculated by using the relevant equations in (4.88)–(4.98) with null phase angles, are given in Table 4.8.

Convergence was obtained in four iterations to a power mismatch tolerance of $\varepsilon \leq 10^{-12}$. The nodal voltage magnitudes and phase angles are given in Table 4.9 and the power flow results are shown in Figure 4.23.

It should be noticed that in this example the UPFC was set to exert its full control potential and that it operated within its design limits. In this case, a power flow solution using the simple model described in Section 4.7.2, where the UPFC is modelled as a combination of a PV node and a PQ node, yields the same result.

The objective to control active and reactive powers and voltage magnitude at the target values was achieved with the following voltage magnitudes and phase angles of the series and shunt sources: $|V_{cR}| = 0.101$ p.u., $\theta_{cR} = -92.73°$, $|V_{vR}| = 1.017$ p.u. and $\theta_{vR} = -6°$.

As expected, the UPFC improved the voltage profile when compared to the original network. It is worth noticing that major changes in the redistribution of

Table 4.8 UPFC initial conditions

Voltage information	Voltage sources	
	Series	Shunt
$|V|$ (p.u.)	0.04	1
θ (degrees)	−87.13	0

Table 4.9 Nodal complex voltages of UPFC upgraded network

Voltage information	System nodes				
	North	South	Lake	Main	Elm
$\lvert V \rvert$ (p.u.)	1.06	1	1	0.992	0.975
θ (degrees)	0	−1.77	−6.02	−3.19	−5.77

active power flow have taken place, particularly in the powers flowing towards Lake node through transmission lines connected between North–Lake and South–Lake. The resulting power flows satisfy the power consumed by the load at Lake node (45 MW) and the active power demanded by the UPFC series converter, which is set to control active power flow at 40 MW as opposed to the 19.38 MW that existed in the original network. The maximum amount of active power exchanged between the UPFC and the AC system will depend on the robustness of the UPFC shunt node, i.e. Lake node. Since the UPFC generates its own reactive power, the generator connected at North node decreases its reactive power generation and the generator connected at South node increases its absorption of reactive power.

As a further exercise, we look at the characteristics of the DVR as a steady state controller. The UPFC model is replaced with a DVR model and the complex voltages are shown in Table 4.10.

The Newton–Raphson algorithm converges in five iterations to a mismatch power tolerance of $\varepsilon \leq 10^{-12}$. The DVR also controls active and reactive power flows through transmission line Lake–Main at 40 MW and 2 MVAr, respectively. The voltage magnitude and phase angle of the series voltage source are: $\lvert V_{cR} \rvert =$
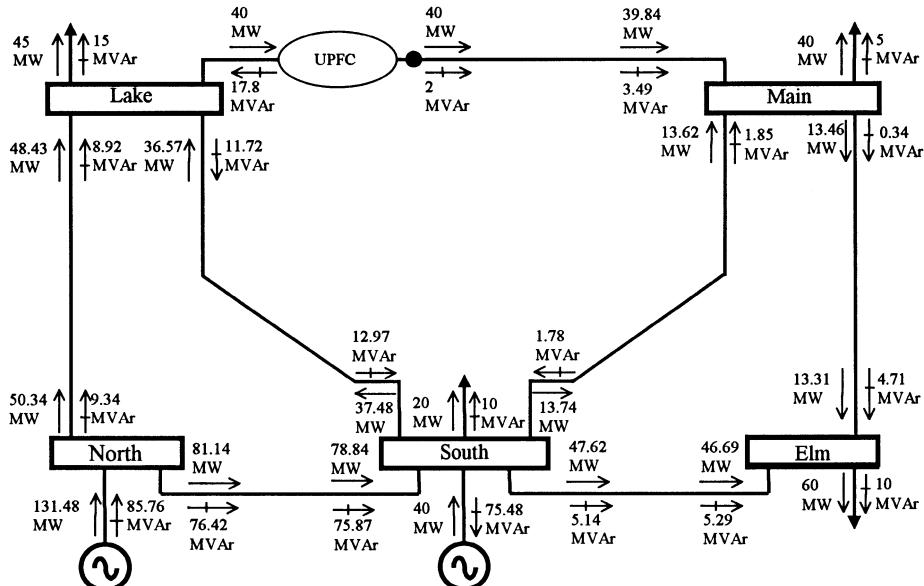
Fig. 4.23 UPFC upgraded test network and power flow results.

Table 4.10 Nodal complex voltages of DVR upgraded network

Voltage information	System nodes				
	North	South	Lake	Main	Elm
$\lvert V \rvert$ (p.u.)	1.06	1	0.987	0.994	0.976
θ (degrees)	0	−1.75	−5.72	−3.18	−4.96

0.059 p.u. and $\theta_{cR} = -115.2°$. Apart from the voltage magnitude at Lake node dropping to 0.987 p.u., the voltage magnitudes at the other nodes do not change noticeably. It is worth noticing that for the conditions set in this example the magnitude of the DVR series voltage source is considerably smaller than the UPFC series voltage source.

4.7.5 HVDC Light power flow modelling

The power flow equations of the HVDC light are closely related to equations (4.71)–(4.72), which are the power flow equations of the STATCOM. The HVDC light comprises two VSCs which are linked to the AC system via shunt connected transformers. Furthermore, the two VSCs are connected in series on the DC side, either back-to-back or through a DC cable (Asplund et al., 1998).

If it is assumed that power flows from nodes l to m, the active and reactive power injections at these nodes are

$$P_l = |V_l|^2 G_{vR1} - |V_l||V_{vR1}|\{G_{vR1}\cos(\theta_l - \theta_{vR1}) + B_{vR1}\sin(\theta_l - \theta_{vR1})\quad (4.100)$$

$$Q_l = -|V_l|^2 B_{vR1} - |V_l||V_{vR1}|\{G_{vR1}\sin(\theta_l - \theta_{vR1}) - B_{vR1}\cos(\theta_l - \theta_{vR1})\quad (4.101)$$

$$P_m = |V_m|^2 G_{vR2} - |V_m||V_{vR2}|\{G_{vR2}\cos(\theta_m - \theta_{vR2}) + B_{vR2}\sin(\theta_m - \theta_{vR2})\}\quad (4.102)$$

$$Q_m = -|V_m|^2 B_{vR2} - |V_m||V_{vR2}|\{G_{vR2}\sin(\theta_m - \theta_{vR2}) - B_{vR2}\cos(\theta_m - \theta_{vR2})\}\quad (4.103)$$

In this situation the rectifier is connected to node l and the inverter to node m. Hence, active and reactive powers for the rectifier are readily available by exchanging subscripts l and $vR1$ in the voltage magnitudes and phase angles in equations (4.100)–(4.101). By the same token, active and reactive powers for the inverter are derived by exchanging subscripts m and $vR2$ in the voltage magnitudes and phase angles in equations (4.102)–(4.103).

An active power constraint equation, similar to equation (4.98) for the UPFC, is also required for the HVDC light. For the case of a back-to-back connected HVDC Light

$$\mathrm{Re}\{V_{vR1}I_l^* - V_{vR2}I_m^*\} = 0 \quad (4.104)$$

Similarly to the STATCOM model presented in Section 4.5.4, it may be assumed that the conductances of the two converters are negligibly small, i.e. $G_{vR1} = 0$ and $G_{vR2} = 0$, but contrary to the STATCOM model, in this case there is active power exchanged with the AC system, hence, $\theta_{vR1} \neq \theta_l$ and $\theta_{vR2} \neq \theta_m$.

Based on equations (4.100)–(4.104), the linearized equation for the HVDC light is given below for the case when nodal voltage magnitude is controlled at node m by the inverter and active power flow is controlled by the rectifier at node l (Acha, 2002)

$$
\begin{bmatrix}
\Delta P_l \\
\Delta Q_l \\
\Delta P_m \\
\Delta Q_m \\
\Delta P_{bb}
\end{bmatrix}
=
\begin{bmatrix}
\frac{\partial P_l}{\partial \theta_l} & \frac{\partial P_l}{\partial |V_l|} & 0 & 0 & \frac{\partial P_l}{\partial \theta_{vR1}} \\
\frac{\partial Q_l}{\partial \theta_l} & \frac{\partial Q_l}{\partial |V_l|} & 0 & 0 & \frac{\partial Q_l}{\partial \theta_{vR1}} \\
0 & 0 & \frac{\partial P_m}{\partial \theta_m} & \frac{\partial P_m}{\partial |V_{vR2}|} & 0 \\
0 & 0 & \frac{\partial Q_m}{\partial \theta_m} & \frac{\partial Q_m}{\partial |V_{vR2}|} & 0 \\
\frac{\partial P_{bb}}{\partial \theta_l} & \frac{\partial P_{bb}}{\partial |V_l|} & \frac{\partial P_{bb}}{\partial \theta_m} & \frac{\partial P_{bb}}{\partial |V_{vR2}|} & \frac{\partial P_{bb}}{\partial \theta_{vR1}}
\end{bmatrix}
\begin{bmatrix}
\Delta \theta_l \\
\Delta |V_l| \\
\Delta \theta_m \\
\Delta |V_{vR2}| \\
\Delta \theta_{vR1}
\end{bmatrix}
\qquad (4.105)
$$

The variable voltage magnitude $|V_{vR2}|$ and the voltage phase angle θ_{vR1} are selected to be the state variables. Also, ΔP_{bb} is the power mismatch given by equation (4.104), which corresponds to the case when the converters are connected back-to-back. If this is not the case and the converters are connected in series via a DC cable then the voltage drop across the cable would be included in the constraint equation. Additional equations become necessary to cater for the increased number of state variables, with the DC equations being used to this end. At the end of iteration (r), the voltage magnitude $|V_{vR2}|$ and phase angle θ_{vR1} are updated

$$
|V_{vR2}|^{(r+1)} = |V_{vR2}|^{(r)} + \Delta |V_{vR2}|^{(r)} \qquad (4.106)
$$

$$
\theta_{vR1}^{(r+1)} = \theta_{vR1}^{(r)} + \Delta \theta_{vR1}^{(r)} \qquad (4.107)
$$

If the converters are connected back-to-back, a simple model based on the concept of PV and PQ nodes may be used instead. For the control case considered in equation (4.105), the rectifier is modelled as a PQ node and the inverter as a PV node. However, it should be noticed that this model may lack control flexibility.

The UPFC in the modified five-node network used in Example 8 was replaced with an HVDC light system to enable 40 MW and 2 MVAr to be transmitted towards Main via the transmission line Lake–Main. Moreover, the rectifier is set to control nodal voltage magnitude at Lake node at 1 p.u. As expected, the power flow solution agrees with the solution given in Example 8.

4.7.6 Numerical example 9

A further power flow solution is carried out for the case when the HVDC light replaces the UPFC in the five-node network. In this example, the active power generated by the generator in South node is specified to increase from 40 to 88.47 MW and the nodal voltage magnitudes at North and South are fixed at 1.036 p.u. and 1.029 p.u., respectively. The active power leaving the HVDC Light towards Main is set at 25 MW. The inverter is set to absorb 6 MVAr and the rectifier to regulate nodal voltage magnitude at Lake at 1 p.u. The nodal voltage magnitudes and phase angles are given in Table 4.11 and the power flow results are shown in Figure 4.24.
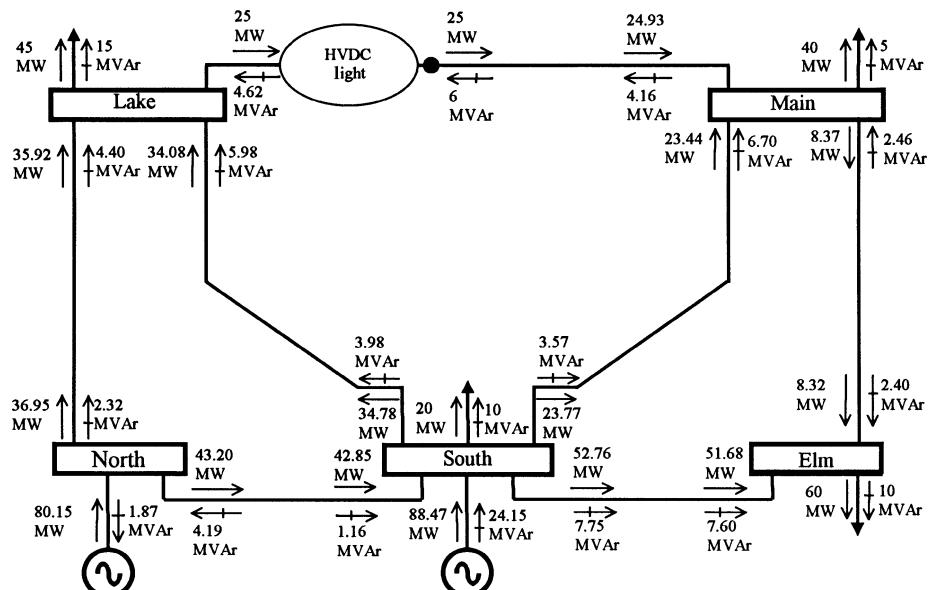
The objective to control active and reactive powers and voltage magnitude at the target values is achieved with the following voltage magnitudes and phase angles of

Table 4.11 Nodal complex voltages of HVDC light upgraded network

Voltage information	System nodes				
	North	South	Lake	Main	Elm
$|V|$ (p.u.)	1.036	1.029	1	1.006	0.999
θ (degrees)	0	−1.402	−4.685	−3.580	−4.722

the rectifier and inverter sources: $|V_{vR1}| = 1.005$ p.u., $\theta_{vR1} = 6.11°$, $|V_{vR2}| = 1.001$ p.u. and $\theta_{vR2} = 1.71°$.

As expected, the HVDC Light improved the voltage profile when compared to the original network but this is also in part due to the higher voltage magnitude specified at South node. It should be noted that the generator in this node is now contributing reactive power to the system and that the generator in North node is absorbing reactive power. In general, the new operating conditions enable a better distribution of active power flows throughout the network. For instance, the largest active power flow in the network decreases from 89.33 MW in the original network to 43.2 MW in this example. The generators share, almost equally, the power demands in Lake node to satisfy a load of 45 MW and the 25 MW required by the HVDC light. Furthermore, the largest reactive power flow in the original network decreases from 73.99 MVAr to 7.75 MVAr in this example. This enables better utilization of transmission assets and reduces transmission losses. The power flow solution presented in this example is based on an optimal power flow solution (Ambriz-Perez, 1998) where generator fuel costs and transmission losses are minimized.

Fig. 4.24 HVDC Light upgraded test network and power flow results.

4.8 Conclusion

This chapter has presented the mathematical modelling of plant components used to control active and reactive power flows and voltage magnitude in high-voltage transmission networks. The emphasis has been on positive sequence power flow modelling of both conventional equipment and modern power systems controllers. The main steady state characteristics of the most prominent FACTS and Custom Power controllers were discussed with a view to developing simple and yet comprehensive power flow models for this new generation of power systems equipment. The following FACTS controllers received attention in this chapter: the SVC, the STATCOM, the SPS, the TCSC, the DVR, the UPFC, and the HVDC Light.

The theory of power flows and the fundamental equations used in electrical power circuits have been covered in depth, with plenty of detailed numerical examples. The Newton–Raphson power flow algorithm has been singled out for full treatment due to its high reliability towards the convergence. Numerical methods with strong convergence characteristics are mandatory when solving FACTS upgraded power systems networks. This is due to the difficulty involved in solving the highly non-linear equations used to represent such equipment and the very large-scale system that the power network represents.

Power semiconductor devices and converter hardware issues

5.1 Introduction

The advances of high voltage/current semiconductor technology directly affect the power electronics converter technology and its progress. The 'perfect' high-power semiconductor is yet to be fully developed and become commercially available. However, new semiconductors have changed the way that power switches are protected, controlled and used and an understanding of the device characteristics is needed before a system is developed successfully.

Technological progress in the power electronics area over the last twenty years or so has been achieved due to the advances in power semiconductor devices. In this chapter, these devices are presented and current developments are discussed.

5.2 Power semiconductor devices

The various semiconductor devices can be classified into three categories with respect to the way they can be controlled:

1. *Uncontrolled.* The diode belongs to this category. Its on or off state is controlled by the power circuit.
2. *Semi-controlled.* The thyristor or silicon controlled rectifier (SCR) is controlled by a gate signal to turn-on. However, once it is on, the controllability of the device is lost and the power circuit controls when the device will turn-off.
3. *Fully-controlled.* Over the last twenty years a number of fully controlled power semiconductors have been developed. This category includes the main kind of

transistors such as the bipolar junction transistor (BJT) and the metal oxide semiconductor field effect transistor (MOSFET). New hybrid devices such as the insulated gate bipolar transistor (IGBT), the gate turn-off thyristor (GTO), the mos-controlled thyristor (MCT), and many others have recently been introduced.

In the next sections the various power semiconductors are presented.

5.2.1 Diode

The circuit symbol of the diode is shown in Figure 5.1(a). The diode as mentioned earlier belongs to the family of uncontrolled devices that allow the current to flow in one direction only, that is from the anode (A) to the cathode (K).

The diode's typical steady-state i–v characteristics along with the ideal ones are depicted in Figure 5.1(b) and (c) respectively. The operation of the device can be described in a simplified way as follows. When the voltage across the diode from the anode to the cathode $v_{AK}(v_{AK} = v_D)$ with the polarity shown in Figure 5.1(a) is positive (forward biased), the diode starts to conduct current whose value is controlled by the circuit itself. Furthermore, a small voltage drop appears across the diode. When the voltage across the diode v_{AK} becomes negative, the device stops conducting with a small current (leakage current) flowing from the cathode to the anode. It should be noted that the ideal i–v characteristics should not be used as part of a design procedure but only to explain the operation of a given circuit.

The typical two-layer structure of the diode is shown in Figure 5.1(d). It is a single junction device with two layers in a silicon wafer, a p-layer lacking electrons and an n-layer doped with a surplus of electrons.

If a diode is conducting and a reverse bias voltage is applied across, it turns off as soon as the forward current becomes zero. However, the process of a diode turning off is not a straightforward one. The extended time required for a diode to turn off and the phenomena happening during such time are known as *diode reverse recovery*. Practically, the time required for a diode to turn off ranges from between a few nanoseconds to a few microseconds. This depends on the technology used to manufacture the device and on the power ratings of the device.

A basic explanation of the reverse recovery phenomena can be given with the assistance of Figure 5.2. The reverse recovery current reaches its maximum value (I_{RM}) after a time interval t_r from the zero crossing point. By then, sufficient carriers have been swept out and recombined and therefore current cannot continue to increase. It starts then to fall during the interval t_f. The sum of the two intervals t_r and t_f is also known as *reverse recovery time* t_{rr}. It is also known as the storage time because it is the required time to sweep out the excess charge from the silicon Q_{rr} due to reverse current. This phenomenon can create large voltage overshoots and losses in inductive circuits. The time t_{rr} characterises the diodes as fast recovery, ultra fast recovery and line frequency diodes. Proper design of the power circuit can influence the behaviour of the device during reverse recovery and limit the negative effect of the described problem.

The diode has no low power control terminal like other semiconductors and therefore is less susceptible to electronic noise problems. However, it still must be protected against overcurrent, overvoltage and transients. For overvoltages, snubber
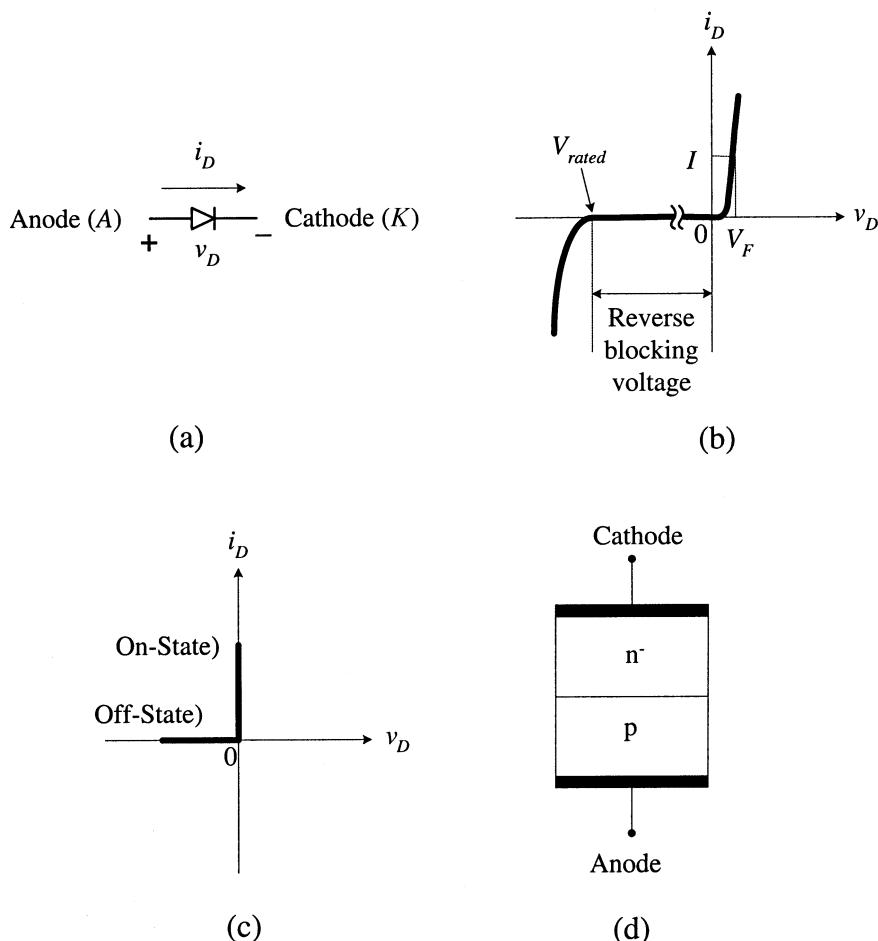
Fig. 5.1 Diode: (a) circuit symbol; (b) typical *i–v* characteristics; (c) ideal *i–v* characteristics; and (d) typical structure.
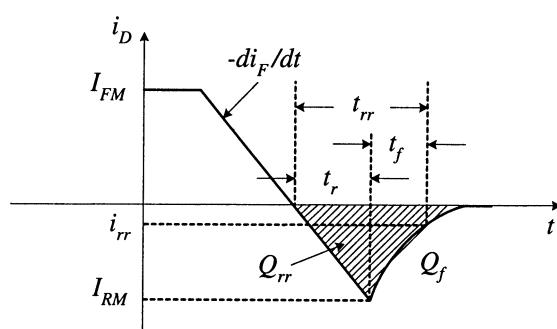
Fig. 5.2 Diode reverse recovery parameters and definitions.

circuits must be used in general to suppress transients which may result in high voltages and ensure that the breakdown voltage (V_{BR}) is not exceeded as shown in Figure 5.1(b). For current, usually the average value, the rms value and the peak value for a given duration are considered. Due to thermal effect on these values, typically the diodes operate below their rated value.

If the circuit requirements for voltage and current are higher than the ratings of a given individual diode, a number of diodes may be connected in series and/or parallel to share the voltage and/or current respectively. Exact voltage and current sharing is not always feasible, since it is impossible that two similar devices exhibit the exact same characteristics. To avoid problems of unequal sharing of voltage and/or current, which in some cases may result in thermal differences and other problems, external resistors or other devices may be used to ensure that the voltage and/or current are shared as required.

5.2.2   Thyristor

The SCR, simply referred to as thyristor is a semi-controlled four-layer power semiconductor with three electrodes, namely, the anode (A), the cathode (K) and the gate (G). The circuit symbol of the thyristor and its structure are shown in Figures 5.3(a) and (b) respectively.

Since it is a four-layer device, it possesses three junctions. A two-transistor based analogy can be used to explain the operating characteristics of the device as shown in Figures 5.3(c) and (d).
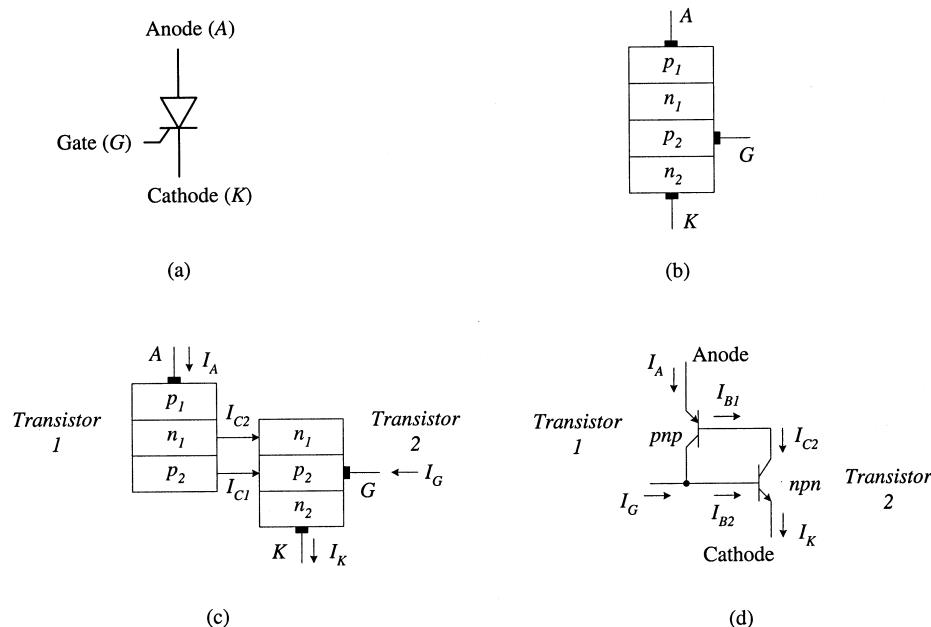
Fig. 5.3 Thyristor: (a) circuit symbol; (b) structure; (c) schematic structure of the two-transistor model; and (d) two transistor equivalent circuit.

An ideal thyristor exhibits infinite resistance to positive anode current unless a positive current pulse I_G is supplied through the gate. Then, the thyristor enters its on state and its resistance becomes zero. It remains at this state till the anode current becomes zero. If the gate current pulse I_G is then zero, the thyristor resumes its initial state of having infinite resistance from the anode to the cathode to positive anode current. However, it should be noted that the anode current does not become zero even when the gate pulse current I_G becomes zero when the thyristor is on. This is the most significant difference between the thyristor and the other fully controlled semiconductors, which will be presented later in this chapter.

The ideal i–v characteristics of the thyristor are plotted in Figure 5.4(a). The current in the thyristor flows from the anode (A) to the cathode (K), like the ordinary diode when it is turned on. Using the two-transistor equivalent circuit shown in Figure 5.3(d), the triggering and the operation of the thyristor can be further explained as follows. When a positive gate current pulse I_G is applied to the p_2 base of the npn transistor (Figure 5.1(c)), the transistor starts to conduct. Negative current flowing through the base of the pnp transistor, also turns the other transistor on. The current flowing through the pnp transistor becomes the base current now of the npn transistor and the whole process described above continues to occur. The regenerative effect turns the thyristor on with a very low forward voltage across. It also leads the two transistors into saturation with all the junctions being forward biased. If the gate pulse is removed, this situation will not change, i.e. the two transistors will remain on. The current flowing through the thyristor is limited only by the external power circuit. Once the thyristor is on, the device behaves as a single junction (although as it was mentioned earlier, there are three junctions). The only way then to turn the thyristor off is to make the anode to cathode current virtually zero.

The operation of the thyristor can be explained with the assistance of the non-ideal i–v characteristics of the device shown in Figure 5.4(b). When the thyristor is in its off state, it can block a positive (forward) polarity voltage from the anode to the
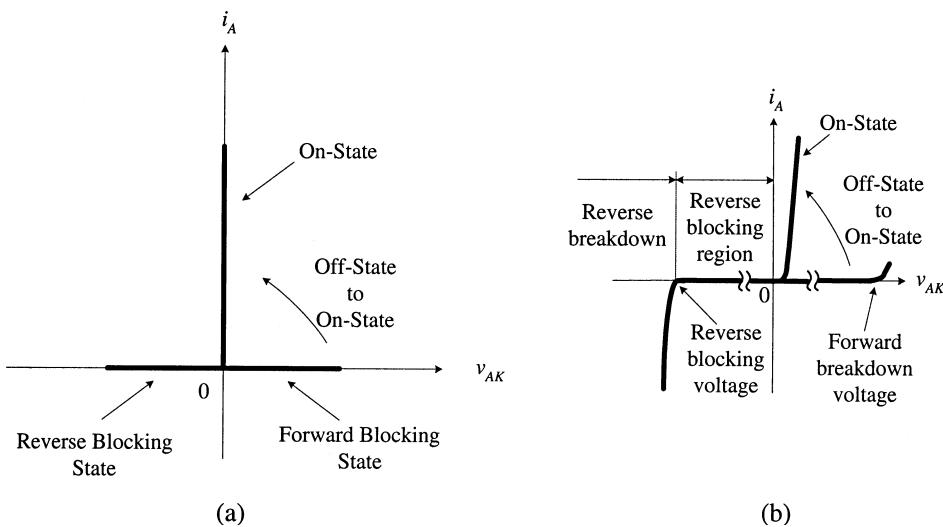
Fig. 5.4 Thyristor i–v characteristics: (a) ideal; and (b) non-ideal.

cathode. There is a need for two conditions to be present simultaneously to turn on the thyristor:

1. forward voltage from the anode (A) to the cathode (K)
2. positive gate current to be applied for a short time.

When the two conditions are met, the thyristor can be triggered or as also referred the thyristor can be fired into its on state. It then behaves almost as a short circuit with a low voltage drop across (typically few Volts depending upon the type of the thyristor and its power ratings). Once the thyristor enters its on state, the controllability of the device through the gate circuit is lost and the thyristor behaves as an ordinary diode. This happens even if the gate current is removed. The thyristor cannot be turned off through the gate. Only if, due to the operation of the power circuit, the current from the anode to the cathode tries to change direction (becomes negative or else flows from the cathode to the anode), the thyristor turns off and the anode to the cathode current becomes eventually zero. This happens under certain conditions and the circuit design must ensure that while the anode to the cathode current is negative and finally becomes zero, a negative voltage must be present across the thyristor to ensure that it turns off completely. Manufacturers' data sheets specify times and requirements for the thyristor to turn off. When the voltage across the thyristor is negative (reverse bias) a very small current (leakage current) flows from the cathode to the anode.

5.2.3   Light-triggered thyristor (LTT)

The thyristor represents a mature technology and is already the most widely used device especially in high and very-high power applications for decades. However, there are a number of developments happening in order to further improve the performance characteristics of the device.

In the early 1970s the electrically triggered thyristor (ETT) was developed. However, when such devices are used in series in large numbers to develop a high-voltage valve, the electrical triggering and the required insulation were complex making the hardware equipment expensive. In the late 1970s, a light-sensitive gating method was developed and the associated amplifying layers were built integrally into the power thyristor to facilitate the light-triggering concept (EPRI, 1978). The main reasons of using LTT technology are as follows:

- Light signals are not affected by ElectroMagnetic Interference (EMI).
- The optical fibre provides one of the best available electrical isolation and transmits the light directly into the gate of the device.

The blocking voltage of the initial devices was relatively low (Temple, 1980; Temple, 1981). Since then continually new devices were manufactured that were able to block higher voltages (Tada et al., 1981; Katoh et al., 1997). Another important aspect was the protection of the device against dv/dt and di/dt (Przybysz et al., 1987). This resulted in the development of the self-protected LTT (Cibulka et al., 1990; Aliwell et al., 1994).

Today, research and development aims mainly at reducing the complexity of the device itself while improving its reliability. Each valve in high-power applications is built with a number of thyristors and work in recent years has resulted in an increase of the blocking voltage level so that the number of thyristors required to build the
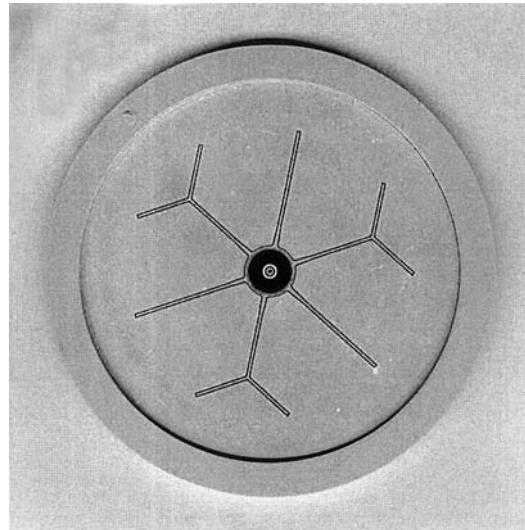
Fig. 5.5 Photograph of a 5-inch light-triggered thyristor with integrated breakover diode. (Courtesy of Siemens and EUPEC.)

same valve from the blocking voltage point of view can be reduced. It is widely accepted by manufacturers that the highest blocking voltage that results in optimized device as far as cost, power losses, reliability and fabrication process are concerned is about 8-kV (Ruff et al., 1999; Asano et al., 1998).

Today, manufacturers try to integrate the drive and protection circuitry within the device. Specifically, the light and overvoltage triggering functions have been integrated with the device. When compared with the ETT, the component count of the drive circuit is reduced substantially (Lips et al., 1997). Furthermore, the overvoltage protection is also integrated into the device which further reduces the complexity of the circuitry arrangement required to ensure safe operating conditions and risk of failure reduction. An improved 8-kV LTT with the overvoltage protection developed by Siemens and EUPEC has become available (Schulze et al., 1996; Schulze et al., 1997; Ruff et al., 1999). An 8-kV LTT with integrated diode (Niedernostheide et al., 2000) is shown in Figure 5.5.

Many LTT devices have been successfully used in Japan (Asano et al., 1998). The recently developed 8-kV LTT by Siemens, AG was tested as commercial product at Bonneville Power Administration's (BPAs), Celilo Converter Station at The Dalles, Oregon, USA in 1997. Celilo is the northern end of BPAs 3.1-MW HVDC line from the Columbia River system to Southern California.

Current R&D work aims at developing fully self-protected devices with break over diode (BOD), forward recovery protection (FRP) and dv/dt protection as a high-power LTT (Ruff et al., 1999).

5.2.4 Desired characteristics of fully-controlled power semiconductors

In switch-mode solid-state converters, the fully controlled power semiconductors can be turned on and off with control signals applied to a third terminal and can

be broadly classified as voltage controlled or current controlled. In the first case, and in simple terms, a voltage signal between two terminals controls the on and off state, whereas in the second case, the injection of current through the third terminal provides such control.

Simplified and linearized voltage and current waveforms during the turn-on and turn-off interval are shown in Figure 5.6. In reality, these waveforms are shaped with snubber networks added in the power circuit to protect the main semiconductor device and to reduce or minimize the switching losses. The overlap between the voltage and current waveforms therefore is greatly dependent upon not only the switching characteristics of the device itself but also on the way the power circuit is designed and controlled.

For instance, there is a family of converters based on resonant concepts where the voltage and current waveforms not only have the shape of sinusoidal signals as opposed to linear waveforms shown in Figure 5.6 but also the overlap is minimal and the respective switching losses quite low.

In the last fifteen years such resonant concepts have been extensively applied in the converter technology and many ideas from the thyristor converters have been used to control the shape of the switching waveforms and reduce the losses. This way the switching frequency of the system can be increased with a number of benefits attached to such improvement. The new family of converters known as *soft-switching* converters or *quasi-resonant* converters with control techniques modified or based on PWM concepts have been the focus of R&D (Divan, 1989; Divan, 1991; Divan et al., 1989; Divan et al., 1993). There are already many products in this area in the market mainly for adjustable speed motor drives and medium power converters for power systems applications.

It is beyond the scope of this book to provide further information on such technology. A review paper of the developments of this technology has been recently written by Bellar et al., 1998.

Before presenting the main semiconductor devices, we will discuss the desired characteristics of the power switches.

The 'perfect' fully controlled power switch would have the following characteristics:

1. *High forward and reverse voltage blocking ratings*. In order to achieve higher power ratings for a given converter, many switches are connected in series to build a
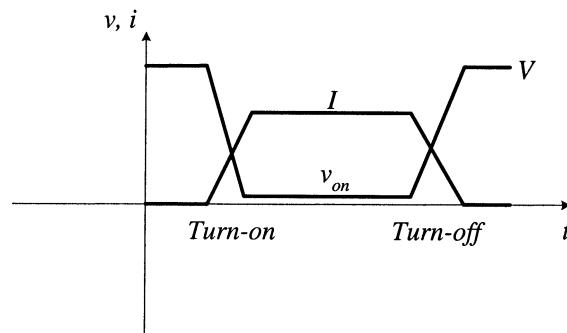
Fig. 5.6 Linear switching voltage and current waveforms for a semiconductor switch.

valve especially for high and ultra-high power applications. If new devices become available with higher voltage ratings, the number of the required switches connected in series to produce the same valve will be reduced. This will minimize the problems with the voltage sharing of the various switches in series, will increase the reliability of the overall system and will minimize the problems with their protection.

2. *High current during conduction state*. At the moment, when the current ratings of a given converter must be met, a number of switches are connected in parallel. If a device is available with high current ratings, the need for parallel connection as well as the problem of current sharing can be eliminated.

3. *Low off-state leakage current*. In most cases such a requirement is not significant as the already available switches exhibit almost negligible off-state leakage current.

4. *Low on-state voltage drop across the switch*. Even a relatively low voltage drop of a few volts across the device at significant current flowing through the device can result in high conduction losses. It is therefore important that such an on-state voltage drop is as low as possible. This becomes more important when a number of switches are connected in series to increase the power handling capability of the converter, as the load current flows through a number of switches generating high conduction losses.

5. *Low turn-on and turn-off losses*. The ability to switch from on to off state and vice versa with minimum overlap between the current and voltage waveforms means that the switching turn-on and off losses are low. When such characteristics are combined with the low conduction losses, cooling requirements and other auxiliary components may be reduced or even eliminated in certain applications making the converter simpler, smaller, more efficient and simply less expensive.

6. *Controlled switching characteristics during turn-on and turn-off*. This means that overcurrent control becomes simpler and easier, the stresses on the device and other parts of the converter such as load, transformers, etc. can be reduced along with EMI generation, the need for filters and snubber circuits.

7. *Capability to handle its rated voltage and current at the same time without the need for derating*. This will mean snubberless design, i.e. the required extra snubber components (resistor–inductor–capacitor–diode) to protect the switch and shape its switching waveforms, can be eliminated. Therefore, if the design does not require all these components, a simpler configuration, more efficient and more reliable will result.

8. *High dv/dt and di/dt ratings*. This will eliminate or reduce the size of the snubber circuits. Of course EMI generation will limit how fast the current and voltage waveforms can change but it is desirable that the switch has large dv/dt and di/dt ratings to eliminate the previously mentioned snubber circuitry.

9. *Ability to operate in high temperatures*. This will also eliminate the cooling requirements and simplify the converter's structure.

10. *Short-circuit fault behaviour*. This will mean that the converter will still be able to operate when a number of switches are connected in series allowing designs that have redundancy factors especially in high and ultra-high power applications.

11. *Light triggering and low power requirements to control the switch*. This will allow fibre optics to be used to control the switch. In most cases the power to drive the switch is taken from the power circuit itself and the low power requirements will minimize the losses of the system.

Having discussed the desired characteristics, we consider the various fully controlled power semiconductors and their realistic characteristics in the next sections.

5.2.5   Gate-turn-off thyristor

This semiconductor device, as the name implies, is a hybrid device that behaves like a thyristor. However, it has an added feature that the provided gate control allows the designer to turn the device on and off if and when desired. It became commercially available during the late 1980s although it was invented a long time ago (Van Ligten et al., 1960). Recently it has undergone a number of improvements and in the next few years may be able to replace the thyristor in the really high power area of applications.

The GTO thyristor is a device similar to the conventional thyristor. However, it is not just a latch-on device but also a latch-off one. The circuit symbol along with the layers are shown in Figures 5.7(a) and (b). The equivalent circuit is depicted in Figure 5.7(c). Its ideal and non-ideal i–v characteristics are plotted in Figures 5.7(d) and (e) respectively.
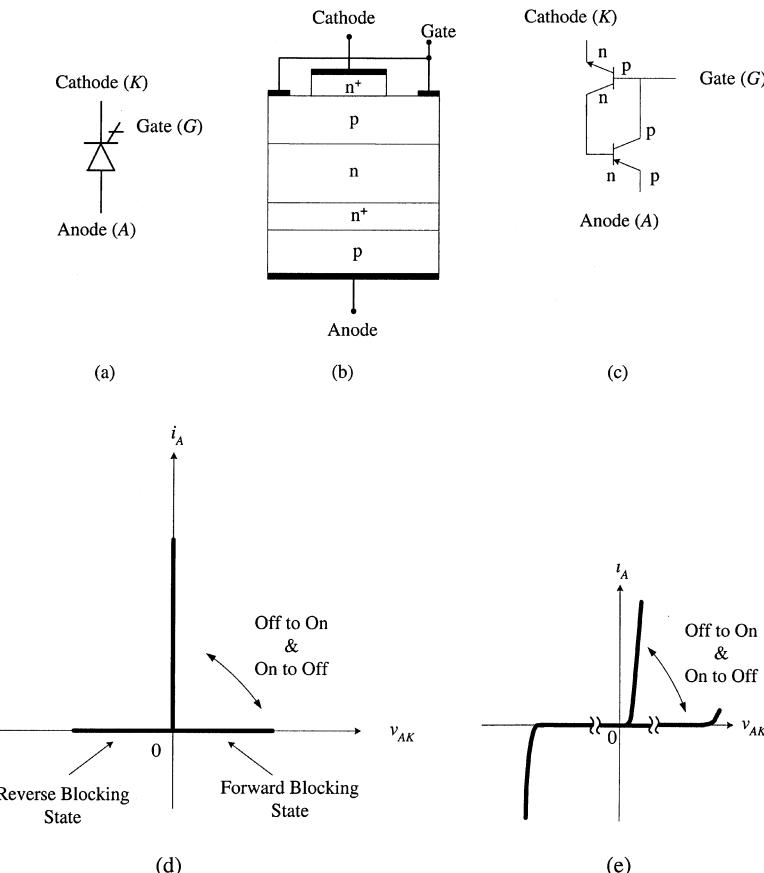
Fig. 5.7 GTO: (a) circuit symbol; (b) device structure; (c) equivalent circuit; (d) ideal i–v characteristics; and (e) non-ideal i–v characteristics.

It should be noted that although the GTO can be turned on like a thyristor, with a low positive gate current pulse, a large negative pulse is required to turn it off. These are relatively slow devices when compared with other fully controlled semiconductors. The maximum switching frequency attainable is in the order of 1 kHz. The voltage and current ratings of the commercially available GTOs are comparable to the thyristors approaching 6.5 kV, 4.5 kA and are expected to increase to cover completely the area occupied by thyristors as shown in Figure 5.12.

5.2.6 Metal-oxide-semiconductor field effect transistor

The metal-oxide semiconductor field effect transistor (MOSFET) is a transistor device capable of switching fast with low switching losses. It cannot handle high power and is mostly suited for low-power applications. These include switch-mode power supplies (SMPS) and low voltage adjustable speed motor drives used in copier machines, facsimiles and computers to name a few. In fact for very low
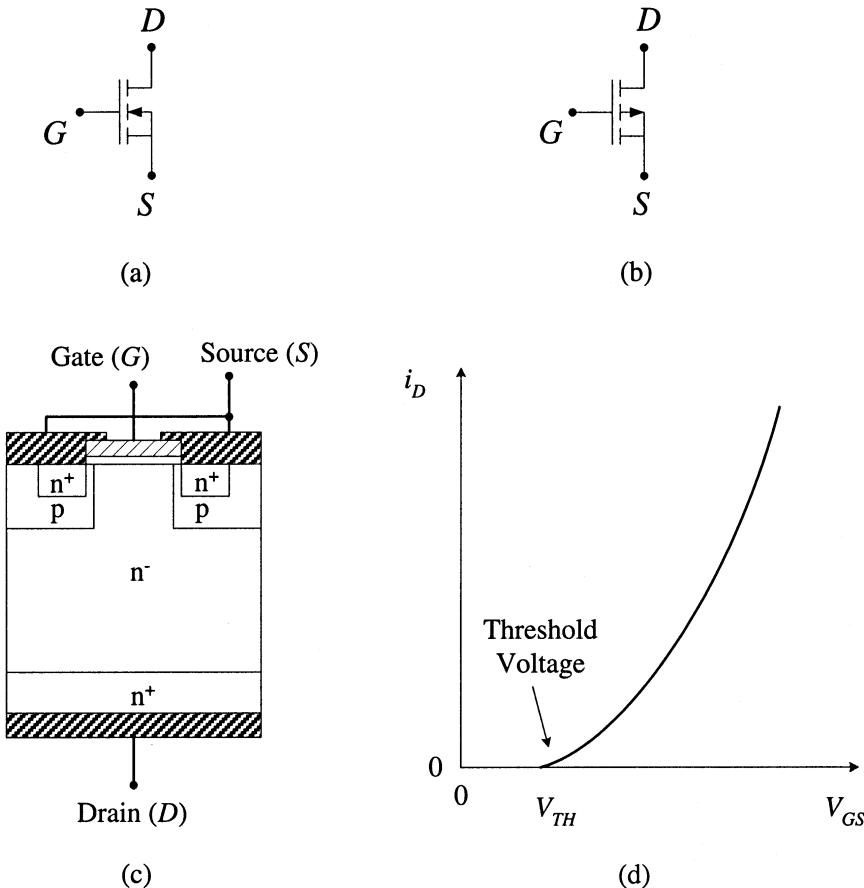
Fig. 5.8 Power MOSFET: (a) circuit symbol for an *n*-channel; (b) circuit symbol for a *p*-channel; (c) basic structure of an *n*-channel device; and (d) voltage signal control of a typical *n*-channel device.

power it is possible to operate the converter in switching frequencies in the MHz region.

This is by far the fastest switching power semiconductor device and this is due to the gate-controlled electric field required to turn the device on and off. In the case of a BJT, a current pulse is required to control it. It is also a slower device when compared with the MOSFET. Although its applications are limited with the lower power handling capability, it is important to understand its operation and structure as many of the new popular devices commercially available are based on MOSFET technology. Figures 5.8(a) and (b) show the circuit symbol for an n-channel and a p-channel MOSFET. The device is controlled by a voltage signal between the gate (G) and the source (S) that should be higher than the threshold voltage as shown in Figure 5.8(d).

5.2.7   Insulated-gate bipolar transistor

The IGBT is the most popular device for AC and DC motor drives reaching power levels of a few hundred kW. It has also started to make its way in the high voltage converter technology for power system applications. It is a hybrid semiconductor device that literally combines the advantages of MOSFETs and BJTs. Specifically, it has the switching characteristics of the MOSFET with the power handling capabilities of the BJT. It is a voltage-controlled device like the MOSFET but has lower conduction losses. Furthermore, it is available with higher voltage and current ratings. There are a number of circuit symbols for the IGBT with the most popular shown in Figure 5.9(a). The equivalent circuit is shown in Figure 5.9(b). The basic structure is then shown in Figure 5.9(c). The typical i–v characteristics are plotted in Figure 5.9(d).

The IGBTs are faster switching devices than the BJTs but not as fast as the MOSFETs. The IGBTs have lower on-state voltage drop even when the blocking voltage is high. Their structure is very similar to the one of the vertical diffused MOSFET, except the p+ layer that forms the drain of the device. This layer forms a junction (p–n).

Most of the IGBTs available on the market are two types as follows:

1. Punch-through IGBTs (PT-IGBTs).
2. Non-punch-through IGBTs (NPT-IGBTs).

Figure 5.10 shows the two basic structures of the two kinds of devices mentioned above.

When comparing the two kinds of devices the following observations can be made.

1. The PT-IGBTs do not have reverse blocking voltage capability.
2. The NPT-IGBTs have better short circuit capability but higher on-state voltage drop. They also have a positive temperature coefficient, which is a great benefit when paralleling devices.

There exist vertically optimized NPT structure based IGBT modules with $6.5\,\mathrm{k}V_{\mathrm{dc}}$ blocking voltage with rated currents up to 600 A. They have positive temperature coefficient of the on-state voltage, short circuit capability and high ruggedness against overcurrent.
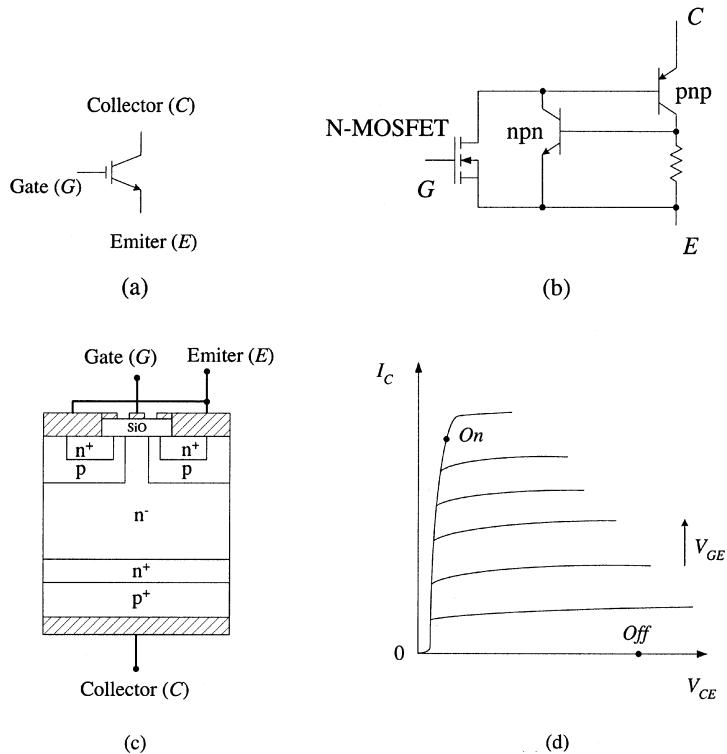
Fig. 5.9 IGBT features: (a) circuit symbol; (b) equivalent circuit; (c) device layer structure; and (d) *i–v* characteristics.
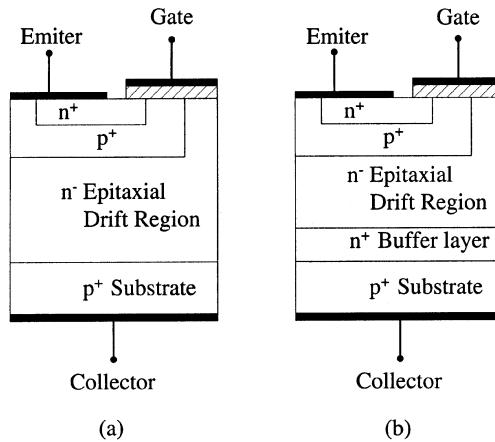
Fig. 5.10 Types of IGBTs: (a) punch-through IGBT; and (b) non-punch-through IGBT.

5.2.8   MOS-controlled thyristor

The MCT is a hybrid device that combines characteristics of two families of technologies, namely MOS and thyristor.
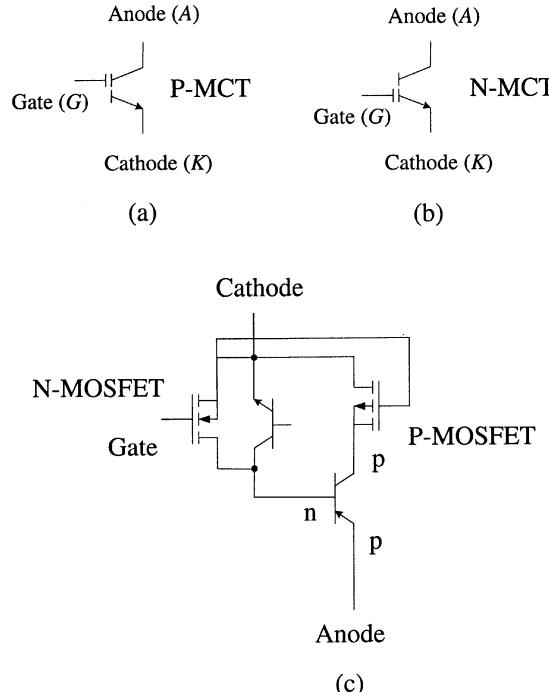
Fig. 5.11 MCT: (a) circuit symbol for a P-MCT; (b) circuit symbol for an N-MCT; and (c) equivalent circuit of an N-MCT.

The basic difference between the previously presented GTO and the MCT is that the second is turned on and off by short pulses of voltage between the gate and anode terminals rather than current pulse used to control the first one. The circuit symbol is shown in Figures 5.11(a) and (b) for a P-MCT and N-MCT respectively. The equivalent circuit is presented in Figure 5.11(c). The MCT exhibits capability to operate at high switching frequencies with low conduction losses.

5.2.9   Other semiconductor devices

There are also many other devices available in the market as a product or at R&D level. Many different names are given to them such as integrated gate-commutated thyristor (IGCT or GCT), emitter turn-off thyristor (ETO) and others. All of them are more or less hybrid versions of the existing devices and effort is spent to make them with higher ratings, better switching characteristics and with reduced conduction and switching losses.

5.2.10   Semiconductor switching-power performance

The power frequency range of the various semiconductors discussed in the previous sections are summarized in Figure 5.12. It is clear that the thyristor dominates the ultra-high power region for relatively low frequencies. The GTO is the next device when it comes to power handling capabilities extending to frequencies of a few hundred Hz. The IGBT occupies the area of medium power with the ability to
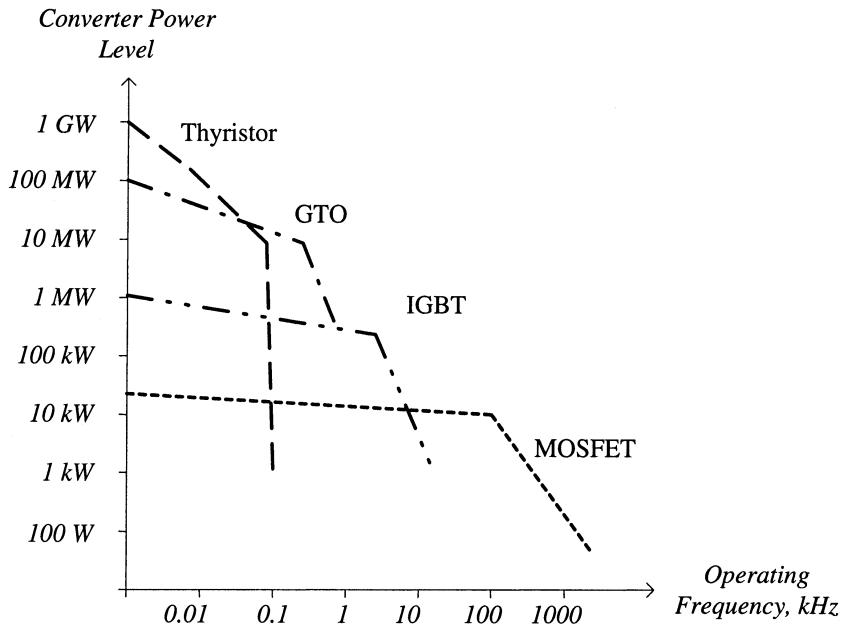
Fig. 5.12 Converter power level and frequency for various semiconductor devices.

operate at relatively higher frequencies, and finally the MOSFET extends its operation to high frequency regions for relatively low power levels. The tendency over the next few years is to have the GTO extend its power area towards the thyristor level. At the same time, the IGBT will also extend its power ability towards the GTO with higher switching frequency.

5.3   Power modules

Manufacturers of high power semiconductor devices offer power modules, which are easy to use to build a power electronics converter. Power modules offer two or more devices typically of the same type interconnected in a certain way to facilitate building a given converter topology. The power modules also naturally have increased voltage and/or current ratings due to internal series and/or parallel connection of several semiconductors. Converter legs for a single-phase and three-phase converter are also available and in many cases a modular converter including not only the three-phase inverter legs, but also the front-end three-phase diode rectifier and other integrated components.

5.4   Passive components

Many other components must be used to make a converter topology function properly to shape the voltage and current supplied from the source to the ones required by the load in a regulated manner and in many cases allow the power flow

to be bidirectional. Components such as inductors, capacitors and resistors must be used not only as part of protection devices in the case of snubbers, but also as filter elements.

Different technologies are available depending upon the power level and the function of the component. For instance, electrolytic, paper, paper–film, film, ceramic, mica, aluminium electrolytic, and oil filled capacitors are widely used in power electronics systems.

In the case of resistors, carbon composition, metal film, low voltage resistors, high voltage resistors, wire-wound resistors, and resistance wire materials are used in various ways and cases.

5.5   Ancillary equipment

A number of ancillary equipment is also used to build power electronics systems. These include support equipment as many of the components of the system are quite heavy. Also included are cabinets, copper bars, heat sinks, drive and control circuits as appropriate, isolation equipment, protection systems, diagnostics, fuses, information and display boards to name a few.

5.6   Cooling systems

Power losses associated with the operation of the semiconductors reduce their thermal capacity. High temperatures of the wafers drastically reduce the electrical characteristics of the devices, namely their maximum blocking voltage, switching times, etc. In order to increase the life expectancy and the reliability of power electronic equipment, adequate cooling means must be provided. Needless to say that overheating may cause total destruction of the device and the converter at large.

The temperature of the semiconductor junction T_j determines its reliability performance. Its maximum allowable value is specified by the manufacturer in the data sheets. It is therefore necessary to keep this temperature within a certain limit and for that reason, depending upon the application, a number of cooling mechanisms are available to the design engineer.

There exist three different mechanisms of heat transfer as follows:

- *Conduction*. The mode of heat transfer in solids or fluids, that are in conduct with one another, and heat can be transferred from the warm object to the cooler one.
- *Convection*. The mode of heat transfer between a solid object and the surrounding air. These mechanisms can be further divided into two subcategories, namely the natural convection and the forced one. The first one occurs naturally when a cooler non-moving air surrounds a warm object. The second one occurs when the air flow around the warm object is forced by a fan or other mechanical means. This method is more efficient and faster when compared with the natural convection. Of course other means such as liquid, i.e. oil or water can be used to remove heat from a given object.
- *Radiation*. The mode of heat transfer due to electromagnetic emission when a transparent medium surrounds a warm object.

The energy flow per unit time by conduction is given by the following formula:

$$P_{\text{conduction}} = \frac{\lambda}{d} \cdot A \cdot (T_1 - T_2) \tag{5.1}$$

where
λ is the thermal conductivity of the material in $[W/m \cdot {}^\circ C]$
T_1, T_2 are the temperatures in $[{}^\circ C]$
A is the surface area in $[m^2]$
d is the length in $[m]$
The energy flow per unit time by convection is

$$P_{\text{convection}} = \alpha \cdot A \cdot (T_1 - T_2) \tag{5.2}$$

where
α is the convection coefficient $[\frac{W}{m^2 \cdot {}^\circ C}]$
A is the surface area in $[m^2]$
T_1, T_2 are the temperatures in $[{}^\circ C]$
Finally, the energy flow per unit time by radiation is

$$P_{\text{radiation}} = S \cdot E \cdot A \cdot (T_1^4 - T_2^4) \tag{5.3}$$

where
S is the Stefan–Boltzmann constant $[5.67 \cdot 10^{-8} \frac{W}{m^2 \cdot K^4}]$
E is the emissivity of the material
A is the area in $[m^2]$
T_1, T_2 are the temperatures in $[{}^\circ K]$
In all previously mentioned cases, the heat transfer is dependent upon the surface area of the object. To increase the surface area, a heat sink is used to mount the device. The heat generated in the device is transferred first from the semiconductor to the heat sink and then to the ambient air if no other means are provided. In heat sinks all modes of heat transfer exist, namely, conduction between the semiconductor, and the heat sink, convection between the heat sink and the air, and radiation from the heat sink and semiconductor to the air. The efficiency of the transfer mode also depends upon the medium used for cooling when forced mechanisms are used. To improve the heat transfer due to conduction, the contact pressure between the semiconductor and the heat sink surface may be increased and conductive grease or soft thermal padding may also be used.

However, in most cases of low power electronic equipment a fan is placed at the bottom of the enclosure and slotted openings are provided to allow circulation of the air. In converters of significant power level and when the power-to-weight-ratio is very high, other means of forced cooling are used. For instance, oil similar to the one used in transformers is used to remove the heat from the converter.

In many cases water forced through hollow pipes is used as a cooling means. The heat-pipe coolers are composed of

- An aluminium base with elements clamped to conduct heat.
- Cooling plates composed of copper or aluminium with surfaces.
- Heat pipes that provide the thermal link between the aluminium base and the plates.

Another kind of heat pipe may include insulation between the evaporator and the condenser allowing water as a coolant or water and glycol and not necessarily chlorofluorocarbons (CFCs).

Figure 5.13 shows some heat sinks with power semiconductors mounted on them to illustrate the previously discussed points.
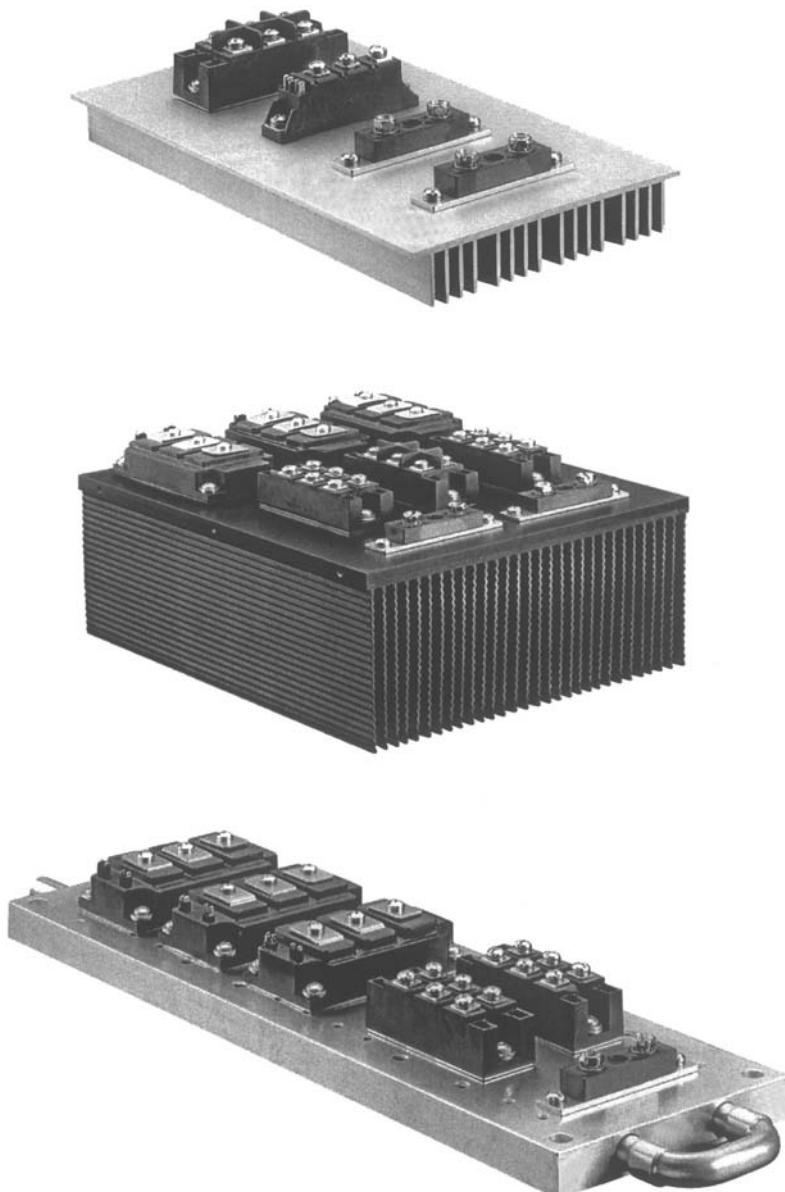
Fig. 5.13 Heat sinks: (a) air cooled extruded heat sink (velocity = 5 m/s, Rsa = 0.2 C/W, weight = 2.6 lb/ft); (b) air cooled fabricated heat sink (velocity = 5 m/s, Rsa = 0.02 C/W, weight = 21 lb/ft); and (c) liquid cooled heat sink (flow rate = 5 lt/s, Rsa = 0.002 C/W, weight = 4.5 lb/ft). (Courtesy of R-Theta, Inc., Mississauga, Ontario, Canada.)

5.7 Component layout

The layout of the converter is very important as high voltage and current are switched at high frequencies. This generates a great deal of EMI and voltage spikes, and care should be taken to minimize the inductance so that the electric noise effect is also kept to the minimum. Of course the worst-case scenario would be wrong triggering of a device that may result in short circuit, which will probably cause destruction of the system.

5.8 Protection of semiconductors – snubber circuits

Proper use of the devices presented so far requires determination of semiconductor losses since adequate cooling means have to be provided to keep the device temperature within rated values.

Generally, the semiconductor losses are grouped into three categories (Rockot, 1987):

1. conduction (on-state and dynamic saturation)
2. switching (turn-on and turn-off)
3. off-state.

The relative magnitudes of the conduction and switching losses are greatly dependent on the type of the converter (i.e. resonant, quasi-resonant, PWM, etc.), the operating frequency, the type of the load (i.e. linear or non-linear, resistive or inductive), and certain characteristics of the switch itself (i.e. turn-on time, turn-off time, etc.). Off-state losses are generally a very small portion of the total losses and are considered negligible.

Snubber circuits are a typical way to minimize switching losses in converters (McMurray, 1972; 1980; 1985). In general, snubber circuits are used for the reduction of switching losses and associated stresses (i.e. protection against high dv/dt and di/dt) of power semiconductor devices. The turn-on and turn-off circuits are placed in series/parallel to the power switching devices, respectively. For instance, one major purpose of using such circuits, especially for BJTs and GTOs is to keep the power device within its safe operating area (SOA).

Two different types of snubber circuits can be considered as follows:

1. dissipative
2. non-dissipative (low-loss snubber).

The basic difference between them is as follows:

- In dissipative snubber circuits, the energy stored in reactive elements (limiting di/dt inductor and limiting dv/dt capacitor) is dissipated in resistors and converted into heat. This type is certainly not the best choice to achieve high switching frequencies and/or high power levels.
- In non-dissipative (low-loss) snubber circuits, there are no substantial losses due to resistors. In this case, losses are only caused by non-ideal device properties, such as conduction and transient switching losses of the switching devices contained in the snubber circuits.

Snubber circuits are employed for the modern semiconductor devices such as power BJTs, MOSFETs, IGBTs, and GTOs. Figure 5.14 shows the conventional dissipative snubber circuits. Specifically, the turn-on snubber R_s–L_s to control the rate of rise of the switch current during turn-on and the turn-off snubber R_s–C_s to control the rise rate of the switch voltage during turn-off are shown. The polarized snubber circuits (turn-on/turn-off) are included. The combined polarized complete turn-on/turn-off snubber circuit is also depicted. The transistor S in each case is the respective semiconductor device that is being protected by the passive snubber components R_s, L_s, C_s and D_s.

With the use of a combined snubber circuit (Figure 5.14), the interaction between the semiconductor device and the snubber circuit is as follows:

- During turn-on the voltage fall is a linear time function completely dictated by the switch characteristics, while the series snubber inductor L_s dictates the current rise.
- During turn-off, the current fall is a linear time function completely determined by the switch characteristics, while the voltage rise is determined by the shunt (parallel) snubber capacitor C_s.

The operation of the combined snubber circuit (Figure 5.14) is described as follows:

After switch turn-on, the snubber capacitor C_s, discharges via the semiconductor device through the C_s–R_s–L_s loop. The discharge current is superimposed on the load current. The snubber capacitor C_s voltage reaches zero afterwards, at which moment the snubber polarizing diode D_s begins to conduct and the remaining overcurrent in the inductor L_s decays exponentially through the L_s–R_s loop. Then after switch turn-off, the series snubber inductor L_s begins to discharge and the snubber diode D_s conducts thus connecting C_s in parallel with the semiconductor device. The discharge voltage of the inductor is superimposed over the input voltage already present across the switch. The discharge circuit consists of the branch L_s–C_s–R_s. The inductor current reaches zero afterwards at which moment the snubber polarizing diode D_s blocks and the remaining overvoltage decays exponentially through the C_s–R_s loop.

The advantages of the conventional dissipative snubber circuits can be summarized as follows:

- Transfer of the switching losses from the semiconductor device to an external resistor;
- Suppression of high voltage transients;
- Control of the rise rate of the current during turn-on and the rise rate of the voltage during turn-off;
- Reduction of the generated 'noise' and the electromagnetic interference;
- Avoidance of the second breakdown in BJT based transistor inverters.

On the other hand, the following disadvantages associated with these snubber circuits can be identified:

- The energy stored in the reactive elements is dissipated in external resistors, thus decreasing overall converter efficiency;
- Overvoltages can still occur as a result of resonances between snubber or stray inductances and snubber or parasitic capacitors;

	Turn-on (Series)	Turn-off (Shunt)
Non Polarized		
Polarized		
Combined		
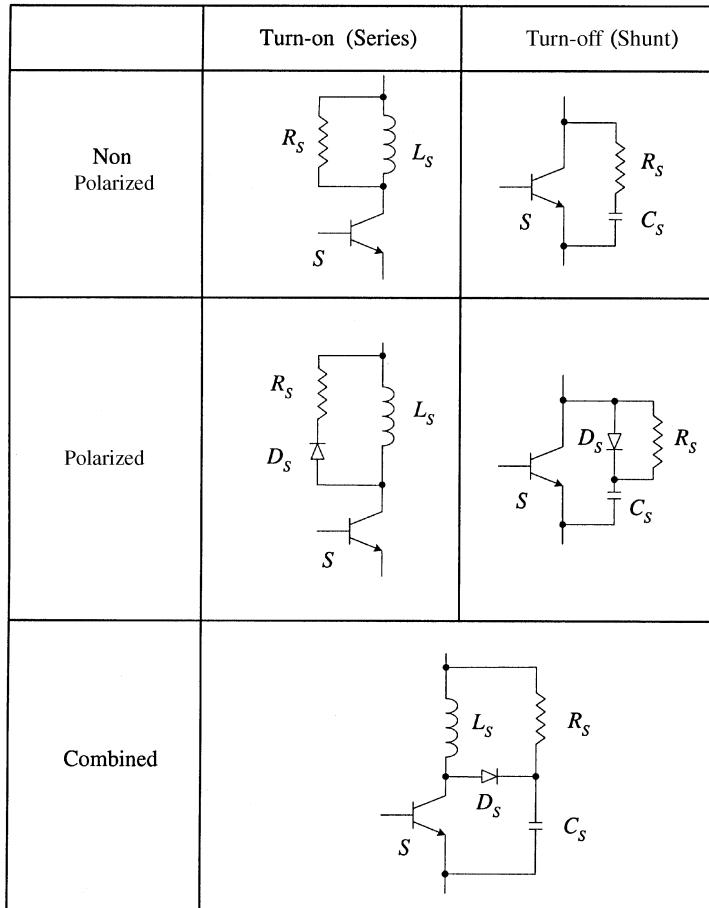
Fig. 5.14 Conventional dissipative snubber circuits.

● Extra components are required, thus increasing power circuit complexity;
● The power losses also complicate the thermal layout and the heat sink design thus leading to an increase in cost.

At higher power levels and switching frequencies, it is more desirable to use non-dissipative (low loss) snubber circuits. The snubber circuits previously presented (Figure 5.14) can be used for each switching device separately. However, it is more efficient to combine components and to use for instance one reactive element (inductor/capacitor) for both switches of a PWM inverter leg.

There are various snubber configurations that improve the overall component count by reducing the number of snubber elements (Undeland, 1976; Undeland et al., 1983; 1984; Zach et al., 1986). In many cases and depending upon the application of the converters, its power level, etc. the snubber circuits maybe more or less complicated. Some snubber configurations proposed for converters are shown in Figures 5.15, 5.16 and 5.17 showing increased complexity and different arrangements
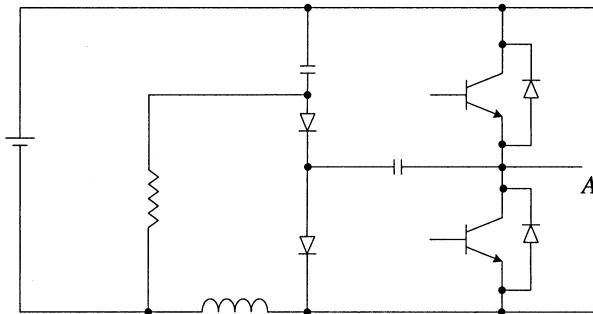
Fig. 5.15 An inverter leg with the improved dissipative snubber circuit.
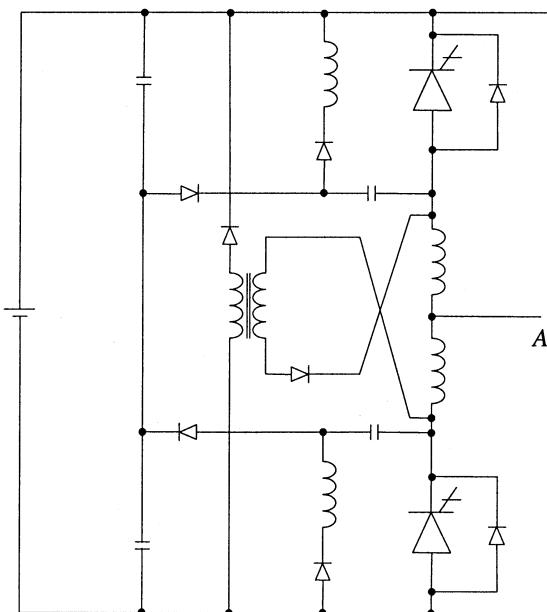
Fig. 5.16 A non-dissipative snubber circuit for high power GTO inverter.

in trying to recover the high energy associated with the operation of the snubber circuit (Holtz et al., 1988; 1989).

5.9   Current trends in power semiconductor technology

In recent years, reports have shown that improvements in the performance of the semiconductors can be achieved by replacing silicon with the following:

- silicon carbide (SiC)
- semiconducting diamond
- gallium arsenide.

The first group of devices is the most promising technology (Palmour et al., 1997).
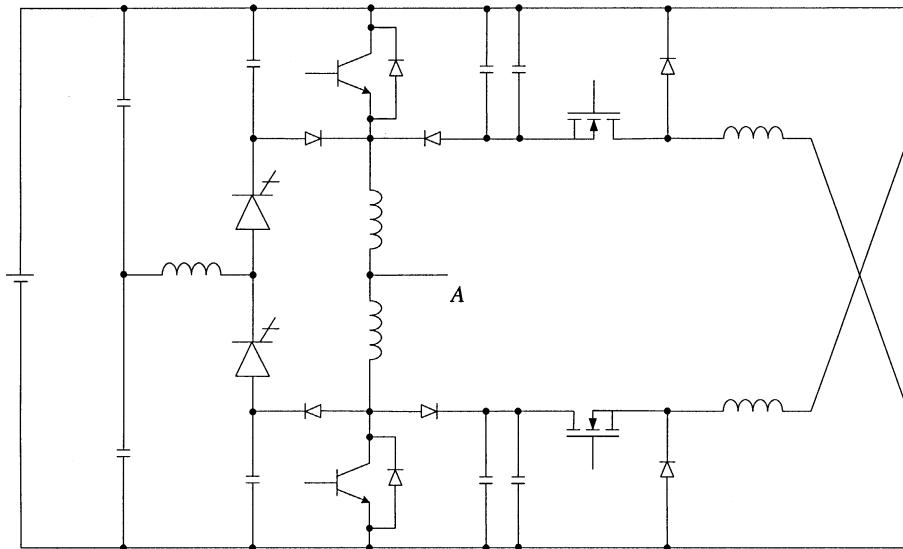
Fig. 5.17 A lossless snubber circuit for an inverter leg.

These new power semiconductor materials offer a number of interesting characteristics, which can be summarized as follows:

● large band gap
● high carrier mobility
● high electrical and thermal conductivity.

Due to the characteristics mentioned above, this new class of power device offers a number of positive attributes such as:

● high power capability
● operation at high frequencies
● relatively low voltage drop when conducting
● operation at high junction temperatures.

Such devices will be able to operate at temperatures up to approximately 600 °C. It is anticipated that this technology will probably offer semiconductors with characteristics closer to the desired ones discussed in the previous section.

Another important development is associated with the matrix converter (direct AC–AC conversion without a DC-link stage). For this converter bidirectional self-commutated devices are needed to build the converter. At the moment research efforts show some promising results (Heinke et al., 2000). However, a commercial product is probably not going to be available before the next decade or so.

5.10 Conclusion

Progress in semiconductor devices achieved over the last twenty years and antici-pated developments and improvements promise an exciting new era in power elec-

tronic systems. Snubberless operation of fully controlled semiconductors at high values of current and voltage and their rates of change will be realizable in the near future. New emerging applications of these semiconductors in areas such as Power Transmission and Distribution and High Voltage Industrial Motor Drives will be possible. The thyristor will remain the only component for certain applications, due to its unmatched characteristics. However, expected improvements of the GTO and IGBT technology and emerging new devices may replace it sooner than later. New applications and use of improved semiconductors may be possible. The next ten to twenty years will therefore see design and use of power electronic systems towards the 'silicon only' with 'no impedance' reactive power compensators and a totally electronically controlled power system as will be discussed in the following chapters.

6

Power electronic equipment

6.1 Introduction

Reactive power compensation in electric power systems is very important as explained in earlier chapters. In this chapter, we examine closer how compensators are realized in practice using the semiconductors and associated technology presented in Chapter 5.

In the first part of the chapter, the *static* compensators are presented. This kind of equipment belongs to the class of active compensators. Furthermore, *static* means that, unlike the synchronous condenser, they have no moving parts. They are used for surge-impedance compensation and for compensation by sectioning in long-distance, high-voltage transmission systems. In addition they have a variety of load-compensating applications. Their practical applications are listed in greater detail in Table 6.1. The main headings in Table 6.1 will be recognized as the fundamental requirements for operating an AC power system, as discussed in previous chapters. Other applications not listed in Table 6.1, but which may nevertheless

Table 6.1 Practical applications of static compensators in electric power systems

---

Maintain voltage at or near a constant level
- under slowly varying conditions due to load changes
- to correct voltage changes caused by unexpected events (e.g. load rejections, generator and line outages)
- to reduce voltage flicker caused by rapidly fluctuating loads (e.g. arc furnaces).

Improve power system stability
- by supporting the voltage at key points (e.g. the mid-point of a long line)
- by helping to improve swing damping.

Improve power factor

Correct phase unbalance

---

be very beneficial, include the control of AC voltage near conventional HVDC converter terminals, the minimization of transmission losses resulting from local generation or absorption of reactive power, and the suppression of subsynchronous resonance. Some types of compensators can also be designed to assist in the limitation of dynamic overvoltages.

In later parts of the chapter some widely used thyristor based controllers, namely the TCR, the thyristor-controlled transformer (TCT), and the TSC are introduced. We then discuss the conventional switch-mode voltage-source converters (VSCs). Some new topologies incorporating solid-state technology to provide multilevel waveforms for high power applications are also presented. Finally, the chapter discusses applications of such technology in energy storage systems, HVDC power transmission systems and active filtering.

6.2   Thyristor-controlled equipment

6.2.1   Thyristor-controlled reactor (TCR)

In this chapter, the IEEE terms and definitions for the various power electronic based controllers are used throughout.

Thyristor-controlled reactor (TCR) is defined as: a shunt-connected thyristor-controlled inductor whose effective reactance is varied in a continuous manner by partial conduction control of the thyristor valve.

Thyristor-switched reactor (TSR) is defined as: a shunt-connected, thyristor-switched inductor whose effective reactance is varied in a stepwise manner by full- or zero-conduction operation of the thyristor valve.

6.2.1.1   Principles of operation of the TCR

The basis of the TCR is shown in Figure 6.1. The controlling element is the thyristor controller, shown here as two back-to-back thyristors which conduct on alternate half-cycles of the supply frequency. If the thyristors are gated into conduction precisely at the peaks of the supply voltage, full conduction results in the reactor, and the current is the same as though the thyristor controller were short-circuited. The current is essentially reactive, lagging the voltage by nearly 90°. It contains a small in-phase component due to the power losses in the reactor, which may be of the order of 0.5–2% of the reactive power. Full conduction is shown by the current waveform in Figure 6.2(a).

If the gating is delayed by equal amounts on both thyristors, a series of current waveforms is obtained, such as those in Figure 6.2(a) through (d). Each of these corresponds to a particular value of the gating angle α, which is measured from the zero-crossing of the voltage. Full conduction is obtained with a gating angle of 90°. Partial conduction is obtained with gating angles between 90° and 180°. The effect of increasing the gating angle is to reduce the fundamental harmonic component of the current. This is equivalent to an increase in the inductance of the reactor, reducing its reactive power as well as its current. So far as the fundamental component of current is concerned, the TCR is a controllable susceptance, and can therefore be applied as a static compensator.
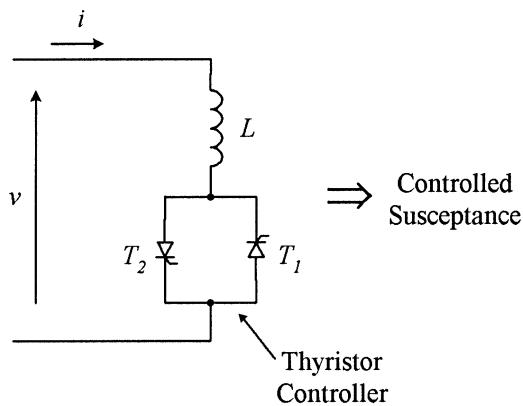
Fig. 6.1 Basic thyristor-controlled reactor.
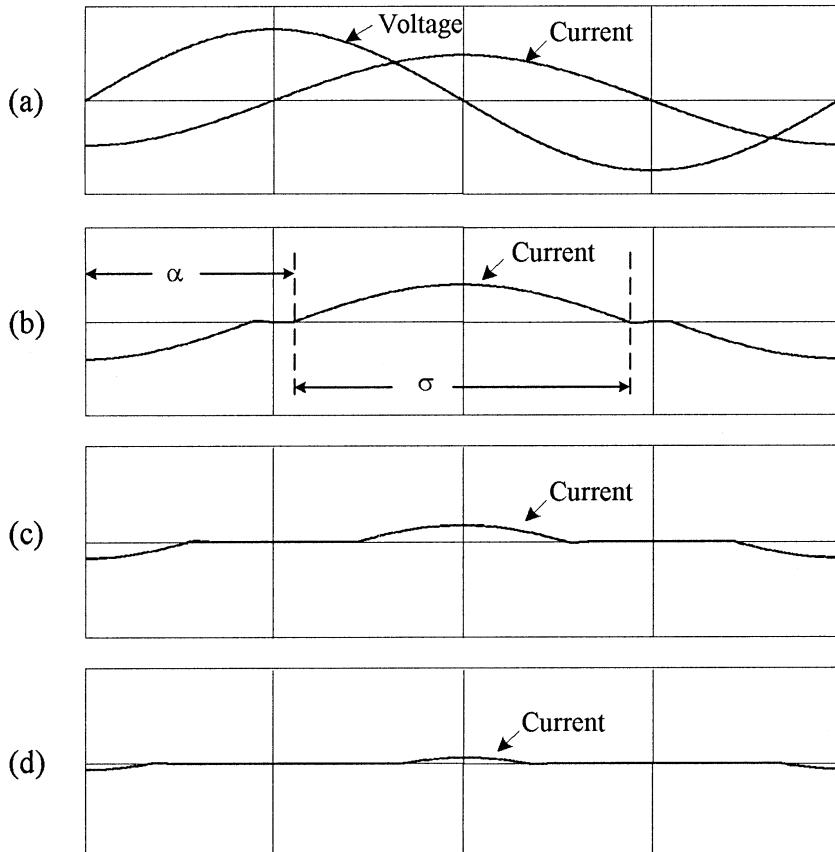
Fig. 6.2 Voltage and line current waveforms of a basic single-phase TCR for various firing angles. (a) $\alpha = 90°$, $\sigma = 180°$; (b) $\alpha = 100°$, $\sigma = 160°$; (c) $\alpha = 130°$, $\sigma = 100°$; (d) $\alpha = 150°$, $\sigma = 60°$.
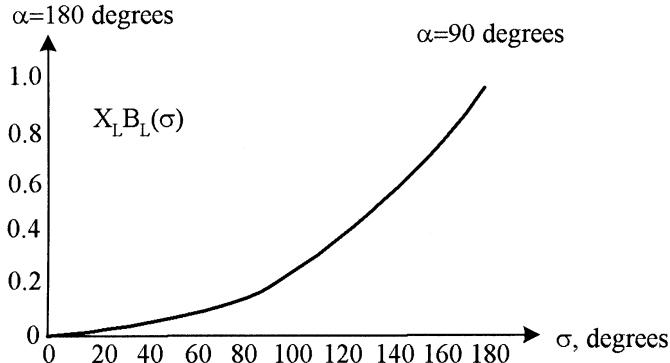
Fig. 6.3 Control law of a basic TCR.

The instantaneous current i is given by

$$i = \begin{cases} \dfrac{\sqrt{2}V}{X_{\mathrm{L}}}(\cos a - \cos \omega t), & a < \omega t < a + \sigma \\ 0, & a + \sigma < \omega t < a + \pi \end{cases} \tag{6.1}$$

where V is the rms voltage; $X_L = \omega L$ is the fundamental-frequency reactance of the reactor (in Ohms); $\omega = 2\pi f$; and α is the gating delay angle. The time origin is chosen to coincide with a positive-going zero-crossing of the voltage. The fundamental component is found by Fourier analysis and is given by

$$I_1 = \frac{\sigma - \sin \sigma}{\pi X_{\mathrm{L}}} V \, \mathrm{A \; rms} \tag{6.2}$$

where σ is the *conduction angle*, related to α by the equation

$$a + \frac{\sigma}{2} = \pi \tag{6.3}$$

Equation 6.2 can be written as

$$I_1 = B_{\mathrm{L}}(\sigma)V \tag{6.4}$$

where $B_{\mathrm{L}}(\sigma)$ is an adjustable fundamental-frequency susceptance controlled by the conduction angle according to the law

$$B_{\mathrm{L}}(\sigma) = \frac{\sigma - \sin \sigma}{\pi X_{\mathrm{L}}} \tag{6.5}$$

This control law is shown in Figure 6.3. The maximum value of B_{L} is $1/X_{\mathrm{L}}$, obtained with $\sigma = \pi$ or $180°$, that is, full conduction in the thyristor controller. The minimum value is zero, obtained with $\sigma = 0$ ($\alpha = 180°$). This control principle is called *phase control*.

6.2.1.2   Fundamental voltage/current characteristic
The TCR has to have a control system that determines the gating instants (and therefore σ), and that issues the gating pulses to the thyristors. In some designs the

control system responds to a signal that directly represents the desired susceptance B_L. In others, the control algorithm processes various measured parameters of the compensated system (e.g. the voltage) and generates the gating pulses directly without using an explicit signal for B_L. In either case the result is a voltage/current characteristic of the form shown in Figure 6.4. Steady-state operation is shown at the point of intersection with the system load line. In the example, the conduction angle is shown as 130°, giving a voltage slightly above 1.0 p.u., but this is only one of an infinite number of possible combinations, depending on the system load line, the control settings, and the compensator rating. The control characteristic in Figure 6.4 can be described by the equation

$$\mathbf{V} = \mathbf{V}_k + jX_S\mathbf{I}_1 \quad 0 < I_1 < I_{max} \tag{6.6}$$

where I_{max} is normally the rated current of the reactors shown here as 1 p.u.
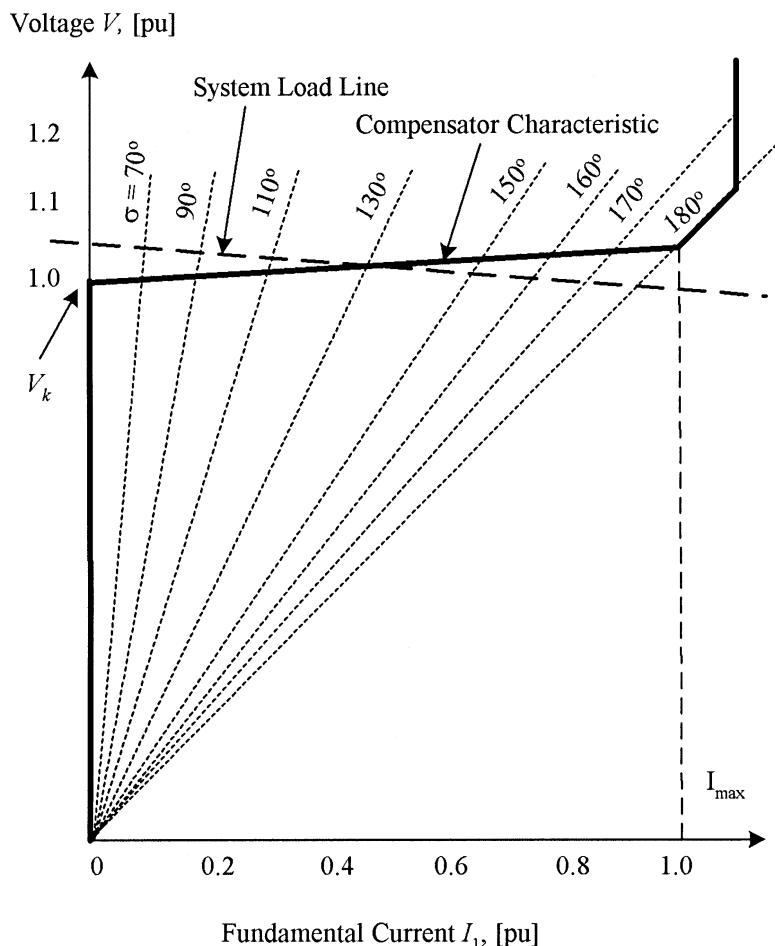
Fig. 6.4 Fundamental voltage/current characteristic in the TCR compensator.

6.2.1.3 Harmonics

Increasing the gating angle (reducing the conduction angle) has two other important effects. First, the power losses decrease in both the thyristor controller and the reactor. Second, the current waveform becomes less sinusoidal; in other words, the TCR generates harmonic currents. If the gating angles are balanced, (i.e. equal for both thyristors), all odd order harmonics are generated, and the rms value of the nth harmonic component is given by

$$I_n = \frac{4}{\pi} \frac{V}{X_L} \left[\frac{\sin(n+1)\alpha}{2(n+1)} + \frac{\sin(n-1)\alpha}{2(n-1)} - \cos\alpha \frac{\sin n\alpha}{n} \right] \quad n = 3, 5, 7\ldots \quad (6.7)$$

Figure 6.5(a) shows the variation of the amplitudes of some of the major (lower-order) harmonics with the conduction angles, and Figure 6.5(b) the variation of the total harmonic content.

Table 6.2 gives the maximum amplitudes of the harmonics down to the 37th. (Note that the maxima do not all occur at the same conduction angle.)

The TCR described so far is only a single-phase device. For three-phase systems the preferred arrangement is shown in Figure 6.6; i.e. three single-phase TCRs connected in delta. When the system is balanced, all the triplen harmonics circulate in the closed delta and are absent from the line currents. All the other harmonics are present in the line currents and their amplitudes are in the same proportions as shown in Figure 6.5 and Table 6.2. However, the waveforms differ from those ones presented in Figure 6.2.

It is important in the TCR to ensure that the conduction angles of the two back-to-back thyristors are equal. Unequal conduction angles would produce even harmonic components in the current, including DC. They would also cause unequal thermal stresses in the thyristors. The requirement for equal conduction also limits σ to a
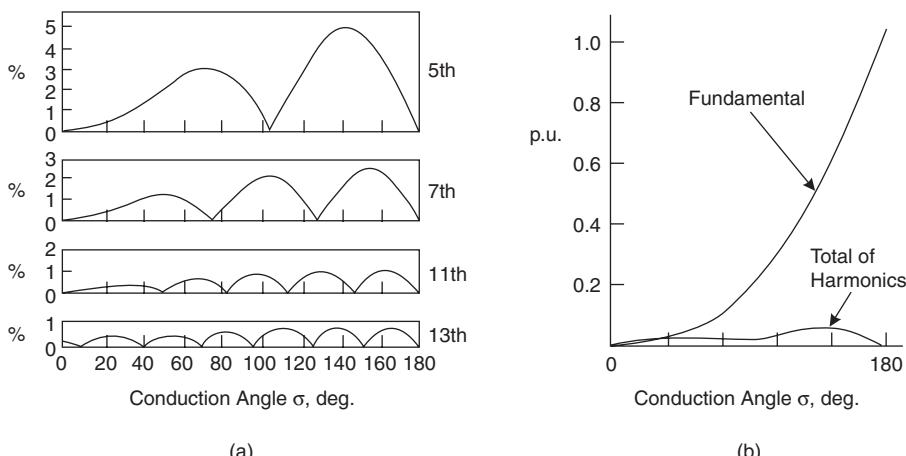
Fig. 6.5 TCR Harmonics. (a) major harmonic current components of TCR. Each is shown as a percentage of the fundamental component at full conduction. The percentages are the same for both phase and line currents; and (b) total harmonic content of TCR current, as a fraction of the fundamental component at full conduction. The percentages are the same for both phase and line currents.

Table 6.2 Maximum amplitudes of harmonic currents in TCR[a]

Harmonic order	Percentage
1	100.00
3	(13.78)[b]
5	5.05
7	2.59
9	(1.57)
11	1.05
13	0.75
15	(0.57)
17	0.44
19	0.35
21	(0.29)
23	0.24
25	0.20
27	(0.17)
29	0.15
31	0.13
33	(0.12)
35	0.10
37	0.09

[a] Values are expressed as a percentage of the amplitude of the fundamental component at full conduction.
[b] The values apply to both phase and line currents, except that triplen harmonics do not appear in the line currents. Balanced conditions are assumed.
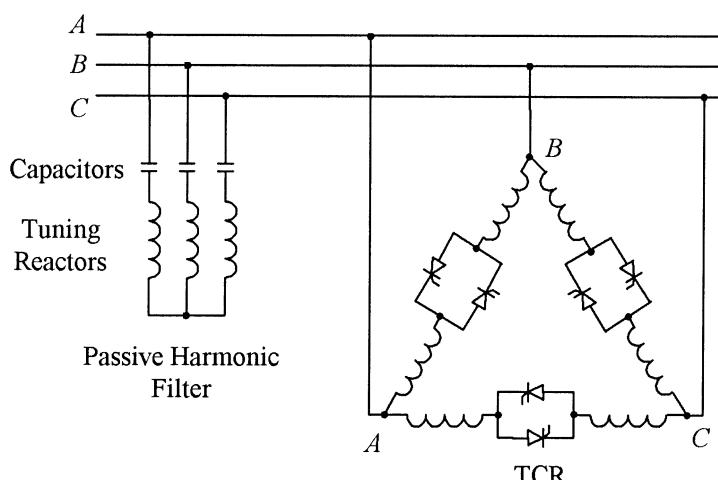
Fig. 6.6 Three-phase TCR with shunt capacitors. The split arrangement of the reactors in each phase provides extra protection to the thyristor controller in the event of a reactor fault.

maximum of 180°. However, if the reactor in Figure 6.1 is divided into two separate reactors (Figure 6.7), the conduction angle in each leg can be increased to as much as 360°. This arrangement has lower harmonics than that of Figure 6.1, but the power losses are increased because of currents circulating between the two halves.
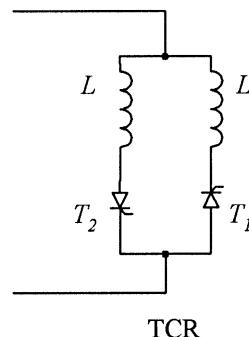
Fig. 6.7 TCR with more than 180° of conduction in each leg to reduce harmonic currents.

As already noted, TCR harmonic currents are sometimes removed by filters (Figure 6.6). An alternative means for eliminating the 5th and 7th harmonics is to split the TCR into two parts fed from two secondaries on the step-down transformer, one being in wye and the other in delta, as shown in Figure 6.8. This produces a 30° phase shift between the voltages and currents of the two TCRs and virtually eliminates the 5th and 7th harmonics from the primary-side line current. It is known as a 12-pulse arrangement because there are 12 thyristor gatings every period. The same phase-multiplication technique is used in conventional HVDC rectifier transformers
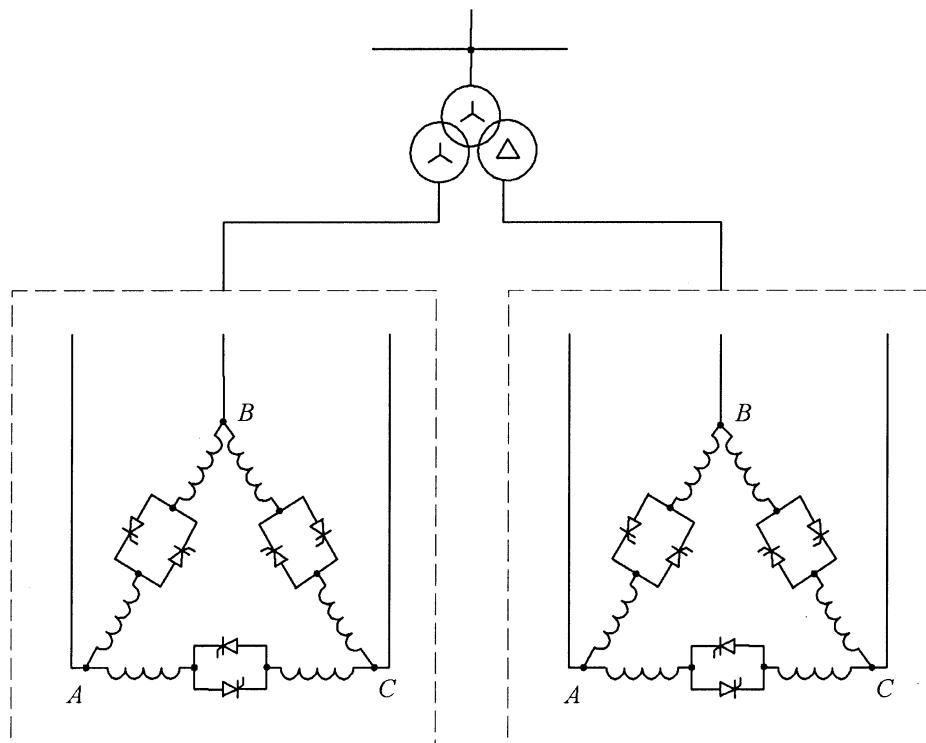
Fig. 6.8 Arrangement of 12-pulse TCR configuration with double-secondary transformer.

for harmonic cancellation. With the 12-pulse scheme, the lowest-order characteristic harmonics are the 11th and 13th. It can be used without filters for the 5th and 7th harmonics, which is an advantage when system resonances occur near these frequencies. For higher-order harmonics a plain capacitor is often sufficient, connected on the low-voltage side of the step-down transformer. Otherwise a high-pass filter may be used. The generation of third-harmonic currents under unbalanced conditions is similar to that in the six-pulse arrangement (Figure 6.6).

With both 6-pulse and 12-pulse TCR compensators, the need for filters and their frequency responses must be evaluated with due regard to the possibility of unbalanced operation. The influence of other capacitor banks and sources of harmonic currents in the electrical neighbourhood of the compensator must also be taken into account. For this purpose, several software packages are available and some examples with a specific one will be provided in Chapter 8.

The 12-pulse connection has the further advantage that if one half is faulted the other may be able to continue to operate normally. The control system must take into account the 30° phase shift between the two TCRs, and must be designed to ensure accurate harmonic cancellation. A variant of the 12-pulse TCR uses two separate transformers instead of one with two secondaries.

6.2.2 The thyristor-controlled transformer (TCT)

Another variant of the TCR is the TCT (Figure 6.9). Instead of using a separate step-down transformer and linear reactors, the transformer is designed with very high
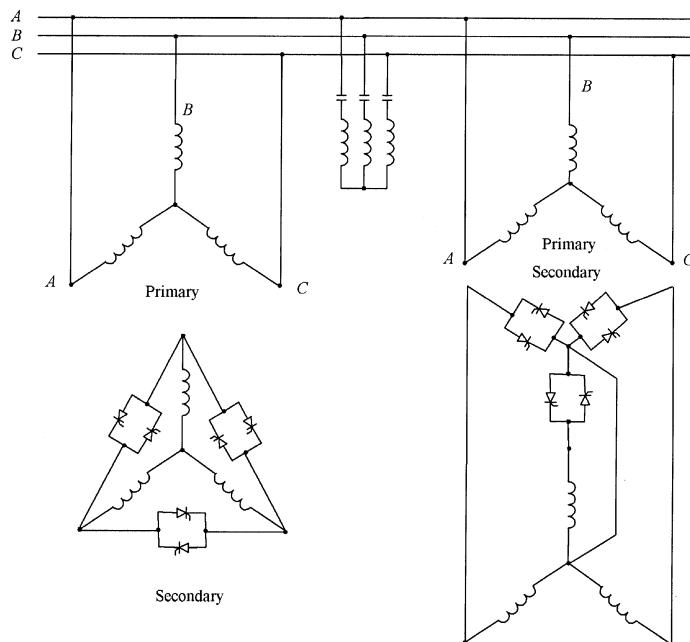
Fig. 6.9 Alternative arrangements of thyristor-controlled transformer compensator. (a) with wye-connected reactors and delta-connected thyristor controller; and (b) wye-connected reactors and thyristor controller (four-wire system).

leakage reactance, and the secondary windings are merely short-circuited through the thyristor controllers. A gapped core is necessary to obtain the high leakage reactance, and the transformer can take the form of three single-phase transformers. With the arrangements in Figure 6.9 there is no secondary bus and any shunt capacitors must be connected at the primary voltage unless a separate step-down transformer is provided. The high leakage reactance helps protect the transformer against short-circuit forces during secondary faults. Because of its linearity and large thermal mass the TCT can usefully withstand overloads in the lagging (absorbing) regime.

6.2.3   The TCR with shunt capacitors

It is important to note that the TCR current (the compensating current) can be varied *continuously*, without steps, between zero and a maximum value corresponding to full conduction. The current is always lagging, so that reactive power can only be absorbed. However, the TCR compensator can be biased by shunt capacitors so that its overall power factor is leading and reactive power is generated into the external system. The effect of adding the capacitor currents to the TCR currents shown in Figure 6.4 is to bias the control characteristic into the second quadrant, as shown in Figure 6.10. In a three-phase system the preferred arrangement is to connect the capacitors in wye, as shown in Figure 6.6. The current in Figure 6.10 is, of course, the fundamental positive sequence component, and if it lies between $I_{C\,max}$ and $I_{L\,max}$ the control characteristic is again represented by equation (6.6). However, if the voltage regulator gain is unchanged, the slope reactance X_s will be slightly increased when the capacitors are added.

As is common with shunt capacitor banks, the capacitors may be divided into more than one three-phase group, each group being separately switched by a circuit
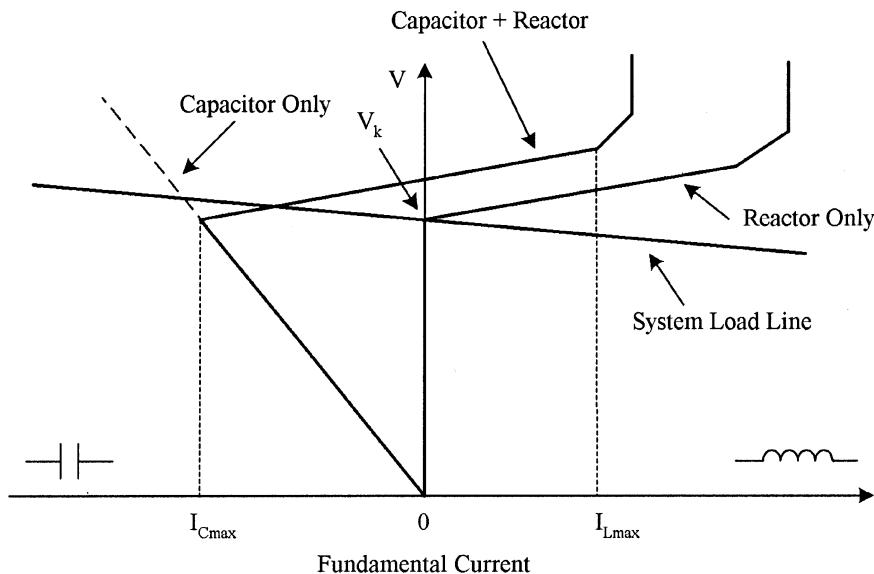
Fig. 6.10 Voltage/current characteristics of TCR.

breaker. The groups can be tuned to particular frequencies by small series reactors in each phase, to filter the harmonic currents generated by the TCR and so prevent them from flowing in the external system. One possible choice is to have groups tuned to the 5th and 7th harmonics, with another arranged as a high-pass filter. The capacitors arranged as filters, and indeed the entire compensator, must be designed with careful attention to their effect on the resonances of the power system at the point of connection.

It is common for the compensation requirement to extend into both the lagging and the leading ranges. A TCR with fixed capacitors cannot have a lagging current unless the TCR reactive power rating exceeds that of the capacitors. The net reactive power absorption rating with the capacitors connected equals the difference between the ratings of the TCR and the capacitors. In such cases the required TCR rating can be very large indeed (up to some hundreds of MVAr in transmission system applications). When the net reactive power is small or lagging, large reactive current circulates between the TCR and the capacitors without performing any useful function in the power system. For this reason the capacitors are sometimes designed to be switched in groups, so that the degree of capacitive bias in the voltage/current characteristic can be adjusted in steps. If this is done, a smaller 'interpolating' TCR can be used.

An example is shown schematically in Figure 6.11, having the shunt capacitors divided into three groups. The TCR controller is provided with a signal representing the number of capacitors connected, and is designed to provide a continuous overall voltage/current characteristic. When a capacitor group is switched on or off, the conduction angle is immediately adjusted, along with other reference signals, so that the capacitive reactive power added or subtracted is exactly balanced by an equal
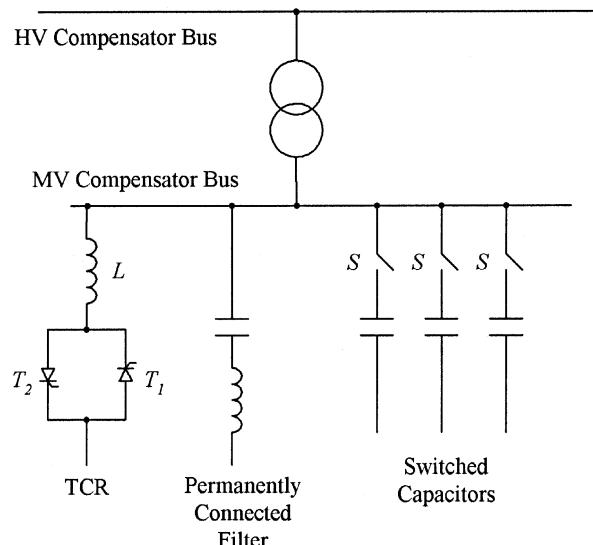
Fig. 6.11 Hybrid compensator with switched capacitors and 'interpolating' TCR. The switches S may be mechanical circuit breakers or thyristor switches.

change in the inductive reactive power of the TCR. Thereafter the conduction angle will vary continuously according to the system requirements, until the next capacitor switching occurs.

The performance of this hybrid arrangement of a TCR and switched shunt capacitors depends critically on the method of switching the capacitors, and the switching strategy. The most common way to switch the capacitors is with conventional circuit breakers. If the operating point is continually ranging up and down the voltage/current characteristic, the rapid accumulation of switching operations may cause a maintenance problem in the circuit breakers. Also, in transmission system applications there may be conflicting requirements as to whether the capacitors should be switched in or out during severe system faults. Under these circumstances repeated switching can place extreme duty on the capacitors and circuit breakers, and in most cases this can only be avoided by inhibiting the compensator from switching the capacitors. Unfortunately this prevents the full potential of the capacitors from being used during a period when they could be extremely beneficial to the stability of the system.

In some cases these problems have been met by using thyristor controllers instead of circuit breakers to switch the capacitors, taking advantage of the virtually unlimited switching life of the thyristors. The timing precision of the thyristor switches can be exploited to reduce the severity of the switching duty, but even so, during disturbances this duty can be extreme. The number of separately switched capacitor groups in transmission system compensators is usually less than four.

6.2.4 The thyristor-switched capacitor (TSC)

Thyristor switched capacitor is defined as 'a shunt-connected, thyristor-switched capacitor whose effective reactance is varied in a stepwise manner by full- or zero-conduction operation of the thyristor valve'.

6.2.4.1 Principles of operation

The principle of the TSC is shown in Figures 6.12 and 6.13. The susceptance is adjusted by controlling the number of parallel capacitors in conduction. Each capacitor always conducts for an integral number of half-cycles. With k capacitors in parallel, each controlled by a switch as in Figure 6.13, the total susceptance can be equal to that of any combination of the k individual susceptances taken $0, 1, 2 \ldots$ or k at a time. The total susceptance thus varies in a stepwise manner. In principle the steps can be made as small and as numerous as desired, by having a sufficient number of individually switched capacitors. For a given number k the maximum number of steps will be obtained when no two combinations are equal, which requires at least that all the individual susceptances be different. This degree of flexibility is not usually sought in power-system compensators because of the consequent complexity of the controls, and because it is generally more economic to make most of the susceptances equal. One compromise is the so-called binary system in which there are $(k-1)$ equal susceptances B and one susceptance $B/2$. The half-susceptance increases the number of combinations from k to $2k$.

The relation between the compensator current and the number of capacitors conducting is shown in Figure 6.14 (for constant terminal voltage). Ignoring switching transients, the current is sinusoidal, that is, it contains no harmonics.
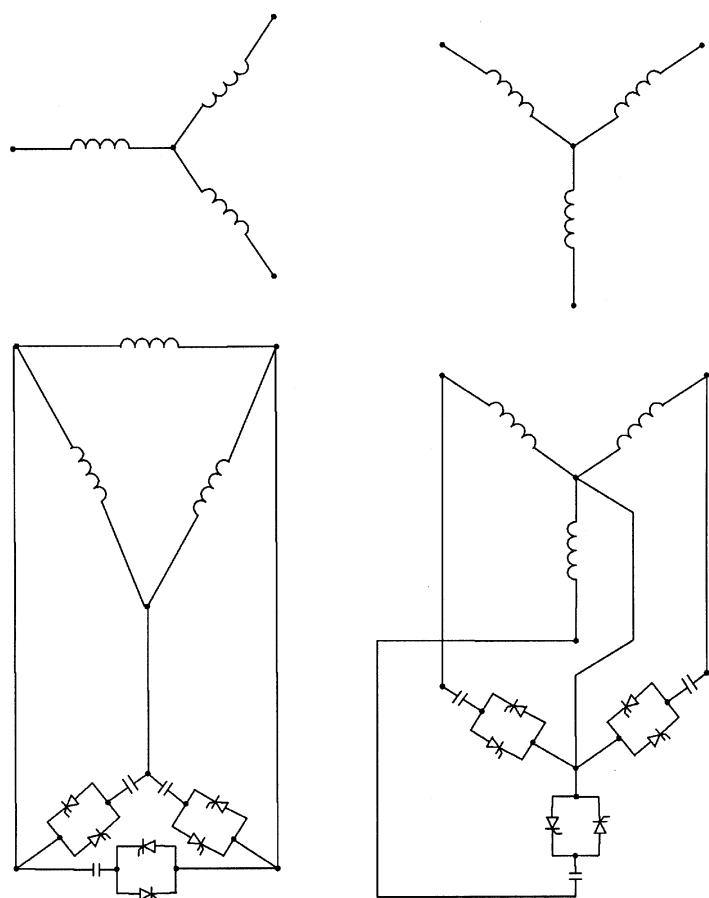
Fig. 6.12 Alternative arrangements of three-phase thyristor-switched capacitor. (a) delta-connected secondary, Delta-connected TSC; and (b) wye-connected secondary, wye-connected TSC (four-wire system).
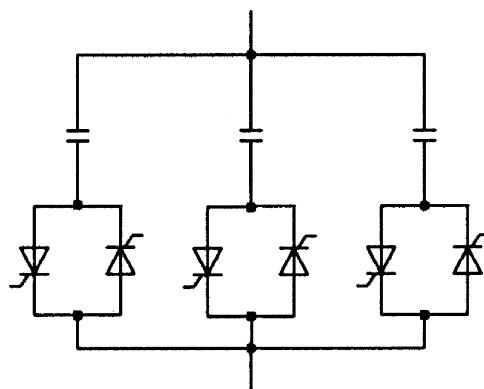
Fig. 6.13 Principles of operation of TSC. Each phase of Figure 6.12 comprises of parallel combinations of switched capacitors of this type.
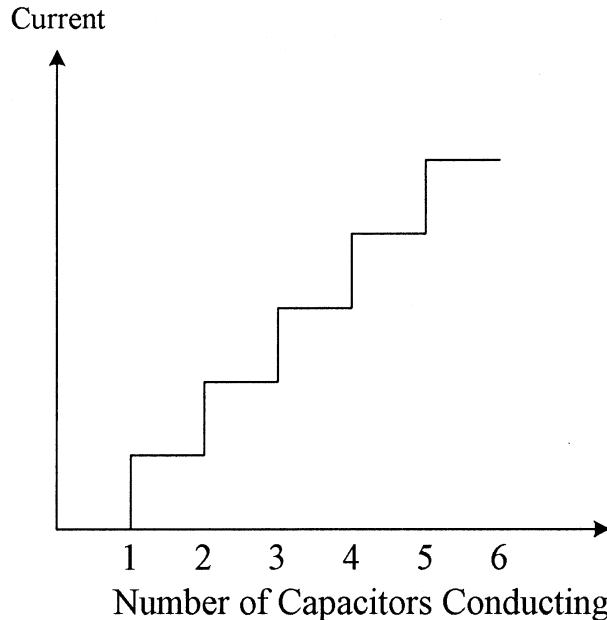
Fig. 6.14 Relationship between current and number of capacitors conducting in the TSC.

6.2.5 Switching transients and the concept of transient-free switching

When the current in an individual capacitor reaches a natural zero-crossing, the thyristors can be left ungated and no further current will flow. The reactive power supplied to the power system ceases abruptly. The capacitor, however, is left with a trapped charge (Figure 6.15(a)). Because of this charge, the voltage across the thyristors subsequently alternates between zero and twice the peak-phase voltage. The only instant when the thyristors can be gated again without transients is when the voltage across them is zero (Figure 6.15(b)). This coincides with peak-phase voltage.

6.2.5.1 Ideal transient-free switching
The simple case of a switched capacitor, with no other circuit elements than the voltage supply, is used first to describe the important concept of transient-free switching. Figure 6.16 shows the circuit.

With sinusoidal AC supply voltage $v = \hat{v}\sin(\omega_0 t + \alpha)$, the thyristors can be gated into conduction only at a peak value of voltage, that is, when

$$\frac{\mathrm{d}v}{\mathrm{d}t} = \omega_0 \hat{v}\cos(\omega_0 t + \alpha) = 0 \tag{6.8}$$

Gating at any other instant would require the current $i = C\mathrm{d}v/\mathrm{d}t$ to have a discontinuous step change at $t = 0^+$. Such a step is impossible in practice because of inductance, which is considered in the next section. To permit analysis of Figure 6.16, the gating must occur at a voltage peak, and with this restriction the current is given by

(a)

(b)
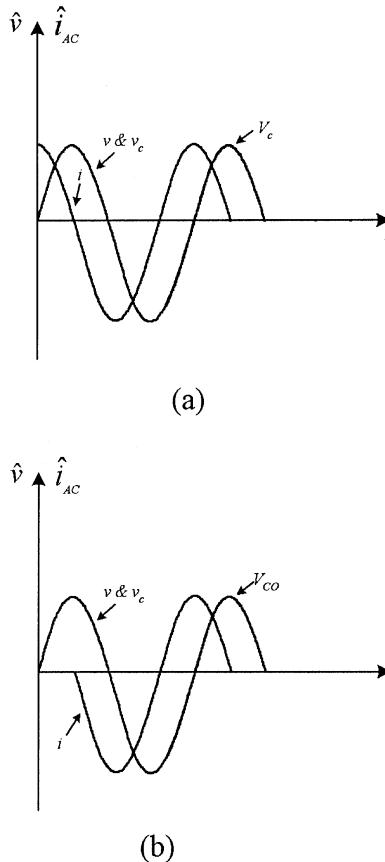
Fig. 6.15 Ideal transient-free switching waveforms. (a) switching on; and (b) switching off.
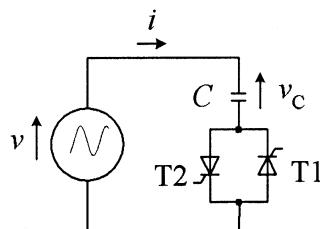
Fig. 6.16 Circuit for analysis of transient-free switching.

$$i = C\frac{\mathrm{d}v}{\mathrm{d}t} = \hat{v}\omega_0 C \cos{(\omega_0 t + \alpha)} \tag{6.9}$$

where $\alpha = \pm\pi/2$. Now $\omega_0 C = B_c$ is the fundamental-frequency susceptance of the capacitor, and $X_c = 1/B_c$ its reactance, so that with $\alpha = \pm\pi/2$

$$i = \pm\hat{v}B_c \sin{(\omega_0 t)} = +\hat{i}_{AC} \sin{(\omega_0 t)} \tag{6.10}$$

where $\hat{i}_{AC}$ is the peak value of the AC current, $\hat{i}_{AC} = \hat{v}B_C = \hat{v}/X_C$.

In the absence of other circuit elements, we must also specify that the capacitor be precharged to the voltage $V_{C0} = \pm\hat{v}$, that is, it must hold the prior charge $\pm\hat{v}/C$. This is because any prior DC voltage on the capacitor cannot be accounted for in the simple circuit of Figure 6.16. In practice this voltage would appear distributed across series inductance and resistance with a portion across the thyristor switch.

With these restrictions, that is, $dv/dt = 0$ and $V_{C0} = \pm\hat{v}$ at $t = 0$, we have the ideal case of transient-free switching, as illustrated in Figure 6.15. This concept is the basis for switching control in the TSC. In principle, once each capacitor is charged to either the positive or the negative system peak voltage, it is possible to switch any or all of the capacitors on or off for any integral number of half-cycles without transients.

6.2.5.2   *Switching transients in the general case*

Under practical conditions, it is necessary to consider inductance and resistance. First consider the addition of series inductance in Figure 6.16. In any practical TSC circuit, there must always be at least enough series inductance to keep di/dt within the capability of the thyristors. In some circuits there may be more than this minimum inductance. In the following, resistance will be neglected because it is generally small and its omission makes no significant difference to the calculation of the first few peaks of voltage and current.

The presence of inductance and capacitance together makes the transients oscillatory. The natural frequency of the transients will be shown to be a key factor in the magnitudes of the voltages and currents after switching, yet it is not entirely under the designer's control because the total series inductance includes the supply-system inductance which, if known at all, may be known only approximately. It also includes the inductance of the step-down transformer (if used), which is subject to other constraints and cannot be chosen freely.

It may not always be possible to connect the capacitor at a crest value of the supply voltage. It is necessary to ask what other events in the supply-voltage cycle can be detected and used to initiate the gating of the thyristors, and what will be the resulting transients.

The circuit is that of Figure 6.17. The voltage equation in terms of the Laplace transform is

$$V(s) = \left[L \cdot s + \frac{1}{C \cdot s} \right] I(s) + \frac{V_{C0}}{s} \tag{6.11}$$
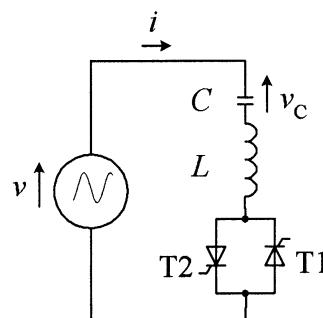
Fig. 6.17 Circuit for analysis of practical capacitor switching.

The supply voltage is given by $v = \hat{v} \sin(\omega_0 t + \alpha)$. Time is measured from the first instant when a thyristor is gated, corresponding to the angle α on the voltage wave-form. By straightforward transform manipulation and inverse transformation we get the instantaneous current expressed as

$$i(t) = \hat{i}_{AC} \cos(\omega_0 t + \alpha) - nB_C \left[V_{C0} - \frac{n^2}{n^2 - 1} \hat{v} \sin \alpha \right] \sin(\omega_n t) - \hat{i}_{AC} \cos \alpha \cos(\omega_n t)$$

(6.12)

where ω_n is the natural frequency of the circuit

$$\omega_n = \frac{1}{\sqrt{LC}} = n\omega_0$$

(6.13)

and

$$n = \sqrt{\frac{X_C}{X_L}}$$

(6.14)

n is the per-unit natural frequency.

The current has a fundamental-frequency component i_{AC} which leads the supply voltage by $\pi/2$ radians. Its amplitude $\hat{i}_{AC}$ is given by

$$\hat{i}_{AC} = \hat{v} B_C \frac{n^2}{n^2 - 1}$$

(6.15)

and is naturally proportional to the fundamental-frequency susceptance of the capacitance and inductance in series, that is, $B_c n^2/(n^2 - 1)$. The term $n^2/(n^2 - 1)$ is a magnification factor, which accounts for the partial series-tuning of the L–C circuit. If there is appreciable inductance, n can be as low as 2.5, or even lower, and the magnification factor can reach 1.2 or higher. It is plotted in Figure 6.18.

The last two terms on the right-hand side of equation (6.12) represent the expected oscillatory components of current having the frequency ω_n. In practice, resistance
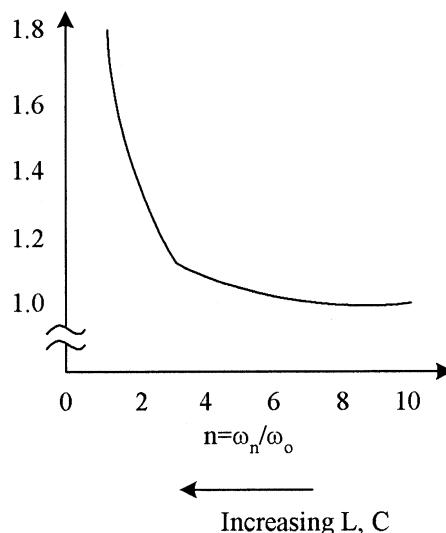
Fig. 6.18 Voltage and current magnification factor $n^2/(n^2 - 1)$.

causes these terms to decay. The next section considers the behaviour of the oscillatory components under important practical conditions.

1. *Necessary condition for transient-free switching*. For transient-free switching, the oscillatory components of current in equation (6.12) must be zero. This can happen only when the following two conditions are simultaneously satisfied:

$$\cos \alpha = 0 \ (i.e. \sin \alpha = \pm 1) \tag{6.16}$$

$$V_{C0} = \pm \hat{v} \frac{n^2}{n^2 - 1} = \pm X_c \hat{i}_{AC} \tag{6.17}$$

The first of these equations means that the thyristors must be gated at a positive or negative crest of the supply voltage sinewave. The second one means that the capacitors must also be precharged to the voltage $\hat{v} n^2 / (n^2 - 1)$ with the same polarity. The presence of inductance means that for transient-free switching the capacitor must be 'overcharged' beyond $\hat{v}$ by the magnification factor $n^2 / (n^2 - 1)$. With low values of n, this factor can be appreciable (Figure 6.18).

   Of the two conditions necessary for transient-free switching, the precharging condition expressed by equation (6.17) is strictly outside the control of the gating-control circuits because V_{C0}, n, and $\hat{v}$ can all vary during the period of non-conduction before the thyristors are gated. The capacitor will be slowly discharging, reducing V_{C0}; while the supply system voltage and effective inductance may change in an unknown way, changing n. In general, therefore, it will be impossible to guarantee perfect transient-free reconnection.

   In practice the control strategy should cause the thyristors to be gated in such a way as to keep the oscillatory transients within acceptable limits. Of the two conditions given by equations (6.16) and (6.17), the first one can in principle always be satisfied. The second one can be approximately satisfied under normal conditions. For a range of system voltages near 1 p.u., equation (6.17) will be nearly satisfied if the capacitor does not discharge (during a non-conducting period) to a very low voltage: or if it is kept precharged or 'topped up' to a voltage near $\pm \hat{v} n^2 / (n^2 - 1)$.

2. *Switching transients under non-ideal conditions*. There are some circumstances in which equations (6.16) and (6.17) are far from being satisfied. One is when the capacitor is completely discharged, as for example when the compensator has been switched off for a while. Then $V_{C0} = 0$. There is then no point on the voltage wave when both conditions are simultaneously satisfied.

In the most general case V_{C0} can have any value, depending on the conditions under which conduction last ceased and the time since it did so. The question then arises, how does the amplitude of the oscillatory component depend on V_{C0}? How can the gating instants be chosen to minimize the oscillatory component? Two practical choices of gating are: (a) at the instant when $v = V_{C0}$, giving $\sin \alpha = V_{C0}/\hat{v}$; and (b) when $dv/dt = 0$, giving $\cos \alpha = 0$. The first of these may never occur if the capacitor is overcharged beyond $\hat{v}$. The amplitude $\hat{i}_{osc}$ of the oscillatory component of current can be determined from equation (6.12) for the two alternative gating angles. In Figures 6.19 and 6.20 the resulting value of $\hat{i}_{osc}$ relative to $\hat{i}_{AC}$ is shown as a function of V_{C0} and n, for each of the two gating angles.

   From these two figures it is apparent that if V_{C0} is exactly equal to $\hat{v}$, the oscillatory component of current is non-zero and has the same amplitude for both gating angles,
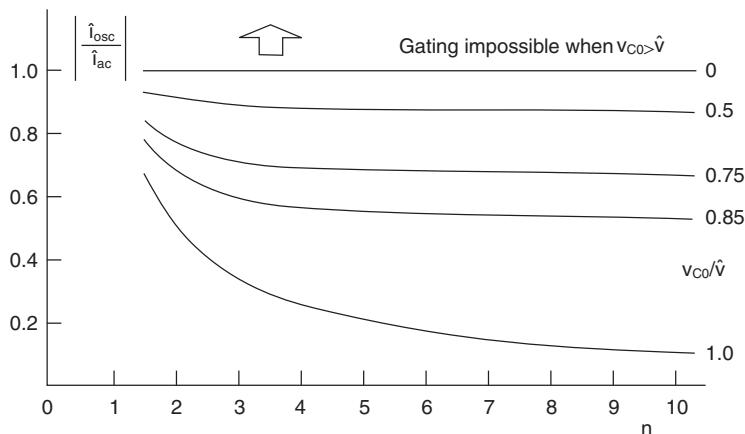
Fig. 6.19 Amplitude of oscillatory current component. Thyristors gated when $v = v_{C0}$.
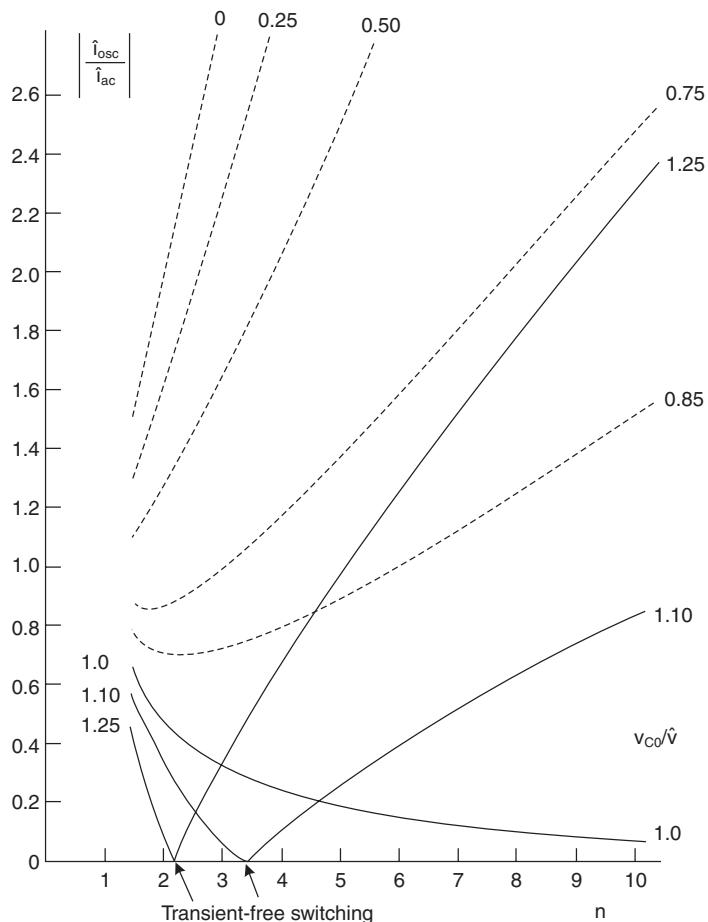
Fig. 6.20 Amplitude of oscillatory current component. Thyristors gated when $dv/dt = 0$.

whatever the value of the natural frequency n. For any value of V_{c0} less than $\hat{v}$, gating with $v = V_{C0}$ always gives the smaller oscillatory component whatever the value of n.

The conditions for transient-free switching appear in Figure 6.20 in terms of the precharge voltage required for two particular natural frequencies corresponding to $n = 2.3$ and $n = 3.6$.

6.2.5.3 *Switching a discharged capacitor*

In this case $V_{C0} = 0$. The two gating angles discussed were: (a) when $v = V_{C0} = 0$; and (b) when $dv/dt = 0$ ($\cos \alpha = 0$). In the former case only equation (6.17) is satisfied. From equation (6.12) it can be seen that in the second case (gating when $dv/dt = 0$) the oscillatory component of current is greater than in the first case (gating when $v = V_{C0} = 0$). An example is shown in Figure 6.21 and Figure 6.22.
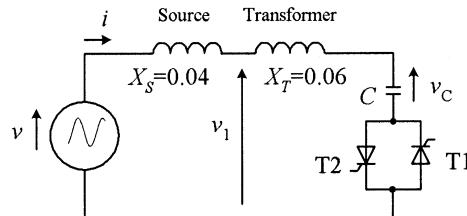
Fig. 6.21 Switching a discharge capacitor; circuit diagram.

(a)

(b)
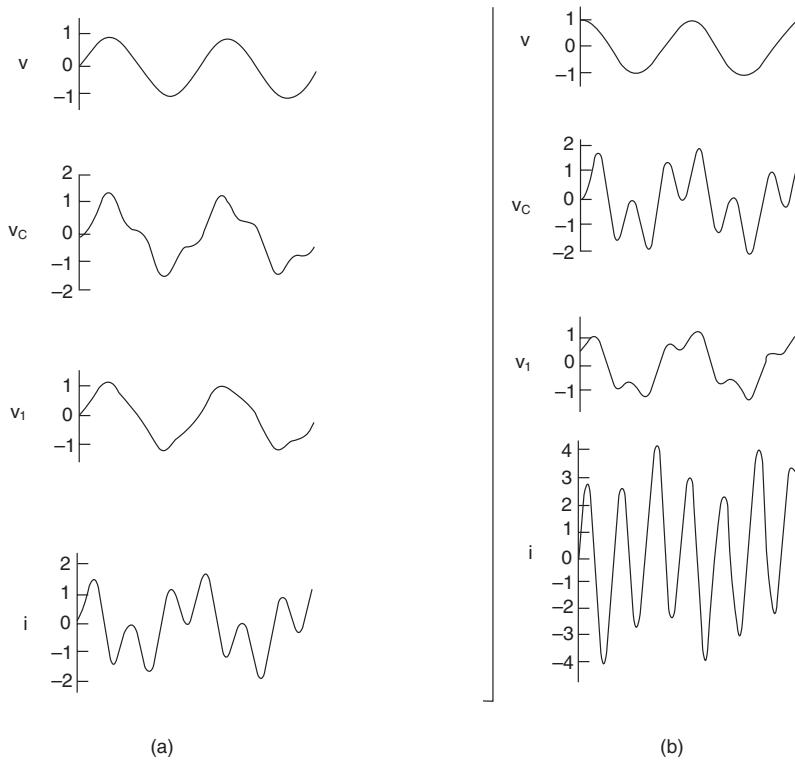
Fig. 6.22 Switching transients with discharge capacitor. (a) gating when $v = v_{C0} = 0$; (b) gating when $dv/dt = 0$.

The reactances are chosen such at $\hat{i}_{AC} = 1$ p.u. and the natural frequency is given by $n = X_C/(X_S + X_T) = 3.6$ p.u. In case (a), the amplitude of the oscillatory component of current is exactly equal to $\hat{i}_{AC}$. In case (b), the oscillatory component has the amplitude $n\hat{i}_{AC}$ and much higher current peaks are experienced. The capacitor experiences higher voltage peaks and the supply voltage distortion is greater.

6.3 Voltage-source converters (VSCs) and derived controllers

The solid-state DC–AC power electronic converters can be classified into two categories with respect to the type of their input source on the DC side being either a voltage- or a current-source:

1. Voltage-source converters or else voltage-source inverters (VSIs): the DC bus input is a voltage source (typically a capacitor) and its current through can be either positive or negative. This allows power flow between the DC and AC sides to be bidirectional through the reversal of the direction of the current.
2. Current-source converters (CSCs) or else current-source inverters (CSIs): the DC bus input is a current source (typically an inductor in series with a voltage source, i.e. a capacitor) and its voltage across can be either positive or negative. This also allows the power flow between the DC and AC sides to be bidirectional through the reversal of the polarity of the voltage.

The conventional phase-controlled thyristor-based converters can only be current source systems. The modern converters based on fully controlled semiconductors can be of either type. In most reactive power compensation applications, when fully controlled power semiconductors are used, the converters then are voltage-source based. However, the conventional thyristor-controlled converters are still used in high power applications and conventional HVDC systems.

In the following sections, we discuss first the half-bridge and the full-bridge single-phase VSC topologies. It is important to understand the operation principles of these two basic converters to fully understand and appreciate all the other derived topologies, namely the conventional six-switch three-phase VSC and other multilevel topologies.

6.3.1 Single-phase half-bridge VSC

Let us consider first the simplest and basic solid-state DC–AC converter, namely the single-phase half-bridge VSC. Figure 6.23 shows the power circuit. It consists of two switching devices (S_1 and S_2) with two antiparallel diodes (D_1 and D_2) to accommodate the return of the current to the DC bus when required. This happens when the load power factor is other than unity. In order to generate a mid-point (O) to connect the return path of the load, two equal value capacitors (C_1 and C_2) are connected in series across the DC input. The result is that the voltage V_{dc} is split into two equal sources across each capacitor with voltage of $V_{dc}/2$. The assumption here is
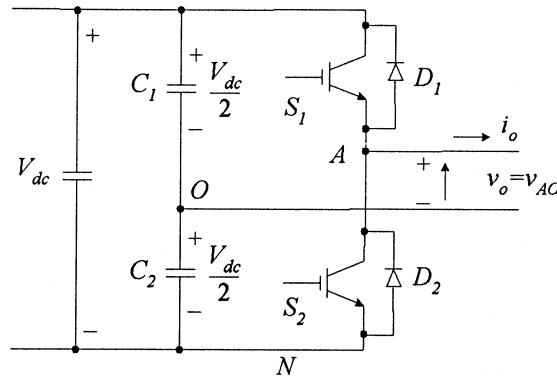
Fig. 6.23 Single-phase half-bridge VSC.

that the value of the capacitors is sufficiently large to ensure a stiff DC voltage source. This simply means that their voltage potential remains unchanged during the operation of the circuit. This also means that the potential of the mid-point (O) is constant with respect to both positive and negative DC bus rails at all times ($V_{dc}/2$ and $-V_{dc}/2$ respectively).

Let us now examine the operation of this circuit. It can be explained in combination with Figure 6.24. The two control signals for turning on and off the switches S_1 and S_2 are complementary to avoid destruction of the bridge. This would happen due to the throughput of high current coming from the low impedance DC voltage sources, if both switches were turned on simultaneously. When the switch S_1 is turned on ($t_3 < t < t_5$), the output voltage $v_o = v_{AO}$ is equal to the voltage $V_{dc}/2$ of the capacitor C_1. The mode of operation of the switching block (S_1 and D_1) is then controlled by the polarity of the output current i_o. If the output current is positive, with respect to the direction shown in Figure 6.23, then the current is flowing through switch S_1 ($t_4 < t < t_5$, Figure 6.24). If the output current is negative, the diode D_1 is conducting, although switch S_1 is turned on ($t_3 < t < t_4$). Similarly, if the switch S_2 is turned on ($t_1 < t < t_3$), the output voltage is equal to the voltage $V_{dc}/2$ of the capacitor C_2 with the polarity appearing negative this time. The output current i_o once again determines the conduction state of the switch and diode. If the output current is positive, the diode D_2 is conducting ($t_1 < t < t_2$). If the output current is negative, the current flows through switch S_2 ($t_2 < t < t_3$). Such states of switches and diodes are clearly marked in the waveforms of Figure 6.24 for the various time intervals. The modes of operation of the half-bridge single-phase VSC are also summarized in Table 6.3.

Figure 6.24(a) shows the output voltage waveform $v_o = v_{AO}$ generated by the converter operation as previously explained. Due to the square-wave generated by the converter, the output voltage waveform is rich in harmonics. Specifically, as shown in Figure 6.24(c) all odd harmonics are present in the spectrum of the output voltage. The fact that the converter cannot control the rms value of the output voltage waveform at fundamental frequency is also a limitation. A separate arrangement must be made to vary the DC bus voltage V_{dc} in order to vary and control the output voltage v_o.
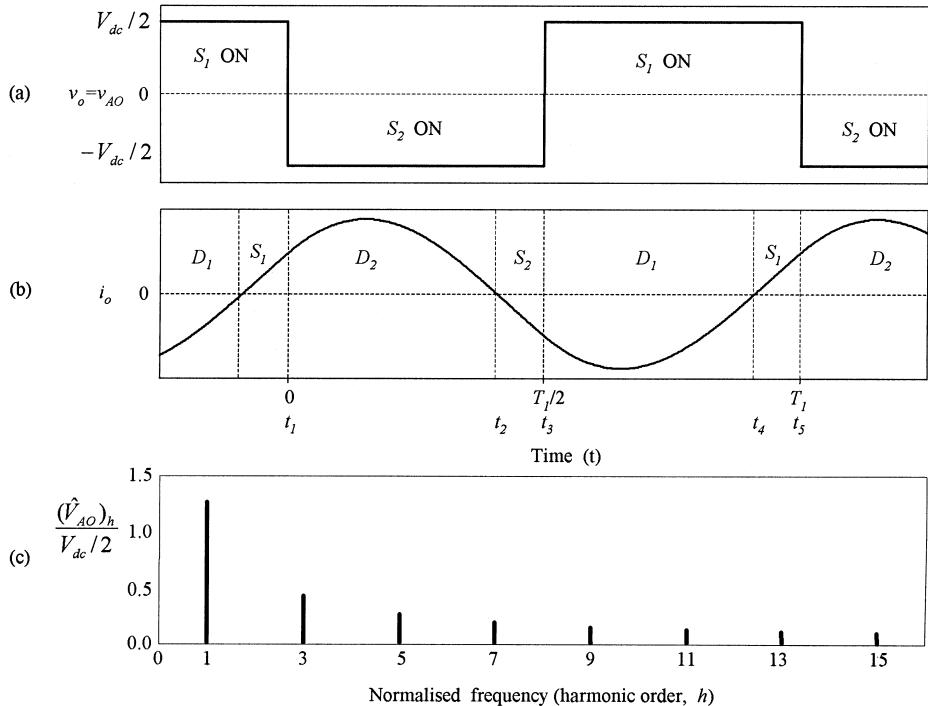
Fig. 6.24 Key waveforms of the single-phase half-bridge VSC circuit operation. (a) output voltage $v_o = v_{AO}$; (b) output current i_o; and (c) harmonic spectrum of the output voltage $v_o = v_{AO}$.

Table 6.3 Modes of operation of the single-phase half-bridge VSC

Switching device state		Output voltage	Output current	Conducting	Power transfer
		$v_o = v_{AO}$	i_o	semiconductor	
S_1	S_2				
1*	0	$V_{dc}/2$	Positive	S_1 $t_4 < t < t_5$	DC → AC
1	0	$V_{dc}/2$	Negative	D_1 $t_3 < t < t_4$	AC → DC
0	1	$-V_{dc}/2$	Positive	D_2 $t_1 < t < t_2$	AC → DC
0	1	$-V_{dc}/2$	Negative	S_2 $t_2 < t < t_3$	DC → AC

* The switch is ON when its state is 1 (one) and is OFF when its state is 0 (zero).

The amplitude of the fundamental component of the output voltage square-wave v_o shown in Figure 6.24(a) can be expressed using Fourier series as follows

$$(\hat{V}_o)_1 = (\hat{V}_{AO})_1 = \frac{4 \cdot V_{dc}}{2 \cdot \pi} \qquad (6.18)$$

The amplitude of all the other harmonics is given by

$$(\hat{V}_o)_h = (\hat{V}_{AO})_h = \frac{4 \cdot V_{dc}}{2 \cdot \pi \cdot h} = \frac{(\hat{V}_o)_1}{h} \qquad h = 3, 5, 7, 9, \ldots \qquad (6.19)$$

where h is the order of the harmonic.

i_o

Rectification	Inversion
Power flow from AC to DC	Power flow from DC to AC
S_2 turned-on & S_1 turned-off	S_1 turned-on & S_2 turned-off
Conducting element: D_2	Conducting element: S_1

$v_o = v_{AO}$

Inversion	Rectification
Power flow from DC to AC	Power flow from AC to DC
S_2 turned-on & S_1 turned-off	S_1 turned-on & S_2 turned-off
Conducting element: S_2	Conducting element: D_1
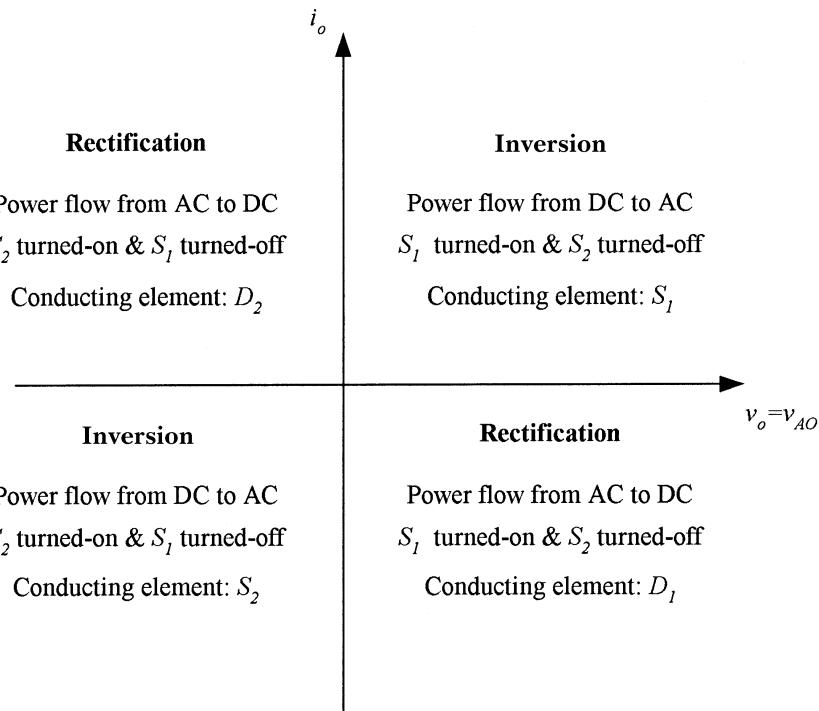
Fig. 6.25 Quadrants of operation of the single-phase half-bridge VSC.

The converter discussed here operates in all four quadrants of output voltage and current as shown in Figure 6.25. There are two distinct modes of operation associated with the transfer of power from the DC to the AC side. When the power flows from the DC bus to the AC side, the converter operates as an inverter. The switches S_1 and S_2 perform this function. In the case that the power is negative, which means power is returned back to the DC bus from the AC side, the converter operates as a rectifier. The diodes D_1 and D_2 perform this function.

The capability of the converter to operate in all four quadrants (Figure 6.25) means that there is no restriction in the phase relationship between the AC output voltage and the AC output current. The converter can therefore be used to exchange leading or lagging reactive power. If the load is purely resistive and no filter is attached to the output the diodes do not take part in the operation of the converter and only real power is transferred from the DC side to the AC one. Under any other power factor, the converter operates in a sequence of modes between a rectifier and an inverter. The magnitude and angle of the AC output voltage with respect to the AC output current control in an independent manner the real and reactive power exchange between the DC and AC sides.

This converter is also the basic building block of any other switch-mode VSC. Specifically, the combination of the switching blocks (S_1 and the antiparallel diode D_1) and (S_2 and D_2) can be used as a leg to build three-phase and other types of converters with parallel connected legs and other topologies. These types of converters will be described in later sections of this chapter.

6.3.2   Single-phase full-bridge VSC

In this section we will examine in detail the single-phase full-bridge VSC. Its power circuit is shown in Figure 6.26. It consists of two identical legs like the half-bridge single-phase converter (Figure 6.23) discussed in Section 6.3.1. Specifically, there are four switching elements (S_1, S_2, S_3, S_4), four antiparallel diodes (D_1, D_2, D_3, D_4) and a DC bus voltage source V_{dc} that can be a single capacitor. The other leg provides the return path for the current this time and the DC bus mid-point does not need to be available to connect the load. The output voltage v_o appears across the two points A and B as shown in Figure 6.26.

The control restriction discussed for the single-phase half-bridge topology (Figure 6.23) applies to this converter as well. Clearly the control signals for the switch pairs (S_1, S_2) and (S_3, S_4) must be complementary to avoid any bridge destruction due to shoot through of infinite current (at least theoretically).

There are two control methods for this topology. The first one treats the switches (S_1, S_4) and (S_2, S_3) as a pair. This means that they are turned on and off at the same time and for the same duration. For square-wave operation the switches S_1 and S_4 are on for half of the period. For the other half, the pair of S_2, S_3 is turned on. Like the single-phase half-bridge VSC, the direction of the output current i_o determines the conduction state of each semiconductor.

When the two switches S_1 and S_4 are turned on, the voltage at the output is equal to the DC bus voltage V_{dc}. Similarly, when the switches S_2 and S_3 are turned on the output voltage is equal to $-V_{dc}$. Such circuit operation is illustrated in Figure 6.27. In the first case, when the direction of the output current i_o is positive as shown in Figure 6.26, the current flows through switches S_1 and S_4 and the power is transferred from the DC side to the AC one ($t_4 < t < t_5$). When the current becomes negative, although the switches S_1 and S_4 are turned on, the diodes D_1 and D_4 conduct the current and return power back to the DC bus from the AC side ($t_3 < t < t_4$). For the other half of the period, when the switches S_2 and S_3 are turned on and the current is positive, the diodes D_2 and D_3 conduct ($t_1 < t < t_2$). In this
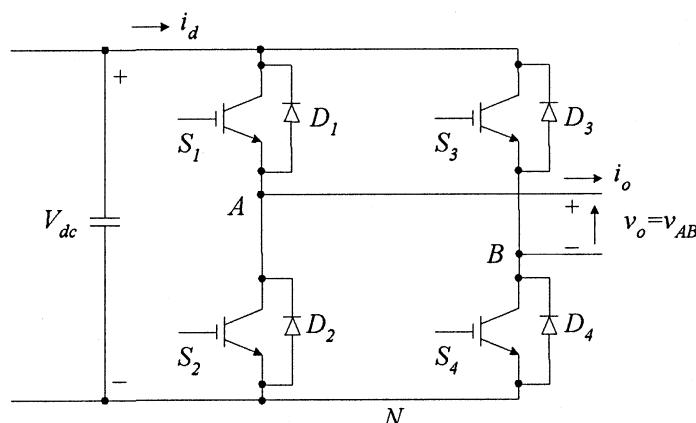
Fig. 6.26 Single-phase full-bridge VSC.
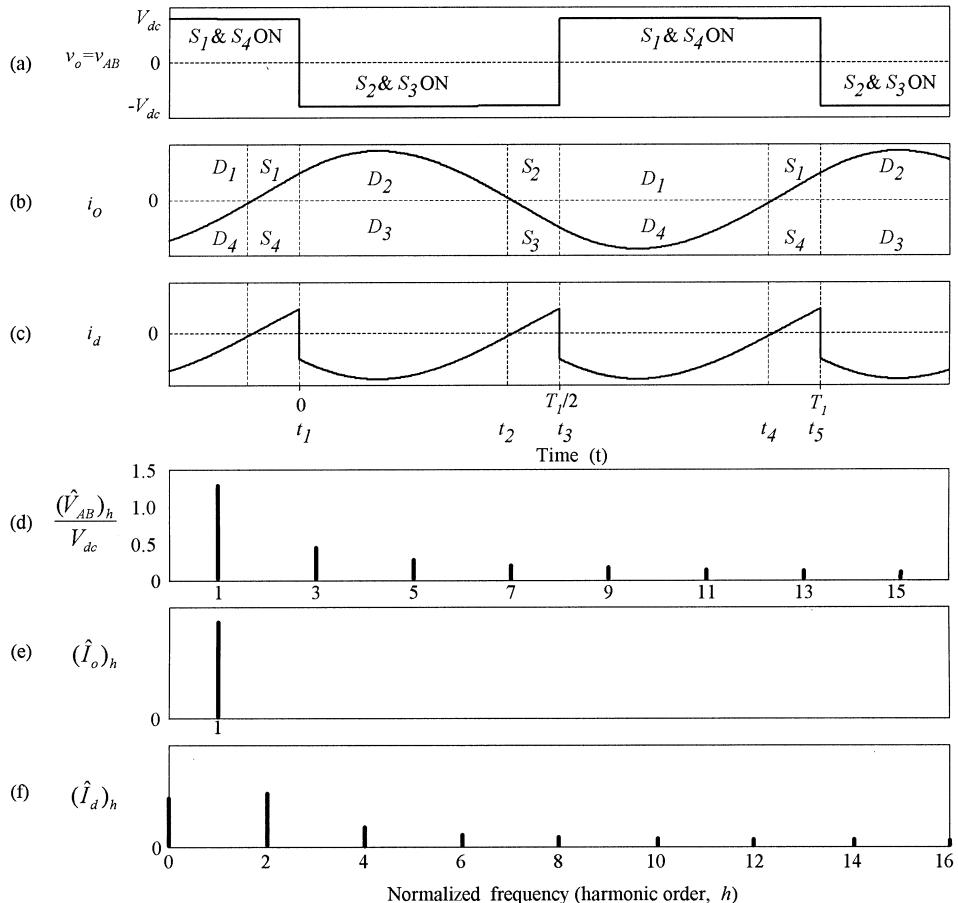
**Fig. 6.27** Key waveforms of the single-phase full-bridge VSC circuit operation. (a) output voltage $v_o = v_{AB}$; (b) output current i_o; (c) input DC bus current i_d; (d) harmonic spectrum of the output voltage $v_o = v_{AB}$; (e) harmonic spectrum of the output current i_o; and (f) harmonic spectrum of the input DC bus current i_d.

instance, power is transferred also back to the DC side from the AC side. Finally, when the current is negative, the switches S_2 and S_3 carry the current and assist the converter to transfer power from the DC bus to the AC side ($t_2 < t < t_3$). In summary, there are four distinct modes of operation for this converter when the control method shown in Figure 6.27 is employed (two inverter modes and two rectifier modes). Simply said, at all times two switches are turned on and the legs are controlled in a synchronized way.

The output voltage $v_o = v_{AB}$ is shown in Figure 6.27(a). The output current i_o and the input DC current i_d are also plotted in Figures 6.27(b) and (c) respectively. Similarly, like the case of the half-bridge topology, the square-wave generated across the AC side includes all odd harmonics and being a single-phase system, the third harmonic is also present (Figure 6.27(d)). These harmonics when reflected back to the DC side source include all even harmonics (Figure 6.27(f)).

i_o

Rectification	Inversion
Power flow from AC to DC	Power flow from DC to AC
S_2 & S_3 turned-on S_1 & S_4 turned-off	S_1 & S_4 turned-on S_2 & S_3 turned-off
Conducting elements: D_2 & D_3	Conducting elements: S_1 & S_4
Inversion	**Rectification**
Power flow from DC to AC	Power flow from AC to DC
S_2 & S_3 turned-on S_1 & S_4 turned-off	S_1 & S_4 turned-on S_2 & S_3 turned-off
Conducting elements: S_2 & S_3	Conducting elements: D_1 & D_4

$v_o = v_{AB}$

Fig. 6.28 Quadrants of operation of the single-phase full-bridge VSC.

The fundamental component of the output voltage v_o waveform has an amplitude value of

$$(\hat{V}_o)_1 = (\hat{V}_{AB})_1 = \frac{4 \cdot V_{dc}}{\pi} \tag{6.20}$$

And its various harmonics are given by

$$(\hat{V}_o)_h = (\hat{V}_{AB})_h = \frac{4 \cdot V_{dc}}{\pi \cdot h} = \frac{(\hat{V}_o)_1}{h} \qquad h = 3,\ 5,\ 7,\ 9,\ \ldots \tag{6.21}$$

where h is the order of the harmonic.

The converter is capable of operating in all four quadrants of voltage and current as shown in Figure 6.28. The various modes and their relationship to the switching and/or conduction state of the semiconductors are also summarized in Table 6.4 for further clarity. The phase relationship between the AC output voltage and AC output current does not have to be fixed and the converter can provide real and reactive power at all leading and lagging power factors. However, the converter itself cannot control the output voltage if the DC bus voltage V_{dc} remains constant. There is a need to adjust the level of the DC bus voltage if one wants to control the rms value of the output voltage v_o.

There is however a way to control the rms value of the fundamental component of the output voltage as well as the harmonic content of the fixed waveform shown in Figure 6.27(a). In this method, the control signals of the two legs are not

Table 6.4 Modes of operation of the single-phase full-bridge VSC

S_1	S_2	S_3	S_4	Output voltage $v_o = v_{AB}$	Output current i_o	Conducting semiconductor	Power transfer
Square-wave method or Phase-shifted method
1	0	0	1	V_{dc}	Positive	$S_1\ S_4\ t_4 < t < t_5$	DC → AC
1	0	0	1	V_{dc}	Negative	$D_1\ D_4\ t_3 < t < t_4$	AC → DC
0	1	1	0	$-V_{dc}$	Negative	$S_2\ S_3\ t_2 < t < t_3$	DC → AC
0	1	1	0	$-V_{dc}$	Positive	$D_2\ D_3\ t_1 < t < t_2$	AC → DC
Phase-shifted method only (extra modes – free-wheeling modes)
1	0	1	0	0	Positive	$S_1\ D_3$	None
1	0	1	0	0	Negative	$S_3\ D_1$	None
0	1	0	1	0	Positive	$S_4\ D_2$	None
0	1	0	1	0	Negative	$S_2\ D_4$	None

synchronized in any way and the switches are not treated as pairs like previously. For the safe operation of the converter, the control signals between (S_1 and S_2) and (S_3 and S_4) must be complementary. In this case, there is a phase-shift between the two legs and this way a zero volts interval can appear across the output.

For instance, if switches S_1 and S_3 are turned on at the same time, the output voltage (v_{AB}) will be zero. The current in the case of other than unity power factor must keep flowing. There is no power exchange between the DC side and the AC one (free-wheeling mode). If the current is positive, the current flows through S_1 and D_3. If the current is negative, it flows through D_1 and S_3. Similarly, when the two bottom switches S_2 and S_4 are turned on at the same time, the output voltage (v_{AB}) is zero and the output current once again determines which element conducts and allows the output current to continue flowing. Specifically, if the current is positive, the diode D_2 and the switch S_4 are conducting. In the case that the current is negative, the switch S_2 and diode D_4 provide a path for the output current. These extra modes of operation for the single-phase full-bridge topology (Figure 6.26) are also included in Table 6.4 as the free-wheeling modes.

For a given phase-shift (α degrees) between the control signals of the two legs, the waveforms are shown in Figure 6.29. It is clear that the output voltage waveform is a three-level one, being able to have the values of V_{dc}, 0 and $-V_{dc}$ as shown in Figure 6.29(a). The control signals are shown in Figures 6.29(b)–(d). It is also clear that between the top and bottom switches of each leg complementary control signals are used. It should be noted that for $\alpha = 0$, the output voltage becomes similar to the previously presented control method (square-wave, Figure 6.27(a)).

The output voltage v_o (v_{AB}) is shown in Figure 6.30(a) along with the output current i_o and the DC bus current i_d in Figures 6.30(b) and (c) respectively. Therefore, by controlling the phase-shift between the two legs (α degrees), the rms value of the fundamental component can be controlled. The amplitude of all odd harmonics, as shown in Figure 6.30(d) for the output voltage, can also be controlled. The output current has only a fundamental component as shown in Figure 6.30(e), where the DC bus current has a DC component and all even harmonics as shown in Figure 6.30(f).
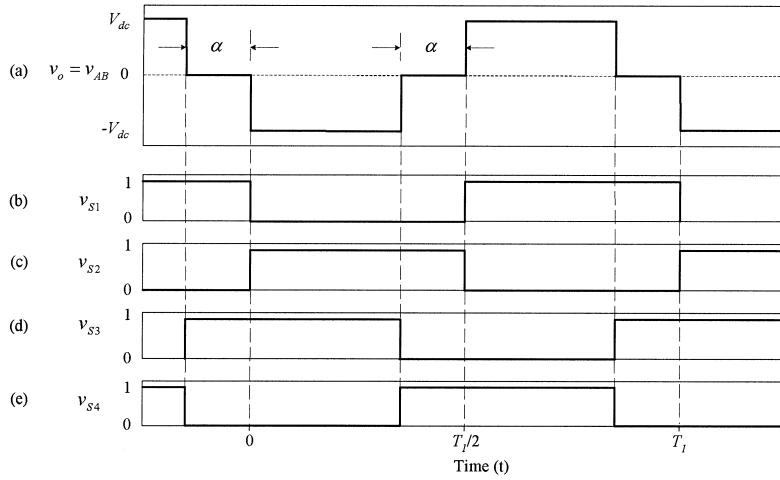
Fig. 6.29 Key waveforms of the single-phase full-bridge phase-shifted controlled VSC circuit operation. (a) output voltage $v_o = v_{AB}$; (b) control signal for switch S_1; (c) control signal for switch S_2; (d) control signal for switch S_3; and (e) control signal for switch S_4.
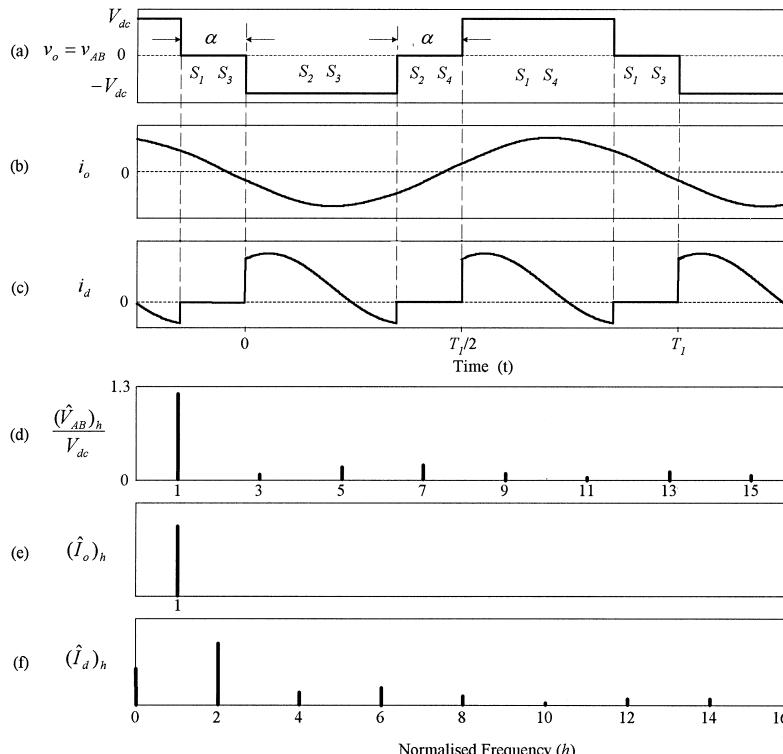
Fig. 6.30 Key waveforms of the single-phase full-bridge phase-shifted controlled VSC circuit operation. (a) output voltage $v_o = v_{AB}$; (b) output current i_o; (c) DC bus current i_d; (d) harmonic spectrum of the output voltage $v_o = v_{AB}$; (e) harmonic spectrum of the output current i_o; and (f) harmonic spectrum of the input DC bus current i_d.

$$\frac{(\hat{V}_{AB})_1}{4 \cdot V_{dc}/\pi}$$

$$\frac{(\hat{V}_{AB})_h}{4 \cdot V_{dc}/\pi} \quad h = 3,5,7,9$$
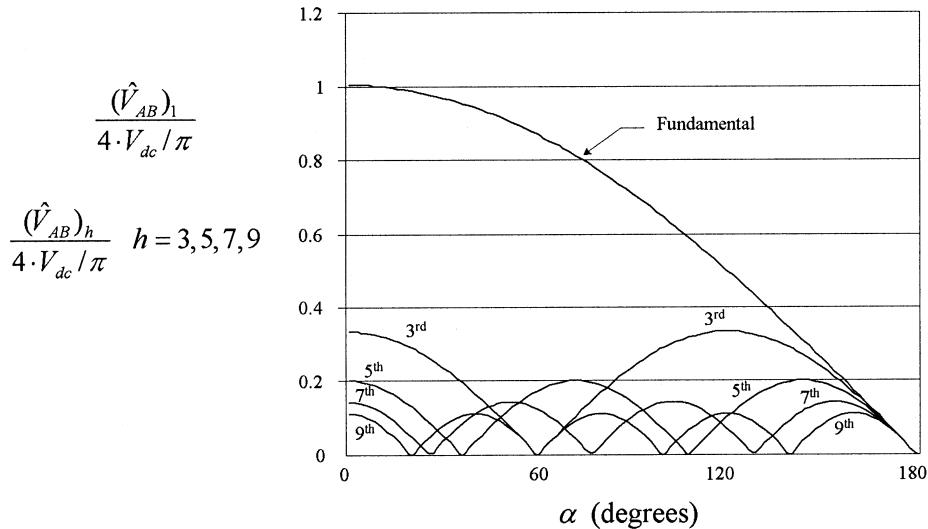
Fig. 6.31 Normalized amplitudes of fundamental and harmonics for the phase-shifted output voltage as a function of α (zero volts interval in degrees).

For a given zero interval α in degrees, as shown in Figures 6.29(a) and 6.30(a), the amplitude of the fundamental and harmonics are as follows

$$(\hat{V}_o)_1 = (\hat{V}_{AB})_1 = \frac{4 \cdot V_{dc}}{\pi} \sin\left[\left(\frac{\pi - \alpha}{2}\right)\right] \tag{6.22}$$

and

$$(\hat{V}_o)_h = (\hat{V}_{AB})_h = \frac{4 \cdot V_{dc}}{\pi \cdot h} \sin\left[h \cdot \left(\frac{\pi - \alpha}{2}\right)\right] \quad h = 3, 5, 7, 9, \ldots \tag{6.23}$$

where h is the order of the harmonic.

When $\alpha = 0$ the converter operates as a square-wave one (Figure 6.27). The normalized amplitude of the fundamental and the most significant harmonics, i.e. 3rd, 5th, 7th and 9th to the output of the square-wave converter as a function of α, are plotted in Figure 6.31.

6.3.3 Conventional three-phase six-step VSC

The conventional three-phase six-switch VSC is shown in Figure 6.32. It consists of six switches S_1–S_6 and six antiparallel diodes D_1–D_6. The number indicates their order of being turned on. A fictitious neutral (O) as a mid-point is also included although in most cases is not available. However, when the converter under consideration is used as an active filter in the case of a four-wire three-phase system, this point (O) is used to connect the fourth-wire. This case will be discussed further in later parts of the chapter.

The three converter legs are controlled with a phase-shift of 120° between them. The basic way to control the three-phase six-switch VSC is to turn on each switch for half of the period (180°) with a sequence 1, 2, 3, ... as they are numbered and shown in Figure 6.32.
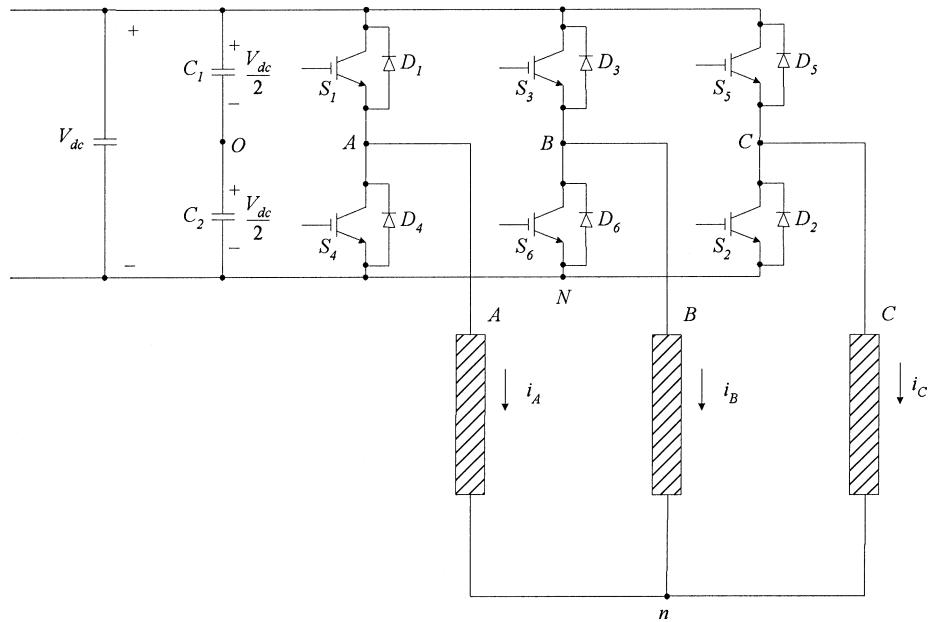
Fig. 6.32 Conventional three-phase six-switch VSC.
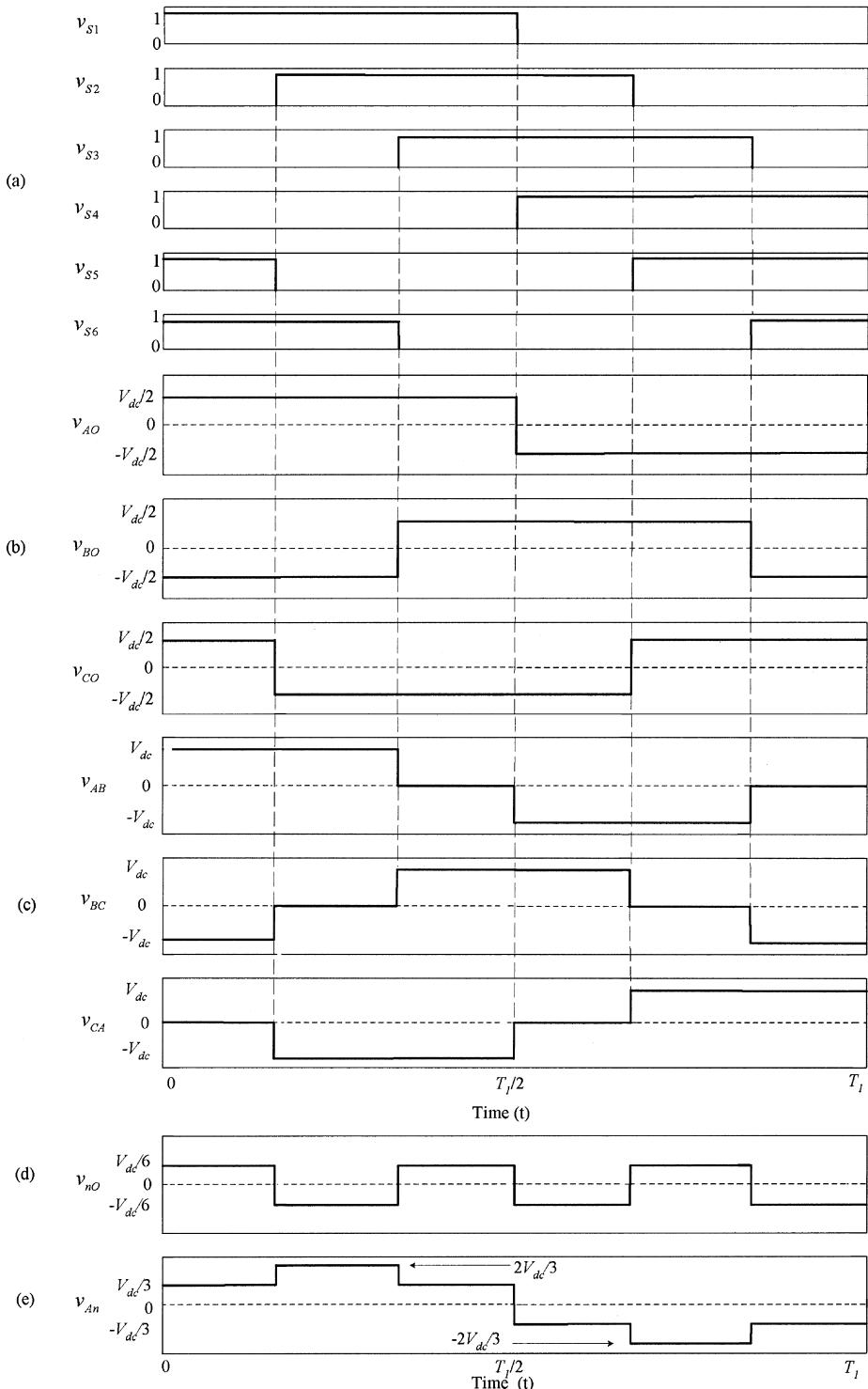
The operation of the converter can be explained with the assistance of Figure 6.33. Specifically, the control signals for each of the six switches are shown in Figure 6.33(a). Clearly, each switch remains on for 180° and every 60° a new switch is turned on and one of the previous group is turned off. At any given time therefore, one switch of each leg is on. Assuming that the fictitious mid-point (O) is available, three square-type waveforms for the voltages v_{AO}, v_{BO}, and v_{CO} can be drawn as shown in Figure 6.33(b). Each of the voltage waveforms has two peak values of $V_{dc}/2$, and $-V_{dc}/2$, and they are displaced by 120° from each other.

From the three waveforms v_{AO}, v_{BO}, and v_{CO}, the line-to-line voltage waveforms can be drawn since

$$v_{AB} = v_{AO} - v_{BO}$$
$$v_{BC} = v_{BO} - v_{CO} \qquad (6.24)$$
$$v_{CA} = v_{CO} - v_{AO}$$

The three resultant line-to-line voltage waveforms are then shown in Figure 6.33(c). It is clear that each waveform takes three values (V_{dc}, 0, $-V_{dc}$) and there is a 120° phase-shift between them. These waveforms have a 60° interval when they are zero for each half of the period, a total of 120° per period. As explained earlier, each leg can handle current in both directions at any time, since either the turned on switch or the antiparallel diode of the other switch can be the conducting element depending upon the polarity of the output line current.

The potential of the load neutral point (n) shown in Figure 6.32 with respect to the mid-point of the DC bus (O) is drawn in Figure 6.33(d). It can be seen that such a waveform has frequency three times the output frequency and the two peak values
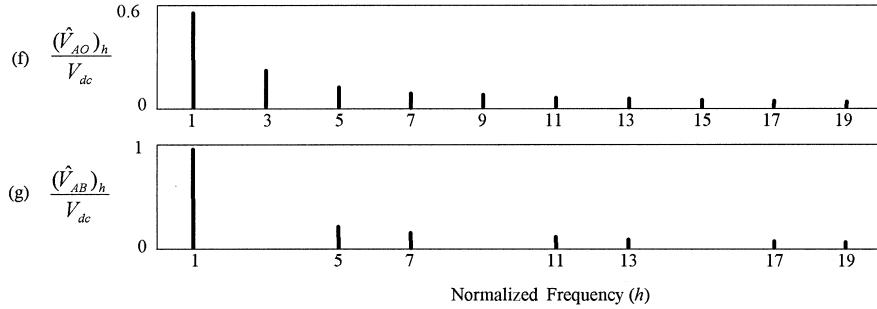
Fig. 6.33 Key waveforms of the three-phase six-step VSC circuit operation. (a) control signals for switches S_1 S_2, S_3, S_4, S_5, S_6; (b) voltage waveforms v_{AO}, v_{BO}, and v_{CO}; (c) output line-to-line voltage waveforms v_{AB}, v_{BC}, v_{CA}; (d) voltage waveform between the load neutral point (n) and the DC bus mid-point (O); (e) voltage waveform between the line point A and the load neutral point n; (f) harmonic spectrum of the line-to-DC bus mid-point; and (g) harmonic spectrum of the line-to-line voltage v_{AB}.

are between $V_{dc}/6$ and $-V_{dc}/6$. Finally, the line-to-load neutral point (n) voltage waveform is illustrated in Figure 6.33(e). Such a voltage waveform has two positive values ($V_{dc}/3$ and $2V_{dc}/3$) and two negative ones ($-V_{dc}/3$ and $-2V_{dc}/3$).

The harmonics of the various waveforms can be calculated using Fourier series. The fundamental amplitude of the voltage waveforms v_{AO}, v_{BO}, and v_{CO} is

$$(\hat{V}_{AO})_1 = (\hat{V}_{BO})_1 = (\hat{V}_{CO})_1 = \frac{4 \cdot V_{dc}}{2 \cdot \pi} \tag{6.25}$$

$$(\hat{V}_{AO})_h = (\hat{V}_{BO})_h = (\hat{V}_{CO})_h = \frac{4 \cdot V_{dc}}{2 \cdot \pi \cdot h} \quad h = 3, 5, 7, \ldots \tag{6.26}$$

where h is the order of the harmonic.

For the line-to-line voltage waveforms v_{AB}, v_{BC}, and v_{CA} then the fundamental amplitude is

$$\hat{V}_{AB1} = \frac{2\sqrt{3}}{\pi} \cdot V_{dc} \tag{6.27}$$

and therefore the rms value of the fundamental component is then

$$V_{AB1,rms} = \frac{2\sqrt{3}}{\pi\sqrt{2}} \cdot V_{dc} = \frac{\sqrt{6}}{\pi} \cdot V_{dc} = 0.78 \cdot V_{dc} \tag{6.28}$$

Similarly, the amplitude of the harmonic voltages is

$$(\hat{V}_{AB})_h = \frac{2\sqrt{3}}{\pi \cdot h} \cdot V_{dc} \quad h = 5, 7, 11, 13, \ldots \tag{6.29}$$

The rms value of the line-to-line voltage including all harmonics is

$$V_{AB,rms} = \sqrt{\frac{1}{\pi} \int_{-\pi/3}^{\pi/3} V_{dc}^2 d\omega t} = \frac{\sqrt{2}}{\sqrt{3}} \cdot V_{dc} = 0.816 \cdot V_{dc} \tag{6.30}$$

The normalized spectrum of the line-to-DC bus mid-point and the line-to-line voltage waveforms are plotted in Figures 6.33(f) and (g) respectively. It can be seen that the voltage waveforms v_{AO}, v_{BO}, and v_{CO} contain all odd harmonics. The load connection as shown in Figure 6.32 does not allow 3rd harmonic and all multiples to flow, and this is confirmed with the spectrum of the line-to-line voltage waveform v_{AB} where 3rd, 9th and 15th harmonics are eliminated as shown in Figure 6.33(g).

6.3.4 Single-phase half-bridge neutral-point-clamped (NPC) VSC

For single-phase applications, so far the half-bridge and the full-bridge conventional topologies have been discussed in detail. These converters have the capability to generate two-level voltage waveforms in both cases where only frequency control is possible and a separate control of the DC bus voltage must be employed to control the output AC voltage waveform (when square-wave control method is considered). Except of course for the case where a phase-shifted control method is used for the single-phase full-bridge VSC topology. In this case, the converter is capable of generating a three-level waveform and with controlled amplitude.

However, there exists a topology that is capable of generating a three-level voltage waveform at the output with a half-bridge version. Such a converter leg has made a significant contribution in the general area of converters, as a building block, especially for high power applications. We present this VSC topology in this section.

A three-level half-bridge VSC based on the NPC topology is shown in Figure 6.34 (Nabae et al., 1981). In this version the neutral point is clamped with diodes.
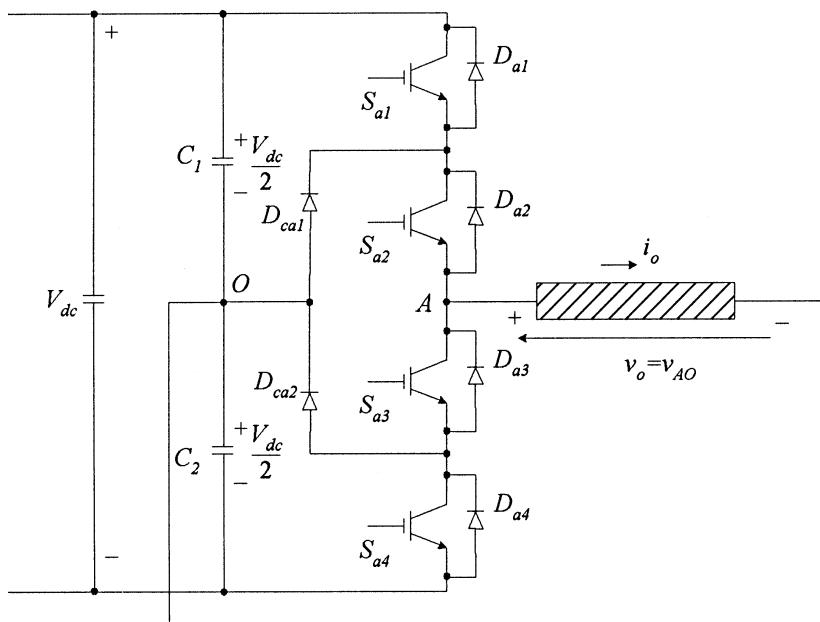
Fig. 6.34 Three-level single-phase half-bridge NPC VSC.

Specifically, the converter consists of four switches (S_{a1}, S_{a2}, S_{a3}, S_{a4}) and the antiparallel diodes (D_{a1}, D_{a2}, D_{a3}, D_{a4}). Due to the nature of the leg being able to generate a three-level voltage waveform between the points A and O, two DC bus voltage sources of equal value are required. This can be accomplished with two equal value capacitors C_1 and C_2 where the initial DC bus voltage V_{dc} is split across to make two voltage sources of $V_{dc}/2$ value available.

In previous sections, the phase-shifted control method (Figures 6.29 and 6.30) for a single-phase full-bridge VSC shown in Figure 6.26 was explained. The interesting point of such a technique is the ability to control the output voltage and its harmonics contents by adjusting the angle α (degrees) where the line-to-line waveform becomes zero.

It has been introduced in the technical literature that the number of levels of the voltage between the mid-point of the converter leg and the DC bus mid-point (line-to-neutral voltage waveform) is used to classify a given multilevel topology. The conventional three-phase VSC as shown in Figure 6.32 is then a two-level converter since it is capable of producing a two-level waveform between the two points mentioned above.

To clamp the voltage, two extra clamping diodes D_{ca1} and D_{ca2} as shown in Figure 6.34 are required to connect the DC bus mid-point to the load applying zero volts. They also allow the current to flow in either direction when the converter operates in the free-wheeling mode (zero volts at the output). For this case the load can be connected between the points A and O like the case of the single-phase half-bridge VSC shown in Figure 6.23.

The control for the three-level half-bridge VSC is slightly different and will be explained next. It can be confirmed with the assistance of Figures 6.34 and 6.35 that
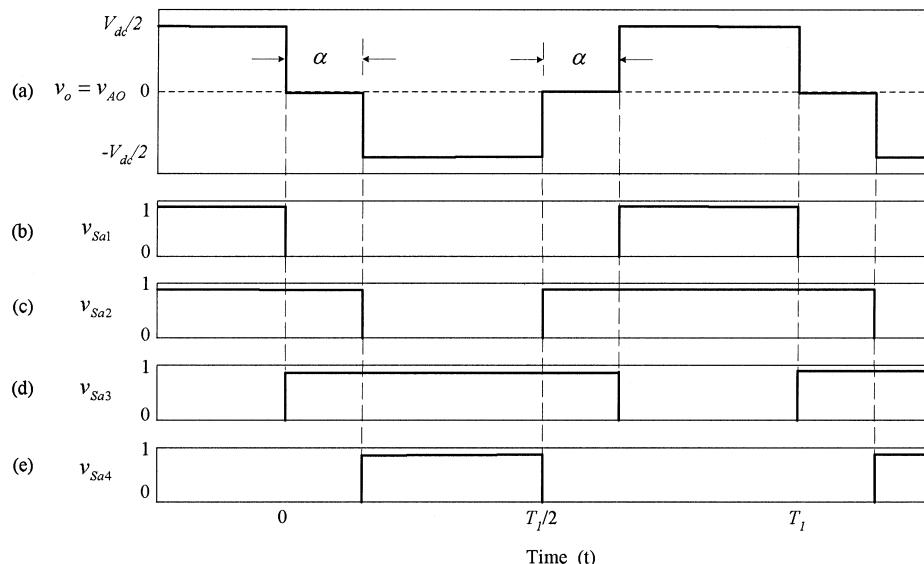
Fig. 6.35 Key waveforms of the three-level single-phase half-bridge NPC VSC circuit operation. (a) output voltage $v_o = v_{AO}$; (b) control signal for the switch S_{a1}; (c) control signal for the switch S_{a2}; (d) control signal for switch S_{a3}; and (e) control signal for switch S_{a4}.

Table 6.5 Modes of operation of the three-level half-bridge NPC VSC

Switching device state				Output voltage	Output current	Conducting semiconductor	Power transfer
S_{a1}	S_{a2}	S_{a3}	S_{a4}	$v_o = v_{AO}$	i_o		
Square-wave method							
1	1	0	0	$V_{dc}/2$	Positive	$S_{a1}\ S_{a2}$	DC → AC
1	1	0	0	$V_{dc}/2$	Negative	$D_{a1}\ D_{a2}$	AC → DC
0	0	1	1	$-V_{dc}/2$	Negative	$S_{a3}\ S_{a4}$	DC → AC
0	0	1	1	$-V_{dc}/2$	Positive	$D_{a3}\ D_{a4}$	AC → DC
0	1	1	0	0	Positive	$S_{a2}\ D_{ca1}$	None
0	1	1	0	0	Negative	$S_{a3}\ D_{ca2}$	None

when switches S_{a1} and S_{a2} are turned on at the same time, the voltage of the capacitor C_1 ($V_{dc}/2$) will be applied across the load. When this pair of switches is turned on, the other pair of switches (S_{a3}, S_{a4}) must be turned off to avoid destruction of the bridge. Similarly when the switches S_{a3} and S_{a4} are turned on simultaneously the output voltage $v_o = v_{AO}$ becomes negative ($-V_{dc}/2$) due to the voltage of capacitor C_2 being applied across the load. Now, in order for the converter to generate zero voltage across the output (the third level of the output voltage waveform), the two switches S_{a2} and S_{a3} are turned on simultaneously and the other two switches S_{a1} and S_{a4} are turned off. This way, through the assistance of the two clamping diodes D_{ca1} and D_{ca2}, the potential of the DC bus mid-point O is across the load generating zero volts in the voltage waveform v_{AO} as shown in Figure 6.35(a). The control signals for the four switches S_{a1}, S_{a2}, S_{a3}, and S_{a4} are plotted in Figures 6.35(b)–(e) respectively. It is clear that the switches S_{a1} and S_{a3} have complementary signals, and the same applies for the control signals between the switches S_{a4} and S_{a2}. The duration that the switch S_{a1} is on simultaneously with S_{a2} controls the length of the output voltage that is positive as explained earlier. The same applies for the interval that the output voltage is negative when the switch S_{a4} is on simultaneously with S_{a3}.

Table 6.5 summarizes the modes of operation of the three-level single-phase half-bridge VSC based on the NPC topology with clamping diodes. This converter is also capable of operating in all four quadrants, since both the output voltage and current can be both positive and negative (bidirectional VSC topology). These quadrants of operation of the three-level single-phase half-bridge NPC VSC are indicated in Figure 6.36.

It should be noted that the waveform generated by the three-level converter (Figure 6.35(a)) and the single-phase full-bridge VSC with the phase-shifted method (Figure 6.29(a)) are identical. Therefore the harmonic content is also identical as analysed in Section 6.3.2 and plotted in a normalized form in Figure 6.31.

6.3.5 Single-phase full-bridge NPC VSC

The converter leg presented in Section 6.3.4 can be used to build full-bridge single-phase and three-phase VSC topologies with the capability of generating three or higher-level voltage waveforms. In this case, the line-to-line voltage waveform will be of a higher than three level. However, the converter in the technical literature is called a three-level one since the number of levels of the line-to-line voltage waveform is *not*

Rectification

Power flow from AC to DC

S_{a3} & S_{a4} turned-on
S_{a1} & S_{a2} turned-off

Conducting elements: D_{a3} & D_{a4}

Inversion

Power flow from DC to AC

S_{a1} & S_{a2} turned-on
S_{a3} & S_{a4} turned-off

Conducting elements: S_{a1} & S_{a2}

Inversion

Power flow from DC to AC

S_{a3} & S_{a4} turned-on
S_{a1} & S_{a2} turned-off

Conducting elements: S_{a3} & S_{a4}

Rectification

Power flow from AC to DC

S_{a1} & S_{a2} turned-on
S_{a3} & S_{a4} turned-off

Conducting elements: D_{a1} & D_{a2}

Fig. 6.36 Quadrants of operation of the three-level single-phase half-bridge NPC VSC.
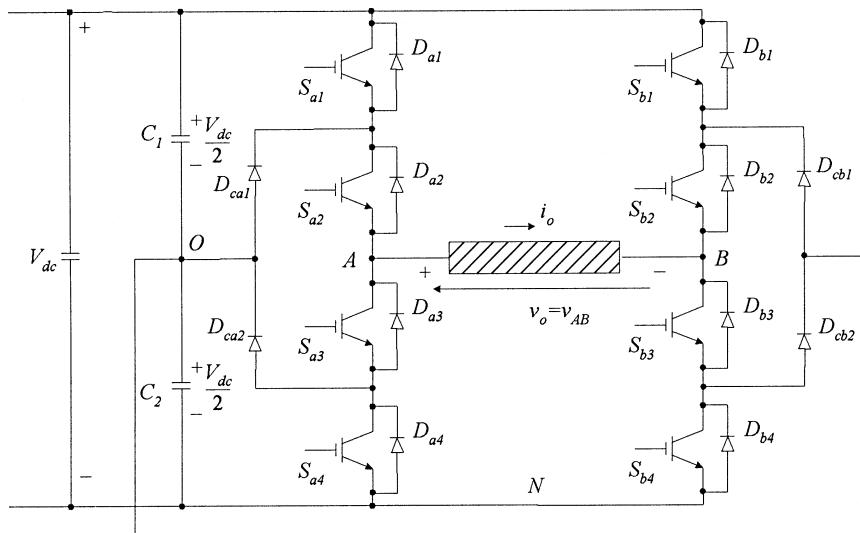
Fig. 6.37 Three-level single-phase full-bridge NPC VSC.

used to name the level of the topologies but rather the line to the DC bus mid-point voltage waveform (line-to-neutral).

A three-level single-phase full-bridge VSC is shown in Figure 6.37. Each leg generates a three-level voltage waveform when it is referred to the mid-point of the
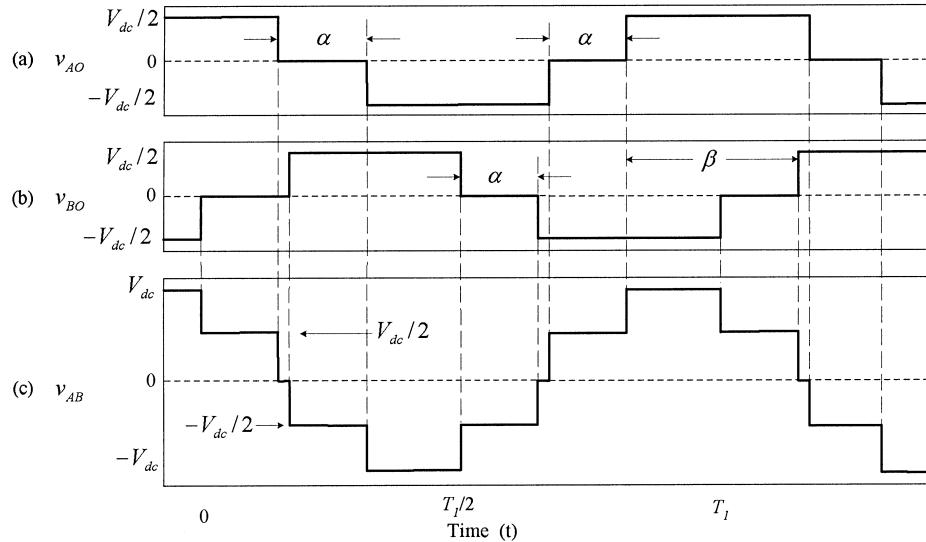
Fig. 6.38 Key waveforms of the three-level single-phase full-bridge NPC VSC circuit operation. (a) line-to-DC bus mid-point voltage waveform v_{AO}; (b) line-to-DC bus mid-point voltage waveform v_{BO}; and (c) line-to-line voltage waveform v_{AB}.

DC bus as shown in Figures 6.38(a) (voltage v_{AO}) and 6.38(b) (voltage v_{BO}). There is a phase-shift between the output voltage waveforms of the two legs in order to be able to generate a five-level line-to-line voltage waveform. The resultant line-to-line voltage waveform ($v_{AB} = v_{AO} - v_{BO}$) is shown in Figure 6.38(c). Clearly, the line-to-line voltage waveform is a five-level waveform, taking values of V_{dc}, $V_{dc}/2$, 0, $-V_{dc}/2$ and $-V_{dc}$. The various modes of operation for the converter under consideration are summarized in Table 6.6.

Higher-level legs can be built in a similar way, which would, of course, require a higher number of DC bus sources. Even and odd numbers of levels can be built depending upon the application. For a given number of levels m, $m-1$ DC bus sources (capacitors) are required. For an even number of levels, the zero level will be missing from the line-to-DC bus mid-point voltage waveform. A five-level leg is

Table 6.6 Modes of operation of the three-level single-phase full-bridge NPC VSC

			Switching device state					Output voltage $v_o = v_{AB}$
S_{a1}	S_{a2}	S_{a3}	S_{a4}	S_{b1}	S_{b2}	S_{b3}	S_{b4}	
1	1	0	0	0	0	1	1	V_{dc}
0	0	1	1	1	1	0	0	$-V_{dc}$
1	1	0	0	0	1	1	0	$V_{dc}/2$
0	1	1	0	0	0	1	1	$V_{dc}/2$
0	1	1	0	1	1	0	0	$-V_{dc}/2$
0	0	1	1	0	1	1	0	$-V_{dc}/2$
0	1	1	0	0	1	1	0	0
1	1	0	0	1	1	0	0	0 (possible)
0	0	1	1	0	0	1	1	0 (possible)

shown in Figure 6.39. Clearly, as described above, four DC bus sources are used and this time more clamping diodes are required.

For the five-level half-bridge leg shown in Figure 6.39, there exist switch pairs that require complementary control signals. These pairs are: (S_{a1}, S_{a5}), (S_{a2}, S_{a6}), (S_{a3}, S_{a7}), and (S_{a4}, S_{a8}). Moreover, the various switches do not have the same switching frequency and as the number of levels increases such a problem becomes more of a drawback.

The states of the switching devices of a five-level single-phase half-bridge VSC as shown in Figure 6.39 are summarized in Table 6.7.

One significant drawback of the NPC topology is the unequal distribution of switching losses among the switches and also the unequal load distribution among the various capacitors. This problem becomes more serious as the number of levels of the converter increases.

6.3.6 Other multilevel converter topologies

So far many power electronics based circuits have been presented which are capable of generating more than two-level voltage waveforms. There is however another converter topology, which is also capable of producing multilevel voltage waveforms. This topology contains two legs per phase as shown in the single-phase version in Figure 6.40. Each phase leg consists of two legs similar to the half-bridge explained earlier and shown in Figure 6.23. Each leg is controlled independently and with a specific phase-shift is able to generate a three-level voltage waveform between the phase point A and the mid-point of the DC bus O. In order to be able to add the waveforms generated by the two legs, an inductor-based configuration is used as shown in Figure 6.40.

For square-wave operation, the voltage waveform between the point A_1 and the DC bus mid-point is a two-level waveform taking values between $V_{dc}/2$ and $-V_{dc}/2$. The same applies for the voltage waveform between the other point of the phase leg A_2 and the point O. These two signals are phase-shifted accordingly and are drawn in Figures 6.41(a) and (b). The potential of point A referred to the point O is the sum of the two waveforms v_{A1O}, and v_{A2O}. This voltage waveform is shown in Figure 6.41(c). It is a three-level waveform taking values of V_{dc}, 0 and $-V_{dc}$. Finally, the voltage across the inductor, that is the potential difference between the two points A_1 and A_2, is illustrated in Figure 6.41(d). Similar arrangements can be used for the other two-phase legs to build a three-phase converter. Furthermore, more legs per phase can be used and more inductor arrangements can be used to sum even more voltage waveforms so that higher numbers of levels for the phase voltage waveform can be generated. This depends upon the application of course. Such arrangements can also offer opportunities to cancel more harmonics with appropriate phase-shifting.

Another circuit to obtain multilevel systems is of course the combination of the NPC converter and the arrangement with inductors to add voltage waveforms. The converter then is three-level with respect to one-phase leg, and becomes a five-level one with respect to the phase. Such a five-level circuit based on inductor summing and the NPC converter is shown in Figure 6.42. In this case appropriate phase-shifted PWM techniques can be used to take advantage of the topology and position the first significant harmonics of the resultant output voltage waveforms to higher frequencies.
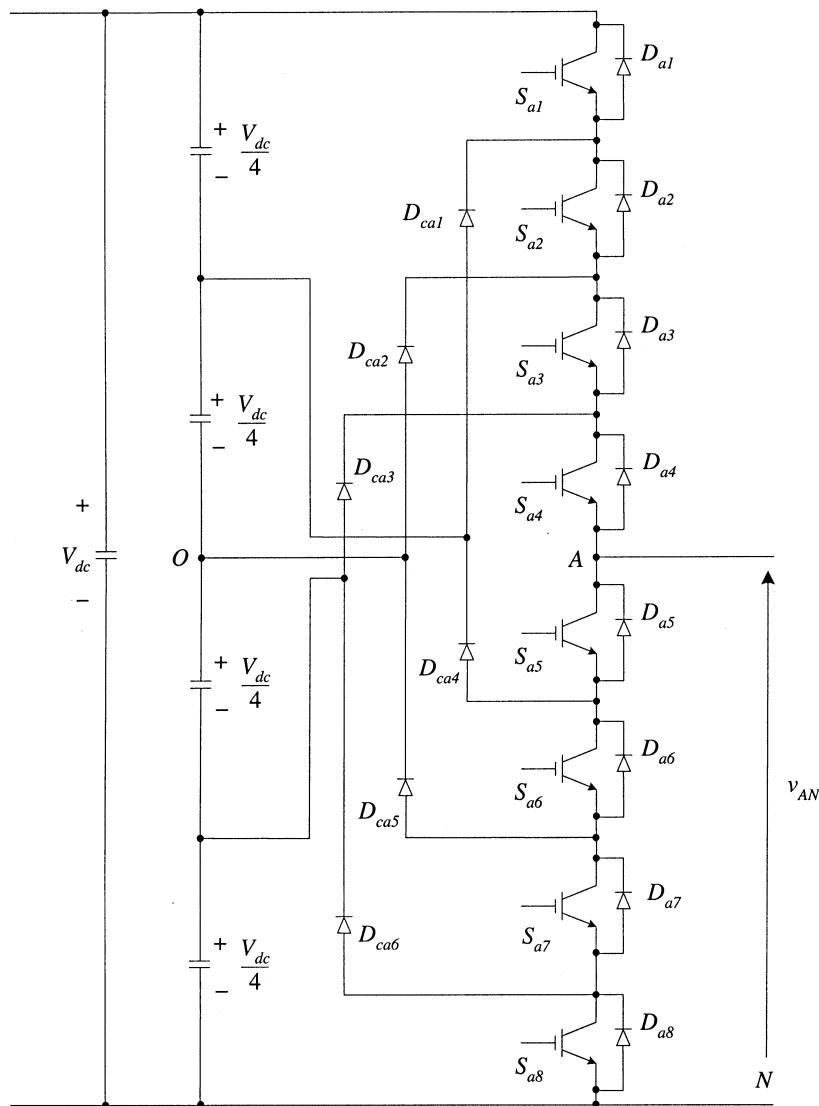
Fig. 6.39 Five-level single-phase half-bridge NPC VSC.

Table 6.7 Modes of operation of the five-level single-phase half-bridge NPC VSC

Switching device state								Output voltage
S_{a1}	S_{a2}	S_{a3}	S_{a4}	S_{a5}	S_{a6}	S_{a7}	S_{a8}	$v_o = v_{AN}$
1	1	1	1	0	0	0	0	V_{dc}
0	1	1	1	1	0	0	0	$3V_{dc}/4$
0	0	1	1	1	1	0	0	$V_{dc}/2$
0	0	0	1	1	1	1	0	$V_{dc}/4$
0	0	0	0	1	1	1	1	0
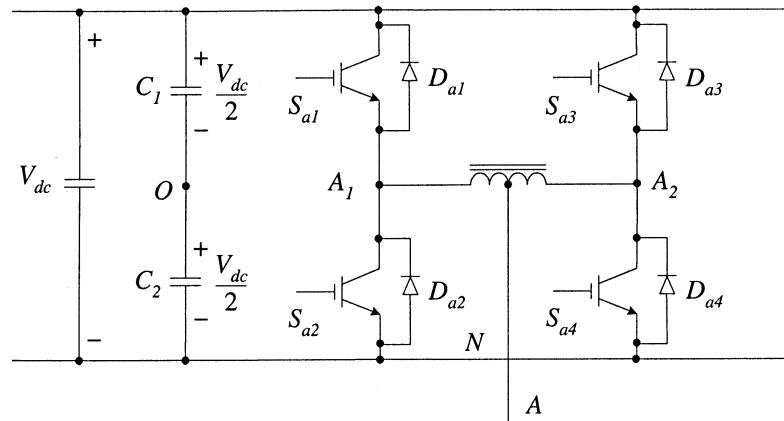
Fig. 6.40 Three-level converter with parallel legs and a summing inductor to generate multilevel voltage waveforms.
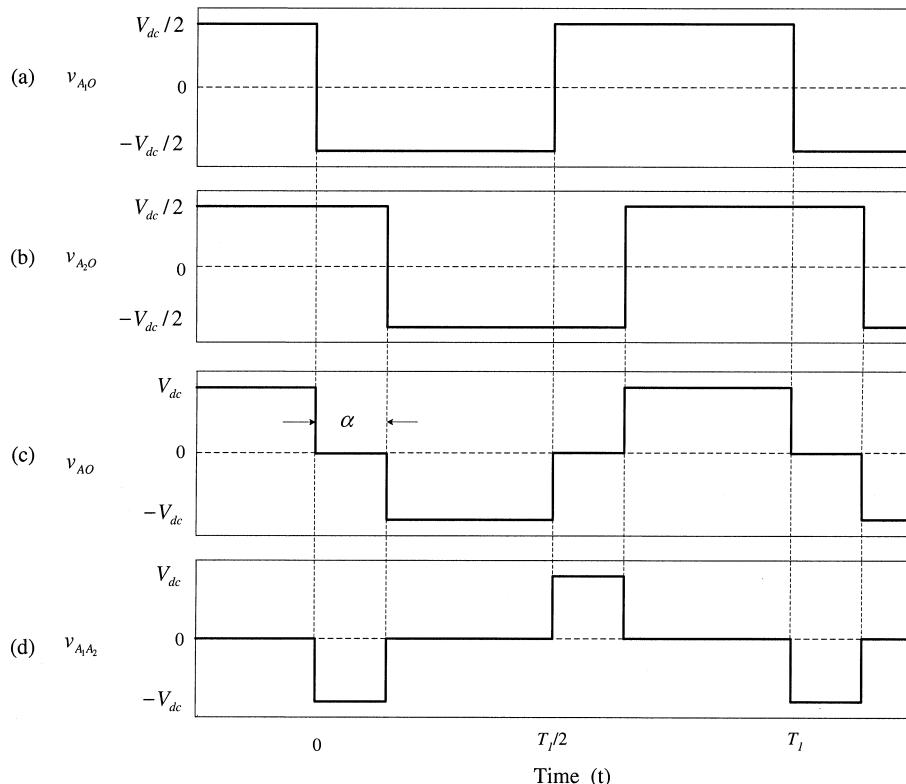
Fig. 6.41 Key waveforms of the three-level converter with parallel legs and a summing inductor circuit operation. (a) voltage waveform between the mid-point of the left phase leg A_1 and the DC bus mid-point O, v_{A10}; (b) voltage waveform between the mid-point of the right phase leg A_2 and the DC bus mid-point O, v_{A20}; (c) voltage waveform between the phase point and the DC bus mid-point, v_{AO}; and (d) voltage waveform across the inductor v_{A1A2}.
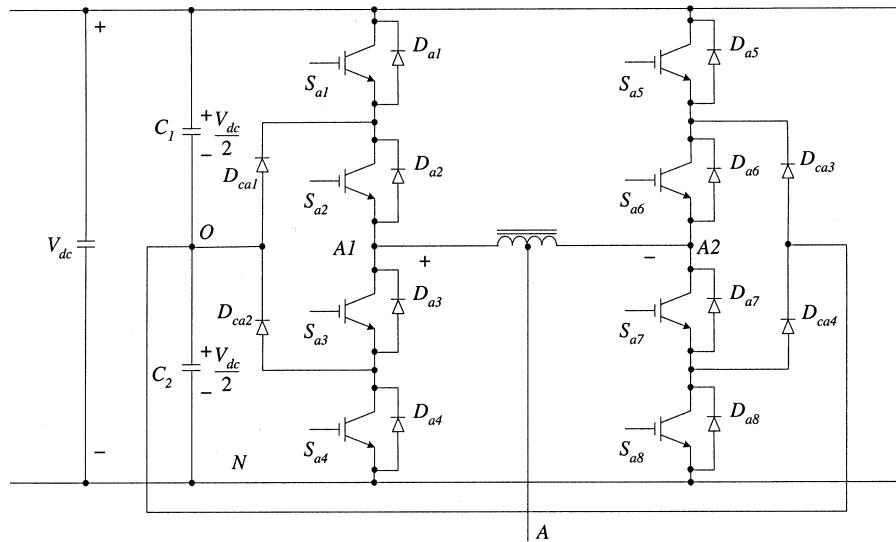
Fig. 6.42 Five-level phase leg with parallel legs based on the NPC VSC.

There are however two other multilevel configurations known as flying capacitor topology and cascaded converter topology. Both of them have merits and drawbacks like all circuits presented so far. And for a different application in reactive compensation a further understanding of the converter and its applicability must be studied and well understood. Switch and other element ratings, cost, and hardware implementation difficulties, control and other issues must be evaluated in order to achieve an optimum topology for the given application. These topologies have been presented in the technical literature mainly as adjustable speed motor drives and they are at the research level for the power system reactive compensation applications. They are presented here due to their possible future applicability in high power applications.

The flying capacitor topology and one of its legs is shown in Figure 6.43. The control technique for this converter is described as follows. It uses a phase-shifted PWM technique. Due to the nature of the multilevel converter, the most significant harmonics of the output voltage waveform are located at a higher frequency typically controlled by the number of carriers used (the harmonic multiplying factor is equal to the number of the level of the converter minus one). For an N-level system, $N-1$ carriers are required. Then the most significant harmonics in the unfiltered output voltage signal are located around frequencies $(N-1)$ times the carrier frequency.

The flying capacitor converter seems to be very attractive for the following reasons:

● A simple PWM phase-shifted technique can be used to generate the control signals for the semiconductors.
● The voltages of the capacitors are automatically balanced under ideal conditions.
● For a more sophisticated system, the capacitor voltages can be actively monitored and controlled by an appropriate DC shifting of the signal generator.
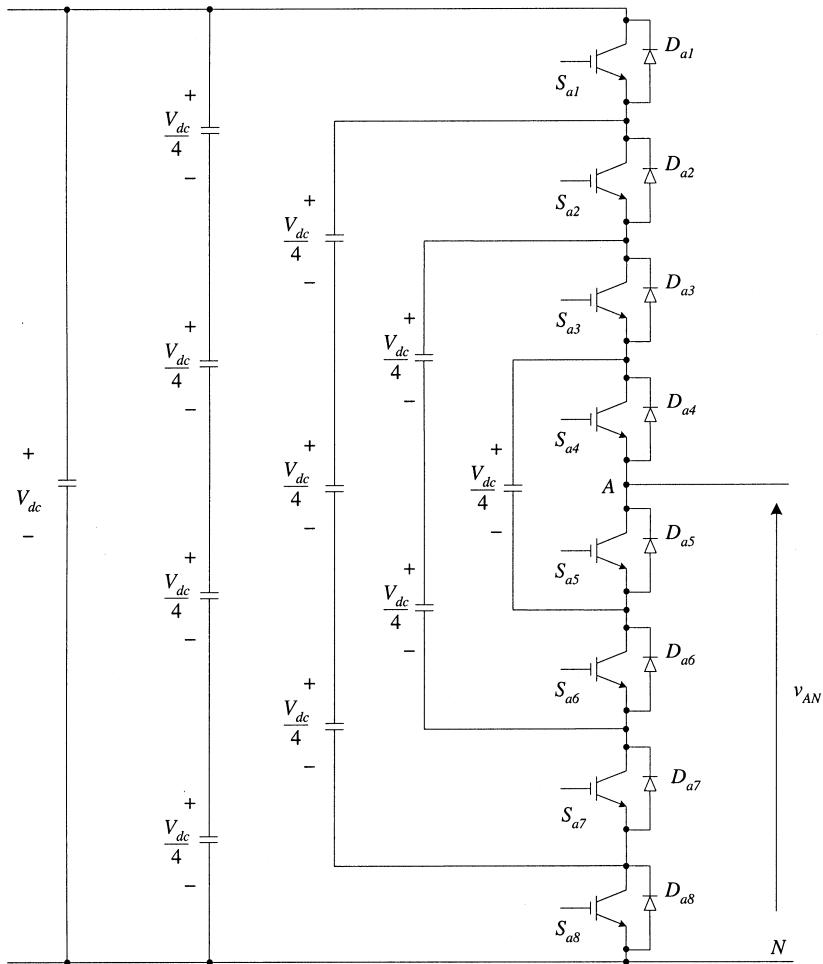
Fig. 6.43 Five-level flying capacitor converter phase leg.

- All semiconductors have equal switching frequency which is equal to the carrier frequency.
- The topology is modular.

However, a number of issues must be resolved in order for such a topology to become a commercially viable alternative to conventional VSC topologies for high power applications. These issues can be summarized as follows:

- The number of high voltage capacitors is considered quite high. Furthermore, taking into account that they need to conduct the full load current at least part of the switching cycle makes them very expensive with high values.
- The topology is subject to faults and does not have tolerance to them, therefore appropriate control and monitoring is required.
- The flying capacitors initially have zero charge and starting the converter is not a trivial issue. This needs to be seriously addressed.
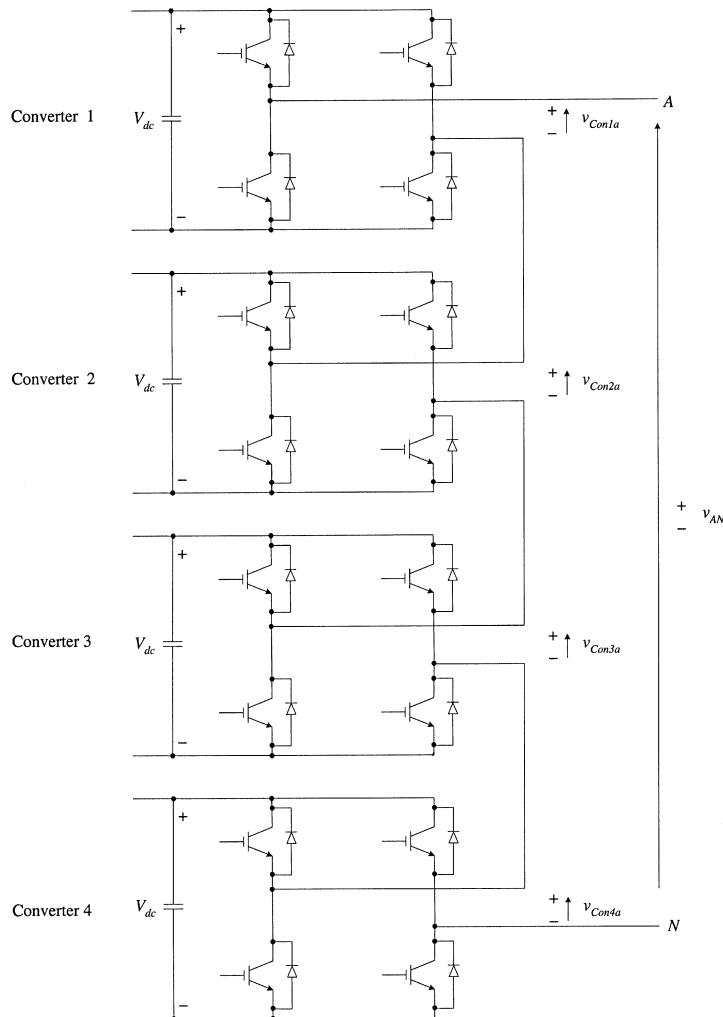
Fig. 6.44 Nine-level cascaded multilevel converter topology based on the single-phase full-bridge VSC.

Finally, the cascaded converter topology is presented in Figure 6.44. This topology offers significant advantages. The first one is the equal switching frequency of each switch. The second one is its ability to employ the phase-shifted control technique, which allows cancellation of more harmonics. This becomes more important when PWM is considered even at a low frequency. The number of the legs is the direct multiple of the carrier frequency to obtain the location of the significant harmonics. This will become clear when the various PWM schemes are introduced in detail.

For fundamental frequency operation, i.e. switches are turned on and off once per cycle, each converter is capable of generating a three-level voltage waveform across the two mid-point legs using the phase-shifted square-wave control method. Due to the nature of the converter phase leg, the phase voltage will be the sum of all converter voltages as follows:

$$v_{AN} = v_{con1a} + v_{con2a} + v_{con3a} + v_{con4a} \tag{6.31}$$

Therefore, the phase voltage v_{AN} will have a total of eight-levels plus the zero level (overall nine-levels converter). For the leg shown in Figure 6.44, the voltage v_{AN} will have values of $4V_{dc}$, $3V_{dc}$, $2V_{dc}$, V_{dc}, 0 and $-V_{dc}$, $-2V_{dc}$, $-3V_{dc}$, and $-4V_{dc}$. Generally speaking, for an m-level converter we need to use $(m-1)/2$ single-phase full-bridge circuits. The line-to-line voltage waveform will have higher numbers of levels. The key waveforms for the nine-level circuit shown in Figure 6.44 are shown in Figure 6.45. Specifically, each converter generates a three-level square-wave signal with a different angle α. The effect of that is that when the four voltage waveforms of each of the four converters are added, a higher level staircase voltage waveform is obtained as shown in Figure 6.45(e). This generates a phase voltage waveform that approaches a sinusoidal looking waveform with minimum harmonic distortion although each individual voltage waveform has a relatively high harmonic distortion (modified square wave).
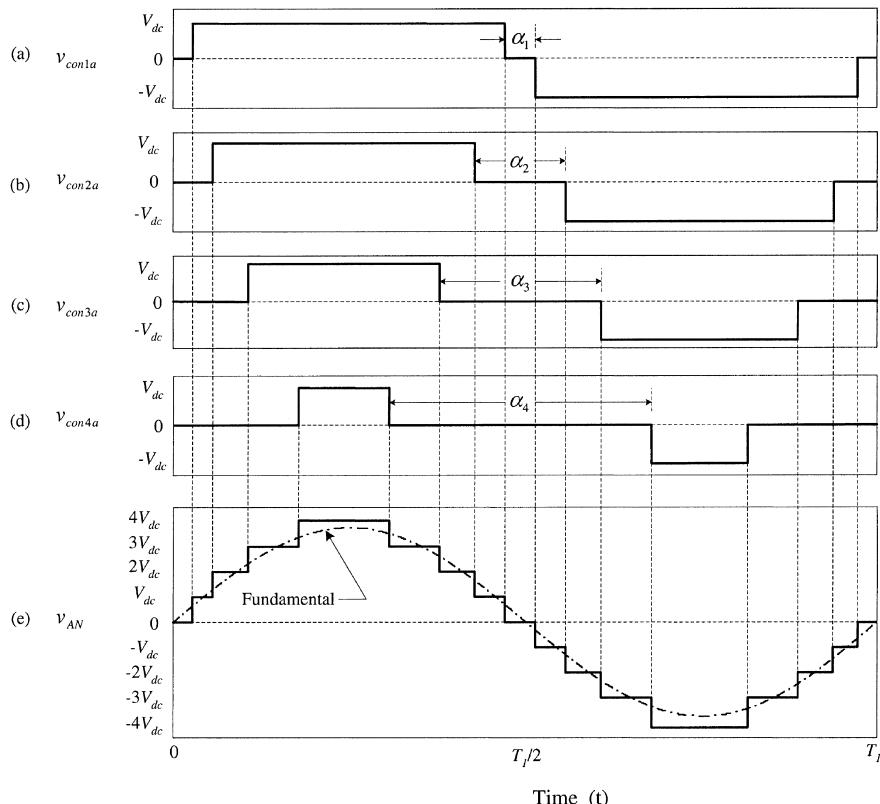
Fig. 6.45 Key waveforms for the nine-level cascaded multilevel converter topology based on the single-phase full-bridge VSC circuit operation. (a) output voltage of converter 1, v_{con1a}; (b) output voltage of converter 2, v_{con2a}; (c) output voltage of converter 3, v_{con3a}; (d) output voltage of converter 4, v_{con4a}; and (e) converter phase voltage v_{AN}.
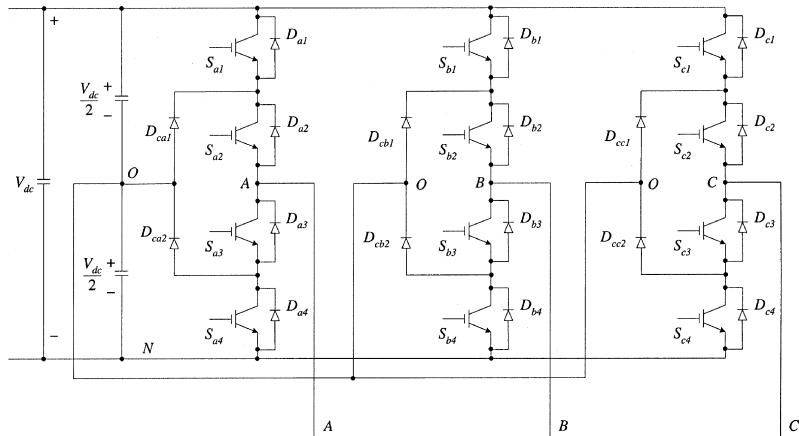
Fig. 6.46 Three-level three-phase NPC VSC.

6.3.7 Three-level three-phase NPC VSC

So far the operation of three-level legs (half-bridge and full-bridge) and a five-level half-bridge one have been described. It is easy therefore to see how a three-phase converter can be built using the legs presented in the previous sections.

A three-level three-phase NPC VSC is shown in Figure 6.46. Each leg is controlled in a similar way as explained before and a 120° phase-shift between each leg is introduced like the case of the conventional three-phase VSC shown in Figure 6.32. Again the number of levels for the line-to-line waveforms will be higher than the level of the converter.

6.3.8 Pulse-width modulated (PWM) VSCs

The square-wave type of control has been presented so far for the VSC topologies. However, if the switch is capable of operating at higher frequencies, which is typically the case with fully controlled semiconductors, PWM concepts can be applied. This control technique is quite an old and proven concept and has dominated the industry since the early 1960s (Schönung, 1964) especially for adjustable speed motor drives.

The thyristor technology was not used with PWM techniques but rather fundamental frequency control based on the square-wave control was used for high power applications. The availability of the GTO and IGBT technology has made it possible for the PWM concepts and topologies known from the adjustable speed motor drives area to now be applied in the reactive power control area and other applications in the power system for energy storage and power quality. These applications will be discussed in detail in later sections of this chapter. In this section, the PWM concepts will be introduced in combination with the VSC topologies presented so far.

The single-phase half-bridge VSC (Figure 6.23) can be controlled using the two-level PWM. As previously discussed, the half-bridge single-phase VSC is a two-level converter as it generates a two-level voltage waveform between the mid-point of the leg and the mid-point of the DC bus (line-to-neutral). Therefore, the two-level PWM method can be used.
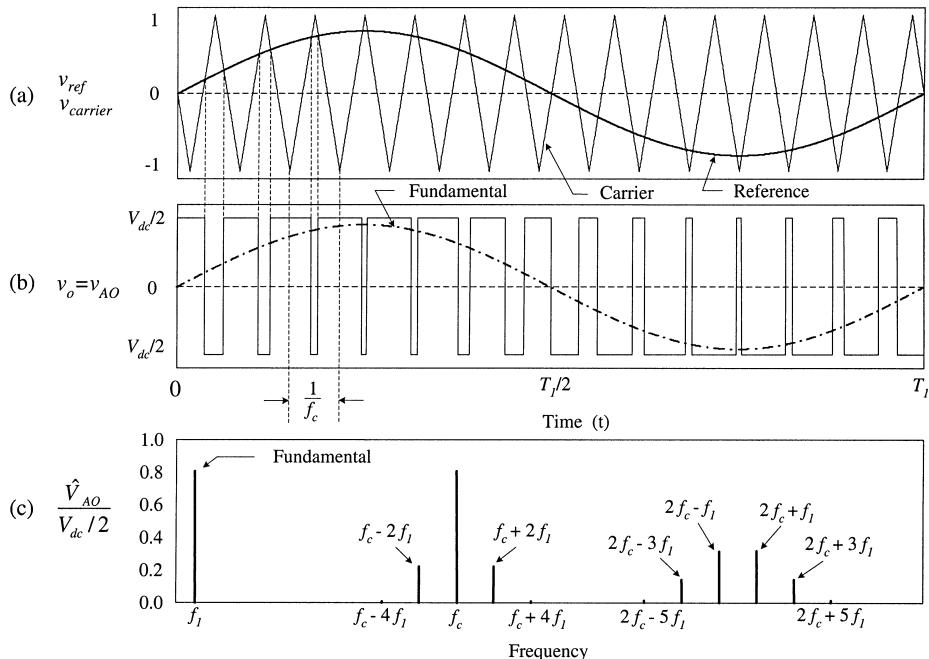
Fig. 6.47 Two-level sinusoidal PWM method. (a) reference (sinusoidal) and carrier (triangular) signals ($f_c = 15 \cdot f_1$ and $M_a = 0.8$); (b) voltage waveform v_{AO}; and (c) normalized harmonic amplitude of the voltage waveform v_{AO}.

The two-level PWM method can be described with the assistance of Figure 6.47. The method is based on the comparison between a reference signal (sinusoidal) having the desired frequency (f_1) and a carrier signal (triangular) with a relatively higher frequency f_c. These signals are shown in Figure 6.47(a). For illustrative purposes, a carrier frequency f_c of 15 times the desired frequency f_1 has been chosen. By varying the amplitude of the sinusoidal signal against the fixed amplitude of the triangular signal kept at 1 p.u. value, the amplitude of the fundamental component at f_1 can be controlled in a linear fashion. This comparison generates a modulated square-wave signal that can be used to control the switches of a given converter topology.

For instance if a leg is considered similar to the converter shown in Figure 6.23, a two-level voltage waveform can be generated between the mid-point of the leg A, and the mid-point of the DC bus O. This waveform has therefore two-levels of $V_{dc}/2$ and $-V_{dc}/2$. Figure 6.47(b) shows the respective waveform. Clearly, the width of the square-wave is modulated in a sinusoidal way and the fundamental component superimposed on Figure 6.47(b) can be extracted with the use of a particular filter. The waveform also contains harmonics associated with the carrier frequency f_c and its multiples, and related sidebands.

It is necessary to define the following amplitude modulation ratio M_a.

$$M_a = \frac{\hat{A}_s}{\hat{A}_c} \tag{6.32}$$

where

$\hat{A}_s$ is the amplitude of the sinusoidal signal and
$\hat{A}_c$ is the amplitude of the triangular signal.

The PWM method shown in Figure 6.47 is presented for an amplitude modulation ratio of 0.8 ($\hat{A}_s = 0.8$ p.u., $\hat{A}_c = 1$ p.u.). When the harmonic content of the resultant voltage waveform is considered, the following observations can be made. The waveform v_{AO} contains a fundamental component with amplitude equal to M_a on a per unit basis as shown in Figure 6.47(c). The harmonics are positioned as sidebands as follows

$$f_h = k \cdot f_c \pm m \cdot f_1 \tag{6.33}$$

where

$k = 1, 3, 5, \ldots$ when $m = 0, 2, 4, 6, \ldots$

and

$k = 2, 4, 6, \ldots$ when $m = 1, 3, 5, \ldots$

When the two-level PWM method is used with a single-phase full-bridge VSC (Figure 6.26), the waveforms are shown in Figure 6.48. When comparing the waveforms of Figure 6.48 with the ones presented earlier in Figure 6.47 for a half-bridge leg, the
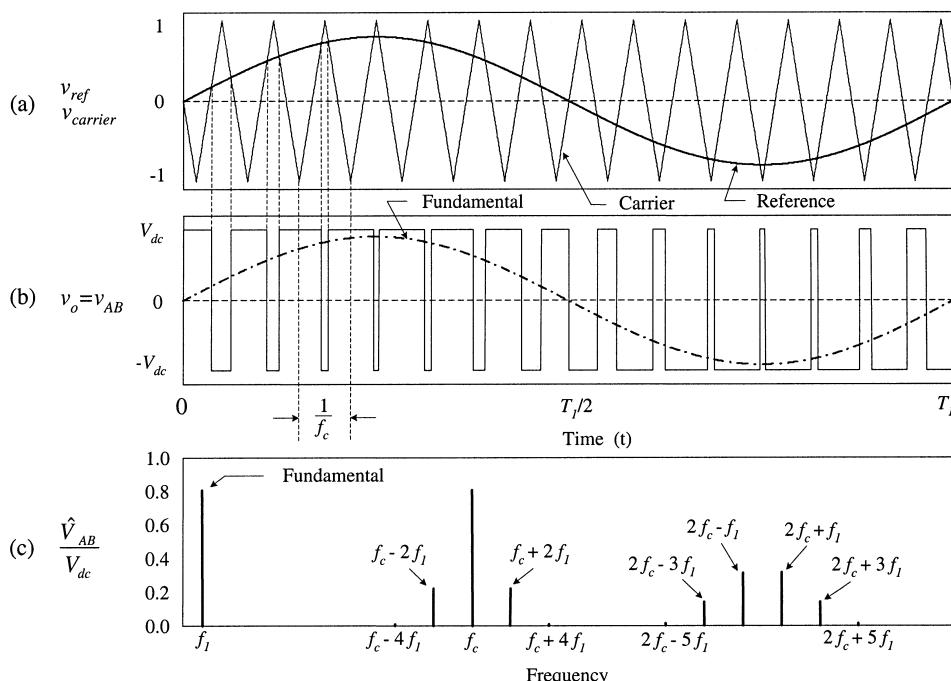
Fig. 6.48 Two-level sinusoidal PWM with a single-phase full-bridge VSC. (a) reference (sinusoidal) and carrier (triangular) signals ($f_c = 15 \cdot f_1$ and $M_a = 0.8$); (b) voltage waveform v_{AB}; and (c) normalized harmonic amplitude of the voltage waveform v_{AB}.

only difference is that the output voltage v_o is taken across points A and B in this case. Therefore, the two-levels of the output waveform take V_{dc} and $-V_{dc}$ values. The control method for the single-phase full-bridge VSC assumes that the switches (S_1, S_4) and (S_2, S_3) are treated as pairs and obviously in a complementary manner (Figure 6.26). The normalized amplitude values of the fundamental and the various harmonics are identical as confirmed with the Figure 6.48(c).

In a previous section, two control methods were presented for a single-phase full-bridge VSC, namely the square-wave method and the phase-shifted square-wave method. The second control method can be extended to include PWM methods.

The phase-shifted PWM method is also known as a three-level PWM method since is it capable of generating a three-level line-to-line voltage waveform. It is also known as unipolar PWM since the line-to-line voltage waveform is either positive and zero or negative and zero for each half of the period.
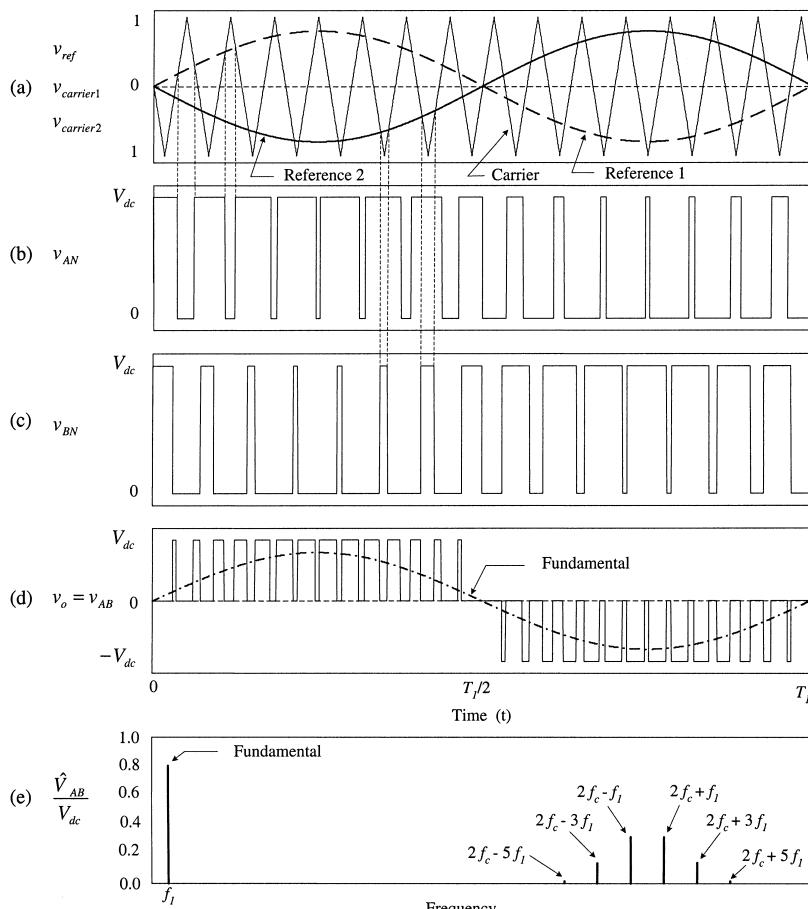
Fig. 6.49 Three-level sinusoidal PWM method for single-phase full-bridge VSC. (a) two reference signals (sinusoidal) and carrier (triangular) signal ($f_c = 15 \cdot f_1$ and $M_a = 0.8$); (b) voltage waveform v_{AN}; (c) line-to-line voltage waveform v_{AB}; and (d) normalized harmonic amplitude of the voltage waveform v_{AB}.

This technique is shown in Figure 6.49. Specifically, in this method two reference signals are used with 180° phase shift as shown in Figure 6.49(a). The same carrier is used to generate the modulated square-waveforms. The direct comparison of the triangular signal with the reference one is used to control one leg. The direct comparison between the other reference and the triangular signal is used to control the other leg. The two voltage waveforms between the mid-point of the leg, say A and B and the negative DC rail point N are shown in Figure 6.49(b) and (c) respectively. The output voltage waveform v_o defined as v_{AB} is drawn in Figure 6.49(d). It can be seen that such voltage waveform has three-levels, namely V_{dc}, 0, and $-V_{dc}$. The frequency of the resultant line-to-line voltage waveform is also twice the carrier frequency. The output voltage waveform contains a fundamental component shown in Figure 6.49(d) as a superimposed waveform and can also be extracted with the appropriate filtering arrangement. The harmonics shown in Figure 6.49(e) are improved when compared with the two-level PWM method shown in Figure 6.48(c). The harmonic components are positioned as follows

$$f_h = k \cdot f_c \pm m \cdot f_1 \tag{6.34}$$

where

$$k = 2, 4, 6, \ldots \text{ when } m = 1, 3, 5, \ldots$$

For a three-phase six-switch VSC (Figure 6.32) the basic sinusoidal PWM technique is illustrated in Figure 6.50. In this case, since there are three legs, three reference (sinusoidal) signals phase-shifted by 120° from one another are used with one carrier (triangular) signal as shown in Figure 6.50(a). The direct comparison between the reference and the carrier generates square-wave signals which are used to drive the six switches. The voltage waveforms between the leg mid-points A and B with respect to the negative DC bus rail point N are given in Figure 6.50(b) and (c). The line-to-line voltage waveform can be simply drawn since

$$\begin{aligned} v_{AB} &= v_{AN} - v_{BN} \\ v_{BC} &= v_{BN} - v_{CN} \\ v_{CA} &= v_{CN} - v_{AN} \end{aligned} \tag{6.35}$$

The resultant line-to-line voltage waveform has three-levels, namely V_{dc}, 0, and $-V_{dc}$.

It should be noted that for as long as the amplitude of the sinusoidal signal remains within the 1 p.u. range, the converter operates in a linear mode. Once the amplitude of the sinusoidal signal becomes higher than 1 p.u., the converter operates in the overmodulation region and certain low order harmonics start to appear in the output voltage waveforms.

In the case of multilevel NPC converter topology, the PWM technique must be adjusted in order to provide the appropriate control. Specifically, for the three-level single-phase half-bridge NPC VSC topology, two carriers are needed. The simple relation between the phase-shift between them is 180° phase shift. This is shown in Figure 6.51(a). Two triangular carriers are used and the comparison between them and the sinusoidal reference generates the control signals for the various switches. The control signals between S_{a1} and S_{a3}, and S_{a2} and S_{a4} must be complementary as discussed earlier. These control signals are plotted in Figure 6.51(b)–(e). The resultant line-to-neutral voltage waveform is then shown in Figure 6.51(g). It is clear that due to
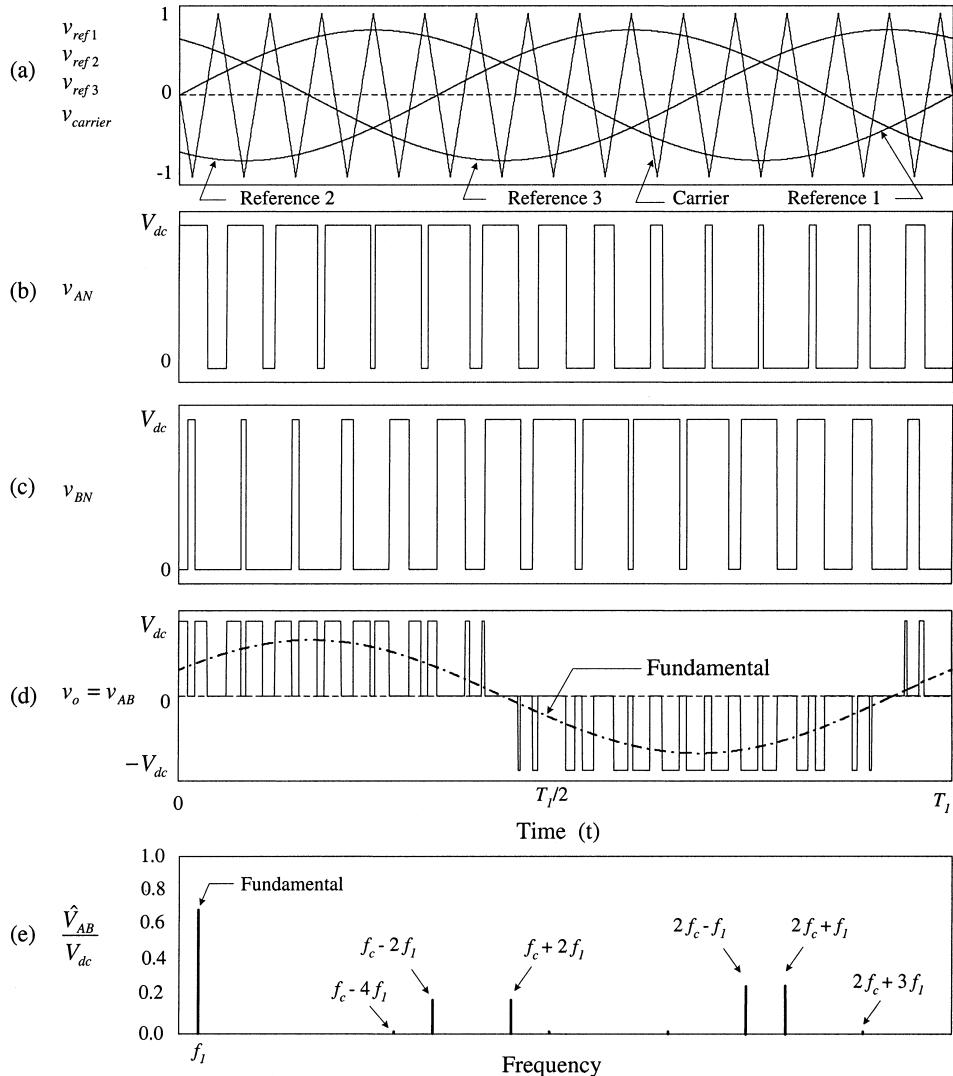
Fig. 6.50 Two-level sinusoidal PWM method for the conventional six-switch three-phase VSC. (a) reference signals and carrier signal (triangular) ($f_c = 15 \cdot f_1$ and $M_a = 0.8$); (b) voltage waveform v_{AN}; (c) voltage waveform v_{BN}; (d) line-to-line output voltage waveform v_{AB}; and (e) normalized harmonic amplitude of the voltage waveform v_{AB}.

PWM operation, the line-to-neutral voltage waveform has three levels, namely, V_{dc}, 0, and $-V_{dc}$. To illustrate the effect of the PWM operation, the harmonic spectrum of the line-to-neutral voltage waveform is given in Figure 6.51(f). The first significant harmonics are located around the carrier frequency as the PWM theory presented in the previous section suggests and as sidebands of that frequency as well.

Based on the PWM operation of the previous converter, a full-bridge version can be built. The PWM control is illustrated in Figure 6.52. Specifically, the two line-to-neutral voltage waveforms as obtained with the previous described method are plotted
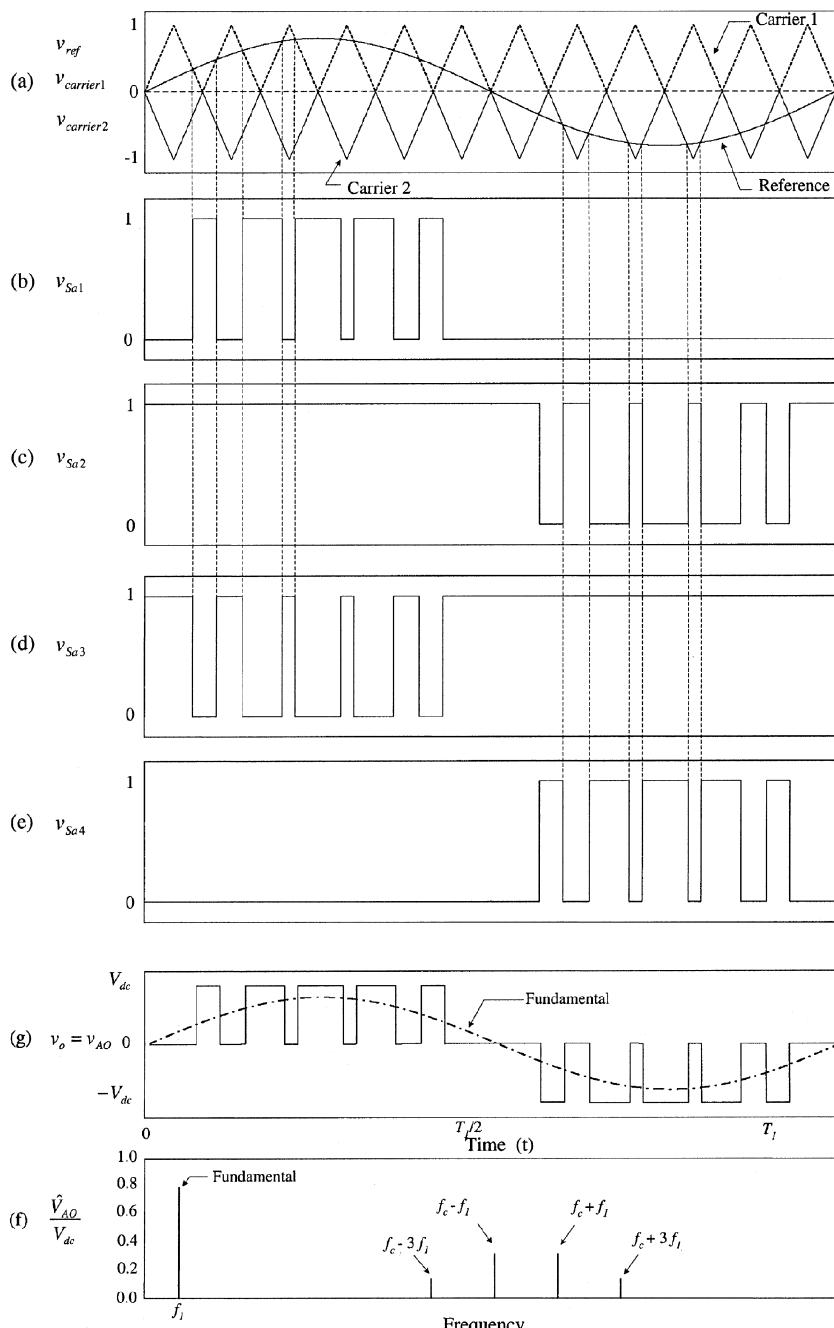
Fig. 6.51 Sinusoidal PWM for the three-level single-phase half-bridge NPC VSC. (a) reference and two carrier waveforms phase-shifted by 180°; (b) control signal for switch S_{a1}; (c) control signal for switch S_{a2}; (d) control signal for switch S_{a3}; (e) control signal for switch S_{a4}; (g) resultant line-to-neutral voltage waveform v_{AO}; and (f) harmonic spectrum of the line-to-neutral voltage waveform v_{AO}.
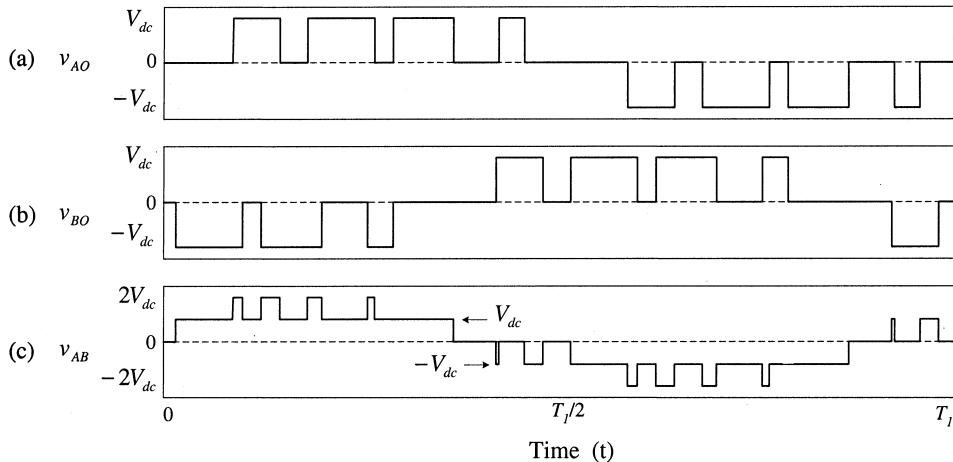
Fig. 6.52 Sinusoidal PWM for the three-level single-phase full bridge NPC VSC. (a) line-to-neutral voltage waveform v_{AO}; (b) line-to-neutral voltage waveform v_{BO}; and (c) resultant line-to-line voltage waveform v_{AB}.

in Figures 6.52(a) and (b) respectively. It is then easy to obtain the resultant line-to-line voltage waveform shown in Figure 6.52(c). It can be observed that this waveform is a multilevel waveform taking five values, namely $2V_{dc}$, V_{dc}, 0, $-V_{dc}$, and $-2V_{dc}$.

Finally it should be added that all these basic topologies presented in this section could be used along with appropriate connections of transformers to generate multi-level voltage waveforms of higher number than the individual converter.

6.4   Uninterruptible Power Supplies (UPSs)

Although the outage of the electricity supply rarely occurs in most developed countries, there exist cases and critical loads that must be protected against such event. The majority of the events that happen are due to extreme weather conditions. Furthermore, the trend is that the average outage times for customers connected to the low voltage levels have been reducing over the last 50 years continually.

However, there are other problems associated with the electricity network such as power line disturbances, namely, voltage spikes, surges and dips, harmonics, and electromagnetic interference. There are critical loads such as computer or information systems which process key data for organizations, medical apparatus, military and government systems that are necessary to be supplied by very high quality of electricity with the highest possible availability factor. For this kind of loads a UPS system is needed.

Large power UPS systems with more than 1 MVA rating are used in large computer rooms by many organizations processing critical data such as banks, government agencies, airlines, and transport and telecommunications companies.

Earlier UPS systems were of rotary design based on DC and AC motor/alternator respectively with a battery for back up. With the advent of the thyristor in the 1960s, static converter based equipment UPS appeared. A block diagram of a basic UPS system is shown in Figure 6.53. The AC mains voltage through a rectifier is converted
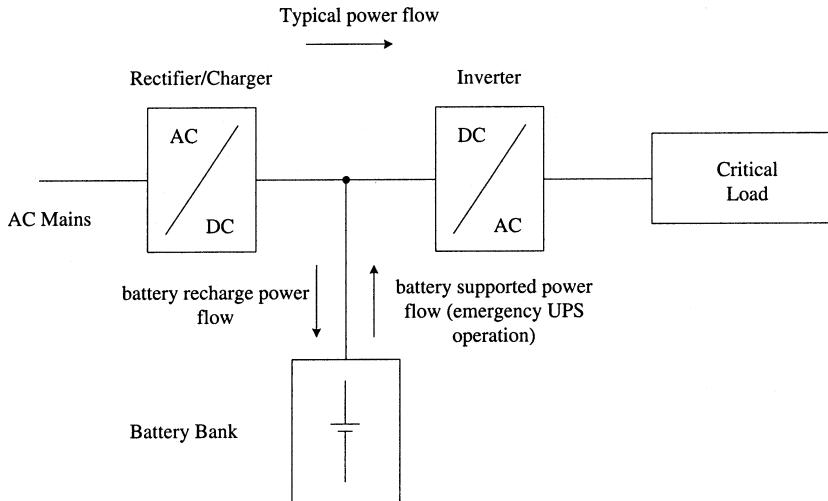
Fig. 6.53 Block diagram of a basic UPS system.

into DC providing a stiff DC bus voltage as an input to the inverter if it is of a voltage source type. A battery is connected across the DC bus to provide the back up power when the AC mains fail through the inverter. When the AC supply becomes available again, power flows through the rectifier/charger to the battery to recharge it and to the critical load via the inverter.

To increase the reliability of the UPS system, the power line can be used as a separate bypass input power supply. In this case, a static transfer switch changes over the power supply to the load from the UPS to the power line. Figure 6.54 shows the circuit arrangement.
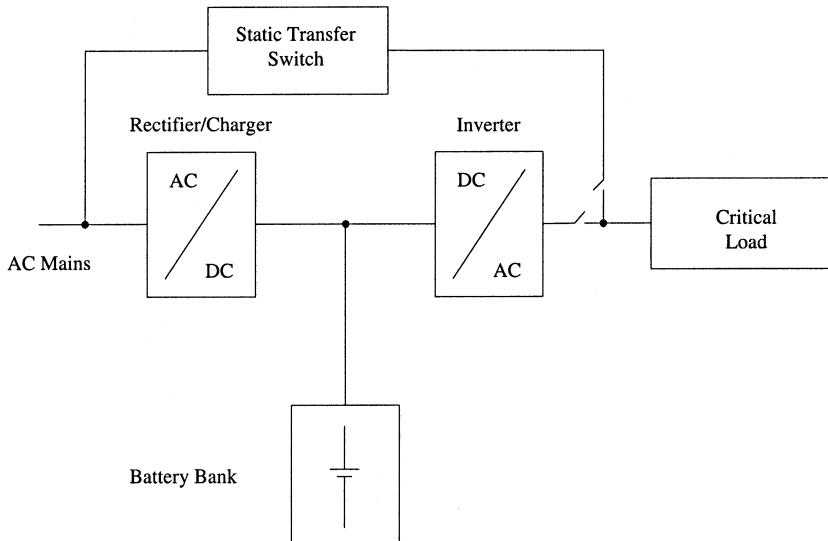
Fig. 6.54 Complementary functions for the UPS and the power line through a static transfer switch arrangement.
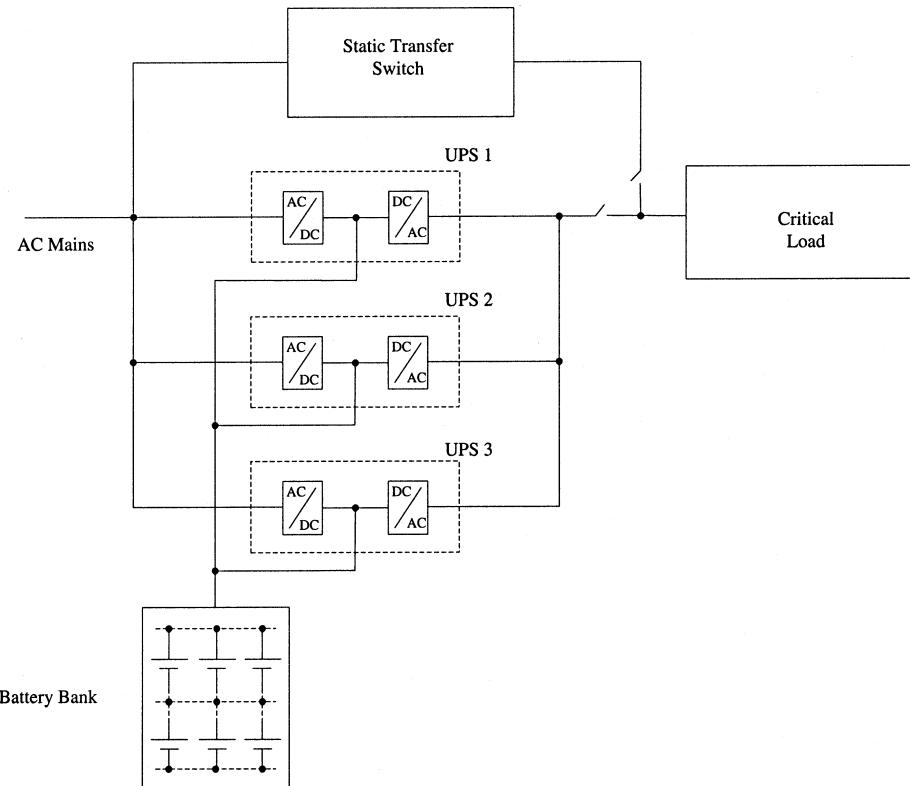
Fig. 6.55 Multi-module based UPS system.

To increase the reliability of a single module UPS system, a redundant system may be considered. It can be designed with the $(N-1)$ concept. Simply said, the total kVA ratings of the overall system with $(N-1)$ units should be equal to the load kVA rating. In this case, the loss of any one UPS unit does not create a problem since the rest of them remaining in service can still supply the load in a satisfactory way. Such a redundant system is shown in Figure 6.55.

For a low kVA rating, the UPS system can be an on-line or an off-line one. In the on-line case, the load is typically supplied through the UPS. If there is a fault with the converter of the UPS system, the AC mains supplies direct the load through the by-pass configuration. In the off-line case, the AC mains supplies the load and the UPS system is on-line when the AC mains fail or under circumstances that the quality of the supply is very low (i.e. under disturbances).

Today, PWM inverters of high frequency are mainly used especially in low and medium power levels. Such systems based on the converter and the technology previously presented in this chapter, have a number of advantages when compared with the thyristor based UPS systems. They include reduced size and weight mainly due to the smaller size of the filter required to meet the THD requirements for the generated supply, lower or even no acoustic noise if the frequencies used are higher than the ones within the audible range (approximately $>18\,\text{kHz}$). Such frequencies are feasible with the use of IGBTs and MOSFETs presented in Chapter 5.

Uninterruptible power supplies systems require an energy storage device to be able to supply the load under power line failure. In most cases, a battery bank is used. The selection of battery is not a hard task although many technologies are available. Specifically, alkaline batteries of the nickel–cadmium type, lead–acid and other more exotic technologies can be theoretically considered. However, the high cost of all the technologies previously mentioned make the lead–acid battery the most common choice for commercial applications. There are a number of drawbacks associated with the lead–acid battery technology including maintenance requirements and environmental concerns. In recent years, new systems based on technologies such as flywheels have been commercially developed even for relatively medium power level applications. These systems are presented in further detail in Section 6.6.1.

6.5 Dynamic voltage restorer (DVR)

Over the last decade and in the twenty-first century, the electricity sector has been going and will go through further deregulation and privatization in the developed world. Competition therefore amongst electricity suppliers with the increased use of power electronics in everyday activities has resulted in increased attention to the issue of power quality.

In Section 6.4, the UPS systems were discussed. In this section, the concept of custom power (CP), proposed to ensure high quality of power supply will be presented briefly. The DVR is such an example. It can be designed to have excellent dynamic performance capable of protecting critical and/or sensitive load against short duration voltage dips and swells. The DVR is connected in series with the distribution line as shown in Figure 6.56. It typically consists of a VSC, energy
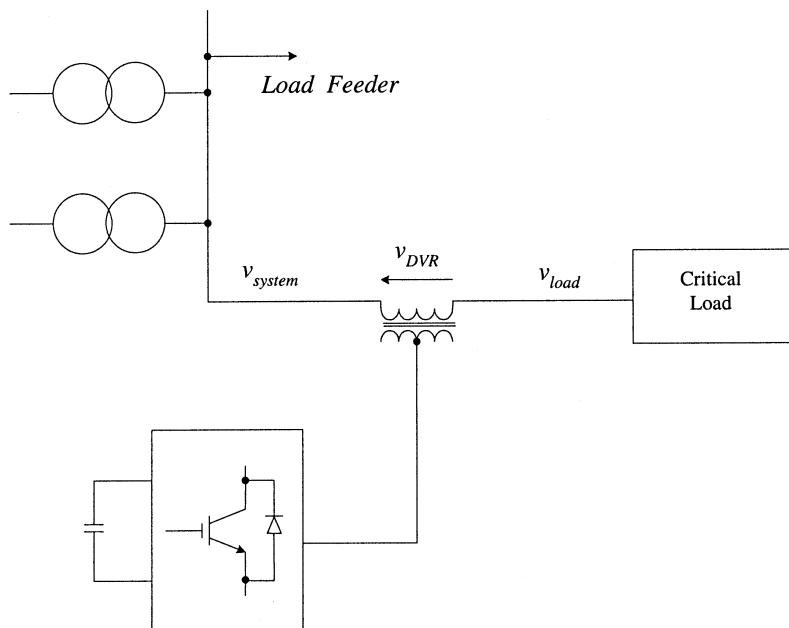
Fig. 6.56 Schematic representation of a dynamic voltage restorer (DVR).
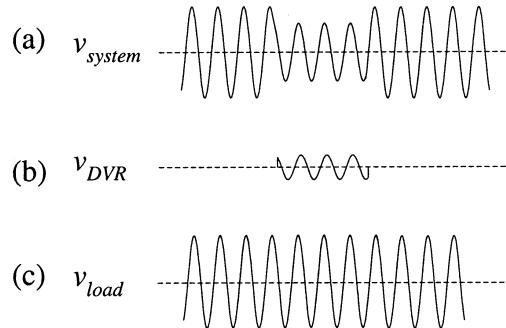
Fig. 6.57 Key waveforms of the DVR operation.

storage capacitor bank, harmonic filters and a connecting transformer. Protection equipment and instrumentation is also part of the system.

But how does the DVR work? The DVR, connected in series as mentioned earlier, injects AC voltage in series with the incoming network voltages. Due to the presence of a PWM VSC, real and reactive power can be exchanged with the system since all DVR injected voltages can be controlled with respect to their amplitude and phase (PWM operation).

When everything is fine with the line voltages, the DVR operates in a standby mode with very low losses. Since no switching takes place and the voltage output is zero (the connecting transformer is seen as a short circuit by the network), the losses in the DVR are conduction losses and relatively very low. If there is a voltage dip, the DVR injects a series voltage to compensate for the dip and restore the required level of the voltage waveform. Such key waveforms are shown in Figure 6.57. In Chapter 8, this system will be further discussed and a simulation example will be provided.

6.6   Energy storage systems

Electrical energy unfortunately is one of the few products, which must be produced almost when it is required for consumption and has no inherent self-life. However, there are a number of energy storage schemes for various purposes and these are discussed in this section.

The continuous demand for uninterrupted and quality power has resulted in a number of smart and alternative energy storage systems. Therefore, some exciting new systems will be introduced first. These include flywheels and superconducting materials. Conventional systems such the hydroelectric pumped storage, batteries and other new technologies with a promising future will also be presented. Some of them may be used in electric utilities applications and some may be more suitable for low power levels such as an electric or hybrid vehicle and other low power demand management applications.

6.6.1   Flywheel energy storage systems

A flywheel energy storage system is an old idea gaining more attention due to technological advances making it a commercially viable solution for the industry.
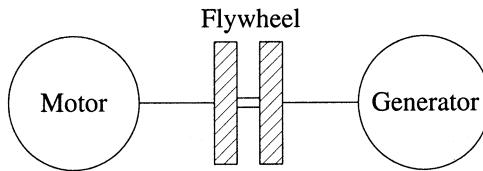
Fig. 6.58 A block diagram of a conventional flywheel system.

Although as previously mentioned, the flywheel is one of the oldest technologies for energy storage – Greek potters still use them today – modern systems based on the same idea incorporate high-tech composite material based wheels and low-friction bearings that operate in extremely high rotational speeds which may reach 100 000 rpm. Of course conventional systems which couple to existing rotating machines are still available.

Electric energy in the form of kinetic energy is stored in a flywheel comprising of a spinning disc, wheel or cylinder. This efficient and quiet way of storing energy offers a reliable source of power which can be accessed to provide an alternative source during electrical outages as a UPS system. A block diagram of a conventional flywheel is shown in Figure 6.58. The two concentric rotating parts of the flywheel are where the energy is stored and retrieved when needed.

In power utility applications, its commercially important application includes peak electricity demand management. Flywheels can be used to store energy generated during periods that electricity demand is low and then access that energy during high peak. The applications of flywheels extend to areas of electric vehicles and satellite control and gyroscopic stabilization.

Modern flywheels use composite materials and power electronics. The ultra-high rotational speeds require magnetic bearings, where magnetic forces are used to 'levitate' the rotor minimizing frictional losses. Such systems operate in partial vacuum which makes the control of the system quite sophisticated.

For power quality applications, cost is a very important consideration and hybrid solutions between the conventional systems and the modern highly sophisticated ones are available. Figure 6.59 shows an exploded view of a modern flywheel motor/generator structure.

Figure 6.60 shows a flywheel system controlled via an IGBT converter. The flywheel absorbs power to charge from the DC bus and when required, power is transferred back to the DC bus since the inverter can operate in the regenerative mode, slowing down the flywheel. Such decision can be based on a minimum acceptable voltage across the DC bus below which the flywheel can start discharging. Like a battery, when the flywheel is fully charged, its speed becomes constant. When the flywheel is discharged, the DC bus voltage is held constant and the flywheel behaves as a generator, transferring power back to the DC bus at an independent rotor speed.

A commercially available flywheel energy storage system of 240 kW for utility applications operating at approximately 7000 rpm is shown in Figure 6.61.

A number of UPS configurations can be considered with the use of flywheels. For instance, in case of critical loads and the availability of a generator, a flywheel system may be used to supply the critical load until the starting and synchronization of the
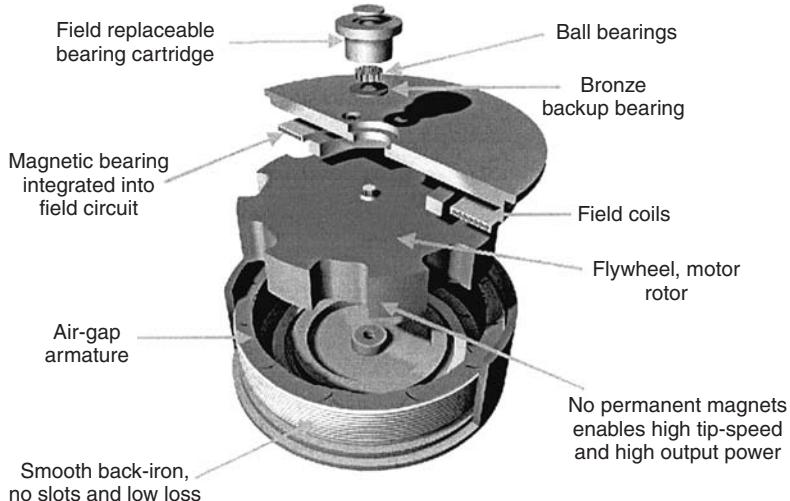
Fig. 6.59 Exploded view of a modern flywheel motor/generator structure. (Courtesy of Active Power Inc., USA.)
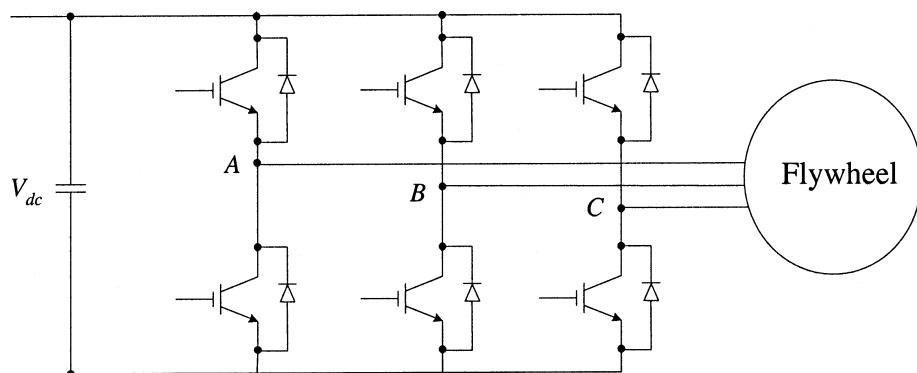
Fig. 6.60 Modern flywheel energy storage system based on VSC.

generator as shown in Figure 6.62. Such a system is called continuous power supply (CPS). It differs from the conventional UPS system as the critical load is connected to the AC mains used as a primary source of power. The static UPS systems use backup battery power and the CPS uses a dynamic energy storage system, a flywheel for example. Finally CPS systems condition the power coming from the utility or in case of emergency from a diesel generator providing also power factor correction and reduction in current harmonics.

A flywheel may be part of a power quality system or else power conditioning system used to eliminate network problems associated with voltage sags, short notches and swells, harmonic distortion and power factor. Figure 6.63 shows a block diagram of a typical configuration based on a flywheel.

Finally in case of a UPS system requiring a battery bank, in order to extend the life of the battery arrangement, a flywheel system maybe used as shown in Figure 6.64. Uninterruptible power supplies systems are designed and used to provide the
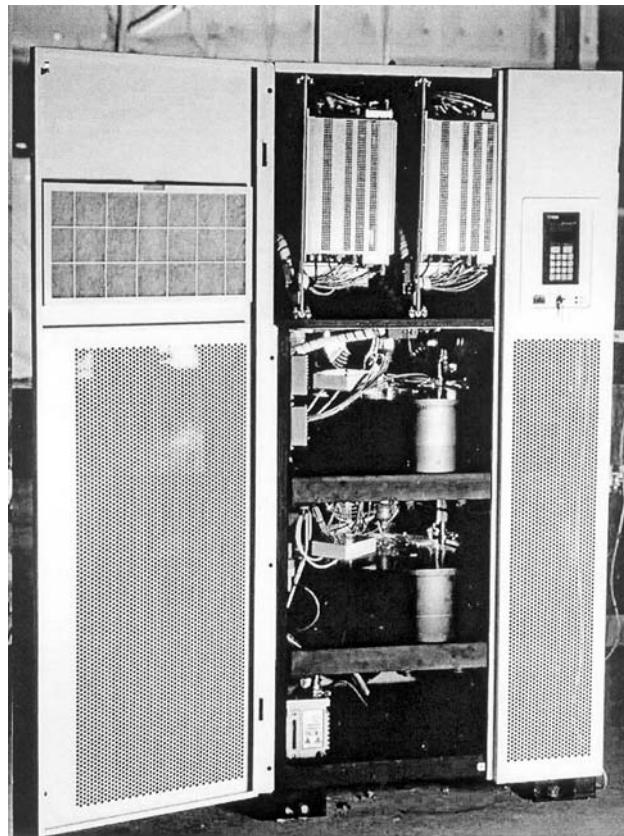
Fig. 6.61 A 240 kW flywheel system. (Courtesy of Active Power Inc., USA.)
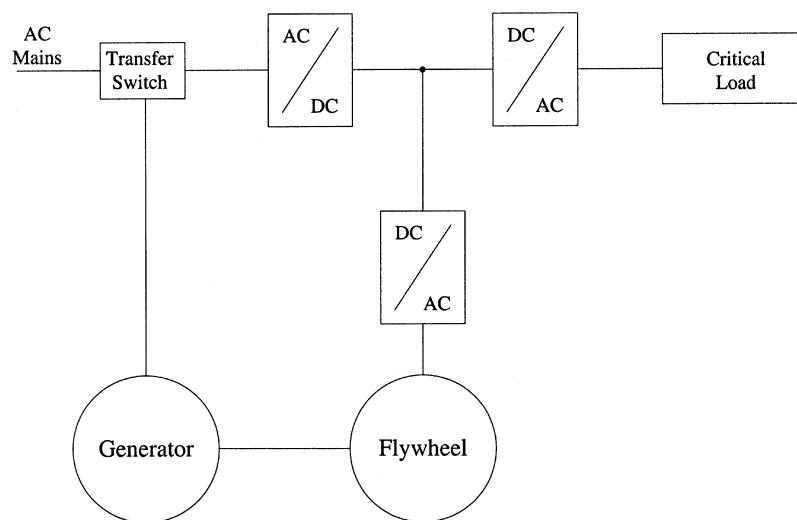
Fig. 6.62 Flywheel based continuous power system.
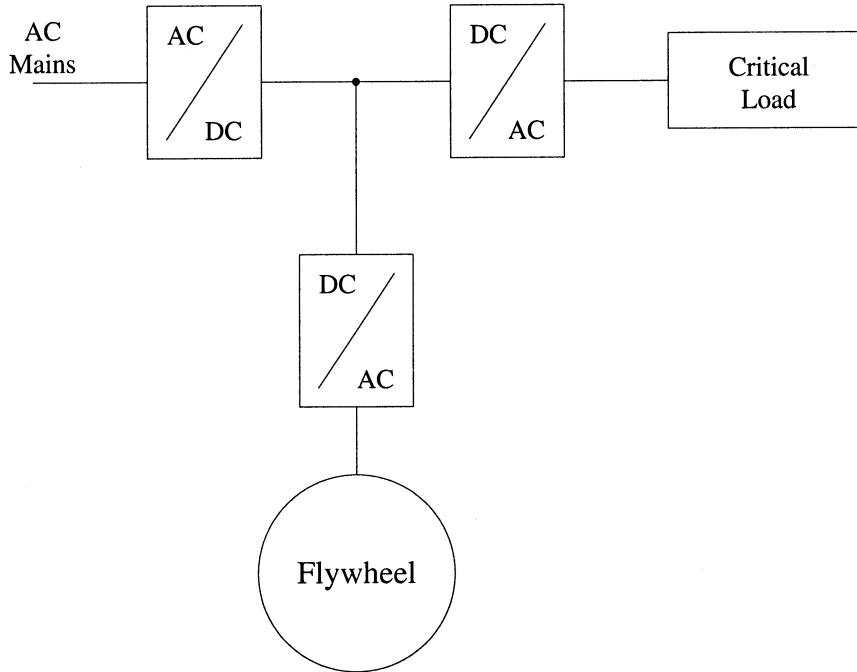
Fig. 6.63 Flywheel based power quality system.
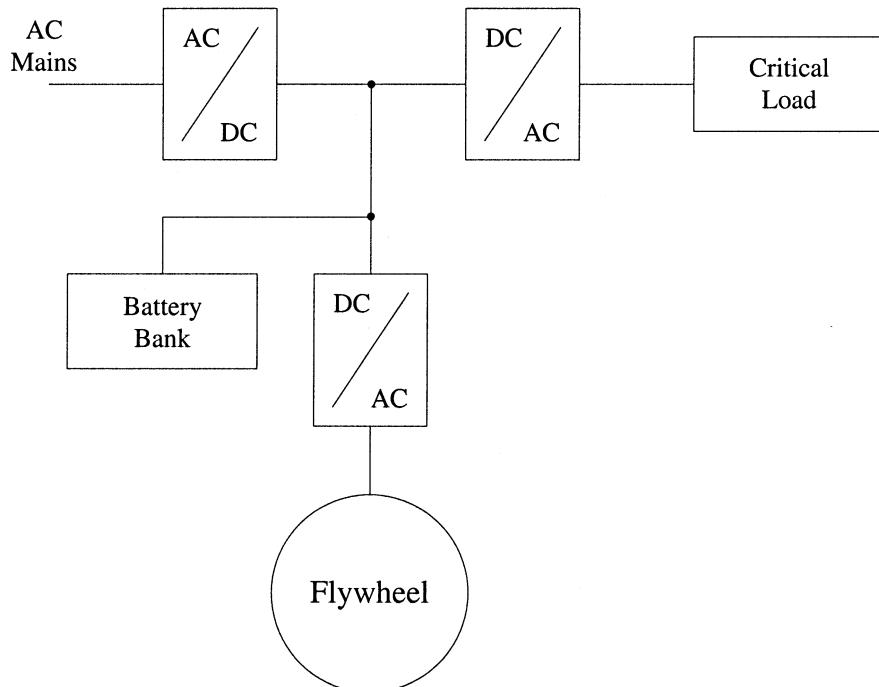
Fig. 6.64 Flywheel based UPS system with battery bank.

power supply during long non-availability of the AC mains. However, the battery depends on the times and duration of charge and discharge and for short voltage sags and other line problems a flywheel can extend its life by dealing with such problems rather than the batteries.

Finally, another potential application for small flywheel systems is renewable energy systems and specifically wind power systems. The flywheel may act as a buffer supplying energy for short intervals of time and mainly between wind gusts since the flywheel systems can charge and discharge quickly. Batteries cannot compete with such short demands of energy supply and take more time to charge.

6.6.2 Superconducting magnetic energy storage (SMES)

Superconducting magnetic energy storage (*SMES*) is defined as: a superconducting electromagnetic energy storage system containing electronic converters that rapidly injects and/or absorbs real and/or reactive power or dynamically controls power flow in an AC system.

A typical SMES system connected to a utility line is shown in Figure 6.65. But before explaining the power electronics technology available for such systems, let's examine first the phenomenon of superconductivity, a natural phenomenon and probably one of the most unusual ones.

Superconductivity is the lack of resistance in certain materials at extremely low temperatures allowing the flow of current with almost no losses. Specifically, super-conductors demonstrate no resistance to DC current and very low to AC current. They also exhibit quite strong diamagnetism, which simply means they are strongly repelled by magnetic fields. The levitating MAGLEV trains are based on this principle. The materials known today as superconductors must be maintained at relatively low temperature. There are two kinds of materials:

1. low temperature superconductor (LTS)
2. high temperature superconductor (HTS).

The latter has been discovered recently and has opened up new opportunities for commercial applications of the SMES systems. Applications of such material range from the microelectronics area such as radio frequency circuits to highly efficient power lines, transformers, motors, and magnetic levitating trains just to name a few.

The Dutch physicist H.K. Onnes first discovered superconductivity in 1911 at the University of Leiden. Progress was made later by others, but it was only in 1957 when the American physicists J. Bardee, L.N. Cooper and J.R. Schrieffer introduced the BCS theory named after their initials which explained the phenomenon for the first time in history. This theory provided the first complete physical description of the
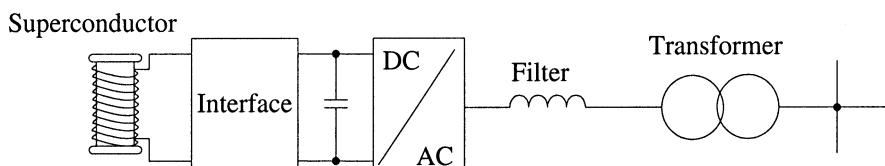
Fig. 6.65 A typical SMES system connected to a power network.

phenomenon known as a quantum phenomenon, in which conduction electrons happen to move in pairs thus showing no electrical resistance. For their work they won the Nobel Prize in 1972. However, until 1985, the highest temperature superconductor was niobium germanium at 23 K (23 K or 418 °F). The temperature of 23 K was very difficult to achieve, as liquid helium is the only gas that can be used to cool the material to that temperature. Due to its nature, liquid helium is very expensive and inefficient and that was the main obstacle for commercial applications of superconductors. In 1986, K.A. Miller and J.G. Bednorz discovered a superconducting oxide material at temperatures higher than ones which had been thought possible. For their discovery they won the Nobel Prize in physics in 1987. They had effectively raised the temperature for a superconductor to 30 K (−406 F). In 1987, P. Chu announced the discovery of a compound (Yttrium Barium Copper Oxide) that became superconducting at 90 K. Even higher temperatures were achieved in later times with bismuth compounds at 110 K and thallium compounds at 127 K. When materials were discovered that their critical temperature to become superconductors was raised above 77 K, the low cost and readily available liquid nitrogen could be used to cool the superconductor. This made some products and applications commercially viable.

Superconductivity offers two interesting and different ways of energy storage, namely SMES systems and flywheels based on superconductive magnetic bearings as presented in the previous section (Hull, 1997).

The characteristics of an SMES system can be summarized as follows:

- Very quick response time (six cycles or simply 100 ms for a 50 Hz system, for large-scale systems, and fewer cycles for smaller-scale units).
- High power (multi-MW systems are possible, for instance 50–200 MW with 30–3000 MJ capacity).
- High efficiency (since no conversion of energy from one form to another, i.e. from mechanical or chemical to electrical and vice versa does not occur, the round trip efficiency can be very high).
- Four quadrant operation.

The above mentioned attributes can provide significant benefits to a utility for a number of cases as follows:

- load levelling
- improve the stability and reliability of the transmission line
- enhance power quality
- extend line transmission capacity
- provide voltage and reactive power control
- spinning reserve.

A SMES system belongs to FACTS, which can exchange both real and reactive power with the grid. Therefore, it can be used successfully to manage the performance of the grid at a given point. It is based on a well-known concept of DC current flowing through a coiled wire (Figure 6.65). However, the wire is not a typical type which has losses through the conduction of current. The wire is made of a superconducting material. An important part of any SMES system is the required cryocooling. A highly efficient cryostat containing the superconductor
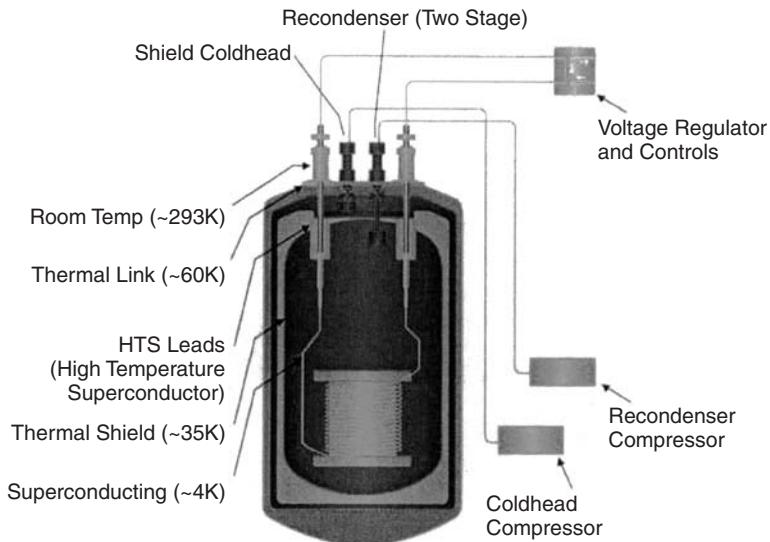
Fig. 6.66 A high efficiency cryostat containing the superconductor magnet. (Courtesy of American Superconductor Inc.)

magnet is shown in Figure 6.66. The three-phase VSC topology (Figure 6.32) can be used to transfer power between the superconductor and the power system/load.

6.6.3 Other energy storage systems

There are a number of other energy storage systems. A hydroelectric pumped-storage plant for instance is a quite popular one with power utilities. It works like the conventional hydroelectric station, except for the fact that the same water is used over and over again to produce electricity. There are two reservoirs at different altitudes. When power from the plant is needed, water from the upper reservoir is released driving the hydro turbines. The water is then stored in the lower reservoir. A pump is used then to pump the water back from the lower reservoir to the upper one, so that it can be used again to generate electricity. Pumped-storage plants generate electricity during peak load demand. The water is generally pumped back to the upper reservoir at night and/or weekends when the demand is lower and hence the operating costs of the plant can be reduced to meet the economics of the method. Of course the advantage of using the water again and again requires the building of a second reservoir therefore increasing the cost of the overall plant. Since the plant uses electricity when the water is pumped into the upper reservoir, the concept behind the development of such plants is based on the conversion of relatively low cost, off-peak electricity generated by thermal plants into high value on-peak electricity when the hydroelectric plant generates electricity to assist with demand management for utilities.

Another energy storage system may be based on batteries. Such a system of course requires a great deal of maintenance and periodic replacement. Furthermore,

supercapacitors represent a state-of-the-art technology with potential applications in power quality. When compared with the lead–acid batteries a supercapacitor is capable of releasing energy a lot more rapidly and can address energy storage applications in the milliseconds to approximately 100 s. The energy storage capability per volume unit is also higher than a conventional capacitor.

Finally, there exist systems based on hydrogen storage and technology associated with double-layer capacitors. All these systems can offer a solution for different energy storage needs and power requirements.

6.7 HVDC

High voltage direct current power transmission, although not part of the grid to distribute power to customers, is a significant technology used successfully to transmit power in a more economic way over long distances, to connect two asynchronous networks and in many other cases. The idea and the relevant technology were under development for many years and started as early as in the late 1920s. However, the application became commercially possible in 1954 when an HVDC link was used to connect the island of Götland and the mainland of Sweden. The power of that project was 20 MW and the DC voltage was 100 kV. At the time, mercury arc valves were used to convert the AC into DC and vice versa. The control equipment used vacuum tubes.

Since then of course, the semiconductor field went through a revolution mainly due to the development of the thyristor and other devices as presented in Chapter 5. It is these continuous developments that drive the changes and the improvements in the HVDC technology.

The thyristor or SCR was developed by General Electric and became commercially available in the early 1960s in ratings of approximately 200 A and 1 kV. However, it took more than a decade for the device to mature and be used successfully in commercial high-power applications such as HVDC. The mercury arc valves then were replaced by thyristor valves, which reduced the complexity and size of the HVDC converter stations a great deal. The introduction of digital control and microcomputers has also made its contribution to the further development of the technology.

Today, further improvements can be expected and some are already in place with the availability of the IGBT to build HVDC systems based on the VSC topologies discussed in an earlier section of this chapter. These state-of-the-art developments will be discussed in the following sections of this chapter.

In simple terms HVDC is the conversion of AC into DC using a phase-controlled converter with thyristors and then transfer the power as DC into the other side which again converts the DC into an AC with a similar converter. A simple diagram representing an HVDC system and its major equipment is shown in Figure 6.67.

There are two AC systems interchanging their role of a sending and receiving end power system shown as *AC System 1* and *AC System 2* (Figure 6.67). These systems are connected through a transformer with the power electronics converter based on thyristor technology. These converters (*Converter 1* and *Converter 2*) operate as a line
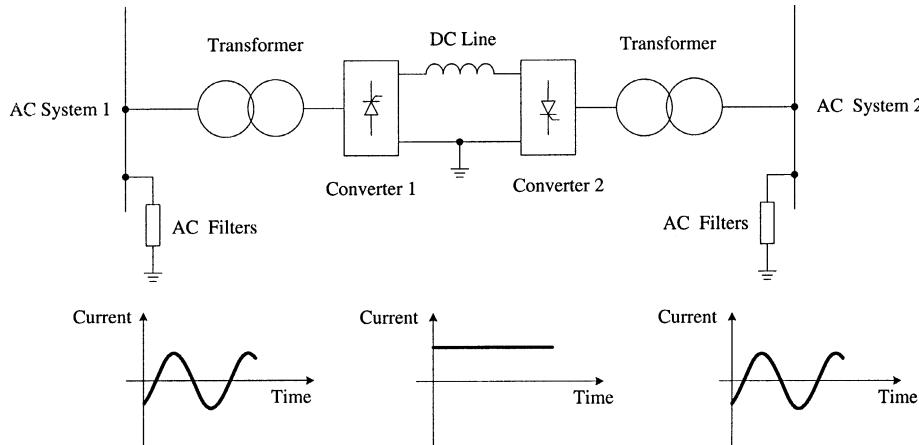
Fig. 6.67 Simple representation of a conventional HVDC power transmission system.

commutated inverter or as a line-commutated rectifier depending upon the way the power flows interchanging their role as well. The AC current is rectified into a DC quantity and the power is transmitted in DC form via a conducting medium. The DC line can be a short length of a busbar if the HVDC system is a back-to-back one, or a long cable or overhead line if the two converters are physically located within some distance between them. On the other end, the DC current is inverted with the assistance of the other converter into an AC waveform. The fundamental frequency switching of the thyristors and the associated phase-control generates waveforms which are rich in low frequency harmonics on the AC side current and on the DC side voltage. These harmonics must be filtered to meet the requirements of specific standards.

It is however very hard to filter such low frequency harmonics and due to the nature of the high power involved, higher order pulse converters are used. If one converter is supplied by voltages generated by a star-connected transformer and the other one by a delta-connected one, the phase-shift of the transformer voltages can suppress the harmonics around the 6th per unit frequency (5th and 7th). This will result in first significant harmonic frequencies around the 12th harmonic (11th and 13th). This converter arrangement is shown in Figure 6.68 and is known as a 12-pulse converter.

Even though the harmonics are shifted at higher frequencies, there is still a need to filter them with appropriate filters on the AC side. These filters are connected in shunt configuration and are built with resistors, capacitors and inductors. They are designed to have the appropriate impedance at specific frequencies. The converters draw from the AC system reactive power and such power must be compensated. Therefore, the filters must have capacitive behaviour at the fundamental frequency to be able to supply and thus compensate the reactive power required by the converter.

Each thyristor as shown in Figure 6.68 drawn as a single one may be built with a number of them in series to be able to block high voltages. The DC voltage levels are not fixed and most projects commissioned today use different voltage levels. For
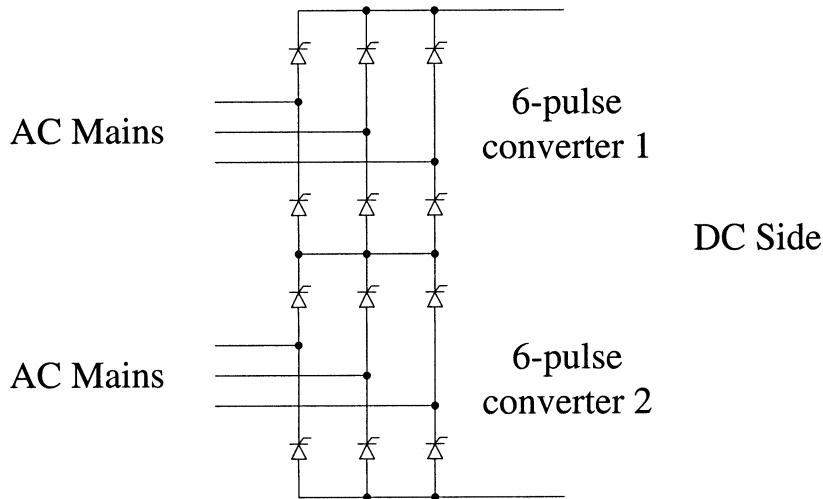
Fig. 6.68 Circuit configuration of a 12-pulse thyristor converter.

instance DC voltage levels as high as 600 kV have been used in projects and taking into account that the thyristor blocking voltage is approximately today 8 kV, one can clearly see that a number of them must be used in series to achieve the required blocking voltage mentioned earlier. A thyristor module based on a LTT device (presented in Chapter 5) is shown in Figure 6.69.

For reliable operation of the HVDC system under all conditions, switchgears are used. These assist the system to clear faults and to re-configure the station to operate in a different way if required. The reliability and the ability to operate in many cases under extreme weather conditions are very important. For instance the design temperature of the AC breakers and the installation at Radisson converter station, James Bay, Canada needs to be $-50\,°C$. Figure 6.70 shows this installation.
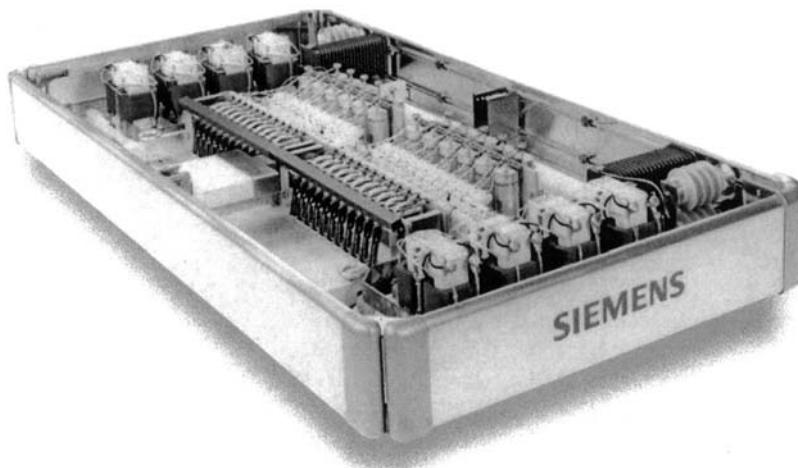
Fig. 6.69 A light triggered thyristor (LTT) valve for conventional HVDC applications. (Courtesy of Siemens.)

Fig. 6.70 AC breakers and current transformers at Radisson converter station, James Bay, Canada. Design temperature is $-50\,^\circ$C. (Courtesy of ABB, Sweden.)

6.7.1 HVDC schemes and control

Depending upon the function and location of the converter stations, various schemes and configurations of HVDC systems can be identified as follows:

1. *Back-to-back HVDC system*. In this case the two converter stations are located at the same site and there is no transmission of power with a DC link over a long distance. A block diagram of a back-to-back system is shown in Figure 6.71. The two AC systems interconnected may have the same or different frequency, i.e. 50 Hz and 60 Hz (asynchronous interconnection). There are examples of such systems in Japan and South America. The DC voltage in this case is quite low (i.e. 50 kV–150 kV) and the converter does not have to be optimized with respect to the DC bus voltage and the associated distance to reduce costs, etc. Furthermore, since both converters are physically located in the same area, the civil engineering costs of the project are lower when compared with a similar HVDC power transmission system where two stations at two different locations must be built.

A 1000 MW back-to-back HVDC link is shown in Figure 6.72. The scheme comprises of two 500 MW poles each operating at 205 kV DC, 2474 A together with conventional switchgears at each end of the link. Fifty-four thyristors, each rated at
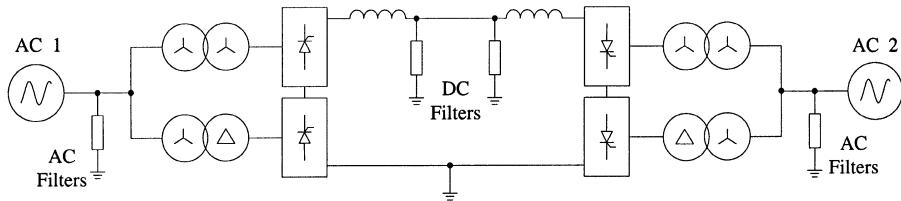
Fig. 6.71 Back-to-back HVDC power system with 12-pulse converters.
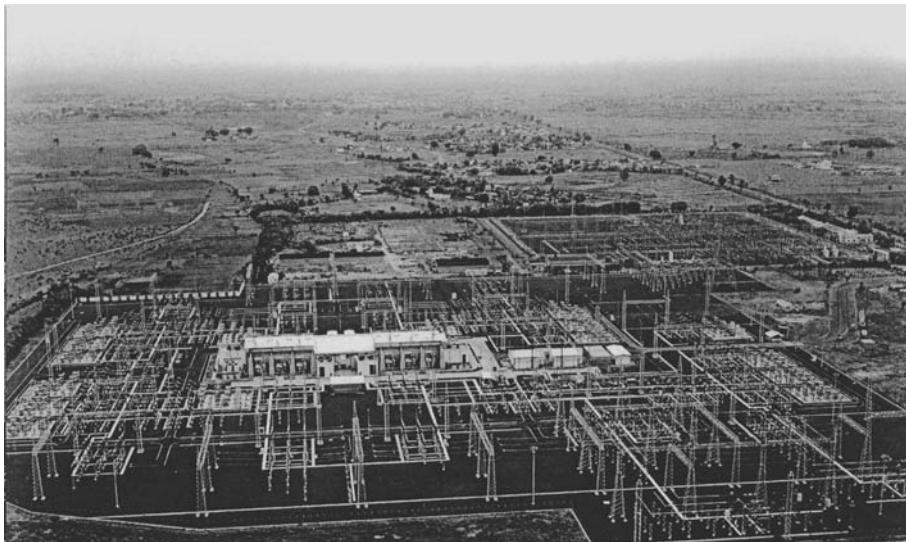
Fig. 6.72 A 1000 MW back-to-back HVDC link, Chandrapur, India. (Courtesy of ALSTOM, Transmission and Distribution, Power Electronic Systems, Stafford, England, UK.)

5.2 kV, are connected in series to form a valve and four valves stacked vertically form a 'quadrivalve' tower. One 'quadrivalve' is approximately $3.8 \times 3.8 \times 6.2$ m high and weighs around 14 tonnes. The six 'quadrivalve' towers are shown in Figure 6.73.

The quadrivalves are arranged in the valve hall with space around them for maintenance access, electrical clearance and connections. The valve hall is designed to provide a temperature and humidity controlled environment and the screened walls contain the radio frequency interference generated by the valve-switching transients.

2. *Monopolar HVDC system*. In this configuration, two converters are used which are separated by a single pole line and a positive or a negative DC voltage is used. Many of the cable transmissions with submarine connections use monopolar systems. The ground is used to return current. Figure 6.74 shows a block diagram of a monopolar HVDC power transmission system with 12-pulse converters.

3. *Bipolar HVDC system*. This is the most commonly used configuration of an HVDC power transmission system in applications where overhead lines are used to transmit power. In fact the bipolar system is two monopolar systems. The advantage of
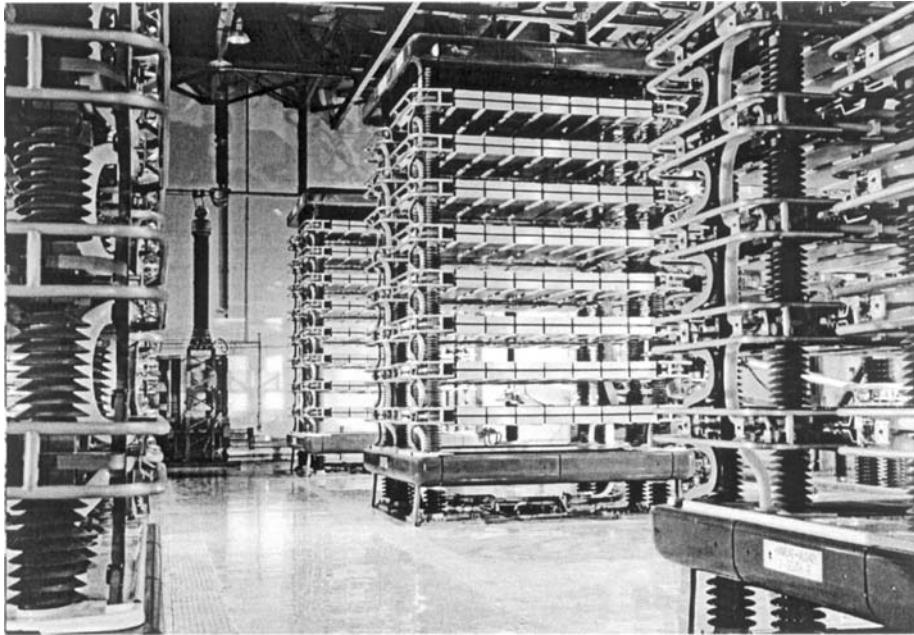
Fig. 6.73 Inside the valve hall, showing its six 'quadrivalve' towers. (Courtesy of ALSTOM, Transmission and Distribution, Power Electronic Systems, Stafford, England, UK.)
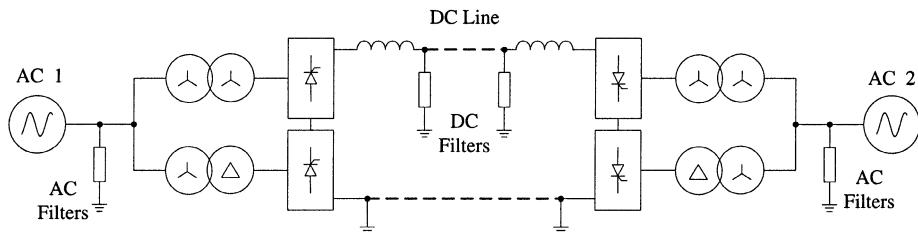
Fig. 6.74 Monopolar HVDC power transmission system based on 12-pulse converters.

such a system is that one pole can continue to transmit power in the case that the other one is out of service for whatever reason. In other words, each system can operate on its own as an independent system with the earth as a return path. Since one is positive and one is negative, in the case that both poles have equal currents, the ground current is zero theoretically, or in practice within a 1% difference. The 12-pulse based bipolar HVDC power transmission system is depicted in Figure 6.75.

4. *Multi-terminal HVDC system*. In this configuration there are more than two sets of converters like the bipolar version (Figure 6.75). A multi-terminal HVDC system with 12-pulse converters per pole is shown in Figure 6.76. For example a large multi-terminal HVDC system is the 2000 MW Quebec–New England power transmission system. In this case, converters 1 and 3 can operate as rectifiers while converter 2
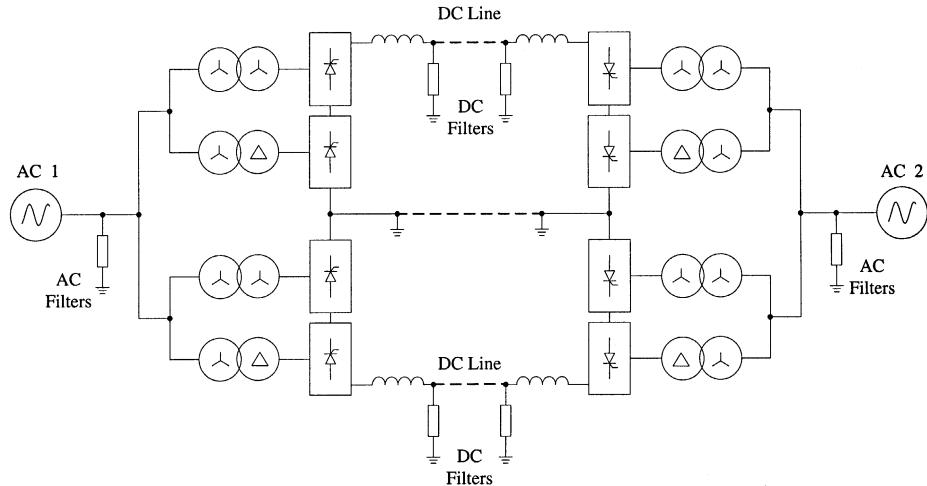
Fig. 6.75 Bipolar HVDC power transmission system based on 12-pulse converter for each pole.
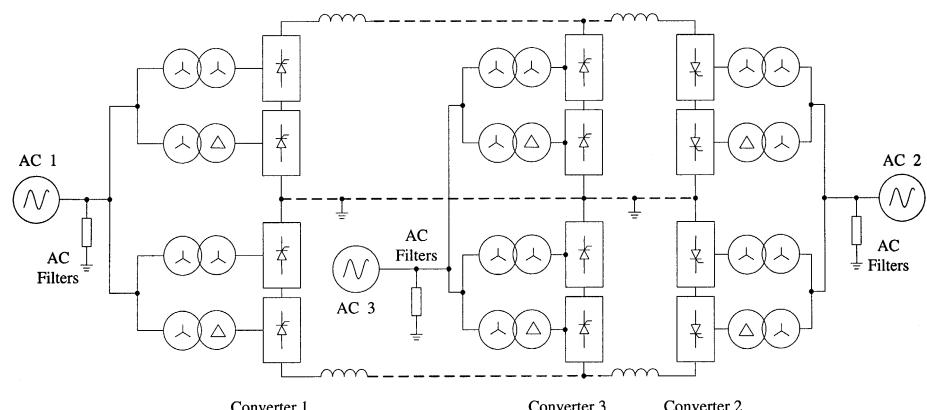
Fig. 6.76 Multi-terminal HVDC power transmission system with 12-pulse converter for each pole parallel connected.

operates as an inverter. Working in the other order, converter 2 can operate as a rectifier and converters 1 and 3 as an inverter. By mechanically switching the connections of a given converter other combinations can be achieved. For example, converters 2 and 3 can operate as an inverter and converter 1 as a rectifier and vice versa.

There is a breakeven point for which the transmission of bulk power with HVDC as opposed to HVAC becomes more economical. Although the projects are evaluated on their own economic terms and conditions, it is widely accepted by industry that the distance that makes HVDC more competitive than HVAC is about 800 km or greater in the case of overhead lines. This distance becomes a lot shorter if submarine or underground cables are used for the transmission bringing it down to approximately 50 km or greater. This allows of course not only the trading of electricity between two networks but also economic exploitation of remote site power generation.

Other advantages include increased capacity for power transmission within a fixed corridor and power transfer between two AC networks that is frequency and phase independent. Finally, due to non-mechanical parts in the power conversion, a fast modulation and reversal of power can be achieved, and due to the nature of the DC link, the fault currents between the two systems are not transferred from one network to another.

Higher order HVDC systems based on 24-pulse or even 48-pulse converter arrangements are also possible. In this case the harmonics can be shifted around the 24th and the 48th harmonics respectively. This means the most significant harmonics will be the 23rd and the 25th harmonics for the 24-pulse converter and 47th and 49th for the 48-pulse one. Clearly such harmonics are easier to filter when compared with the 11th and 13th harmonics of the 12-pulse system. However, in this case, the transformer must be designed to have phase-shifting properties other than the star–delta connection (30°). Being a high voltage transformer, this makes it quite costly to the point that AC side and DC side filters are an easier and cheaper way to use to filter the low order harmonics (at least the 11th and the 13th harmonics due to the 12-pulse converter). A bipolar HVDC system based on 24-pulse converters per pole is drawn in Figure 6.77.
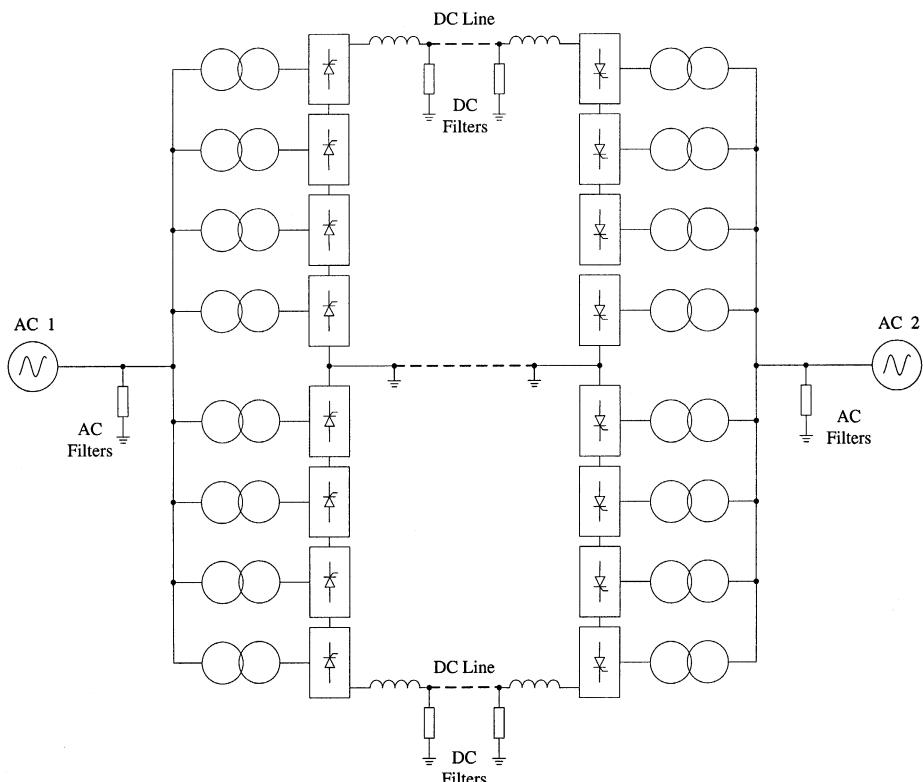
Fig. 6.77 Bipolar HVDC power transmission system based on 24-pulse converter for each pole.

6.7.2 Advanced concepts in conventional HVDC applications

Although thyristor-based HVDC systems represent mature technology, there are still exciting developments worth mentioning such as (Arrillaga, 1998):

● active AC and DC filtering (Figure 6.79)
● capacitor commutated converter (CCC) based systems
● air-insulated outdoor thyristor valves
● new and advanced cabling technology
● direct connection of generators to HVDC converters.

In the case of a thyristor-based converter for HVDC, series capacitors can be used to assist the commutations. Such a single-line diagram of a monopolar converter HVDC system is shown Figure 6.78. Such capacitors are placed between the converter valves and the transformer. A major advantage for using such approach is that the reactive power drawn by the converter is not only lower when compared with conventional line commutated converters but also fairly constant over the full load range. Furthermore, such HVDC system can be connected to networks with a much lower short-circuit capacity. Finally, Figure 6.79 shows an active DC filter installation.

6.7.3 HVDC based on voltage-source converters

The HVDC systems presented in the previous section were based on thyristor technology. The phase-controlled converters require reactive power which flows in one direction only. This is shown in Figure 6.80(a). The flow of the real power across the DC bus can be potentially in both directions.

HVDC systems based on the technology of VSCs described earlier in this chapter is also possible with the use of IGBT or GTO switches. In this case the real power flow remains unchanged and is in both directions like before. This is shown
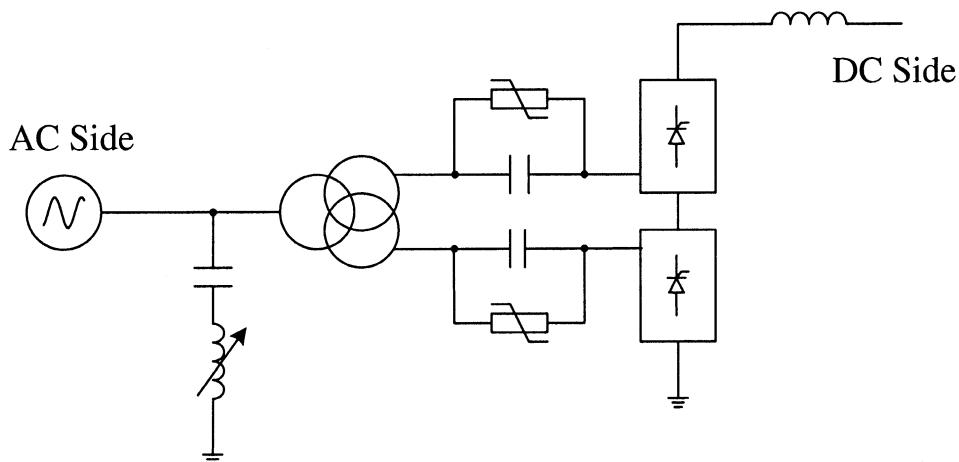
Fig. 6.78 Single-line diagram of a monopolar HVDC power transmission system with capacitor commutated converter (CCC).

Fig. 6.79 Active DC filter at the Swedish terminal of the Baltic cable link. (Courtesy of ABB, Sweden.)

(a)

(b)
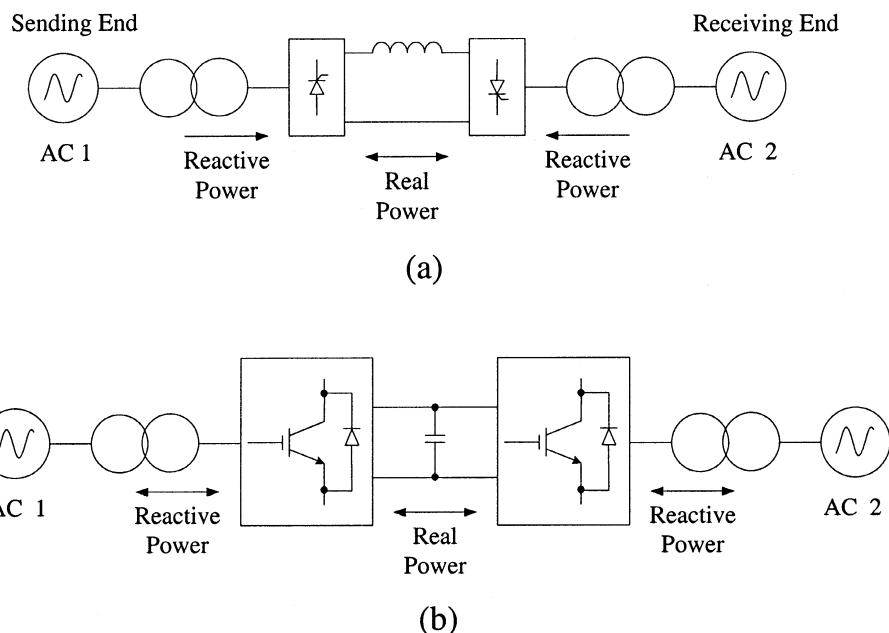
Fig. 6.80 Power flow in HVDC systems. (a) conventional; and (b) VSC based.

in Figure 6.80(b). However, the reactive power flow is improved and can be in both directions mainly due to the independent control of the amplitude and phase of the converter output voltage due to PWM operation.

There are a number of significant advantages gained from the application of PWM VSC technology into the HVDC transmission systems. These can be summarized as follows:

1. Independent control of both real and reactive power almost instantaneously.
2. Minimum contribution of the converter to the short-circuit power.
3. Transformerless applications may be possible if the voltage handling capacity of the semiconductors is high enough to be connected directly to the AC system.
4. The system can be connected to an AC weak grid without the presence of generators, as the voltages are not required for the commutation of the thyristors which are replaced by fully controlled devices.
5. Reduction of the size of the installation since the AC filters are smaller, and the reactive power compensators are not required.

The converter is a typical six-switch three-phase VSC as shown in Figure 6.32 where transistors are used to represent the switches. A number of IGBTs of course are connected in series to make up one switch.

There are a number of potential applications for the HVDC systems based on IGBT or similar technology to build the converter. For instance with the continuous push for renewable technology systems, it is important that these applications are exploited further. Wind farms can be located either off-shore or away from communities for various reasons including minimum environmental impact on local communities, maximization of the resource available, building of large plants, etc. Such relatively large-scale power generation can be connected to the grid via an HVDC system with VSCs. This will potentially reduce the cost of the investment by cutting down transmission costs. Of course the same concept can be applied to other sources of power such as hydro. In the case of small islands, like Greece for instance, where diesel generators are used, VSC-based HVDC technology can be used to connect them to the mainland's grid and this way the dependency on non-renewable energy sources can be eliminated.

Moreover, upgrading AC lines for the same power capacity can be difficult these days mainly for environmental reasons. The AC cables from existing transmission lines can be replaced by DC cables to increase the transmission capability of the line without adding extra cable towers that would be difficult to build. Furthermore, upgrading AC lines into cities' centres is costly and permits for the right of way may be difficult to obtain. If more high-rise buildings cause power demand increases, HVDC can be used as an alternative in competitive terms against AC power transmission.

This technology is relatively new. Specifically, the first VSC based PWM HVDC system has been in operation since March 1997 (Helljsön project, Sweden, 3 MW, 10 km distance, ±10 kV). The installation of this project is shown in Figure 6.81. Another one is the Götland project (Sweden) commissioned recently (50 MW, 70 km distance, ±80 kV).

There are currently three similar projects under construction or just completed recently as follows:

1. The HVDC connection between Texas and Mexico at Eagle Pass.
2. The DirectLink between Queensland and New South Wales in Australia (180 MW, 65 km distance).
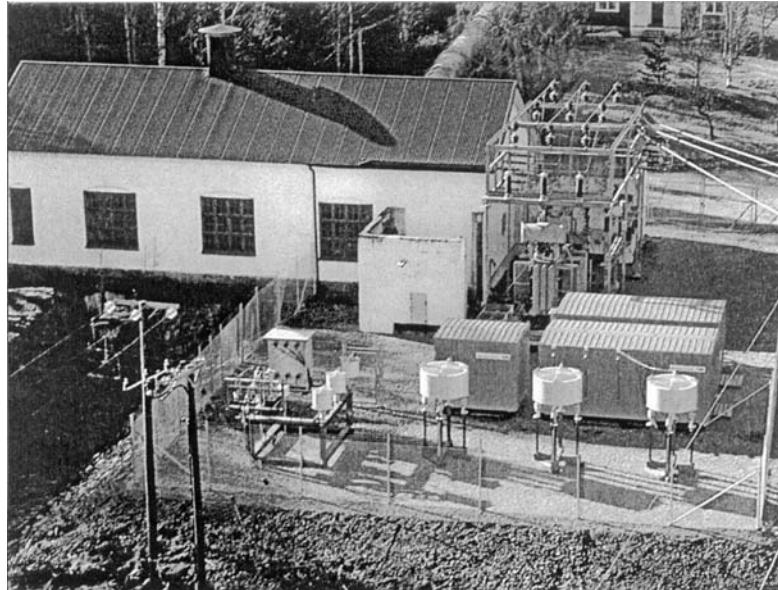
Fig. 6.81 The Hellsjön VSC-based HVDC system. (HVDC light, Courtesy of ABB, Sweden.)

3. The cross-sound cable subsea power interconnection linking Connecticut and
   Long Island in New York, USA.

As the ratings of the IGBTs increase further and the technology of connecting
these devices in series improves, it is likely that most HVDC links will be based on
VSCs.

6.7.4   Multilevel VSCs and HVDC

The multilevel VSC topologies have been successfully investigated and developed for
adjustable speed electric motor drives of high power (Holtz et al., 1988), and AC
heavy traction drives (Ghiara et al., 1990) and mainly as three-level systems.

It is only natural that such topologies and concepts can be extended to use them as
a basic block in a multilevel HVDC system with VSCs. The main obstacles are always
cost and reliability and when these factors are addressed the technology can be
developed commercially. Such a system has been proposed and studied (Lipphardt,
1993).

The advantage of such an approach would be the use of lower voltage switches to
handle higher power. An important advantage of course would be the benefit of
shifting the harmonics of the output of the converter at higher frequencies without
having to operate the PWM controller at high frequencies. It is simply the same
advantage of shifting the harmonics by transformers as in the old systems. The only
difference here would be that the PWM controllers will be able to do that within the
converter and the summation of the waveforms will be done again by reactive
elements whose size will be a lot smaller.

6.8   Active filters (AFs)

The solid-state power electronic converters can be used as part of an apparatus to control electric loads such as adjustable speed electric motor drives, to create regulated power supplies, etc. The same equipment however generates harmonics and the currents drawn from the AC mains are highly reactive. The harmonics injected back into the AC system create serious problems and the 'pollution' of the supply networks has become a major concern for all utilities and power engineers.

There are ways to rectify the problems associated with 'polluted' power networks. Filtering or power conditioning which may include other more sophisticated functions for the equipment used is therefore not only required in electric power systems but is also considered a mature technology as far as passive elements are concerned.

A combination of inductive–capacitive networks has been used successfully in most cases to filter harmonics and capacitor banks have been employed to improve the power factor of a plant. Such conventional solutions have fixed levels of performance, are usually bulky and create resonance phenomena.

The requirements for harmonics and reactive power compensation along with the continuous development of power electronics have resulted in dynamic and adjustable solutions for the pollution of the AC networks. Such equipment is based on power electronic converters. The converters interacting with the network to filter harmonics or compensate for reactive/real power they are known as active filters or power conditioners or power quality equipment.

In this section we present the various converter-based topologies used as active filters or power conditioners in schematic form only. It is beyond the scope of this book to provide any more detailed information on this subject, but rather show the potential of the VSC technology for power system applications.

Converter based active filtering topologies are used to provide compensation for:

- harmonics
- reactive power
- neutral currents
- unbalanced loads.

The applications include different cases such as:

- single-phase
- three-phase with floating neutral (three wires only)
- three-phase with neutral (four wire).

A number of topologies are used as active filters in series or shunt connection along with a combination of them as well in series/shunt configuration. The series topologies are normally used to deal with:

- voltage harmonics
- spikes
- sags
- notches
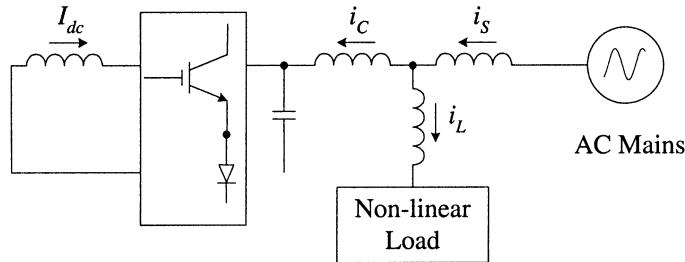
Fig. 6.82 CSC based shunt connected active filter.

The shunt topologies are normally used to deal with:

● current harmonics
● reactive power compensation.

There are two types of topologies used as AFs, namely the current-source and the voltage-source based. Figure 6.82 shows a current-source single-phase inverter in shunt connection used as an active filter.

The voltage-source converter based shunt-connected active filter is shown in Figure 6.83. This topology typically has a large DC capacitor and it can be used in expandable multilevel or multistep versions to increase power ratings or improve the performance operating at lower switching frequency and in many cases with fundamental frequency modulation. The same hardware can be used as an active filter connected in series as shown in Figure 6.84. The next step is a natural extension of the two systems previously mentioned to arrive at the unified series/shunt
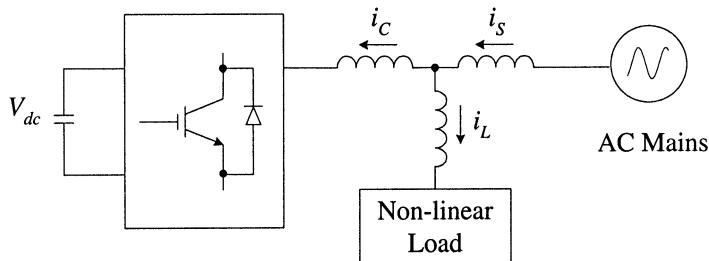
Fig. 6.83 VSC based shunt connected active filter.
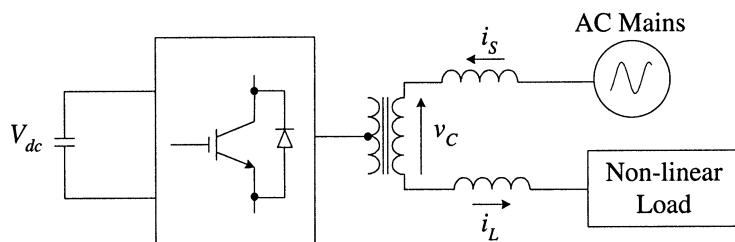
Fig. 6.84 VSC based series connected active filter.
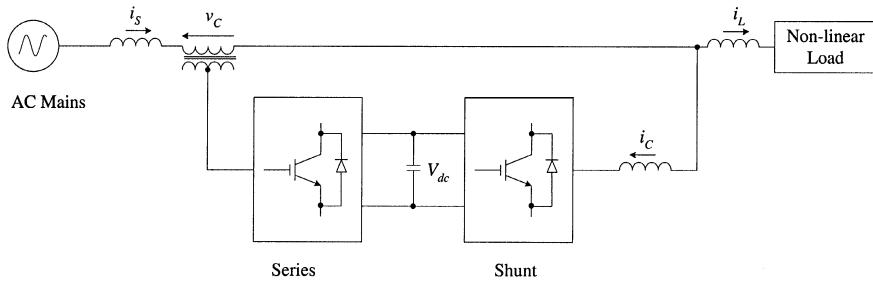
Fig. 6.85 VSC based series/shunt combined active filter.
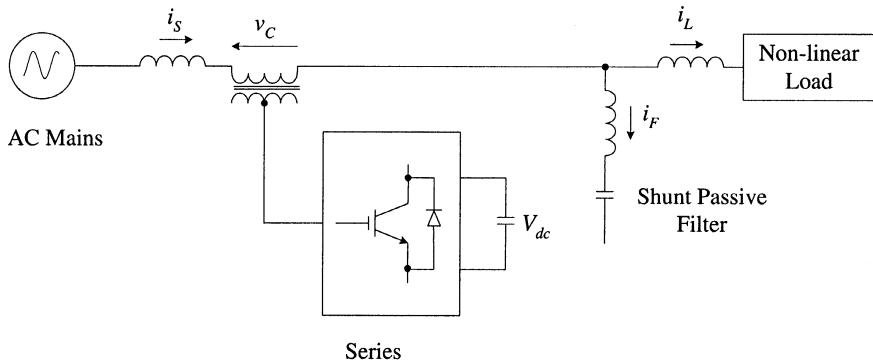
Fig. 6.86 VSC based series active filter combined with shunt passive one.
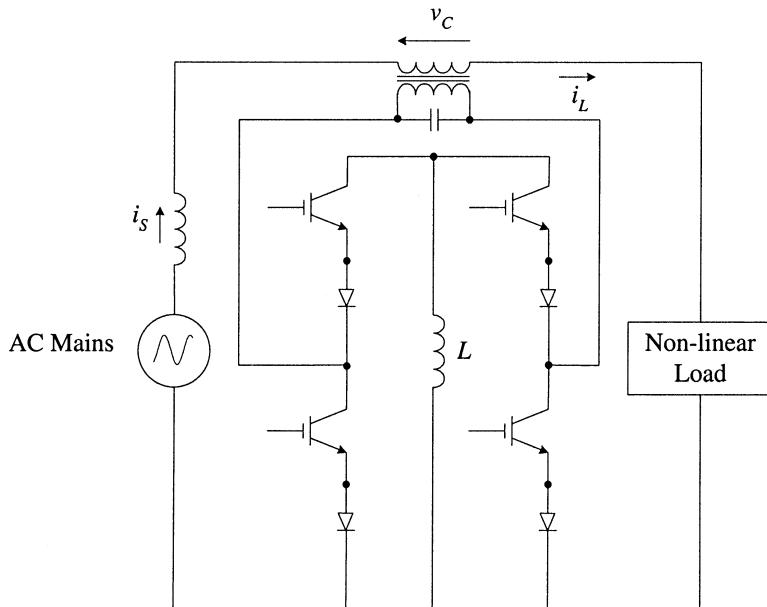
Fig. 6.87 CSC based single-phase series connected active filter.
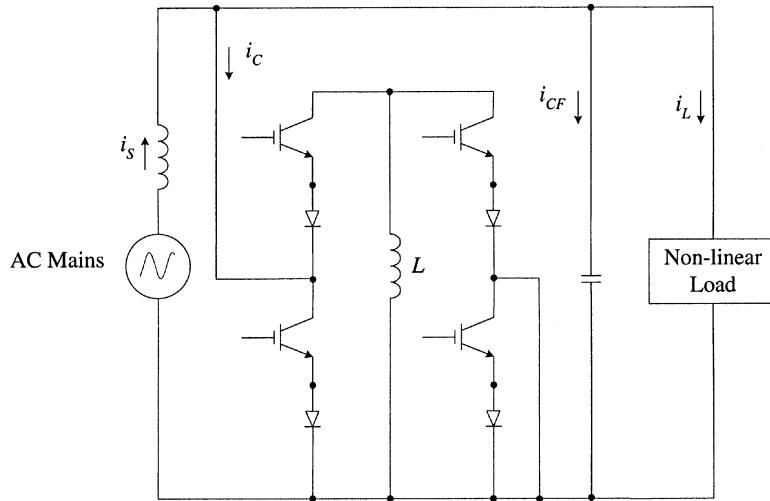
Fig. 6.88 CSC based single-phase shunt connected active filter.
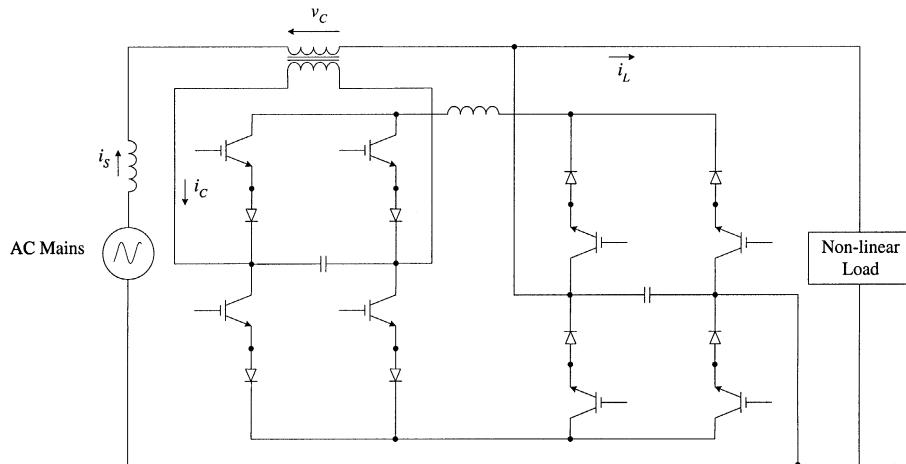
Fig. 6.89 CSC based single-phase combined series/shunt connected active filter.

VSC-based active filter as shown in Figure 6.85. The power circuit shown in Figure 6.83 is used mainly as a shunt compensator and it is known as a STATCOM. Its basic function in utility applications is to provide reactive power compensation, eliminate the line current harmonics and balance the three-phase loads in a three-phase configuration. It can be used to restore the voltage in a series connection as a DVR shown in Figure 6.84. In all figures where a converter is used as an active filter, the AC mains is shown as a voltage source with series inductance, and at the point of connection, an inductor is also used on the side of the converter. The only difference is that if the converter is of a current-source type, a capacitor is connected prior to the inductor as square-wave currents are generated at the output of the converter which
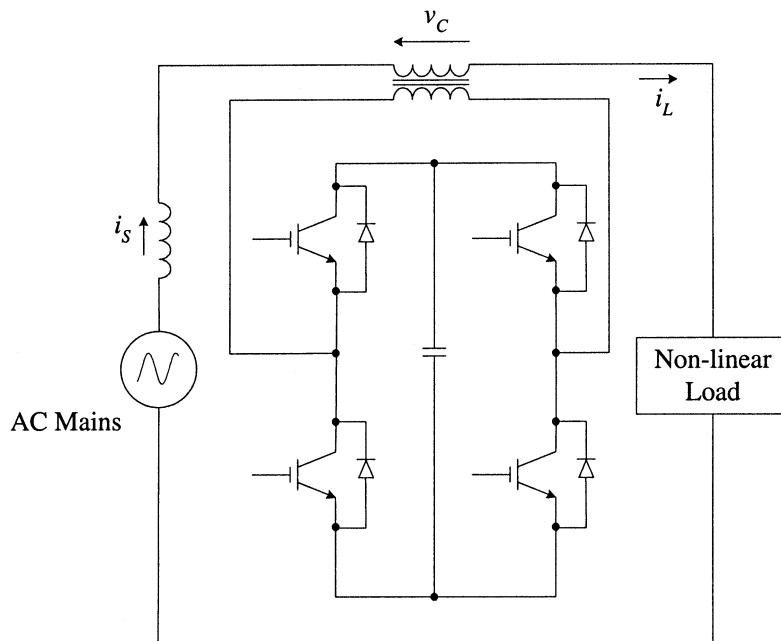
Fig. 6.90 VSC based single-phase series connected active filter.
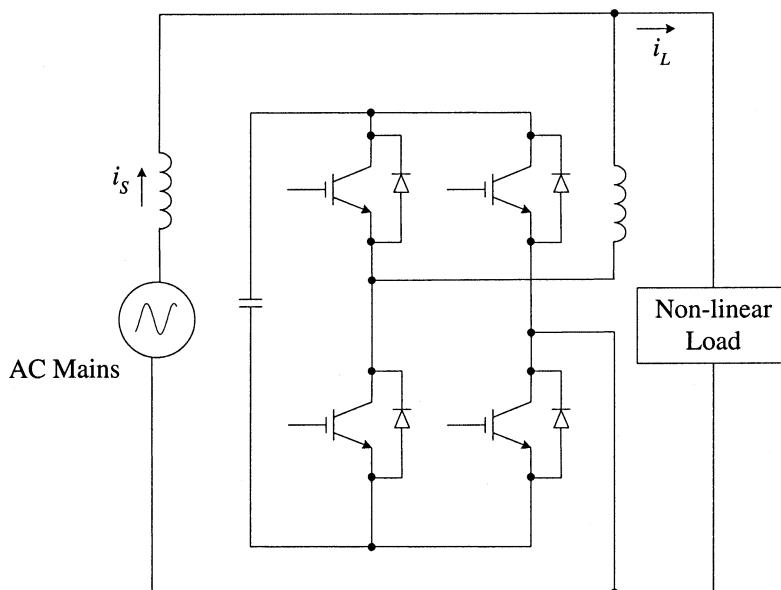
Fig. 6.91 VSC based single-phase shunt connected active filter.
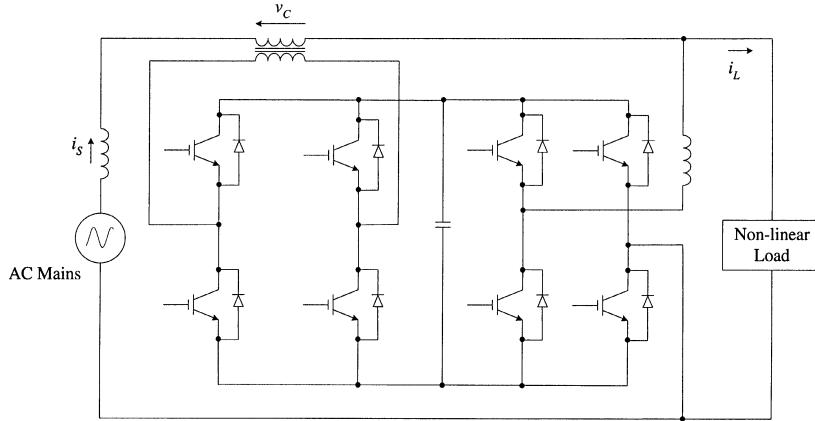
Fig. 6.92 VSC based single-phase combined series/shunt connected active filter.

need to be filtered and become sinusoidal waveforms. Furthermore, in the case of a voltage-source type converter being used, the inductor is connected at the output of the converter as the voltage waveforms created are of a square-wave type and also need to be filtered and become sinusoidal prior to being fed into the line.

In the case of the converter being connected in series, a transformer is used to connect the output of the converter in series with the line. Once again both load and mains have an inductor in series.

The unified active filter that has a series and shunt connected VSCs is shown in Figure 6.85. The two converters share the same DC bus and the same rules to connect them into the line are followed.

The next step is to combine the active filters with passive ones as a series and/or parallel. These filters are discussed in the following section (Figures 6.93–6.95).
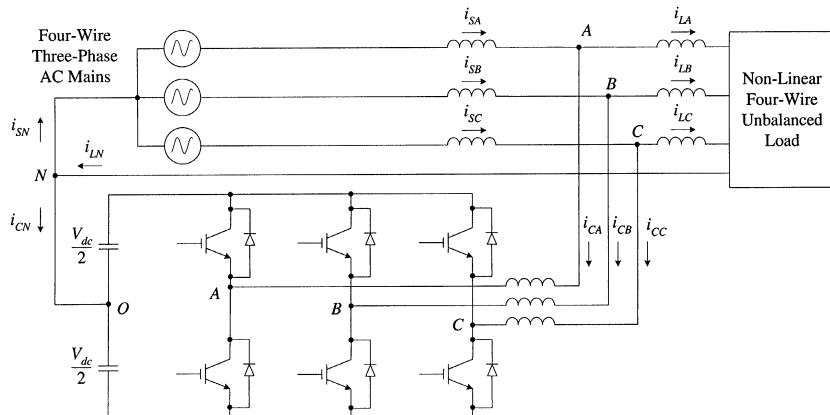
Fig. 6.93 Four-wire three-phase VSC based shunt connected active filter.
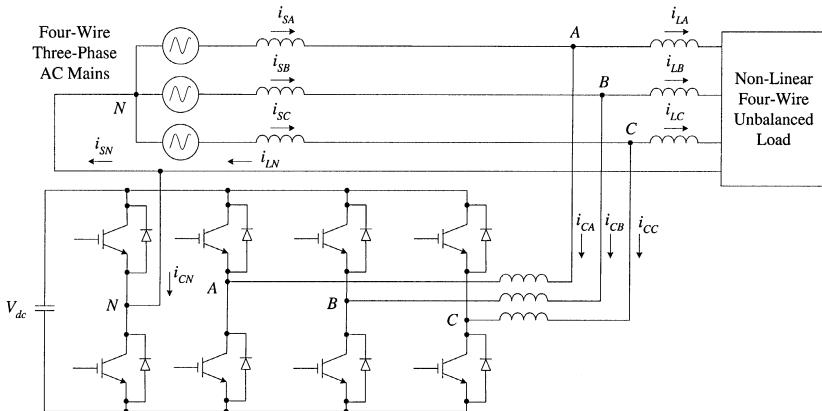
Fig. 6.94 Four-wire four-pole VSC based shunt connected active filter.
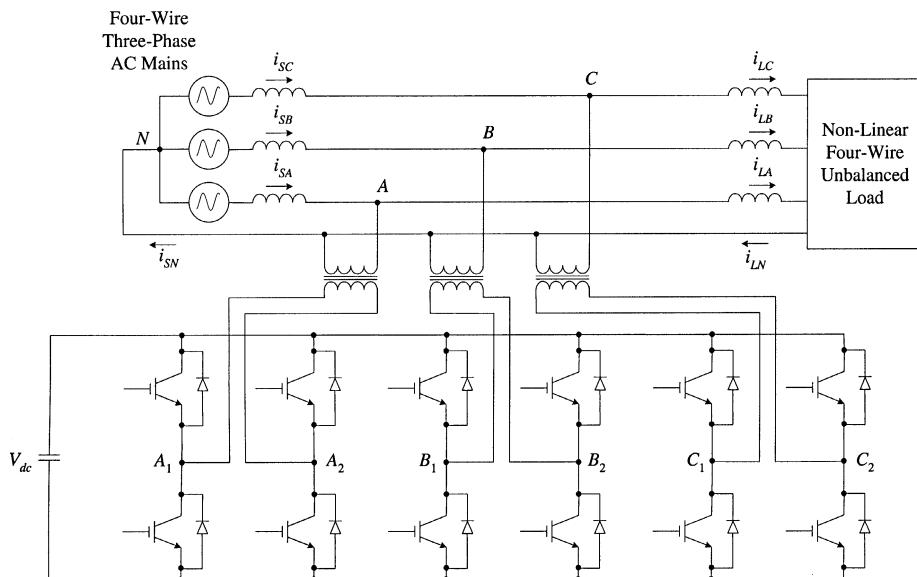
Fig. 6.95 Four-wire three-phase three bridge VSC shunt connected active filter.

6.9 Combined active and passive filters

In high power applications with DC and AC motor drives, DC power supplies or HVDC conventional thyristor-based systems 12-pulse rectifier loads are widely used. Such configurations are typically used because they generate significantly lower harmonic currents when compared to a six-pulse rectifier circuit.

In order to meet harmonic requirements (i.e. IEEE 519) although the 12-pulse system offers improved harmonics it still requires filtering. Only an 18-pulse rectifier circuit can meet IEEE 519 requirements without any additional filtering. In conventional
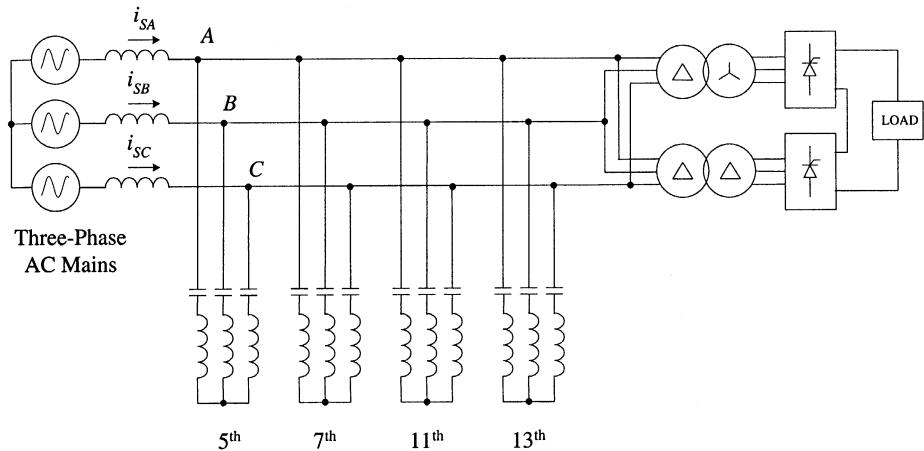
Fig. 6.96 Typical passive filter based arrangement for a 12-pulse rectifier system.
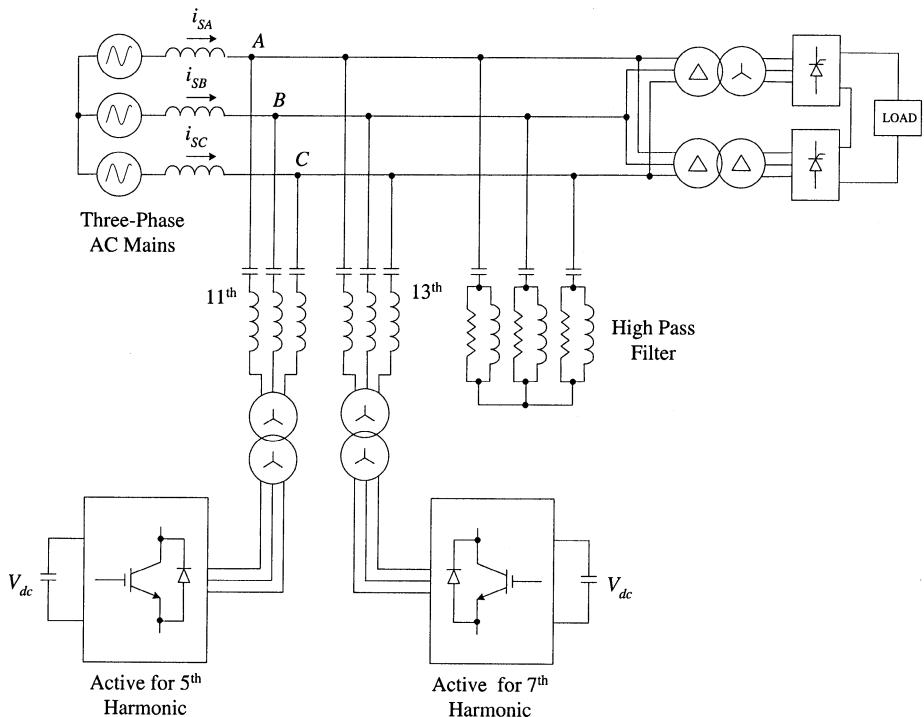
Fig. 6.97 Hybrid active/passive shunt filter for 12-pulse rectifier system.

filtering arrangements, L–C tuned filters at 5th, 7th, 11th, and 13th harmonic frequencies are employed. The 12-pulse rectifier does not generate significant 5th and 7th harmonics. However, one cannot ignore them as resonances between passive filter components and line impedances are likely to increase the amplitude of the

harmonics at 5th and 7th frequencies. Moreover, 11th and 13th harmonic frequencies must be dealt with via the design of tuned passive filters. Figure 6.96 shows a typical passive filter configuration for a 12-pulse rectifier with shunt filters tuned at 5th, 7th, 11th, and 13th harmonics.

The application of active filtering as shunt configuration based on a VSC technology has the advantage of low converter ratings and simplicity. Such systems of course for high power applications are not feasible, as most active filtering schemes presented in the previous section require high bandwidth PWM converters to successfully eliminate harmonics below the 13th. Simply said such a solution is also not cost effective for high power applications (>10 MW).

Hybrid topologies can be considered. The main motivation to use hybrid solution is to reduce the ratings of the active filter. Figure 6.97 shows a hybrid active/passive shunt filter system suitable for 12-pulse rectifiers. Specifically, two VSC based active filters for the 5th and 7th harmonics are used in combination with series connected passive filters tuned at 11th and 13th harmonic frequencies. Because the application involves high power, six-step three-phase inverters can be employed. The rating for the inverters is no more than approximately 2% of the load kVA rating.

6.10   Advanced concepts in reactive power control equipment

Many new reactive power control equipment based on the VSC topologies presented earlier have been under research and development over the last decade. A number of them have been developed and successfully implemented. These include the UPFC, and the interline power flow controller (IPFC). The UPFC is not discussed in this chapter, but it is treated in other parts of the book.

6.11   Conclusion

In this chapter, the conventional thyristor-controlled equipment for reactive power control in power systems has been presented first. The voltage source converter topologies were then presented in detail including multilevel converter topologies. Such topologies will have a major impact on the applications of reactive control and power quality equipment in the industry. New systems based on energy storage, namely the flywheel technology and superconductor energy storage systems were then briefly discussed to highlight the potential of this technology. HVDC systems with conventional technology and using VSC technology and PWM systems were also presented as a significant application area of high power electronics in the electric power systems. Finally, active and hybrid filters based on active and passive technologies were also discussed where the VSC technology will have a major impact and significant improvements in performance. Many new applications will become possible in the near future once the limitations of fully controlled devices such as the IGBT are overcome. This will potentially allow the full replacement of the thyristor

in the future systems even in very high power applications. This may seem quite speculative today, but if one looks back at the developments that have happened in the semiconductor area in the last 40 years one can hopefully visualize that such advancements may only be a matter of time.

Harmonic studies of power compensating plant

The use of power electronics-based equipment in high-voltage power transmission and in low-voltage distribution has increased steadily over the last three decades. Notwithstanding their great many operational benefits, they also have increased the risk of introducing harmonic distortion in the power system because several of these devices achieve their main operating state at the expense of generating harmonic currents. In the early days, most applications of this technology were in the area of HVDC transmission (Arrillaga, 1999). However, the SVC which is a more recent development, has found widespread use in the area of reactive power management and control (Miller, 1982). In the last 20 years or so, a substantial number of SVCs have been incorporated into existing AC transmission systems (Erinmez, 1986; Gyugyi, 1988). Many utilities worldwide now consider the deployment of the newest and most advanced generation of power electronics-based plant components, FACTS and Custom Power equipment (Hingorani, 1993; 1995), a real alternative to traditional equipment based on electromechanical technologies (IEEE/CIGRE, 1995).

Over the years, many adverse technical and economic problems have been traced to the existence of harmonic distortion. Professional bodies have long recognized harmonics as a potential threat to continuity of supply and have issued guidelines on permissible levels of harmonic distortion (IEEE IAS/PES, 1993). However, it is generally accepted that this problem, if left unchecked, could get worse. Hence, great many efforts are being directed at finding new measuring, simulation and cancellation techniques that could help to contain harmonic distortion within limits. Substantial progress has been made in the development of accurate instrumentation to monitor the harmonic behaviour of the network at the point of measurement (Arrillaga et al., 2000). However, in planning and systems analysis the problem must

be addressed differently because measurements may not be economic or the network may not exist. In such cases, digital simulations based on mathematical modelling provide a viable alternative to actual measurements (Dommel, 1969). Research efforts worldwide have produced accurate and reliable models for predicting power systems harmonic distortion. Time and frequency domain solutions have been used for such a purpose. Owing to its popularity, most frequency domain techniques use Fourier's transform (Semlyen et al., 1988) but alternative transforms such as Hartley (Acha et al., 1997), Walsh (Rico and Acha, 1998) and Wavelets can also be used for alternative harmonic solutions.

The thrust of this chapter is to present harmonic models of power plant compensation equipment, but it is useful to set the scene by first examining some of the adverse effects caused by the existence of harmonics and the potential harmonic magnification problems which may be introduced by a bank of capacitors, together with the beneficial effects brought about by the use of tuning reactors.

Models of TCR, SVC and TCSC are presented in Sections 7.4, 7.5 and 7.6, respectively. These models use Fourier's transform and are used to solve harmonic distortion problems in power systems containing electronic compensation. They come in the form of harmonic admittance and impedance matrices, respectively. In the absence of harmonics build up due to, for instance, resonance conditions, these plant components may be considered linear, time-variant. The harmonic admittance and impedance models are derived by 'linearizing' the TCR equations, in a manner that resembles the linearization exercise associated with, say, the non-linear equations of magnetic iron cores (Semlyen and Rajakovic, 1989).

It should be noted that linear, time-invariant components generate no harmonic distortion whereas non-linear and linear, time-variant components do generate harmonic distortion. Examples of linear, time-invariant components are banks of capacitors, thyristor-switched capacitors, air-core inductors, transmission lines and cables. Examples of non-linear components are, saturated transformers and rotating machinery, salient pole synchronous generators feeding unbalanced systems, electric arc furnaces, fluorescent lamps, microwave ovens, computing equipment and line commutated AC–DC converters (Acha and Madrigal, 2001). Time-variant components are, for instance, SVCs and TCSCs operating under medium to low harmonic voltage distortion, VSC-based equipment with PWM control, e.g. STATCOM, DVR, UPFC and HVDC light.

7.2   Effect of harmonics on electrical equipment

In industrial installations, the first evidence of excessive harmonic levels is blown capacitor fuses or failed capacitors in capacitor banks. Current standards cover the characteristics of shunt power capacitors (IEEE IAS/PES, 1993). It is well known that continuous operation with excessive harmonic current leads to increased voltage stress and excessive temperature rises, resulting in a much reduced power plant equipment's useful life. For instance, a 10% increase in voltage stress will result in 7% increase in temperature, reducing the life expectancy to 30% (Miller, 1982). More severe capacitor failure may be initiated by dielectric corona, which depends on both intensity and duration of excessive peak voltages.

Harmonic currents are also known to cause overheating in rotating machinery, particularly synchronous generators. This applies to both solid-rotor synchronous generators and salient-pole synchronous generators feeding unbalanced networks. Harmonic currents produce an electromagnetic force that causes currents to flow in the rotor adding to the heating. Positive sequence harmonics, e.g. 7th, 13th, rotate in the same direction as the fundamental frequency and induce harmonic orders 6th, 8th, 12th, 14th, in the rotor. Negative sequence harmonics, e.g. 5th, 11th, rotate against the direction of the rotor and produce harmonic orders 4th, 6th, 10th, 12th, and so on, in the rotor. The resulting pulsating magnetic fields caused by the opposing rotating pairs, e.g. 6th and 12th, may require a derating of the machine. To illustrate the point, the derating of a synchronous generator operating near a six-pulse rectifier, can be quite considerable, depending on the particular machine design. On the other hand, derating for balanced 12-pulse rectifier operation is, on average, minimal (Miller, 1982).

Induction motors are much less affected by harmonics than are synchronous generators. However, excessive harmonic currents can lead to overheating, particularly in cases when they are connected to systems where capacitors in resonance with the system are aggravating one or more harmonics.

Harmonic currents carried by transformers will increase the load loss, $I^2 R$, by a factor greater than the mere increase in RMS current. The increase depends on the proportion of $I^2 R$ loss proportional to frequency squared (eddy current loss), and the amount proportional to the first power of frequency (stray load loss). The same rule-of-thumb holds for current limiting and tuning reactors. Precise information about the amount and order of each significant harmonic is mandatory in reactor design practise.

7.3 Resonance in electric power systems

Banks of capacitors are very often added to power systems to provide reactive power compensation, with voltage support and power factor correction being two popular applications. An issue of great importance to bear in mind is that the capacitor bank and the inductance of the system will be in parallel resonance in one or more frequency points, and that harmonics injected into the system at coincident frequencies will be amplified.

The small system shown in Figure 7.1 is used to illustrate the principle of harmonic current flow and resonance. To simplify the explanation, it is assumed that the harmonic source generates constant harmonic currents. The one-line diagram of Figure 7.1(a) may be represented on a per-phase basis by the equivalent circuit in Figure 7.1(b).

The n-th harmonic current divides between the capacitor and the supply according to the equation

$$I_n = I_{sn} + I_{fn} \tag{7.1}$$

The impedance of the capacitor branch at any frequency is given by

$$Z_f = Z_{fc} + Z_{fl} \tag{7.2}$$
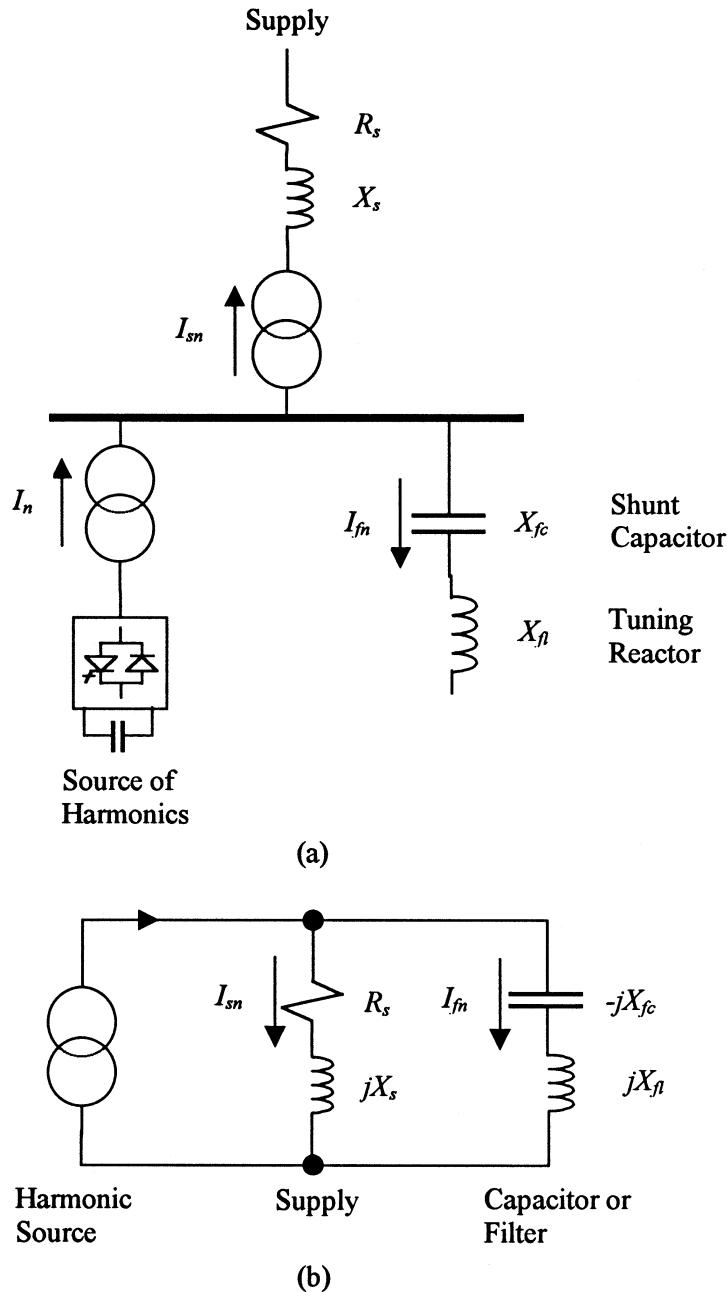
Fig. 7.1 (a) One-line diagram of small system; and (b) per-phase equivalent circuit.

where Z_{fc} is the impedance of the capacitor and Z_{fl} is the impedance of a tuning reactor. The subscript f alludes to the filtering action of the capacitor branch.

The harmonic current I_n divides between the capacitor and the supply in proportion to the admittance of these parallel branches. If Z_s is the equivalent

impedance of the supply, including the transformer, then the following relations will apply

$$I_{\text{f}n} = \frac{Z_\text{s}}{Z_\text{f} + Z_\text{s}} I_n = \rho_\text{f} I_n \tag{7.3}$$

$$I_{\text{s}n} = \frac{Z_\text{f}}{Z_\text{f} + Z_\text{s}} I_n = \rho_\text{s} I_n \tag{7.4}$$

From these equations, it is not difficult to see that if the distribution factor ρ_s is large at a particular harmonic frequency coincident with one of the harmonics generated by a harmonic source, then amplification of the harmonic current will occur and the currents in the capacitor and the supply may become excessive. This would particularly be the case if $Z_\text{f} + Z_\text{s} \to 0$ at some harmonic frequency. Hence, ρ_s must be kept low at these frequencies if excited by coincident harmonic currents.

The function of the tuning reactor shown in series with the capacitor in Figure 7.1(a) is to form a series-resonant branch or filter, for which $Z_\text{f} \to 0$ at the resonant frequency. As a result, $\rho_\text{s} \to 0$ thus minimizing the possibility of harmonic currents flowing into the utility network. The ideal outcome is when $\rho_\text{f} \to 1$ so that $I_{\text{f}n} = I_n$, meaning that all the harmonic current generated enters the filter.

7.3.1   Numerical example 1

A simple numerical example may be used to illustrate the performance of a detuned and a tuned capacitor filter. Assume that the step-down transformer impedance is much greater than the source impedance so that for a narrow range of frequencies the approximation $X_\text{s}/R_\text{s} = $ constant may be used. Assume the following parameters

Bus voltage $= 13.8\,\text{kV}$
Short circuit MVA $= 476$
Capacitor reactive power $= 19.04\,\text{MVAr}$
$X_\text{s}/R_\text{s} = 10$

Knowing that inductive reactance is directly proportional to frequency and that capacitive reactance is inversely proportional to frequency
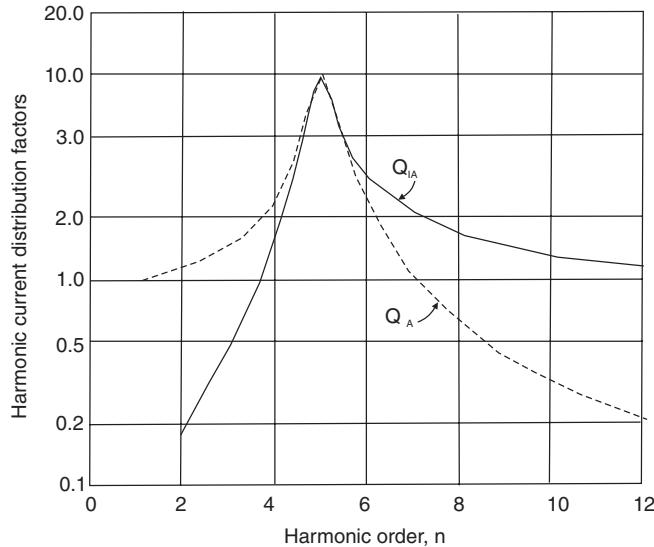
$$X_\text{s} = \frac{n(13.8)^2}{476} = 0.4n \tag{7.5}$$

$$X_\text{fc} = \frac{(13.8)^2}{19.04n} = \frac{10}{n} \tag{7.6}$$
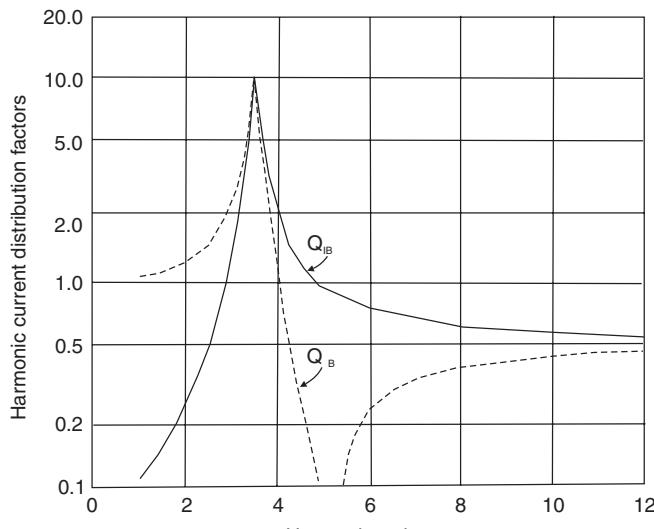
$$R_\text{s} = \frac{X_\text{s}}{10} = 0.04n \tag{7.7}$$

$$\rho_\text{f} = \frac{0.04 + \text{j}0.4}{0.04 + \text{j}(0.4 - 10/n^2)} \tag{7.8}$$

In Figure 7.2, ρ_f and ρ_s are plotted against the harmonic order n. There is a parallel resonance between the capacitor and the supply at the 5th harmonic. It should be noted that at that point $\rho_\text{s} \approx \rho_\text{f}$.

Fig. 7.2 Harmonic current distribution factors versus harmonic order: (a) capacitor bank with no tuning reactor; and (b) capacitor bank with tuning reactor.

If a tuning reactor X_{fl} is added to the capacitor to form a series 5th harmonic filter, and if the resistance of the reactor is considered negligible in comparison with the system resistance, then at 60 Hz

$$X_{fl} = \frac{X_{fc}}{5^2} = \frac{10}{25} = 0.4\,\Omega \tag{7.9}$$

The equation for ρ_f becomes

$$\rho_f = \frac{R_s + jX_s}{R_s + j(X_s + X_{fl} - X_{fc})} \tag{7.10}$$

Figure 7.2(b) shows the response in terms of ρ_f and ρ_s with the tuning reactor. Note that $\rho_f = 1$ at the 5th harmonic, i.e. $\rho_s = 0$, and is maximum (parallel resonance) at a lower harmonic order, about 3.54.

7.4 Thyristor-controlled reactors

7.4.1 TCR periodic characteristics

The instantaneous v–i characteristics exhibited by a TCR acting under sinusoidal AC excitation voltage are a family of ellipses, which are a function of the conduction angle σ, as shown in Figure 7.3.

The firing angle δ can be controlled to take any value between 90° and 180° corresponding to values of σ between 180° and 0°. The former case corresponds to the TCR in a fully conducting state whilst the latter corresponds to the TCR in a completely non-conducting state. Both operating conditions are free from harmonics, whereas any other condition in between will be accompanied by the generation of harmonics.

For the case, when the TCR is fully conducting and driven by a periodic voltage source the relationship between the excitation voltage and TCR current can be written as

$$\frac{d}{dt} i_R(t) = \frac{1}{L_R} v(t) \tag{7.11}$$
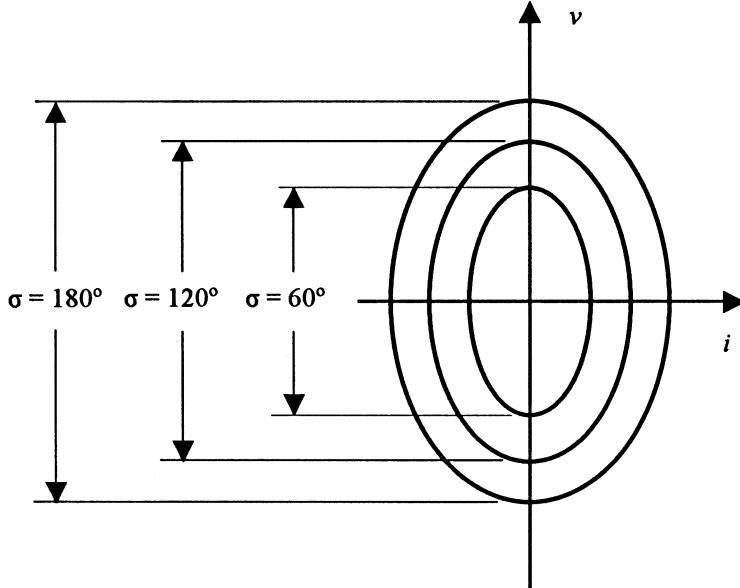
Fig. 7.3 A family of instantaneous $v$$-$$i$ characteristics of a single-phase TCR.
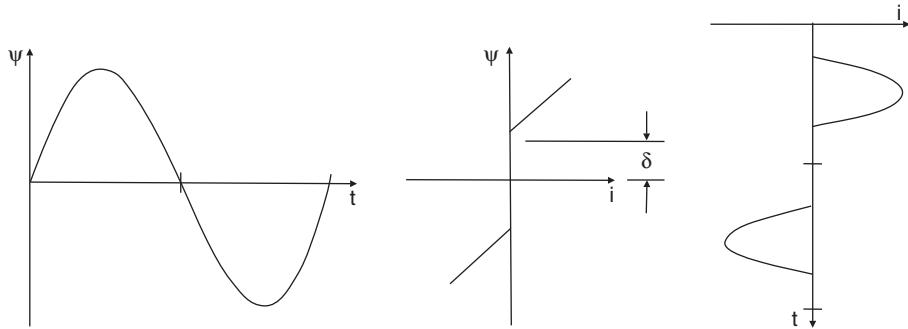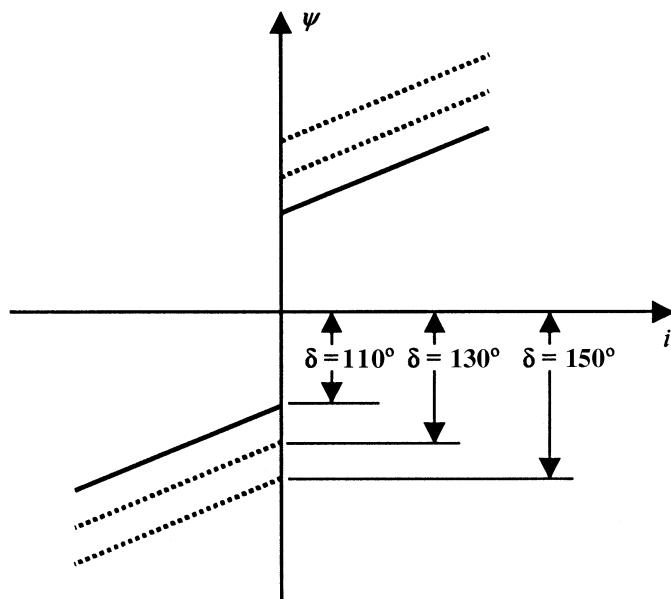
Fig. 7.4 A full cycle of the TCR current and flux excitation.

$\delta = 110°$ $\delta = 130°$ $\delta = 150°$

Fig. 7.5 A family of instantaneous $\psi - i$ characteristics of a single-phase TCR.

However, this relationship does not hold at conduction angles σ smaller than 180°. In such a situation, the current will exhibit dead-band zones and becomes non-sinusoidal. This effect is clearly shown in Figure 7.4, where the ψ–i characteristic relates a full cycle of the excitation flux to a full cycle of the TCR current.

More generally, the characteristics exhibited by a single-phase TCR, acting under a sinusoidal AC excitation flux, are a family of straight lines which are a function of the flux-based firing angle δ_ψ, as shown in Figure 7.5.

Furthermore, numeric differentiation can be used to obtain a full cycle of the derivative of the TCR current with respect to the flux with respect to time.

It is noted from Figure 7.6 that when the TCRs are conducting the magnitude of the derivative is inversely proportional to the reactor's inductance L_R and it is zero if no conduction takes place. Also, the conduction angles σ_1 and σ_2 may differ.
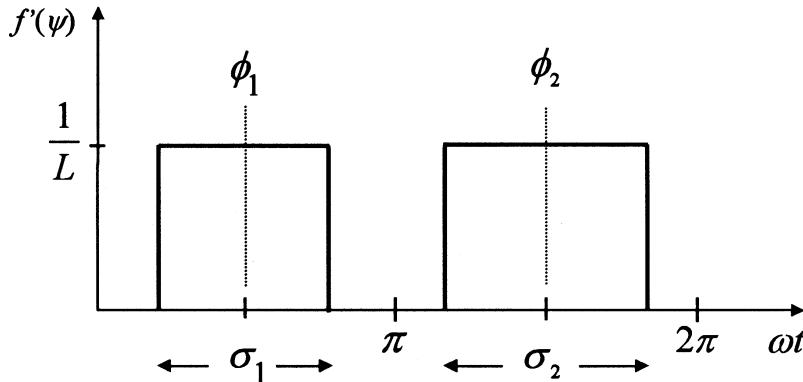
Fig. 7.6 A full cycle of derivative $f'(\psi)$.

In a thyristor-controlled, inductive circuit the flux-based relationship between the firing angle and the conduction angle is given by the following expression

$$\sigma = \pi - 2\delta_\psi \tag{7.12}$$

It should be noted that this expression differs from the conventional voltage-based relation (Miller, 1982)

$$\sigma = 2(\pi - \delta) \tag{7.13}$$

In equation (7.12), the flux-based firing angle δ_ψ can be controlled to take any value between $0°$ and $90°$, corresponding to values of σ between $180°$ and $0°$.

7.4.2   TCR currents in harmonic domain

Early representations of the TCR involved simple harmonic currents injections. They were a function of the firing angle, and were made to include imbalances, but no voltage dependency was accounted for (Mathur, 1981).

A more realistic representation in the form of a voltage-dependent harmonic currents injection was derived to account for the facts that TCRs are not always connected to strong network points and that both, network and TCR imbalances, may be an important part of the problem under study (Yacamini and Resende, 1986). A more advanced model is derived below, it comes in the form of a harmonic admittance matrix, which shows to be a special case of the harmonic Norton equivalent normally associated with non-linear plant component representation (Semlyen et al., 1988). The derivation follows similar principles as the work presented in (Bohmann and Lasseter, 1989).

Currents exhibiting dead-band zones, such as the one shown in Figure 7.4, can be conveniently expressed by the time convolution of the switching function, $s_R(t)$, with the excitation flux, $\psi(t)$

$$i_R(t) = \frac{1}{L_R} \int_0^T s_R(\tau)\psi(\tau)d\tau \tag{7.14}$$

The function $s_R(t)$ takes values of one whenever the thyristor is on and zero whenever the thyristor is off. Like the TCR derivative shown in Figure 7.6, $s_R(t)$ is also a function of the conduction periods σ_1 and σ_2.

Applying a Fourier transform to both sides of equation (7.14), and taking the Integration and Frequency Convolution theorems into account, it is possible to write an expression in the frequency domain for the TCR current, $\mathbf{I_R}$

$$\mathbf{I_R} = \frac{1}{L_R}\mathbf{S_R}\Psi \tag{7.15}$$

where $\mathbf{S_R}$ and Ψ are the switching function and the excitation flux vectors, respectively.

7.4.2.1 Harmonic switching vectors

One way to obtain the harmonic coefficients of the switching vector, $\mathbf{S_R}$, is by drawing a fundamental frequency cycle of the derivative of the TCR current with respect to the flux with respect to time and then using an FFT routine (Acha, 1991). The harmonic content of $\mathbf{S_R}$ would then be obtained by multiplying this result by L_R, the inductance of the linear reactor. However, this is an inefficient and error prone option. A more elegant and efficient alternative to determine the harmonic coefficients of the switching function was put forward by Rico et al. (1996).

The more efficient formulation uses a periodic train of pulses to model the switching function $s_R(t)$, which in the frequency domain is well represented by a complex harmonic vector, $\mathbf{S_R}$, with the following structure

$$\mathbf{S_R} = \begin{bmatrix} \frac{a_h}{2} - j\frac{b_h}{2} \\ \vdots \\ \frac{a_1}{2} - j\frac{b_1}{2} \\ a_0 \\ \frac{a_1}{2} + j\frac{b_1}{2} \\ \vdots \\ \frac{a_h}{2} + j\frac{b_h}{2} \end{bmatrix} \tag{7.16}$$

where the vector accommodates the complex harmonic coefficients from $-h$ to $+h$. Also, the generic coefficient S_h is

$$S_h = \frac{a_h}{2} + j\frac{b_h}{2} = \frac{1}{\pi}\int_{-\pi}^{\pi} s(t)e^{-jh\omega t}d\omega t \tag{7.17}$$

The Fourier coefficients a_h and b_h are calculated from equations (7.18) to (7.20), which take into account the fact that the switching function has a value of one in the following intervals $[-\pi/2 - \sigma_1/2, -\pi/2 + \sigma_1/2]$ and $[\pi/2 - \sigma_2/2, \pi/2 + \sigma_2/2]$

$$a_0 = \frac{1}{\pi}\left[\int_{-\frac{\pi}{2}-\frac{\sigma_1}{2}}^{-\frac{\pi}{2}+\frac{\sigma_1}{2}} d\omega t + \int_{\frac{\pi}{2}-\frac{\sigma_2}{2}}^{\frac{\pi}{2}+\frac{\sigma_2}{2}} d\omega t\right] = \frac{\sigma_1 + \sigma_2}{2\pi} \tag{7.18}$$

$$a_h = \frac{1}{\pi}\left[\int_{-\frac{\pi}{2}-\frac{\sigma_1}{2}}^{-\frac{\pi}{2}+\frac{\sigma_1}{2}} \cos(h\omega t)d\omega t + \int_{\frac{\pi}{2}-\frac{\sigma_2}{2}}^{\frac{\pi}{2}+\frac{\sigma_2}{2}} \cos(h\omega t)d\omega t\right]$$
$$= \frac{2}{h\pi}\left[\sin\left(\frac{h\sigma_2}{2}\right) + \sin\left(\frac{h\sigma_1}{2}\right)\right]\cos\left(\frac{h\pi}{2}\right) \tag{7.19}$$

$$b_h = \frac{1}{\pi} \left[\int_{-\frac{\pi}{2}-\frac{\sigma_1}{2}}^{-\frac{\pi}{2}+\frac{\sigma_1}{2}} \sin(h\omega t)\mathrm{d}\omega t + \int_{\frac{\pi}{2}-\frac{\sigma_2}{2}}^{\frac{\pi}{2}+\frac{\sigma_2}{2}} \sin(h\omega t)\mathrm{d}\omega t \right]$$

$$= \frac{2}{h\pi} \left[\sin\left(\frac{h\sigma_2}{2}\right) - \sin\left(\frac{h\sigma_1}{2}\right) \right] \sin\left(\frac{h\pi}{2}\right) \tag{7.20}$$

The harmonic switching vector can handle asymmetrically gated, reverse-parallel thyristors since the conduction angles σ_1 and σ_2 can take independent values. Hence, equation (7.15), incorporating the switching vector, as given in equation (7.16), provides an effective means of calculating TCR harmonic currents for cases of both equal and unequal conduction angles. This is a most desirable characteristic in any TCR model, since TCRs are prone to exhibit imbalances due to manufacturing tolerances in their parts.

7.4.2.2 Harmonic admittances

Similarly to the harmonic currents, the TCR harmonic admittances are also a function of the conduction angles σ_1 and σ_2. In cases when the TCR is fully conducting, i.e. $\sigma_1 = \sigma_2 = 180°$, only the DC term exists. Smaller values of conduction angles lead to the appearance of harmonic admittance terms: the full harmonic spectrum is present when $\sigma_1 \neq \sigma_2$ but only even harmonics and the DC term appear in cases when $\sigma_1 = \sigma_2$.

The TCR harmonic admittances, when combined with the admittances of the parallel capacitor and suitably inverted, provide a means for assessing SVC resonant conditions as a function of firing angle operation. As an extension, the SVC harmonic admittances can be combined with the admittances of the power system to assess the impact of the external network on the SVC resonant characteristics.

The current derivative, with respect to the flux, is expressed as follows

$$\mathbf{f}'(\mathbf{\Psi}) = \frac{1}{L_R} \mathbf{S_R} \tag{7.21}$$

In the time domain, the magnitude of the derivative is inversely proportional to the reactor's inductance L_R during the conduction period and it is zero when no conduction takes place. In the frequency domain, the harmonic admittances are inversely proportional to the magnitude of the harmonic terms contained in the switching vector.

7.4.2.3 Harmonic Norton and Thévenin equivalent circuits

An incremental perturbation of equation (7.15) around a base operating point $\mathbf{\Psi_b}, \mathbf{I_b}$ leads to the following linearized equation (Semlyen et al., 1988),

$$\Delta \mathbf{I_R} = \mathbf{f}'(\mathbf{\Psi}) \cdot \Delta \mathbf{\Psi} \tag{7.22}$$

where $\mathbf{f}'(\mathbf{\Psi})$ is a harmonic vector of first partial derivatives.

The evaluation of the rhs term in equation (7.22) may be carried out in terms of conventional matrix operations, as opposed to convolutions operations, if the harmonic vector $\mathbf{f}'(\mathbf{\Psi})$ is expressed as a band-diagonal Toeplitz matrix, $\mathbf{F_R}$, i.e.

$$
\begin{bmatrix}
\vdots \\
\varphi_{-2} \\
\varphi_{-1} \\
\varphi_0 \\
\varphi_1 \\
\varphi_2 \\
\vdots
\end{bmatrix}
\Rightarrow
\begin{bmatrix}
\ddots & \ddots & \ddots & & & & \\
\ddots & \varphi_0 & \varphi_{-1} & \varphi_{-2} & & & \\
\ddots & \varphi_1 & \varphi_0 & \varphi_{-1} & \varphi_{-2} & & \\
& \varphi_2 & \varphi_1 & \varphi_0 & \varphi_{-1} & \varphi_{-2} & \\
& & \varphi_2 & \varphi_1 & \varphi_0 & \varphi_{-1} & \ddots \\
& & & \varphi_2 & \varphi_1 & \varphi_0 & \ddots \\
& & & & \ddots & \ddots & \ddots
\end{bmatrix}
\tag{7.23}
$$

The alternative harmonic domain equation

$$
\Delta \mathbf{I_R} = \mathbf{F_R} \Delta \mathbf{\Psi}
\tag{7.24}
$$

is well suited to carry out power systems harmonic studies. This expression may also be written in terms of the excitation voltage as opposed to the excitation flux

$$
\Delta \mathbf{I_R} = \mathbf{H_R} \Delta \mathbf{V}
\tag{7.25}
$$

The following relationship exists between $\mathbf{F_R}$ and $\mathbf{H_R}$

$$
\mathbf{H_R} = \mathbf{F_R} D \left(\frac{1}{\mathrm{j}\omega h} \right)
\tag{7.26}
$$

where $D(\,\cdot\,)$ is a diagonal matrix with entries $1/\mathrm{j}\omega h$.

By incorporating the base operating point $\mathbf{V_b}, \mathbf{I_b}$ in equation (7.24), the resultant equation may be interpreted as a harmonic Norton equivalent

$$
\mathbf{I_R} = \mathbf{H_R} \mathbf{V} + \mathbf{I_N}
\tag{7.27}
$$

where $\mathbf{I_N} = \mathbf{I_b} - \mathbf{H_R} \mathbf{V_b}$.

Alternatively, a representation in the form of a harmonic Thévenin equivalent may be realized from the Norton representation

$$
\mathbf{V} = \mathbf{Z_R} \mathbf{I_R} + \mathbf{V_T}
\tag{7.28}
$$

where $\mathbf{V_T} = \mathbf{V_b} - \mathbf{Z_R} \mathbf{I_b}$ and $\mathbf{Z_R} = 1/\mathbf{H_R}$.

7.4.2.4 Constraint equations

In the presence of low to moderate levels of harmonic voltage distortion, the TCR is a linear plant component, albeit a time-variant one, and the harmonic Norton current source in equation (7.27) will have null entries, i.e. the TCR is represented solely by a harmonic admittance matrix. Likewise, if the TCR is represented by a Thévenin equivalent, equation (7.28), the harmonic Thévenin source does not exist. The engineering assumption here is that the TCR comprises an air-core inductor and a phase-locked oscillator control system to fire the thyristors. In such a situation, the reactor will not saturate and the switching function will be constant.

For TCR operation under more pronounced levels of distortion, the switching function can no longer be assumed to remain constant, it becomes voltage dependent instead. This dependency is well represented by the periodic representation of

equation (7.11), beginning at the time when the thyristor is turned on, at $\phi_1 - \sigma_1/2$, and with an initial condition that the current is zero

$$I_R(\omega t) = \frac{1}{L_R} \int_{\phi_1 - \frac{\sigma_1}{2}}^{t} V(\omega t) \mathrm{d}\omega t \tag{7.29}$$

If the voltage is assumed to be a harmonic series then the current will have a similar representation

$$I_R(\omega t) = \sum_{-\infty}^{\infty} \frac{1}{h\omega L_R} V \left(\frac{\mathrm{e}^{\mathrm{j}h\omega t} - \mathrm{e}^{-\mathrm{j}h\omega t}}{\mathrm{j}2} \right) \Bigg|_{\phi_1 - \frac{\sigma_1}{2}}^{t} \tag{7.30}$$

This equation describes the current until the thyristor turns off. Just after the first zero crossing, at $\phi_1 + \sigma_1/2 \rightarrow I_R(\omega t) = 0$

$$0 = \sum_{-\infty}^{\infty} \frac{2V}{h\omega L_R} \mathrm{e}^{\mathrm{j}h\phi_1} \sin\left(\frac{h\sigma_1}{2}\right) \tag{7.31}$$

Similarly

$$0 = \sum_{-\infty}^{\infty} \frac{2V}{h\omega L_R} \mathrm{e}^{\mathrm{j}h\phi_2} \sin\left(\frac{h\sigma_2}{2}\right) \tag{7.32}$$

The constrained equations (7.31) and (7.32) are solved by iteration. Each is dependent on two angles, σ_1 and ϕ_1 for equation (7.30) and σ_2 and ϕ_2 for equation (7.31). The angles σ_1 and σ_2 may be used to determine the switching vector in equation (7.16).

7.4.3　Three-phase TCRs

A three-phase TCR normally consists of three delta connected, single-phase TCRs in order to cancel out the 3rd, 9th and 15th harmonic currents. Banks of capacitors and TSCs produce no harmonic distortion and there is no incentive for them to be connected in delta. The admittance matrix of equation (7.27) can be used as the basic building block for assembling three-phase TCR models. Linear transformations can be used for such a purpose.

The combined harmonic equivalent of three single-phase TCRs is

$$\begin{pmatrix} \mathbf{I_{R,1}} \\ \mathbf{I_{R,2}} \\ \mathbf{I_{R,3}} \end{pmatrix} = \begin{pmatrix} \mathbf{H_{R,1}} & \mathbf{0} & \mathbf{0} \\ \mathbf{0} & \mathbf{H_{R,2}} & \mathbf{0} \\ \mathbf{0} & \mathbf{0} & \mathbf{H_{R,3}} \end{pmatrix} \begin{pmatrix} \mathbf{V_1} \\ \mathbf{V_2} \\ \mathbf{V_3} \end{pmatrix} \tag{7.33}$$

In a power invariant, delta connected circuit the relationships between the unconnected and connected states are

$$\begin{pmatrix} I_A \\ I_B \\ I_C \end{pmatrix} = \frac{\angle 30°}{\sqrt{3}} \begin{pmatrix} 1 & 0 & -1 \\ -1 & 1 & 0 \\ 0 & -1 & 1 \end{pmatrix} \begin{pmatrix} I_1 \\ I_2 \\ I_3 \end{pmatrix} \tag{7.34}$$

and

$$\begin{pmatrix} V_1 \\ V_2 \\ V_3 \end{pmatrix} = \frac{\angle -30°}{\sqrt{3}} \begin{pmatrix} 1 & -1 & 0 \\ 0 & 1 & -1 \\ -1 & 0 & 1 \end{pmatrix} \begin{pmatrix} V_A \\ V_B \\ V_C \end{pmatrix} \tag{7.35}$$

Premultiplying equation (7.33) by the matrix term of equation (7.34), suitably modified to account for the higher order dimensions associated with the harmonic problem, and substituting equation (7.35) into the intermediate result, the following solution is arrived at

$$\begin{pmatrix} \mathbf{I_{R,A}} \\ \mathbf{I_{R,B}} \\ \mathbf{I_{R,C}} \end{pmatrix} = \frac{1}{3} \begin{pmatrix} \mathbf{H_1 + H_2} & \mathbf{-H_2} & \mathbf{-H_1} \\ \mathbf{-H_2} & \mathbf{H_2 + H_3} & \mathbf{-H_3} \\ \mathbf{-H_1} & \mathbf{-H_3} & \mathbf{H_3 + H_1} \end{pmatrix} \begin{pmatrix} \mathbf{V_A} \\ \mathbf{V_B} \\ \mathbf{V_C} \end{pmatrix} \tag{7.36}$$

7.4.3.1   *Numerical example 2*

The three-phase TCR harmonic model is used to calculate the harmonic currents drawn by a TCR installed in a 400 kV substation. The static compensator draws a net $35 + 10\%$ MVAr inductive at the tertiary terminal of a 240 MVA, 400/230/33 kV autotransformer.

The network is assumed to have 2% negative sequence voltage unbalance and the average system frequency is taken to be 50 Hz. The three-phase fault level at the 400 kV side is 11 185 MVA, while that on the 230 kV side is 6465 MVA. The short-circuit parameters of the transformer are 12.5%, 81.2% and 66.3% for the HV/MV, HV/LV and MV/LV sides, respectively. The TCR inductance per phase is $L = 90$ mH.

Norton equivalent representations that vary linearly with frequency are used for both the 400 kV network and the 230 kV network, A T-representation is used for the three-winding transformer. The linear Norton equivalents and the transformer admittances are combined with the harmonic domain admittance of the TCR. The overall representation is a nodal admittance matrix that contains information for the nodes, phases, harmonics and cross-couplings between harmonics. Table 7.1 gives the magnitudes of the harmonic current (rms values) drawn by the delta connected TCR when conduction angles of 120° are applied to all six thyristors.

It should be noted that the 2% negative sequence in the excitation voltage leads to unequal current magnitudes in phase A from those in phases B and C. Also, the delta

Table 7.1 Harmonic currents drawn by the TCR

Harmonic	Phase A (A rms)	Phase B (A rms)	Phase C (A rms)
1	268.79	260.81	260.81
3	5.54	3.20	3.20
5	17.63	18.91	18.91
7	6.93	6.30	6.30
9	1.59	0.81	0.81
11	2.86	3.56	3.56
13	2.05	1.81	1.81
15	0.85	0.43	0.43
17	0.98	1.53	1.53
19	0.84	0.77	0.77
21	0.49	0.25	0.25
23	0.39	0.93	0.93
25	0.33	0.36	0.36

connected TCR does not prevent completely the third harmonic currents and their multiples from reaching the network. It should be remarked that under balanced operation, these harmonic currents should be confined within the delta connected circuit. Also, as expected, TCR currents above the 13th harmonic term are quite small and may be ignored in most network harmonic studies.

Sometimes it is useful to use simplified expressions to check the sanity of the results. In this case, we shall calculate the fundamental frequency, positive sequence component of the TCR current by using the following equation (Miller, 1982)

$$I_1 = \frac{(\sigma - \sin \sigma)}{\pi} \cdot \frac{V}{X_L} \text{ A rms}$$ (7.37)

which gives the following result

$$I_1 = \frac{(120° \times \frac{\pi}{180°}) - \sin 120°}{\pi(2\pi \cdot 50 \times 0.09)} \times \frac{33 \times 10^3}{\sqrt{3}} = 263.48 \text{ A rms}$$ (7.38)

This value agrees rather well with the positive sequence value derived from applying symmetrical components to the fundamental frequency three-phase currents given in Table 7.1, i.e. 263.47 A rms.

7.4.3.2   Numerical example 3

A portion of a 220-kV power system for which complete information exists in the open literature (Acha et al., 1989) is used to illustrate the results produced by the three-phase TCR model. The system is shown in Figure 7.7. This is a well-studied test network, which shows a parallel resonance laying between the 4th and 5th harmonic frequencies, i.e. 200–250 Hz, as shown by the frequency response impedance in Figure 7.8.

A delta connected three-phase TCR is connected at busbar 1. Transmission lines are modelled with full frequency-dependence, geometric imbalances and long-line effects. Generators, transformers and loads have been assumed to behave linearly.
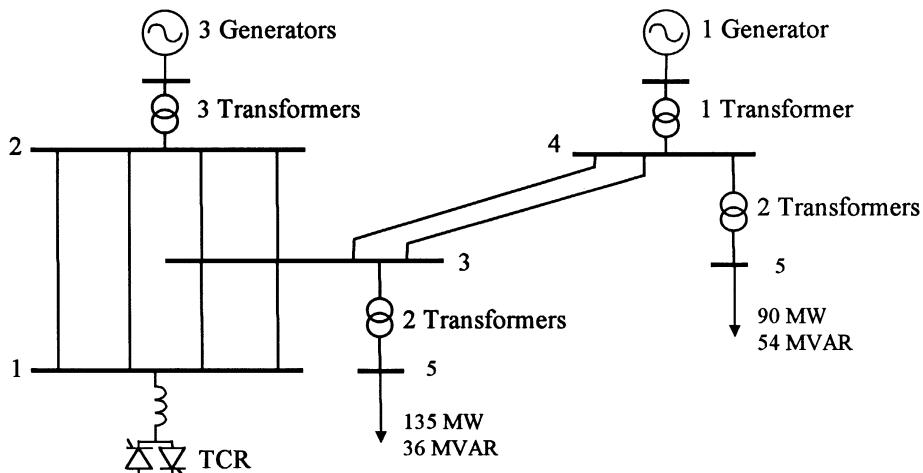
Fig. 7.7 Test system.

Fig. 7.8 Frequencey response impedance as seen from node 1.

It is well known that the TCRs will inject maximum 5th harmonic current when the conduction angle is 140° (Miller, 1982). In the case being analysed, this condition is compounded with the parallel resonance at near the 5th harmonic frequency exhibited by the network to give rise to a distorted voltage waveform at busbar 1. Figures 7.9(a) and (b) show the voltage waveform and the harmonic content for the three phases. Large harmonic voltage imbalances are shown in this result where the percentage of the 5th harmonic reaches almost 8% for phase B and 12% for phase C. The remaining harmonic voltages are well below recommended limits and are cause

(a)

(b)

Fig. 7.9 Voltage waveform and harmonic content at the TCR.

of no concern. However, filtering equipment would have to be connected at busbar 1 to provide a low impedance path for the 5th harmonic current.

Alternatively, the 5th and 7th TCR harmonic currents can be removed very effectively from the high voltage side of the network by employing two identical half-sized TCR units and a three phase transformer with two secondary windings.

7.5   SVC representations

The model of a single-phase SVC is readily assembled by adding up the harmonic admittance of the TCR in equation (7.27) and the harmonic admittance of the capacitor, $\mathbf{Y_C}$. The latter is a diagonal matrix with entries $j\omega hC$ and will hold for both banks of capacitors and thyristor-switched capacitors

$$\mathbf{I_{SVC}} = (\mathbf{H_R} + \mathbf{Y_C})\mathbf{V} = \mathbf{Y_{SVC}}\mathbf{V} \tag{7.39}$$

where $\mathbf{Y_{SVC}}$ and $\mathbf{I_{SVC}}$ are the equivalent admittance and the current drawn by the SVC, respectively. It should be noted that $\mathbf{Y_{SVC}}$ is a function of the conduction angles σ via $\mathbf{H_R}$.

Since the three-phase banks of capacitors, or thyristor-switched capacitors, are effectively connected in a grounded star configuration, the harmonic admittance model of the three-phase SVC is easily obtained

$$\begin{pmatrix} \mathbf{I_{SVC,A}} \\ \mathbf{I_{SVC,B}} \\ \mathbf{I_{SVC,C}} \end{pmatrix} = \frac{1}{3} \begin{pmatrix} \mathbf{H_1} + \mathbf{H_2} + 3\mathbf{Y_{C,1}} & -\mathbf{H_2} & -\mathbf{H_1} \\ -\mathbf{H_2} & \mathbf{H_2} + \mathbf{H_3} + 3\mathbf{Y_{C,2}} & -\mathbf{H_3} \\ -\mathbf{H_1} & -\mathbf{H_3} & \mathbf{H_3} + \mathbf{H_1} + 3\mathbf{Y_{C,3}} \end{pmatrix} \begin{pmatrix} \mathbf{V_A} \\ \mathbf{V_B} \\ \mathbf{V_C} \end{pmatrix} \tag{7.40}$$

7.6   Thyristor-controlled series compensation

The TCSC steady-state response may be calculated by solving the TCSC differential equations using a suitable numeric integration method or by expressing the TCSC equations in algebraic form and then using a phasorial method. The former approach involves the integration of the differential equations over many cycles until the transient response dies out. This solution method is rich in information since the full evolution of the response is captured, from transient inception to steady-state operation, but problems may arise when solving lightly damped circuits because of the low attenuation of the transient response. Two different solution flavours emerge from the phasor approach: (i) A non-linear equivalent impedance expression is derived for the TCSC and solved by iteration. The solution method is accurate and converges very robustly towards the convergence, but it only yields information about the fundamental frequency, steady-state solution; and (ii) Alternatively, the TCSC steady-state operation may be determined by using fundamental and harmonic frequency phasors leading to non-iterative solutions in the presence of low to moderate harmonic voltage distortion. The solution takes place in the harmonic domain and this is the approach presented in Section 7.6.2. The method yields full information for the fundamental and harmonic frequency TCSC parameters but no transient information is available.

7.6.1   Main parameters and operating modes

A basic TCSC module consists of a single-phase TCR in parallel with a fix capacitor. An actual TCSC comprises one or more modules. Figure 7.10 shows the layout of one phase of the TCSC installed in the Slatt substation (Piwko et al., 1996).

   As previously discussed in Section 7.4.1, the TCR achieves its fundamental frequency operating state at the expense of generating harmonic currents, which are a function of the thyristor's conduction angle. Nevertheless, contrary to the SVC application where the harmonic currents generated by the TCR tend to escape towards the network, in the TCSC application the TCR harmonic currents are trapped inside the TCSC due to the low impedance of the capacitor, compared to
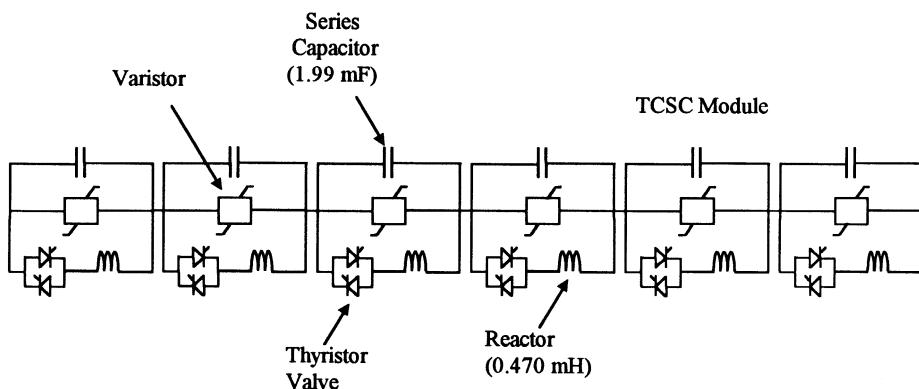
Fig. 7.10 Layout of one phase of the ASC installed in the Slatt substation.

the network equivalent impedance. This is at least the case for well-designed TCSCs operating in capacitive mode. Measurements conducted in both the Slatt and the Kayenta TCSC systems support this observation. For instance, the Kayenta system generates at its terminals, a maximum THD voltage of 1.5% when operated in capacitive mode and firing at an angle of 147° (Christl et al., 1991). It should be noted that there is little incentive for operating the TCSC in inductive mode since this would increase the electrical length of the compensated transmission line, with adverse consequences on stability margins and extra losses.

By recognizing that the thyristor pair in the TCSC module has two possible operating states, namely off and on (Helbing and Karady, 1994) developed equations for the TCSC voltage and current:

1. Thyristors off:

$$V_C^{\mathrm{off}}(t, \alpha) = \frac{I_M \sin \alpha}{\omega C}[1 - \sin(\omega t + \alpha)] - \frac{I_M \cos \alpha}{\omega C} \cos(\omega t + \alpha) + V_{\mathrm{st}'} \qquad (7.41)$$

where I_M is the peak line current and $V_{\mathrm{st}'}$ is the voltage across the capacitor at thyristor commutation time.

$$I_C^{\mathrm{off}}(t, \alpha) = I_M \sin \omega t \qquad (7.42)$$

In this situation, the inductor and thyristor current are zero, and the capacitor current equals the load current.

2. Thyristors on:

During conduction the inductor voltage equals the capacitor voltage.

$$
\begin{aligned}
V_C^{\mathrm{on}}(t, \alpha) = &\, I_M \frac{\omega_0^2 L \cos \alpha}{\omega^2 - \omega_0^2} \left\{ \omega \cos(\omega t - \alpha) - \omega_0 \sin\left[\omega_0 t - \frac{\omega_0}{\omega}\left(\alpha - \frac{\pi}{2}\right)\right] \right\} \\
&- I_M \frac{\omega_0^2 \omega L \cos \alpha}{\omega^2 - \omega_0^2} \left\{ \sin(\omega t - \alpha) + \cos\left[\omega_0 t - \frac{\omega_0}{\omega}\left(\alpha - \frac{\pi}{2}\right)\right] \right\} \\
&+ V_{\mathrm{st}''} \cos\left[\omega_0 t - \frac{\omega_0}{\omega}\left(\alpha - \frac{\pi}{2}\right)\right]
\end{aligned}
\qquad (7.43)
$$

where $V_{\mathrm{st}''}$ is the capacitor voltage at the time of thyristor firing.

$$
\begin{aligned}
I_L^{\mathrm{on}}(t, \alpha) = &\, I_M \frac{\omega \omega_0^2 \sin \alpha}{\omega^2 - \omega_0^2} \left\{ \frac{\sin\left(\omega_0 t - \frac{\omega}{\omega_0}\left(\alpha - \frac{\pi}{2}\right)\right)}{\omega_0} - \frac{\cos(\omega t - \alpha)}{\omega} \right\} \\
&- I_M \frac{\omega_0^2 \cos \alpha}{\omega^2 - \omega_0^2} \left\{ \cos\left(\omega_0 t - \frac{\omega}{\omega_0}\left(\alpha - \frac{\pi}{2}\right)\right) + \sin(\omega t - \alpha) \right\}
\end{aligned}
\qquad (7.44)
$$

where $\omega_0 = \frac{1}{\sqrt{LC}}$.

The capacitor current comprises the line current plus the inductor current

$$I_C^{\mathrm{on}}(t, \alpha) = I_L^{\mathrm{on}}(t, \alpha) + I_M \sin \omega t \qquad (7.45)$$

These equations are useful for calculating on a cycle-by-cycle basis the currents and voltages in the inductor, thyristor and capacitor. For instance (Helbing and Karady,

1994), give results for a TCSC module with the following parameters, $C = 212\,\mu\text{F}$ and $L = 15\,\text{mH}$, a line current of 2000 A and a firing angle of 133°.

The steady-state waveforms of the voltages and currents associated with the various TCSC components are shown in Figures 7.11, 7.12 and 7.13. Figure 7.11 shows the voltage and current waveforms in the capacitor, whereas Figures 7.12 and 7.13 show similar information in the inductor and in the bidirectional thyristors, respectively.

Figure 7.14(a) and (b) give information of the harmonic behaviour of the TCSC module under analysis. The result shows that the only harmonic of concern is the third harmonic as the firing angle decreases, i.e. the conduction angle increases. Careful design should ensure that the third harmonic voltage is kept at manageable levels.
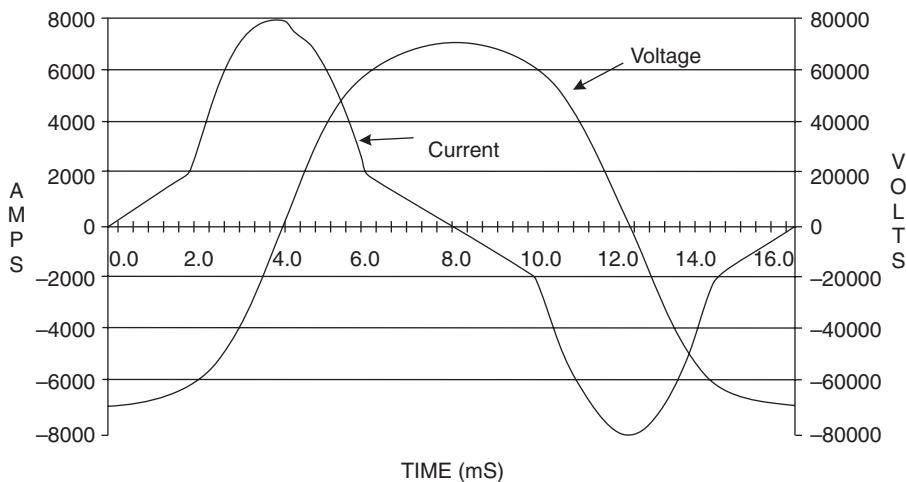
Fig. 7.11 Voltage and current waveforms in the TCSC capacitor.
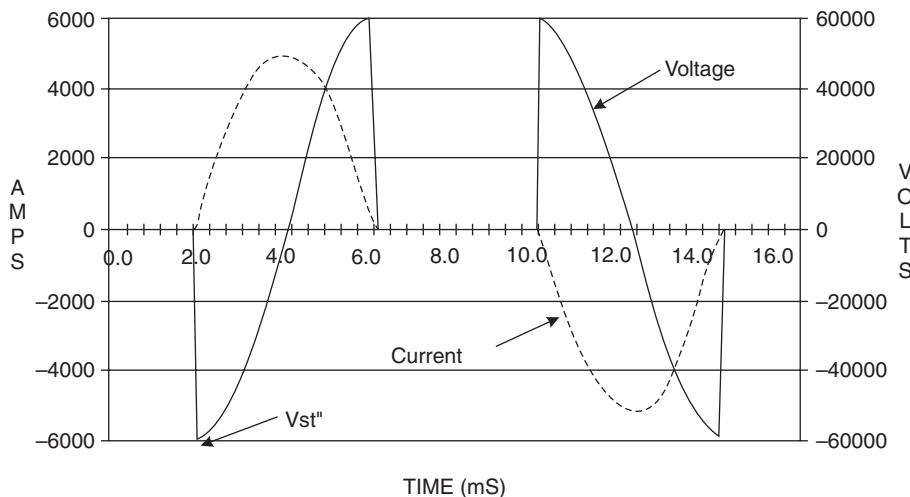
Fig. 7.12 Voltage and current waveforms in the TCSC inductor.
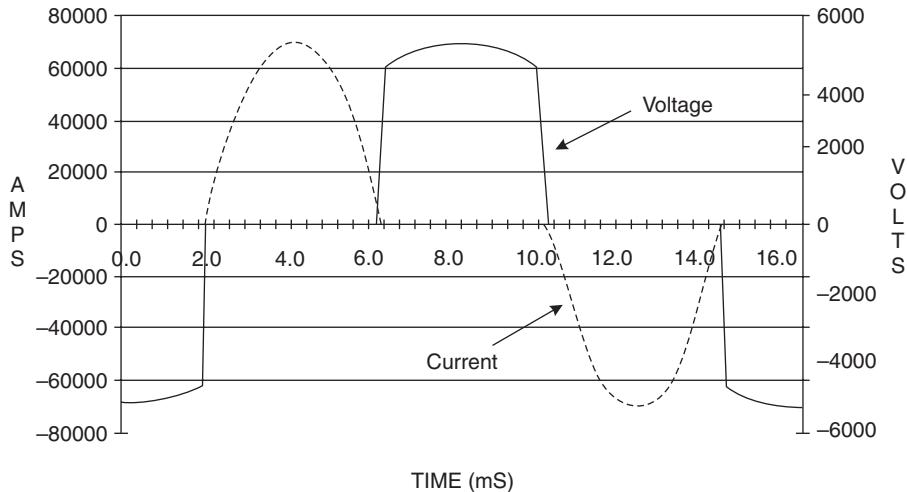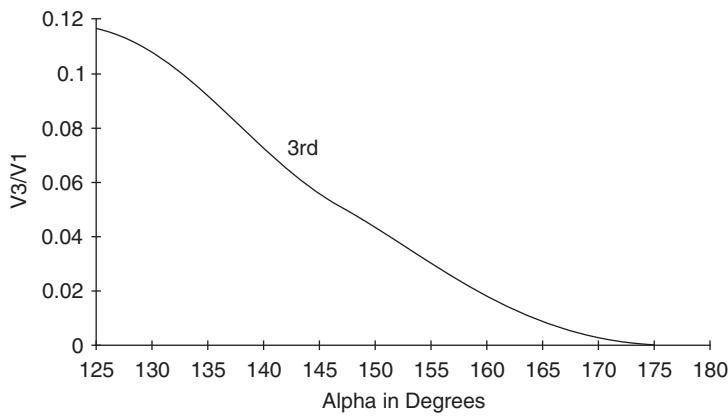
Fig. 7.13 Voltage and current waveforms in the bidirectional thyristors.

The TCSC has three basic operating modes: (i) the thyristor blocked mode; (ii) the thyristor bypassed mode; and (iii) the thyristor vernier mode. In (i), the thyristors do not conduct at all, and the transmission line current follows exclusively the TCSC capacitive path. The condition in (ii) corresponds to the case when the thyristors are conducting current continuously, with most of the transmission line current flowing through the thyristors. The TCSCs with realistic inductive and capacitive parameters have a small, net inductive reactance when operated in bypassed mode. In (iii), the thyristors are operated with phase control delay, leading to partial thyristor conduction. Two distinct operating characteristics will result from operating the TCSC in vernier mode, one inductive and one capacitive. In TCSCs with realistic *LC* parameters, low levels of thyristor conduction, i.e. large firing angle delays, will establish a net capacitive reactance making the TCSC to operate in the capacitive operating region. Conversely, high levels of thyristor conduction, i.e. low firing angle delays, will result in a net inductive reactance leading to TCSC operation in the inductive

(a)
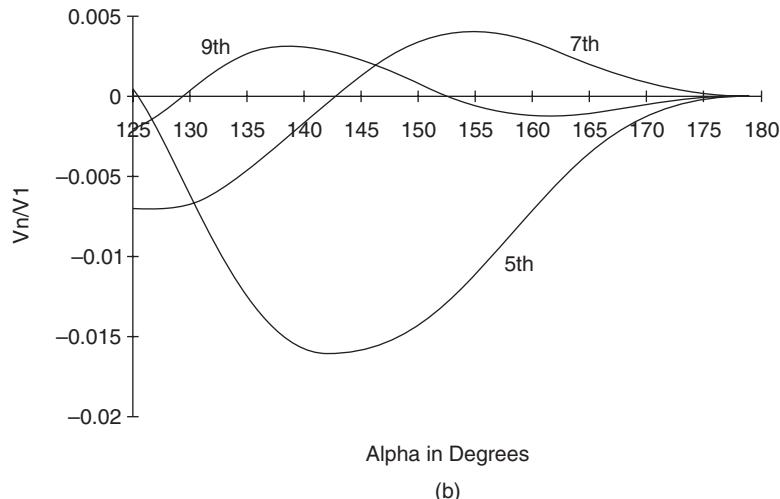
Fig. 7.14 Harmonic generation in per unit of fundamental frequency voltage as a function of firing angle.

region. For the case of the TCSC Kayenta scheme, with $X_C = 15\,\Omega$ and $X_L = 2.6\,\Omega$, firing angles of 90° to approximately 139° will lead to operation in the inductive region. On the other hand, firing angles of approximately 147° to 180° will lead to operation in the capacitive region. As shown in Figure 7.15, the fundamental frequency resonant point is centred at around 143°.

The TCSC impedance of the Kayenta scheme is also used to emphasize the importance of including all the relevant harmonic terms in the calculations, in
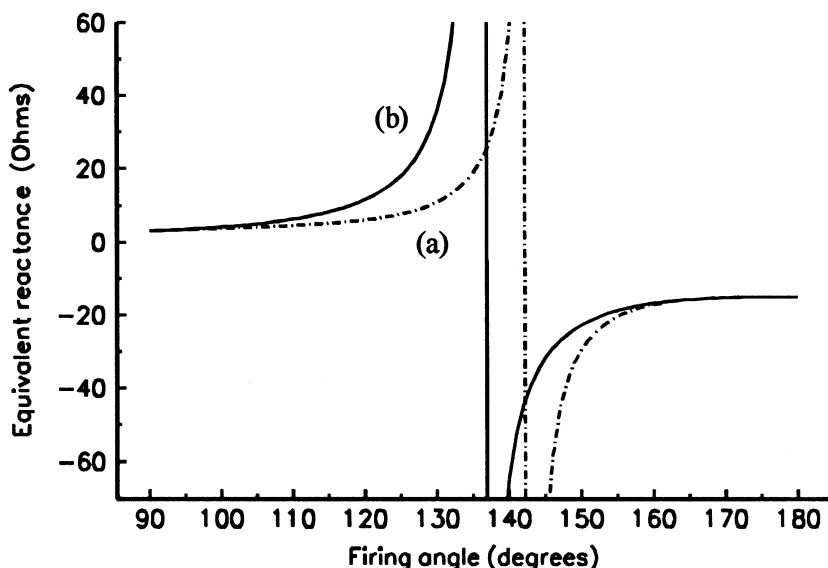
Fig. 7.15 TCSC impedance characteristic as a function of firing angle: (a) correct steady-state impedance; and (b) *understated* steady-state impedance.

addition to the fundamental frequency component. Figure 7.15(a) corresponds to the accurate solution whereas the result in Figure 7.15(b) was obtained by using only the fundamental frequency component, i.e. the harmonic terms were neglected.

Figure 7.16 shows the voltage across the TCSC capacitor for different values of firing angles. From Figure 7.16(a) and (b), it is observed that the distortion in the capacitor voltage waveform is larger when the TCSC operates in the inductive region of vernier operation. As expected the voltage magnitude increases as the resonant point is approached. The voltage across the capacitor is sinusoidal when the TCSC is operating in both thyristor bypassed mode, i.e. $\alpha = 90°$, and thyristor blocked mode, i.e. $\alpha = 180°$. Figures 7.17 and 7.18 show the current through the TCR and capacitor for different values of firing angles, respectively. The value of firing angle determines the direction of the current through the TCR and capacitor. Both plots show that the current magnitude increases as the resonant point is approached. As shown in

(a) Inductive region. (b) Capacitive region.
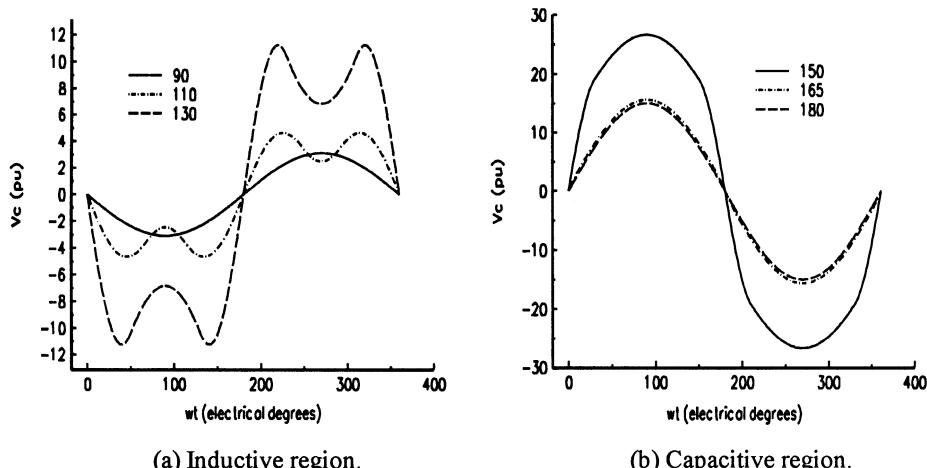
Fig. 7.16 Voltage across the TCSC capacitor for different values of firing angle.

(a) Inductive region. (b) Capacitive region.
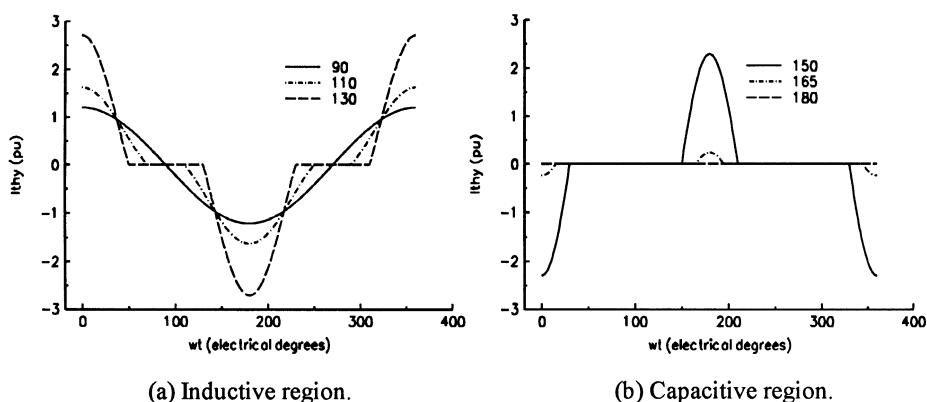
Fig. 7.17 Current waveform through the TCR for different values of firing angle.

(a) Inductive region.   (b) Capacitive region.
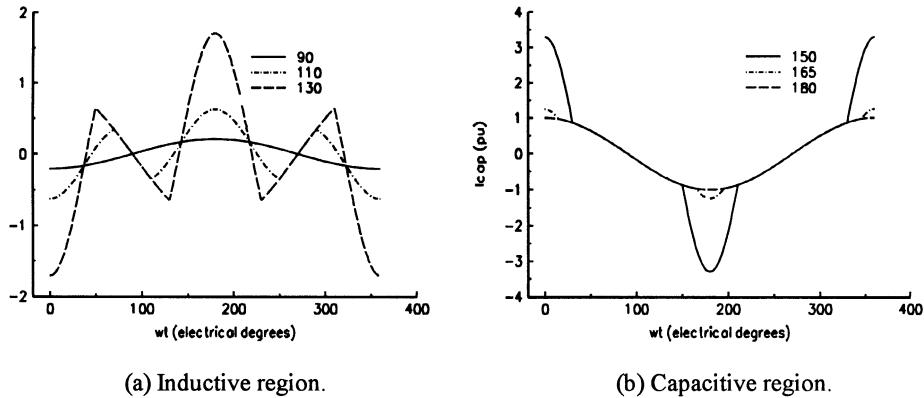
Fig. 7.18 Current waveform through the capacitor for different values of firing angle.

Figures 7.17(a) and (b) and 7.18(a) and (b), TCSC operation in the inductive region produces larger currents flowing through the thyristors than through the capacitors. The opposite situation occurs when the TCSC operates in the capacitive region.

7.6.2   TCSC harmonic domain modelling

Due to the circulating currents inside the TCSC module, intrinsic in the working mechanism of this equipment, the TCR representation based on harmonic currents injections is of limited use. Instead, the TCR is well modelled by a harmonic admittance matrix, which can then be combined with the admittance of the capacitive element to give the overall admittance representation of a single TCSC module. From the modelling viewpoint, this is the basic block, which may be used to build models for the three-phase TCSC systems. The basic building block is also useful to conduct fundamental studies of how the TCSC harmonic impedances and cross-coupling impedances vary as a function of the conduction angle.

7.6.2.1   Single-phase TCSC representation

In principle, equation (7.39) is valid for both the single-phase SVC and the TCSC, but the latter is better represented as a two-port circuit because it is a series connected element, that would be interfaced at both ends with transmission network plant, i.e. high-voltage transmission lines. Using the result in equation (7.39), the nodal transfer admittance matrix of the TCSC is built with ease

$$\begin{pmatrix} \mathbf{I_s} \\ \mathbf{I_r} \end{pmatrix} = \begin{pmatrix} \mathbf{Y_{TCSC}} & -\mathbf{Y_{TCSC}} \\ -\mathbf{Y_{TCSC}} & \mathbf{Y_{TCSC}} \end{pmatrix} \begin{pmatrix} \mathbf{V_s} \\ \mathbf{V_r} \end{pmatrix} \tag{7.46}$$

where $\mathbf{Y_{TCSC}} = \mathbf{Y_{SVC}} = (\mathbf{H_R} + \mathbf{Y_C})$, $\mathbf{V_s}$ and $\mathbf{V_r}$ are the voltages at the sending and receiving ends, $\mathbf{I_s}$ and $\mathbf{I_r}$ are the currents at the sending and receiving ends, respectively.

7.6.2.2   Impedance characteristics

The voltage drop expression for the single-phase TCSC may be derived using the result in equation (7.39)

$$\Delta\mathbf{V} = (\mathbf{H_R} + \mathbf{Y_C})^{-1}\mathbf{I_{TCSC}} = \mathbf{Z_{TCSC}}\mathbf{I_{TCSC}} \tag{7.47}$$

where the voltage drop is $\Delta\mathbf{V} = \mathbf{V_s} - \mathbf{V_r}$. Also, $\mathbf{Z_{TCSC}}$ and $\mathbf{I_{TCSC}}$ are the equivalent impedance and the current across the TCSC, respectively. It should be noted that $\mathbf{Z_{SVC}}$ is a function of the conduction angle σ via $\mathbf{H_R}$.

7.6.2.3   Three-phase TCSC representation

Equation (7.46) represents a single-phase TCSC in harmonic domain. However, expanding this model to encompass three-phase TCSCs is straightforward because of the decoupled nature of the three phases

$$\begin{pmatrix} \mathbf{I_{A,s}} \\ \mathbf{I_{B,s}} \\ \mathbf{I_{C,s}} \\ \mathbf{I_{A,r}} \\ \mathbf{I_{B,r}} \\ \mathbf{I_{C,r}} \end{pmatrix} = \begin{pmatrix} \mathbf{Y_{TCSC,A}} & \mathbf{0} & \mathbf{0} & -\mathbf{Y_{TCSC,A}} & \mathbf{0} & \mathbf{0} \\ \mathbf{0} & \mathbf{Y_{TCSC,B}} & \mathbf{0} & \mathbf{0} & -\mathbf{Y_{TCSC,B}} & \mathbf{0} \\ \mathbf{0} & \mathbf{0} & \mathbf{Y_{TCSC,C}} & \mathbf{0} & \mathbf{0} & -\mathbf{Y_{TCSC,C}} \\ -\mathbf{Y_{TCSC,A}} & \mathbf{0} & \mathbf{0} & \mathbf{Y_{TCSC,A}} & \mathbf{0} & \mathbf{0} \\ \mathbf{0} & -\mathbf{Y_{TCSC,B}} & \mathbf{0} & \mathbf{0} & \mathbf{Y_{TCSC,B}} & \mathbf{0} \\ \mathbf{0} & \mathbf{0} & -\mathbf{Y_{TCSC,C}} & \mathbf{0} & \mathbf{0} & \mathbf{Y_{TCSC,C}} \end{pmatrix} \begin{pmatrix} \mathbf{V_{A,S}} \\ \mathbf{V_{B,s}} \\ \mathbf{V_{C,s}} \\ \mathbf{V_{A,r}} \\ \mathbf{V_{B,r}} \\ \mathbf{V_{C,r}} \end{pmatrix} \tag{7.48}$$

7.7   TCSC systems

Equation (7.46) represents one single-phase TCSC module in the harmonic domain. If the TCSC comprises more than one module, or if the TCSC module is part of a series compensation scheme comprising conventional capacitor banks, then two-port representations may be used instead. The former case corresponds to the series compensation scheme found in the Slatt substation, where six identical TCSC modules are used (Piwko et al., 1996). This compensating scheme has been dubbed, Advanced Series Compensator (ASC). The latter compensation scheme is found in the Kayenta substation, where one $15\,\Omega$ TCSC module is connected in tandem with two capacitor banks, with values of $40\,\Omega$ and $55\,\Omega$, respectively (Christl et al., 1991).

The two-port, ABCD representation of a generic transmission element connected between nodes **s** and **r** is

$$\begin{pmatrix} \mathbf{V_s} \\ \mathbf{I_s} \end{pmatrix} = \begin{pmatrix} \mathbf{A} & \mathbf{B} \\ \mathbf{C} & \mathbf{D} \end{pmatrix} \begin{pmatrix} \mathbf{V_r} \\ -\mathbf{I_r} \end{pmatrix} \tag{7.49}$$

Due to the lumped nature of the TCSC module, as opposed to a transmission line or a cable, where the distributed inductive and capacitive effects are very pronounced, the ABCD representation of one TCSC module is very simple

$$\begin{pmatrix} \mathbf{V_s} \\ \mathbf{I_s} \end{pmatrix} = \begin{pmatrix} \mathbf{1} & \mathbf{Z_{TCSC}} \\ \mathbf{0} & \mathbf{1} \end{pmatrix} \begin{pmatrix} \mathbf{V_r} \\ -\mathbf{I_r} \end{pmatrix} \tag{7.50}$$

where **1** and **0** are the unity and null matrices, respectively.

A similar representation exists for the conventional series capacitor bank in this frame of reference, i.e.

$$\begin{pmatrix} \mathbf{V_s} \\ \mathbf{I_s} \end{pmatrix} = \begin{pmatrix} \mathbf{1} & \mathbf{Z_{SC}} \\ \mathbf{0} & \mathbf{1} \end{pmatrix} \begin{pmatrix} \mathbf{V_r} \\ -\mathbf{I_r} \end{pmatrix} \tag{7.51}$$

where $\mathbf{Z_{SC}}$ is the impedance of the series capacitor.

For completeness, the ABCD parameters of a transmission line with long-line effects, i.e. distributed parameters, are given below

$$
\begin{aligned}
\mathbf{A} &= \mathbf{T_i} \times D(\cos h(\gamma_m l)) \times \mathbf{T_v}^{-1} \\
\mathbf{B} &= \mathbf{T_v} \times D(z_{0m} \times \sin h(\gamma_m l)) \times \mathbf{T_i}^{-1} \\
\mathbf{C} &= -\mathbf{T_i} \times D\left(\frac{1}{z_{0m}} \times \sin h(\gamma_m l)\right) \times \mathbf{T_i}^{-1} \\
\mathbf{D} &= \mathbf{A}^t
\end{aligned}
\tag{7.52}
$$

where $\mathbf{T_v}$ and $\mathbf{T_i}$ are linear transformation matrices that require the eigen-solution of the products $\mathbf{ZY}$ and $\mathbf{YZ}$, respectively. $\mathbf{Z}$ and $\mathbf{Y}$ are the series impedance and the shunt admittance of the pi-nominal circuit per-unit length of a transmission line. As an extension, $\mathbf{Z_m} = \mathbf{T_v}^{-1}\mathbf{ZT_i}$ and $\mathbf{Y_m} = \mathbf{T_i}^{-1}\mathbf{YT_v}$. Also, l is the length of the line and $D(\cdot)$ is a diagonal matrix. $\gamma_m = \sqrt{z_m y_m}$ and $z_{0m} = \sqrt{z_m/y_m}$ are the propagation constant and the characteristic impedance of the transmission line, where $z_m \epsilon \mathbf{Z_m}$ and $y_m \sin \mathbf{Y_m}$. This model includes full frequency dependence and long-line effects.

For the case when n TCSC modules are connected in tandem, such as the Slatt compensation scheme, which comprises six modules, the equivalent TCSC system is

$$
\begin{aligned}
\begin{pmatrix} \mathbf{V_s} \\ \mathbf{I_s} \end{pmatrix} &= \begin{pmatrix} 1 & \mathbf{Z_{TCSC,1}} \\ 0 & 1 \end{pmatrix} \times \begin{pmatrix} 1 & \mathbf{Z_{TCSC,2}} \\ 0 & 1 \end{pmatrix} \times \cdots \times \begin{pmatrix} 1 & \mathbf{Z_{TCSC,6}} \\ 0 & 1 \end{pmatrix} \begin{pmatrix} \mathbf{V_r} \\ -\mathbf{I_r} \end{pmatrix} \\
&= \begin{pmatrix} 1 & \mathbf{Z_{TCSC,1}} + \mathbf{Z_{TCSC,2}} + \cdots + \mathbf{Z_{TCSC,6}} \\ 0 & 1 \end{pmatrix} \begin{pmatrix} \mathbf{V_r} \\ -\mathbf{I_r} \end{pmatrix}
\end{aligned}
\tag{7.53}
$$

The case of the Kayenta compensation scheme consists of three modules, of which only one module is TCSC and the other two are conventional capacitor banks, i.e.

$$
\begin{aligned}
\begin{pmatrix} \mathbf{V_s} \\ \mathbf{I_s} \end{pmatrix} &= \begin{pmatrix} 1 & \mathbf{Z_{TCSC}} \\ 0 & 1 \end{pmatrix} \times \begin{pmatrix} 1 & \mathbf{Z_{SC,1}} \\ 0 & 1 \end{pmatrix} \times \begin{pmatrix} 1 & \mathbf{Z_{SC,2}} \\ 0 & 1 \end{pmatrix} \begin{pmatrix} \mathbf{V_r} \\ -\mathbf{I_r} \end{pmatrix} \\
&= \begin{pmatrix} 1 & \mathbf{Z_{TCSC}} + \mathbf{Z_{SC,1}} + \mathbf{Z_{SC,2}} \\ 0 & 1 \end{pmatrix} \begin{pmatrix} \mathbf{V_r} \\ -\mathbf{I_r} \end{pmatrix}
\end{aligned}
\tag{7.54}
$$

The attractiveness of the ABCD representation is that it is quite compact, compared to say, network nodal analysis, and it still allows each individual TCSC module to incorporate its own firing angle. Moreover, the approach allows for a direct incorporation of the compensated transmission line and the external network, albeit in equivalent form, e.g. Norton and Thévenin equivalents.

Some application studies require information of the voltages at intermediate points of the compensation scheme, and nodal analysis provides a systematic tool for achieving such a result. For instance, for the case of the Kayenta scheme, the nodal admittance matrix equation is

$$
\begin{pmatrix} \mathbf{I_s} \\ 0 \\ 0 \\ \mathbf{I_r} \end{pmatrix} = \begin{pmatrix} \mathbf{Y_{TCSC}} & -\mathbf{Y_{TCSC}} & 0 & 0 \\ -\mathbf{Y_{TCSC}} & \mathbf{Y_{TCSC}} + \mathbf{Y_{SC,1}} & -\mathbf{Y_{SC,1}} & 0 \\ 0 & -\mathbf{Y_{SC,1}} & \mathbf{Y_{SC,1}} + \mathbf{Y_{SC,2}} & -\mathbf{Y_{SC,2}} \\ 0 & 0 & -\mathbf{Y_{SC,2}} & \mathbf{Y_{SC,2}} \end{pmatrix} \begin{pmatrix} \mathbf{V_s} \\ \mathbf{V_1} \\ \mathbf{V_2} \\ \mathbf{V_r} \end{pmatrix}
\tag{7.55}
$$

where $\mathbf{V_1}$ and $\mathbf{V_2}$ are the nodal voltages at the junctions of the TCSC module and the capacitor bank 1, and the capacitor banks 1 and 2, respectively.

7.8   Conclusion

This chapter has discussed the main adverse effects caused by harmonics in electrical equipment, in particular in industrial installations where capacitors used for power-factor correction become severely affected by the presence of harmonics. The all-important problem of parallel resonances caused when banks of capacitors are combined with the inductance of the AC system, is discussed in some detail. Simple equations are used to examine this problem from the quantitative point of view and a numerical example is presented.

Comprehensive harmonic domain models are presented for the TCR, the SVC and the TCSC. The SVC achieves fast and accurate voltage magnitude control at its point of connection with the AC network due to the TCR, which can be set to absorb a variable amount of reactive power with very little delay. However, an operational drawback of this scheme is that the TCR achieves its main operating point at the expense of generating harmonic currents. The order and magnitude of these harmonics being a function of the thyristors' firing angles. The harmonic domain models presented in this chapter enable realistic studies of both TCR and SVC equipment connected to AC networks of any size and complexity. The models are developed in the phase domain to incorporate frequency dependent, multiphase transmission systems, which may be very unbalanced at harmonic frequencies. Furthermore, the three-phase SVC representation also caters for TCR imbalances in either its firing angle control or in the linear inductors or capacitors. Numerical examples are provided to illustrate the usefulness of these models in power systems harmonic studies.

The discussion also applies to the TCSC, where the fast acting, regulating characteristic of the TCR enables the TCSC to shorten or to lengthen the electrical distance of the compensated transmission line with almost no delay. This characteristic of the TCSC is being exploited in high-voltage transmission installations to provide instantaneous active power flow regulation. However, TCSC harmonic generation and the existence of resonant conditions inside the TCSC call for accurate and comprehensive analysis tools. The harmonic domain models presented in this chapter are suitable to study such complex phenomena.

8

Transient studies of FACTS and Custom Power equipment

8.1 Introduction

Electromagnetic transient studies have always played an essential role in the analysis of electrical power systems. They provide priceless information relating to the behaviour of the system in the event of different forms of transient phenomena, which can hardly be achieved by other means. This chapter addresses the transient studies of electrical networks with embedded, power electronics-based, FACTS and Custom Power (CP) controllers. The FACTS controllers considered here are:

- SVC
- TCSC
- STATCOM.

The CP controllers include:

- D-STATCOM
- DVR
- PFC
- Shunt-Connected VSC-based AF
- Solid-State Transfer Switch (SSTS).

The transient analysis and modelling is performed with the state-of-the-art digital simulator PSCAD/EMTDC v2.00 (Manitoba, 1996) for UNIX, unless otherwise stated. The appendix at the end of this chapter presents the settings of the most relevant blocks used in the digital implementations developed in PSCAD/EMTDC, for each of the FACTS and CP controllers considered here.

8.2   Electromagnetic transient analysis

The transient response of any natural system is the way in which the response of the system behaves as a function of time. Mathematically, the transient behaviour of a given system is modelled by differential equations. However, this approach can be reasonably applied to systems where the underlying principles are clear and where the system is sufficiently elementary, so that a 'basic' approach can be used. Due to the high complexity involved in the solution of differential equations by hand-methods, it has been imperative to develop efficient and reliable numerical techniques implemented on digital computers, which reproduce confidently the transient response of almost every system provided that these are modelled appropriately.

Electrical power networks like other physical systems are exposed to various forms of transient phenomena; nowadays, fast variations of electrical parameters such as voltage or current are very common due to the elaborated equipment and configurations used in the power systems. Bearing this in mind, digital tools have become an invaluable resource when the transient response of the electrical network is required. When used for this purpose, digital tools are commonly labelled as electromagnetic transient simulators.

A considerable percentage of power systems studies rely on electromagnetic transient simulations. They provide substantial information associated with the performance of the network under any operating condition and enable the user to identify and assess the interaction between the various elements encompassing the network. This information can be used for miscellaneous purposes such as evaluation, planning, operation, design, commissioning, characterization, etc.

Generally, power networks are very complex all around the world. The enhancement of transmission and distribution systems by means of high-power electronics technology, such as FACTS and CP controllers has increased considerably the complexity of electrical networks. Consequently, the development of power systems studies has become more difficult. Moreover, in some cases the only possible way to carry out the analysis of a given network is by means of electromagnetic transient simulators. Fortunately, for the electricity supply industry, digital simulators have equally been developing in order to meet the new system requirements. They are powerful and provide the user with friendly interface environments. Some of them have already incorporated models of power electronics-based controllers so that transient analysis results can be achieved accurately and with high reliability. Some of the most popular electromagnetic transient simulators currently available are as follows:

- EMTP/ATP (Electromagnetic Transient Program)
- PSCAD/EMTDC (Power Systems Computer Aided Design/Electromagnetic Transient Direct Current)
- NETOMAC
- SPICE
- SABER

These simulators provide built-in models for a wide variety of power system components, which assist users to easily study electrical networks. Although all

the above simulators can be used to model a power system network, different difficulty in developing appropriate models for the system can be experienced. The reason being that they have been designed for various purposes. For instance, some have been designed for electronic circuits and their models for the various semiconductors can be more sophisticated (i.e. SPICE) than the ones provided by other simulators specifically designed for power system simulations (i.e. PSCAD/ EMTDC).

As mentioned before, PSCAD/EMTDC has been used here to carry out the transient analysis of FACTS and CP controllers. Therefore, in the following subsection we present a tutorial-like introduction to this digital tool in order to familiarize the reader with it and thus, facilitate the understanding of models and analysis presented in this chapter.

8.3 Electromagnetic transient simulator PSCAD/EMTDC

PSCAD/EMTDC is a general-purpose time domain simulation tool for examining the transient behaviour of electrical networks. Since it was first developed in 1976, the EMTDC simulation program has constantly been evolving in its scope and capabilities. PSCAD provides a flexible user interface to make use of EMTDC, enabling an integrated visual environment that supports all aspects associated with the simulation, including circuit assembly, run-time control, analysis and reporting (Gole, Nayak et al., 1996; Manitoba, 1994).

The following list summarizes the main studies that can be conducted with EMTDC:

- contingency studies of AC networks containing rotating machines, exciters, governors, turbines, transformers, transmission lines and cables
- sub-synchronous resonance studies of networks with rotating machines, controls, transmission lines and HVDC systems
- design and evaluation of filter performance and harmonic analysis
- control system design and co-ordination of HVDC, FACTS and CP controllers
- optimal design of controller parameters
- investigation of new circuits and control concepts.

PSCAD/EMTDC has a comprehensive palette of components. Circuits are built by dragging and dropping the appropriate model block onto the drawing canvas, and using drag and stretch wires to connect it to the circuit under construction. The process of circuit construction is thus similar to that of drawing a schematic diagram of the power circuit under study. The main components available in PSCAD/ EMTDC are as follows:

- resistors (R), inductors (L), capacitors (C)
- single-phase transformers, i.e. mutually coupled windings
- transmission lines and cables
- current and voltage sources
- switches and circuit breakers
- diodes, thyristors and GTOs
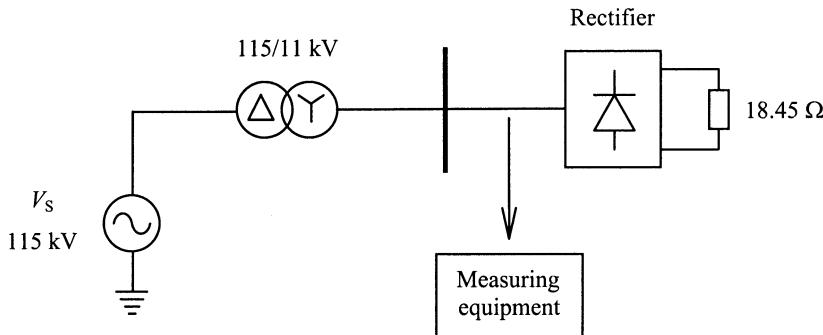
Fig. 8.1 Test circuit to be built in PSCAD.

- analogue and digital control functions
- AC machines, exciters, governors, stabilizers and inertial models
- meters and measuring functions
- generic DC and AC controls
- HVDC, SVC and other FACTS and CP controllers.

Once the construction of the circuit schematic diagram has been completed, it is run using the module `RunTime Executive`. The simulation results to be captured are selected using the `RunTime Executive` module. It is possible to observe these results as the simulation progresses. This module allows for the use of sliders, push buttons, dials and meters that permit the user to control the program in an interactive manner. The process required for graphically building a circuit and simulating its transient response in PSCAD/EMTDC is explained next in a very illustrative and comprehensive fashion.

Figure 8.1 shows the one-line diagram of the electrical circuit used in this tutorial. It comprises of a three-phase AC voltage source feeding into a six-pulse diode rectifier, via a delta–star connected transformer.

The process may be divided into four major steps:

1. creation of a new project and data entry
2. generation of the circuit schematic diagram using `Draft`
3. transient simulation using `RunTime Executive`
4. plotting and analysis of results using `MultiPlot`.

8.3.1 Creation of a new project and data entry

1. Start the PSCAD graphical user interface by typing `PSCAD` in the shell command. A window like the one shown in Figure 8.2 appears. At this point a new project is created using the `CREATE PROJECT` option under the `File Manager`. Figure 8.2 already shows this project which in this exercise is called 'ACSYSTEM'.
2. The next step is to create a study case that will contain all the files relating to the circuit. Open the project 'ACSYSTEM' by choosing the `OPEN` option under the pull down menu in the 'ACSYSTEM' icon. Using the `CREATE CASE` option under
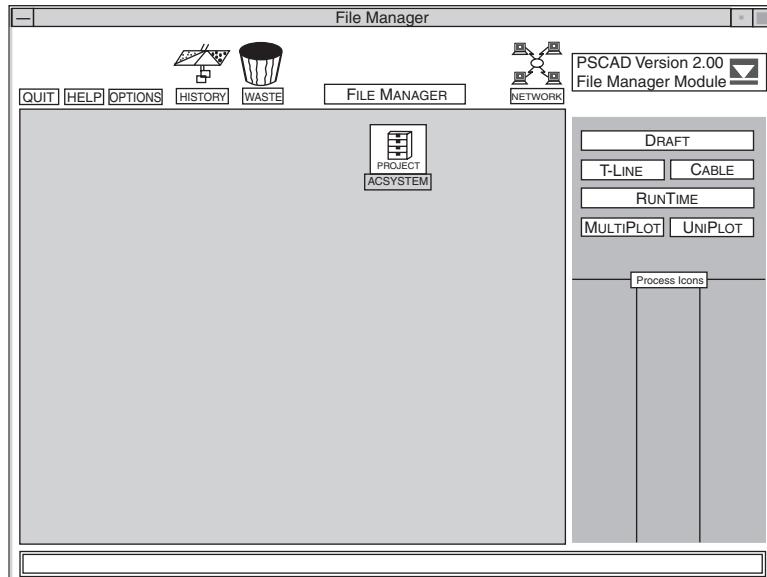
Fig. 8.2 PSCAD window appearing once the project 'ACSYSTEM' has been created.
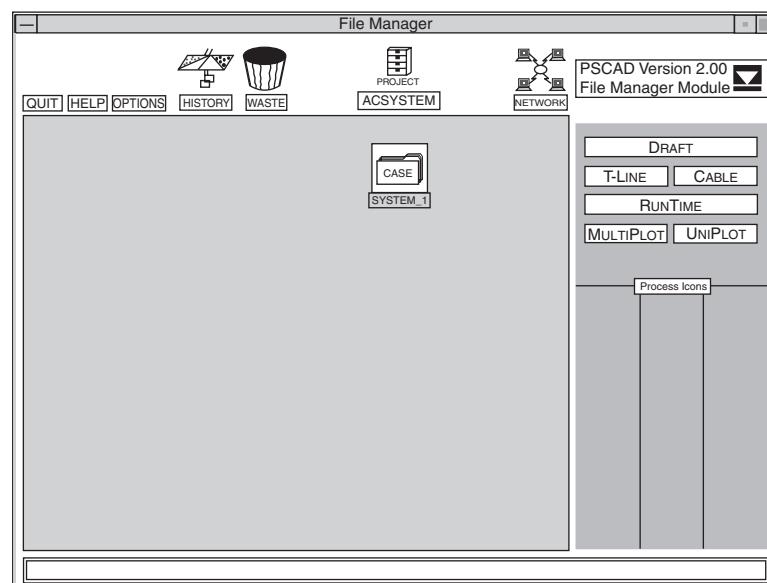
Fig. 8.3 PSCAD window appearing once the case 'SYSTEM_1' has been created.

the pull down menu in the project icon create a case called 'SYSTEM_1'. The window looks like the one shown in Figure 8.3.

3. The Draft tool is used to create the circuit file. The 'SYSTEM_1' case is opened using the OPEN option from the pull down menu of the project icon. The procedure is
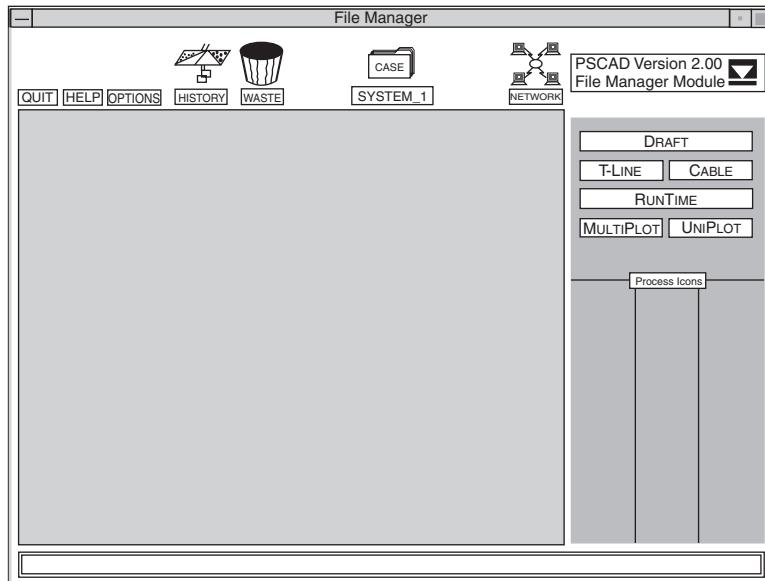
Fig. 8.4 PSCAD window appearing once the case 'SYSTEM_1' has been opened.

the same as in step 2. Once the case is opened, the window looks like the one shown in Figure 8.4. Now we proceed to draw the schematic diagram of the model circuit.

8.3.2 Generation of the circuit schematic diagram using `Draft`

The process required for drawing the circuit schematic diagram is as follows:

1. Select the action box labelled `Draft` to start the module. A window similar to the one shown in Figure 8.5 appears. This window shows the `Draft` module bar of menus, part of the drawing canvas and the library of components.
2. There is a pull down menu for each component in the library located at the right-hand side of the screen. Select the COPY option under the pull down menu of the required library component and drag it on to the work sheet. For this example, it is necessary to copy the components shown in Figure 8.6 to the drawing canvas. These include:
   - *Three-phase source* model with built-in controls for adjusting the magnitude and/or phase of the source.
   - *Three-phase, two-winding transformer model* with built-in controls to define transformer parameters such as capacity, operating frequency, winding data, and saturation among others.
   - *Real/Reactive power meter* that measures the three-phase real and/or reactive power flow into three nodes from three network branches. The instantaneous power signals are smoothed through a first order lag to simulate transducer delays.
   - *Signal plotting block* that causes `Draft` to add code to the EMTDC program which will record the signal flowing into the component.
   - *Wire connectors* and *label,* a *diode and* a *resistor.*
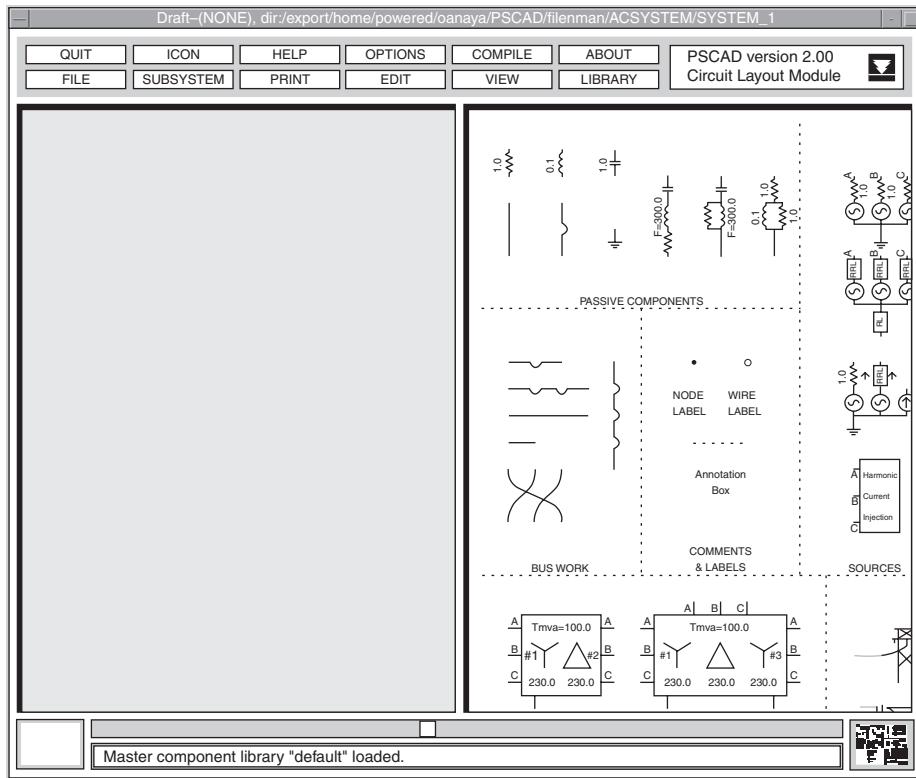
Fig. 8.5 `Draft` tool window.
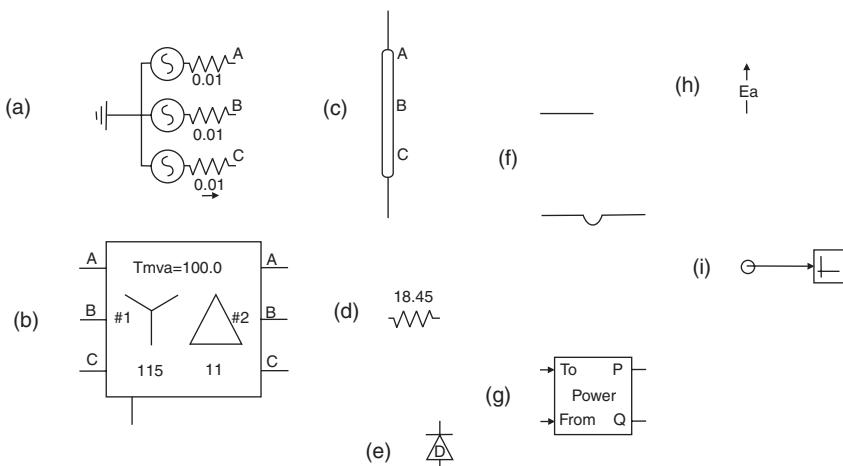
Fig. 8.6 Set of components required for the circuit of the example: (a) three-phase voltage source; (b) three-phase wye–delta transformer; (c) three-phase voltage signal sensor; (d) resistor; (e) diode; (f) wires; (g) active and reactive power meter; (h) voltage signal meter; and (i) signal plotting block.
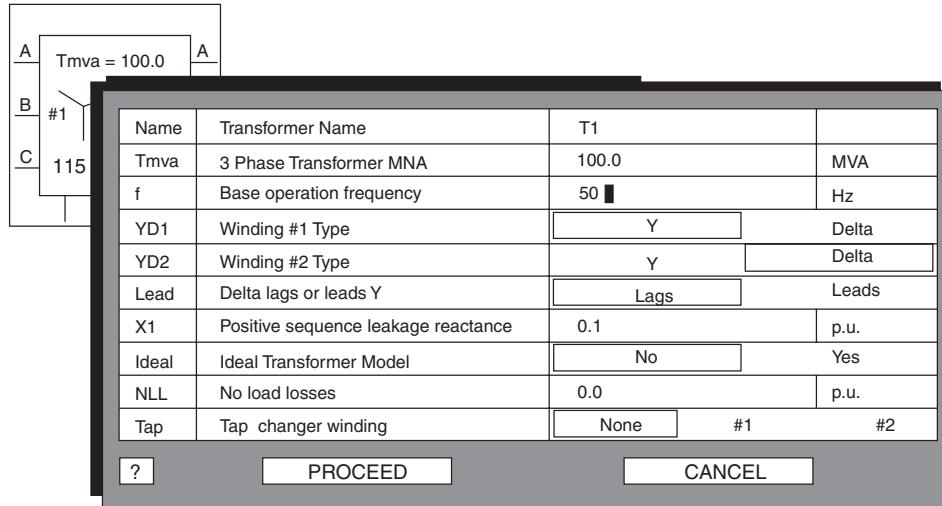
Fig. 8.7 Window to enter the parameters of the two-winding transformer model.

3. Select suitable parameters for each component. Choose the EDIT option in the pull down menu of each selected component and set the appropriate parameters. Figure 8.7 shows the window menu for the two-winding transformer.
4. Connect the components using the stretching wires. After completing the schematic drawing, the circuit must look like the one shown in Figure 8.8.
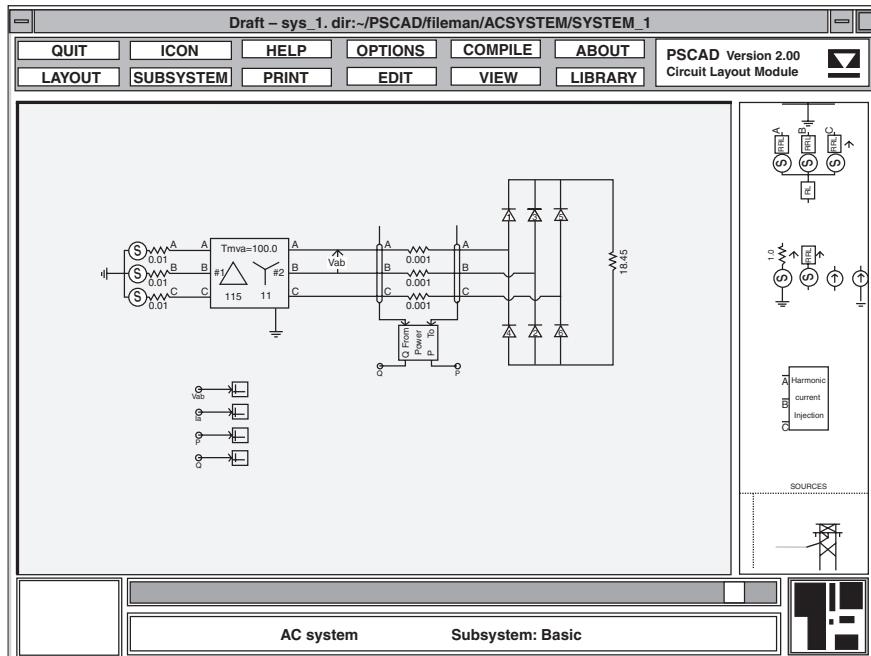
Fig. 8.8 Draft tool after completing the schematic drawing.

5. To save the circuit just created, select the SAVE AS option from the pull down menu found in the FILE box located near the top left of the Draft window. Save the current file as 'sys_1'.
6. Select the COMPILE option to compile the circuit. Provided the circuit has been properly created, the message: *Compile complete 0 error(s), 0 warning(s)* should appear in the bottom box.
7. Use either the QUIT or ICON options to exit the Draft window.

After the circuit schematic diagram has been completed, the transient simulation is performed using the module RunTime Executive. The RunTime Executive palette allows the user to customize the appearance of the console and to show as many waveform outputs as required. Also, control devices such as sliders, push-buttons and dials, can be opened for interactive control of the simulation.

8.3.3   Transient simulation using RunTime Executive

1. Start the RunTime Executive by selecting it from the corresponding box in the File Manager.
2. Use the LOAD option in the BATCH pull down menu to load the file 'sys_1'.
3. Select the PLOT option in the CREATE pull down menu to create the plots. Use graph 1 to display the line voltage, graph 2 to display the load current and graphs 3 and 4 to display the active and reactive power respectively.
4. Push the PLAY button to start the simulation. While the simulation is running, it is possible to click the [A/S] icon at the right-hand side of the plot to auto scale the graph.
5. Once the simulation has finished the window looks similar to the one shown in Figure 8.9. This figure shows the waveforms of the line voltage V_{ab} at the secondary of the transformer, the line current in phase a, I_a, the active power P, and the reactive power Q.
6. Use either the ICON or QUIT options to minimize or exit RunTime Executive respectively.

It should be noted that while the simulation is in progress, it may be paused, single-stepped through or restarted, using the tape recorder type buttons on the menu bar located immediately above the graphs. Also, cursors and zoom in-out features are available for closer inspection of the traces.

8.3.4   Plotting and analysis of results using MultiPlot

1. Select the MultiPlot module in the File Manager. The window must look similar to the one shown in Figure 8.10.
2. Create an empty graph using the pull down option in the CREATE menu.
3. Position the mouse on the empty graph, click the right button in the mouse and select ADD CURVE from the options presented in the menu box.
4. Select the desired signal you wish to display.

At the end of the simulation session, the File Manager window should look like the one shown in Figure 8.11. It shows the icons for the various files created for a given simulated circuit. To end the session, close down all the applications, e.g. Draft, RunTime Executive and MultiPlot, and then press the QUIT button.
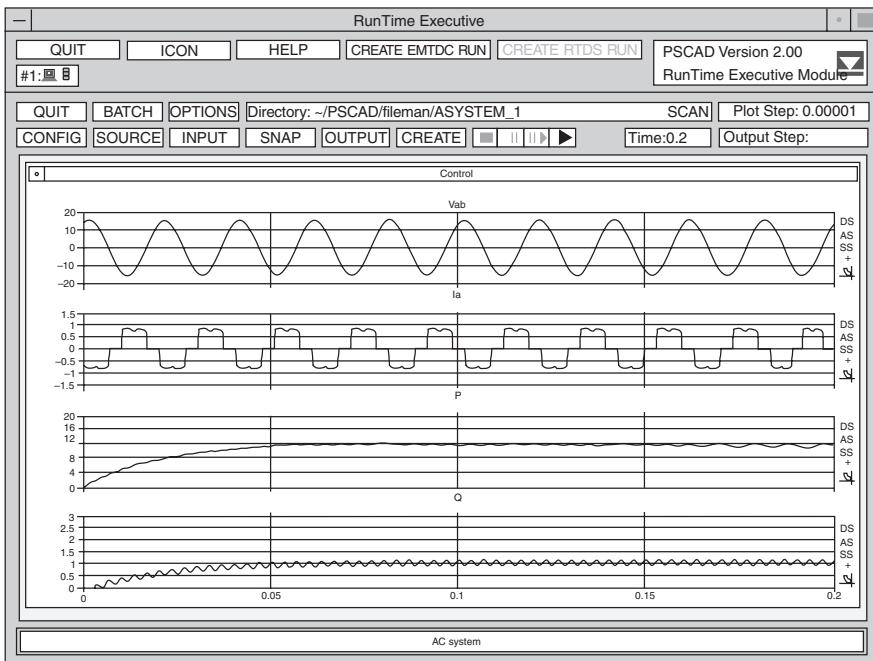
Fig. 8.9 Transient simulation using `RunTime Executive`.
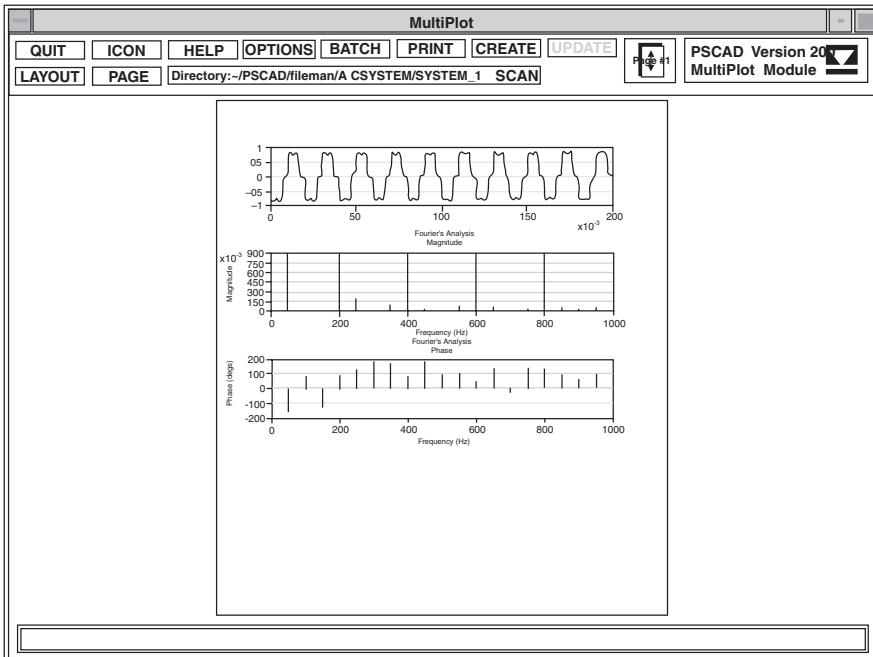
Fig. 8.10 `Multiplot` module used for further analysis of output waveforms.
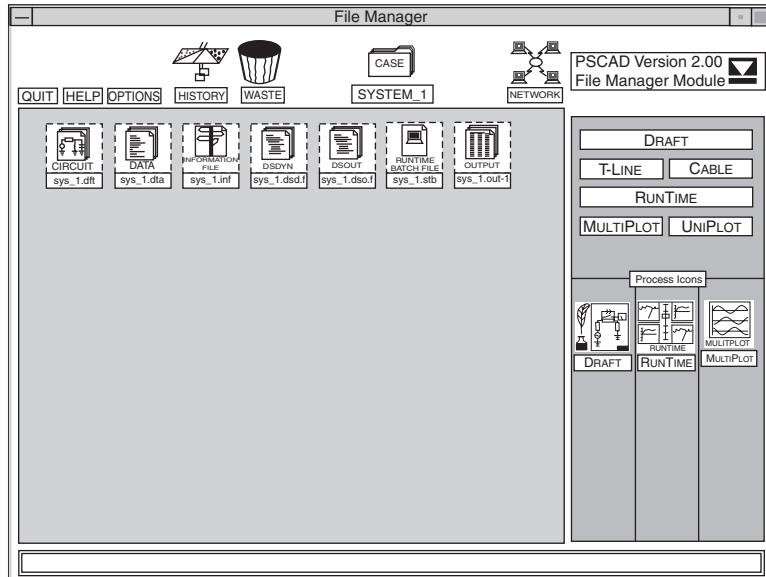
Fig. 8.11 `File Manager` window and files created for a given simulated circuit.

8.4 Static Var Compensator (SVC)

At this point in time, SVCs are the most widely installed FACTS equipment. They mimic the working principles of a variable shunt susceptance and use fast thyristor controllers with settling times of only a few fundamental frequency periods. From the operational point of view, the SVC adjusts its value automatically in response to changes in the operating conditions of the network. The SVC has the ability to either draw capacitive or inductive current from the network. By suitable control of this equivalent reactance, it is possible to regulate the voltage magnitude at the SVC point of connection, thus enhancing significantly the power system's performance.

More specifically, as discussed in Chapter 3, voltage regulation at a key location of the transmission system should provide the following benefits:

- prevention of large voltage variations
- prevention of voltage instability (voltage collapse)
- enlargement of transient (first swing) stability limits
- provision of power oscillations damping.

The SVC may be designed in many different ways. Figure 8.12 shows the schematic diagrams of the most typical arrangements for continuously controlled SVCs i.e. fixed capacitors (FC) with TCR and TSC with TCR. The thyristors are the controllable elements enabling smooth control of the TCR when operated in the range of 90–180°. On the other hand, the TSC is a fast-switched element that achieves voltage regulation in a stepwise fashion.

When the SVC is operated in a voltage control mode, it is the fastest thyristor-controlled FACTS controller, with settling times of almost one period in the case of
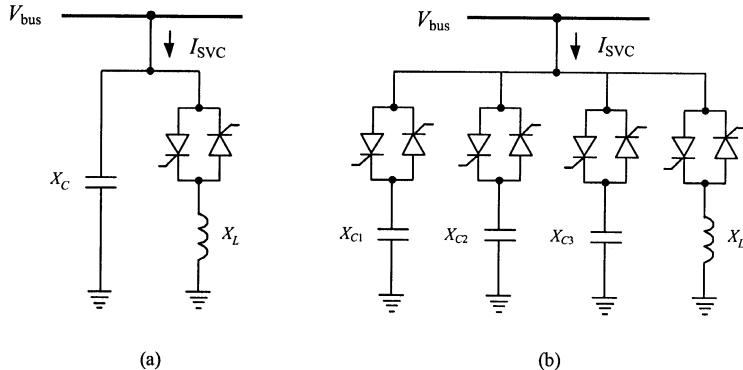
Fig. 8.12 Typical SVC's structures: (a) a TCR with a fixed capacitor; and (b) a TCR with a TSC.

the FC/TCR arrangement. In the case of switched elements (TSC/TCR), the response time is usually 30–60 µs depending upon the SVC configuration and system strength. In order to achieve such a high-speed response, it is necessary to properly assess the type and size of the power components as well as the control scheme according to the specific network configuration and operation requirements.

Figure 8.13 shows a simplified block diagram of a voltage control scheme for a typical SVC application (Tyll, 1992; Shen, 1998). Essential elements in this control scheme are: the measuring circuits, the voltage regulator, the allocator, the linearizer, and the TCR and TSC firing circuits.

Measuring circuits. The main function of these circuits is to measure the voltages and currents at different points of the power network, which provide relevant
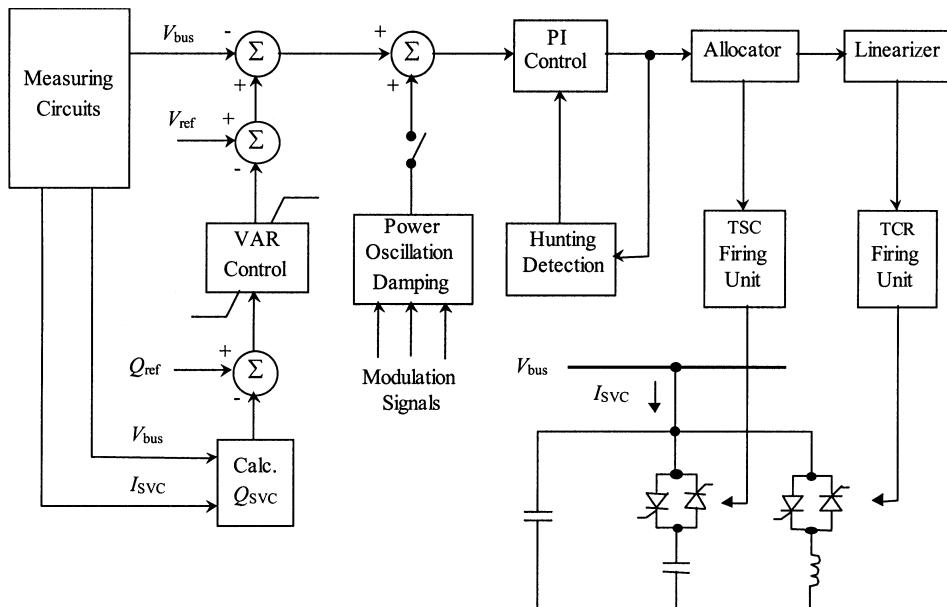
Fig. 8.13 Simplified voltage control block diagram of a typical SVC application.

information for SVC control and protection purposes. The measured signals are conditioned to provide suitable control to the other blocks of the control system.

Voltage regulator. The voltage regulator performs the closed loop voltage control. The difference between the voltage reference and the voltage measured at the point of connection of the SVC is fed as the control error signal to a PI (proportional-integral) regulator that provides the total SVC susceptance reference required to minimize the error.

Power oscillation damping. When a power modulation control circuit is included in the SVC controller, this high-level control function utilizes the power system response as the input and acts on the voltage regulation to provide damping for slow electro-mechanical swings in the power system.

Allocator. This block has the function of converting the susceptance reference from the voltage regulator into specific information which is then processed in order to determine the number of reactive banks that must be switched on and the required firing angle.

Linearizer. The linearizer converts the susceptance from the allocator to a firing angle α. To maintain the same control response over the entire SVC operating range, the angle α is determined as a non-linear function of the susceptance reference order. This function is normally given as a table that is derived from the following formula

$$1 - X_L B(\alpha) = \alpha + \frac{\sin(\pi\alpha)}{\pi} \tag{8.1}$$

where $B(\alpha)$ is the susceptance of the TCR fired at the angle α.

Hunting detection and gain adjustment. The stability controller supervises the operation of the voltage controller. Unstable operation (hunting), which may take place during weak system operating conditions, will be detected and the gain of the PI controller would be reduced by half to try to achieve stable operation.

TSC–TCR firing units. These units compute the angles α and generate firing pulses for the TSC and TCR thyristor valves.

Other control elements that can be added to the control circuit are the DC and reactive power controllers. With the addition of these elements the control system becomes more robust and efficient; however, its complexity increases considerably. Then, it is necessary to design the control system according to application requirements bearing in mind simplicity, efficiency and reliability. To illustrate the design and implementation of the SVC control system, a simple single-phase circuit is selected, where the SVC is connected between the source and the load. The FC/TCR topology is used as shown in the test system in Figure 8.14.

The aim of the SVC in this application is to provide voltage regulation at the point of connection, following load variations. Initially the SVC is operated in open-loop mode and for this condition, the power exchange between the SVC and the AC system should be zero. When breaker *Brk* is closed, the load is increased and the voltage at the load point experiences a voltage sag of nearly 16%. When the load is increased, the SVC controller operation changes to closed-loop mode in order to adjust the SVC effective impedance X_{SVC} so that it injects capacitive current into the system to restore the voltage back to the target value.

The SVC parameters have been determined according to the compensation requirements for the case when the second load is connected. Based on the reactive
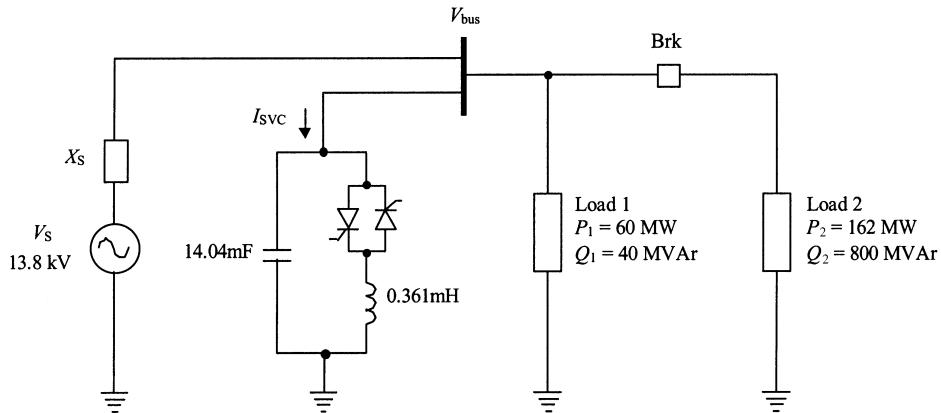
Fig. 8.14 Test system implemented to carry out time domain analysis of the SVC.

(a)   (b)
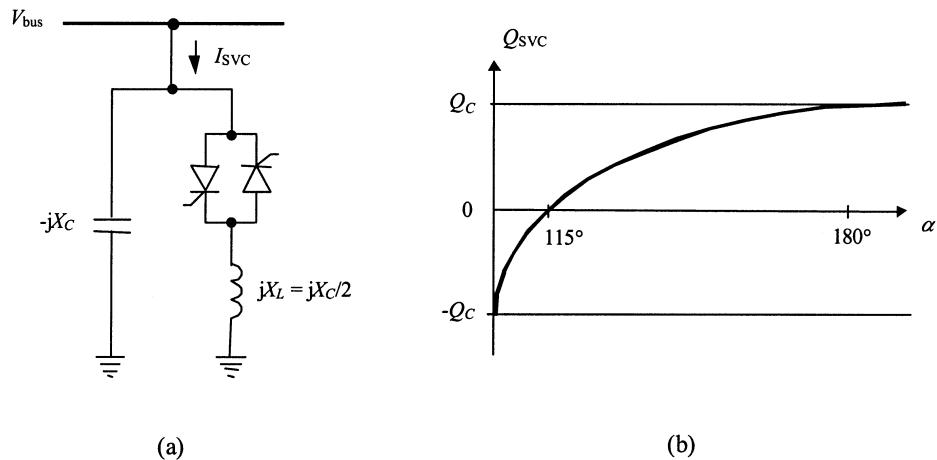
Fig. 8.15 (a) SVC capacitance and inductances values; and (b) characteristic plot $Q_{SVC}(\alpha)$.

power required by *Load* 2, the SVC is sized with enough capacity to supply at least this reactive power in order to drive the voltage V_{bus} back to the reference, that is

$$Q_{SVC} > 800 \, \text{MVAr} \tag{8.2}$$

In this example, the maximum reactive capacity of the SVC is set at $Q_{SVC} = 840 \, \text{MVAr}$. The values for the capacitance and the TCR inductance are then calculated based on this setting.

With reference to Figure 8.15(a)

$$X_C = \frac{(V_{bus})^2}{Q_{SVC}} = \frac{(13.8 \, \text{kV})^2}{840 \, \text{MVAr}} = 0.226714 \, \Omega \tag{8.3}$$

and

$$X_L = \frac{X_C}{2} \tag{8.4}$$

From Equations 8.3 and 8.4 and considering a fundamental frequency of $f = 50\,\text{Hz}$, the capacitance and inductance values are

$$C = 14.04\,\text{mF}$$

$$L = 0.361\,\text{mH}$$

Once the capacitance and inductance have been sized, it is necessary to determine the initial operating condition of the SVC. Initially, *Brk* is open and there is no need for the SVC to be in operation. However, it is already connected and interacting with the AC system. Then the selection of the initial firing angle α must be such that under this operating condition the SVC does not exchange any power with the AC system.

This firing angle corresponds to the case when the effective reactances X_C and X_L cancel each other out. In this case, the SVC effective reactance X_{SVC} is infinite and there is no current leaving or entering the SVC, i.e. the power exchange between the SVC and the AC system is zero.

According to the inductive and capacitive reactances, each SVC has its own firing angle-reactive power characteristic, $Q_{SVC}(\alpha)$ which is a function of the inductive and capacitive reactances. The firing angle initial condition may be determined using a graph similar to that shown in Figure 8.15(b). The following steps may be used to determine this plot. Firstly, it is necessary to obtain the effective reactance X_{SVC} as a function of the firing angle α, using the fundamental frequency TCR equivalent reactance X_{TCR}

$$X_{TCR} = \frac{\pi X_L}{\sigma - \sin \sigma} \tag{8.5}$$

and

$$\sigma = 2(\pi - \alpha) \tag{8.6}$$

where X_L is the reactance of the linear inductor, and σ and α are the thyristors' conduction and firing angles, respectively.

At $\alpha = 90°$ the TCR conducts fully and the equivalent reactance X_{TCR} becomes X_L. At $\alpha = 180°$, the TCR is blocked and its equivalent reactance becomes extremely large, i.e. infinite.

The total effective reactance of the SVC, including the TCR and capacitive reactances, is determined by the parallel combination of both components

$$X_{SVC} = \frac{X_C X_{TCR}}{X_C + X_{TCR}} \tag{8.7}$$

which as a function of the conduction angle σ becomes

$$X_{SVC} = \frac{\pi X_C X_L}{X_C(\sigma - \sin \sigma) - \pi X_L} \tag{8.8}$$

And finally as a function of the firing angle α becomes

$$X_{SVC} = \frac{\pi X_C X_L}{X_C[2(\pi - \alpha) + \sin 2\alpha] - \pi X_L} \tag{8.9}$$
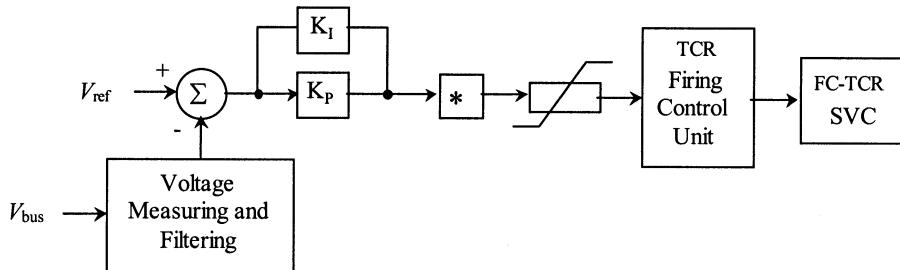
Fig. 8.16 Basic control scheme designed for the FC/TCR topology of the example.

As expected, the effective reactance of the SVC is a function of the firing angle α. Equation 8.9 may be used to plot $Q_{SVC}(\alpha)$ and to determine the angle α for which $Q_{SVC}(\alpha) \approx 0$, using the following fundamental relationship

$$Q_{SVC} = V_{bus}^2 \cdot \frac{X_C[2\pi - \alpha + \sin 2\alpha] - \pi X_L}{\pi X_C X_L} \tag{8.10}$$

As indicated by Equation 8.10, Q_{SVC} takes a value of zero when the effective reactance X_{SVC} is extremely large, i.e. infinite. This condition is satisfied when the following relationship approaches zero

$$X_C[2(\pi - \alpha) + \sin 2\alpha] - \pi X_L \to 0 \tag{8.11}$$

With the SVC parameters used in this example, the value of the firing angle α that satisfies Equation 8.11 is found to be $\alpha \approx 115°$. This angle is used as the initial condition for α in the open-loop control of the SVC.

To illustrate the SVC's ability to provide voltage regulation at the point of connection, a simplified control scheme has been implemented for the single-phase SVC circuit shown in Figure 8.14. The block diagram is shown in Figure 8.16. This control scheme works as follows: The amplitude of the bus voltage V_{bus} is measured and filtered. Then it is compared against the voltage reference V_{ref}. The voltage difference (error) between the two signals is processed by a PI controller which causes a corresponding change in the firing angle α. The value provided by the PI controller is used as the input to the TCR firing angle control unit where the firing pulse is calculated. The zero-crossing of the V_{bus} voltage signal is taken as the reference for the firing angle. Figures 8.17 and 8.18 show the digital implementation of the power circuit and control scheme respectively. Both diagrams were developed using PSCAD/EMTDC v3.04 for PCs.

Two experiments are carried out as follows:
In experiment 1 the constant AC voltage source V_S feeds *Load 1* only. The SVC is connected in parallel with the load and it is controlled in open-loop mode. The firing angle α for the thyristors is set at 115°. As mentioned above, with $\alpha = 115°$ the power exchange between the SVC and the AC system is close to zero for the SVC parameters and load conditions shown in Figure 8.17. The voltage V_{rms} at the load point is close to 0.96 p.u. At a time $t = 0.6$ s, *Load 2* is switched on by closing *Brk*, with the load overall increasing. Under the new load conditions the voltage at the load point drops by as much as 16%, giving a V_{rms} value equal to 0.8 p.u., as shown in Figure 8.19(a).
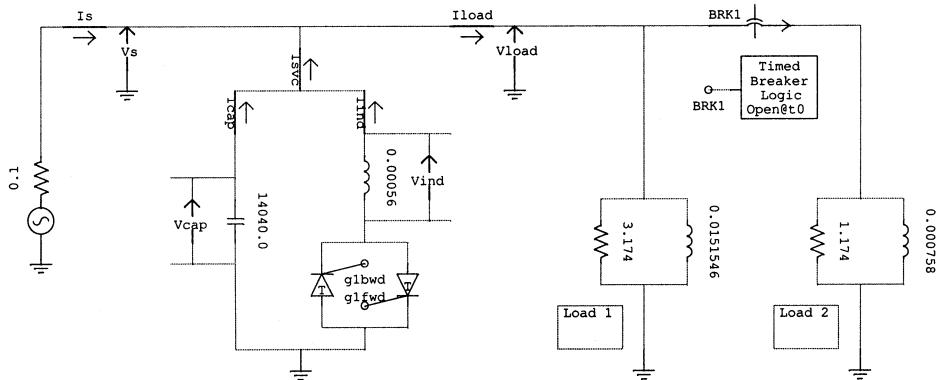
Fig. 8.17 SVC power circuit implemented in PSCAD/EMTDC.
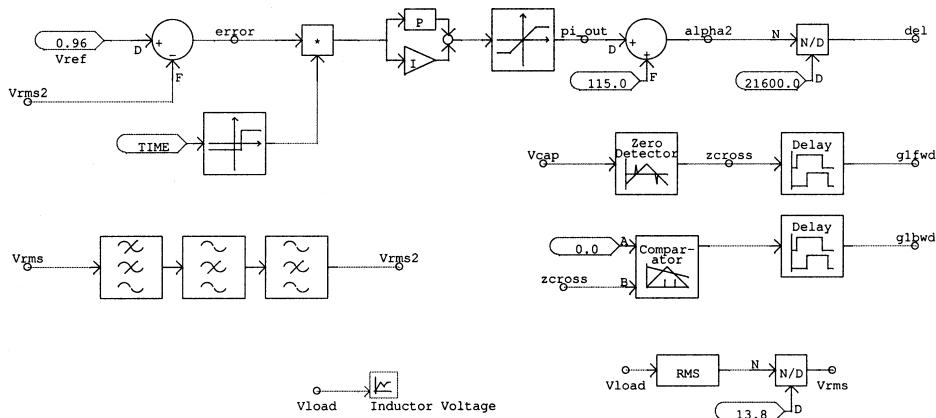
Fig. 8.18 SVC control scheme implemented in PSCAD/EMTDC.

In experiment 2, the SVC is controlled in closed-loop mode, in order to restore the voltage back to the original value of 0.96 p.u. At $t = 0.6$ s, the SVC begins to control the firing angle α of the back-to-back thyristors, changing the effective reactance X_{SVC} in such a way that the SVC injects capacitive current into the AC system. By using this reactive compensation control scheme the voltage is regulated and driven back to the original value as shown in Figure 8.19(b).

Figure 8.20 shows the voltage V_{load} waveform at the load point for both operating conditions, with no reactive compensation (Figure 8.20(a)) and with the SVC injecting capacitive current (Figure 8.20(b)). It can be observed that when the SVC is operating in closed-loop mode the voltage is kept constant, at the reference value, even when the load has increased. A delay of almost two cycles due to the parameters selected for the controller can be seen in the response.

The waveform of the SVC current I_{SVC} is shown in Figure 8.21. It should be noted that the current I_{SVC} increases considerably when the SVC starts voltage regulation. Due to variations in the firing angle α, the effective impedance X_{SVC} changes and
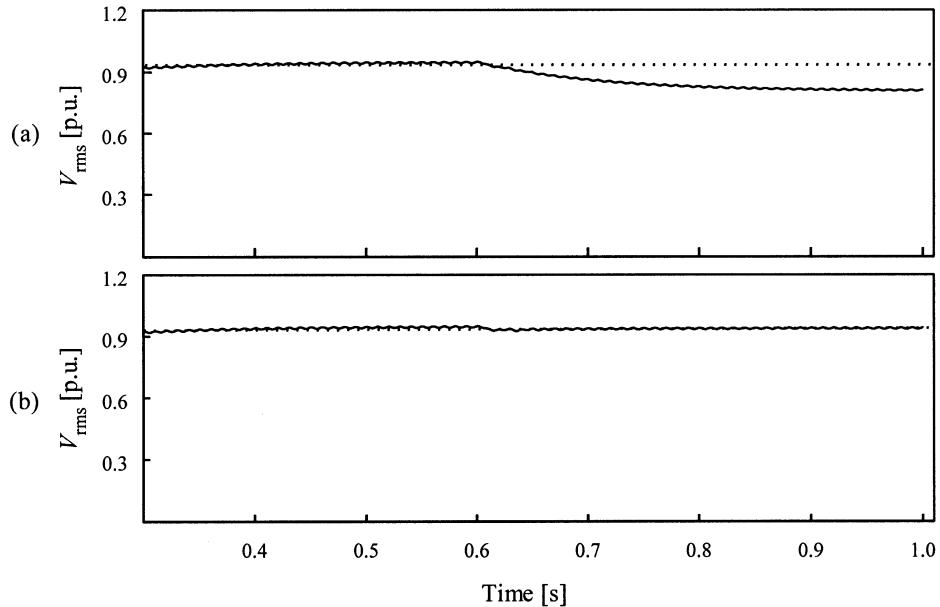
Fig. 8.19 Voltage V_{rms} at the load point: (a) with SVC operating in open-loop mode; and (b) with SVC operating in closed-loop mode.
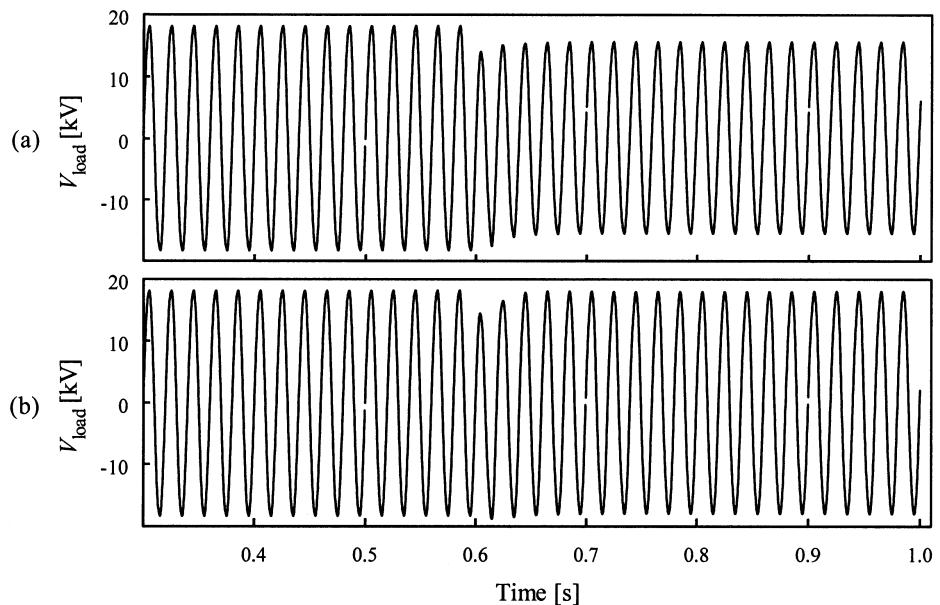
Fig. 8.20 Voltage V_{load} at the load point: (a) with SVC operating in open-loop mode; and (b) with SVC operating in closed-loop mode.
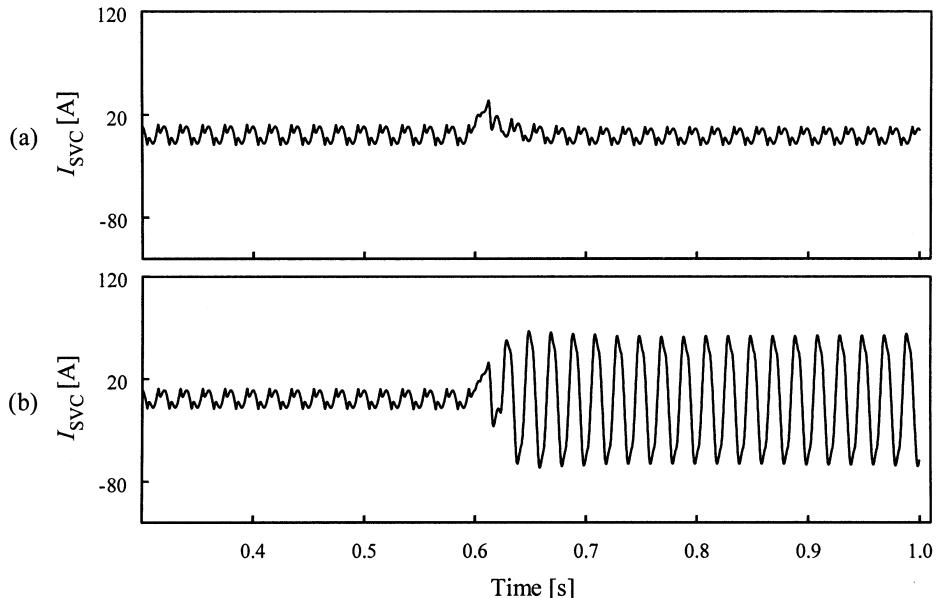
Fig. 8.21 SVC current I_{SVC}: (a) with the SVC operating in open-loop mode; and (b) with the SVC operating in closed-loop mode.
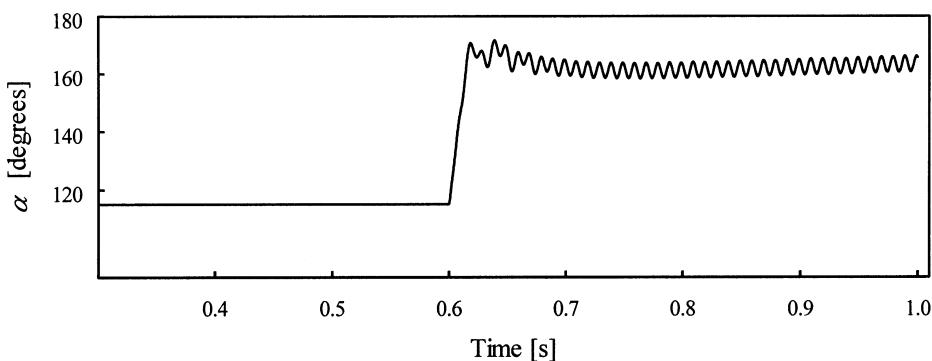
Fig. 8.22 Firing angle α with SVC operating in closed-loop mode.

consequently the current I_{SVC} rises abruptly to meet the compensation requirements. Figure 8.22 illustrates the response of the firing angle α. As mentioned above, when the SVC operates in open-loop mode α has a fixed value of 115°. When the closed-loop control is enabled the angle α changes abruptly to nearly 170° in order to supply the reactive power required by the AC system and then it decreases to a steady state value of $\alpha \approx 162°$.

Figures 8.23 and 8.24 show the waveforms in each element of the SVC, with the SVC controller in open-loop and in closed-loop modes, respectively. These figures show the behaviour of the currents and voltages in both the TCR and in the capacitor for the two different operating conditions. Specifically, in Figure 8.23, when the SVC
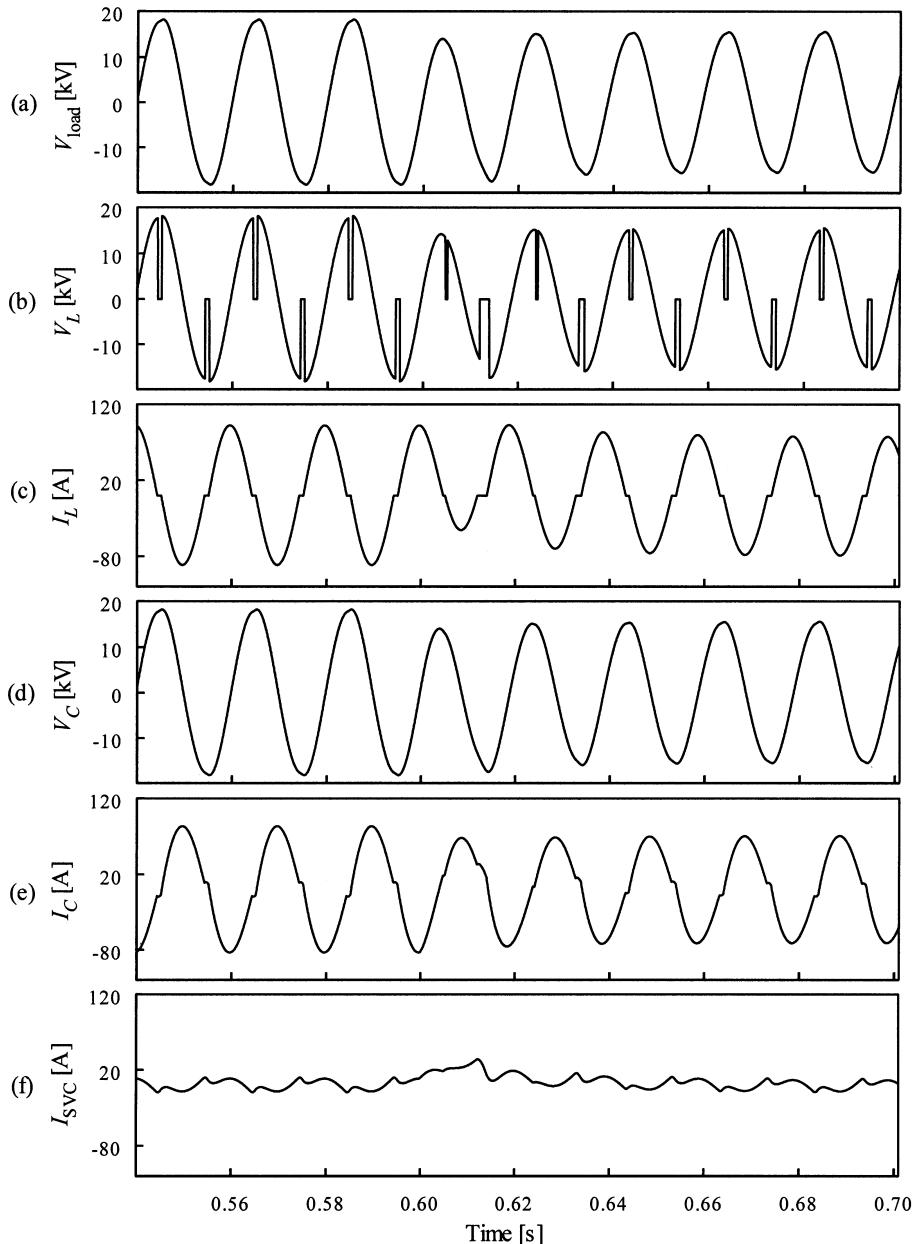
Fig. 8.23 SVC characteristic waveforms in open-loop mode: (a) voltage V_{load} at the load point; (b) voltage V_L at the SVC inductor; (c) current I_L through the SVC inductor; (d) voltage V_C through the SVC capacitor; (e) current I_C through the SVC capacitor; and (f) total current I_{SVC} through the SVC.

is in open-loop mode, the currents and voltages in the SVC decrease in response to an increase in load. However, after a small transient period, the current I_{SVC} recovers to the same wave shape that it had before the load change at $t = 0.6$ s. On the other
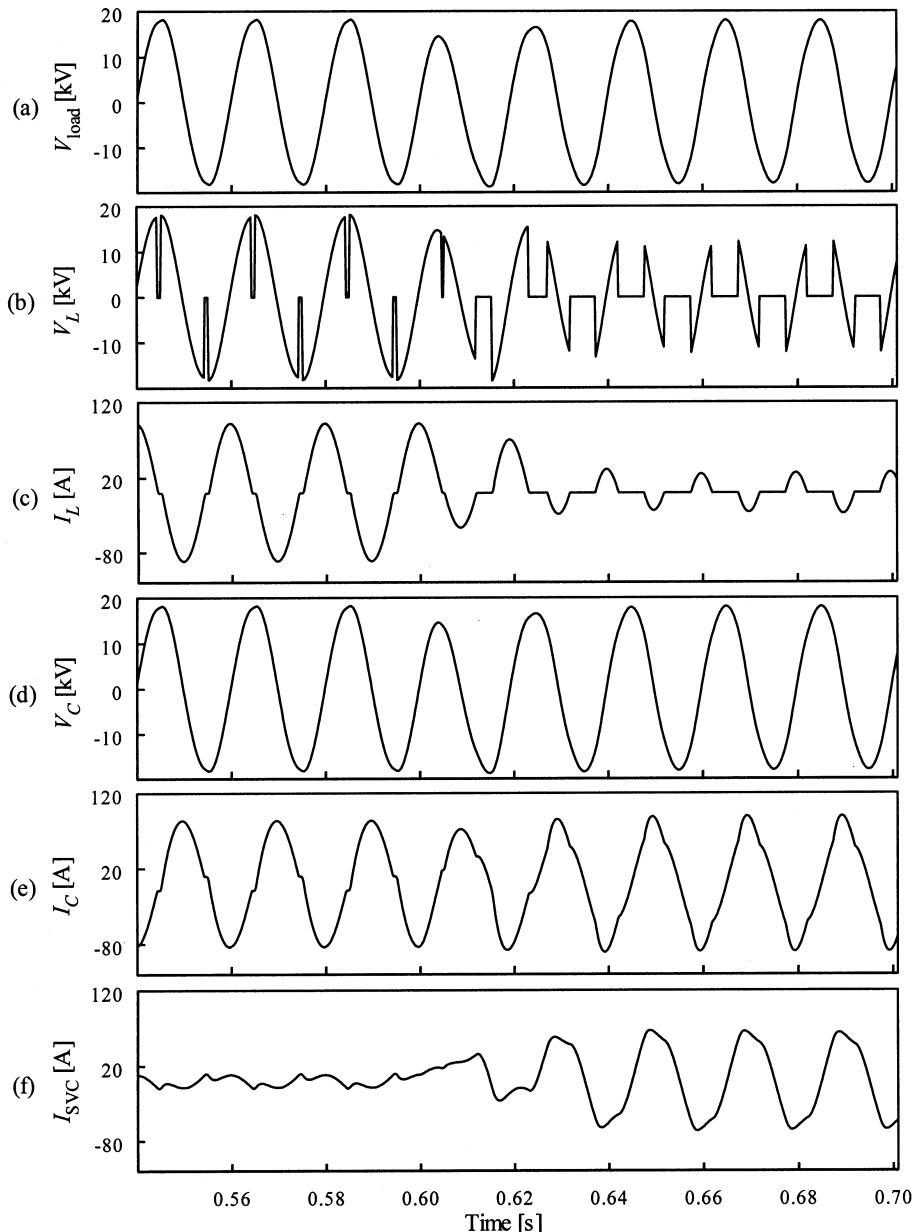
Fig. 8.24 SVC characteristic waveforms in closed-loop mode: (a) voltage V_{load} at the load point; (b) voltage V_L at the SVC inductor; (c) current I_L through the SVC inductor; (d) voltage V_C at the SVC capacitor; (e) current I_C through the SVC capacitor; and (f) total current I_{SVC} through the SVC.

hand, when the SVC is in closed-loop mode, the current through the reactor decreases considerably to the point that most of the SVC current flows through the capacitive element, as shown in Figure 8.24.

It is clear from these results that the SVC is an effective system controller which may be used to provide voltage regulation at the point of connection and to improve substantially the voltage quality in power systems. In most three-phase applications the SVC uses symmetrical voltage control (average value of 3 phases). However, the SVC can also be used to provide compensation to unbalanced three-phase loads and, at the same time, to restore voltage balance. This is achieved with a more sophisticated SVC control module.

8.5 Thyristor-Controlled Series Compensator (TCSC)

This section presents time domain simulations of the TCSC circuit and its implementation in PSCAD/EMTDC v3.04 for PCs. Two examples are presented:

1. Firstly, the basic model of the TCSC is implemented in PSCAD/EMTDC in order to identify its main characteristics.
2. Secondly, a test system representing a transmission network with an embedded TCSC system is implemented to show the effectiveness of the TCSC to provide line impedance compensation.

The TCSC is a key member of the FACTS family of power electronic controllers that provides smooth, rapid and continuous adjustment of the transmission line impedance. Figure 8.25 shows the equivalent circuit representation of the basic TCSC scheme, where a TCR is placed in parallel with a fixed capacitor. The controlling elements are the two back-to-back thyristors, connected in series with the linear reactor.

The TCSC has three fundamental modes of operation as follows:

1. thyristor-blocked mode
2. thyristor-bypassed mode
3. thyristor operating in phase-controlled mode.

In thyristor-blocked mode, the current through the TCR is zero and the TCSC functions as a capacitive reactance X_C. In thyristor-bypassed mode, the thyristor valves are fired with no delay and the TCSC has small inductive impedance. When the thyristor operates in phase-controlled mode, the value of the firing angle
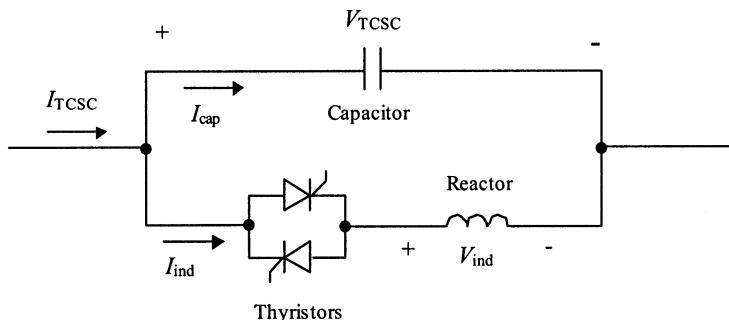
Fig. 8.25 TCSC basic scheme.

determines the direction of the current through the TCR and the capacitor, enabling the TCSC to work as either a capacitive or an inductive reactance. In this mode, the thyristor firing mechanism is controlled to vary the amount of effective reactance connected to the system (Jalali et al., 1994; Helbing and Karaday, 1994; Zhou, Liang, 1999).

The series capacitive compensation is bypassed during minimum loading in order to avoid transmission line overvoltages resulting from excessive capacitive effects in the system. Conversely, series capacitive compensation is fully utilized during maximum loading. The purpose of this operating strategy is to increase the transfer of power from generating sites to load centres, without overloading transmission lines.

8.5.1   Example 1

From the operational point of view, the TCSC shown in Figure 8.25 may be interpreted as a variable impedance which is a function of the thyristor firing angle α. In most applications, the voltage across the capacitor V_{TCSC} is taken as the reference voltage for the purpose of determining the thyristor firing angle α. The thyristors are fired when the capacitor voltage and current are opposite in polarity. This gives a range of 90–180° for the firing angle of the forward-connected thyristor. Firing the thyristors in this range results in a current flow through the inductor that opposes that in the capacitor, creating a loop flow. This loop current increases the voltage across the capacitor and the overall series compensation. This loop current increases as α decreases from 180 to 90°.

The main characteristics and waveforms of each element of the TCSC are obtained for the circuit shown in Figure 8.26. For the purpose of the simulation, a constant AC voltage source $V_{\text{S}} = 1\,\text{kV}$ is used to supply a series R–L load.

In order to perform the time domain analysis the circuit shown in Figure 8.26 is implemented in PSCAD/EMTDC, as shown in Figure 8.27. This figure shows both the power circuit and the open-loop control of the TCSC. The controller generates the firing signals for the thyristors based on a zero-crossing detector and a delay function block. In this case the TCSC is only connected between the constant AC voltage source and the linear series R–L load. The source voltage signal V_{S} provides a
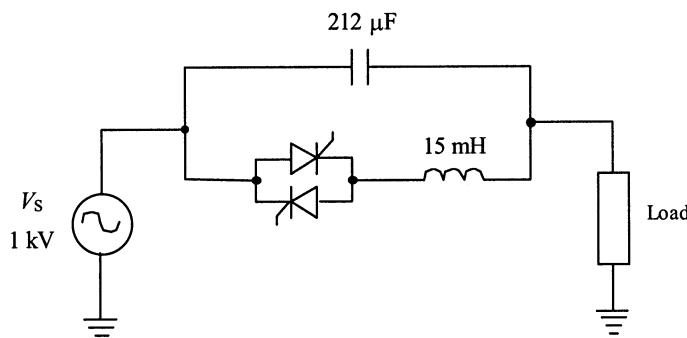
Fig. 8.26 Single-phase diagram used to simulate the operation of the TCSC and identify its main characteristics.
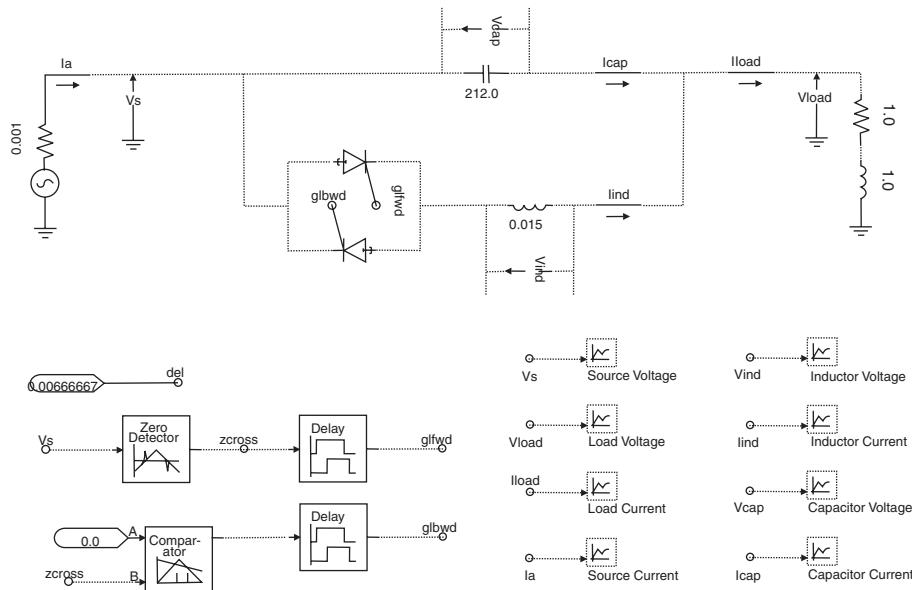
Fig. 8.27 TCSC basic circuit implemented in PSCAD/EMTDC.

constant and stable reference and it is taken as the input signal to the zero-crossing detector. Taking a fundamental frequency of $f = 50$ Hz, the delay function in the controller is adjusted in order to obtain a firing angle of $\alpha = 130°$.

The waveforms of the simulated TCSC model are shown in Figure 8.28 for a firing angle of $\alpha = 130°$ and a fundamental frequency of $f = 50$ Hz. Specifically, Figure 8.28(a) shows the source voltage and Figures 8.28(b) and 8.28(c) show the inductor voltage and current, respectively. Figures 8.28(d) and 8.28(e) show the voltage and current of the capacitor respectively. Note that the voltages V_S, V_L and V_C are in phase. It should also be noted that the zero-crossing of the source voltage V_S coincides with the negative peak of the inductor current I_L and with the positive peak of the capacitor current I_C.

The characteristic waveforms shown in Figure 8.28 can be obtained for any firing angle α in the range $90° < \alpha < 180°$. It is important to mention that in general the TCSC performance in the inductive region is not as smooth as in the capacitive region. In inductive operation conduction, the inductive current and the active losses are greater than in the capacitive region. Also, the capacitor current and voltage waveforms present higher harmonic distortion.

8.5.2   Example 2

The test system used in the example 2 is shown in Figure 8.29. Only one phase of the test system is used. It comprises of a constant AC voltage source feeding a linear series R–L load through three parallel branch transmission circuits. The equivalent impedance of each transmission path is adjusted to be equal, with one of them including a TCSC. As shown in Figure 8.29, the top branch contains a breaker, *Brk*, which is used to simulate the opening of this branch at a given point in time of
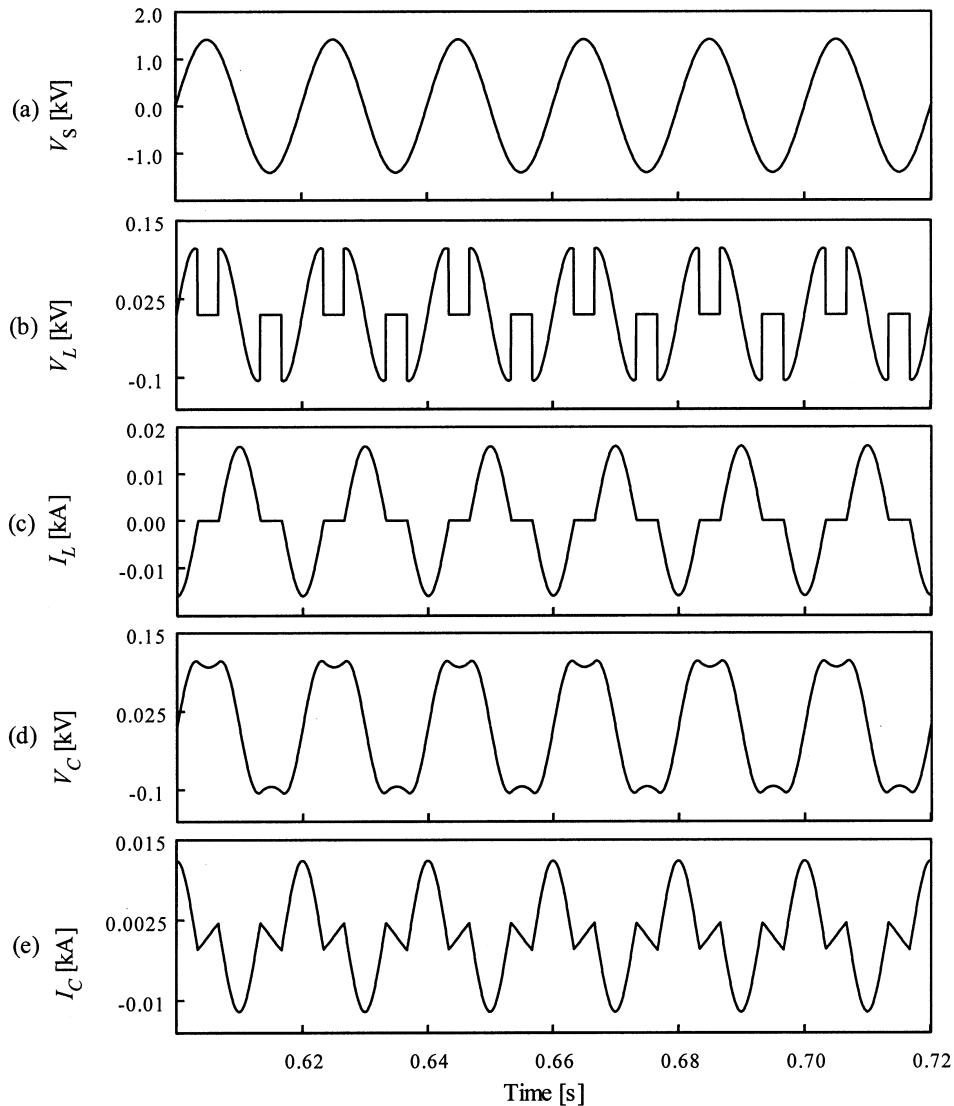
Fig. 8.28 TCSC characteristic waveforms for the model circuit with $\alpha = 130°$. (a) voltage V_S of the source; (b) voltage V_L at the TCSC inductor; (c) current I_L through the TCSC inductor; (d) voltage V_C at the TCSC capacitor; and (e) current I_C through the TCSC capacitor.

the transient simulation and to analyse the dynamic performance of the TCSC under the new operating condition. When *Brk* opens the equivalent impedance of the transmission system increases and consequently the current supplied to the load drops. Thus, the aim of the TCSC and its controller is to provide capacitive compensation to the remaining circuit consisting of two parallel inductive branches in such a way that the power flows and the current fed to the load remains at the same level as before.
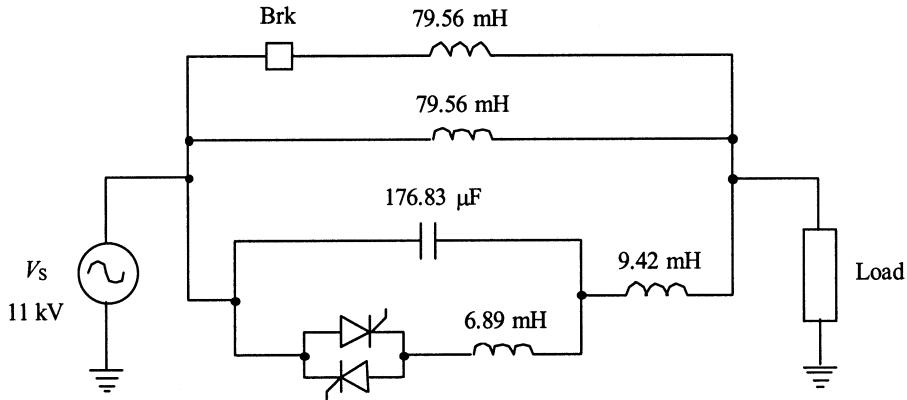
Fig. 8.29 Test system used to simulate the transient response of the TCSC in a medium-voltage transmission system.
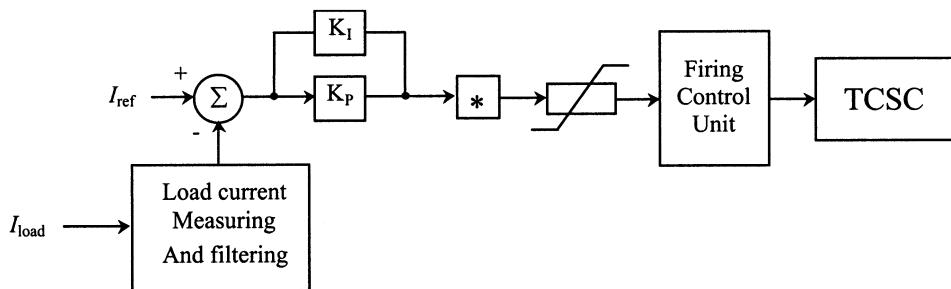
Fig. 8.30 A typical PI controller for a TCSC.

This application requires the TCSC to be controlled in a closed-loop fashion. For the purposes of this example the TCSC is operated by means of the control scheme shown in Figure 8.30. This particular scheme is based on measurements of the *rms* load current I_{load} which is compared against a reference value I_{ref} in order to obtain an error signal. Before the comparison is carried out, the *rms* current is filtered to eliminate any high-order harmonic which may exist in the signal and that may lead to the controller's spurious operation. The error signal is then processed by a PI controller that generates the appropriate thyristor's firing angle required to adjust the equivalent impedance of the TCSC and to drive the load current back to the reference or prefault value.

Before the firing signals are sent to the thyristors, the output of the PI controller is converted to angle units and properly conditioned to keep this angle within the limits. This is also required to avoid operation near resonant points. The firing control unit shown in Figure 8.30 includes the zero-crossing and delay functions. Also, the initial condition for the firing angle α may be set in this unit. In these simulations the thyristors are initially operated at a firing angle of $\alpha = 130°$, with no closed-loop control. Once the system reaches steady state, an electrical disturbance is created by opening *Brk*. Following this condition, the TCSC is operated with the closed-loop
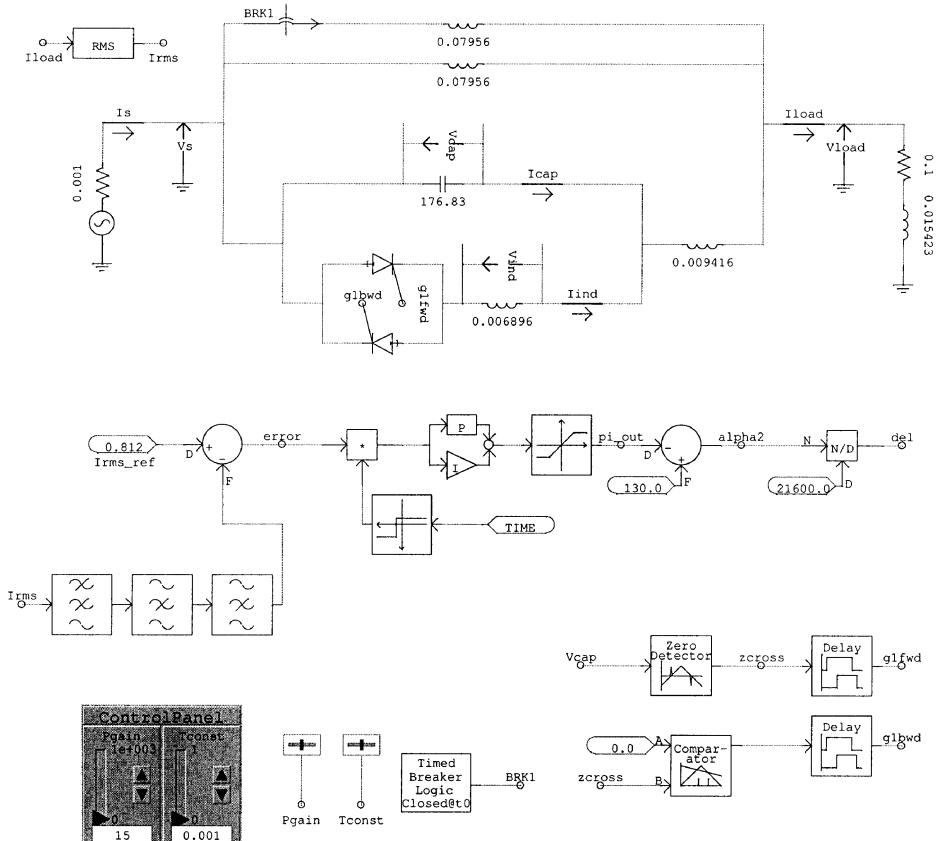
Fig. 8.31 Digital implementation in PSCAD/EMTDC of the test system used to simulate the TCSC in a line-impedance compensation application.

control mentioned above. PSCAD/EMTDC is used to implement the test system and the TCSC controller, resulting in the digital implementation shown in Figure 8.31.

The results of the simulation for this test system are presented in several figures as follows: Figure 8.32 shows the *rms* load current $I_{load, rms}$. Its steady-state value is approximately 0.8 p.u. Specifically, Figure 8.32(a) shows the *rms* load current $I_{load, rms}$ for the case when the TCSC is operated with open-loop control. Its new steady-state value drops to nearly 70% when *Brk* is opened at $t = 1.8$ s. Figure 8.32(b) shows once again the load current when the TCSC controller is in operation. It can be seen that the equivalent impedance of the transmission system is rapidly adjusted by the TCSC and that the load current is driven back to the reference value with almost no delay. The TCSC control scheme is shown to be effective for the requirements of this example. The waveforms of the load current and voltage at the load point are shown in Figures 8.33 and 8.34 for both operating conditions.

Figure 8.35 shows the characteristic of the firing angle α generated by the control scheme. It can be seen that before *Brk* opens the TCSC operates with a firing angle of $\alpha = 130°$ in open-loop fashion. At $t = 1.8$ s, when *Brk* opens and the TCSC
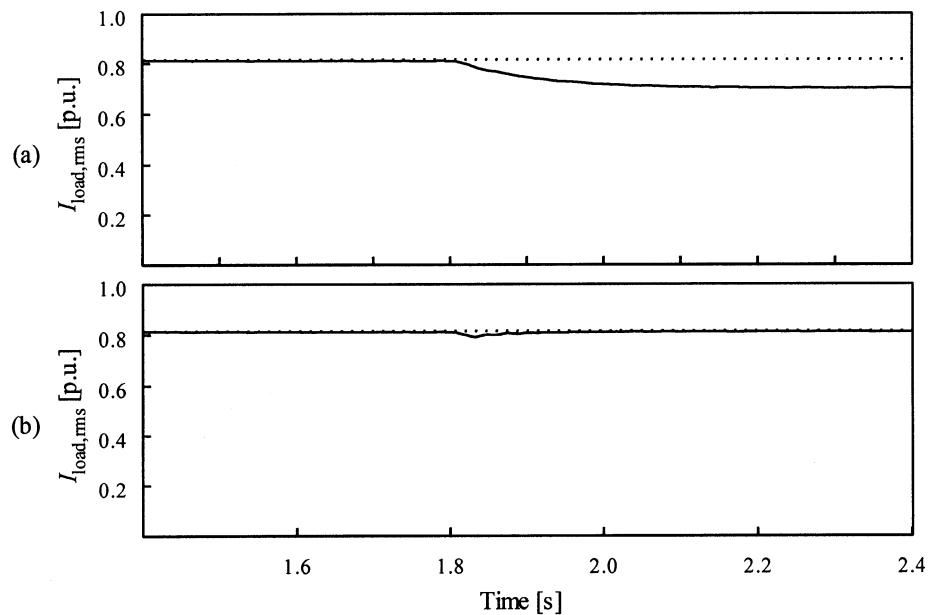
Fig. 8.32 Current $I_{load, rms}$ supplied to the load: (a) with TCSC in open-loop mode; and (b) with TCSC in closed-loop mode.
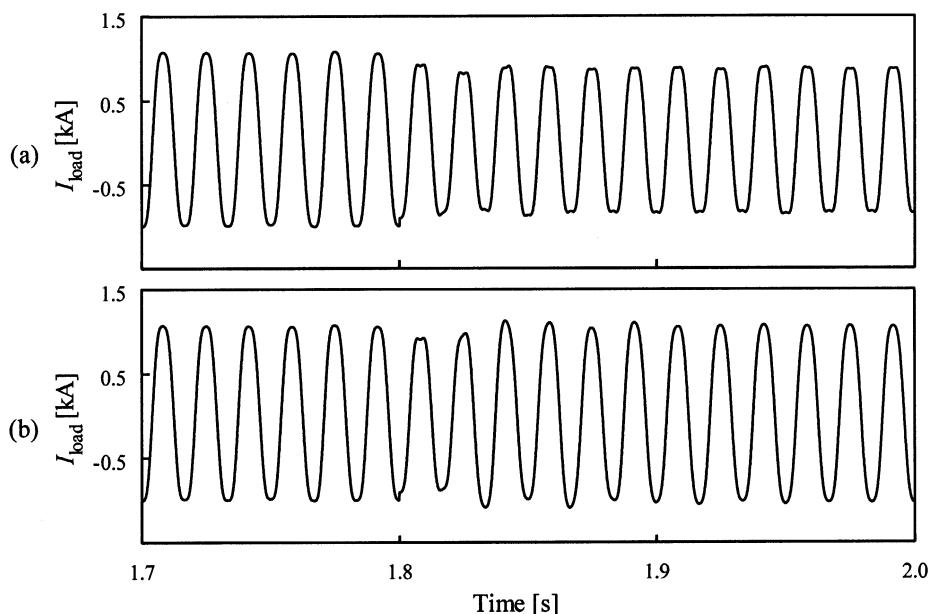
Fig. 8.33 Waveform of the current I_{load} supplied to the load: (a) with TCSC in open-loop mode; and (b) with TCSC in closed-loop mode.
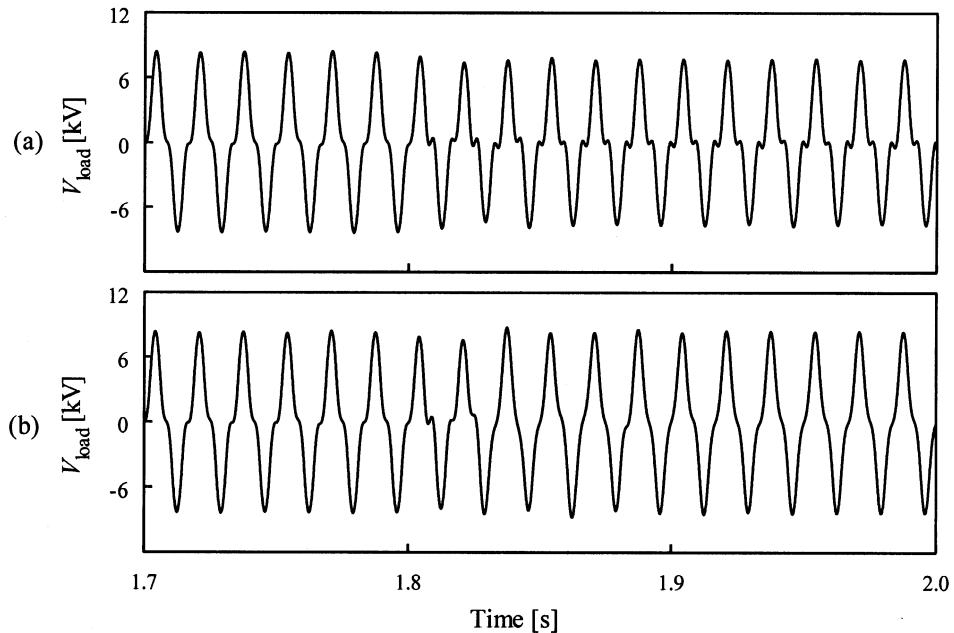
Fig. 8.34 Waveform of the voltage V_{load} at the load point: (a) with TCSC in open-loop mode; and (b) TCSC in closed-loop mode.

controller is set in operation, the angle α decreases from 130° to nearly 113° and it then settles down to a new steady-state value of approximately 117°.

By decreasing α the equivalent impedance of the TCSC becomes more capacitive thus reducing the inductive impedance of the overall transmission circuit.

Figure 8.36 shows the TCSC waveforms when it is operated in open-loop fashion. As a result of the rise in equivalent reactance both the capacitor and inductor voltages increase.

Figure 8.37 shows the TCSC waveforms operating in closed-loop mode. It can be seen in this figure that just after the disturbance has occurred, the capacitor and
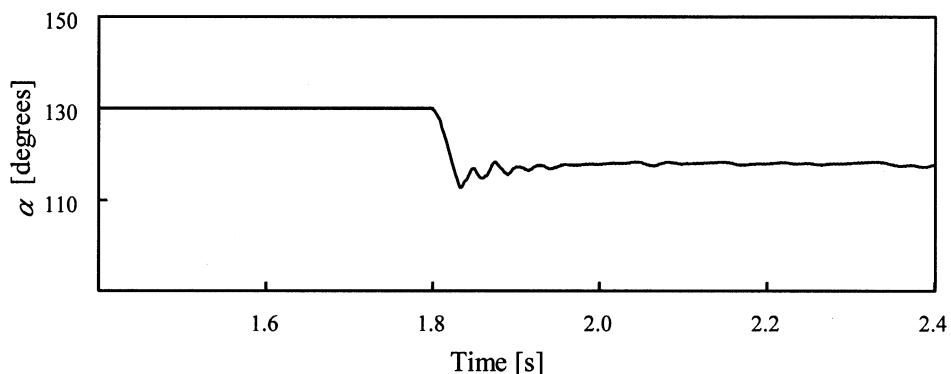
Fig. 8.35 Firing angle α processed by the TCSC closed-loop controller.
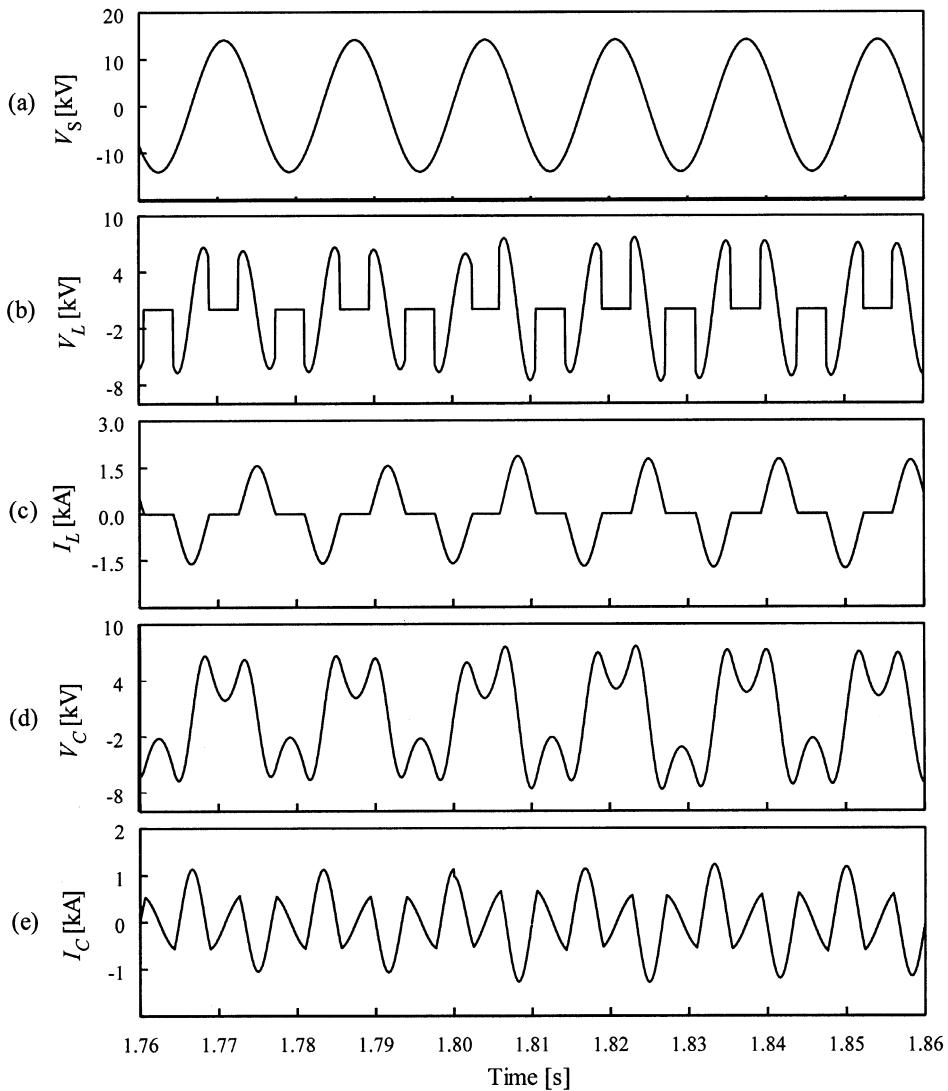
Fig. 8.36 Waveforms in the TCSC operating with open-loop control. Disturbance occurs at $t = 1.8$ s: (a) voltage V_S of the source; (b) voltage V_L at the TCSC inductor; (c) current I_L through the TCSC inductor; (d) voltage V_C at the TCSC capacitor: and (e) current I_C through the TCSC capacitor.

inductor voltages start to decrease and have no longer half- and quarter-wave symmetry. This is mainly due to the sudden change in firing angle value from 130° to 113°. Nevertheless, as the system reaches the new steady-state condition, these voltages waveforms recover their symmetry.

These time-domain results show the effectiveness of the TCSC circuit to improve the transmission branch performance by means of rapid and smooth adjustment of the effective transmission circuit impedance. The main factors that affect the TCSC
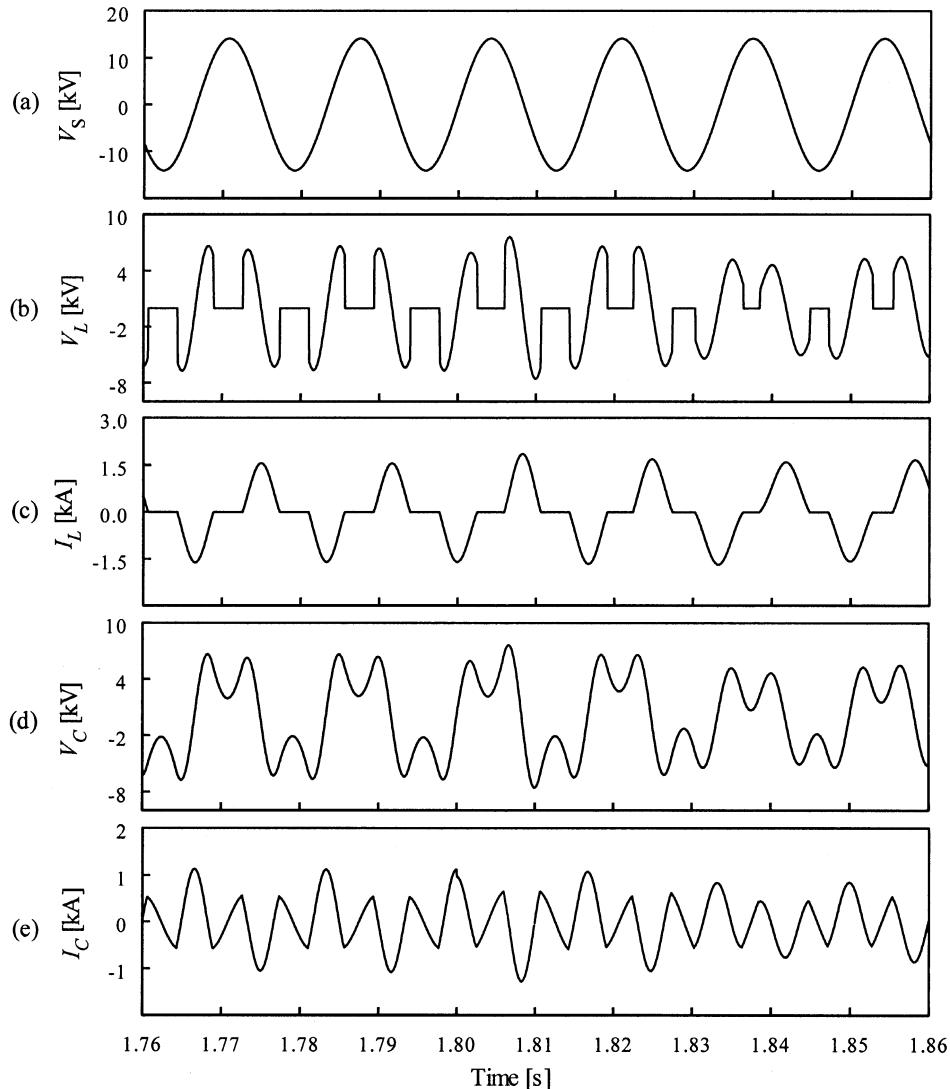
Fig. 8.37 Waveforms in the TCSC operating with closed-loop control. Disturbance occurs at $t = 1.8$ s: (a) voltage V_S of the source; (b) voltage V_L at the TCSC inductor; (c) current I_L through the TCSC inductor; (d) voltage V_C at the TCSC capacitor; and (e) current I_C through the TCSC capacitor.

response are the initial operating point for the firing angle α, the amount of change required, and the amount of net series compensation involved between operating points.

8.6 Static Compensator (STATCOM)

The STATCOM belongs to a family of power electronics controllers that base their operation on the VSC principle. These converter topologies have been presented in
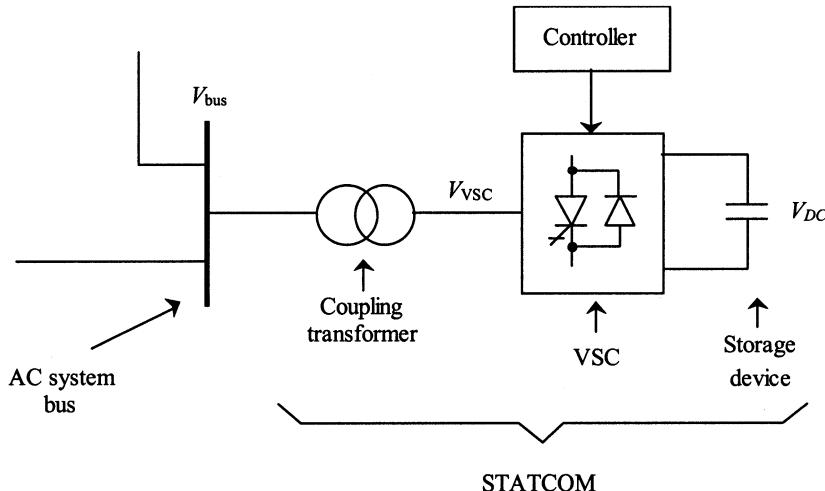
Fig. 8.38 Connection of the STATCOM with the AC system.

Chapter 6. Its performance is analogous to that of the rotating synchronous condenser. It may be used for the dynamic compensation of power transmission systems, providing voltage support and increased transient stability margins (Zhuang et al., 1996).

This section presents the modelling of the STATCOM used in both, transmission (FACTS) and distribution (CP) systems applications to provide reactive power compensation and voltage regulation at the point of connection. The principle of operation and main characteristics of the STATCOM are described followed by particular example cases of its use as a FACTS and CP controller.

The most basic configuration of the STATCOM consists of a two-level VSC with a DC energy storage device, a coupling transformer connected in shunt with the AC system, and the associated control circuits. Figure 8.38 depicts the schematic diagram of the STATCOM. The DC energy storage device may be a battery, whose output voltage remains constant, or it may be a capacitor, whose terminal voltage can be raised or lowered by inverter control, in such a way that its stored energy is either increased or decreased.

The VSC converts the DC voltage across the storage device into a set of three-phase AC output voltages that are in phase and coupled with the AC system through the reactance of the coupling transformer, discussed in detail in Chapter 6. A key characteristic of this controller is that the active and reactive powers exchanged between the converter and the AC system, can be controlled by changing the phase angle between the converter output voltage and the bus voltage at the point of common coupling (PCC) (Ma et al., 1997; Han et al., 1998).

The single-phase equivalent circuit of a power system with a STATCOM controller is shown in Figure 8.39. If the magnitude of V_{VSC} is greater than that of V_{bus} then the STATCOM supplies reactive power to the AC system, and it draws reactive power from the AC system if the magnitude of V_{bus} is greater than that of V_{VSC}. With suitable variation of the phase angle between the STATCOM output voltage and the AC system voltage, the STATCOM can exchange active power with the AC system.
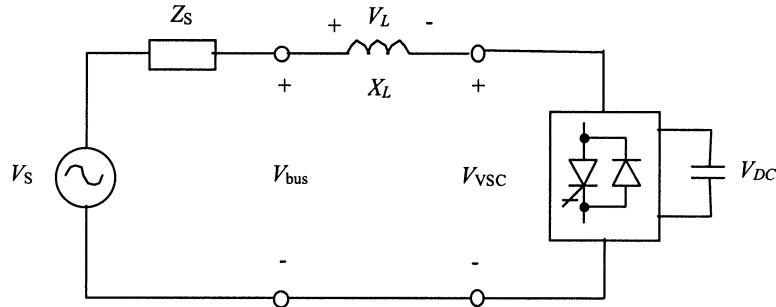
Fig. 8.39 Single-phase equivalent circuit of a power system with a STATCOM controller.

This exchange can be used to replenish the internal losses of the VSC and to keep the DC capacitor charged to the appropriate DC voltage, or to increase/decrease the capacitor voltage and thereby the magnitude of the output voltage of the STATCOM.

Figure 8.40 shows the steady state vector representation at the fundamental frequency for capacitive and inductive modes, and for the transition states from capacitive to inductive and vice versa. The terminal voltage V_{bus} is equal to the sum of the inverter voltage V_{VSC} and the voltage across the coupling transformer reactance V_L in both capacitive and inductive modes. The transition from capacitive to
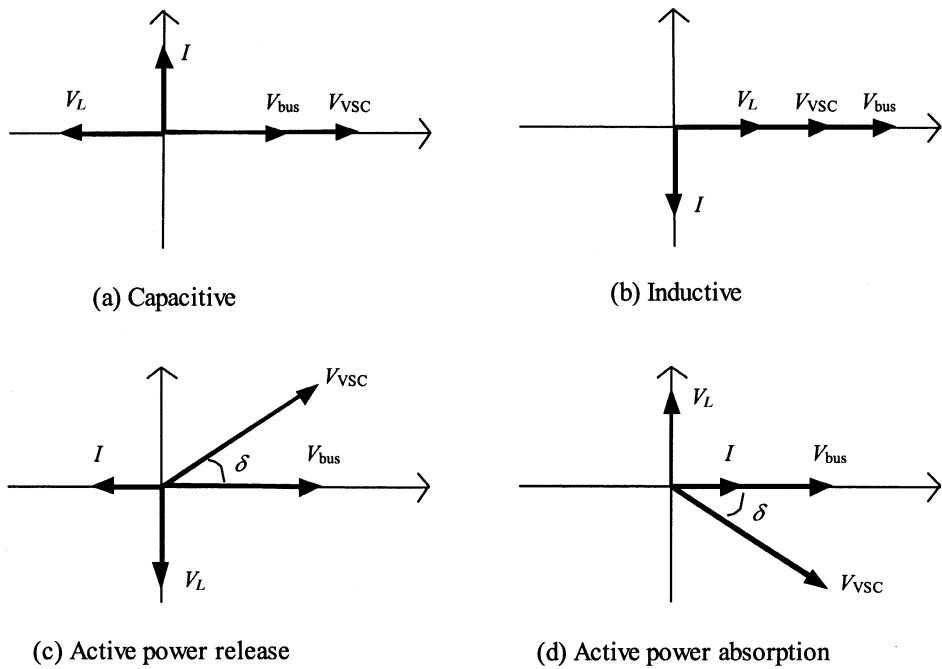
Fig. 8.40 STATCOM vector representation.

inductive mode occurs by changing the angle δ from zero to a positive value. The active power is transferred from the DC capacitor to the AC terminal and causes the DC link voltage to drop. The transition from inductive to capacitive mode occurs by changing the angle δ from zero to a negative value. The active power is transferred from the AC terminal to the DC capacitor and causes the DC link voltage to rise.

With reference to Figure 8.39 and Figure 8.40, the active and reactive power may be expressed by the following equations

$$P = \frac{V_{\text{bus}} V_{\text{VSC}}}{X_L} \sin \delta \tag{8.12}$$

$$Q = \frac{V_{\text{bus}}^2}{X_L} - \frac{V_{\text{bus}} V_{\text{VSC}}}{X_L} \cos \delta \tag{8.13}$$

In any practical STATCOM there are losses in the transformer windings and in the converter switches. These losses consume active power from the AC terminals. Accordingly, a small phase difference always exists between the VSC voltage and the AC system voltage. A summary of the power exchanges between the STATCOM and the AC system as a function of the STATCOM output voltage V_{VSC} and the AC system voltage V_{bus} is presented in Table 8.1.

From the analysis shown above it can be seen that the STATCOM can be controlled essentially by a single parameter: the phase angle between the VSC output voltage and the AC system voltage. Moreover, if the converter is restricted to reactive power exchange, then the AC output voltage is governed by only controlling the magnitude of the DC link voltage. This is possible due to the fact that the magnitude of the AC output voltage is directly proportional to the DC capacitor voltage.

The DC capacitor size may be selected by analytical methods (Moran et al., 1989) considering DC voltage ripple constraints and power rating. The use of analytical equations to determine the most appropriate DC capacitor size may be an involved task. Moreover, the DC capacitor size has a direct impact on the performance of the closed-loop controller and there will always exist a compromise between the VSC harmonic generation and the controller's speed of response (Xu et al., 2001). It is in this respect that electromagnetic transient simulators are very useful, providing an alternative way to select the size of the capacitor. This involves a straightforward trial and error process where the ripple constraint and the speed of response required in the controller are taken into account. The capacitor size is determined below using the transient simulator.

Table 8.1 Power exchange as a function of STATCOM voltage V_{VSC} and the AC system voltage V_{bus}

Voltage relation	Power exchange		
	STATCOM	⇔	AC system
$|V_{\text{VSC}}| > |V_{\text{bus}}|$	Q	⇒	
$|V_{\text{VSC}}| < |V_{\text{bus}}|$		⇐	Q
$\delta < 0$	P	⇒	
$\delta > 0$		⇐	P

The switching control of the VSC valves can be executed using two different techniques:

1. *Fundamental frequency switching* (*FFS*), where the switching of each semiconductor device is limited to one turn-on and one turn-off per cycle. With this technique the conventional six-pulse VSC produces a quasi-square-wave output with the inherent high harmonic content, as previously discussed in Chapter 6. As will be described later, when FFS is chosen, several six-pulse units are combined to form a multi-pulse structure in order to achieve better waveform quality and higher power ratings.

2. *Pulse-width-modulation* (*PWM*), where the semiconductor switches are turned on and off at a rate considerably higher than the power frequency. The output waveform is chopped and the width of the resulting pulses is modulated. This shifts the undesirable harmonics in the output to higher frequencies and filtering is possible with smaller components as was also illustrated in Chapter 6.

Both, the fundamental frequency and PWM switching approaches suffer from certain drawbacks for utility applications:

- The fundamental frequency switching approach requires complex transformer configurations to achieve low waveform distortion. In addition, the low switching frequency constrains the response rate and precludes incorporation of active harmonic filtering. Nevertheless, this is currently the preferred approach because of lower losses and higher semiconductor switch utilization. Present implementations of the STATCOM in high-voltage applications employ fundamental frequency switching.

- The PWM approach results in high switching losses and the fundamental frequency output obtainable is somewhat reduced. Consequently, at present PWM is less attractive for utility applications that require high efficiency and large power ratings. However, it has certain advantages such as faster response and capability for harmonic elimination, which could be exploited in the future with semiconductor switch improvements. However, PWM is preferred for CP low-voltage applications.

In low-to-medium voltage CP applications of VSC, PWM is widely used for suppression of harmonics and control of DC to AC voltage ratio. However, for FACTS applications, the high ratings of the converter will require valves of high power ratings, dictating slow switching speed and increased switching losses. With regards to the VSC electronic valves, VSCs using GTOs as the power devices are preferred for FACTS applications whereas VSCs using IGBTs are preferred for low-voltage CP applications (Zaho and Iravani, 1994; Edwards and Nannery, 1998; Raju et al., 1997).

8.6.1   STATCOM used as a FACTS controller

The output voltage waveform of the conventional six-pulse VSC contains harmonic components with frequencies of $[6k \pm 1] f$ (and its input current has related harmonic components with frequencies of $6kf$), where f is the fundamental output frequency and $k = 1, 2, 3, \dots$ The high harmonic content of the output voltage makes this simple inverter impractical for high-power applications.

Using the principle of *harmonic reduction*, the input and output of *n* basic six-pulse inverters (which are operated with appropriate relative phase-displacements) can be combined so as to obtain an overall $P = 6n$ multipulse structure. The frequencies of the harmonics present in the output voltage and input current of this *P-pulse* inverter are $[Pk \pm 1]f$ and Pkf, respectively. As can be seen, the harmonic spectrum improves rapidly with increasing pulse number. In addition, the amplitude of these harmonics is inversely related to the pulse number; that is, the amplitude of the *k-th* harmonic of the output voltage waveform is proportional to $1/[Pk \pm 1]$ and that of the DC supply current to $1/Pk$ (Gyugyi, 1994).

Consequently, the FACTS STATCOM uses many six-pulse VSCs, appropriately phase shifted, with their output combined electromagnetically to produce a nearly sinusoidal resultant waveform. The pulse number of such an arrangement is generally quoted as six times the number of basic inverters used, and provides an indication of the level of harmonic reduction achieved. For transmission line applications, a pulse number of 24 or higher is required to achieve adequate waveform quality without large passive filters. A single line diagram of a STATCOM system is shown in Figure 8.41. The VSC combines eight three-phase inverters into a 48-pulse
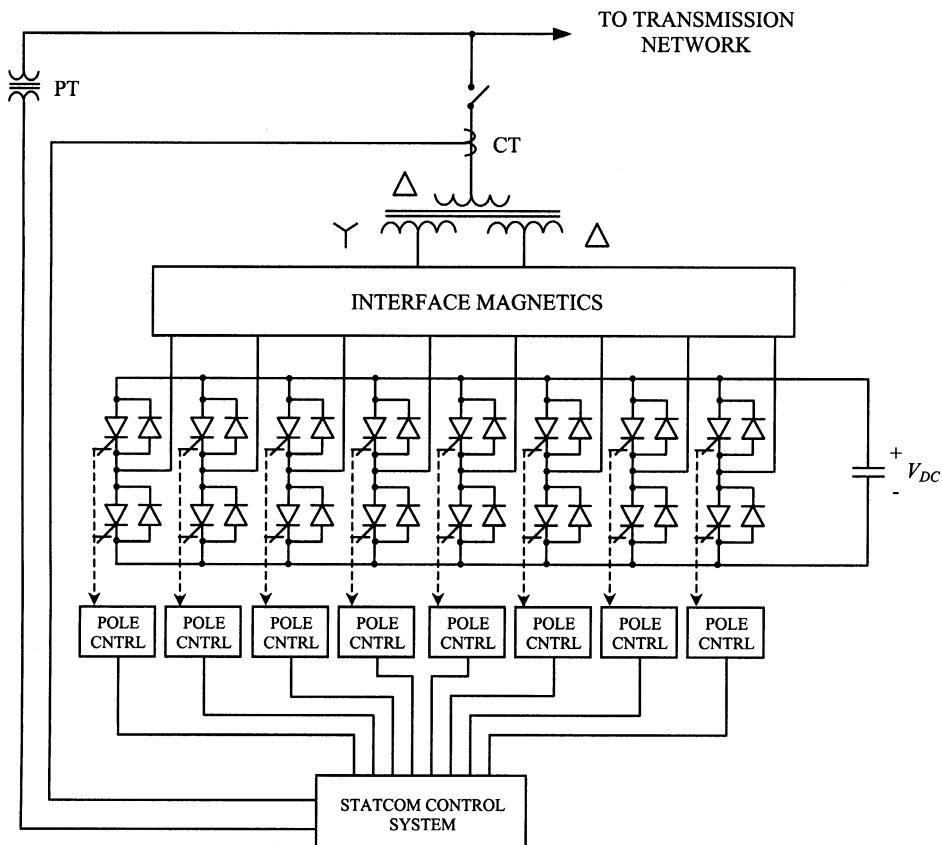
Fig. 8.41 Single-line diagram of a 48-pulse VSC-based STATCOM.
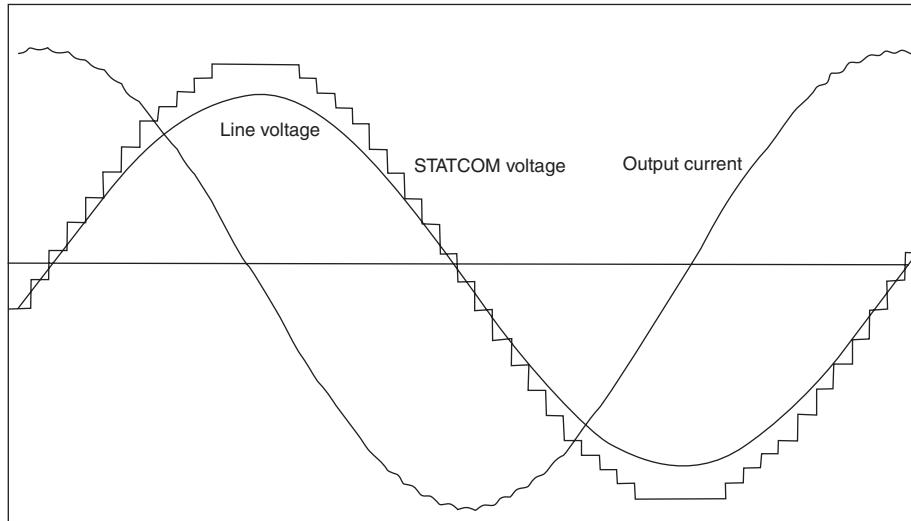
Fig. 8.42 Output voltage and current waveforms for a 48-pulse STATCOM generating reactive power.

configuration. The eight-inverter poles comprising sixteen GTO valves, depicted symbolically, are associated with one of the three output phases the STATCOM generates. Each inverter pole produces a square voltage waveform, progressively phase-shifted from one pole to the next by an appropriately chosen angle. These eight square-wave pole voltages are combined by magnetic summing circuits into two voltage waveforms displaced by 30°. One of these waveforms feeds the wye and the other the delta secondary of the main coupling transformer. The final 48-pulse output voltage waveform is obtained at the transformer primary. The voltage and current output waveforms are shown in Figure 8.42 (Schauder, 1997).

A simplified block diagram of the control system used for the 48-pulse STATCOM is shown in Figure 8.43. An inner feedback loop is used to regulate the STATCOM instantaneous reactive current. Note that this control is achieved by varying the phase angle α, of the inverter output voltage relative to the transmission line voltage. This technique makes it possible to maintain a constant maximum ratio between the converter output voltage and the DC capacitor voltage. The reference value for the reactive current control loop is generated by an outer loop responsible for the system voltage control. This outer control loop is similar to that used in conventional static var compensators, and includes an adjustable slope setting that defines the voltage error at full STATCOM reactive output.

A simple example is presented in this section where a 12-pulse STATCOM is implemented in PSCAD/EMTDC to illustrate the waveforms generated by the multipulse topology. The circuit used for this purpose is shown in Figure 8.44. The PSCAD/EMTDC implementations of this circuit and the switching controller are shown in Figures 8.45 and 8.46 respectively.

Figure 8.47 shows the output voltage and current waveforms generated by the 12-pulse VSC-based STATCOM of the example.
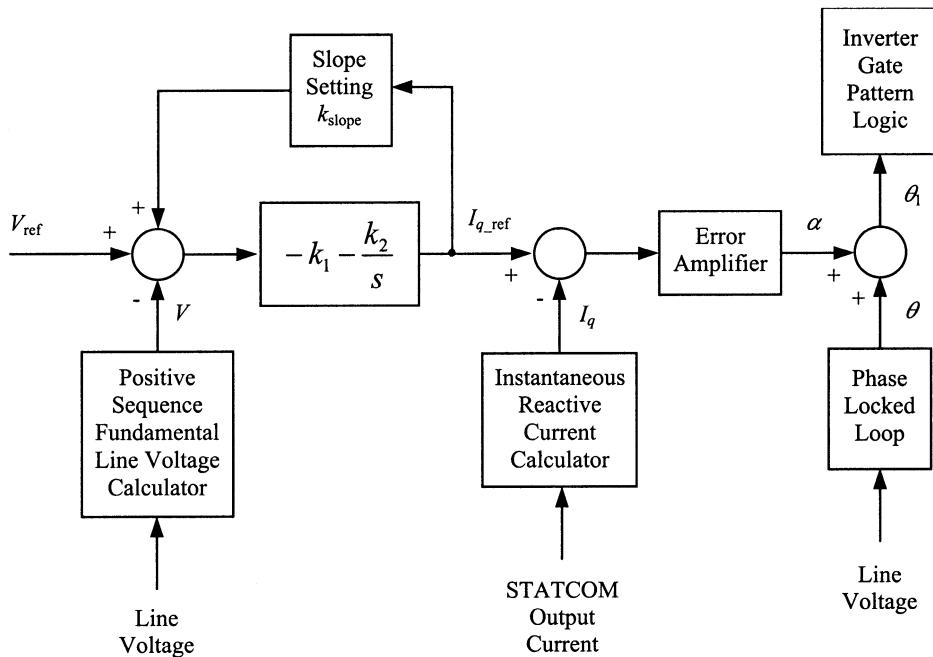
Fig. 8.43 Simplified block diagram of a typical STATCOM control system.
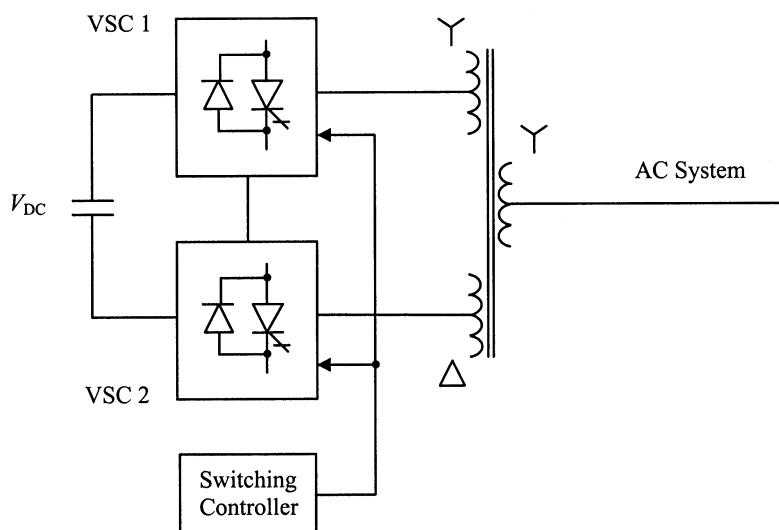
Fig. 8.44 Circuit used to implement a 12-pulse VSC-based STATCOM.
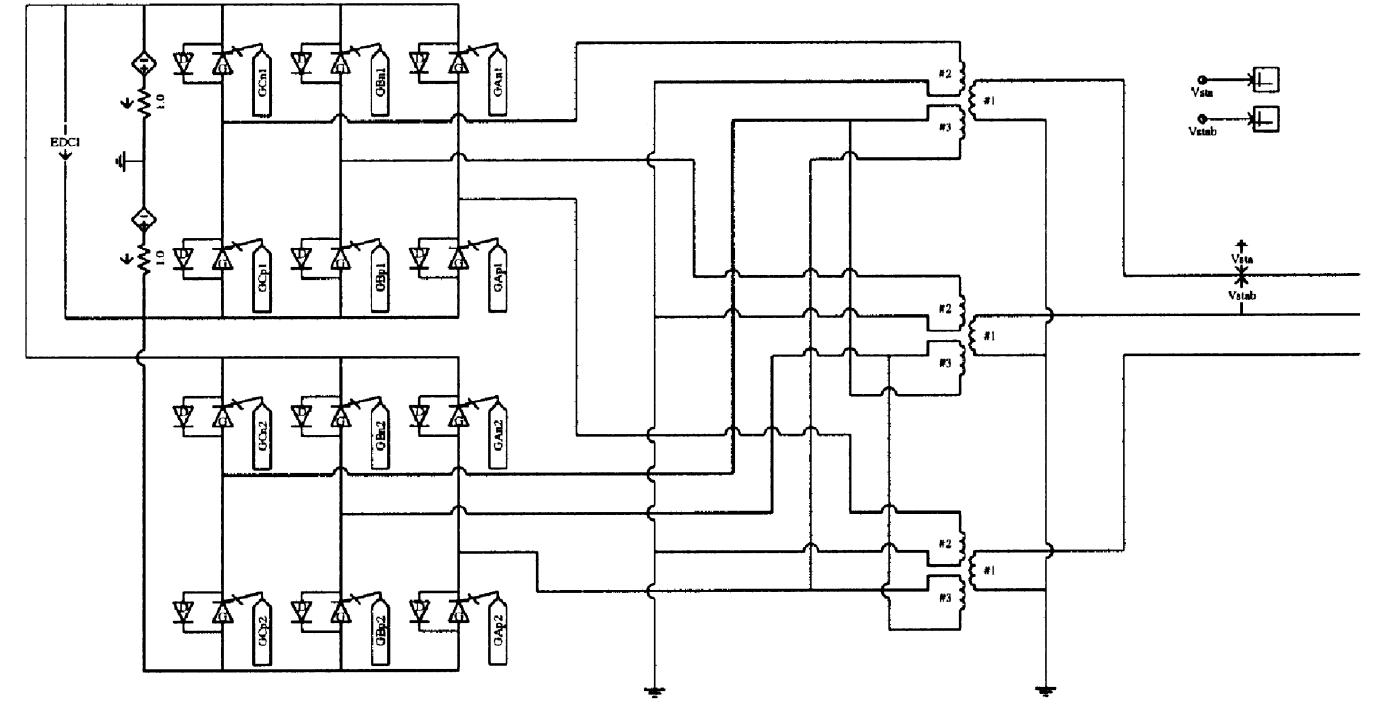
Fig. 8.45 Circuit of a 12-pulse VSC-based STATCOM implemented in PSCAD/EMTDC.
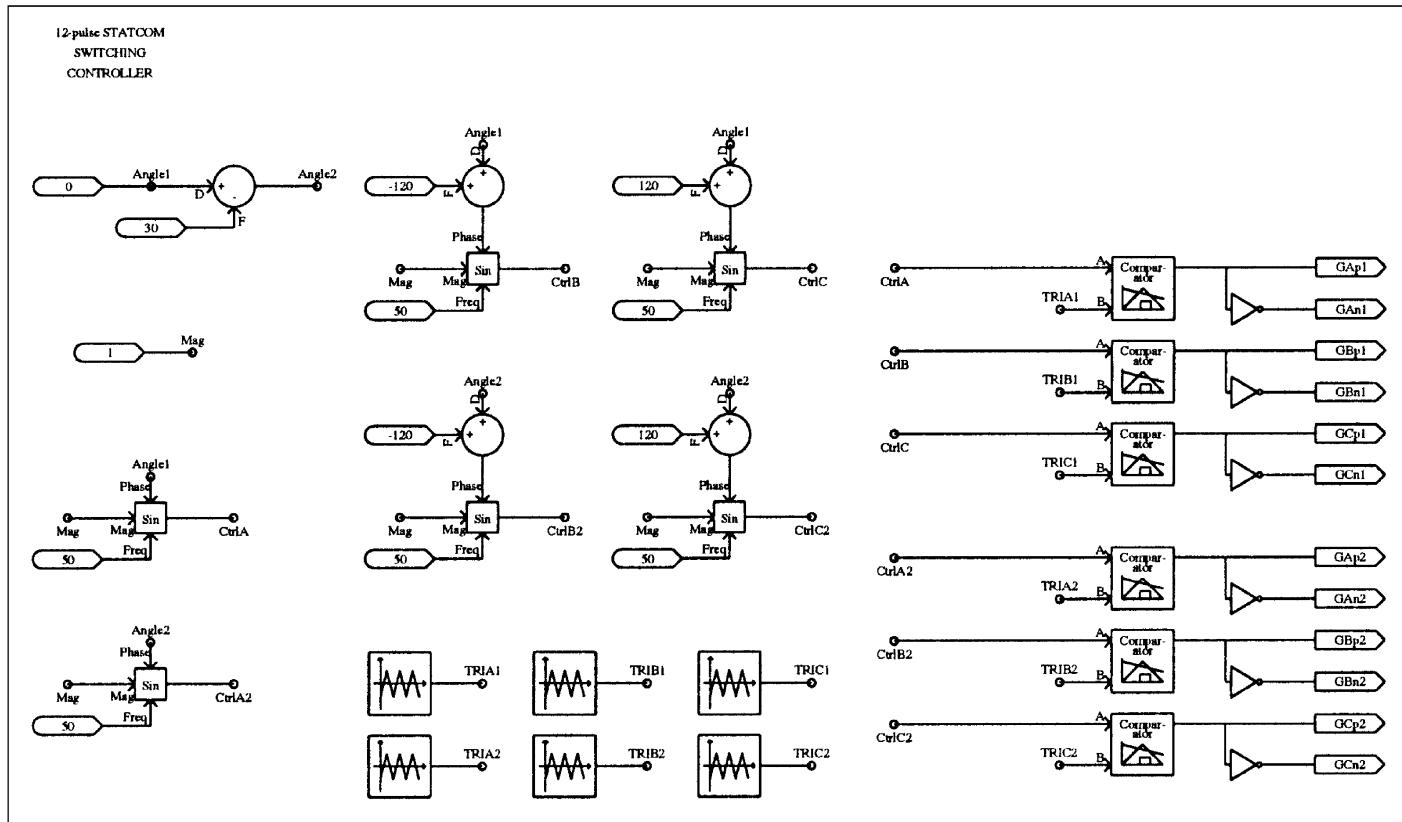
Fig. 8.46 Switching controller for the 12-pulse STATCOM implemented in PSCAD/EMTDC.

8.6.2 Distribution Static Compensator (D-STATCOM)

When used in low-voltage distribution systems the STATCOM is normally identified as Distribution STATCOM (D-STATCOM). It operates in a similar manner as the
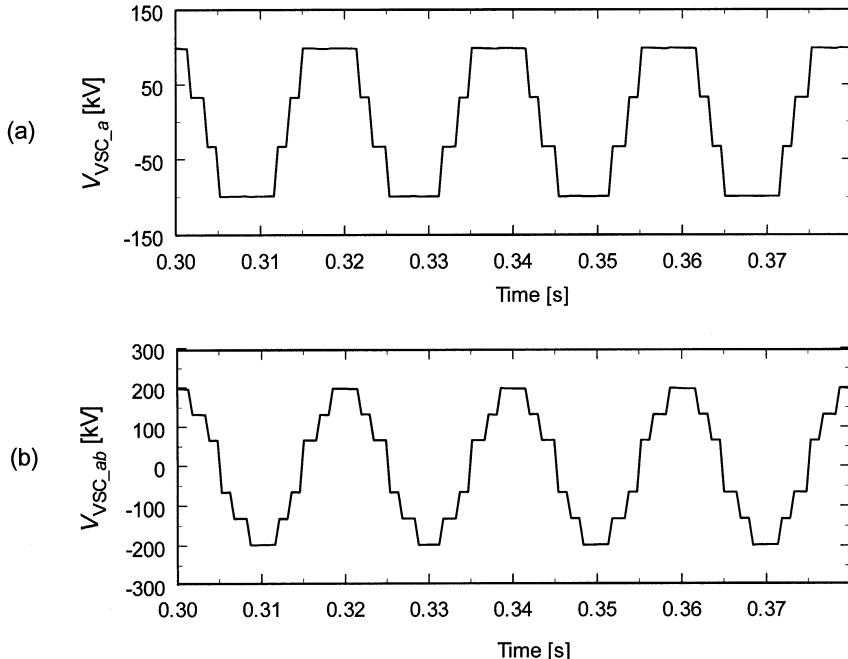
Fig. 8.47 Voltage generated by the 12-pulse VSC-based STATCOM: (a) phase voltage V_{VSC_a}; and (b) line voltage V_{VSC_ab}.
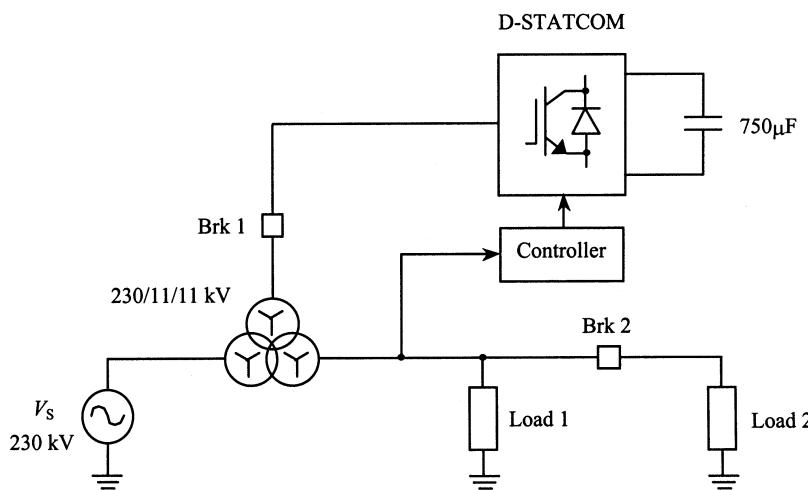
Fig. 8.48 Schematic diagram of the test system used to carry out transient analysis of the D-STATCOM.

STATCOM (FACTS controller), with the active power flow controlled by the angle between the AC system and VSC voltages and the reactive power flow controlled by the difference between the magnitudes of these voltages. As with the STATCOM, the capacitor acts as the energy storage device and its size is chosen based on power ratings, control and harmonics considerations. The D-STATCOM controller continuously monitors the load voltages and currents and determines the amount of compensation required by the AC system for a variety of disturbances. In this section, the D-STATCOM is modelled using the digital simulator PSCAD/EMTDC.

Figure 8.48 shows the schematic diagram of the test system used to carry out the transient modelling and analysis of the D-STATCOM. The test system comprises of a 230 kV three-phase transmission system, represented by a Thévenin equivalent feeding into the primary side of a three-winding transformer. A varying load is connected into the 11 kV, secondary side of the transformer. A two-level VSC-based D-STATCOM is connected to the 11 kV tertiary winding to provide instantaneous voltage support at the load point. A 750 μF capacitor on the DC side provides the D-STATCOM energy storage capabilities. Breaker *Brk1* is used to control the period of operation of the D-STATCOM and *Brk2* controls the connection of *Load 2* to the system.

In this particular example the aim of the D-STATCOM is to provide voltage regulation at the load point and mitigate the voltage sag generated when the load is increased. The system is considered to be operating under balanced conditions and both loads are linear. The D-STATCOM structure is based on a simple two-level VSC which is controlled using conventional sinusoidal PWM. Filtering equipment is not included in the design.

A block diagram of the control scheme designed for the DSTATCOM is shown in Figure 8.49. It is based only on measurements of the voltage V_{rms} at the load point. The voltage error signal is obtained by comparing the measured V_{rms} voltage against a reference voltage, V_{rms_ref}. The difference between these two signals is processed by a PI controller in order to obtain the phase angle δ required to drive the error to zero. The angle δ is used in the PWM generators as the phase angle of the sinusoidal control signal. The switching frequency used in the sinusoidal PWM generators is $f_{sw} = 1050$ Hz and the modulation index is $M_a \approx 1$. The digital implementation in PSCAD/EMTDC of the power system and D-STATCOM controller for this example are shown in Figures 8.50 and 8.51.

Simulations were carried out for both cases where the D-STATCOM was connected into the system and not. In the simulation interval 0.8–1.0 s the load is increased by closing *Brk2*.
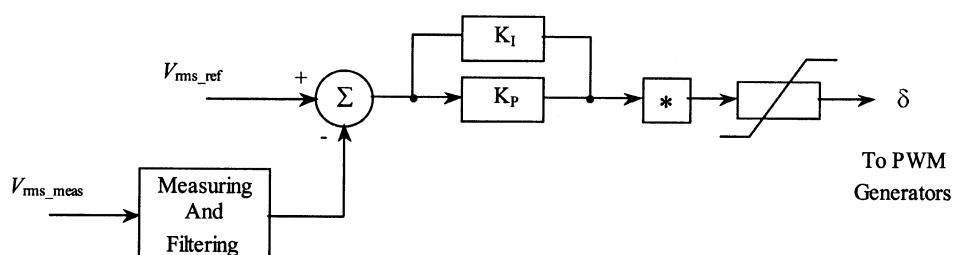
Fig. 8.49 Control scheme designed for the D-STATCOM.
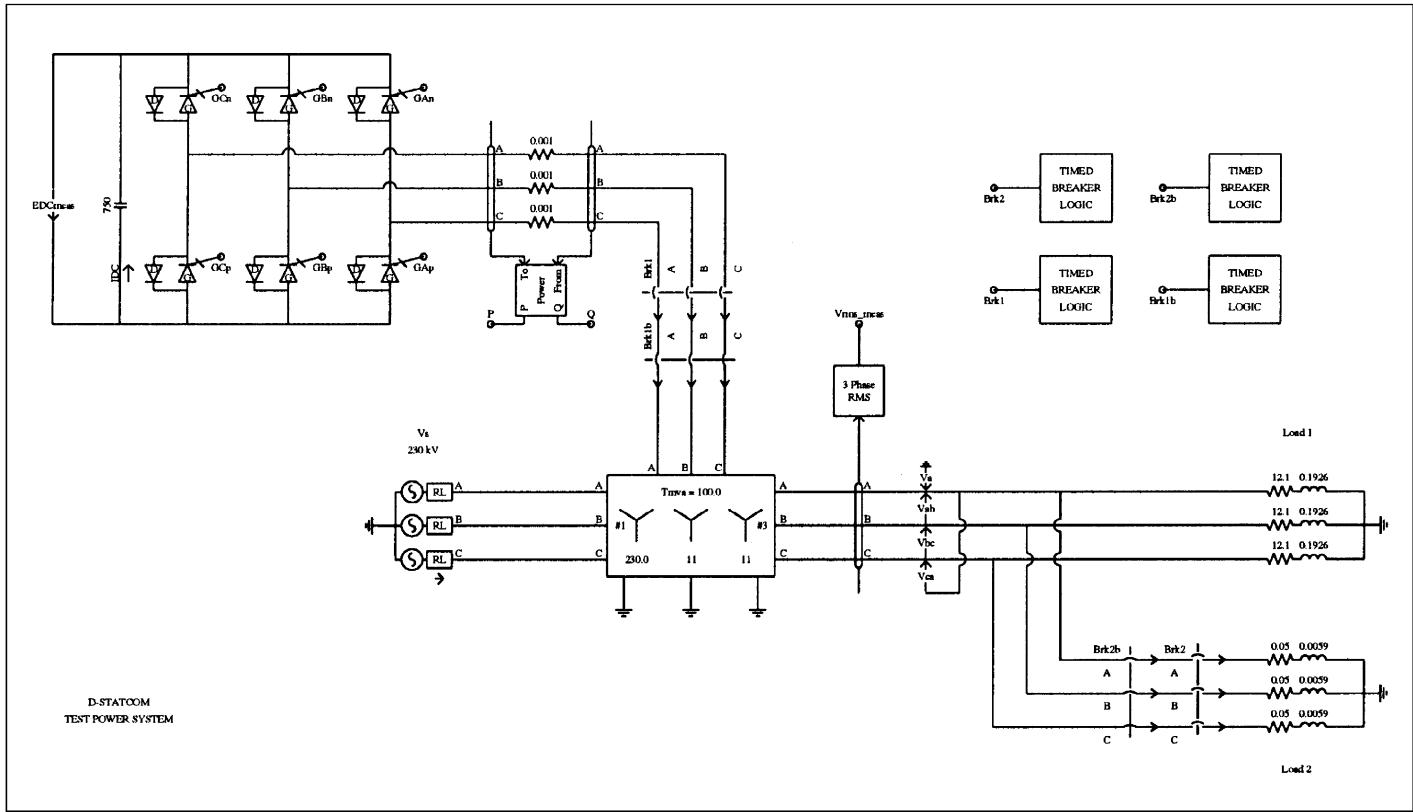
**Fig. 8.50** D-STATCOM test system implemented in PSCAD/EMTDC.
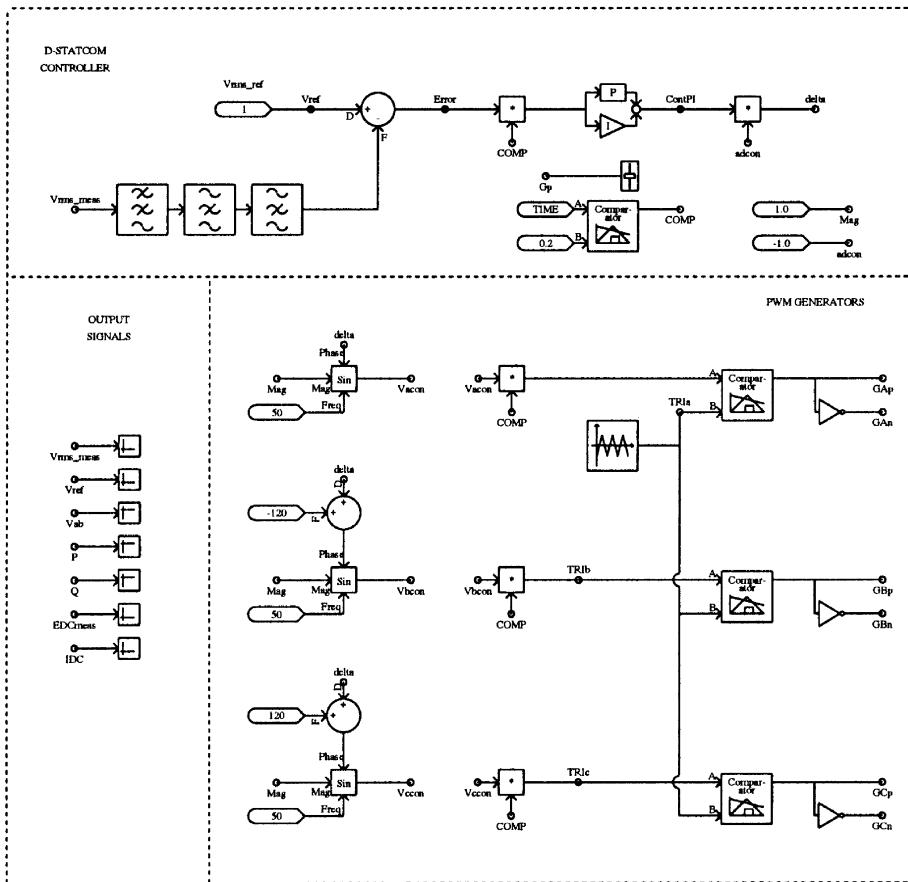
**Fig. 8.51** D-STATCOM controller implemented in PSCAD/EMTDC.
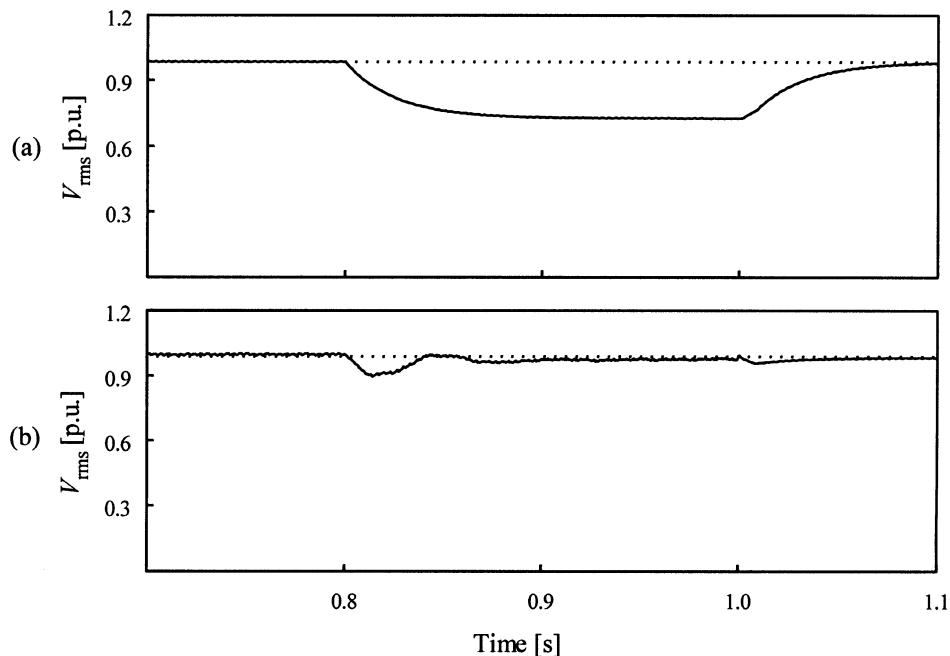
**Fig. 8.52** Voltage V_{rms} at the load point: (a) without D-STATCOM; and (b) with D-STATCOM operating.
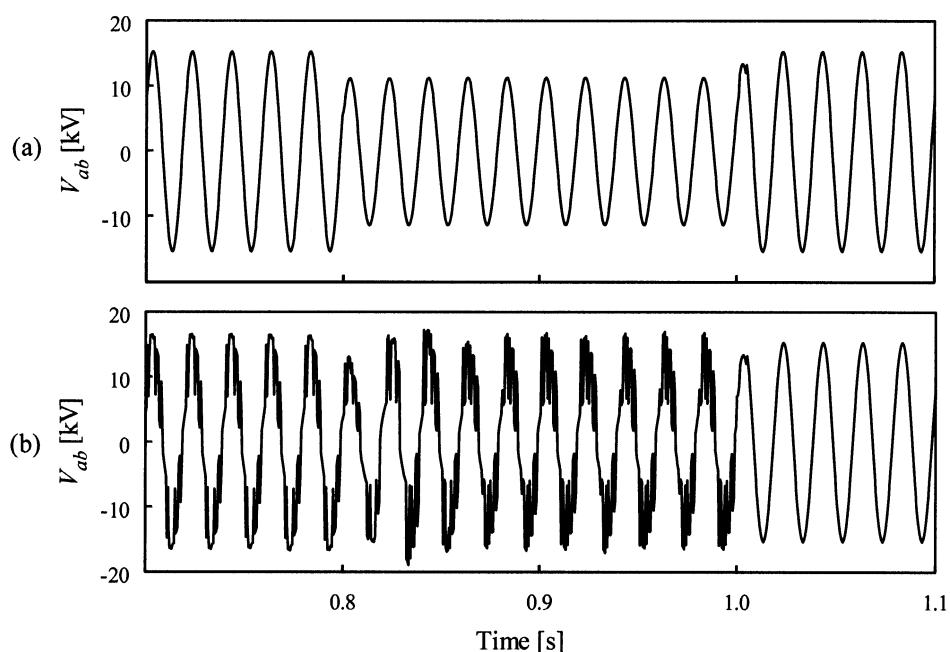
**Fig. 8.53** Voltage V_{ab} at the load point: (a) without D-STATCOM; and (b) with D-STATCOM operating.
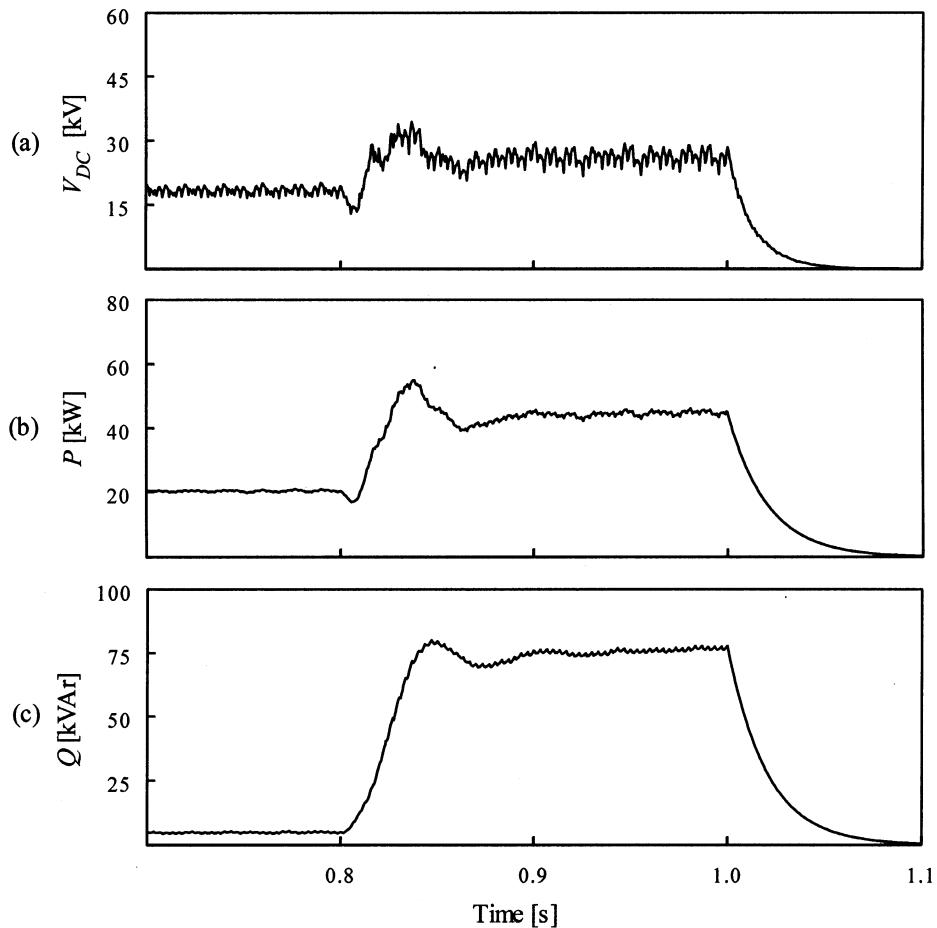
Fig. 8.54 (a) DC link voltage. Power exchange between the AC system and the D-STATCOM: (b) active power; and (c) reactive power.

Under this new operating condition the voltage at the load point experiences a voltage sag of 26% with respect to the reference value which is adjusted to be unity. In this same interval *Brk1* is closed and the D-STATCOM starts operating to mitigate the voltage sag and restore the voltage back to the reference value. Figure 8.52(a) shows the voltage V_{rms} at the load point without D-STATCOM and Figure 8.52(b) with the D-STATCOM in operation. It is possible to observe that the voltage sag is being minimized almost completely.

The regulated V_{rms} voltage shows a reasonably smooth profile. Figure 8.53 shows the line voltage V_{ab} at the load point for both operating conditions. As mentioned before, no filtering equipment has been used throughout the simulation. Figure 8.54(a) shows the DC voltage of the VSC. Before the D-STATCOM starts operating the capacitor is charged to a steady state voltage level of approximately 19 kV. This initial condition of the capacitor improves the response of the D-STATCOM and simplifies the requirements of the control system.

When the D-STATCOM is in full operation, the DC voltage increases to nearly 28 kV. As shown in Figure 8.54(b), in this period the D-STATCOM absorbs active power from the AC system to charge the capacitor and maintain the required DC link voltage level. The reactive power exchange between the AC system and the compensator is shown in Figure 8.54(c).

The results achieved through the digital simulations clearly show the capability of the D-STATCOM to mitigate voltage sags providing a continuously variable level of shunt compensation. The response of the controller is fast, and even when simple, it is effective for the operating conditions considered in the example.

The D-STATCOM has plenty of applications in low-voltage distribution systems aimed to improve the quality and reliability of the power supplied to the end-user. It can be used to prevent non-linear loads from polluting the rest of the distribution system. The rapid response of the D-STATCOM makes it possible to provide continuous and dynamic control of the power supply including voltage and reactive power compensation, harmonic mitigation and elimination of voltage sags and swells.

There are several factors that must be considered when designing the STATCOM and associated control circuits. In relation to the power circuit the following issues are of major importance:

- DC link capacitor size
- coupling transformer reactance and transformation ratio
- output filter equipment.

These elements must be properly selected bearing in mind the application's require-ments, voltage regulation and power compensation. The DC capacitor has direct influence on the harmonic distortion of the output voltage generated by the STAT-COM and the speed of response of the controller. If the capacitor is undersized the controller's response will be fast but the DC link voltage will have excessive ripple and consequently the output voltage will contain high levels of harmonic distortion. Moreover, high transient overshoots will exist. On the other hand, an oversized capacitor will improve the output voltage waveform shape and reduce the transient overshoots but at the expense of a sluggish controller's response. Besides, some oscillations will appear in the STATCOM response and if care is not taken in the adjustment of the PI parameters, the system may become unstable.

The selection of the coupling transformer parameters has a large impact on the performance of the STATCOM. It plays an important role in the value of voltage regulation and power compensation that the STATCOM can provide. In essence, the amplitude and the phase angle of the voltage drop across the transformer reactance define the active and reactive power flows between the STATCOM and the AC system. This reactance can be seen as a smoothing reactor that will attenuate medium and high order harmonics in the STATCOM output voltage.

8.7 Dynamic Voltage Restorer (DVR)

Similarly to the D-STATCOM, the DVR consists of a VSC, a switching control scheme, a DC energy storage device and a coupling transformer that in this case, is
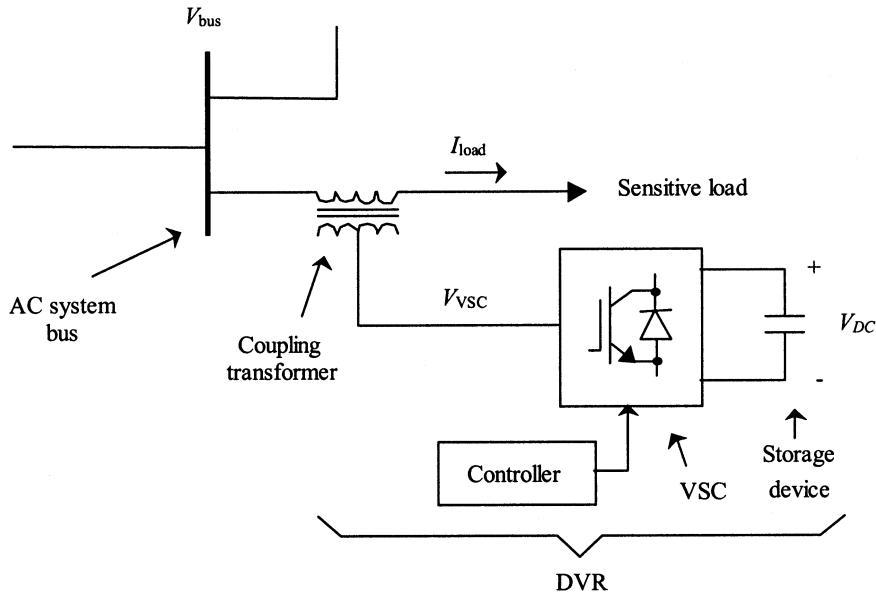
Fig. 8.55 Schematic representation of the DVR.

connected in series with the AC system, as illustrated in Figure 8.55. This controller is suited for solving a variety of power quality and reliability problems including (Osborne et al., 1995; Taylor, 1995; Chan and Kara, 1998):

- voltage sags and swells
- voltage unbalances
- voltage harmonics
- power factor correction
- outages.

The DVR injects a set of three-phase AC voltages in series and synchronized with the distribution feeder voltages of the AC system. The amplitude and phase angle of the injected voltages are variable thereby allowing control of the active and reactive power exchanges between the DVR and the AC system within predetermined positive (power supply), and negative (power absorption) limits.

   This section presents the time domain analysis of the DVR for the case when it is used to maintain constant voltage at the point of connection. The test system used to carry out the transient studies is shown in Figure 8.56. The DVR is connected in series with *Load 1* in order to protect this load against any disturbance that could appear in the system. In this example, the DVR must keep the voltage at *Load 1* point constant under a three-phase fault at point A. The DVR coupling transformer is connected in delta in the DVR side. It has a leakage reactance of 10% and unity turns ratio (no booster capabilities exist). The DC link voltage is assumed to be 2.5 kV.
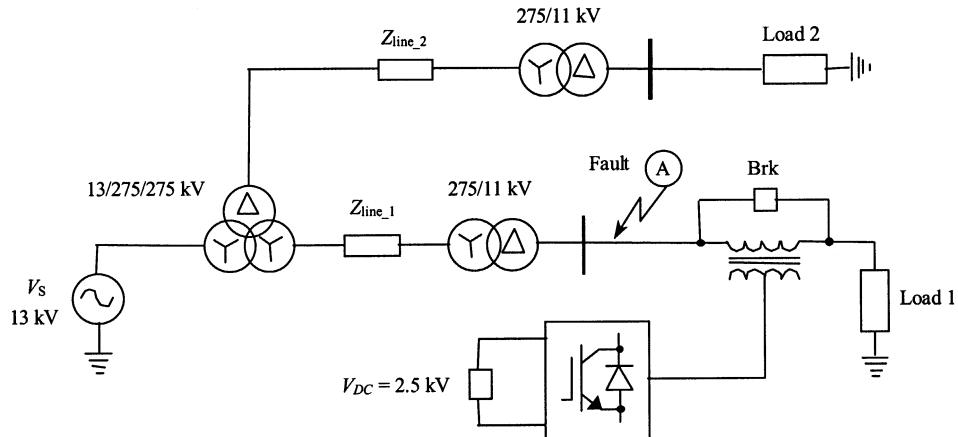
Fig. 8.56 Test system used to carry out the DVR transient analysis.

The simulation scenarios are as follows:

(i) In the first simulation the DVR is disconnected and a three-phase short-circuit fault is applied at point A, via a fault resistance of $0.66\,\Omega$, during the interval 0.8–1.0 s. The voltage sag at the load point is 25% with respect to the reference value.

(ii) The second simulation is carried out using the same scenario as above but now with the DVR in operation.

Figures 8.57 and 8.58 show the digital implementation in PSCAD/EMTDC of the power system and the DVR controller. Using the facilities available in the simulator, the DVR is simulated to be in operation only for the duration of the fault, as it is expected in a practical situation. The results for both simulations are shown in Figure 8.59. When the DVR is in operation, the voltage sag is mitigated almost completely, and the voltage V_{rms} at the load point is driven back to the reference as shown in Figure 8.59(b). The PWM control scheme controls the magnitude and the phase of the injected voltages, restoring V_{rms}. The sag mitigation is performed with a smooth, stable and rapid DVR response; acceptable overshoots are observed when the DVR comes in and out of operation. Figure 8.60 shows the V_a voltage at the sensitive load point. Figure 8.60(a) shows the voltage V_a when the DVR is not in operation (*Brk1* open). When *Brk1* is closed and the DVR is connected in series with *Load* 1 the voltage sag is mitigated as shown in Figure 8.60(c). A slight increase in the peak value of the waveform is observed compared to the case when the DVR is not in operation.

This effect is purely due to the harmonic distortion generated by the DVR. However, the rms voltage is kept very close to the reference value as shown in Figure 8.59(b). The voltage injected by the DVR in phase *a* is shown in Figure 8.60(b). It should be noted that no filters are used in the simulations with a switching frequency of $f_{sw} = 450\,Hz$.
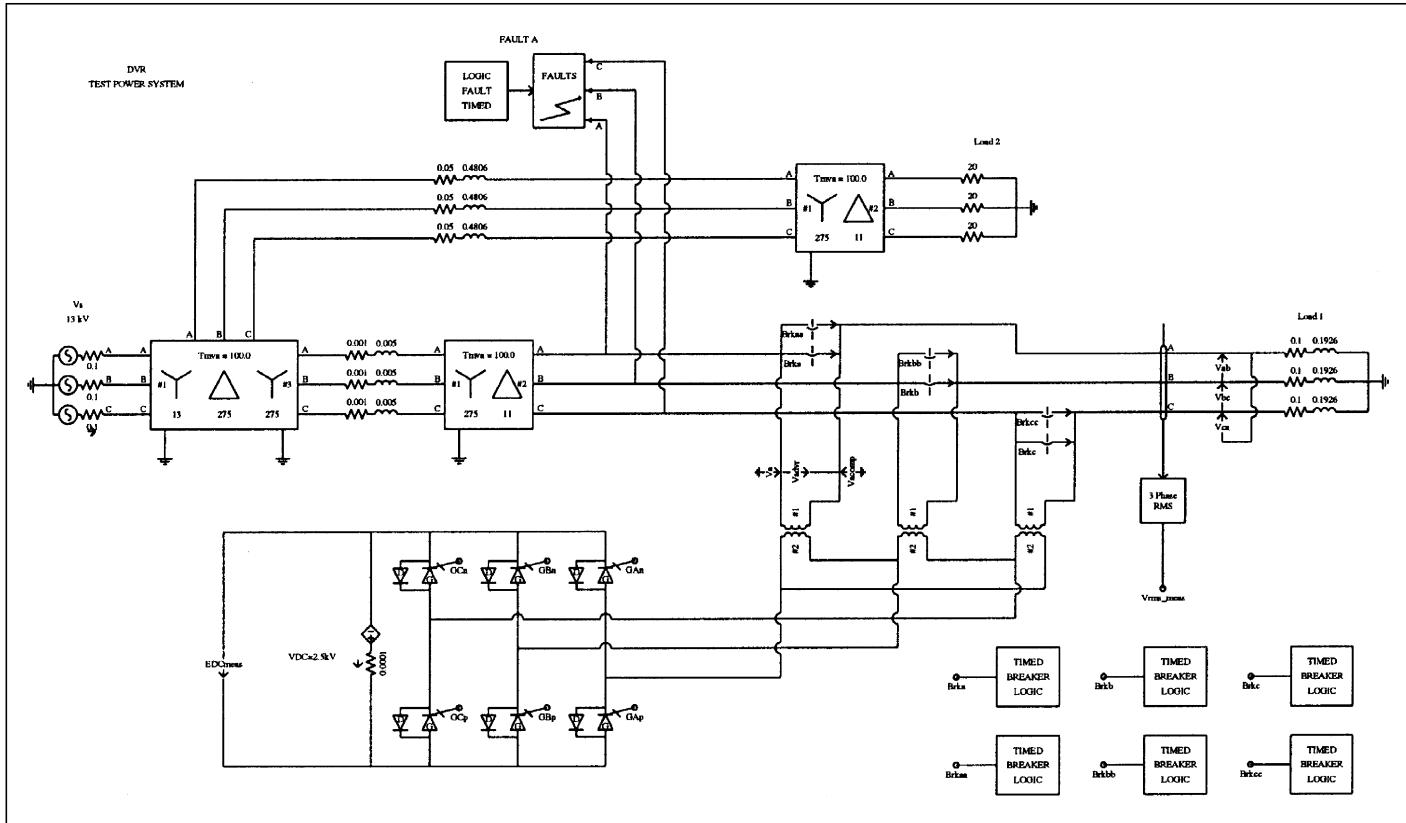
Fig. 8.57 DVR test system implemented in PSCAD/EMTDC.
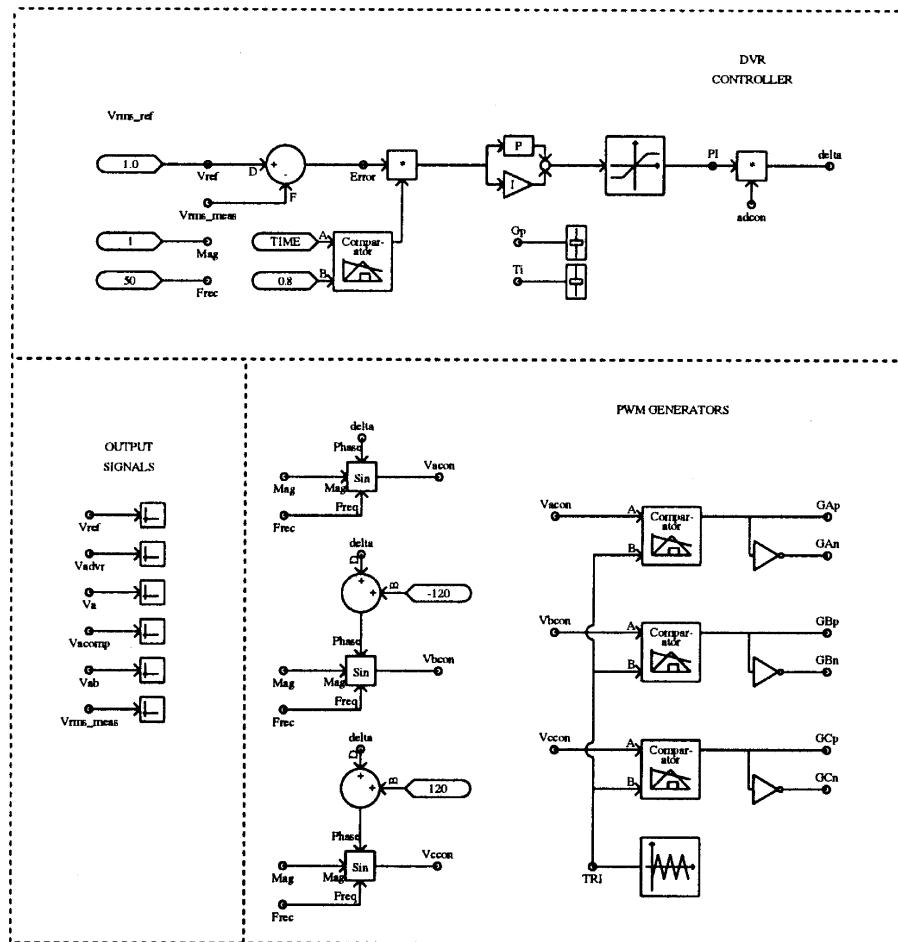
Fig. 8.58 DVR controller implemented in PSCAD/EMTDC.

The simulations carried out showed that the DVR provides excellent voltage regulation capabilities. It must be observed that its capacity for power compensation and voltage regulation depends mainly on two factors: the rating of the DC storage device and the characteristics of the coupling transformer. These two factors determine the maximum value of series compensation that the DVR can provide.

In similar way as with the D-STATCOM, the coupling transformer plays a very important role in the behaviour and performance of the DVR. Thus, it is necessary to select the transformer properly. In order to avoid saturation under every condition, the coupling transformer must be sized to handle at least twice the normal steady-state flux requirement at maximum *rms* injection voltage, without saturation. Normally a high reactance is necessary to filter out the harmonic distortion introduced by the PWM action of the inverter. However, a high reactance of the coupling transformer will slow down the response of the DVR and fast transients will be difficult to identify and correct.
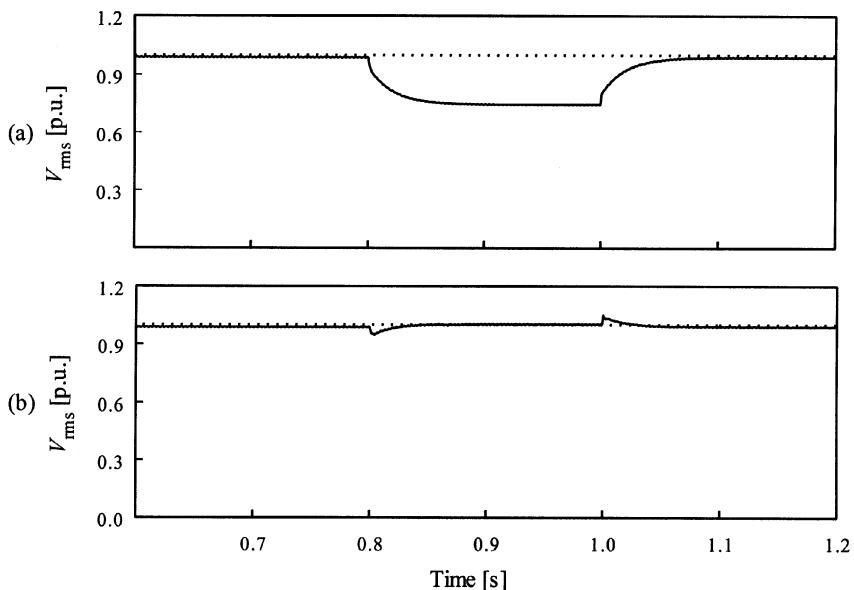
Fig. 8.59 Voltage V_{rms} at the load point: (a) without the DVR; and (b) with the DVR operating.
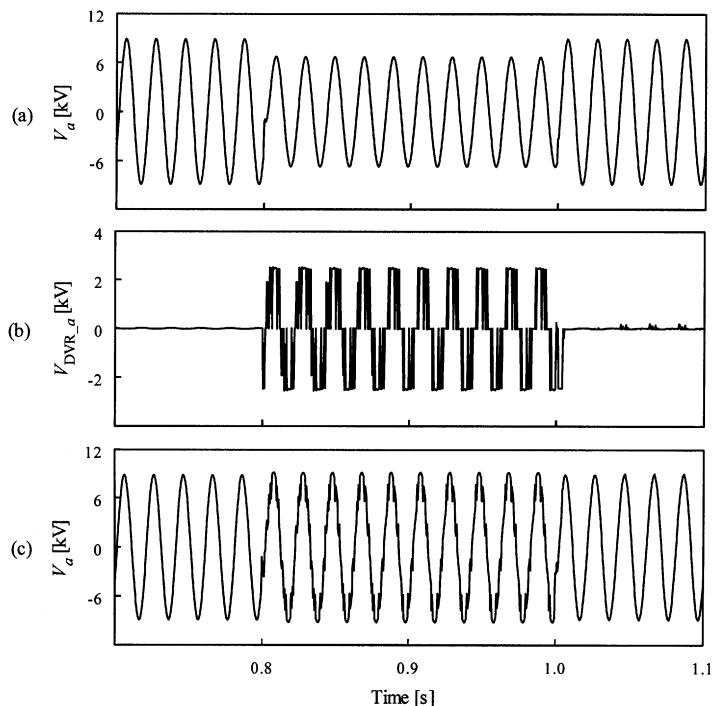
Fig. 8.60 (a) Phase voltage V_a at the load point without DVR; (b) phase voltage supplied by the DVR in phase a; and (c) phase voltage V_a at the load point with the DVR operating.

8.8   Power Factor Corrector (PFC)

Power factor correction usually means the practice of generating reactive power as close as possible to the load that requires it, rather than supplying it from a remote power station. Most industrial loads have lagging power factors; that is, they absorb reactive power. The load current therefore tends to be larger than is required to supply the real power alone. Only the real power is ultimately useful in energy conversion and the excess load current represents a waste to the consumer, who has to pay not only for the excess cable capacity to carry it but also for the excess heat loss produced in the supply cables. The supply utilities also have good reasons for not transmitting unnecessary reactive power from generators to loads: their generators and distribution networks cannot be used at full capacity, and the control of voltage in the supply system can become more difficult. Supply tariffs to industrial customers almost always penalize low power factor loads, and have done so for many years (Miller, 1982).

These aspects and the current power quality regulations have led to the extensive development of power factor correction systems which have lately been an active research topic in power electronics. Conventional techniques for power factor correction involve the use of fixed capacitor banks and reactors with electromechanical controllers. However, the advances in the power electronics technology have enabled the development of new techniques and systems to improve the power factor. In this point the research has been heavily focused on inverter applications (Mao, 1997).

Several VSC topologies can be used to implement a PFC where the most appropriate topology is dictated by the requirements of the specific application. The topology used to implement the PFC presented in this section is based on a VSC connected in shunt with the AC system (Tepper et al., 1996; Moran et al., 1995; Zargari et al., 1995) as shown in Figure 8.61. This topology can be used either individually or simultaneously for three different purposes:
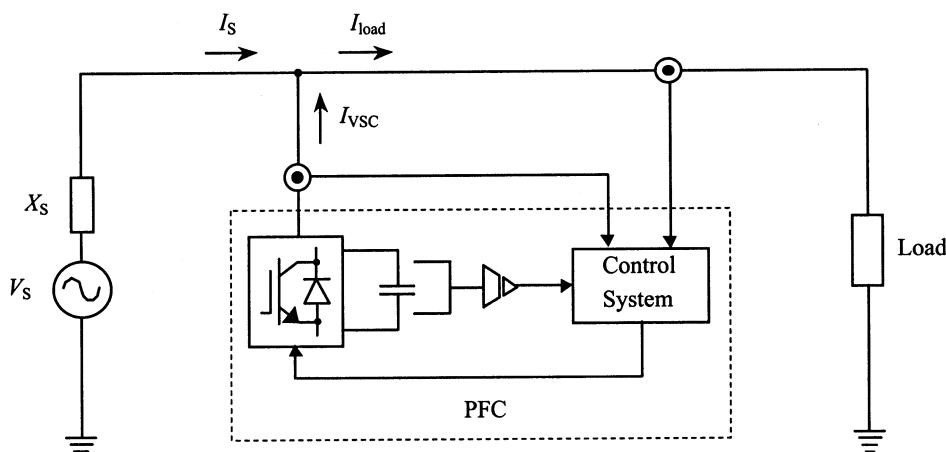

Fig. 8.61 Schematic diagram of the PFC.

1. voltage regulation and compensation of reactive power (STATCOM)
2. correction of power factor (PFC)
3. elimination of undesirable current harmonics (shunt active filter).

The design approach of the control system determines the priorities and functions developed by the shunt-connected VSC in each case. In section 8.4 this topology was used as a STATCOM to provide voltage regulation and compensation of reactive power at the point of connection. In that case a simple control strategy based on voltage measurements was implemented to control the operation of the shunt-connected VSC. However, for the PFC model the implementation of the control strategy is based on a current-controlled VSC scheme. The VSC is controlled as a current source using PWM. Controlled in this way the VSC injects the proper amount of reactive current required by the load so that the main supply delivers only the required active current thus improving the power factor.

The principle of operation of the PFC can be explained using the schematic diagram of Figure 8.61. Without compensation the load current I_{load} is commonly made up of the following terms:

$$I_{\text{load}} = I_{\text{load\_0}} + I_{\text{load\_p}} + I_{\text{load\_q}} + I_{\text{load\_h}} \qquad (8.14)$$

where

$I_{\text{load\_0}}$ DC component
$I_{\text{load\_p}}$ in-phase line current
$I_{\text{load\_q}}$ reactive current
$I_{\text{load\_h}}$ harmonic currents.

Normally, the DC component is very small or it does not exist at all, then $I_{\text{load\_0}}$ is excluded from Equation 8.14. For the specific case of power factor correction and assuming a linear load, the term $I_{\text{load\_h}}$ can be considered zero and Equation 8.14 finally reduces to

$$I_{\text{load}} = I_{\text{load\_p}} + I_{\text{load\_q}} \qquad (8.15)$$

In order to achieve unity power factor operation the mains supply must only deliver $I_{\text{load\_p}}$ in Equation 8.15. This can be achieved if the PFC is controlled to generate and inject into the system the reactive current $I_{\text{load\_q}}$ required by the load. From Equation 8.15 the reactive current $I_{\text{load\_q}}$ is calculated by subtracting the active current component $I_{\text{load\_p}}$ from the measured current I_{load} as

$$I_{\text{load\_q}} = I_{\text{load}} - I_{\text{load\_p}} \qquad (8.16)$$

In order to generate $I_{\text{load\_q}}$ the VSC must be provided with an appropriate current control loop. At present there are several current control techniques available such as hysteresis, predictive and indirect current control techniques which are implemented using a stationary (abc) frame of reference. These techniques can be further explained as follows:

1. Hysteresis current control keeps the error within a specified band. The advantages of this technique are simplicity, good accuracy, and high robustness. The major drawback is that the switching frequency varies within one load cycle; this results

in a higher switching frequency than other techniques and the average varies with operating conditions, thus resulting in additional stresses on switching devices and difficulties in designing the appropriate filtering equipment.

2. Predictive current control with fixed switching frequency is based on prediction of the current error from a load model. The advantages are speed and accuracy in tracking the reference waveform; however, it is sensitive to parameter variations, inaccuracies, and delays.

3. Indirect current control eliminates the need for current transducers and employs a standard sinusoidal PWM pattern. However, system parameter values are required and the stability region is more restricted as compared to the hysteresis controller.

The current controller designed for the PFC presented in this section is developed using a rotating ($dq0$) frame of reference that offers higher accuracy than the stationary frame techniques. The block diagram of the overall control system is shown in Figure 8.62.

As illustrated in the block diagram of Figure 8.62 the inputs to the control system are the load currents I_{load_a}, I_{load_b} and I_{load_c}, the converter currents I_{VSC_a}, I_{VSC_b} and I_{VSC_c}, and the voltage V_{DC} of the DC link.

Two control loops are used in this controller, a current control loop and a voltage control loop for the DC link voltage. The measured DC link voltage is first filtered and then compared with a voltage reference. The error is fed to a PI controller in order to reduce the steady-state error. The load and inverter currents are transformed to the rotating ($dq0$) frame and filtered to extract the fundamental components. The currents are transformed to the ($dq0$) frame using the following transformation
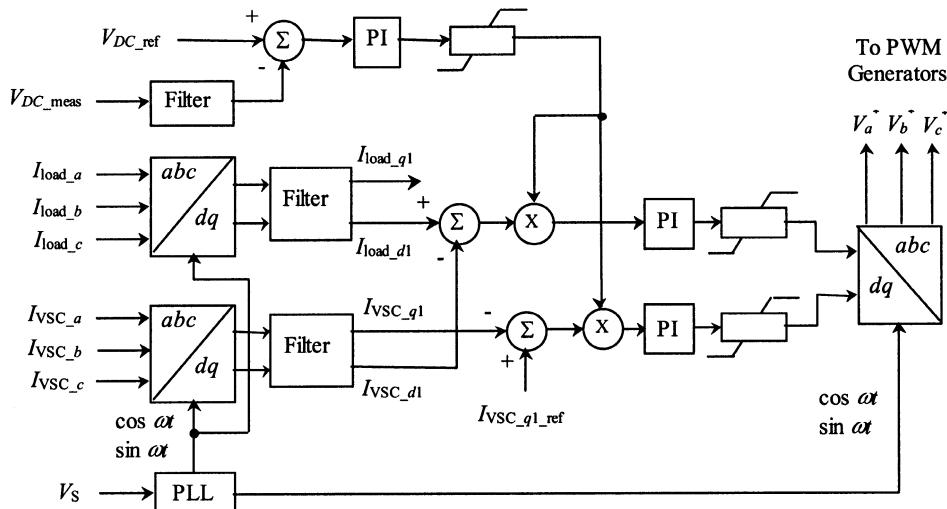
Fig. 8.62 Current controller in the *dq0* frame.

$$\begin{bmatrix} f_\alpha \\ f_\beta \end{bmatrix} = \frac{2}{3} \begin{bmatrix} 1 & -1/2 & -1/2 \\ 0 & \sqrt{3}/2 & -\sqrt{3}/2 \end{bmatrix} \begin{bmatrix} f_a \\ f_b \\ f_c \end{bmatrix} \qquad (8.17)$$

where the function f in this case represents the instantaneous current. The transformation from the $\alpha\beta$ reference frame to the rotating $(dq0)$ frame is achieved by means of the following transformation

$$\begin{bmatrix} f_d \\ f_q \end{bmatrix} = \begin{bmatrix} \cos \omega t & \sin \omega t \\ -\sin \omega t & \cos \omega t \end{bmatrix} \begin{bmatrix} f_\alpha \\ f_\beta \end{bmatrix} \qquad (8.18)$$

where ω is the synchronous angular frequency of the mains supply. The DC components in the rotating $(dq0)$ frame f_d and f_q correspond to the positive sequence fundamental components of f_α and f_β. Since the dq transformation is one that converts frequency dependant signals into ones with constant value, an ideal three-phase system yields constant f_d and f_q. The relation between the dq and active and reactive components depends on the frame of reference selected.

The rotating frame of reference can be chosen arbitrarily. However, once it is chosen every following calculation must be done with respect to the selected frame. As an example, Figure 8.63 shows two different rotating frames; any of these can be selected as the reference. In this example, the rotating frame is selected such that the q-axis is in phase with the phase a as shown in Figure 8.63(b). The reference signals are the load current dq components that are compared with the measured converter currents. The error signals are then fed to the PI controllers and the output is used as the control signals in the PWM generators. Before the control signals are sent to the PWM generators they are converted back into the stationary (abc) frame of reference using the inverse transformation of Equations 8.17 and 8.18 in the following way
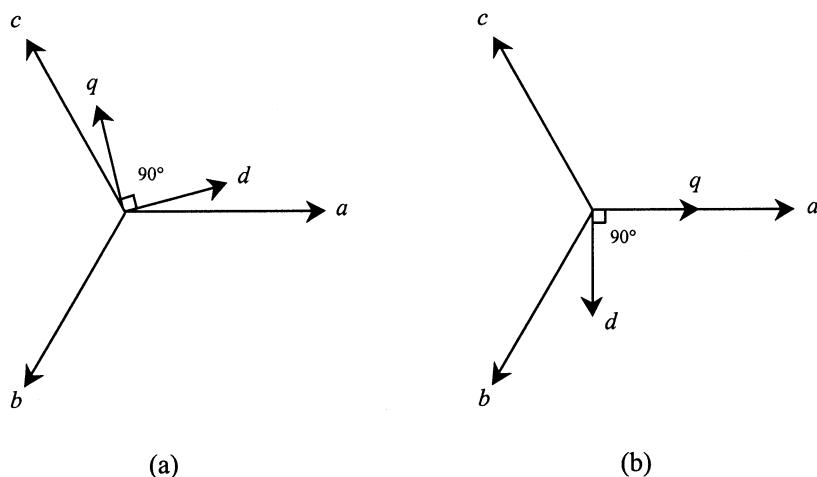
Fig. 8.63 (a) An arbitrary rotating frame; and (b) chosen rotating frame of reference.
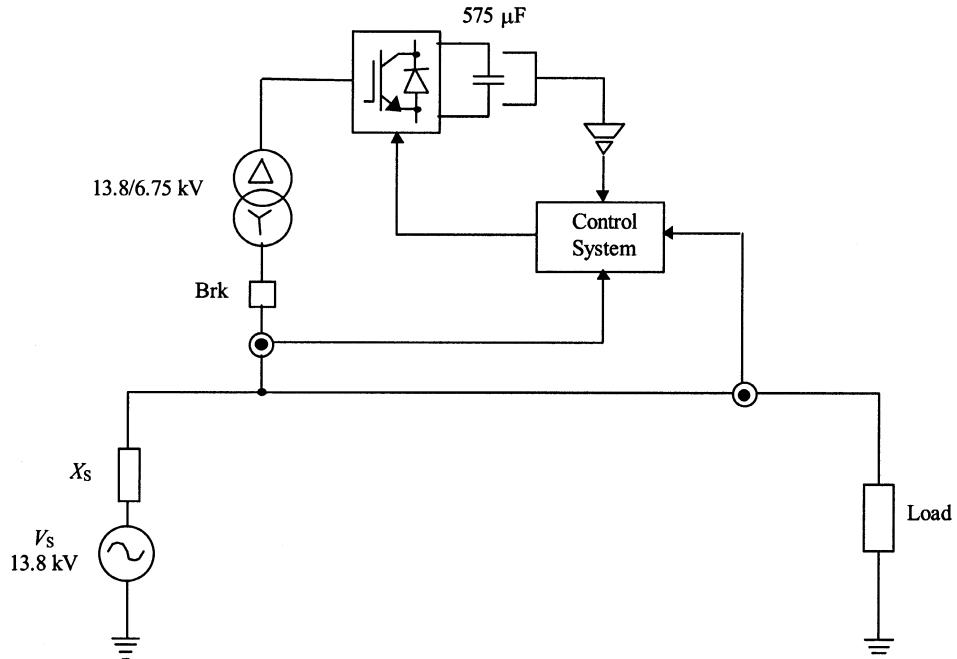
Fig. 8.64 Schematic diagram of the test system used to carry out transient analysis of the PFC.

$$
\begin{bmatrix} f_a^* \\ f_b^* \\ f_c^* \end{bmatrix} = \begin{bmatrix} 1 & 0 \\ -1/2 & \sqrt{3}/2 \\ -1/2 & -\sqrt{3}/2 \end{bmatrix} \begin{bmatrix} \cos \omega t & -\sin \omega t \\ \sin \omega t & \cos \omega t \end{bmatrix} \begin{bmatrix} f_d^* \\ f_q^* \end{bmatrix} \tag{8.19}
$$

where f_a^*, f_b^*, f_c^* are the commands in the PWM generators.

The electrical system used to carry out the transient simulations of the PFC is shown in Figure 8.64. It comprises of a simple three-phase system where an AC constant source is supplying a linear R–L load. The PFC is connected in shunt with the AC system between the source and the *load* through the reactance of a Y–Δ coupling transformer. The breaker *Brk* controls the connection of the PFC to the AC system. The PFC is provided with a control system that measures the load current I_{load}, the VSC output current I_{VSC}, and the voltage of the DC link V_{DC}. The control logic is then derived based on these measurements as previously explained. A 575 μF is connected on the DC side of the VSC to provide the energy storage capability. Figure 8.65 illustrates the digital implementation developed in PSCAD/EMTDC of the test system. The controller is shown in Figures 8.66 and 8.67.

Under normal operating conditions the power factor of the load is at an extremely low value of 0.35 lagging. The PFC is connected to raise the power factor and bring the whole system into unity power factor operation. The simulations were run for a long period of time but only a few cycles are presented for clarity.

Figure 8.68 shows the source current I_S, the load current I_{load}, and the converter output current I_{VSC}. These waveforms are plotted together with the source voltage V_S. The simulation begins with the PFC disconnected from the network and both, I_S
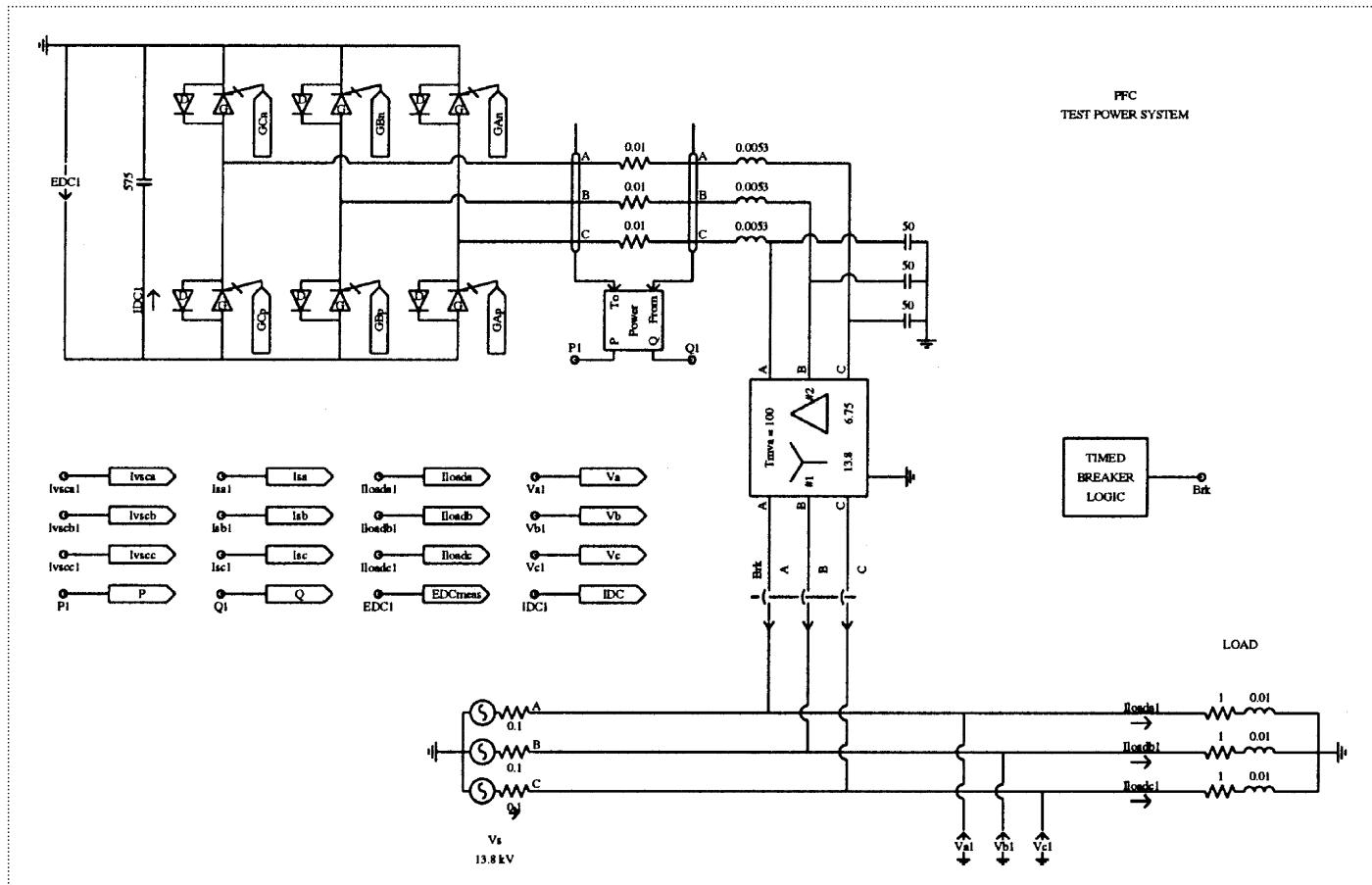
Fig. 8.65 PFC test system implemented in PSCAD/EMTDC.
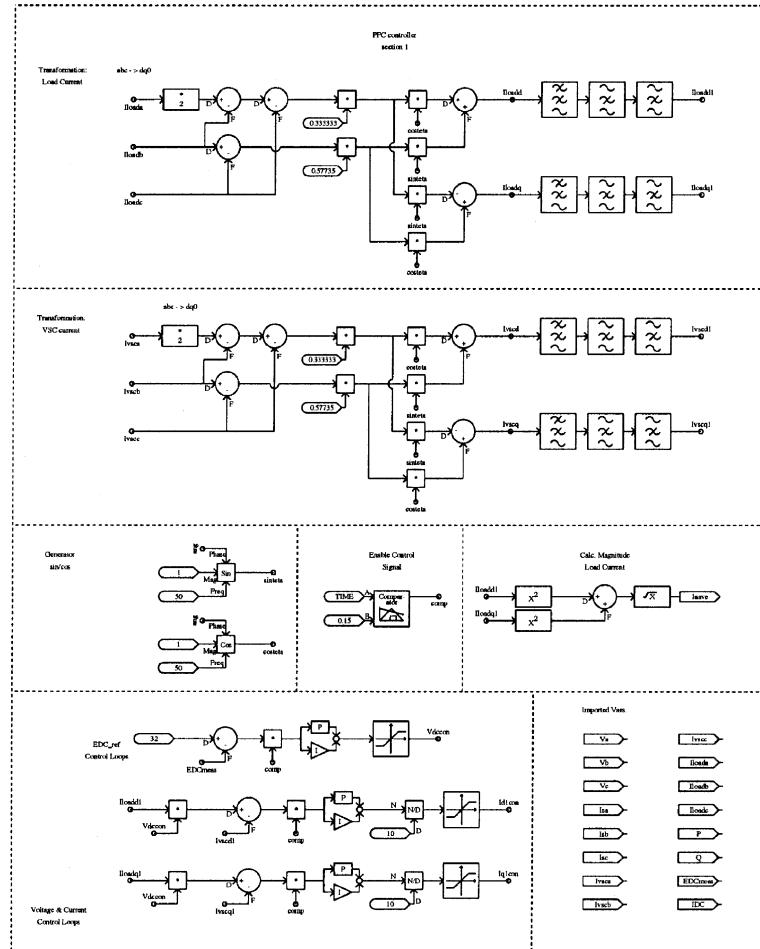
Fig. 8.66 PFC controller implemented in PSCAD/EMTDC: Transformation of variables to the *dq0* frame, and control loops.

and I_{load} lag V_{S} as shown in Figures 8.68(a) and 8.68(b) respectively. At $t = 0.15$ s the breaker *Brk* is closed and the PFC is connected to the AC system. As soon as the PFC starts operating the power factor increases very rapidly and it only takes a couple of cycles until the input power factor is driven to unity as illustrated in Figure 8.68(a).

Observe that the phase relation between I_{load} and V_{S} remains unaltered even when the PFC is in operation. As shown in Figure 8.68(b), the load current I_{load} keeps on lagging V_{S} by the same initial angle. However, the power factor as seen by the AC source has been improved to a unity value, i.e. the AC source is not supplying any reactive power to the load, as it is seen by the source as a purely resistive one.

In order to improve the power factor to the desired value, the PFC injects into the AC system the appropriate amount of reactive power required by the load which otherwise, has to be delivered by the AC source. As mentioned before, the PFC controller splits the load current into its active and reactive components by
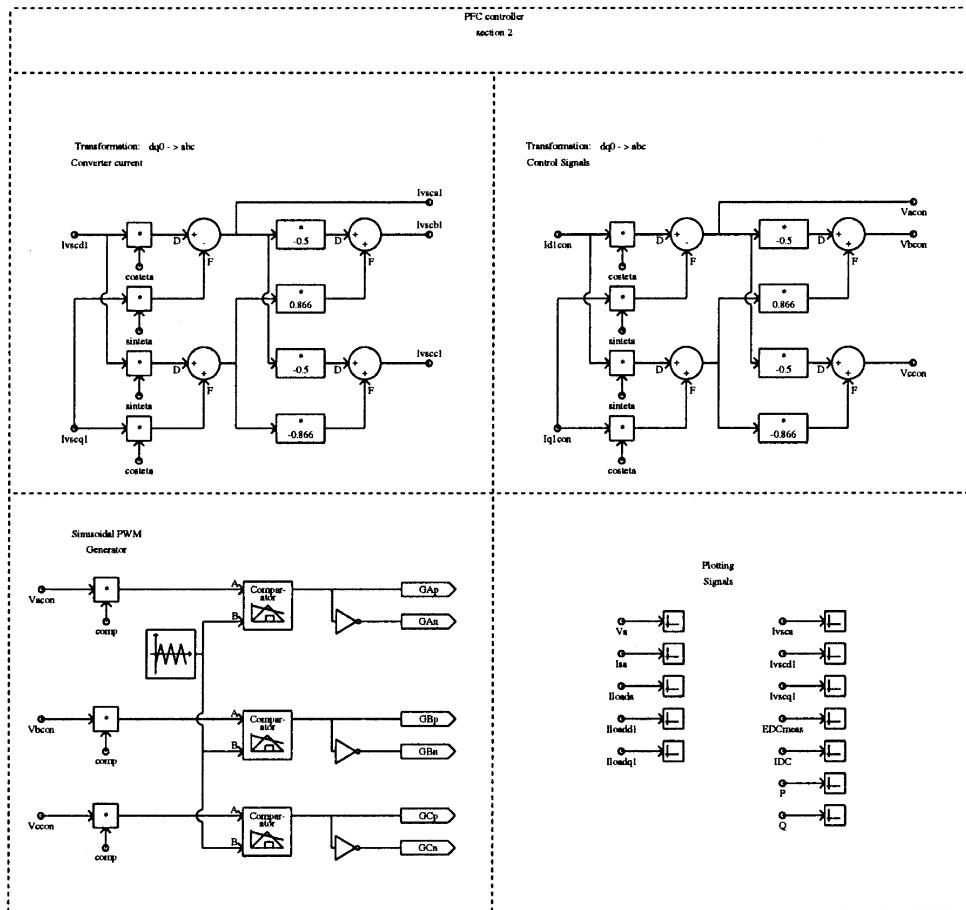
Fig. 8.67 PFC controller implemented in PSCAD/EMTDC: Transformation of command signals back to the *abc* frame, and PWM generators.
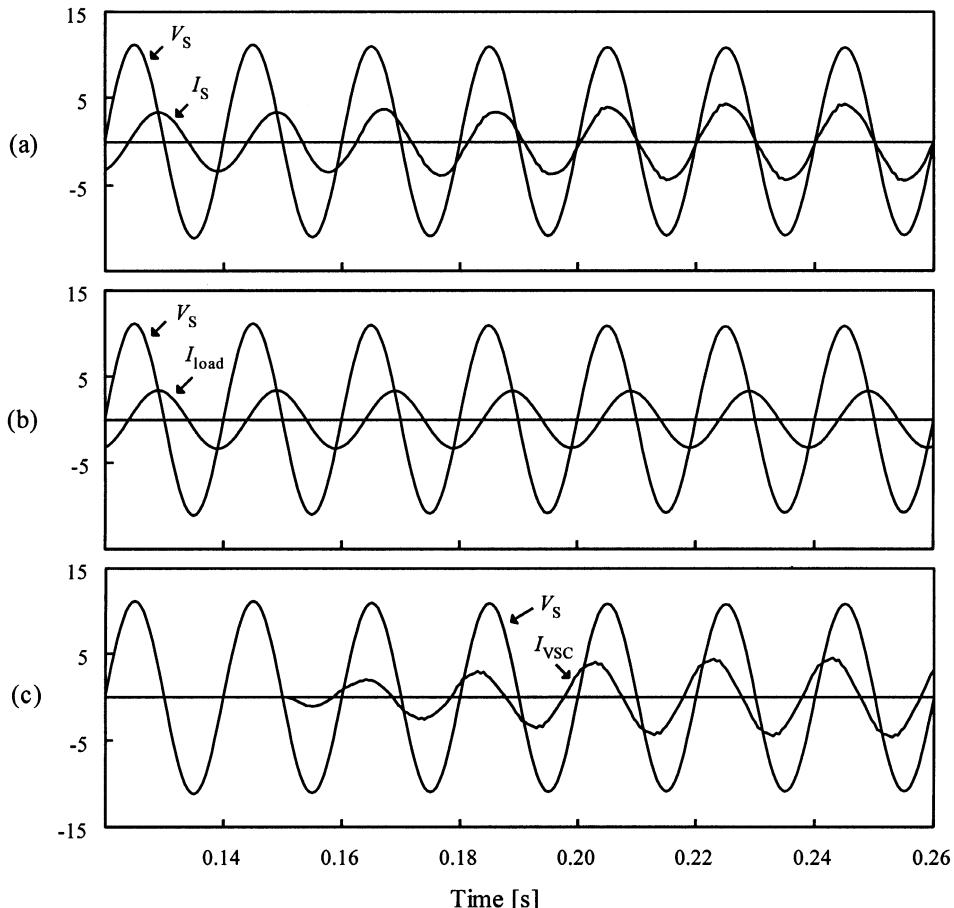
Fig. 8.68 Key waveforms for the PFC circuit: (a) source voltage V_S and current I_S; (b) source voltage V_S and load current I_{load}; and (c) source voltage V_S and converter current I_{VSC}.

a transformation into the rotating $dq0$ frame. These dq-components are used as reference input values in the closed loop control scheme. According to the selected rotating $dq0$ frame shown in Figure 8.63 the reactive components of I_{load}, I_S and I_{VSC} are shown in Figure 8.69. At $t = 0.15$ s the PFC is connected to the network and the reactive current required by the load is supplied by the PFC as shown in Figure 8.69(c). Figure 8.69(b) shows the reactive current supplied by the source which decreases rapidly very close to zero. In this way, the power factor increases significantly and becomes practically unity.

Figure 8.70 shows the corresponding DC link voltage V_{DC} which is maintained at 33 kV. The response of the controller can be appreciated in this plot, and it can be seen that it takes almost two cycles before the DC voltage is driven from an initial zero value to the required 33 kV. The size of the DC capacitance is selected sufficiently large to minimize the DC voltage ripple without slowing the response of the controller. The DC voltage ripple can be further reduced by connecting an appro-
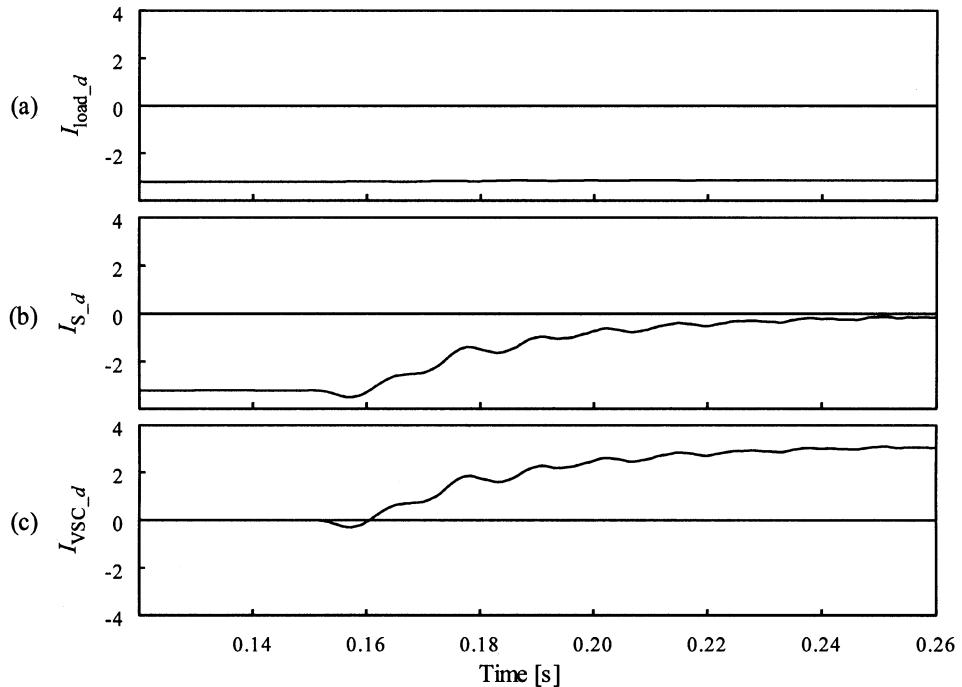
Fig. 8.69 Reactive components in the rotating frame: (a) load current I_{load_d}; (b) source current I_{S_d}; and (c) converter current I_{VSC_d}.

priate filter at the VSC output terminals. However, for the purpose of this example filtering has not been included.

Figure 8.71 shows the current through the DC link capacitor, I_{DC}. The current I_{DC} has the typical pattern for the case of lagging power factor compensation. When the compensation is for a leading power factor the orientation of the waveform is in the opposite direction. It shows low current harmonic distortion that is reflected in the
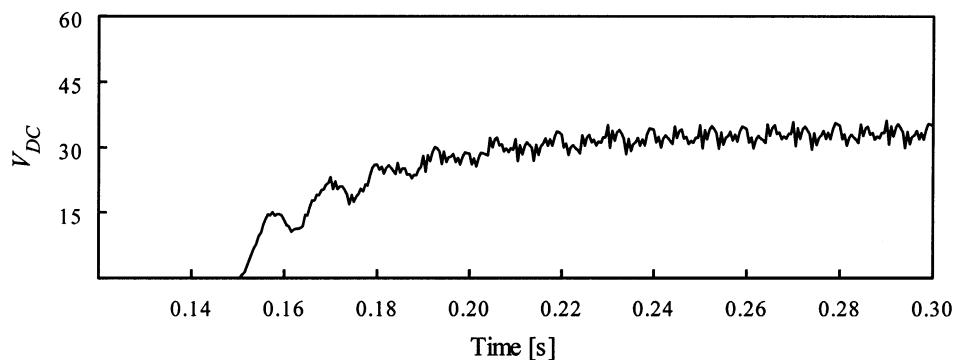
Fig. 8.70 DC link voltage V_{DC}.
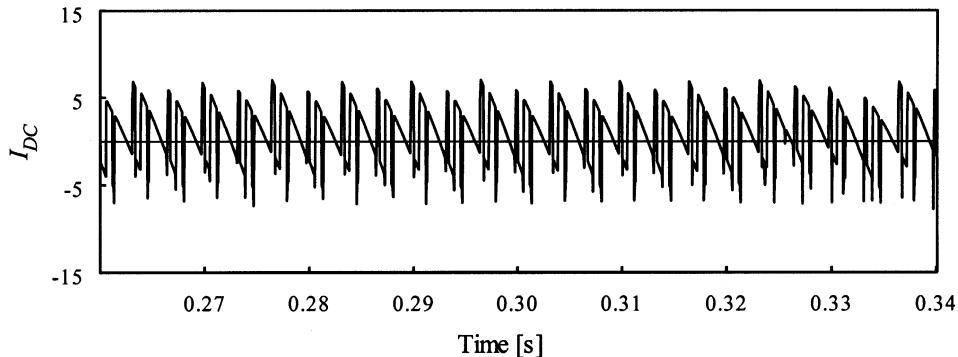
Fig. 8.71 DC link current I_{DC}.

current injected by the converter I_{VSC}, and the resulting compensated source current I_S shown in Figure 8.68.

8.9 Active Filters (AFs)

In Chapter 6, various converter topologies have been introduced as a way to improve the quality of the power supply. The reason being that the composition of electric utility systems' elements has gone through a gradual change from being largely linear to partially or dominantly non-linear during the past 30 years or so. The proliferation of non-linear loads and sources, such as power electronic based equipment, has led to a serious problem of power quality for both, utilities and customers, as these non-linear elements are the main contributors of harmonic pollution in the system.

This situation has become a major concern for power system specialists due to the effects of non-sinusoidal voltages and currents on sensitive loads and on the overall distribution system. For example, harmonic current components increase power system losses, cause excessive heating in rotating machinery, create significant interference with communication circuits that shared common right-of-ways with AC power lines, and can generate noise on regulating and control circuits causing erroneous operation of such equipment. On the other hand, among other components, rotating machinery can be significantly impacted by the harmonic voltage distortion as it translates into harmonic fluxes that induce additional losses. Decreased efficiency, along with heating, vibration, and high-pitched noises, are clear symptoms of harmonic voltage distortion (Singh et al., 1999).

A common source of harmonic currents is the phase-controlled thyristor rectifier where the current waveform distortion, i.e. the generation of harmonics, results from the phase delay control method. The details of these harmonics depend on the rectifier's firing angle, the inductance of the power supply, the DC load, and other circuit parameters. Figure 8.72(a) shows a typical thyristor rectifier and Figure 8.73 shows the source voltage and rectifier current waveforms. Because the harmonic current contents and characteristics are less dependent upon the AC side, this type of harmonic source behaves like a current source. Therefore, they are called harmonic

(a)

(b)
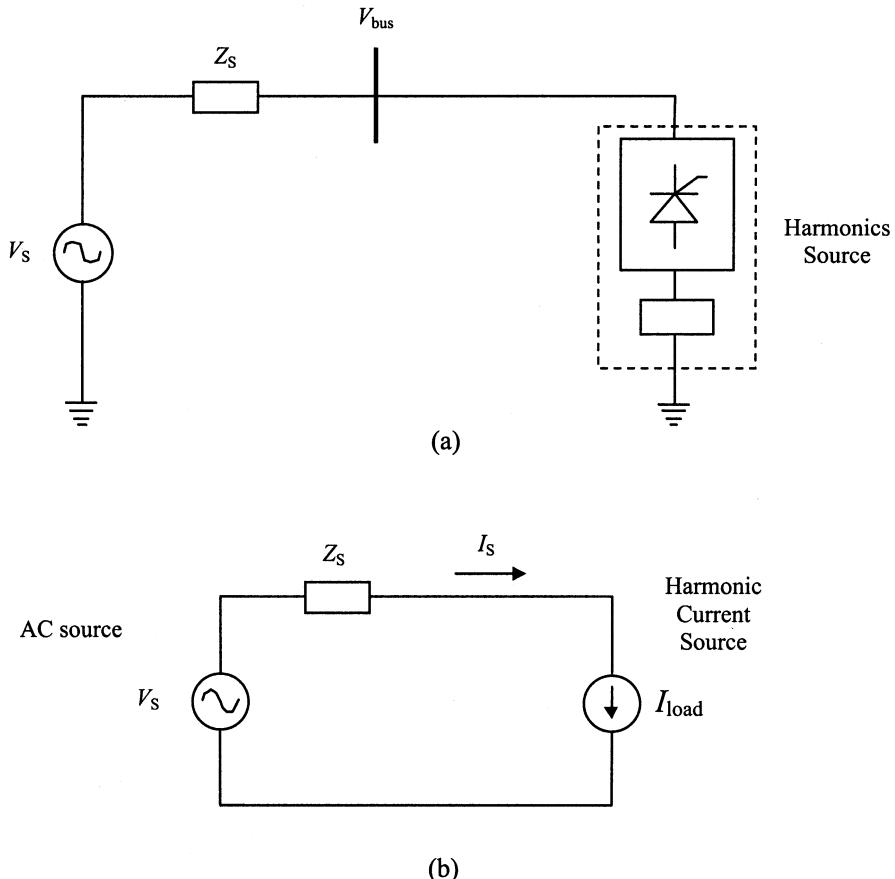
Fig. 8.72 Typical type of harmonic current source: (a) phase-controlled thyristor rectifier; and (b) single-phase equivalent circuit.

current source and represented as a current source shown in Figure 8.72(b). Other common sources of periodic, non-sinusoidal signals, and hence harmonics, are adjustable speed drives, inverters, and compact fluorescent lamps (Peng, 1998).

At present, another common harmonic source is that of diode rectifiers with 'smoothing' DC capacitors as shown in Figure 8.74(a). Figure 8.75 shows the current and voltage waveforms. Although the current is highly distorted, its harmonic amplitude is greatly affected by the impedance of the AC side whereas the voltage at the rectifier's input terminals is characteristic and less dependent upon the AC impedance.

Therefore, a diode rectifier with a 'smoothing' capacitor behaves like a voltage source rather than a current source. Figure 8.74(b) shows the equivalent circuit of the diode rectifier system, where the diode rectifier is represented as a harmonic voltage source. Accordingly, the harmonic current originates from the rectifier voltage, and its content is determined by, and dependent, upon the rectifier voltage and the AC impedance. Conventionally, passive L–C filters have been used to eliminate line
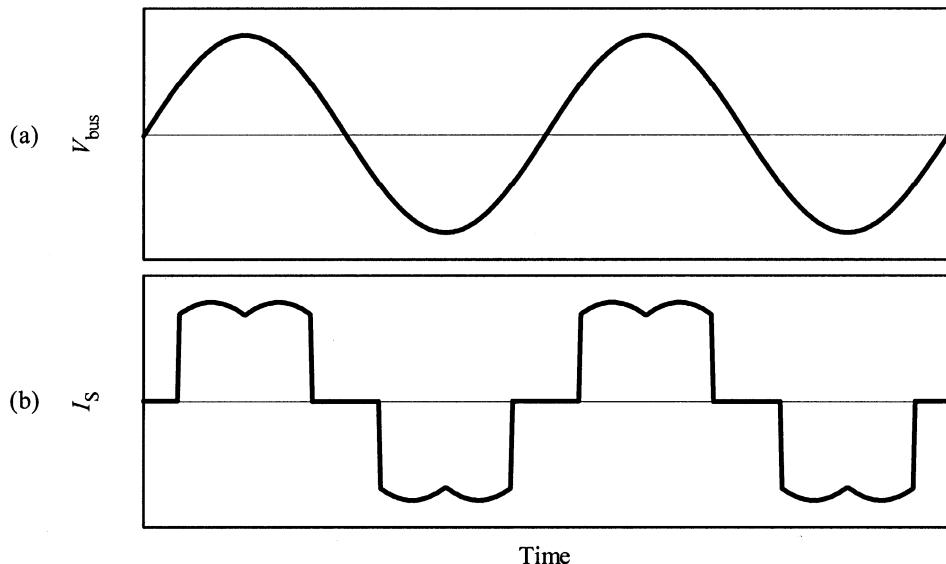
Fig. 8.73 Typical waveforms of phase-controlled rectifiers: (a) voltage V_{bus}; (b) current I_S.
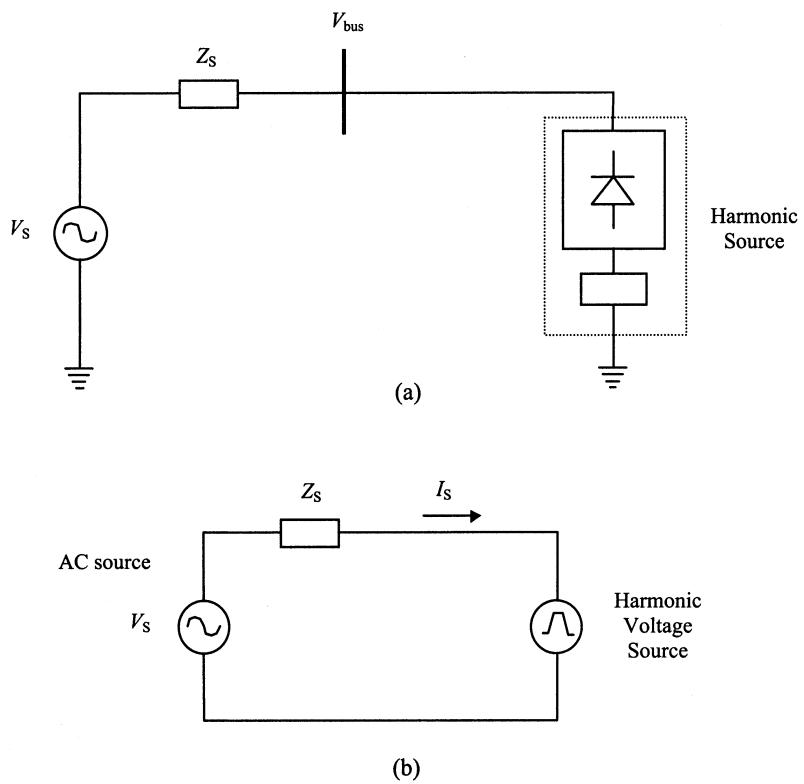

Fig. 8.74 Typical type of harmonic voltage source: (a) diode rectifier; and (b) single-phase equivalent circuit.
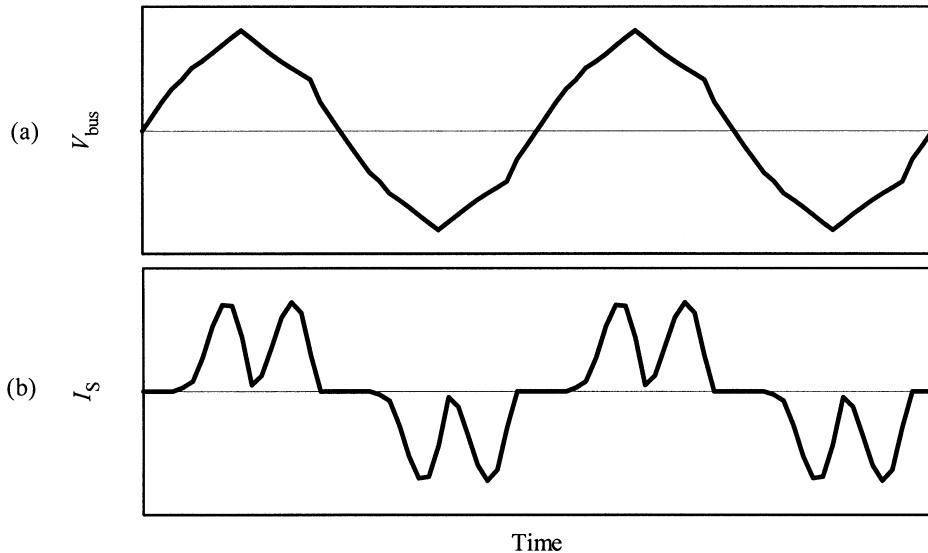
Fig. 8.75 Typical waveforms of diode rectifiers: (a) voltage V_{bus}; and (b) current I_S.

harmonic pollution and to increase the line power factor. However, in practical applications passive filters have the demerits of fixed compensation, being relatively bulky, and resonating with other system elements. The increased severity of harmonic pollution in power networks has attracted the attention of power electronics and power system engineers to develop dynamic and adjustable solutions to the power quality problems giving rise to the active power filters technology.

Active filtering provides compensation for harmonics, reactive power, and/or neutral current in AC networks. It is also used to eliminate voltage harmonics, to regulate terminal voltage, to suppress voltage flicker, and to improve voltage balance in three-phase systems. This wide range of objectives is achieved either individually or in combination, depending upon the requirements and control strategy and configuration that have to be selected appropriately.

Active filters are based on sophisticated power electronics and can be much more expensive than passive filters depending upon the application. However, they have the distinctive advantage that they do not resonate with the system. They can be used in very difficult circumstances where passive filters cannot operate successfully due to parallel resonance complications. They can also address more than one harmonic at a time and combat other power quality problems such as flicker. They are particularly useful for large, distorting loads fed from relatively weak points on the power system. The basic idea behind the active power filters is to replace the portion of the sine waveform that is missing in the current and/or voltage in a non-linear load. An electronic control monitors the line voltage and/or current, switching the power electronics very precisely to track the load current or voltage and force it to be sinusoidal. Many circuit topologies for series and/or shunt active filtering exist and have been presented in Chapter 6.

8.9.1 Shunt active filter

The topology of a VSC connected in shunt with the AC system was used in previous sections as a STATCOM and PFC for power factor improvement. This section presents the time domain analysis of this topology when used as shunt active filter for the elimination of current harmonics. A simple control scheme is developed to regulate the operation of the active filter and transient simulations are carried out in PSCAD/EMTDC.

As mentioned above the shunt AF is a PWM VSC that is placed in shunt with a load (or a harmonic current source) and has the capability to inject into the AC system a harmonic current with the same amplitude but opposite phase than that of the load. Figure 8.76 illustrates the schematic representation of the shunt AF. The principal components are the VSC, a DC energy storage device that in this case is a capacitor, a coupling transformer (not shown in the Figure) and associated control circuits.

The control scheme developed for the shunt AF is based on the determination of the load current harmonic components. With this information the control system drives the VSC in such a way that it generates and injects into the AC system a current with the appropriate harmonic content to neutralize the current harmonics due to the load. Without compensation the load current I_{load} can be split into two terms as

$$I_{load} = I_{load\_1} + I_{load\_h} \qquad (8.20)$$

where I_{load_1} and I_{load_h} represent the fundamental and harmonic components of the load current respectively. The controller developed for the shunt AF is very similar to the one used for the PFC. In the last section the control scheme of the PFC was focussed on controlling the active and reactive parts of the fundamental component. For the shunt AF the control scheme concentrates on the harmonic component of the load current that can be obtained from Equation 8.20 as

$$I_{load\_h} = I_{load} - I_{load\_1} \qquad (8.21)$$
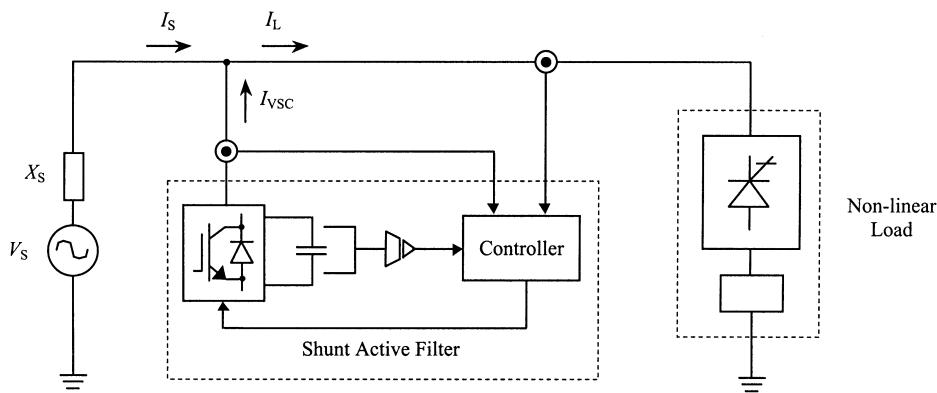
**Fig. 8.76** Schematic diagram of a shunt AF and associated control circuit.
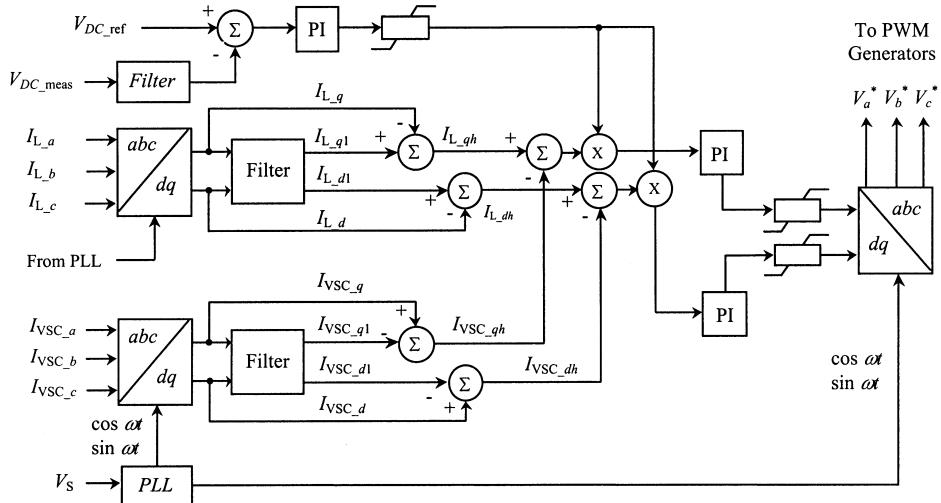
Fig. 8.77 Block diagram of the control scheme designed for the shunt AF.

Equation 8.21 implies first the determination of the fundamental component I_{load_1} and then the subtraction of I_{load_1} from the total load current I_{load} in order to isolate the harmonic component I_{load_h}. Figure 8.77 shows the block diagram of the shunt AF controller. As can be seen in this figure, two control loops are used i.e. a DC link voltage control loop and a current loop in a similar way as with the PFC.

Direct generation of a VSC 'average voltage' reference for current regulation can also be achieved by stationary or rotating frame PI-based current controllers. This last option was selected in this example.

Figure 8.78 shows the schematic diagram of the test system used to carry out the time domain analysis of the shunt AF. The system comprises of a three-phase system where a constant AC source is supplying a non-linear load represented by a phase-controlled rectifier. The shunt AF is connected with the AC system between the source and the non-linear load through the reactance of a Y–Δ coupling transformer. The connection of the shunt AF to the AC system is controlled by means of breaker *Brk*. The shunt AF is provided with a control system that measures the load current I_{load}, the VSC output current I_{VSC}, and the DC link voltage V_{DC}. The control logic is then derived based on these measurements. A 175 μF capacitor is connected in the DC side of the VSC to provide the energy storage capability. A firing angle control scheme was designed for the operation of the phase-controlled rectifier. By controlling the instant at which the thyristors are gated, the average current in the rectifier can be controlled in a continuous manner. The control is based on comparison of a saw-tooth waveform V_{st} (synchronized with the AC source voltage) against a control signal $V_{control}$. The thyristor firing angle α with respect to the positive zero crossing of the AC source voltage is obtained in terms of $V_{control}$ and the peak of the saw-tooth waveform V_{st_peak} as (Mohan et al., 1995)

$$\alpha^\circ = 180^\circ \frac{V_{control}}{V_{st\_peak}} \tag{8.22}$$
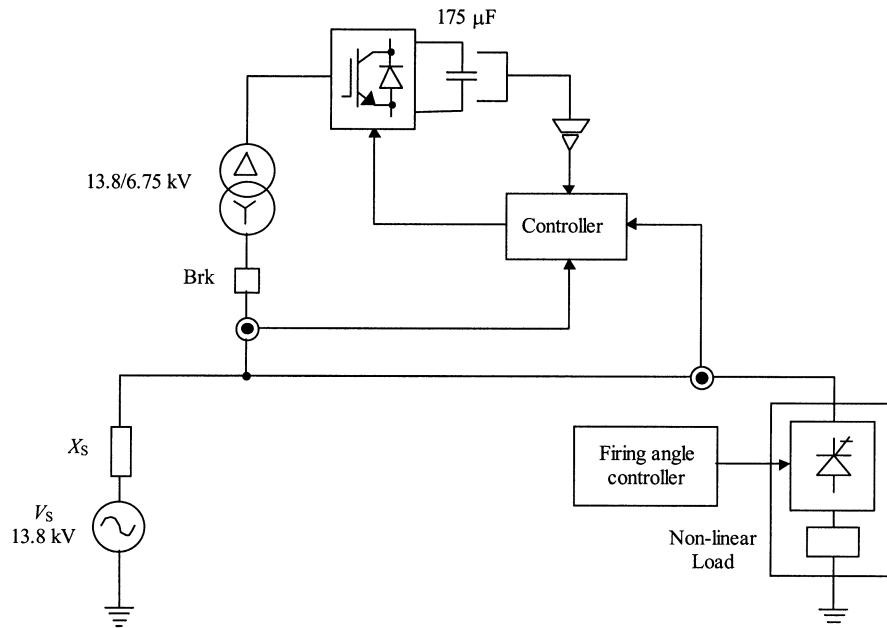
Fig. 8.78 Schematic diagram of the test system used to carry out transient analysis of the shunt AF.


(a)

(b)
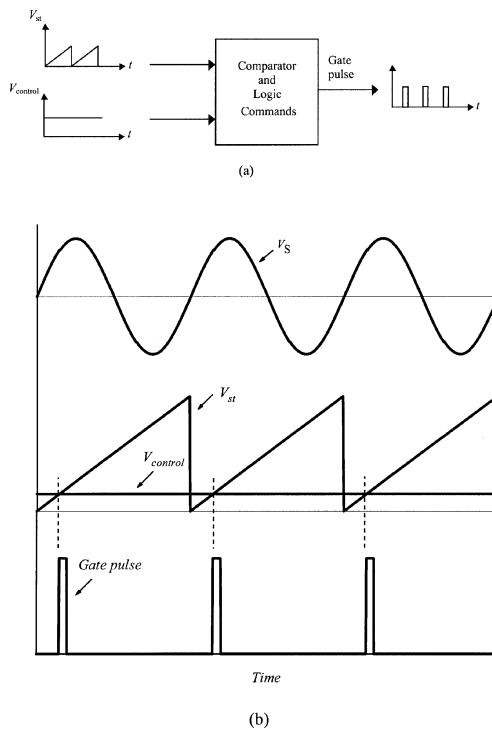
Fig. 8.79 Firing angle control of the phase-controlled rectifier; (a) block diagram; and (b) control signals.

Another gate trigger signal can be obtained, delayed with respect to the zero crossing of the AC source voltage. The control scheme diagram is shown in Figure 8.79.

The implementation of the test power system in PSCAD/EMTDC is shown in Figures 8.80–8.84.

The results obtained through the transient simulation are presented for the time interval of 0.06–0.18 s. At the beginning of the simulation the shunt AF is disconnected from the AC system, i.e. *Brk* is in the open state. At $t = 0.1$ s *Brk* is closed and the active filter is connected to the AC system and starts operating. Figure 8.85 shows the source current I_S, the load current I_L and the VSC current I_{VSC} for both operating conditions. It can be seen in Figure 8.85(a) that when the shunt AF starts operating at $t = 0.1$ s the source current recovers its sinusoidal waveform as the shunt AF is blocking properly the low order current harmonics generated by the load.
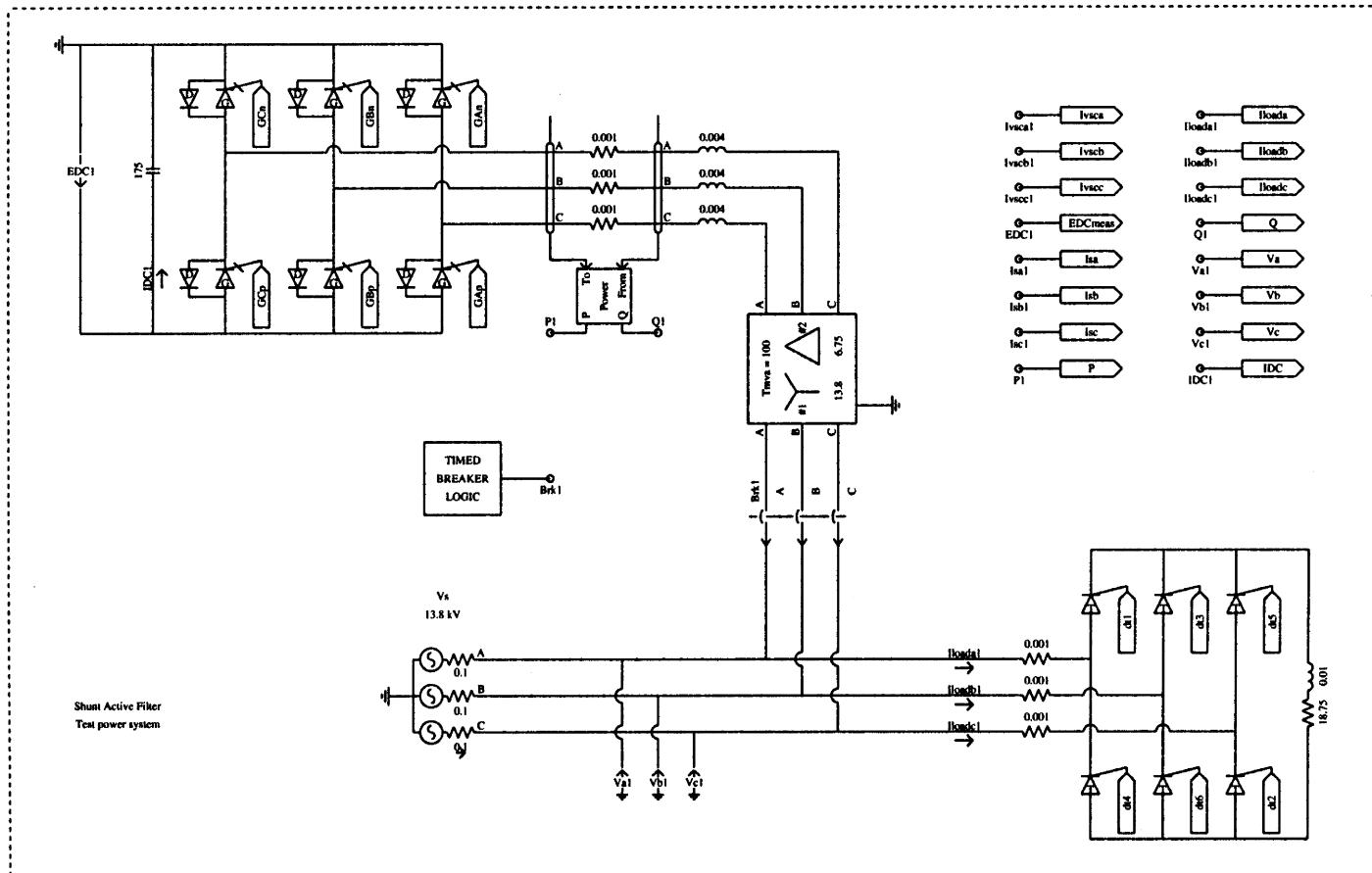
It is important to observe in Figure 8.85(b), that the line current drawn by the load remains unchanged even when the filter operates. The effect of the filter is to block the line current harmonics generated by the load from flowing back into the distribution network and disturb other network components in the vicinity.

Figure 8.86 shows the harmonic spectrum of the source current I_S before and after the shunt AF operates. Without filtering, I_S has a current total harmonic distortion ITHD $= 30.52\%$ with high contents of low order harmonics such as the 5th, 7th, 11th and 13th. With the shunt AF in operation, the total harmonic distortion of the source current decreases to ITHD $= 8.73\%$ as the content of the low order harmonics is significantly reduced as shown in Figure 8.86(b). It must be observed that the fundamental component of the source current is different before and after the filter operation. The fundamental component value is greater when the filter is in operation. This can be explained bearing in mind that the VSC of the active filter has a DC link capacitor whose voltage must be kept constant for the correct operation of the filter. That is, the source current increases as the active filter is drawing active power from the AC system to charge the capacitor and maintain constant DC link voltage.

Figure 8.87 shows the harmonic current component of the load current I_L, the active filter VSC current I_{VSC} and the source current I_S. It can be clearly appreciated in this figure how the harmonic current component generated by the active filter and the harmonic current component due to the load have the same wave shape but opposite direction. The response of the filter controller is fast and it only needs half a cycle to start tracking the reference currents and drive the filter to generate the appropriate harmonic currents to cancel those of the load current. Figures 8.88 and 8.89 show the harmonic current components of the load, filter and source currents in the rotating *dq0* frame.

Specifically, the harmonic current components in the rotating frame *q*-axis are shown in Figure 8.88 and the harmonic current components in the *d*-axis are shown in Figure 8.89. Once again, it can be seen that the harmonic current *dq* components generated by the active filter and the harmonic current *dq* components due to the load have the same wave shapes but opposite directions.

The voltage V_{DC} through the DC link capacitor of the active filter is shown in Figure 8.90(a) and the active and reactive powers absorbed by the shunt AF are shown in Figures 8.90(b) and 8.90(c) respectively. After the transient period when the filter is connected to the network, the shunt AF absorbs active power to

Fig. 8.80 Test system implemented in PSCAD/EMTDC to carry out transient analysis of the shunt AF.
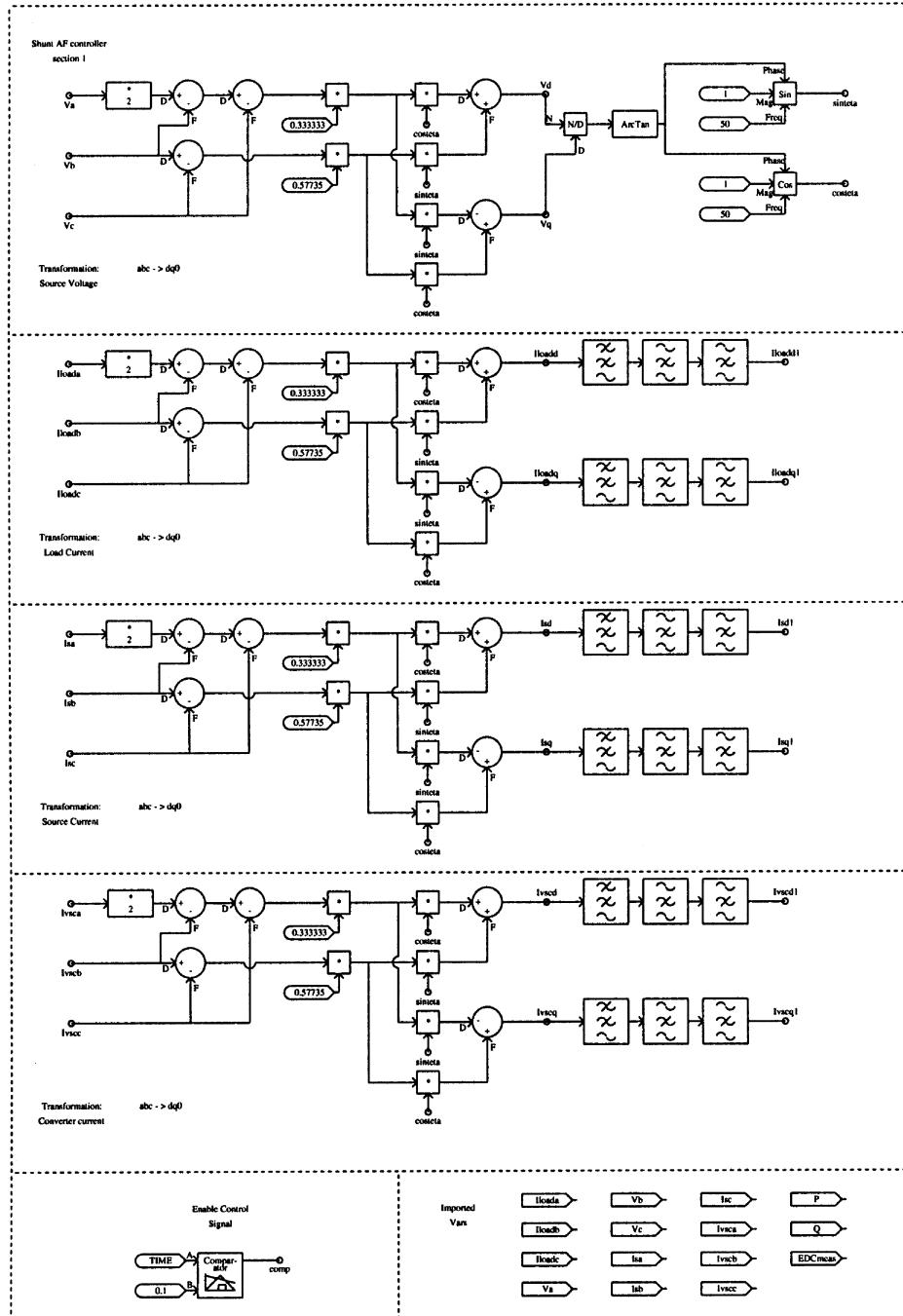
Fig. 8.81 Shunt AF controller implemented in PSCAD/EMTDC: Transformation of variables to the *dq0* frame.
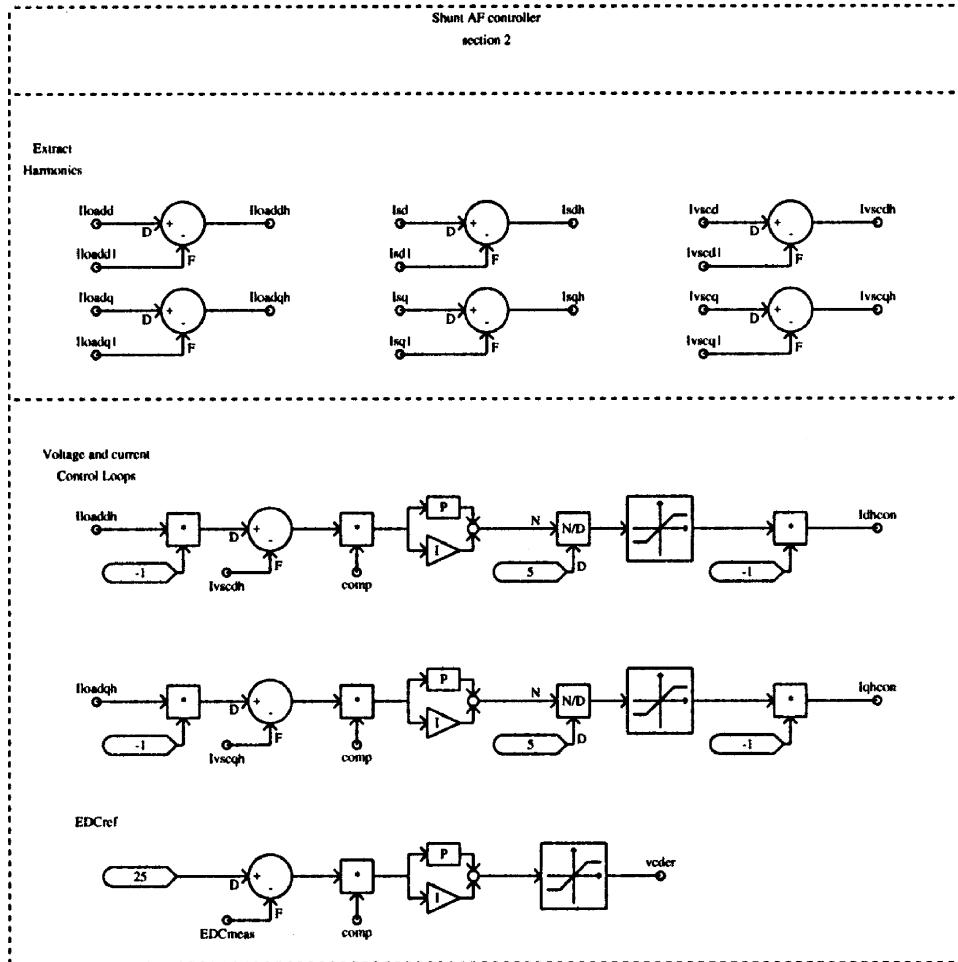
Fig. 8.82 Shunt AF controller implemented in PSCAD/EMTDC: Control loops.

charge the capacitor to a constant value of almost 33 kV for the rest of the simulations. The DC link voltage is not completely constant and presents significant ripple component.

In order to decrease the DC voltage ripple, it is possible to select a larger value for the DC capacitance but this compromises the controller response, as a larger DC capacitance will result in a more sluggish system. Another solution to minimize the DC voltage ripple is the use of switching ripple filter topology at the output of the shunt active filter in order to provide a sink for the dominant inverter switching frequencies that cause the DC voltage ripple. If properly designed, switching ripple filters can also provide attenuation for higher harmonic supply currents that are above the current regulator bandwidth of shunt AF inverter (Bhattacharya et al., 1998).
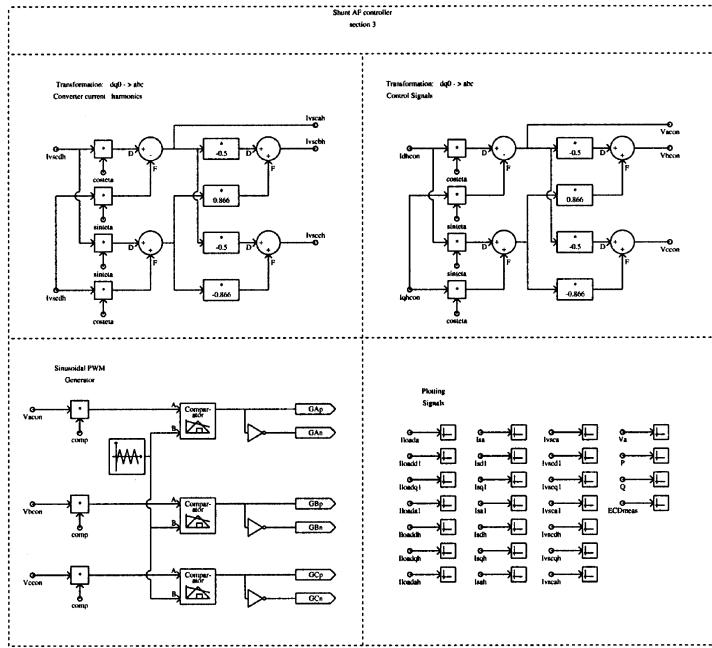
Fig. 8.83 Shunt AF controller implemented in PSCAD/EMTDC: Transformation of command signals back to the *abc* frame, and PWM generators.
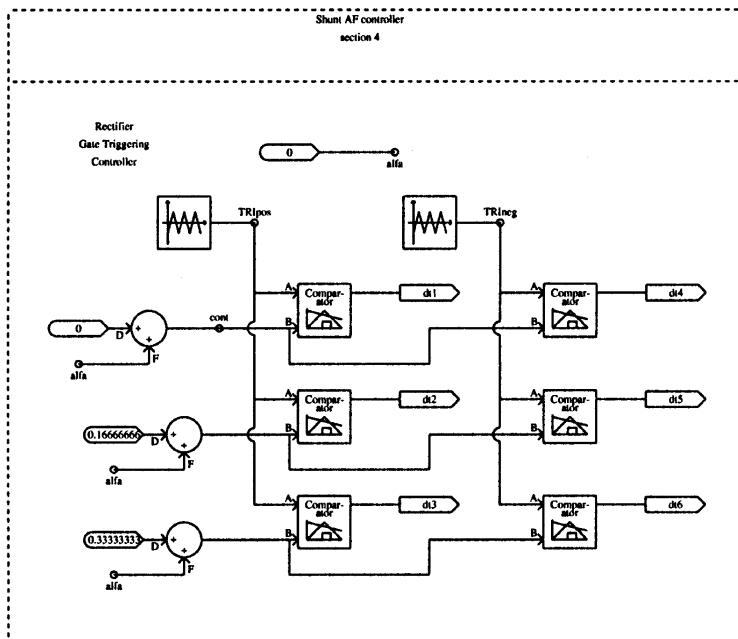

**Fig. 8.84** Shunt AF controller implemented in PSCAD/EMTDC: Firing angle module of the phase-controlled rectifier.
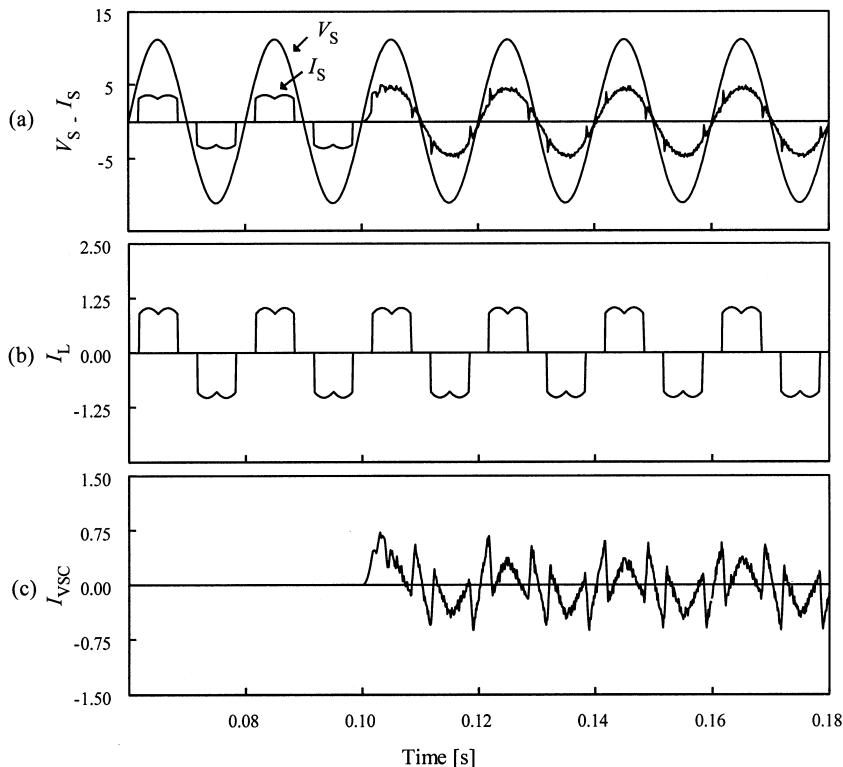
Fig. 8.85 Current waveforms in the shunt AF model circuit: (a) source voltage V_S and current I_S; (c) current I_L; and (c) converter current I_{VSC}.
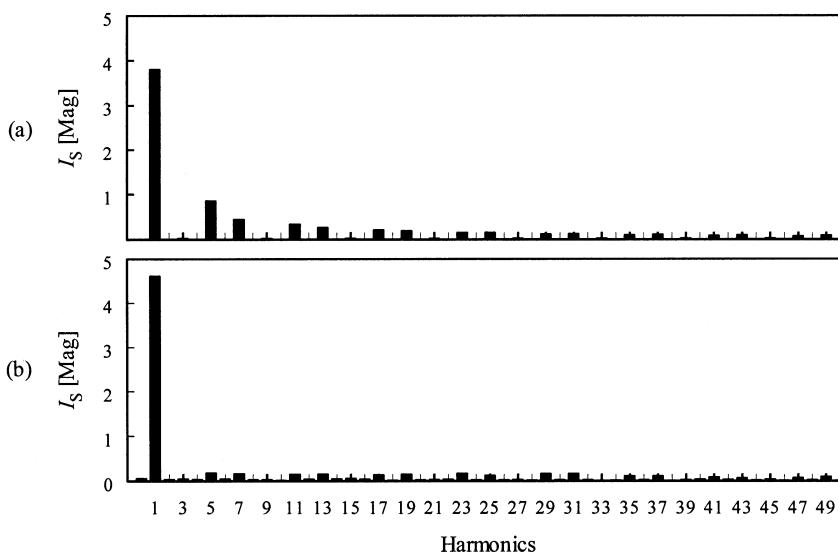

Fig. 8.86 Harmonic spectrum of the source current I_S: (a) without shunt AF; and (b) with shunt AF operating.
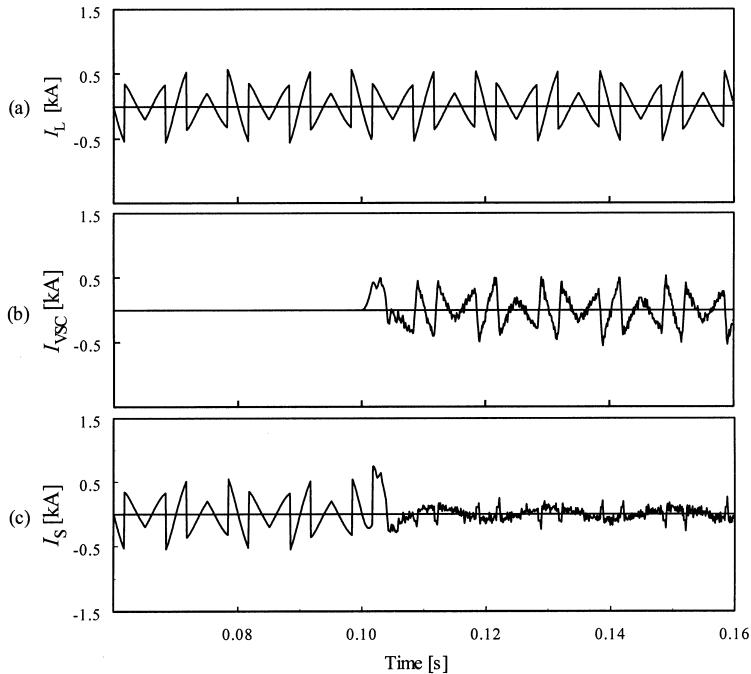
Fig. 8.87 Current harmonic components: (a) current I_L; (b) converter current I_{VSC}; and (c) source current I_S.
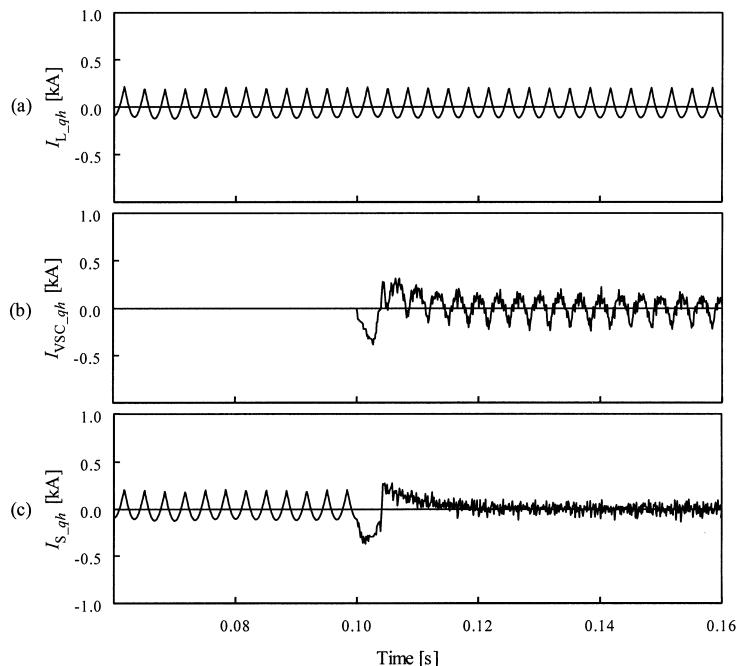

Fig. 8.88 Current harmonic components in the q-axis: (a) current I_{L_qh}; (b) converter current I_{VSC_qh}; and (c) source current I_{S_qh}.
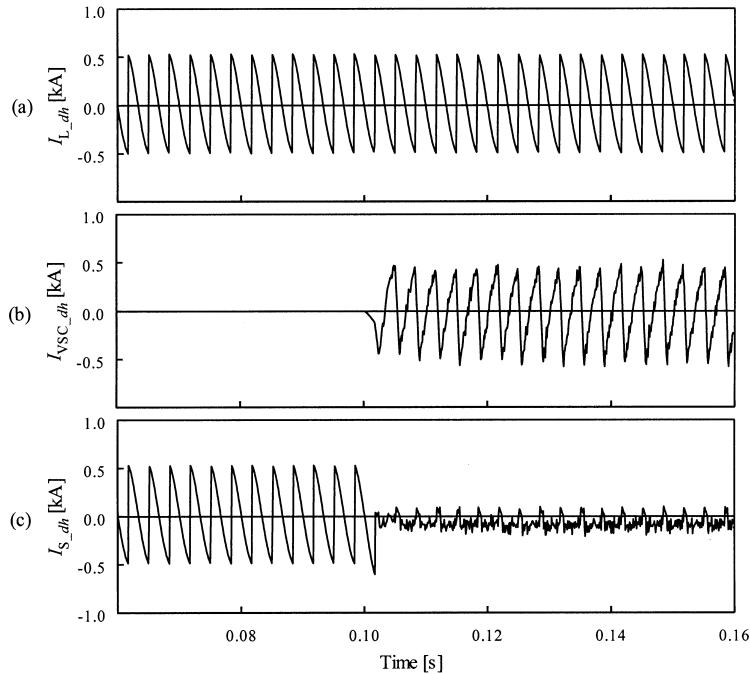
Fig. 8.89 Current harmonic components in the d-axis: (a) current I_{L_dh}; (b) converter current I_{VSC_dh}; and (c) source current I_{S_dh}.
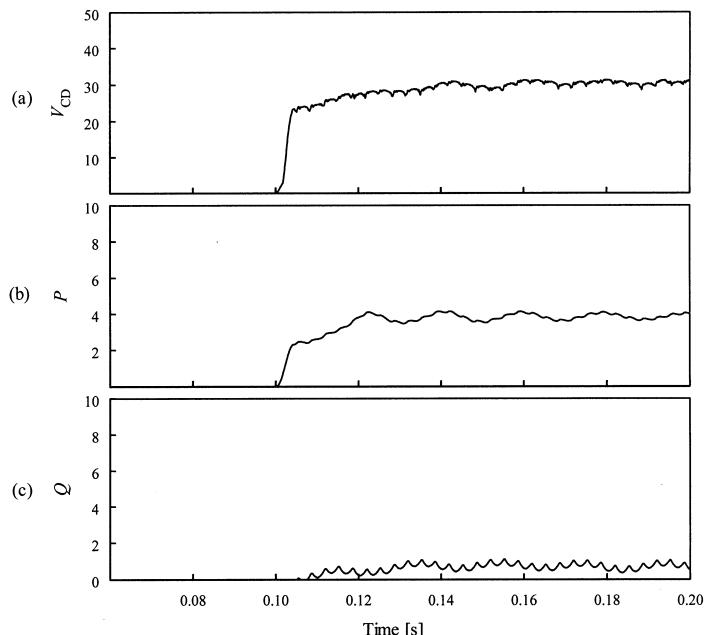

Fig. 8.90 (a) DC link voltage V_{DC}. Power exchange between the AC system and the shunt AF; (b) active power P; and (c) reactive power Q.

8.10   Solid-State Transfer Switch (SSTS)

The SSTS is a high-speed, open-transition switch that enables the transfer of electrical loads from one AC power source to another within a few milliseconds. It is designed to replace the mechanical auto-transfer equipment currently used to switch major industrial and commercial facilities from one feeder to another. The open-transition property of the SSTS means that the switch breaks contact with one source before it makes contact with the other source.

The advantage of this transfer scheme over the closed-transition mechanical switch is that the electrical sources are never cross-connected unintentionally. The cross connection of independent AC sources, with the alternate source switching on to a faulted system is discouraged by electrical utilities (Chan, Kara and Kieboom, 1998). The SSTS can be used very effectively to protect sensitive loads against voltage sags, swells and other electrical disturbances. The basic configuration of this device consists of two three-phase solid-state switches, one for the main feeder and one for the backup feeder. These switches have an arrangement of back-to-back connected thyristors, as illustrated in the one-line diagram shown in Figure 8.91. If a voltage sag or interruption is detected on the main feeder that is supplying the load, then that switch is opened and the load is transferred to the backup feeder within a very short time (Gole and Palav, 1998).

This section presents the time domain analysis of the SSTS system using the electromagnetic transient simulator PSCAD/EMTDC. The test system shown in Figure 8.92 is used in order to carry out transient analysis of the SSTS. The system comprises of two identical feeders feeding into a 13 kV-bus. A sensitive load is connected to the bus.
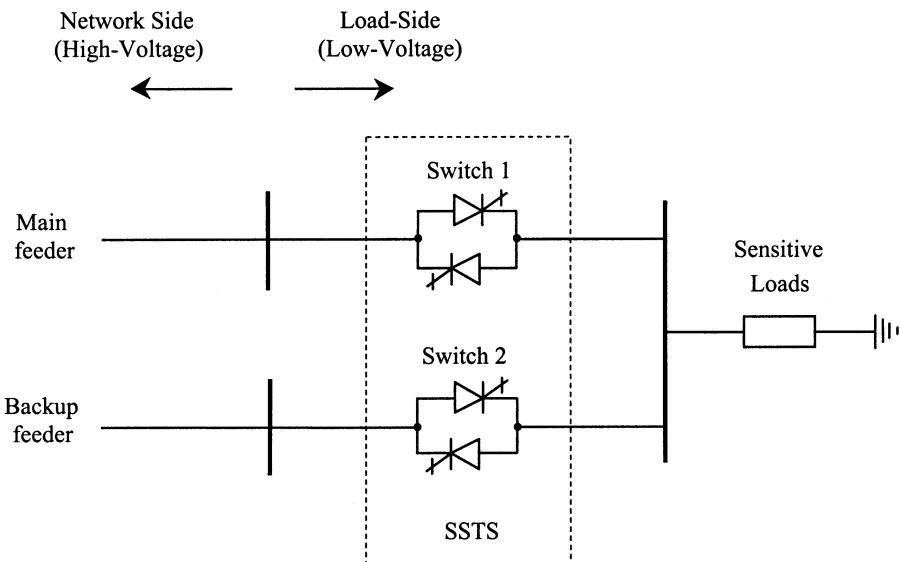

**Fig. 8.91** Schematic representation of the SSTS.
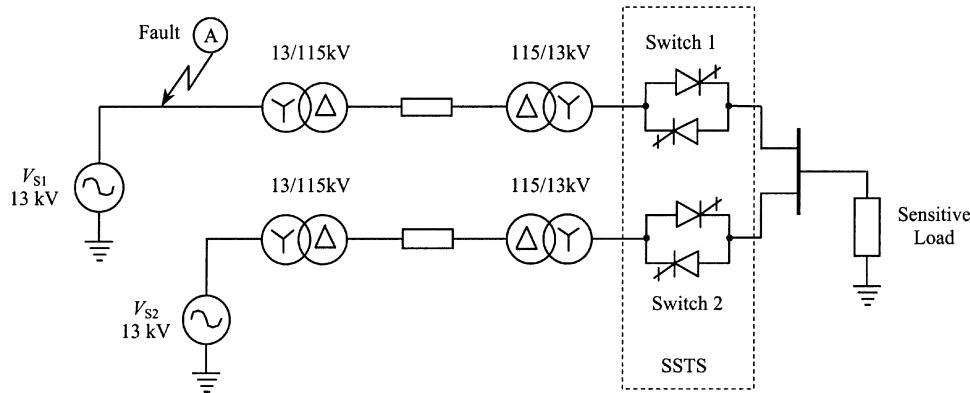
Fig. 8.92 Schematic diagram of the test system used to carry out transient analysis of the SSTS.
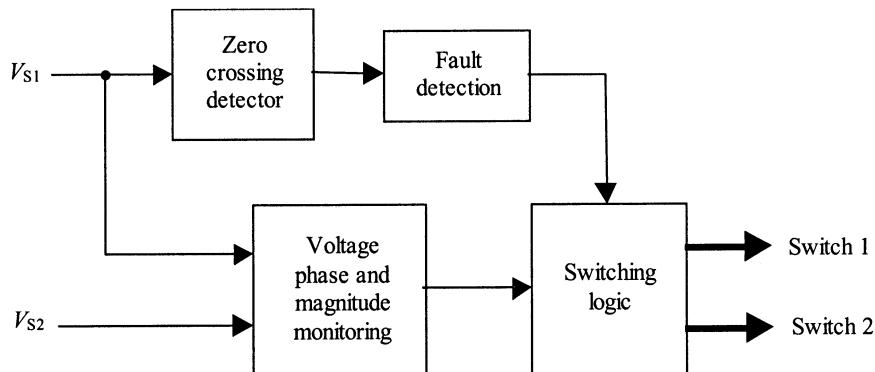

Fig. 8.93 Control circuit designed for the SSTS.

Figure 8.93 shows the block diagram of a simple control strategy that can be used to operate the SSTS for the application illustrated in the example. Each time a fault condition is detected in the main feeder, the control system swaps the firing signals to the thyristors in both switches, *Switch 1* in the main feeder is deactivated and *Switch 2* in the backup feeder is activated.

The control system measures the peak value of the voltage waveform at every half-cycle and checks whether or not it is within a prespecified range. If it is outside limits, an abnormal condition is detected and the firing signals to the thyristors are changed to transfer the load to the healthy feeder. The digital implementation in PSCAD/EMTDC of the test system is shown in Figure 8.94. The following simulations were carried out to perform the time domain analysis of the SSTS:

- In the first experiment the SSTS is disconnected and a three-phase fault is applied at the main feeder in point A as shown in Figure 8.92. The fault is applied at a time
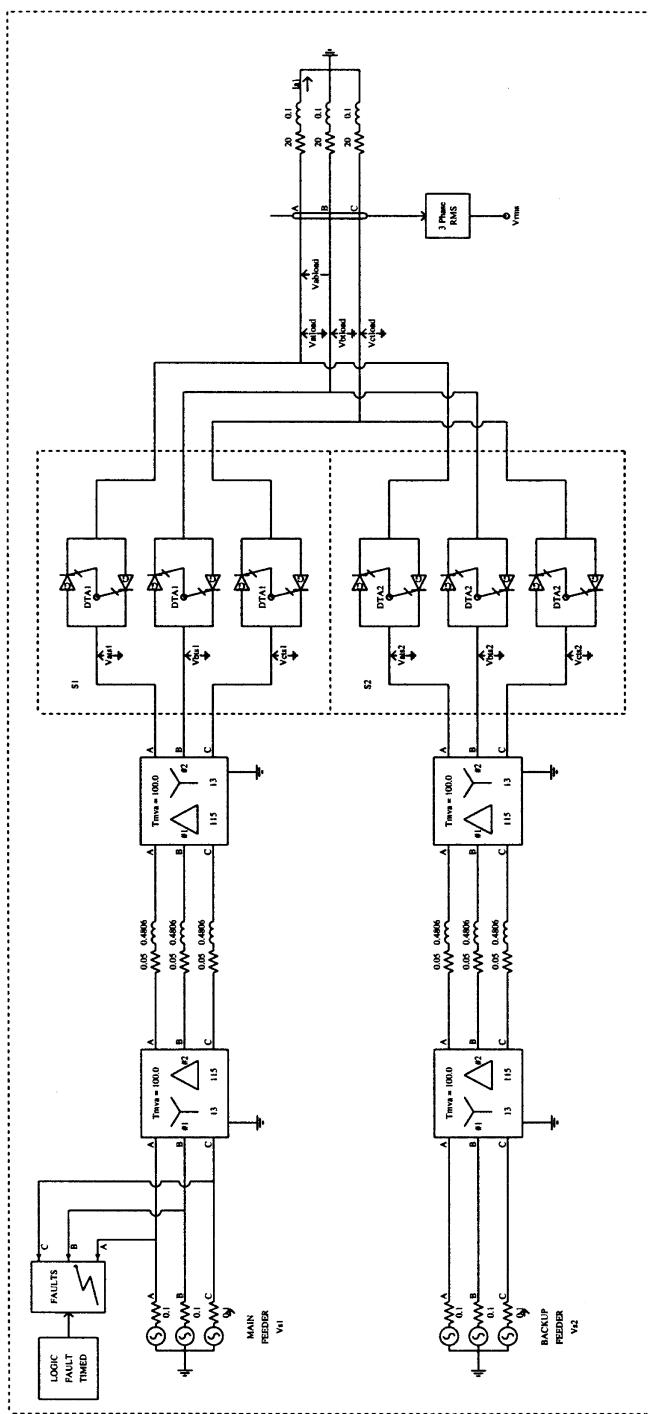
Fig. 8.94 SSTS test system implemented in PSCAD/EMTDC.
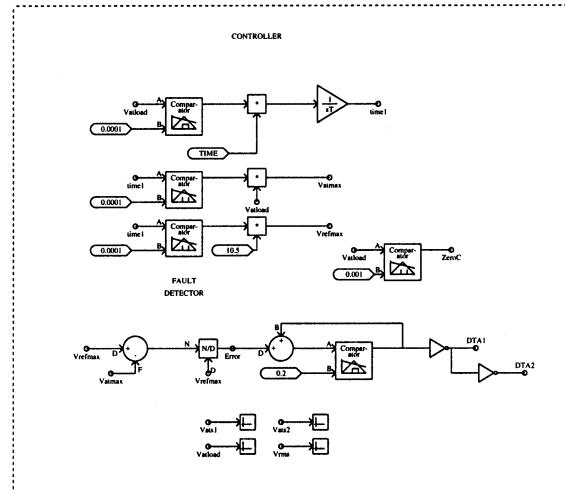
Fig. 8.95 SSTS controller implemented in PSCAD/EMTDC.
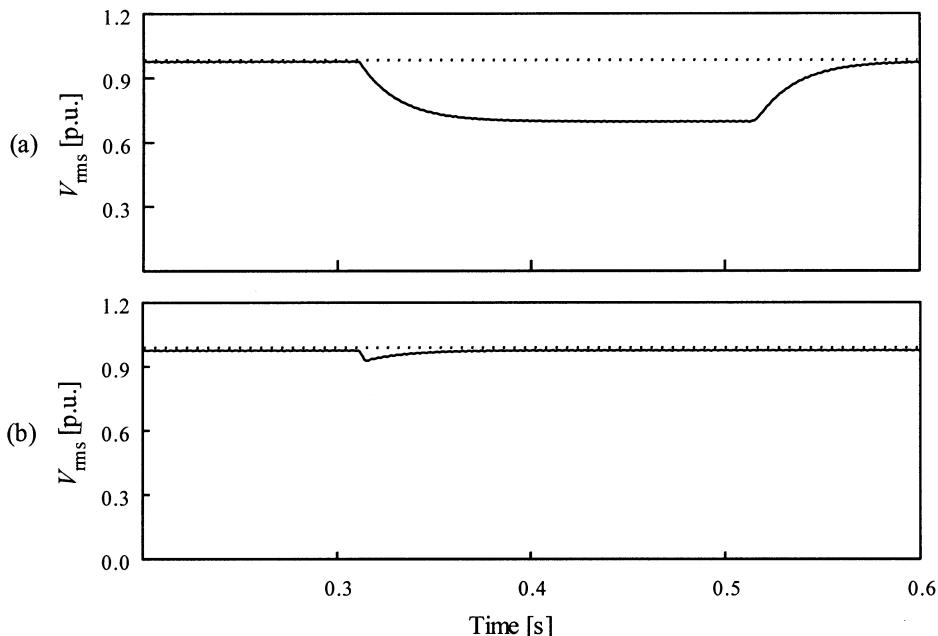
Fig. 8.96 Voltage V_{rms} at the load point. The fault is applied at $t = 0.31$s: (a) without SSTS; and (b) with SSTS operating.

0.31 s with fault duration of 0.2 s. The magnitude of the voltage sag due to the fault is 30%, as seen from the voltage V_{rms} shown in Figure 8.96(a).

- A second experiment was carried out using a similar scenario as above but now with the SSTS in operation. The voltage V_{rms} at the load point is shown in Figure 8.96(b).

As mentioned before, the control system monitors the maximum and minimum values of the voltage waveform at the load point every half-cycle. Whenever a faulted condition in the electrical supply is detected, the triggering signals to both switches are reversed. Figure 8.96(b) shows that after the disturbance has occurred the *rms* voltage at the load point is driven back to the prefault value very rapidly.

It should be noted that the SSTS does not regulate voltage neither generate or absorb reactive power. Its only function is to deactivate a faulty feeder in favour of a fault-free one. The waveform of the voltage V_a at the load point for both operating conditions is shown in Figure 8.97.

It can be seen that when the faulted condition is registered, it only takes a fraction of a cycle (less than 4 ms at 50 Hz fundamental frequency) for the SSTS to perform the transfer of load to the backup feeder, and restore the voltage to the prefault condition. Figure 8.98 shows a few cycles of the voltage waveform to observe in detail the moment of the load transfer between the faulty feeder and the healthy one.

Arguably, there is always a load transfer delay associated with SSTS applications which is a function of the fault detection technique used. In this example, the quality of the voltage waveform is checked at every peak and trough, with respect to a reference voltage value, e.g. 90% of rated value. Besides, monitoring the voltage at peak values reduces the possibility of the control scheme being adversely affected by the presence of large harmonic distortion.

The circuit configurations of an SSTS installation are dependent on several factors such as the availability of an existing alternate source, the size of critical loads, and the need to protect single or several separate critical loads among others. The dual
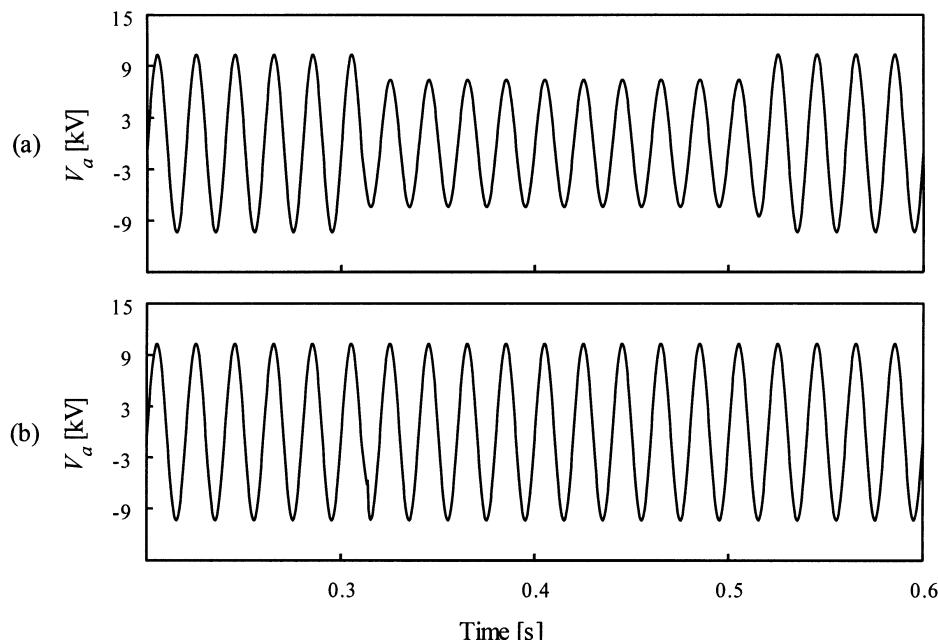
**Fig. 8.97** Phase voltage V_a at the load point. The fault is applied at $t = 0.31$s: (a) without SSTS; and (b) with SSTS operating.
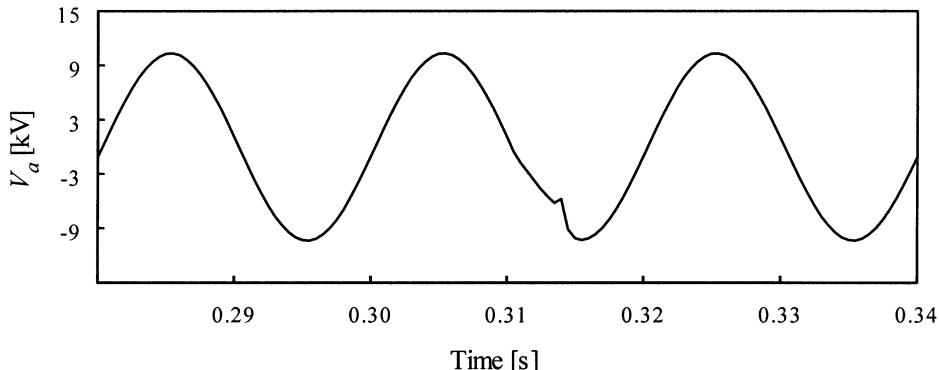
Fig. 8.98 Waveform of the phase voltage V_a at the load point. The fault is applied at $t = 0.31$s.

service circuit configuration shown in Figure 8.91 is the most widely used implementation of the SSTS system. In some application the SSTS is used in conjunction with the D-STATCOM in order to provide sag and swell protection, as well as supply continuous power in the presence of an upstream fault.

8.11   Conclusion

The use of computer programs in the simulation of FACTS and CP controllers, including their controls, is extremely important for the development and understanding of this power electronics-based technology. They yield key information relating to the performance of the system under any operating condition, which is not possible to achieve by analytical means. They allow to identify and to assess the interaction between the various elements in the network. This chapter has presented time-domain results for several FACTS and CP controllers. The highly developed graphics facilities available in the electromagnetic transient simulator PSCAD/ EMTDC were used to conduct all aspects of model implementation and to carry out simulation studies.

The basic control schemes presented in this chapter are simple and easy to implement in any transient simulator. Of course, they may be made to operate more efficiently but this will be at the expense of added control complexity. The reader should have no difficulties in exploring more advanced control aspects in the superb environment afforded by PSCAD/EMTDC.

Examples, problems and exercises

9.1 Simple exercises[1]

1. Draw a diagram of a transmission tower for a high-voltage overhead transmission line.
2. What is the function of a transformer?
3. What parameters are used to describe 'power quality'?
4. What is the minimum number of conductors required for a three-phase overhead transmission line?
5. How is *power factor* defined when the voltage or current is not sinusoidal?
6. Thomas Edison is credited with the invention of 'the electric light bulb'. In the early days of the electricity supply industry (roughly 100 years ago), when the new electric companies were expanding and promoting the use of electric power, Edison believed that DC was superior to AC. On the other hand, George Westinghouse took the opposite view. For low-voltage (i.e. residential) and medium-voltage (industrial) supplies, the argument is obviously well settled in favour of AC, but for very high voltage transmission it is not always a straightforward choice.

   Moreover, in the case of small isolated power systems such as the power system of a *car* or an *aircraft*, the argument is being re-opened. Whereas most cars use 12 VDC and most commercial aircraft use 115-V three-phase AC at 400 Hz, these standards may be replaced within the next decade or two.

   Table 9.1 summarizes some of Edison's and Westinghouse's arguments, along with some additional ones that are relevant today. An additional column is provided for you to add your own comments.

---

[1] The exercises in this section can be used for classwork, either with a whole class or in small groups.

Table 9.1 AC vs. DC: some points for argument and discussion

DC (Edison)	AC (Westinghouse)	Your opinion (DC or AC)
DC requires only two conductors, and in certain cases you can even use a single conductor with 'ground return'. This is obviously cheaper.	AC is more 'natural' than DC because it is what you get when you rotate a magnet inside a coil, and that is really what you have in a power-station generator.	
	It is easier to make switchgear (especially contactors and circuit-breakers) for AC, because you have a natural current-zero every half-cycle, where the current can be interrupted easily without striking a massive arc.	
AC can be easily 'transformed' from low-voltage to high-voltage and back again. This is an advantage in long-distance transmission, or in transmitting high power levels, because you can use a lower current and therefore thinner conductors (and less copper or aluminium).	Westinghouse has Stanley's patents on the transformer, and GE doesn't.[a]	
DC is perfectly smooth and, unlike AC, does not produce 'lamp flicker' or 'AC hum' in telephone and signalling circuits.	DC is perfectly smooth.	
DC is better for lighting, especially public lighting with arc lamps.	AC is better for supplying industry with motive power, because you can use induction motors which are self-starting, highly efficient, and very inexpensive and rugged. Besides, Westinghouse has Tesla's patents on the induction motor, and GE doesn't.	
DC is better for supplying electric railways, because the traction motors are DC motors with very smooth torque control and torque/speed characteristics ideally suited to traction requirements.	With modern field-oriented AC drives, the torque control with AC motors is as good as it is with DC motors.	
DC is better for connecting two large power networks together (e.g. Britain and France, or USA and Canada), because you don't need to synchronize the two networks.	With polyphase AC (i.e. two or three phases) you can run different loads off different phases, so the security of supply is better.	
With AC you have reactance in the circuit, and therefore a larger voltage drop in the cables or overhead lines.	With AC you have reactance in the circuit, and when there is a fault, the reactance limits the fault current.	
With DC and modern power electronics you can create a power supply of any voltage waveform (including sinewave AC, if that is what you want).	With DC motors you need a commutator and brushes, which need frequent maintenance and cause radio interference.	

[a] GE was founded by Thomas Edison.

9.2 A basic worked example – leading and lagging loads

Figure 9.1 shows a circuit with a supply system whose open-circuit voltage is $\mathbf{E}$ and short-circuit impedance is $\mathbf{Z}_s = 0 + jX_s$, where $X_s = 0.1\,\Omega$. The load impedance is $Z = 1\,\Omega$ but the power factor can be unity, 0.8 lagging, or 0.8 leading. For each of these three cases, the supply voltage E must be adjusted to keep the terminal voltage $V = 100\,\mathrm{V}$. For each case determine E, the power-factor angle ϕ, the load angle δ, the power P, the reactive power Q, and the volt-amperes S.
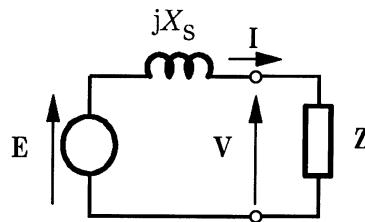

Fig. 9.1 Simple AC circuit.

Unity power-factor. Referring to Figure 9.2, we have $E \cos \delta = V = 100$ and $E \sin \delta = X_s I = 0.1 \times 100/1 = 10\,\mathrm{V}$. Therefore $\mathbf{E} = 100 + j10 = 100.5\mathrm{e}^{j5.71°}\,\mathrm{V}$. The power-factor angle is $\phi = \cos^{-1}(1) = 0$, $\delta = 5.71°$, and $\mathbf{S} = P + jQ = \mathbf{V}\mathbf{I}^* = 100 \times 100\mathrm{e}^{j0} = 10\,\mathrm{kVA}$, with $P = 10\,\mathrm{kW}$ and $Q = 0$.
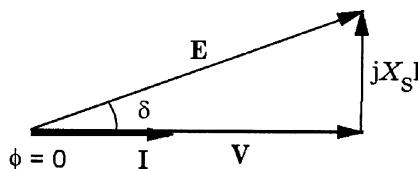

Fig. 9.2 Unity PF.

Lagging power-factor. Referring to Figure 9.3, the current is rotated negatively to a phase angle of $\phi = \cos^{-1}(0.8) = -36.87°$. Although $I = 100\,\mathrm{A}$ and $X_s I$ is still $10\,\mathrm{V}$, its new orientation 'stretches' the phasor $\mathbf{E}$ to a larger magnitude: $\mathbf{E} = \mathbf{V} + jX_s\mathbf{I} =$
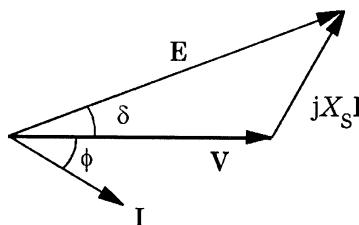
Fig. 9.3 Lagging PF.

$(100 + \mathrm{j}0) + \mathrm{j}0.1 \times 100\mathrm{e}^{-\mathrm{j}36.87°} = 106.3\mathrm{e}^{\mathrm{j}4.32°}$ V. Note that the supply voltage E has to be higher to achieve the same load voltage when the power-factor is lagging. The load angle is $\delta = 4.32°$ and $\mathbf{S} = \mathbf{VI}^* = 100 \times 100\mathrm{e}^{+\mathrm{j}36.87°} = 8000 + \mathrm{j}6000$ VA. Thus $S = 10\,\mathrm{kVA}$, $P = 8\,\mathrm{kW}$ and $Q = +6\,\mathrm{kVAr}$ (absorbed).

Leading power-factor. The leading power-factor angle causes a reduction in the value of E required to keep V constant: $\mathbf{E} = 100 + \mathrm{j}0.1 \times 100\mathrm{e}^{+\mathrm{j}36.87°} = 94.3\mathrm{e}^{\mathrm{j}4.86°}$ V. The load angle is $\delta = 4.86°$, and $\mathbf{S} = 10\,000\mathrm{e}^{-\mathrm{j}36.87°} = 8000 - \mathrm{j}6000$; i.e. $P = 8\,\mathrm{kW}$ and $Q = 6\,\mathrm{kVAr}$ (generated).
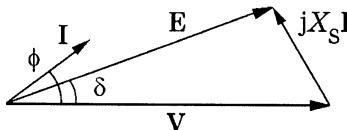

Fig. 9.4 Leading PF.

We have seen that even though the power and the current are the same in all cases, the inductive load with its lagging power factor requires a higher source voltage E. The capacitive load with its leading power factor requires a lower source voltage.

If the source voltage E were kept constant, then the inductive load would have a lower terminal voltage V and the capacitive load would have a higher terminal voltage. As an exercise, repeat the calculations for $E = 100$ V and determine V in each case, assuming that $Z = 1\,\Omega$ with each of the three different power-factors.

We can see from this that power-factor correction capacitors (connected in parallel with an inductive load) will not only raise the power factor but will also increase the voltage. On the other hand, if the voltage is too high, it could conceivably be reduced by connecting inductors in parallel. In modern high-voltage power systems at locations far from the generating stations, it is possible to control the voltage by varying the amount of inductive or capacitive current drawn from the system at the point where the voltage needs to be adjusted. This is called *reactive compensation* or *static VAr control*. In small, isolated power systems (such as an automotive or aircraft power system supplied from one or two generators) this is not generally necessary because the open-circuit voltage of the generator E can be varied by field control, using a *voltage regulator*.

9.3 Simple basic problems

1. A single-phase power system has an open-circuit voltage $E = 6.35\,\mathrm{kV}$ and a fault level of 16 MVA. Calculate the short-circuit current I_{sc} in kA, and the Thévenin internal reactance X_{s} in ohms. (See Figures 2.1 and 9.1).
2. What value of resistance R would draw 1.5 MW when connected to the power system of Question 1? (See Figures 2.1 and 9.2). Calculate also the terminal voltage V, the voltage drop $X_{\mathrm{s}}I$, and the load angle δ.
3. What value of inductive reactance X_{L} would be needed to reduce the voltage by 3% in the power system of Question 1 (assuming that no other loads are

     connected)? (See Figures 2.3 and 9.3). Express the answer in ohms and also *per unit* of X_s (i.e. the ratio X_L/X_s).

4. What value of capacitive reactance X_C would be needed to raise the voltage by 3% in the power system of Question 1 (assuming that no other loads are connected)? (See Figures 2.4 and 9.4). Express the answer in ohms and also *per unit* of X_s (i.e. the ratio X_C/X_s).

5. In the symmetrical power system shown in Figure 2.5a, $E_s = E_r = 6.35\,\text{kV}$ and $X = 2.52\,\Omega$. If the voltage-drop XI is 40% of E_s, calculate the current I, the power transmitted, the power factor at both ends of the line, and the load angle δ between $\mathbf{E}_s$ and $\mathbf{E}_r$.

6. A three-phase delta-connected induction motor is fed from a supply of 440 V line–line, and delivers 225 kW to a water pump. Calculate the line current, assuming 90% for the efficiency and 85% for the power factor.

7. Each phase of a three-phase delta-connected load comprises a capacitor of 40 µF in series with a resistor of 100 Ω. This load is connected to a three-phase supply at 440 V and 50 Hz. Calculate (a) the rms phase current in the load; (b) the line current; and (c) the total power taken from the supply.

8. The load of Question 7 is to be dismantled and shipped to a far-off country, where the local power company has declared that all electrical goods of foreign origin must be connected in star (i.e. wye). Calculate the new line currents and the power taken from the supply, if the phases that were originally connected in delta are reconnected in star. Comment on the result. The supply is still 440 V at 50 Hz.

9. Three impedances, each comprising a resistance of 40 Ω in series with an inductance of 95.5 mH, are connected in wye to a 400 V, 50 Hz, three-phase AC supply. Calculate (a) the supply line current; and (b) the resistance R and inductance L (in series) of a balanced delta-connected load that takes the same line current at the same power factor.

10. Three identical inductive impedances are connected in delta to a 415 V, 50 Hz, three-phase supply of sequence RYB. The current in the R *line* is 4.8 A and it leads the voltage $\mathbf{V}_{YB}$ by 53°. Determine (a) the rms phase current; and (b) the resistance and inductance of each phase-impedance. (*Do* be careful with subscripts, arrows, etc. in this one.)

11. Three single-phase loads are connected to a 250 V, three-phase, three-wire supply of sequence RYB:

      6 kW at unity PF between R and Y;
      4 kW at 0.8 PF leading between Y and B;
      2 kW at 0.5 PF lagging between B and R.

Taking $\mathbf{V}_{RY}$ as reference phasor, calculate all three line-currents. (*Hint:* use $\mathbf{S} = \mathbf{V}\mathbf{I}^*$ and calculate the phase currents first. Watch the asterisks as well as the subscripts and arrows.)

9.3.1 Answers to problems in Section 9.3

1. 2.52 kA; 2.52 Ω.
2. $R = 26.643\,\Omega$ or 0.238 Ω; $V = 6.322\,\text{kV}$ or 0.5979 kV; $X_s I = 0.5979\,\text{kV}$ or 6.322 kV; and δ = 5.403° or 84.597°.

3. $81.48\,\Omega$; 32.33 p.u.
4. $86.52\,\Omega$; 34.33 p.u.
5. $1.008\,\text{kA}$; 6.271 MW; 0.980 lagging at the sending end (E_s); 0.980 leading at the receiving end (E_r).
6. 386 A.
7. (a) $I_{\text{phase}} = 3.44\,\text{A}$; (b) $I_{\text{line}} = 5.96\,\text{A}$; (c) $P = 3.56\,\text{kW}$.
8. $I_{\text{line}} = 1.99\,\text{A}$; $P = 1.19\,\text{kW}$ (*both reduced to one-third*).
9. (a) 4.62 A; (b) $120\,\Omega$; 286 mH.
10. (a) 2.77 A; (b) $120\,\Omega$; 286 mH.
11. $\mathbf{I_R} = 16.0 - \text{j}13.9\,\text{A}$; $\mathbf{I_Y} = -21.6 - \text{j}19.9\,\text{A}$; $\mathbf{I_B} = 5.6 + \text{j}33.7\,\text{A}$.

9.4   Worked examples

1. An inductive three-phase wye-connected load is supplied at $4160\,\text{V}$ and takes $1400\,\text{kW}$ of real power and $700\,\text{kW}$ of reactive power. The supply system impedance is $\text{j}0.9\,\Omega$/phase. Calculate

  (i) the current;
  (ii) the power factor;
  (iii) the open-circuit voltage (i.e. the supply voltage E) if the load voltage $V = 4160\,\text{V}$;
  (iv) the ratio of the open-circuit voltage E to the load voltage V; and
  (v) the load angle (i.e. the phase angle between $\mathbf{E}$ and $\mathbf{V}$).

  (i) $P + \text{j}Q = \sqrt{3}\mathbf{V_L}\mathbf{I_L^*}$
  (ii) $\therefore \mathbf{I_L} = (1400 + \text{j}700) \times 10^3/(\sqrt{3} \times 4160) = 217.23\text{e}^{\text{j}26.56°}\,\text{A}$
  (iii) $\Delta V = \dfrac{X_s Q}{V} + \text{j}\dfrac{X_s P}{V} = \dfrac{0.9 \times 700/3}{4160/\sqrt{3}} + \text{j}\dfrac{0.9 \times 1400/3}{4160/\sqrt{3}}$

  $\qquad = 87.435 + \text{j}174.87 = 195.51\text{e}^{\text{j}63.43°}\,\text{V}.$

  (iv) $\mathbf{E} = (4160/\sqrt{3} + \text{j}87.435) + \text{j}174.87 = 2489.2 + \text{j}174.87 = 2495.3\text{e}^{\text{j}4.02°}\,\text{V}.$

  (v) $\dfrac{E}{V} = \dfrac{2495.3}{4160/\sqrt{3}} = 1.039$

2. For the system in Problem 1, use the equation $V = E(1 - Q/S)$ to estimate the ratio E/V, where S is the short-circuit level.

  $S = 2495^2/0.9 = 6917\,\text{kVA/phase}$, so

  $$V = E\left(1 - \frac{Q}{S}\right) = E\left(1 - \frac{700/3}{6917}\right) = 0.9663$$

  whence $E/V = 1/0.9663 = 1.035$ (Unlike the result of Problem 1, this result is only approximate).

3. For the system in Problem 1, find the capacitance/phase and the total reactive power of a capacitor that will make $E = V = 4160\,\text{V}$, if the load is constant at $1400 + \text{j}700\,\text{kVA}$. The frequency is 50 Hz.

With $E = V$

$$V^2 = \left(V + \frac{X_s Q}{V}\right)^2 + \left(\frac{X_s P}{V}\right)^2$$

$$V^4 = (V^2 + X_s Q)^2 + (X_s P)^2$$

$$\therefore \quad Q^2 + \frac{2V^2}{X_s} Q + P^2 = 0$$

whence $Q = -S \pm \sqrt{S^2 - P^2}$

Now $S = 4.16^2/0.9 = 19.288$ MVA (all three phases) and $P = 1.40$ MVA, so the net reactive power required to make $E = V$ is

$$Q = Q_{\text{load}} + Q_\gamma = -19.2884 \pm \sqrt{19.2884^2 - 1.40^2}$$

$$= -19.2884 \pm 19.2375 = -38.5259 \quad \text{or} \quad -0.0509 \text{ MVA}$$

The correct solution is -0.0509 MVA so that with $Q_{\text{load}} = 0.70$ MVAr we get $Q_\gamma = -0.7509$ MVAr. Then the capacitor current is

$$I_\gamma = \frac{0.7509 \times 10^6}{\sqrt{3} \times 4160} = 104.2 \text{ A}$$

The capacitor reactance must be $(4160/\sqrt{3})/104.2 = 23.047 \, \Omega$/phase (assuming wye connection), and therefore at 50 Hz the required capacitance is $10^6/(2\pi \times 50 \times 104.2) = 138 \, \mu\text{F}$.

4. An unbalanced delta-connected load draws the following power and reactive power from a three-phase supply whose line–line voltage is 560 V:

   200 kW between lines a, b
   170 kW at 0.85 power-factor lagging between lines b, c
   170 kW at 0.85 power-factor leading between lines c, a.

   Determine the susceptances of a purely reactive delta-connected compensating network that will balance this load and correct its power factor to unity. Also determine the resulting line currents.

   General result is

$$B_{\gamma ab} = -B_{ab} + (G_{ca} - G_{bc})/\sqrt{3}$$

$$B_{\gamma bc} = -B_{bc} + (G_{ab} - G_{ca})/\sqrt{3}$$

$$B_{\gamma ca} = -B_{ca} + (G_{bc} - G_{ab})/\sqrt{3}$$

   leaving $G = G_{ab} + G_{bc} + G_{ca}$ in each phase of a wye-connected resulting network. In each phase $P + jQ = VI^* = V^2 Y^*$ so $Y = (P - jQ)/V^2$ so

   in phase ab, $\mathbf{Y}_{ab} = (200 - j0) \times 10^3/560^2 = 0.638 + j0$ S

   in phase bc, $\mathbf{Y}_{bc} = (170 - j105.357)/560^2 = 0.542 - j0.336$ S

   in phase ca, $\mathbf{Y}_{ca} = (170 + j105.357)/560^2 = 0.542 + j0.336$ S

$$B_{\gamma ab} = -0 + (0.542 - 0.542)/\sqrt{3} = 0$$
$$B_{\gamma bc} = -(-0.336) + (0.638 - 0.542)/\sqrt{3} = 0.391 \, \text{S (capacitor)}$$
$$B_{\gamma ca} = -0.336 + (0.542 - 0.638)/\sqrt{3} = -0.391 \, \text{S (inductor)}$$

The resulting impedance in each phase is $0.638 + 0.542 + 0.542 = 1.722 \, \Omega$, so the line current is $(560/\sqrt{3})/1.722 = 187.8 \, \text{A}$.

5. A transmission cable has a sending-end voltage $E_s = 345 \, \text{kV}$ line–line. Losses may be neglected. The cable has an inductive reactance per unit length of $0.60 \, \Omega/\text{km}$ and a capacitive admittance of $50.0 \, \mu\text{S/km}$ at 50 H, and its length is $a = 54.8 \, \text{km}$. Assuming that the receiving-end is open-circuited, calculate

   (i) the surge impedance Z_0;
   (ii) the electrical length θ in degrees;
   (iii) the receiving-end voltage expressed in per-unit with E_s as reference;
   (iv) the sending-end current;
   (v) the reactive power at the sending end, in MVAr; and
   (vi) the reactive power at the sending end, expressed as a fraction of the surge-impedance loading.

   (i) $Z_o = \sqrt{(x_L \cdot x_C)} = \sqrt{(x_L/y_C)} = \sqrt{(0.60/50 \times 10^{-6})} = 109.55 \, \Omega$
   (ii) $\beta = \sqrt{(x_L/x_C)} = \sqrt{(x_L \cdot y_C)} = \sqrt{(0.60 \times 50 \times 10^{-6})} = 5.477 \times 10^{-3}$ radians/km
   $= 0.3138°/\text{km}$, so $\theta = \beta a = 0.3138 \times 54.8 = 17.2°$
   (iii) $\mathbf{V}_r = \dfrac{E_s}{\cos \theta} = \dfrac{1.0}{\cos 17.2°} = 1.0468$
   (iv) $\mathbf{I}_s = j\dfrac{E_s}{Z_o} \tan \theta = \dfrac{345/\sqrt{3}}{109.55} \tan 17.2° \, \text{kA} = j563 \, \text{A}$
   (v) $Q_s = \sqrt{3} \times 345 \times 0.563 = 336 \, \text{MVAr}$
   (vi) $P_o = 345^2/109.55 = 1086.5 \, \text{MVA}$, so $Q_s/P_o = 336/1086.5 = 0.309$ p.u.

6. A transmission cable has a receiving end voltage $V_r = 345 \, \text{kV}$ line–line. The load is 900 MVA with a lagging power factor of 0.88, and is wye-connected. Find the value of the line current, expressed as a phasor. Take $\mathbf{V}_r$ as reference. The cable may be assumed lossless.

   $$P = 900 \times 0.88/3 = 264 \, \text{MW/phase}$$
   $$Q = 300 \times \sin(\cos^{-1}(0.88)) = 300 \times \sin 28.3576° = 142.492 \, \text{MVAr}$$
   Load is lagging or inductive, so $Q > 0$.

   $$\mathbf{I}_r = (P - jQ)/\mathbf{V}_r = (264 - 142.492)/(345/\sqrt{3})$$
   $$= 1.32540 - j0.71537 = 1.50613e^{-j28.3576°} \, \text{kA}$$

7. The cable in Problem 6 has an inductive reactance per unit length of $0.60 \, \Omega/\text{km}$ and a capacitive admittance of $50.0 \, \mu\text{S/km}$ at 50 Hz. The cable length is $a = 14.8 \, \text{km}$. Calculate

   (i) the surge impedance Z_0;
   (ii) the electrical length θ in radians and degrees;

(iii) the sending end voltage when the load is 900 MVA with a lagging power factor of 0.88;
(iv) the transmission angle δ in degrees;
 (v) the sending-end current;
(vi) the power and reactive power at the sending end; and
(vii) draw the phasor diagram showing the phase voltage and current at both ends.

$$\omega\ell = 0.60\,\Omega/\text{km and } \omega c = 50 \times 10^{-6}\,\text{S/km}$$

(i) $Z_0 = \sqrt{(\ell/c)} = \sqrt{(\omega\ell/\omega c)} = \sqrt{(0.60/(50 \times 10^{-6}))} = 109.545\,\Omega$

(ii) $\beta = \sqrt{(\omega\ell \times \omega c)} = \sqrt{(0.60 \times 50 \times 10^{-6})} = 0.005477$ radians/km
$\quad = 0.31382°/\text{km}$
$\quad \theta = \beta a = 0.005477 \times 14.8 = 0.08106$ radians $= 4.64456°$

(iii) $\mathbf{E}_s = \mathbf{V}_r \cos\theta + jZ_0\mathbf{I}_r \sin\theta$
From Question 6, $\mathbf{I}_r = 1.50613e^{-j28.3576°}$ kA

$\therefore \mathbf{E}_s = (345/\sqrt{3})\cos 4.64456° + j109.545 \times \sin 4.64456° \times 1.50613e^{-j28.3576°}$ kV

$\quad = 198.532 + 13.35984\,e^{j(90 - 28.3576)°}$

$\quad = 198.532 + 6.34556 + j11.757 = 204.878 + j11.757$

$\quad = 205.214e^{j3.2843°}$ kV l–n, i.e. 355.442 kV line–line

Thus if $V_r = 1.0$ p.u, $E_s = 205.215/(345/\sqrt{3}) = 1.0303$ p.u.

(iv) Transmission angle $\delta = 3.2843°$.
Check the power transmission: $Z_0 \sin\theta = 109.545\ \sin 4.64456° = 8.87031$
$P = (205.215 \times 345\sqrt{3}/8.87031)\sin 3.2843° = 264.0$ MW/phase.

(v) $\mathbf{I}_s = j(\mathbf{V}_r/Z_0)\sin\theta + \mathbf{I}_r \cos\theta$

$\quad = j(345/\sqrt{3})/109.545 \sin 4.64456° + 1.50613e^{-j28.3576°} \times \cos 4.64456°$

$\quad = 1.32104 - j0.56579$ kA $= 1.43710e^{-j23.1850°}$ kA

(vi) $P_s + jQ_s = \mathbf{E}_s\mathbf{I}_s^* = 3 \times 205.214e^{j3.2843°} \times 1.43710e^{j23.1850°}$
$\quad = 792.0 + j394.3$ MVA.

(vii)

$$\mathbf{E}_s = 205.214\ e^{\,j3.2843}\ \text{kV}$$
$$\mathbf{V}_r = 199.186\ e^{\,j0}\ \text{kV}$$
$$\mathbf{I}_s = 1.43710\ e^{\,j23.185}\ \text{kA}$$
$$\mathbf{I}_r = 1.50613\ e^{\,j28.3576}\ \text{kA}$$
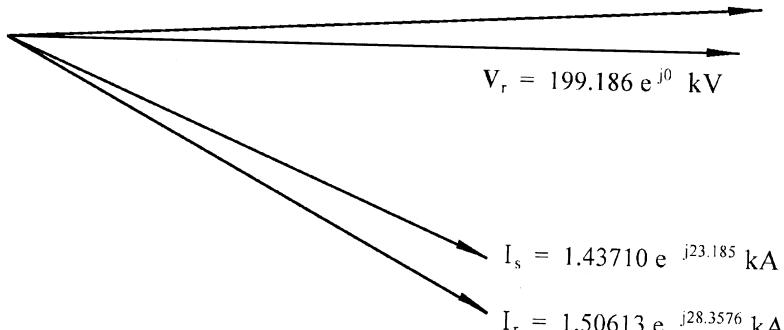
Fig. 9.5

8. If the load in Problem 7 is disconnected, and no change is made to the sending-end voltage, what will be the value of the receiving-end voltage? Also calculate the charging current and the charging MVAr at the sending end.

   With $I_r = 0, E_s = V_r \cos\theta$ so $V_r = 355.442/\cos 4.64456° = 356.613\,\text{kV} = 1.03366\,\text{p.u.}$ Charging current is $\mathbf{I}_s = j(E_s/Z_o)\tan\theta = j(205.214/109.545)\tan 4.64456° = j0.15219\,\text{kA}$. Charging MVAr $= \sqrt{3} \times 355.442 \times 0.15219 = 93.695\,\text{MVAr}$.

9. A 29.6-km lossless transmission cable has synchronous machines at both ends, which maintain the terminal voltages at 345 kV line–line. If the inductive reactance per unit length is 0.60 Ω/km and the capacitive admittance is 50.0 μS/km at 50 Hz, calculate

   (i) the Surge Impedance Load P_0;
   (ii) the maximum transmissible power P_{max};
   (iii) the reactive power requirements at both ends, when the load power is $0.23P_0$ and the mid-point voltage is held at 1.0 p.u. by adjusting the sending- and receiving-end voltages; and
   (iv) the values of the sending- and receiving-end voltages required to maintain 1.0-p.u. voltage at the mid-point.
   The surge impedance Z_0 is the same as the cable in Question 7, i.e. $Z_0 = 109.545\,\Omega$.

   (i) $P_0 = V_0^2/Z_0 = 345^2/109.545 = 1086.54\,\text{MW}$
   (ii) Electrical length $\theta = 2 \times 4.64456° = 9.28912°$ $P_{\text{max}} = P_0/\sin\theta = 1086.54/\sin 9.28912° = 6731.28\,\text{MW}$
   (iii) $Q_s = P_0 \left[\dfrac{P^2}{P_o^2}\dfrac{V_o^2}{V_m^2} - \dfrac{V_m^2}{V_o^2}\right]\dfrac{\sin\theta}{2} = 1086.54 \times [0.23^2 - 1]\dfrac{\sin 9.28912°}{2} = -83.054\,\text{MVA}$

   $Q_s < 0$, i.e. absorbing reactive power. At the receiving end $Q_r = -Q_s$, also absorbing.
   (iv) $E_s = E_r = \sqrt{1 - \left[1 - \dfrac{P^2}{P_0^2}\right]\sin^2\dfrac{\theta}{2}} = \sqrt{1 - [1 - 0.23^2]\sin^2 4.64456°} = 0.99689\,\text{p.u.}$

10. (i) Define the terms *surge impedance loading, transmission angle* and *electrical length* in relation to an electrical transmission line or cable.
    (ii) Write an equation for the phasor voltage $\mathbf{E}_s$ at the sending end of a lossless cable, in terms of the voltage $\mathbf{V}_r$, power P_r and reactive power Q_r at the receiving-end, if the electrical length is θ radians. Include the transmission angle δ in the expression for $\mathbf{E}_s$, and use it to derive an equation for the reactive power requirements Q_s and Q_r in terms of the transmission angle δ, the electrical length θ, and the voltages E_s and E_r.
    (iii) A cable having an electrical length of 8.7° has a rated voltage of 500 kV line–line, and a surge impedance $Z_0 = 50.4\,\Omega$. (i) Determine the maximum transmissible power P_{max} when it is operated as a symmetrical line with $E_s = E_r = 500\,\text{kV}$; and (ii) Determine the transmission angle δ and the reactive power requirements at both ends of the cable when the power transmission is 47% of the surge impedance load.

    (i) Surge impedance load = that load which produces a flat voltage profile, i.e. V_0^2/Z_0.
    Transmission angle δ = angle between E_s and E_r.

Electrical length θ = phase angle between E_s and E_r at the surge-impedance load.

(ii) $\mathbf{E}_s = \mathbf{E}_s e^{j\delta} = \mathbf{V}_r \cos\theta + jZ_0 \dfrac{P_r - jQ_r}{V_r} \sin\theta$

... use this to derive

$$Q_s = -Q_r = -\frac{E_s^2(\cos\delta - \cos\theta)}{Z_0 \sin\theta}$$

(iii) (a) Surge impedance load $P_0 = V_0^2/Z_0 = 500^2/50.4 = 4960\,\text{MW}$ $P_{\max} = P_0/\sin\theta = 4960/\sin 8.7° = 32\,793\,\text{MW}$.

(b) $P/P_0 = \sin\delta/\sin\theta = 0.47$, so $\sin\delta = 0.47 \times \sin 8.7°$, i.e. $\delta = 4.07674°$.
$Q_s = -Q_r = -500^2(\cos 4.07674° - \cos 8.7°)/(50.4 \sin 8.7°)$
$= -294.3\,\text{MVAr} -$ absorbing at both ends.

11. (i) What are the functions of *reactive compensation* applied to electrical transmission systems?

(ii) What are the differences between *passive* and *active* compensators? Give examples of both.

(iii) By means of a sketch showing V_r/E_s vs. P/P_0, illustrate how the receiving-end voltage of a transmission cable can be maintained within a narrow range near 1.0 p.u. by means of switched shunt compensating devices. E_s is the sending-end voltage, P is the power transmission, and P_0 is the natural load.

(i) (a) to produce a flat voltage profile at all levels of power transmission;

(b) to improve stability by increasing the maximum transmissible power $P_{\max}$; and

(c) to provide the most economical means for meeting the reactive power requirements.

(ii) Passive compensation = fixed or switched reactors and capacitors
Active compensation = continuously variable devices: e.g. thyristor-controlled reactors, synchronous condensers, AVRs used with turbine-generators; 'FACTS' devices.

(iii)
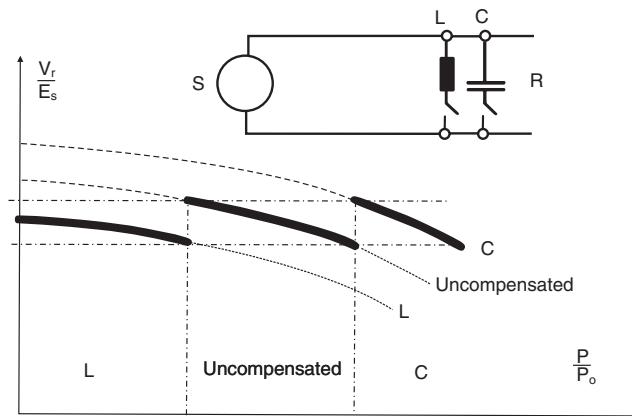
Fig. 9.6

12. (i) Write an equation for the phasor voltage $\mathbf{E}_s$ at the sending end of a lossless cable, in terms of the voltage $\mathbf{V}_r$, power P_r and reactive power Q_r at the receiving end, if the electrical length is θ radians. Use this equation to derive an expression for the reactance X required to make the no-load voltage at the receiving end of a radial transmission cable equal to the sending-end voltage.

(ii) Using the theory of part (i) and any necessary development thereof, determine the values of four reactors equally spaced along a 500 kV, 80-km symmetrical line such that the no-load voltage profile is substantially flat. Of the four reactors, one is at the sending end and one at the receiving end, and the synchronous machines at the two ends contribute no reactive power. The line series inductive reactance is $0.60\,\Omega/\text{km}$ and shunt capacitive susceptance is $50.0\,\mu\text{S/km}$.

(iii) What is the maximum voltage in the compensated line of part (b) at no-load, and where does it occur?

(iv) What is the total combined reactive power of the four reactors at no-load and rated voltage?

(i) $\mathbf{E}_s = \mathbf{V}_r \cos\theta + j Z_o \mathbf{I}_r \sin\theta = \mathbf{V}_r \left[\cos\theta + \dfrac{Z_o}{X}\sin\theta\right]$

so that for $E_s = V_r$

$$X = Z_o \frac{\sin\theta}{1 - \cos\theta}$$

(ii) $\theta = 80 \times \sqrt{(0.60 \times 50 \times 10^{-6})} = 0.43818$ radians $= 25.1°$

$Z_0 = \sqrt{(0.60/(50 \times 10^{-6}))} = 109.545\,\Omega$

(iii) $2X$ at the ends and X at two intermediate locations (26.7 km from each end).
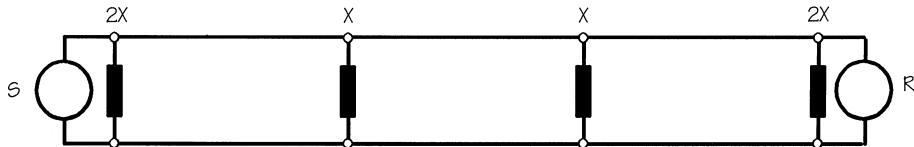

Fig. 9.7

$$X = \frac{Z_0}{2}\frac{\sin(\theta/n)}{1 - \cos(\theta/n)} = \frac{109.545}{2}\frac{\sin(25.1/3)}{1 - \cos(25.1/3)} = 748\,\Omega$$

Maximum voltage is at the mid-point and at $80/6 = 13.3$ km from each end:
$V_m = E_s/\cos(\theta/2n)$ with $n = 3$; i.e. $V_m = 500/\cos(25.1/6) = 500 \times$
1.00267 kV line–line or 1.00267 p.u.

(iv) Total compensating reactive power $= (500/\sqrt{3})^2/748 \times 3 \times (1+1+1/2+1/2) =$
1.003 MVAr.

13. A 500-kV cable is 80 km long and has a mid-point dynamic shunt compensator that maintains the voltage at its terminals equal to 1.0 p.u. under all loading

conditions. The series inductive reactance of the line is $X_{\mathrm{L}} = 48.0\,\Omega$ and the shunt capacitive susceptance is $B_{\mathrm{c}} = 4000\,\mu\mathrm{S}$. Calculate

(i) the transmission angle δ when the load is $1540\,\mathrm{MW}$;
(ii) the value of the compensating susceptance B_{γ} and reactance X_{γ} at this load.

(i) $P = \dfrac{2E^2}{X_{\mathrm{L}}}\sin\dfrac{\delta}{2} = 1540 = \dfrac{2 \times 500^2}{48}\sin\dfrac{\delta}{2}$

so $\delta = 17.0°$.

(ii) $B_{\gamma} = \dfrac{B_{\mathrm{c}}}{2} - \dfrac{4}{X_{\mathrm{L}}}\left[1 - \dfrac{E}{E_{\mathrm{m}}}\cos\dfrac{\delta}{2}\right]$

$\quad = \dfrac{4000 \times 10^{-6}}{2} - \dfrac{4}{48}\left[1 - \cos\dfrac{17°}{2}\right] = 0.00108\,\mathrm{S}$

so $X_{\gamma} = 1/0.00108 = 922\,\Omega$.

Problem 13 – alternative solution (i)
In this solution, we represent the inductance and capacitance of the line by 'lumped parameters' distributed as shown in Fig. 9.8. The phasor diagram is shown in Fig. 9.9. Note the extensive use of symmetry in drawing these diagrams. Each half of the line is represented by a π equivalent circuit. The phasor diagram emphasizes the sending-end half of the line, with $\mathbf{E}_{\mathrm{s}}$ at one end and $\mathbf{V}_{\mathrm{m}}$ at the other; the receiving-end
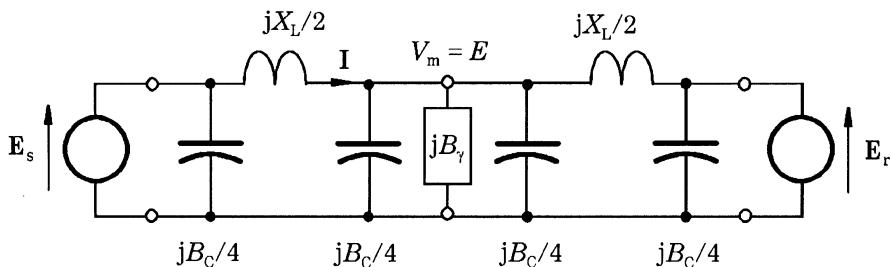

Fig. 9.8 Lumped-parameter representation of line with mid-point compensator.
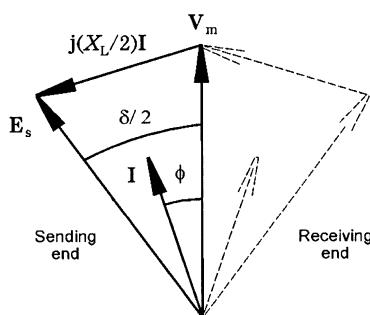
Fig. 9.9 Phasor diagram.

half is similar, with $\mathbf{V}_m$ at one end and $\mathbf{E}_r$ at the other. The voltages E_s and E_r are both equal to E and the reactive compensator maintains $V_m = E$.

For the sending-end half of the line we can write

$$P = \frac{E^2}{X_L/2} \sin \frac{\delta}{2}$$

so that $1540 = 500^2/24 \sin (\delta/2)$, giving $\delta/2 = 8.50177°$. This is the transmission angle over each half of the line, so the total transmission angle is $\delta = 17.0°$. By symmetry, the current phasor is at right-angles to the voltage-drop phasor joining $\mathbf{V}_m$ and $\mathbf{E}_s$, so that the power-factor angle between $\mathbf{I}$ and $\mathbf{V}_m$ is $\phi = \delta/4 = 4.25089°$. The same power-factor angle is between $\mathbf{E}_s$ and $\mathbf{I}$, but it is a lagging angle at the sending end and leading at the mid-point. This indicates that the line inductance is absorbing reactive power at both points. The reactive power absorbed by $X_L/2$ is $I^2 X_L/2$/phase. Since $P = \sqrt{3}V_{LL}I_L \cos \phi$, $I_L = 1540/(\sqrt{3} \times 500 \times \cos 4.25089°) = 1.78314\,\text{kA}$, so that the total reactive power absorbed is $3I^2 X_L/2 = 228.93143\,\text{MVAr}$ in each half of the line, or $457.86286\,\text{MVAr}$ over the whole line. Of this, 25% is absorbed at the two ends and 50% ($228.93143\,\text{MVAr}$) at the mid-point. However, the shunt capacitance at the mid-point is *generating* $2 \times E^2 B_c/4 = 2 \times 500^2 \times (4000 \times 10^{-6}/4) = 500\,\text{MVAr}$. Therefore, the *net* reactive power at the mid-point is $500 - 228.93143 = 271.06857\,\text{MVAr}$, and this must be *absorbed* by the compensator. The compensator must therefore have an inductive susceptance $B_\gamma = 271.06857/500^2 = 0.00108\,\text{S}$, or a reactance $X_\gamma = 922.2\,\Omega$. At the sending end, the generator absorbs $271.06857/2 = 135.5\,\text{MVAr}$, and the same at the receiving end.

Problem 13 – alternative solution (*ii*)
We can treat the line as a 'long line' and use the distributed-parameter equations based on Z_0, θ, etc. Thus, $Z_0 = \sqrt{(X_L X_C)}$ where $X_L = 48\,\Omega$ and $X_C = 1/4000 \times 10^{-6} = 250\,\Omega$, so $Z_0 = 109.545\,\Omega$.[2] Also the electrical length is $\theta = \sqrt{(X_L/X_C)} = \sqrt{(48/250)} = 0.43818$ radians $= 25.10575°$. Taking just one half of the line, with equal voltages at both ends, we can use the equation

$$P = \frac{E^2}{Z_0 \sin \dfrac{\theta}{2}} \sin \frac{\delta}{2}$$

i.e. $1540 = 500^2/(109.545 \sin 25.10575°/2) \sin (\delta/2)$, giving $\delta = 16.87°$. (Note the slight difference from the $17.0°$ obtained with the 'lumped-parameter' method in solution (i) above.)

We can now find the reactive power required at each end of each half of the line:

$$Q_s = -\frac{E^2(\cos \delta - \cos \theta)}{Z_0 \sin \theta} = \frac{500^2(\cos 8.43346° - \cos 12.55288°)}{109.545 \sin 12.55288°} = -137.46\,\text{MVAr}$$

with the same at the receiving end and twice this value at the mid-point, i.e. $274.93\,\text{MVAr}$. The compensator must have a susceptance equal to $274.93/500^2 = 0.00110\,\text{S/phase}$, i.e. a reactance of $909.35\,\Omega$/phase. Again note the slight difference from the $922.2\,\Omega$/phase calculated with the lumped-parameter model.

---

[2] Note that X_L is proportional to the line length, whereas X_C is inversely proportional to the line length, so that $Z_0 = \sqrt{(X_L X_C)} = \sqrt{(x_L x_C)}$, where X is total reactance and x is reactance per unit length.

In this solution, the line capacitance and inductance do not appear explicitly since they are incorporated in the constants Z_0 and θ.

The two ends of the line and the compensator in the middle are all absorbing reactive power, indicating that the line is working below its surge impedance loading. To check this, note that $P_0 = 500^2/109.545 = 2282$ MW, which is indeed greater than the power transmission of 1540 MW.

14. (i) What is meant by the *system load line* in relation to the voltage at a busbar in a power transmission system?
   (ii) A power transmission system with a high $X{:}R$ ratio has a short-circuit level of 14 500 MVA. What is slope of the system load line in p.u./MVAr?

   (i) The system load line shows the relation between V/E and Q/S, where V is the actual bus voltage, E is the no-load voltage, Q is the reactive power drawn from the bus, and S is the short-circuit level. The equation of the load line is approximately $V/E = 1 - Q/S$.
   (ii) Slope of load-line $= \mathrm{d}(V/E)/\mathrm{d}(Q/S) = -1$.

15. An unbalanced three-phase load is delta-connected to a balanced power supply at 415 V line–line. The impedances are $Z_{ab} = 0.9584\,\Omega$ at unity power-factor; $Z_{bc} = 0.9584\,\Omega$ at 0.9 power-factor leading; and $Z_{ca} = 0.9584\,\Omega$ at 0.7 power-factor lagging. Determine the impedances of three reactive compensating capacitors or reactors connected in parallel with the three load impedances, such that the resulting load is balanced and has unity power factor. What is the line current of the compensated load?

$$Y_{ab} = G_{ab} + jB_{ab} = 1/0.9584 = 1.04341\ \text{S}$$

$$Y_{bc} = G_{bc} + jB_{bc} = 1/[0.9584\mathrm{e}^{-j\,\mathrm{Arc\,cos}\,(0.9)}] = 0.93907 + j0.45481\ \text{S}$$

$$Y_{ca} = G_{ca} + jB_{ca} = 1/[0.9584\mathrm{e}^{j\,\mathrm{Arc\,cos}\,(0.7)}] = 0.73038 - j0.74514\ \text{S}$$

$$B_{\gamma ab} = -B_{ab} + (G_{ca} - G_{bc})/\sqrt{3} = (0.73038 - 0.93907)/\sqrt{3}$$
$$= -0.12049\ \text{(inductive)}$$

$$B_{\gamma bc} = -B_{bc} + (G_{ba} - G_{ca})/\sqrt{3} = -0.45481 + (1.04341 - 0.73038)/\sqrt{3}$$
$$= -0.27408\ \text{(inductive)}$$

$$B_{\gamma ca} = -B_{ca} + (G_{bc} - G_{ab})/\sqrt{3} = 0.74514 + (0.93907 - 1.04341)/\sqrt{3}$$
$$= 0.68490\ \text{(capacitive)}$$

$$Z_{\gamma ab} = 1/(-j0.12049) = j8.30\,\Omega\ \text{(inductive)}$$
$$Z_{\gamma bc} = 1/(-j0.27408) = j3.65\,\Omega\ \text{(inductive)}$$
$$Z_{\gamma ca} = 1/(j0.68490) = -j1.46\,\Omega\ \text{(capacitive)}$$

Line current $I_L = (V_{LL}/\sqrt{3})/G$
where $G = G_{ab} + G_{bc} + G_{ca} = 1.04341 + 0.93907 + 0.73038 = 2.71286$.
Thus $I_L = (415/\sqrt{3})/2.71286 = 88.3$ A.

16. (i) Explain the difference between a *wye* connection and a *delta* connection, and mention one advantage of each connection.

(ii) Draw the circuit diagram of a wye-connected supply with a delta-connected load. Also draw two separate phasor diagrams, one for the voltages and currents of the supply, and the other for the voltages and currents of the load. Use the phasor diagrams to show that under balanced conditions

$$V_{LL} = \sqrt{3}V_{ph} \quad \text{and} \quad I_L = I_{ph} \text{ at the supply, and}$$
$$V_{LL} = V_{ph} \quad \text{and} \quad I_L = \sqrt{3}I_{ph} \text{ at the load;}$$

where I_L is the line current, I_{ph} is the phase current, V_{LL} is the line–line voltage, and V_{ph} is the phase voltage.

(iii) A 415-V, three-phase, three-wire supply has phase sequence RYB, with the following loads:

6.0 kW at unity power-factor between lines R,Y;
4.5 kW at 0.8 power-factor lagging between lines Y,B;
2.7 kW at 0.5 power-factor leading between lines B,R.

Taking $\mathbf{V}_{RY}$ as reference phasor, calculate all three-phase currents and all three-line currents. Hence, calculate the ratio of the average-line current to the average-phase current.

(i) Advantage of wye: provides earthing point. If three-wire, it suppresses triplen-harmonic currents and permits two-wattmeter method to be used. Advantage of delta: provides path for triplen currents.
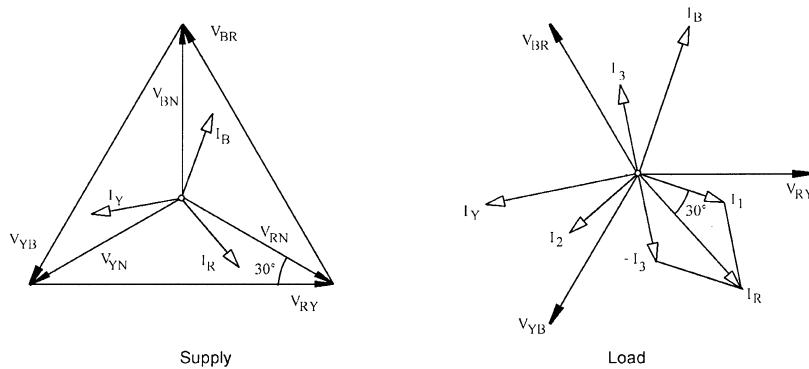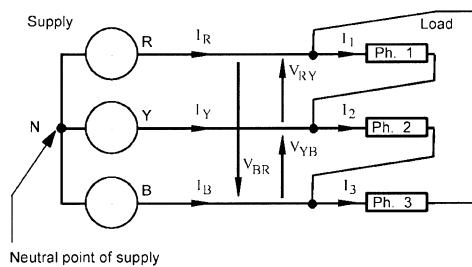
Fig. 9.10

(ii) From supply diagram, $\mathbf{I_L} = \mathbf{I_{ph}}$ in all three lines/phases. From the voltage diagram, $V_{RY} = 2\cos 30° \times V_{RN} = \sqrt{3}V_{RN}$; other lines/phases likewise. From load diagram, $\mathbf{I_R} = \mathbf{I_1} - \mathbf{I_3}$ and if balanced, $I_L = 2 \times \cos 30° \, I_{ph} = \sqrt{3}I_{ph}$.

(iii) $6000 + j0 = \mathbf{V_{RY}I^*_{RY}} = 415e^{j0}\mathbf{I^*_{RY}}$ so $\mathbf{I_{RY}} = 14.458\text{A} = \mathbf{I_1}$

$(4500/0.8)e^{j\cos^{-1}(0.8)} = 415e^{-j120°}\mathbf{I^*_{YB}}$ so $\mathbf{I_{YB}} = 13.554e^{-j156.87°}\text{A} = -12.464 - j5.324\text{A} = \mathbf{I_2}$

$(2700/0.5)e^{-j\cos^{-1}(0.5)} = 415e^{j120°}\mathbf{I^*_{BR}}$ so $\mathbf{I_{BR}} = -13.012\text{A} = \mathbf{I_3}$

$\mathbf{I_R} = \mathbf{I_1} - \mathbf{I_3} = 27.470\text{A}$

$\mathbf{I_Y} = \mathbf{I_2} - \mathbf{I_1} = -26.922 - j5.324\text{A} = 27.444e^{-j168.813°}\text{A}$

$\mathbf{I_B} = \mathbf{I_3} - \mathbf{I_2} = -0.548 - j5.324\text{A} = 5.352e^{j95.877°}\text{A}$

Average line current/Average phase current $= (27.470 + 27.444 + 5.352)/(14.458 + 13.554 + 13.012) = 1.469$.

17. (i) Draw a circuit diagram showing the connection of two wattmeters to measure the power in a three-wire supply to a three-phase load.

(ii) Using a suitable phasor diagram for the two-wattmeter connection, prove that the power-factor angle ϕ of a balanced load can be determined from the equation

$$\tan\phi = \sqrt{3}\frac{P_1 - P_2}{P_1 + P_2}$$

where P_1 and P_2 are the readings on the individual wattmeters.

(iii) A three-phase AC motor draws balanced currents from a three-phase supply. Its power factor is 0.85 lagging. The output power of the motor is 9.7 kW and the efficiency is 92%. Determine the individual readings P_1 and P_2 of two wattmeters measuring the input power to the motor in the two-wattmeter connection.

(i)
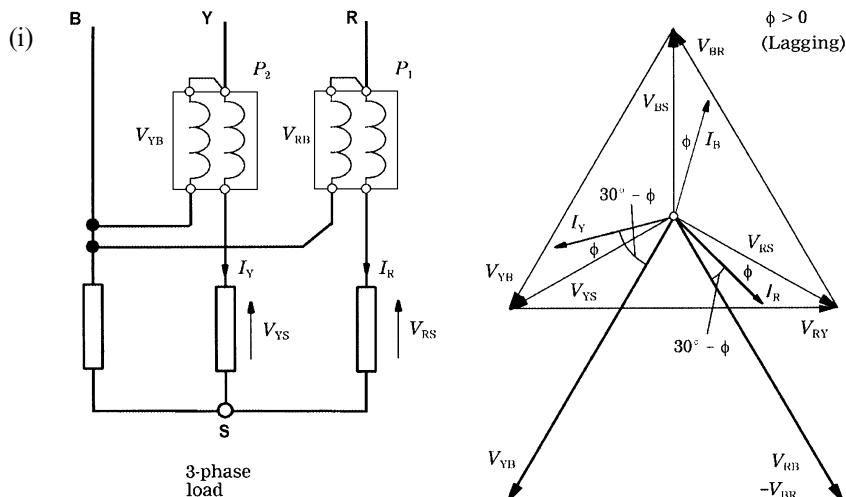
Fig. 9.11

(ii) $P_1 = V_{RB}I_R \cos(30° - \phi) = V_{LL}I_L(\cos 30° \cos \phi + \sin 30° \sin \phi)$
 $P_2 = V_{YB}I_Y \cos(30° + \phi) = V_{LL}I_L(\cos 30° \cos \phi - \sin 30° \sin \phi)$
 $P_1 + P_2 = V_{LL}I_L \times 2\cos 30° \cos \phi = \sqrt{3}V_{LL}I_L \cos \phi = P$ (total power)
 $P_1 - P_2 = V_{LL}I_L \times 2\sin 30° \sin \phi = V_{LL}I_L \sin \phi$

Hence

$$\tan \phi = \sqrt{3}\frac{P_1 - P_2}{P_1 + P_2}$$

(iii) $P = 9700/0.92 = 10\,543\text{W} = P_1 + P_2$
 $\tan \phi = \tan(\arccos(0.85)) = 0.620$

$$\therefore P_1 - P_2 = 0.620/\sqrt{3} \times 10\,543 = 3.773\text{W}$$
$$P_1 + P_2 = 10\,543\text{W}$$
$$2P_1 = 10\,543 + 3773 = 14\,316 \text{ so } P_1 = 7158\text{W}$$
$$2P_2 = 10\,543 - 3773 = 6770 \text{ so } P_2 = 3385\text{W}.$$

18. (i) State four distinct functions of power transformers.
 (ii) Draw the equivalent circuit of one phase of a three-phase power transformer, with all impedances referred to the HV (high-voltage) side.
 (iii) A 250-kVA, 10-kV/400-V, three-phase Yy0 transformer gave the following standard test data for the line–line voltage, line current, and total three-phase input power:

Input to HV winding; LV short-circuited : $V_{LL} = 1005\,\text{V}$, $I_L = 14.4\,\text{A}$, $P = 2.49\,\text{kW}$.
Input to LV winding; HV open-circuited: $V_{LL} = 400\,\text{V}$, $I_L = 3.886\,\text{A}$, $P = 2.50\,\text{kW}$.

Make a neat sketch of an approximate equivalent circuit for one phase of this transformer, in which all the impedances R_1, R_2', jX_{L1}, jX_{L2}', R_c and jX_m are referred to the HV winding. Determine the values of these parameters.

(i)
- Transform voltage level for optimum transmission
- Transform current level for measurement (C.T.); or voltage (P.T. or V.T.)
- Isolate coupled circuits
- Impedance matching
- Introduce series impedance (to limit fault current)
- Create a neutral point (e.g. ground connection remote from power station)
- Suppress harmonics (especially triplen harmonics)
- Provide tappings for loads along a transmission line
- Produce phase shift or multiple phases (e.g. for multiple-pulse converters)
- Produce frequency-multiplication (saturated core)
- Constant-voltage reactive compensation (saturated core).

(ii)
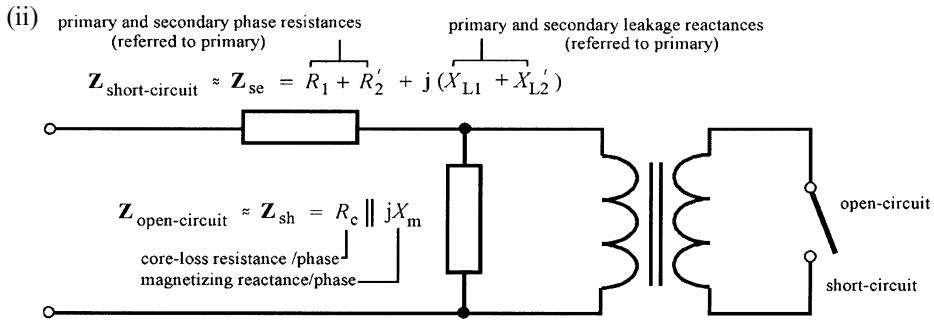
Fig. 9.12

(iii) In short-circuit test: $2490 = \sqrt{3} \times 1005 \times 14.4 \cos \phi$, so $\phi = 84.299°$ (current lags voltage). Neglecting $\mathbf{Z}_{sh}$, $\mathbf{Z}_{se} = (1005/\sqrt{3})/(14.4e^{-84.299°}) = 40.294 e^{j84.299°}$ $\Omega = 4.00 + j40.0 \, \Omega$ (referred to HV).

In open-circuit test: $2500 = \sqrt{3} \times 400 \times 3.886 \cos \phi$, so $\phi = 21.786°$
$\mathbf{Z}''_{sh} = (400/\sqrt{3})/(3.886e^{-21.786°}) = 59.429 e^{j21.786°}$ ohm ($''$ means referred to LV)
$\mathbf{Z}_{sh} = (10\,000/400)^2 \mathbf{Z}''_{sh} = 37\,143 e^{j21.786°}$ (referred to HV)
$\mathbf{Y}_{sh} = 1/\mathbf{Z}_{sh} = (1/37\,143)e^{-j21.786°} = 0.000025 - j0.00000992 \, \text{S}$

$\therefore R_c = 1/0.000025 = 40\,000\,\Omega;$
$X_m = 1/0.00000992 = 100\,000\,\Omega,$
both referred to HV.

19. (i) Draw a circuit diagram *and* a phasor diagram showing how third-harmonic voltages cause oscillation of the star point in a three-phase electrical network.
   (ii) A delta-connected three-phase load has the following harmonic components of voltage and current in each phase:

Harmonic	rms voltage, V	rms current, A	Phase angle (deg.)
1	220	12.5	15
3	0	11.5	–
5	19	4.5	21
7	15	6	−26.0

Calculate

(a) the rms line current;
(b) the rms line–line voltage;
(c) the total mean power supplied; and
(d) the ratio of the actual $I^2 R$ losses to the $I^2 R$ losses that are attributable to the fundamental alone.

(i)   Oscillation of the star point when the neutral is not connected
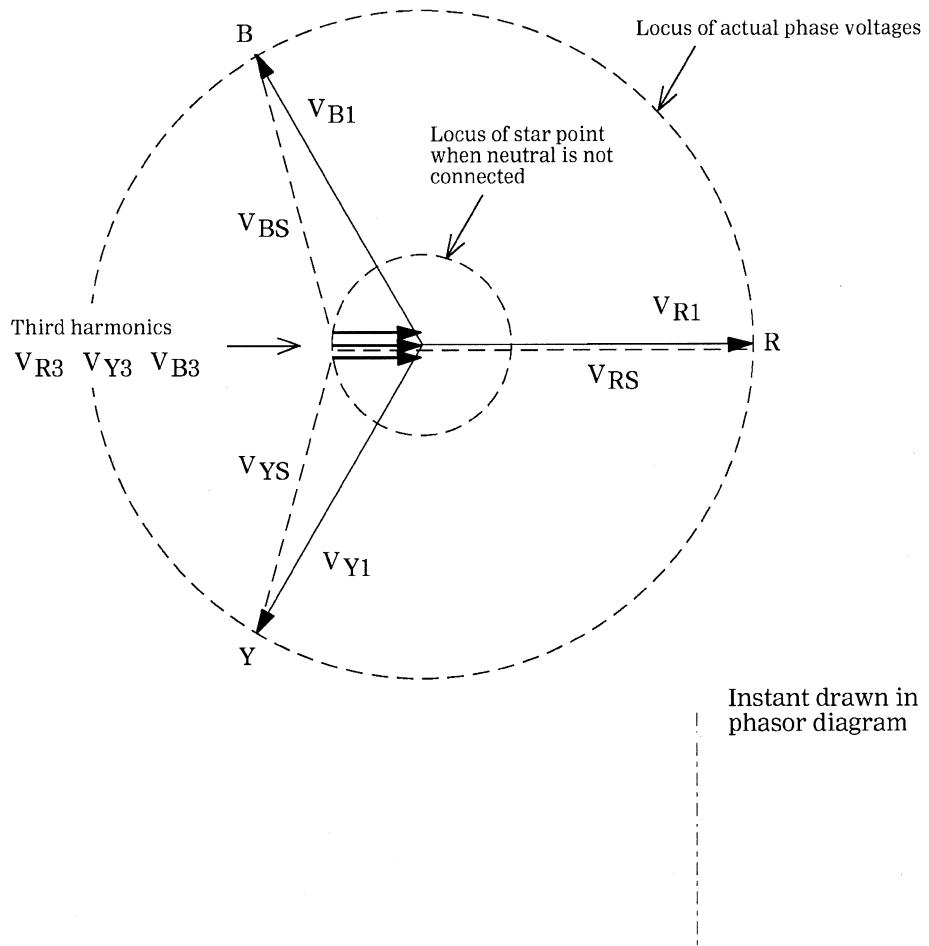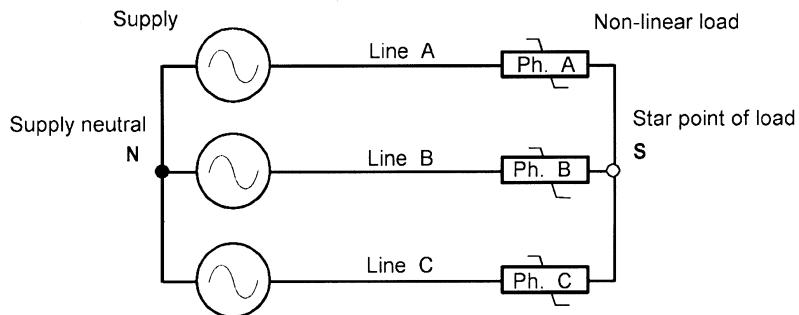
Fig. 9.13

(ii) (a) $I_{L(rms)} = \sqrt{[(\sqrt{3} \times 12.5)^2 + 0 + (\sqrt{3} \times 4.5)^2 + (\sqrt{3} \times 3.0)^2]}$

$= \sqrt{[468.75 + 0 + 60.75 + 27.0]}$

$= 23.59\,\text{A(rms)}$

(b) $V_{L(rms)} = \sqrt{[220^2 + 19.0^2 + 15.0^2]}$

$= 221.33\,\text{V(rms)}$

(c) $P = 3 \times [220 \times 12.5\cos 15.0° + 19.0 \times 4.5\cos 21.0°$

$+ 15.0 \times 6.0\cos(-26.0°)]$

$= 2656.30 + 79.82 + 80.89$

$= 2817.00\,\text{W}$

(d) Cable loss ratio $= I_{L(rms)}^2/I_{1(rms)}^2 = 23.59^2/(\sqrt{3} \times 12.5)^2 = 1.187$

20. (i) Draw the EMF phasor diagram for a Yd1 transformer. Also draw the configuration of the primary and secondary windings on a three-limb core. Include all internal connections and correct terminal labels.

(ii) A 230/66-kV Yd1 transformer gave the following test results:

Test	Line Current, A	Power factor	Condition
Open circuit	20	0.45	HV winding open 25% voltage on LV winding
Short circuit	120	0.08	LV winding shorted 2% voltage on HV winding

Draw an equivalent circuit for one phase and calculate the series impedance $\mathbf{Z}_{se} = R_e + jX_e$ and shunt admittance $\mathbf{Y}_{sh} = 1/R_c + 1/jX_m$, both referred to the HV side.

(i)
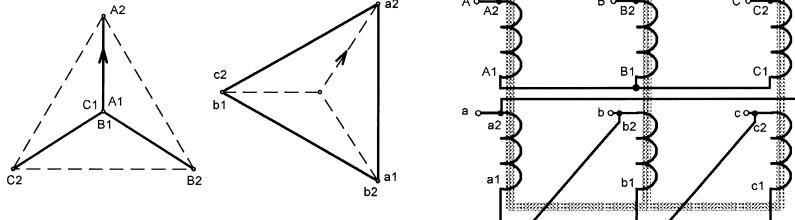
Fig. 9.14

(ii)
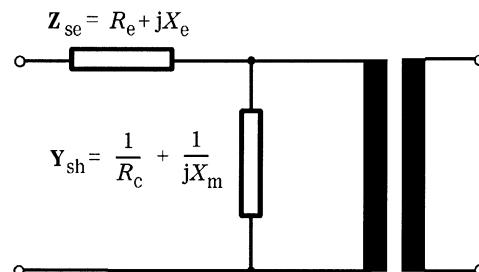
Fig. 9.15

From open-circuit test

$$\mathbf{Y}_{\text{sh}} = \frac{20e^{-j\arccos(0.5)}}{0.25 \times \dfrac{66}{\sqrt{3}} \times 10^3} \times \left[\frac{230}{66}\right]^2 = 0.01148 - j0.02276\text{S}$$

giving $R_c = 87.11\,\Omega$ and $X_m = 43.94\,\Omega$.
From short-circuit test

$$\mathbf{Z}_{\text{se}} = \frac{0.02 \times \dfrac{230}{\sqrt{3}}}{120} e^{j\arccos(0.08)} = 0.02213e^{j85.411^\circ} = 0.00177 + j0.02206\,\Omega$$

giving $R_e = 0.00177\,\Omega$ and $X_e = 0.002206\,\Omega$.

21. (i) Draw a circuit diagram and a phasor diagram showing the use of two
    wattmeters to measure the total power in a three-phase three-wire AC load.
   (ii) Derive an expression for the power factor of a balanced three-phase AC load
    in terms of the wattmeter readings P_1 and P_2.
  (iii) An unbalanced delta-connected load on a three-phase 415-V 50-Hz supply
    has the following impedances in each phase:

$$\mathbf{Z}_{ab} = 15 + j0\,\Omega \quad \mathbf{Z}_{bc} = 1.2 + j16.5\,\Omega \quad \mathbf{Z}_{ca} = -j18.2\,\Omega.$$

   Determine the three-line currents in magnitude and phase, and the readings
   of two wattmeters connected such that P_1 measures I_a and V_{ac}, while P_2
   measures I_b and V_{bc}. Take $\mathbf{V}_{ab}$ as reference phasor.
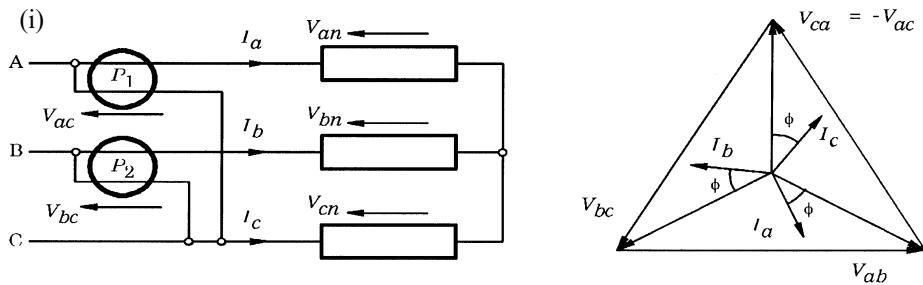

Fig. 9.16

(ii) $P_1 = \text{Re}\{\mathbf{V}_{ac}\mathbf{I}_a^*\} = V_L I_L \cos(30^\circ - \phi)$

   $P_2 = \text{Re}\{\mathbf{V}_{bc}\mathbf{I}_b^*\} = V_L I_L \cos(30^\circ + \phi)$
   $P_1 + P_2 = V_L I_L \times 2\cos 30^\circ \cos(-\phi) = \sqrt{3}V_L I_L \cos\phi$
   $P_1 - P_2 = -V_L I_L \times 2\sin 30^\circ \sin(-\phi) = V_L I_L \sin\phi$
   $\therefore \tan\phi = \sqrt{3}(P_1 - P_2)/(P_1 + P_2)\ldots$ then power factor $= \cos\phi$.

(iii) $\mathbf{I}_{ab} = 415/(15 + j0) = 27.6667 + j0\,\text{A}$

   $\mathbf{I}_{bc} = 415e^{-j120^\circ}/(1.2 + j16.5) = 415e^{-120^\circ}/16.54e^{j85.84^\circ} = 25.085e^{-j205.84^\circ}\,\text{A}$
   $\mathbf{I}_{ca} = 415e^{j120^\circ}/(-j18.2) = 22.80e^{j210^\circ} = -19.75 - j11.40\text{A}$

$$\mathbf{I}_a = \mathbf{I}_{ab} - \mathbf{I}_{ca} = 47.41 + j11.40 = 48.76e^{j13.52°}\,A$$
$$\mathbf{I}_b = \mathbf{I}_{bc} - \mathbf{I}_{ab} = -50.24 + j10.94 = 51.42e^{j167.72°}\,A$$
$$\mathbf{I}_c = \mathbf{I}_{ca} - \mathbf{I}_{bc} = 2.83 - j22.33 = 22.51e^{-j82.78°}\,A$$

$$P_1 = \text{Re}\{\mathbf{V}_{ac}\mathbf{I}_a^*\} = 415e^{-j60°} \times 48.76e^{-j13.52°} = 5741\,W$$

$$P_2 = \text{Re}\{\mathbf{V}_{bc}\mathbf{I}_b^*\} = 415e^{-j120°} \times 51.42e^{-j167.72°} = 6496\,W$$

Check: $P_1 + P_2 = 12\,237\,W$

$$|\mathbf{I}_{ab}|^2 R_{ab} + |\mathbf{I}_{bc}|^2 R_{bc} + |\mathbf{I}_{ca}|^2 R_{ca} = 27.6667^2 \times 15 + 25.085^2 \times 1.2 = 12\,237\,W.$$

22. (i) What are the main disadvantages of *single-phase* distribution of AC electric power?
    (ii) Explain the methods used to reduce or eliminate the following harmonics in AC power systems:

      (i) odd triplen harmonics, i.e. 3rd, 9th, 15th etc.
      (ii) odd non-triplen harmonics, i.e. 5th, 7th, 11th, 13th etc.

    (iii) A star-connected, three-phase AC load is supplied with 415 V three-phase sinewave AC power at a frequency f Hz, and the star point is solidly connected to the supply neutral. The load impedances at 50 Hz (in ohms) are as follows:

$$\mathbf{Z}_a = 9.184 + j0 \quad \mathbf{Z}_b = 3 + j17 \quad \mathbf{Z}_c = 3 - j17.$$

    Calculate the rms values and phase angles of the line currents and the neutral current when the frequency f is

    (a) 50 Hz
    (b) 150 Hz

  (i) Unbalance; 100-Hz oscillation in the power flow causes vibration, noise, and lamp flicker. Single phase cannot by itself produce a rotating ampere-conductor distribution in electric motors (it needs a capacitor and a split-phase winding).
  (ii) (a) Triplen harmonics are suppressed by star connection or trapped by delta connection; or taken by neutral wire.
       (b) Non-triplen harmonics. In electric machines, they are minimized by winding design (harmonic winding factors) and by having a sine-distributed magnetic flux around the airgap. In transformers, they are minimized by limiting the flux to a level below saturation. In non-linear power-electronic loads such as rectifiers, the 5th and 7th can be cancelled by using a 12-pulse rather than 6-pulse circuit. This requires a transformer with two secondaries, one wye and the other delta. Otherwise, the 5th and 7th can be filtered by damped or tuned filters built up from L, C and R elements.
  (iii) (a) $\mathbf{I}_a = 415/\sqrt{3}/9.184 = 26.088\,A$
        $\mathbf{I}_b = 415/\sqrt{3}e^{-j120°}/(3 + j17) = 415/\sqrt{3}e^{-j120°}/17.263e^{j80°}$
        $= 13.880e^{-j200.0°} = -13.044 + j4.745\,A$
        $\mathbf{I}_c = 415/\sqrt{3}e^{j120°}/(3 - j17) = 415/\sqrt{3}e^{j120°}/17.263e^{-j80°}$
        $= 13.880e^{j200.0°} = -13.044 - j4.745\,A$
        $\mathbf{I}_n = \mathbf{I}_a + \mathbf{I}_b + \mathbf{I}_c = 0$
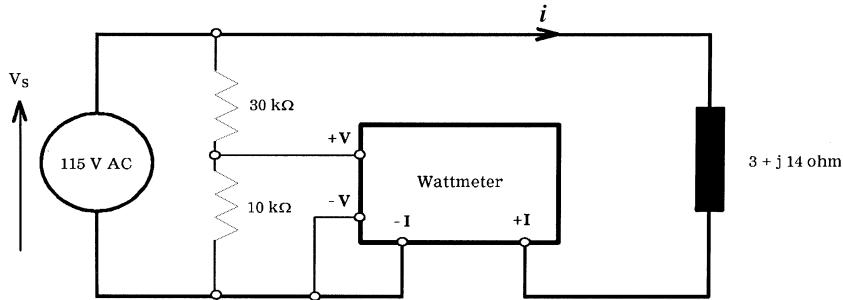
**Fig. 9.17**

(b) $I_a = 415/\sqrt{3}/9.184 = 26.088\,A$ (unchanged)

$I_b = 415/\sqrt{3}e^{-j120°}/(3+j17 \times 150/50) = 415/\sqrt{3}e^{-j120°}/51.088e^{j86.634°}$
   $= 4.690e^{-j206.634°} = -4.192 + j2.102\,A$

$I_c = 415/\sqrt{3}e^{j120°}/(3 - j17 \times 50/150) = 415/\sqrt{3}e^{j120°}/6.412e^{-j62.103°}$
   $= 37.369e^{j182.103°} = -37.344 - j1.371\,A$

$I_n = I_a + I_b + I_c = -15.448 + j0.731 = 15.465e^{j177.29°}\,A.$

23. (i) Draw a circuit diagram and a phasor diagram showing the two-wattmeter method of measuring power in a three-phase system.

 (ii) Prove from first principles that the two-wattmeter method is valid for instantaneous power and not just for average power.

(iii) Figure 9.17 shows a single-phase load of $3 + j14\,\Omega$ supplied from a sinusoidal voltage source of rms value 115 V and frequency 50 Hz. A single-phase wattmeter is connected with its current coil in series with the load. The voltage coil is connected via a voltage divider circuit comprising resistors of $10\,k\Omega$ and $30\,k\Omega$ as shown.

Calculate

 (a) the current
 (b) the real and reactive power $P + jQ$ at the terminals
 (c) the reading W on the wattmeter
 (d) the wattmeter reading if the $10\,k\Omega$ resistor is replaced by a capacitor whose impedance at 50 Hz is $-j6.429\,k\Omega$.
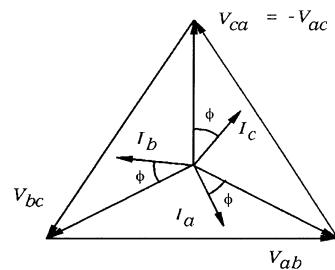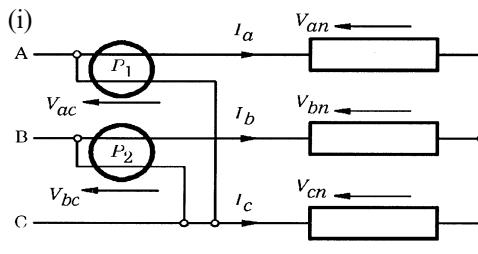
**Fig. 9.18**

 (ii) Total instantaneous power $p = v_a i_a + v_b i_b + v_c i_c$

With three-wire connection, $i_a + i_b + i_c = 0$

$$\therefore p = v_a i_a + v_b i_b - v_c(i_a + i_b)$$
$$= (v_a - v_c)i_a + (v_b - v_c)i_b$$
$$= v_{ab}i_a + v_{bc}i_b$$

(iii) (a) $\mathbf{I} = 115/(3 + j14) = 115/(14.318e^{j77.905°}) = 8.032e^{-j77.905°}$ A

(b) $P + jQ = \mathbf{VI}^* = 115 \times 8.032e^{j77.905°} = 193.537 + j903.171$ VA

(c) Wattmeter voltage coil reads only 1/4 of the load voltage, so the reading is
$W = 193.537/4 = 48.38$ W.

(d) Wattmeter voltage coil voltage is

$$115 \times \frac{-j6.429}{30 - j6.429} = 24.097e^{-j77.904°} \text{ V}$$

Wattmeter coil current is $8.032e^{-j77.905°}$ A.

$\therefore$ Wattmeter reads Re $\{\mathbf{VI}^*\} = \text{Re}\{24.097e^{-j77.904°} \times 8.032e^{j77.905°}\}$
$$= 193.55 \text{ W}$$

24. (i) Draw the phasor diagram of induced voltages for a Yd11 transformer. Also draw the configuration of the primary and secondary windings on a three-limb core. Include all internal connections and correct terminal labels.

(ii) Draw the equivalent circuit for one phase of a three-phase transformer, including the total series resistance R_e and total series leakage reactance X_e referred to the primary, and the core-loss resistance R_c and magnetizing reactance X_m, also referred to the primary.

(iii) A 400-MVA, 230/66-kV Yy6 transformer has series impedances of $R_e = 2.0 \, \Omega$/phase, and shunt impedances of $X_e = 20.0 \, \Omega$/phase, $R_c = 13\,000 \, \Omega$/phase and $X_m = 6\,500 \, \Omega$/phase, all referred to the high-voltage winding. Calculate the three-phase power and reactive power supplied under the following test conditions:

| Test	Condition
Open circuit	HV winding open
	25% voltage on LV winding
Short circuit	LV winding shorted
	2% voltage on HV winding

(i)
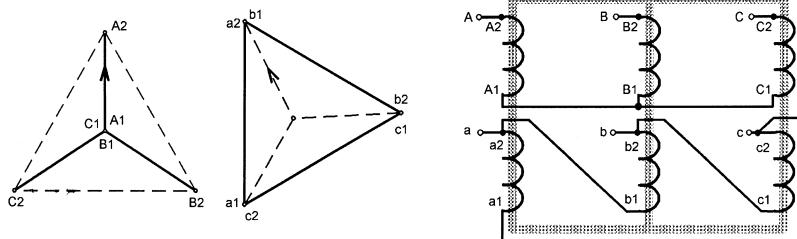
Fig. 9.19

(ii)
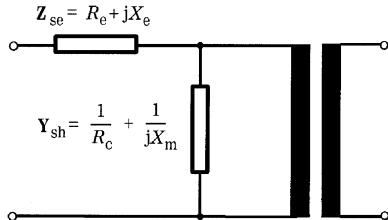
Fig. 9.20

(iii) In the *open-circuit test* with no current at the HV terminals, the impedance looking in to the LV terminals is $[(R_e + jX_e) + (R_c \| jX_m)] \times (66/230)^2$, i.e.

$$\mathbf{Z}_{LV} = [2 + j20 + 13\,000 \times j6500/(13\,000 + j6500)] \times (66/230)^2$$
$$= 214.259 + j429.836\,\Omega$$
$$= 480.277e^{j63.505°}\,\Omega/\text{phase(equivalent star)}$$

The line current is $\mathbf{I} = 0.25 \times 66 \times 10^3/\sqrt{3}/480.277e^{j63.505°} = 19.835e^{-j63.505°}\,\text{A}$.

$\therefore P + jQ = 0.25 \times \sqrt{3} \times 66 \times 10^3 \times 19.835e^{j63.505°} = 252.886 + j507.326\,\text{kVA}$.

In the *short-circuit test* the impedance looking in at the HV terminals is $(R_e + jX_e) \| (R_c \| jX_m) = (2 + j20) \| (13\,000 \| j6500) = 20.035e^{j84.219°}\,\Omega$
The current is $\mathbf{I} = 0.02 \times 230/\sqrt{3}/20.035e^{j84.219°} = 132.559e^{-j84.219°}\,\text{A}$.

$\therefore P + jQ = 0.02 \times \sqrt{3} \times 230 \times 132.559e^{j84.219°} = 106.38 + j1050.8\,\text{kVA}$.

25. (i) Define the *surge impedance* of a transmission line or cable. Describe the operation of a power transmission cable under the following conditions:

   (a) when the load is *less than* the surge impedance load; and
   (b) when the load *exceeds* the surge impedance load.

   Assume that the voltage is maintained constant at rated value at both ends, and make particular reference to the voltage profile and the reactive power requirements at the ends.

(ii) A transmission cable has a sending-end voltage $E_s = 245\,\text{kV}$ line–line. Losses may be neglected. The cable has an inductive reactance per unit length of $0.60\,\Omega/\text{km}$ and a capacitive admittance of $50.0\,\mu\text{S/km}$ at $60\,\text{Hz}$, and its length is $a = 74.8\,\text{km}$. Assuming that the receiving end is open-circuited, calculate
   (a) the surge impedance Z_0;
   (b) the electrical length θ in degrees;
   (c) the receiving-end voltage expressed in per-unit with E_s as reference;
   (d) the sending-end current;

(e) the reactive power at the sending end, in MVAr; and

(f) the reactive power at the sending end, expressed as a fraction of the surge-impedance loading.

(i) The surge impedance load P_0 is equal to V_0^2/Z_0 where $Z_0 = \sqrt{(l/c)} = \sqrt{(x_L x_C)}$, l being the inductance per unit length, c the capacitance per unit length, x_L the series inductive reactance per unit length, and x_C the shunt capacitive reactance per unit length along the line; and V_0 is the rated voltage. If V_0 is the line–line voltage, P_0 is the total power over all three phases. If V_0 is the line-neutral voltage, it is the power per phase. When the transmitted power P is equal to the surge impedance load, the voltage profile is flat and the reactive power requirements at the ends are zero.

(a) When $P < P_0$ the voltage rises towards the mid-point and reactive power must be absorbed at both ends to maintain the voltage equal to V_0.

(b) When $P > P_0$ the voltage falls towards the mid-point and reactive power must be generated at both ends to maintain the voltage equal to V_0.

(ii) (a) $Z_0 = \sqrt{(x_L \cdot x_C)} = \sqrt{(x_L/y_C)} = \sqrt{(0.60/50 \times 10^{-6})} = 109.55\,\Omega$

(b) $\beta = \sqrt{(x_L/x_C)} = \sqrt{(x_L \cdot y_C)} =$
$\sqrt{(0.60 \times 50 \times 10^{-6})} = 5.477 \times 10^{-3}$ radians/km $= 0.3138°/$km
so $\theta = \beta a = 0.3138 \times 74.8 = 23.47°$

(c) $\mathbf{V}_r = \dfrac{\mathbf{E}_s}{\cos\theta} = \dfrac{1.0}{\cos 23.47°} = 1.0902$ p.u. $= 267$ kV

(d) $\mathbf{I}_s = j\dfrac{\mathbf{E}_s}{Z_0}\tan\theta = \dfrac{245/\sqrt{3}}{109.55}\tan 23.47°$ kA $= j561$ A

(e) $Q_s = \sqrt{3} \times 245 \times 0.561 = 238$ MVAr

(f) $P_0 = 245^2/109.55 = 548$ MVA, so $Q_s/P_0 = 238/548 = 0.434$ p.u.

26. (i) Explain why the TCR is preferred over the TSC when it is desired to have a reactive compensator with continuous control of the current.

 (ii) Draw the complete power circuit diagram for a three-phase TCR, including shunt capacitors/filters, and a step-down transformer.

(iii) Draw the phase current waveform in relation to the phase voltage waveform, for a typical conduction angle of, say, $\sigma = 120°$.

(iv) A delta-connected TCR is connected to a 400-kV transmission line through a 7:1 step-down transformer. Its maximum reactive power at rated voltage is 100 MVAr. For a conduction angle of 115°, calculate

(a) the rms fundamental component of the line current at the high-voltage terminals of the transformer; and

(b) the peak current in each thyristor.

 (i) The TCR permits continuous control of the fundamental component of line current by phase control, whereas the TSC can only adjust the current by switching between discrete values.

(ii)

Capacitors for PF
correction
and harmonic
filtering
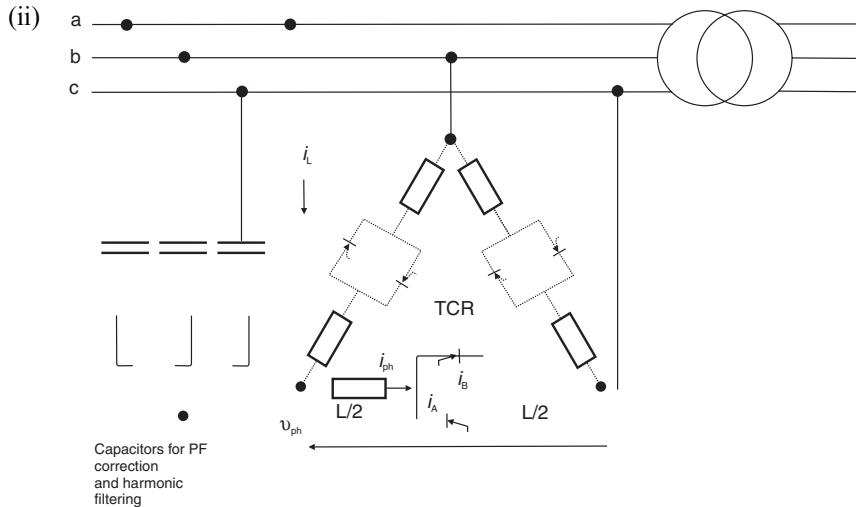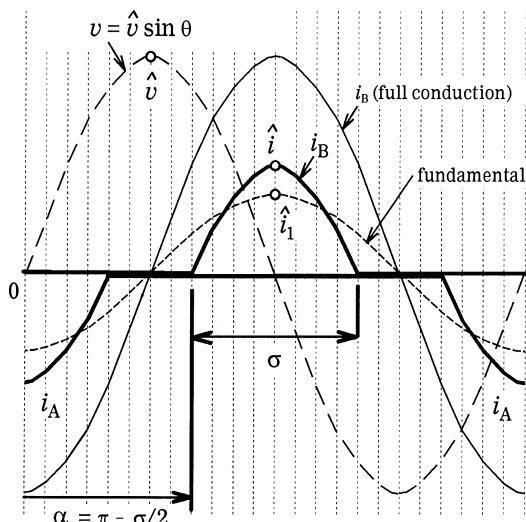
Fig. 9.21

(iii)

Phase voltage and current waveforms

Fig. 9.22

(iv) (a) First calculate X_L: $100 \times 10^6 = \sqrt{3} \times (400 \times 10^3/7) \times I_L$ so $I_L = 1010\,\text{A}$ and $I_{ph} = 583.3\,\text{A}$.

$\therefore X_L = (400 \times 10^3/7)/583.3 = 97.96\,\Omega$ in each phase.

$$I_{1L} = \sqrt{3} \times I_1 ph = \sqrt{3} \times \frac{V_{ph}}{X_L} \frac{\sigma - \sin \sigma}{\pi}$$

$$= \sqrt{3} \times \frac{400 \times 10^3}{7 \times 97.96} \times \frac{115 \times \dfrac{\pi}{180} - \sin 115°}{\pi} = 354\,\text{A}$$

at the low-voltage terminals of the transformer, i.e. $354/7 = 50.6$ A at the high-voltage terminals. (Note that this gives a total reactive power of $\sqrt{3} \times 400 \times 0.506 = 35.0$ MVAr, which corresponds to the fraction $(\sigma - \sin\sigma)/\pi$ of the rated MVAr, since $(\sigma - \sin\sigma)/\pi = 0.350$.)

(b) The phase delay angle is $\alpha = 180° - \sigma/2 = 122.5°$, so the peak phase current (occurring at 180°) is

$$\hat{\imath} = \frac{\sqrt{2} \times V_{\text{LLrms}}}{X_\text{L}} \times (\cos\alpha - \cos\pi) = \frac{\sqrt{2} \times 400 \times 10^3}{7 \times 97.96}$$
$$\times (\cos 122.5° + 1) = 382 \text{ A}$$

27. (i) Explain with your own words and diagrams how the *frequency* and the *voltage* are controlled in an isolated power plant with a local load. Assume that the generator is a conventional wound-field synchronous machine driven by a diesel engine.

   (ii) Prove by means of a series of diagrams, or otherwise, that an unbalanced linear ungrounded three-phase load can be transformed into a balanced, real three-phase load without changing the power exchange between source and load, by connecting an ideal reactive compensating network in parallel with it. Assuming a delta-connected unbalanced load $\mathbf{Y}_{ab} = G_{ab} + jB_{ab}$, $\mathbf{Y}_{bc} = G_{bc} + jB_{bc}$, $\mathbf{Y}_{ca} = G_{ca} + jB_{ca}$, derive expressions for the susceptances of the compensating network.

   (iii) An unbalanced delta-connected load draws the following power and reactive power from a three-phase supply whose line–line voltage is 560 V:

   200 kW between lines a, b
   170 kW at 0.85 power-factor lagging between lines b, c
   170 kW at 0.85 power-factor leading between lines c, a.

   Determine the susceptances of a purely reactive delta-connected compensating network that will balance this load and correct its power factor to unity. Also determine the resulting line currents.

   (i) Frequency is controlled by the speed governor on the prime mover. Voltage is controlled by the excitation in the generator.

   (ii) See Figure 9.23. General result is

$$B_{\gamma ab} = -B_{ab} + (G_{ca} - G_{bc})/\sqrt{3}$$
$$B_{\gamma bc} = -B_{bc} + (G_{ab} - G_{ca})/\sqrt{3} \qquad (9.23)$$
$$B_{\gamma ca} = -B_{ca} + (G_{bc} - G_{ab})/\sqrt{3}$$

   leaving $G = G_{ab} + G_{bc} + G_{ca}$ in each phase of a wye-connected resulting network.

   (iii) In each phase $P + jQ = \mathbf{VI}^* = V^2\mathbf{Y}^*$ so $\mathbf{Y} = (P - jQ)/V^2$ so

   in phase ab, $\mathbf{Y}_{ab} = (200 - j0) \times 10^3/560^2 = 0.638 + j0$ S $= G_{ab} + jB_{ab}$
   in phase bc, $\mathbf{Y}_{bc} = (170 - j105.537) \times 10^3/560^2 = 0.542 - j0.336$ S $= G_{bc} + jB_{bc}$

original
unbalanced
load

$\mathbf{Y}_{ab} = G_{ab} + jB_{ab}$
$\mathbf{Y}_{bc} = G_{bc} + jB_{bc}$
$\mathbf{Y}_{ca} = G_{ca} + jB_{ca}$

real but
unbalanced

connect capacitor and
inductor to
compensate Gab

equivalent
network is
real and
balanced
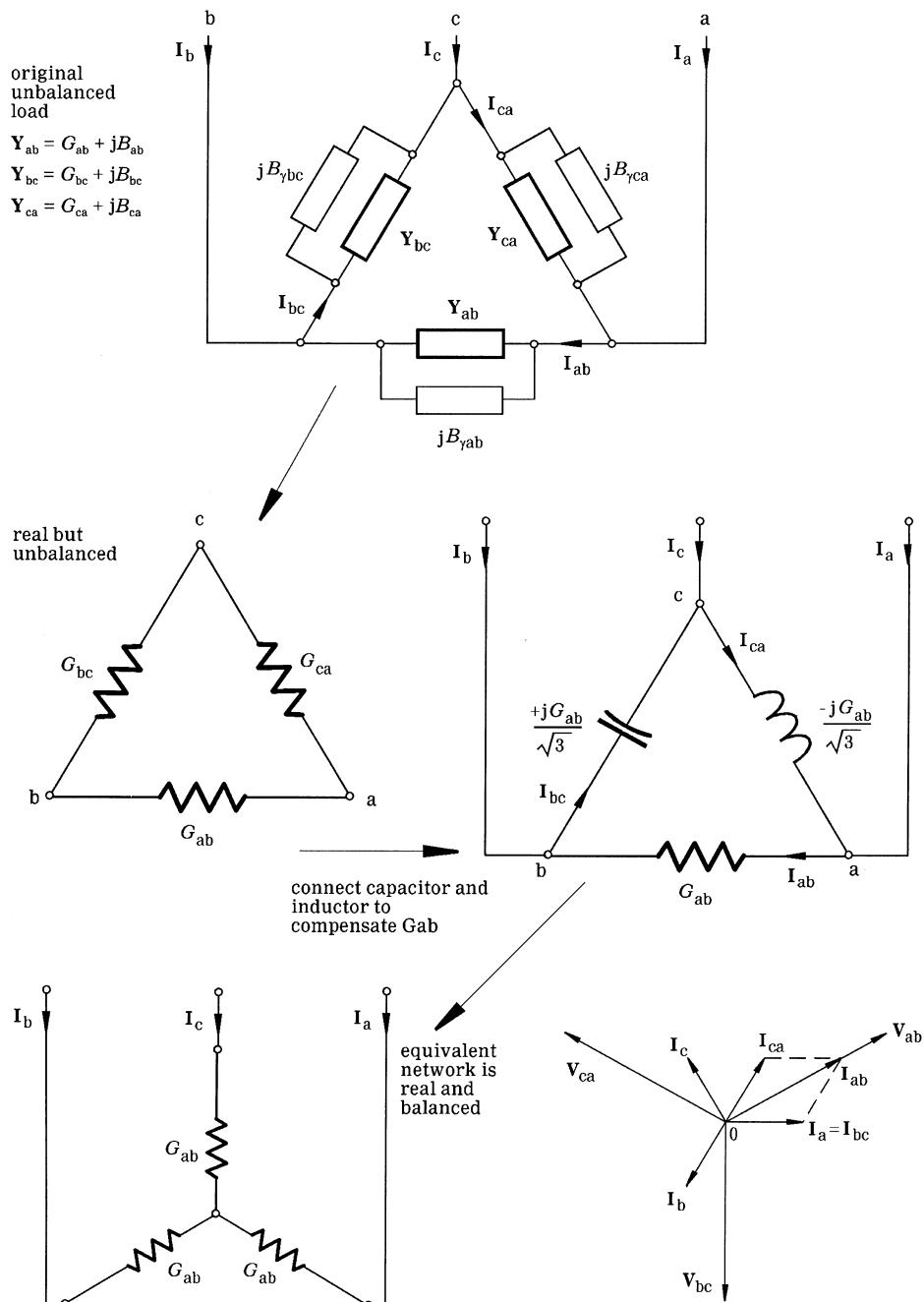
Fig. 9.23

in phase ca, $\mathbf{Y}_{ca} = (170 + \mathrm{j}105.537) \times 10^3/560^2 = 0.542 + \mathrm{j}0.336\,\mathrm{S} = G_{ca} + \mathrm{j}B_{ca}$

$$B_{\gamma ab} = -0 + (0.542 - 0.542)/\sqrt{3} = 0\,\mathrm{S}$$

$$B_{\gamma bc} = -(-0.336) + (0.638 - 0.542)/\sqrt{3} = 0.391\,\mathrm{S}$$

$$B_{\gamma ca} = -0.336 + (0.542 - 0.638)/\sqrt{3} = -0.391\,\mathrm{S}$$

The resultant $G_{ph} = G_{ab} + G_{bc} + G_{ca} = 0.638 + 0.542 + 0.542 = 1.722\,\mathrm{S}$

$$I_{ph} = I_L = (560/\sqrt{3}) \times 1.722 = 556.75\,\mathrm{A}$$

and the total power is $\sqrt{3} \times 560 \times 556.75 = 540\,\mathrm{kW}$ (same as original unbalanced load).

28. (i) Write down the equations for the voltage and current profiles of a lossless power transmission line in terms of the receiving-end voltage $\mathbf{E}_r$, the receiving-end current $\mathbf{I}_r$, the surge impedance Z_0, and the wavenumber β. Also give formulas for β and Z_0 in terms of x_L, the series inductive reactance per unit length, and x_C the shunt capacitive reactance per unit length.

   (ii) Using the equations in part (a), prove that the current at the sending-end of a symmetrical line is given by

$$\mathbf{I}_s = \mathrm{j}\frac{\mathbf{E}_s}{Z_0}\frac{\sin\theta}{1 + \cos\theta}$$

   where $\theta = \beta a$ is the electrical length of the line and a is the actual length. Also derive an equation for the mid-point voltage $\mathbf{V}_m$ in terms of $\mathbf{E}_s$ and θ. Sketch the profiles of $|\mathbf{V}(x)|$ and $|\mathbf{I}(x)|$ for $0 \le x \le a$, where x is distance along the line measured from the sending end.

   (iii) A symmetrical cable line operates at no load with terminal voltages of 345 kV line–line. It has an inductive reactance of $0.56\,\Omega/\mathrm{km}$ and a capacitive admittance of $50.0\,\mu\mathrm{S/km}$ at 50 Hz. The cable length is $a = 19.8\,\mathrm{km}$. Calculate and draw to scale the phasor diagrams of line-to-neutral voltage and current

   (a) at the sending end;
   (b) at the mid-point; and
   (c) at the receiving end.

   Use the sending-end voltage $\mathbf{E}_s$ as the reference phasor for all three cases, in order to show the relative phase angles of the voltages and currents at the three positions.

(i) $\mathbf{V}(x) = \mathbf{V}_r \cos\beta(a - x) + \mathrm{j}Z_0\mathbf{I}_r \sin\beta(a - x)$

$\mathbf{I}(x) = \mathrm{j}\dfrac{\mathbf{V}_r}{Z_0}\sin\beta(a - x) + \mathbf{I}_r \cos\beta(a - x)$

where $\beta = \omega\sqrt{(lc)} = \sqrt{(x_L/x_C)}$ and $Z_0 = \sqrt{(l/c)} = \sqrt{(x_L x_C)}$.

(ii) From equations (a) with $x = 0$, using the symbol **E** for terminal (fixed) voltages

$$\mathbf{E}_s = \mathbf{E}_r \cos\theta + jZ_0\mathbf{I}_r \sin\theta$$

$$\mathbf{I}_s = j\frac{\mathbf{E}_r}{Z_0}\sin\theta + \mathbf{I}_r \cos\theta$$

By symmetry $\mathbf{I}_s = -\mathbf{I}_r$ and from the equation for $\mathbf{E}_s$ we get

$$-\mathbf{I}_r = j\frac{\mathbf{E}_r}{Z_0}\frac{\sin\theta}{1 + \cos\theta} = j\frac{\mathbf{E}_r}{Z_0}\tan\frac{\theta}{2}$$

[Note the alternative form using $\tan(\theta/2)$]. With $\mathbf{E}_s = \mathbf{E}_r$ we get

$$\mathbf{I}_s = j\frac{\mathbf{E}_s}{Z_0}\frac{\sin\theta}{1 + \cos\theta}$$

Also the mid-point voltage is given by

$$\mathbf{V}_m = \mathbf{V}_r \cos\theta/2 + jZ_0\mathbf{I}_r \sin\theta/2$$

$$= \mathbf{E}_s(\cos\theta/2 + \sin\theta/2 \tan\theta/2) = \mathbf{E}_s\left(\cos\theta/2 + \frac{\sin^2\theta/2}{\cos\theta/2}\right) = \frac{\mathbf{E}_s}{\cos\frac{\theta}{2}}$$
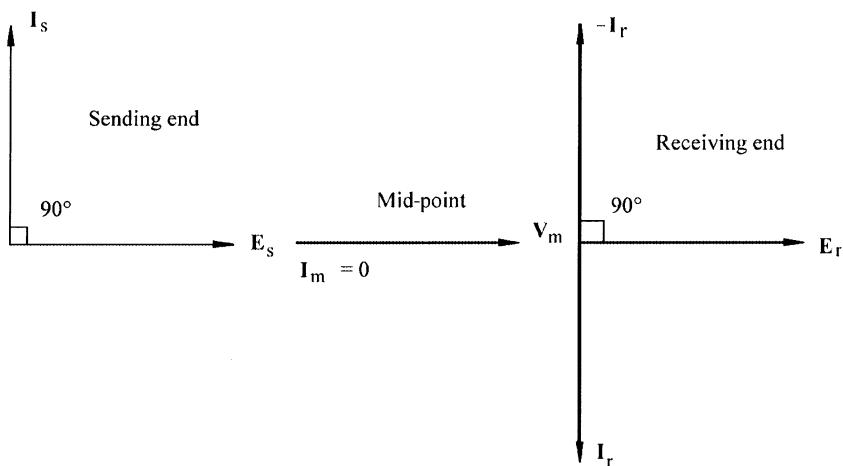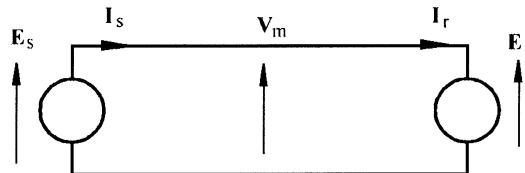
Fig. 9.24

(iii) We have $\mathbf{E}_s = 345/\sqrt{3} = 199.2e^{j0°}$ kV line-neutral and $\theta = \beta a = \sqrt{(0.56 \times 50 \times 10^{-6})} \times 19.8 = 0.105$ radians $= 6.003°$, and $Z_0 = \sqrt{(0.56/50 \times 10^{-6})} = 105.83\,\Omega$, so

$$\mathbf{I}_s = -\mathbf{I}_r = j\frac{345 \times 10^3/\sqrt{3}}{105.83} \times \frac{e^{j0} \sin 6.003°}{1 + \cos 6.003°} = j98.7\,\text{A}$$

At the mid-point, $\mathbf{V}_m = 199.2e^{j0°}/\cos(6.003/2°) = 199.46$ kV line-neutral, hardly changed from the sending-end and receiving-end values, since this is quite a short line. Also $\mathbf{I}_m = 0$.

Supplementary problems (*no solutions*)

29. (i) What are the functions of reactive compensation applied to electrical transmission systems? Distinguish between active and passive compensation.

(ii) By means of a sketch showing V_r/E_s vs. P/P_0, illustrate how the receiving-end voltage of a transmission cable can be maintained within a narrow range near 1.0 p.u. by means of switched shunt compensating devices. E_s is the sending-end voltage, P is the power transmission, and P_0 is the natural load.

(iii) Write an equation for the phasor voltage $\mathbf{E}_s$ at the sending end of a lossless cable, in terms of the voltage $\mathbf{V}_r$, power P_r and reactive power Q_r at the receiving end, if the electrical length is θ radians. Use this equation to derive an expression for the reactance X required to make the no-load voltage at the receiving end of a radial transmission cable equal to the sending-end voltage.

(iv) (a) Determine the value of a reactor placed at the mid-point of a 500 kV, 80-km symmetrical line such that the mid-point voltage is 1.0 p.u. The synchronous machines at the two ends maintain the voltage equal to 1.0 p.u. at both ends. The line series inductive reactance is $0.60\,\Omega$/km and shunt capacitive susceptance is $50.0\,\mu$S/km.

(b) What is the maximum voltage in the compensated line at no-load, and where does it occur?

(c) What is the reactive power of the mid-point reactor?

30. (i) Define the term *surge impedance* as used with electrical power transmission lines and cables. Briefly describe the properties of the voltage and current along a line that is operating at the so-called *surge-impedance load*.

(ii) Write down an equation for the sending-end voltage of a transmission line in terms of the receiving-end voltage $\mathbf{V}_r$, the receiving-end current $\mathbf{I}_r$, the surge impedance Z_0, and the electrical length of the line θ.

(iii) A transmission cable has a receiving end voltage $V_r = 345$ kV line–line. The load is wye-connected and is $264 + j142.5$ MVA/phase. Losses may be neglected. The cable has an inductive reactance per unit length of $0.60\,\Omega$/km and a capacitive admittance of $50.0\,\mu$S/km at 50 Hz. The cable length is $a = 14.8$ km. Calculate

(a) the receiving-end current, expressed as a phasor with $\mathbf{V}_r$ as reference;

(b) the surge impedance Z_0;

(c) the electrical length θ in radians and degrees;
(d) the sending-end voltage expressed as a phasor with $\mathbf{V}_r$ as reference;
(e) the sending-end current, expressed as a phasor with $\mathbf{V}_r$ as reference; and
(f) the power and reactive power at the sending end.

Appendix

This appendix presents the settings of the most relevant blocks used in the digital implementations developed in PSCAD/EMTDC, for each of the FACTS and Custom Power controllers considered in Chapter 8.

SVC

TITLE: SVC_FACTS
TIME-STEP: 3.5e-05
FINISH-TIME: 0.4
PRINT-STEP: 0.0005
RTDS-RACK: 0
RTDS REAL-TIME: Yes

SVC test power circuit (Figure 8.17)

Single-Phase Source
Mag	: 13.8 kV
f	: 50
Initial Phase	: 0.0
Ramp up time	: 0.0001 [sec]

Timed Breaker Logic
Initial State	: Open
Time of First Breaker Operation	: 0.6 [sec]

SVC controller (Figure 8.18)

PI Controller
Gp	: 2500
Ti	: 0.001

Hard Limiter
Upper limit	: 65.0
Lower limit	: −20

Filtering Blocks
```
NAME      : FIL1
G         : 1.0
DR        : 0.7
F         : 90
HP        : No
MP        : No
LP        : Yes

NAME      : FIL2
G         : 1.0
DR        : 0.16
F         : 120
HP        : Yes
MP        : No
LP        : Yes

NAME      : FIL3
G         : 1.0
DR        : 0.16
F         : 60
HP        : Yes
MP        : No
LP        : Yes
```

END

TCSC

TITLE: TCSC_FACTS
TIME-STEP: 3.5e-05
FINISH-TIME: 0.4
PRINT-STEP: 0.0005
RTDS-RACK: 0
RTDS REAL-TIME: Yes

TCSC test circuit example 1 (Figure 8.27)

Single-Phase Source
```
Mag           : 1 kV
f             : 50
Initial Phase : 0.0
Ramp up time  : 0.0001 [sec]
```

TCSC test circuit example 2 (Figure 8.31)

Single-Phase Source
```
Mag           : 11 kV
f             : 50
```

Initial Phase   : 0.0
Ramp up time   : 0.0001 [sec]

PI Controller
Gp   : 15
Ti   : 0.001

Hard Limiter
Upper limit   : 38.0
Lower limit   : 0

Filtering Blocks
NAME   : FIL1
G   : 1.0
DR   : 0.7
F   : 90
HP   : No
MP   : No
LP   : Yes

NAME   : FIL2
G   : 1.0
DR   : 0.16
F   : 120
HP   : Yes
MP   : No
LP   : Yes

NAME   : FIL3
G   : 1.0
DR   : 0.16
F   : 60
HP   : Yes
MP   : No
LP   : Yes

Timed Breaker Logic
Initial State   : Open
Time of First Breaker Operation   : 1.8 [sec]

END

STATCOM

XDRAFT Version 4.2.2
EMTDC
TITLE: STATCOM_FACTS
TIME-STEP: 3.5e-05
FINISH-TIME: 0.4
PRINT-STEP: 0.0005

RTDS-RACK: 0
RTDS REAL-TIME: Yes

12-Pulse vsc-based STATCOM: power circuit (Figure 8.45)

Three-Phase Three-Winding Transformer (3)

Tmva	: 5
f	: 50
Xl12	: 0.1
Xl13	: 0.1
Xl23	: 0.1
V1	: 115
V2	: 115
V3	: 115

GTOs

RD	: 5000.0
CD	: 0.05
RON	: 0.01
ROFF	: 1.0E6
EFVD	: 0.001
EBO	: 1.0E5

Freewheeling Diodes

RD	: 5000.0
CD	: 0.05
RON	: 0.01
ROFF	: 1.0E6
EFVD	: 0.001
EBO	: 1.0E5

DC Voltage Source (2)

Ctrl	: RunTime
Vm	: 66
F	: 60.0
Tc	: 0.05
Imp	: RRL Values
ACDC	: DC

12-Pulse VSC-based STATCOM: switching controller (Figure 8.46)

Sine Modulators (6)

Type	: Sin
FMod	: Hertz
PMod	: Degrees

Triangle Generator TRIB1

F	: 50
P	: −210
Type	: Triangle
Duty	: 50
Max	: 1
Min	: −1

Triangle Generator TRIC1
    F   : 50
    P   : 30
    Type   : Triangle
    Duty   : 50
    Max   : 1
    Min   : −1

Triangle Generator TRIA1
    F   : 50
    P   : −90
    Type   : Triangle
    Duty   : 50
    Max   : 1
    Min   : −1

Triangle Generator TRIA2
    F   : 50
    P   : −120
    Type   : Triangle
    Duty   : 50
    Max   : 1
    Min   : −1

Triangle Generator TRIB2
    F   : 50
    P   : −240
    Type   : Triangle
    Duty   : 50
    Max   : 1
    Min   : −1

Triangle Generator TRIC2
    F   : 50
    P   : 0
    Type   : Triangle
    Duty   : 50
    Max   : 1
    Min   : −1

Comparators (6)
    Pulse   : Level
    OPos   : 1
    ONone   : 0
    ONeg   : 1
    OHi   : 1
    OLo   : 0

END

D-STATCOM

XDRAFT Version 4.2.2
EMTDC
TITLE: DSTATCOM_CUSTOM POWER
TIME-STEP: 5e-05
FINISH-TIME: 1.4
PRINT-STEP: 0.0005
RTDS-RACK: 0
RTDS REAL-TIME: Yes

D-STATCOM test power system (Figure 8.50)

Three-phase Voltage Source

Type	: R//L
Ctrl	: RunTime
MVA	: 100.0
Vm	: 230.0
F	: 50
Tc	: 0.0001
ZSeq	: No
Imp	: RRL Values
NHarm	: 0
R1s	: 26.45
R1p	: 1.0
L1p	: 0.1

Three-phase three-winding transformer

Tmva	: 100.0
f	: 50
YD1	: Y
YD2	: Y
YD3	: Y
Lead	: Leads
Xl12	: 0.1
Xl13	: 0.1
Xl23	: 0.1
V1	: 230.0
V2	: 11
V3	: 11

Breakers

NAME	: Brk1
OPEN	: Open
ROFF	: 1.0E6
RON	: 0.005

NAME	: Brk1b
OPEN	: Closed
ROFF	: 1.0E6
RON	: 0.005

NAME   : Brk2
OPEN   : Open
ROFF   : 1.0E6
RON   : 0.01

NAME   : Brk2b
OPEN   : Closed
ROFF   : 1.0E6
RON   : 0.01

Timed Breaker Logic
NAME   : Brk1
TO   : 0
TC   : 5

NAME   : Brk1b
TO   : 1.0
TC   : 5

NAME   : Brk2
TO   : 0.0
TC   : 0.8

NAME   : Brk2b
TO   : 1.0
TC   : 5

Active/Reactive Power meter
P   : Yes
Q   : Yes
TS   : 0.02

Three-phase rms calculator
Ts   : 0.025
Scale   : 11

GTOs
RD   : 5000.0
CD   : 0.05
RON   : 0.01
ROFF   : 1.0E6
EFVD   : 0.001
EBO   : 1.0E5

Freewheeling Diodes
RD   : 5000.0
CD   : 0.05
RON   : 0.01
ROFF   : 1.0E6
EFVD   : 0.001
EBO   : 1.0E5

D-STATCOM controller (Figure 8.51)

Filtering Blocks
    NAME   : FIL1
    G   : 1.0
    DR   : 0.7
    F   : 90
    HP   : No
    MP   : No
    LP   : Yes

    NAME   : FIL2
    G   : 1.0
    DR   : 0.16
    F   : 120
    HP   : Yes
    MP   : No
    LP   : Yes

    NAME   : FIL3
    G   : 1.0
    DR   : 0.16
    F   : 60
    HP   : Yes
    MP   : No
    LP   : Yes

PI Controller
    GP   : Gp
    TI   : 0.001
    YHI   : 50
    YLO   : -10
    YINIT   : 5

Proportional Gain Gp
    Desc   : Gp
    Value   : 350
    Max   : 6000
    Min   : 0.0

Sine Modulator
    Type   : Sin
    FMod   : Hertz
    PMod   : Degrees

Triangle Generator
    F   : 450
    P   : -95
    Type   : Triangle
    Duty   : 50

Max	: 1
Min	: −1

END

DVR

XDRAFT Version 4.2.2
EMTDC
TITLE: DVR_CUSTOM POWER
TIME-STEP: 5e-05
FINISH-TIME: 1.4
PRINT-STEP: 0.0005
RTDS-RACK: 0
RTDS REAL-TIME: Yes

DVR test power system (Figure 8.57)

Three-Phase Voltage Source

Type	: R
Ctrl	: RunTime
MVA	: 100.0
Vm	: 13.0
F	: 50.0
Tc	: 0.02
ZSeq	: No
Imp	: RRL Values
NHarm	: 0
R1s	: 0.1
R1p	: 1.0
L1p	: 0.1
Z1	: 1.0

DC Voltage Source

Ctrl	: RunTime
Vm	: 2.5
F	: 0.0
Tc	: 0.05
Imp	: RRL Values
ACDC	: DC

Three-Phase Three-Winding Transformer

Tmva	: 100.0
f	: 50.0
YD1	: Y
YD2	: Delta
YD3	: Y
Lead	: Lags
Xl12	: 0.1

    Xl13   : 0.1
    Xl23   : 0.1
    V1   : 13
    V2   : 275
    V3   : 275

Three-phase Two-Winding Transformers (2)
    Tmva   : 100.0
    f   : 50
    YD1   : Y
    YD2   : Delta
    Lead   : Lags
    Xl   : 0.1
    V1   : 275
    V2   : 11

Single-Phase Transformers (3)
    Tmva   : 100
    f   : 50
    Xl   : 0.10
    V1   : 11
    V2   : 11

Breakers
    NAME   : Brka, Brkb, Brkc
    OPEN   : Closed
    ROFF   : 1.E6
    RON   : 0.005

    NAME   : Brkaa, Brkbb, Brkcc
    OPEN   : Open
    ROFF   : 1.E6
    RON   : 0.005

Timed Breaker Logic
    NAME   : Brka, Brkb, Brkc
    TO   : 0.8
    TC   : 5

    NAME   : Brkaa, Brkbb, Brkcc
    TO   : 0
    TC   : 1.0

Logic Faulted Timed
    TF   : 0.8
    DF   : 0.2

Fault Specifications
    RON   : 1.6
    ROFF   : 1.0E6
    A   : Yes
    B   : Yes
    C   : Yes
    G   : Yes

Three-Phase RMS calculator
   Ts   : 0.02
   Scale   : 11

GTOs
   RD   : 5000.0
   CD   : 0.05
   RON   : 0.01
   ROFF   : 1.0E6
   EFVD   : 0.001
   EBO   : 1.0E5

Freewheeling Diodes
   RD   : 5000.0
   CD   : 0.05
   RON   : 0.01
   ROFF   : 1.0E6
   EFVD   : 0.001
   EBO   : 1.0E5

DVR controller (Figure 8.58)

PI Controller
   GP   : Gp
   TI   : Ti
   YHI   : 100
   YLO   : -100
   YINIT   : 85

Proportional Gain Gp
   Desc   : Gp
   Value   : 350
   Max   : 6000
   Min   : 0.0

Sine Modulator
   Type   : Sin
   FMod   : Hertz
   PMod   : Degrees

Triangle Generator
   F   : 1250
   P   : -95
   Type   : Triangle
   Duty   : 50
   Max   : 1
   Min   : -1

Comparators (3)
   Pulse   : Level
   OPos   : 1
   ONone : 0
   ONeg   : 1

OHi   : 1
OLo   : 0

END

PFC

XDRAFT Version 4.2.2
EMTDC
TITLE: PFC_CUSTOM POWER
TIME-STEP: 5e-05
FINISH-TIME: 0.35
PRINT-STEP: 5e-05
RTDS-RACK: 0
RTDS REAL-TIME: Yes

PFC test power system (Figure 8.65)

Three-Phase Voltage Source
    Ctrl   : RunTime
    MVA   : 100
    Vm   : 13.8
    F   : 50
    Tc   : 0.0001
    ZSeq   : No
    Imp   : RRL Values
    NHarm   : 0
    R1s   : 0.1
    R1p   : 10
    L1p   : 0.001
    Z1   : 1.0

Three-Phase Two-Winding Transformer
    Tmva   : 100
    f   : 50
    YD1   : Y
    YD2   : Delta
    Lead   : Leads
    Xl   : 0.1
    V1   : 13.8
    V2   : 6.75

Breakers
    NAME   : Brk
    OPEN   : Open
    ROFF   : 1.0E6
    RON   : 0.08

Timed Breaker Logic
   NAME   : Brk
   TO   : 0
   TC   : 0.15

Active/Reactive Power Meter
   P   : Yes
   Q   : Yes
   TS   : 0.02

GTOs
   RD   : 5000.0
   CD   : 0.05
   RON   : 0.01
   ROFF   : 1.0E6
   EFVD   : 0.001
   EBO   : 1.0E5

Freewheeling Diodes
   RD   : 5000.0
   CD   : 0.05
   RON   : 0.01
   ROFF   : 1.0E6
   EFVD   : 0.001
   EBO   : 1.0E5

PFC controller: transformation abc → dq0 and control loops (Figure 8.66)

Filtering Blocks (3)
   NAME   : Fil1
   G   : 1.0
   DR   : 0.7
   F   : 85
   HP   : No
   MP   : No
   LP   : Yes

   NAME   : Fil2
   G   : 1.0
   DR   : 0.16
   F   : 100
   HP   : Yes
   MP   : No
   LP   : Yes

   NAME   : Fil3
   G   : 1.0
   DR   : 0.16
   F   : 50
   HP   : Yes
   MP   : No
   LP   : Yes

Modulators
Type   : Cos
FMod   : Hertz
PMod   : Degrees

Type   : Sin
FMod   : Hertz
PMod   : Degrees

PI Controller d
GP   : 0.8
TI   : 0.001
YHI   : 25
YLO   : −25
YINIT   : 25

PI Controller q
GP   : 0.8
TI   : 0.0001
YHI   : 24
YLO   : −24
YINIT   : 25

PI Controller DC
GP   : 0.8
TI   : 0.01
YHI   : 10
YLO   : −10
YINIT   : 0.0

PFC controller: transformation dq0 → abc and PWM generators (Figure 8.67)

Triangle Generator
F   : 1050
P   : 35
Type   : Triangle
Duty   : 50
Max   : 1
Min   : −1

Comparators (3)
Pulse   : Level
OPos   : 1
ONone   : 0
ONeg   : 1
OHi   : 1
OLo   : 0

END

SHUNT AF

XDRAFT Version 4.2.2
EMTDC
TITLE: Shunt AF_Custom Power
TIME-STEP: 5e-05
FINISH-TIME: 0.4
PRINT-STEP: 0.0001
RTDS-RACK: 0
RTDS REAL-TIME: Yes

Shunt AF test power system (Figure 8.80)

Three-Phase Voltage Source
    Ctrl   : RunTime
    MVA   : 100
    Vm   : 13.8
    F   : 50
    Tc   : 0.0001
    ZSeq   : No
    Imp   : RRL Values
    NHarm : 0
    R1s   : 0.1
    R1p   : 10
    L1p   : 0.001
    Z1   : 1.0

Three-Phase Two-Winding Transformer
    Tmva   : 100
    f   : 50
    YD1   : Y
    YD2   : Delta
    Lead   : Leads
    Xl   : 0.1
    V1   : 13.8
    V2   : 6.75

Breaker
    NAME   : Brk1
    OPEN   : Open
    ROFF   : 1.0E6
    RON   : 0.08

Timed Breaker Logic
    NAME   : Brk1
    TO   : 0
    TC   : 0.1

Active/Reactive Power Meter
    P   : Yes
    Q   : Yes
    TS   : 0.02

GTOs

RD	: 5000.0
CD	: 0.05
RON	: 0.01
ROFF	: 1.0E6
EFVD	: 0.001
EBO	: 1.0E5

Thyristors

RD	: 5000.0
CD	: 0.05
RON	: 0.01
ROFF	: 1.0E6
EFVD	: 0.001
EBO	: 1.0E5

Freewheeling Diodes

RD	: 5000.0
CD	: 0.05
RON	: 0.01
ROFF	: 1.0E6
EFVD	: 0.001
EBO	: 1.0E5

Shunt AF controller: transformation abc → dq0 (Figure 8.81)

Modulators

Type	: Cos
FMod	: Hertz
PMod	: Degrees
Type	: Sin
FMod	: Hertz
PMod	: Degrees

Filtering Blocks (6)

G	: 1.0
DR	: 0.7
F	: 85
HP	: No
MP	: No
LP	: Yes
G	: 1.0
DR	: 0.16
F	: 100
HP	: Yes
MP	: No
LP	: Yes
G	: 1.0
DR	: 0.16
F	: 50

HP   : Yes
MP   : No
LP   : Yes

Shunt AF controller: control loops (Figure 8.82)

PI Controller d
GP   : 80
TI   : 0.0001
YHI   : 25
YLO   : −25
YINIT   : −10

PI Controller q
GP   : 80
TI   : 0.000075
YHI   : 25
YLO   : −25
YINIT   : −10

PI Controller CD
GP   : 1
TI   : 0.001
YHI   : 10
YLO   : −10
YINIT   : 0.0
COM   : PI Controller

Shunt AF controller: PWM generators (Figure 8.83)

Triangle Generator
F   : 1050
P   : 35
Type   : Triangle
Duty   : 50
Max   : 1
Min   : −1

Comparators (3)
Pulse   : Level
OPos   : 1
ONone   : 0
ONeg   : 1
OHi   : 1
OLo   : 0

Shunt AF controller: rectifier firing angle control (Figure 8.84)

Triangle Generator Pos
F   : 50
P   : 0.0

Type   : Triangle
Duty   : 99.5
Max   : 1
Min   : 0

Comparator Pos
Pulse   : Level
OPos   : 1
ONone   : 0
ONeg   : 0
OHi   : 1
OLo   : 0

Triangle Generator Neg
F   : 50
P   : 180
Type   : Triangle
Duty   : 99.5
Max   : 1
Min   : 0

Comparator Neg
Pulse   : Level
OPos   : 1
ONone   : 0
ONeg   : 1
OHi   : 1
OLo   : 0

END

SSTS

XDRAFT Version 4.2.2
EMTDC
TITLE: SSTS_CUSTOM POWER
TIME-STEP: 5e-05
FINISH-TIME: 0.7
PRINT-STEP: 0.0005
RTDS-RACK: 0
RTDS REAL-TIME: Yes

SSTS test power system (Figure 8.94)

Three-Phase Voltage Source (2)
Ctrl   : RunTime
MVA   : 100.0
Vm   : 13
F   : 50
Tc   : 0.0

```
ZSeq        : No
Imp         : RRL Values
NHarm       : 0
R1s         : 0.1
R1p         : 1.0
L1p         : 0.1
Z1          : 1.0
```

Transformers
```
Step-Up Three-Phase Three-Winding (2)
Tmva        : 100.0
f           : 50.0
YD1         : Y
YD2         : Delta
Lead        : Lags
Xl          : 0.1
V1          : 13
V2          : 115

Step-Down Three-Phase Three-Winding (2)
Tmva        : 100.0
f           : 50.0
YD1         : Delta
YD2         : Y
Lead        : Lags
Xl          : 0.1
V1          : 115
V2          : 13
```

Fault Specifications
```
RON         : 1.0
ROFF        : 1.0E6
A           : Yes
B           : Yes
C           : Yes
G           : Yes
```

Logic Fault Timed
```
TF          : 0.3108
DF          : 0.2
```

Three-Phase RMS Meter
```
Ts          : 0.02
Scale       : 13
```

Thyristors
```
RD          : 5000.0
CD          : 0.05
RON         : 0.01
ROFF        : 1.0E6
EFVD        : 0.001
EBO         : 1.0E5
```

SSTS controller (Figure 8.95)

Integrator
Extrn	: Internal
Reset	: No
COM	: Integrator
T	: 0.0001
Yo	: 0.01
YRst	: 0.0
YHi	: 10
YLo	: -10

*Comparator time*1
Pulse	: Pulse
OPos	: 1
ONone	: 0
ONeg	: 1
OHi	: 1
OLo	: 0

Comparator Vatmax
Pulse	: Level
OPos	: 1
ONone	: 0
ONeg	: 1
OHi	: 1.0
OLo	: -1.0

Comparator Vrefmax
Pulse	: Pulse
OPos	: 1
ONone	: 0
ONeg	: 1
OHi	: 1.0
OLo	: 1.0

Comparator ZeroC
Pulse	: Pulse
OPos	: 1
ONone	: 0
ONeg	: -1
OHi	: 1.0
OLo	: -1

*Comparator DTA*1
Pulse	: Level
OPos	: 1
ONone	: 0
ONeg	: 1
OHi	: 1
OLo	: 0

END

Bibliography

Acha, E., Harmonic Domain Representation of Thyristor Controlled Reactors, *Proceedings of the IEE 5th International Conference on AC and DC Power Transmission*, London, UK, pp. 404–406, 17–20 September 1991.

Acha, E., Flexible HVDC Light Model for Large Scale Power Flows. *Internal Report*, University of Glasgow, Glasgow, UK, 2001.

Acha, E. and Abur, A., Flexible HVDC Light Model for Large Scale Power Flows and State Estimation Studies, to be presented at *5th International Conference on Power System Management and Control*, London, UK, 16–19 April 2002.

Acha, E., Ambriz-Perez, H. and Fuerte-Esquivel, C.R., Advanced Transformer Control Modelling in an Optimal Power Flow Using Newton's Method, *IEEE Transactions on Power Systems*, Vol. 15, No. 1, pp. 290–298, February 2000.

Acha, E., Arrillaga, J., Medina, J.A. and Semlyen, A., A General Frame of Reference for the Analysis of Harmonic Distortion with Multiple Transformer Non-Linearities, *IEE Proceedings on Generation, Transmission and Distribution*, Part C, Vol. 136, No. 5, pp. 271–278, September 1989.

Acha, E., Rico, J.J., Acha, S. and Madrigal, M., Harmonic Modelling in Hartley's Domain with Particular Reference to Three Phase Thyristor-Controlled Reactors, *IEEE Transactions on Power Delivery*, Vol. 12, No. 4, pp. 1622–1628, October 1997.

Acha, E. and Madrigal, M., *Power Systems Harmonics: Computer Modelling and Analysis*, John Wiley & Sons, Chichester, England, 2001.

Agelidis, V.G. and Calais, M., Application Specific Harmonic Performance Evaluation of Multicarrier PWM Techniques, *IEEE Power Electronics Specialists Conference*, Fukuoka, Japan, pp. 172–178, June 1998.

Agelidis, V.G., Keerthipala, W.W.L. and Lawrance, W.B., Multi-Modular Multilevel PWM Converter Systems, *Nordic Workshop on Power and Industrial Electronics*, Espoo, Finland, pp. 56–60, August 1998.

Agelidis, V.G. and Xu, L., A Novel HVDC System Based on Flying Capacitor Multilevel PWM Converters, *Paper presented at the International Conference on Power Systems 2001, Organised by CIGRE Study Committee 14*, Wuhan, China, September 2001.

Agrawal, B. and K. Shenoi, Design Methodology for $\Sigma\Delta M$, *IEEE Transactions on Communications*, Vol. 31, No. 3, pp. 360–370, March 1983.

Akagi, H., Utility Applications of Power Electronics in Japan. *Proceedings of IEEE Industrial Electronics Conference (IECON)*, Vol. 2, pp. 409–416, 1997.

Akagi, H., New Trends in Active Filters for Power Conditioning, *IEEE Transactions on Industry Applications*, Vol. 32, No. 6, November–December 1996.

Aliwell, R.W. and Crees, D.E., Development of a Self-Protected Light-Triggered Thyristor. *Proceedings of IEE Colloquium No. 104*, 7.1–7.3, April 1994.

Ambriz-Perez, H., Flexible AC Transmission Systems Modelling in Optimal Power Flows Using Newton's Method, PhD Thesis, The University of Glasgow, Glasgow, UK, December 1998.

Ambriz-Perez, H., Acha, E. and Fuerte-Esquivel, C.R., Advanced SVC Models for Newton-Raphson Load Flow and Newton Optimal Power Flow Studies, *IEEE Transactions on Power Systems*, Vol. 15, No. 1, pp. 129–136, February 2000.

Anderson, P.M., *Analysis of Faulted Power Systems*, the Iowa State University Press, 1973.

Anderson, P.M. and Fouad, A.A., *Power System Control and Stability*, the Iowa State University Press, 1977.

Aree, P., Small-Signal Stability Analysis of Electronically Controlled Power Networks, PhD Thesis, The University of Glasgow, Glasgow, UK, April 2000.

Arrillaga, J., *HVDC Transmission*, IEE Publications, London, 1999.

Arrillaga, J. and Watson, N.R., *Computer Modelling of Electrical Power Systems*, John Wiley & Sons, 2nd edition, Chichester, England, 2001.

Arrillaga, J., Watson, N.R. and Chan, S., *Power System Quality Assessment*, Wiley & Sons, Chichister, England, 2000.

Asano, K. and Sugawara, Y., Unified Evaluation and Figure of Merit for 8-kV 3.5-kA Light-Triggered Thyristor. *Proceedings of International Symposium on Power Semiconductors and Devices (ISPSD)*, Kyoto, Japan, 229, 1998.

Asplund, G., Application of HVDC Light to Power System Enhancement, *IEEE Winter Meeting, Session: Development and Application of Self-Commutated Converters in Power Systems*, Singapore, January 2000.

Asplund, G., Eriksson, K. and Svensson, K., HVDC Light – DC Transmission Based on Voltage Sourced Converters, *ABB Review*, No. 1, pp. 4–9, 1998.

Baliga, B.J., Power Semiconductor Devices for Variable Frequency Drives. Chapter 1, *Power Electronics and Variable Frequency Drives – Technology and Applications*, edited by B.K. Bose, IEEE Press, New York, NY, USA, 1997.

Bellar, M.D., Wu, T.S., Tchamdjou, A., Mahdavi, J. and Ehsani, M., A Review of Soft–Switched DC–AC Converters. *IEEE Transactions on Industry Applications*, Vol. 34, No. 4, pp. 847–860, July/August 1998.

Bhagwat, P.M. and Stefanovic, V.R., Generalised Structure of a Multilevel PWM Inverter, *IEEE Transactions on Industry Applications*, Vol. 19, No. 6, pp. 1057–1069, November/December, 1983.

Blaabjerg, F., Snubbers in PWM-VSI-Inverter, *Proceedings of IEEE Power Electronics Specialists Conference* (PESC), pp. 104–111, 1991.

Blackburn, D.L., Status and Trends in Power Semiconductor Devices, *Record of IEEE Conference on Industrial Electronics, Control and Instrumentation* (IECON), Vol. 2, pp. 619–625, 1993.

Bohmann, L. and Lasseter, R.H., Harmonic Interactions in Thyristor Controlled Reactor Circuits, *IEEE Transactions on Power Delivery*, Vol. 4, No. 3, pp. 1919–1926, July 1989.

Borgard, L., Grid Voltage Support. *Transmission & Distribution World*, October 1999.

Bornhardt, K., Novel Modulation Techniques for DC-Side Commutated Inverters, *Record of European Power Electronics Conference* (EPE), pp. 92–97, 1987.

Bornhardt, K., New Possibilities for DC-Side Commutated Inverter Circuits, *Record of European Power Electronics Conference* (EPE), pp. 549–554, 1989.

Bornhardt, K., Novel Soft-Switched GTO Inverter Circuits, *Record of IEEE Industry Applications Society Annual Meeting*, pp. 1222–1227, 1990.

Bose, B.K., Power Electronics: A Technology Review, *Proceedings of the IEEE*, Vol. 80, No. 8, pp. 1303–1334, August 1992.

Bose, B.K. (ed.), *Power Electronics and Variable frequency Drives: technology and Applications*, IEEE Press, 1997.

Bose, B.K., Evaluation of Modern Power Semiconductor Devices and Future Trend of Converters, *Record of IEEE Industry Applications Society Annual Meeting*, pp. 790–797, 1989.

Bose, B.K., Power Electronics: An Emerging Technology, *IEEE Transactions on Industrial Electronics*, Vol. 36, No. 3, pp. 403–412, August 1989.

Bose, B.K., Evaluation of Modern Power Semiconductor Devices and Future Trends of Converters, *IEEE Transactions on Industry Applications*, Vol. 28, No. 2, pp. 403–413, 1992.

Bose, B.K., Power Electronics and Motion Control – Technology Status and Recent Trends, *Proceedings of IEEE Power Electronics Specialists Conference (PESC)*, pp. 3–10, 1992.

Bose, B.K., Recent Advances in Power Electronics, *IEEE Transactions on Power Electronics*, Vol. 7, No. 1, pp. 2–16, January 1992.

Bose, B.K., Power Electronics and Motion Control – Technology Status and Recent Trends, *IEEE Transactions on Industry Applications*, Vol. 29, No. 5, pp. 902–909, September/October 1993.

Bowes, S.R., Advanced Regular-Sampled PWM Control Techniques for Drives and Static Power Converters, *IEEE Transactions Industrial Electronics*, Vol. 42, No. 4, pp. 367–373, August 1995.

Bowes, S.R. and Clark, P.R., Regular-Sampled Harmonic-Elimination PWM Control of Inverter Drives, *IEEE Transactions on Power Electronics*, Vol. 10, No. 5, pp. 521–531, September 1995.

Bowes, S.R. and Grewal, S., Novel Harmonic Elimination PWM Control Strategies for Three-Phase PWM Inverters Using Space Vector Techniques, *IEE Proceedings: Electric Power Applications*, Vol. 146, No. 5, pp. 495–514, 1999.

Bowes, S.R. and Lai, Y.S., Investigation into Optimising High Switching Frequency Regular Sampled PWM Control for Drives and Static Power Converters, *IEE Proceedings: Electric Power Applications*, Vol. 143, No. 4, pp. 281–293, July 1996.

Bowes, S.R. and Lai, Y.S., The Relationship between Space-Vector Modulation and Regular-Sampled PWM, *IEEE Transactions on Industrial Electronics*, Vol. 44, No. 5, pp. 670–679, October 1997.

Bremner, J.J., Torque Coefficient Analysis of Multi-Device Power Systems, PhD Thesis, The University of Glasgow, Glasgow, UK, September 1996.

Brown, H.E., *Solution of Large Networks by Matrix Methods*, John Wiley & Sons, New York, 1975.

Calais, M., Agelidis, V.G. and Meinhardt, M., Multilevel Converters for Single-Phase Grid-Connected Photovoltaic Systems: An Overview. *Solar Energy*, Vol. 66, No. 5, pp. 325–335, 1999.

Carrera, G., Marchesoni, M., Salutari, R. and Sciutto, G., A New Multilevel PWM Method: A Theoretical Analysis, *IEEE Transactions Power Electronics*, Vol. 7, No. 3, pp. 497–505, July 1992.

Chen, Y., Mwinyiwiwa, B., Wolanski, Z. and Ooi, B.T., Unified Power Flow Controller (UPFC) based on Chopper Stabilised Diode-Clamped Multilevel Converters, *IEEE Transactions on Power Electronics*, Vol. 15, No. 2, pp. 258–267, March 2000.

Chen, Y. and Ooi, B.T., Advanced Static Var-Compensator using Multimodules of Multilevel Converters with Equalisation Control of DC Voltage Levels, *Proceedings of IEEE PESC '96*, Baveno, pp. 747–752, Italy, 1996.

Chen, Y., Mwinyiwiwa, B., Wolanski, Z. and Ooi, B.T., A Regulating and Equalising DC Capacitor Voltages in Multilevel Advanced Static VAR Compensator, *IEEE Transactions on Power Delivery*, Vol. 12, pp. 901–907, April 1997.

Cheng, P.T., Bhattacharya, S. and Divan, D.M., Application of Dominant Harmonic Active Filter System with 12 Pulse Nonlinear Loads. *IEEE Transactions on Power Delivery*, Vol. 14, No. 2, pp. 642–647, April 1999.

Cho, J.G., Kim, H.S. and Cho, G.H., Novel Soft Switching PWM Converter using a New Parallel Resonant DC-Link, *Record of IEEE Power Electronics Specialists Conference (PESC)*, pp. 241–247, 1991.

Choi, J.W. and Sul, S.K., Resonant Link Bidirectional Power Converter without Electrolytic Capacitor, *Record of IEEE Power Electronics Specialists Conference (PESC)*, pp. 293–299, 1993.

Choi, N.S., Cho, G.C. and Cho, G.H., Modelling and Analysis of a Static Var Compensator using Multilevel Voltage Source Inverter, *Proceedings of IEEE Industry Applications Annual Meeting*, pp. 901–908, 1993.

Christl, N., Hedin, R., Johnson, R., Krause P. and Montoya, A., Power System Studies and Modelling for Kayenta 230 kV Substation Advanced Series Compensation, *Proceedings of the IEE 5th International Conference on AC and DC Power Transmission*, London, UK, pp. 33–37, 17–20, September 1991.

Cibulka, Frank, Crane, Lynn, Marks and John, Field Evaluation of Industry's First Self-Protected Light-Triggered Thyristor. *IEEE Transactions on Power Delivery*, Vol. 5, No. 1, pp. 110–116, January 1990.

Dehmlow, M., Heumann, K. and Sommer, R., Losses in Active Clamped Resonant DC-Link Inverter Systems, *Record of IEEE Power Electronics Specialists Conference (PESC)*, pp. 496–502, 1993.

de Mello, F.P., Power System Dynamics Overview, IEEE 75 CH070-4-PWR, Winter Power Meeting, 1975.

Dewan, S.B. and Straughen, A., Power Semiconductor Circuits, J. Wiley & Sons, Inc., 1975.

Dewinkel, C. and Lamoree, J.D., Storing Power for Critical Loads, *IEEE Spectrum*, Vol. 30, No. 6, pp. 38–42, June 1993.

Divan, D.M., Inverter Topologies and Control Techniques for Sinusoidal Output Power Supplies, *Record of IEEE Applied Power Electronics Conference and Exposition (APEC)* pp. 81–87, 1991.

Divan, D.M., The Resonant DC Link Converter – A New Concept in Static Power Conversion, *IEEE Transactions on Industry Applications*, Vol. 25, No. 2, pp. 317–325, March/April 1989.

Divan, D.M. and Skibinski, G., Zero-Switching-Loss Inverters for High Power Applications, *IEEE Transactions on Industry Applications*, Vol. 25, No. 4, pp. 634–643, July/August 1989.

Divan, D.M., Venkataramanan, G. and De Doncker, R.W., Design Methodologies for Soft Switched Inverters, *IEEE Transactions on Industry Applications*, Vol. 29, No. 1, pp. 126–135, January/February 1993.

Divan, D.M., Malesani, L., Tenti, P. and Toigo, V., A Synchronised Resonant DC Link Converter for Soft-Switched PWM, *IEEE Transactions on Industry Applications*, Vol. 29, No. 5, pp. 940–948, September/October 1993.

Divan, D.M., Venkataramanan, V., Malesani, L. and Toigo, V., Control Strategies for Synchronized Resonant Link Inverters, *Record of International Power Electronics Conference (IPEC)*, pp. 338–345, 1990.

Dommel, H.W., Digital Computer Solution of Electromagnetic Transients in Single and Multiphase Networks, *IEEE Transactions on Power Apparatus and Systems*, Vol. PAS-88, pp. 388–399, April 1969.

Edris, A., FACTS Technology Development: An Update, *IEEE Power Engineering Review*, Vol. 20, No. 3, pp. 4–9, March 2000.

Ekanayake, J.B. and Jenkins, N., Selection of Passive Elements for a Three-Level Inverter Based Static Synchronous Compensator, *IEEE Transactions on Power Delivery*, Vol. 14, No. 2, pp. 655–661, April 1999.

Ekanayake, J.B. and Jenkins, N., A Three-Level Advanced Static Var Compensator, *IEEE Transactions on Power Delivery*, Vol. 11, No. 1, pp. 540–545, January 1996.

Ekanayake, J.B. and Jenkins, N., Mathematical Models of a Three-Level Advanced Static Var Compensator, *IEE Proceedings, Generation, Transmission and Distribution*, Vol. 144, No. 2, pp. 201–206, March 1997.

EPRI, Light-Triggered Thyristors for Electric Power Systems, 932, November 1978.

Erinmez, I.A. (ed.), Static Var Compensators, Working Group 38-01, Task Force No. 2 on SVC, *CIGRE*, 1986.

Evans, P.D. and Mestha, L.K., Analysis of Conventional Snubber Circuits for PWM Inverters using Bipolar Transistors, *IEE Proceedings*, Vol. 135, Part. B, No. 4, pp. 180–192, July 1988.

Fairnley, W., Myles, A., Whitelegg, T.M. and Murray, N.S., Low Frequency Oscillations on the 275 kV Interconnectors between Scotland and England, *CIGRE Conference*, Paper 31-08, 1982.

Ferraro, A., An Overview of Low-Loss Snubber Technology for Transistor Converters, *Record of IEEE Power Electronics Specialists Conference (PESC)*, pp. 466–477, 1982.

Finney, S.J., Green, T.C. and Williams, B.W., Spectral Characteristics of Resonant Link Inverters, *Record of IEEE Power Electronics Specialists Conference (PESC)* 1992, pp. 607–614.

Fitzgerald, A.E., Kingsley, C. and Umans, S.D., *Electrical Machinery*, 4th edition, McGraw-Hill, New York, 1983.

Freris, L.L. and Sasson, A.M., Investigation of the Load Flow Problem, *Proceedings of IEE*, Vol. 115, No. 10, pp. 1459–1470, October 1968.

Fuerte-Esquivel, C.R., Modelling and Analysis of Flexible AC Transmission Systems, PhD Thesis, The University of Glasgow, Glasgow, UK, September 1997.

Fuerte-Esquivel, C.R. and Acha, E., A Newton-Type Algorithm for the Control of Power Flow in Electrical Power Networks, *IEEE Transactions on Power Systems*, Vol. 12, No. 4, pp. 1474–1480, November 1997.

Fuerte-Esquivel, C.R., Acha, E. and Ambriz-Perez, H., A Comprehensive UPFC Model for the Quadratic Load Flow Solution of Power Networks, *IEEE Transactions on Power Systems*, Vol. 15, No. 1, pp. 102–109, February 2000.

Ghiara, T., Marchesoni, M. and Sciutto, G., High Power Factor Control System in Multilevel Converters for AC Heavy Traction Drives. *Proceedings of IEEE Applied Power Electronics Conference*, pp. 672–680, 1990.

Gönen, T., *Electric Power Distribution System Engineering*, McGraw-Hill, New York, 1986.

Grant, D.A. and Gowar, J., *Power MOSFETs: Theory and Applications*, John Wiley & Sons, Inc., 1989.

Gross, G. and Galiana, F.D., Short-Term Load Forecasting, *Proceedings of the IEEE*, Vol. 75, No. 12, pp. 1558–1572, December 1987.

Gyugyi, L, Power Electronics in Electric Utilities: Static Var Compensators, *Proceedings of the IEE*, Vol. 76, No. 4, pp. 483–494, April 1988.

Gyugyi, L, A Unified Power Flow Control Concept for Flexible AC Transmission Systems, *IEE Proceedings*, Part C, Vol. 139, No. 4, pp. 323–331, July 1992.

Gyugyi, L., Schauder, S.L., Williams, S.L., Rietmann, T.R., Torgerson, D.R. and Edris, A., The Unified Power Flow Controller: A New Approach to Power Transmission Control, *IEEE Transactions on Power Delivery*, Vol. 10, pp. 1085–1097, April 1995.

Gyugyi, L. and Schauder, C., US Patent, 5, 343, 139, August 30, 1994.

Habelter, T. and Divan, D.M., Performance Characterization of a New Discrete Pulse Modulated Current Regulator, *Record of IEEE Industry Applications Society Annual Meeting*, pp. 395–405, 1988.

Hansen, A. and Havemann, H., Design of Snubber Circuits for a Transistor-Inverter using a Minimum Number of Components, *Record of IFAC Control in Power Electronics and Electrical Drives*, Lausanne, Switzerland, pp. 165–171, 1983.

Hasegawa, T., Yamaji, K., Irokawa, H., Shirahama, H., Tanaka, C. and Akabane, K., Development of a Thyristor Value for Next Generation 500-kV HVDC Transmission Systems, *IEEE Transactions on Power Delivery*, Vol. 11, No. 4, pp. 1783–1788, October 1996.

Hayashi, T. and Takasaki, M., Transmission Capability Enhancement using Power Electronics Technologies for the Future Power System in Japan, *Electric Power Systems Research*, 44, pp. 7–14, (1998).

He, J., Mohan, N. and Wold, B., Zero-Voltage-Switching PWM Inverter for High-Frequency DC–AC Power Conversion, *IEEE Transactions on Industry Applications*, Vol. 29, No. 5, pp. 959–968, September/October 1993.

Heier, S., *Grid Integration of Wind Energy Conversion Systems*, John Wiley & Sons, Chichester, England, 1998.

Heinke, F. and Sittig, R., Monolithic Bidirectional Switch, MBS, *International Symposium on Semiconductor Power Devices & ICs, ISPSD*, Toulouse, May 22–26, 2000.

Helbing, S.G. and Karady, G.G., Investigation of an Advanced Form of Series Compensation, *IEEE Transactions on Power Delivery*, Vol. 9, No. 2, pp. 939–947, April 1994.

Heumann, K., Power Electronics – State of the Art, *Record of International Power Electronics Conference (IPEC)*, pp. 1–10, 1990.

Hingorani, N.G., Power Electronics in Electric Utilities: Role of Power Electronics in Future Power Systems, *Proceedings of the IEEE*, Vol. 76, No. 4, pp. 481–482, April 1998.

Hingorani, N.G., High Power Electronics and Flexible AC Transmission System, *IEEE Power Engineering Review*, pp. 3–4, July 1998.

Hingorani, N.G., Flexible AC Transmission Systems, *IEEE Spectrum*, Vol. 30, No. 4, pp. 41–48, April 1993.

Hingorani, N.G., Introducing Custom Power, *IEEE Spectrum*, Vol. 32, No. 6, pp. 41–48, June 1995.

Hingorani, N.G., High-Voltage DC Transmission: A power electronics workhorse, *IEEE Spectrum*, Vol. 33, No. 4, pp. 63–72, April 1996.

Hingorani, N.G. and Gyugyi, L., *Understanding FACTS: Concepts and Technology of Flexible AC Transmission Systems*, The Institute of Electrical and Electronics Engineers, Inc., New York, 2000.

Hochgraf, C., Lasseter, R., Divan, D. and Lipo, T.A., Comparison of Multilevel Inverters for Static Var Compensation, *Proceedings of IEEE Industry Applications Annual Meeting* pp. 921–928, 1994.

Hoft, R.G., Semiconductor Power Electronics, Van Nostrand Reinhold, 1986.

Holtz, J. and Salama, S.F., Megawatt GTO-Inverter with Three-Level PWM Control and Regenerative Snubber Circuits, *Proceedings of IEEE Power Electronics Specialists Conference*, pp. 1263–1270, 1988.

Holtz, J., Salama, S. and Werner, K.H., A Nondissipative Snubber Circuit for High-Power GTO Inverters, *IEEE Transactions on Industry Applications*, Vol. 25, No. 4, pp. 620–626, July/August, 1989.

Hull, J.R., *IEEE Spectrum*, Vol. 20, July 1997.

IEEE Power Engineering Society, FACTS Overview, *International Conference on Large High Voltage Electric Systems*, 1995.

IEEE/CIGRE Working Group, FACTS Overview, *IEEE PES Special Publication* 95-TP-108, 1995.

IEEE/CIGRE, FACTS Overview, Special Issue, 95-TP-108, *IEEE Service Center*, Piscataway, NJ, 1995.

IEEE Industry Applications Society/Power Engineering Society, IEEE Recommended Practices and Requirements for Harmonic Control in Electrical Power Systems, *IEEE Std 519–1992*, April 1993.

IEEE Special Stability Controls Working Group, Static Var Compensator Models for Power Flow and Dynamic Performance Simulation, *IEEE Transactions on Power Systems*, Vol. 9, No. 1, pp. 229–240, February 1995.

Kassakian, J.G., Schlecht, M.F. and Verghese, G.V., *Principles of Power Electronics*, Addison-Wesley, 1991.

Katoh, S., Choi, J.H., Yokota, T., Watanabe, A., Yamaguchi, T. and Saito, K., 6-kV, 5.5-kA Light-Triggered Thyristor, *Proceedings of IEEE International Symposium on Power Semiconductor Devices (ISPSD)*, pp. 73–76, 1997.

Kheraluwala, M. and Divan, D.M., Delta Modulation Strategies for Resonant Link Inverters, *Record of IEEE Power Electronics Specialists Conference (PESC)*, pp. 271–278, 1987.

Kimbark, E.W., *Power System Stability. Volume III: Synchronous Machines*, IEEE Press Power Systems Engineering Series, The Institute of Electrical and Electronic Engineers, New York, 1995.

Kinney, S.J., Mittelstadt, W.A. and Suhrbier, R.W., The Results and Initial Experience for the BPA 500 kV Thyristor Controlled Series Capacitor Unit at Slatt Substation, Part I – Design, Operation and Fault Test Results, *Flexible AC Transmission Systems: The Future in High Voltage Transmission Conference, EPRI*, Baltimore, Maryland, October 1994.

Kundur, P., *Power Systems Stability and Control*, the EPRI Power System Engineering Series, McGraw-Hill, New York, 1994.

Lai, J. and Peng, F.Z., Multilevel Converters – A New Breed of Power Converters. *IEEE Transactions on Industry Applications*, Vol. 32, No. 3, pp. 509–517, May/June 1996.

Lai, J.S. and Bose, B.K., High Frequency Quasi-Resonant DC Voltage Notching Inverter for AC Motor Drives, *Record of IEEE Industry Applications Society Annual Meeting*, pp. 1202–1207, 1990.

Lai, Y.S. and Bowes, S.R., New Suboptimal Pulse-Width Modulation technique for Per-Phase Modulation and Space Vector Modulation, *IEEE Transactions on Energy Conversion*, Vol. 12, No. 4, pp. 310–316, December 1997.

Lander, C.W., Power Electronics, McGraw Hill, 1993.

Larsen, E.V., Bowler, C., Damsky, B. and Nilsson, S., Benefits of Thyristor Controlled Series Compensation, *International Conference on Large High Voltage Electric Systems (CIGRE)*, Paper 14/37/38-04, Paris, September 1992.

Ledu, A., Tontini, G. and Winfield, M., Which FACTS Equipment for Which Need?, *International Conference on Large High Voltage Electric Systems (CIGRE)*, Paper 14/37/38-08, Paris, September 1992.

Lipo, T.A., Recent Progress in the Development of Solid-State AC Motor Drives, *IEEE Transactions on Power Electronics*, Vol. 3, No. 2, pp. 105–117, April 1988.

Lipphardt, G., Using a Three-Level GTO Voltage Source Inverter in a HVDC Transmission System, *Proceedings of European Power Electronics and Applications Conference*, pp. 151–155, 1993.

Lips, H.P., Matern, R., Neubert, R., Popp, L. and Uder, M., Light-Triggered Thyristor Valve for HVDC Application, *Proceedings of 7th European Conference on Power Electronics and Applications EPE97*, Trondheim, Norway, Vol. 1, No. 287, 1997.

Lorenz, R.D. and Divan, D.M., Dynamic Analysis and Experimental Evaluation of Delta Modulators for Field Oriented AC Machine Regulators, *Record of IEEE Industry Applications Society Annual Meeting*, pp. 196–201, 1987.

Lund, R., Manjrekar, M.D., Steimer, P. and Lipo, T.A., Control Strategies for a Hybrid Seven-Level Inverter, *Conference Record of EPE*, pp. 1–10, 1999.

Malesani, L., Tenti, P., Divan, D.M. and Toigo, V., A Synchronized Resonant DC Link Converter for Soft-Switched PWM, *Record of IEEE Industry Applications Society Annual Meeting*, pp. 1037–1044, 1989.

Malesani, L., Tomasin, P. and Toigo, V., Modulation Techniques for Quasi Resonant DC Link PWM Converters, *Record of IEEE Industry Applications Society Annual Meeting*, pp. 789–795, 1992.

Manias, S. and Ziogas, P.D., A Novel Current Impulse Commutation Circuit for Thyristor Inverters, *IEEE Transactions on Industry Applications*, Vol. IA-19, No. 2, pp. 244–249, March/April, 1983.

Manjrekar, M. and Venkataramaan, G., Advanced Topologies and Modulation Strategies for Multilevel Inverters, *Conference Proceedings of IEEE PESC*, Vol. 2, pp. 1013–1018, 1996.

Manjrekar, M.D. and Lipo, T.A., A Hybrid Multilevel Inverter for Drive Applications, *Conference Record of IEEE Applied Power Electronics Conference*, pp. 523–529, 1998.

Marchesoni, M., High Performance Current Control Techniques for Applications to Multilevel High-Power Voltage Source Inverters, *IEEE Transactions on Power Electronics*, Vol. 7, No. 1, pp. 189–204, January 1992.

Martinez, S. and Aldana, F., Current-Source Double DC-Side Forced Commutated Inverter, *IEEE Transactions on Industry Applications*, Vol. IA-14, No. 6, pp. 581–593, November/December 1978.

Mathur, R.M., A Study of Noncharacteristic Harmonics Generated by Thyristor Phase Controlled Reactors, *IEE Conference Publication 205*, pp. 117–120, 1981.

Matthias, J., Improved Snubber for GTO Inverters With Energy Recovery by Simple Passive Network, *Record of European Power Electronics Conference (EPE)*, pp. 15–20, 1987.

Mazda, F.F., *Power Electronics Handbook, Components, Circuits and Applications*, Butterworth, 1993.

McHattie, R., Dynamic Voltage Restorer: The Customer's Perspective, *IEE Colloquium on Dynamic Voltage Restorers*, Digest No. 98/189, Glasgow, Scotland, UK, 1998.

McMurray, W., Feasibility of GTO Thyristors in a HVDC Transmission System, EPRI EL-5332, Project 2443-5, Final Report, August 1987.

McMurray, W., Optimum Snubbers for Power Semiconductors, *IEEE Transactions on Industry Applications*, Vol. IA-8, No. 5, pp. 593–600, September/October 1972.

McMurray, W., Selection of Snubbers and Clamps to Optimize the Design of Transistor Switching Converters, *IEEE Transactions on Industry Applications*, Vol. IA-16, No. 4, pp. 513–523, July/August 1980.

McMurray, W., Efficient Snubbers for Voltage-Source GTO Inverters, *Record of IEEE Power Electronics Specialists Conference (PESC)*, pp. 20–27, 1985.

Menzies, R.W. and Zhuang, Y., Advanced Static Compensation using a Multilevel GTO Thyristor Inverter, *IEEE Transactions on Power Delivery*, Vol. 10, pp. 732–738, April 1995.

Mertens, A. and Divan, D.M., A High Frequency Resonant DC Link Inverter using IGBT's, *Record of International Power Electronics Conference (IPEC)*, pp. 152–160, 1990.

Mertens, A. and Skudelny, H.Ch., Calculations on the Spectral Performance of Discrete Pulse Modulation Strategies, *Record of IEEE Power Electronics Specialists Conference (PESC)*, pp. 357–365, 1991.

Mestha, L.K. and Evans, P.D., Analysis of On-State Losses in PWM Inverters, *IEE Proceedings*, Vol. 136, Part B, No. 4, pp. 189–195, July 1989.

Meynard, T., Fadel, M. and Aouda, N., Modelling of Multilevel Converters, *IEEE Transactions on Industrial Electronics*, Vol. 44, No. 3, pp. 356–364, 1997.

Meynard, T.A. and Foch, H., Multilevel Conversion: High Voltage Choppers and Voltage Source Inverters. *IEEE Transactions on Power Electronics*, No. 3, pp. 397–403, 1992.

Miller, T.J.E. (ed.), *Reactive Power Control in Electric Systems*, John Wiley & Sons, New York, 1982.

Mohan, N., Undeland, T.M. and Robbins, W.P., *Power Electronics: Converters, Applications and Design*, 2nd edition, John Wiley & Sons, 1995.

Mwinyiwiwa, B., Wolanski, Z. and Ooi, B.T., Current Equalisation in SPWM FACTS Controllers at Lowest Switching Rates, *IEEE Transactions on Power Electronics*, Vol. 14, No. 5, pp. 900–905, 1999.

Mwinyiwiwa, B., Wolanski, Z., Chen, Y. and Ooi, B.T., Multimodular Multilevel Converters with Input/Output Linearity, *IEEE Transactions on Industry Applications*, Vol. 33, No. 5, pp. 1214–1219, September/October 1997.

Nabae, A., Takahashi, I. and Akagi, H., A New Neutral-Point-Clamped PWM Inverter. *IEEE Transactions on Industry Applications*, Vol. 17, No. 5, pp. 518–523, September/October 1981.

Nabavi-Niaki, A. and Iravani, M.R., Steady-State and Dynamic Models of Unified Power Flow Controller (UPFC) for Power System Studies, IEEE Transactions on Power Systems, Vol. 11, No. 4, pp. 1937–1943, November 1996.

Newton, C. and Sumner, M., Neutral Point Control for Multi-Level Inverters: Theory, Design and Operational Limitations, *Proceedings of the IEEE Industry Applications Annual Meeting*, pp. 1336–1343, 1997.

Newton, C., Sumner, M. and Alexander, T., The Investigation and Development of a Multi-Level Voltage Source Inverter, *Conference Proceedings of IEE/PEVD '96*, Nottingham, UK, pp. 317–321, September 1996.

Niedernostheide, F.J., Schulze, H.-J., Dorn, J., Kellner-Werdehausen, U. and Westerholt, D., Light-Triggered Thyristors with Integrated Protection Functions, *Proceedings of the ISPSD 2000*, Toulouse, May 22–25, in press.

Niedernostheide, F.J., Schulze, H.J. and Kellner-Werdehausen, U., High-Power Thyristors with Integrated Functions, *Proceedings of the ISPSD 2000*, Prague, August 30–September 1.

Nishihara, M., Power Electronics Diversity, *Record of International Power Electronics Conference (IPEC)*, 21–28, 1990.

Noroozian, M. and Andersson, G., Power Flow Control by Use of Controllable Series Components, *IEEE Transactions on Power Delivery*, Vol. 8, No. 3, pp. 1420–1429, July 1993.

Ohno, E., The Semiconductor Evolution in Japan – A Four Decade Long Maturity Thriving to an Indispensable Social Standing, *Record of International Power Electronics Conference (IPEC)*, 11–20, 1990.

Ooi, B.T., Dai, S.Z. and Galiana, F.D., A Solid-State PWM Phase Shifter, *IEEE Transactions on Power Delivery*, Vol. 8, pp. 573–579, April 1993.

Ooi, B.T., Joos, G. and Huang, X., Operating Principles of Shunt STATCOM based on 3-Level Diode-Clamped Converters, *Proceedings of IEEE PES Winter Meeting*, New York, February 1999.

Paice, D.A., *Power Electronic Converter Harmonics: Multipulse Methods for Clean Power*. IEEE Press, 1996.

Palmour, J.W., Singh, R., Glass, R.C., Kordina, O. and Carter, C.H. Jr., Silicon Carbide for Power Devices, *IEEE ISPSD 1997*, Weimar, pp. 25–32, May 26–29.

Peng, F.Z., Lai, J., McKeever, J.W. and VanCoevering, J., A Multilevel Voltage-Source Inverter with Separate DC Sources for Static Var Generation, *IEEE Transactions on Industry Applications*, Vol. 32, No. 5, pp. 1130–1138, September/October 1996.

Peng, F.Z., McKeever, J.W. and Adams, D.J., Cascade Multilevel Inverters for Utility Applications, *IEEE IECON Proceedings of 1997*, pp. 437–442.

Peng, F.Z., McKeever, J.W. and Adams, D.J., Power Line Conditioner using Cascade Multilevel Inverters for Distribution Systems, *IEEE Transactions on Industry Applications*, Vol. 34, No. 6, pp. 1293–1298, November/December 1998.

Peng, F.Z., McKeever, W. and Adams, D.J., A Power Line Conditioner using Cascade Multilevel Inverter for Distribution Systems, *IEEE Transactions on Industry Applications*, Vol. 34, No. 6, pp. 1293–1298, November/December 1998.

Peterson, N.M. and Scott-Meyer, W., Automatic Adjustment of Transformer and Phase Shifter Taps in the Newton Power Flow, *IEEE Transactions on Power Apparatus and Systems*, Vol. PAS-90, No. 1, pp. 103–108, January/February 1971.

Piwko, R.J., Wegner, C.A., Kinney, S.J. and Eden, J.D., Subsynchronous Resonance Performance Test of the Slatt Thyristor-Controlled Series Capacitor, *IEEE Transactions on Power Delivery*, Vol. 11, No. 2, pp. 1112–1119, April 1996.

Przybysz, J.X., Miller, D.L., Leslie, S.G. and Kao, Y.C., High di/dt Light-Triggered Thyristors. *IEEE Transactions on Electron Devices*, ED-34, 10, pp. 2192–2199, October 1987.

Rice, J.B., Design of Snubber Circuits for Thyristor Converters, *Record of IEEE Industry General Applications Annual Meeting*, pp. 485–589, 1969.

Rico, J.J. and Acha, E., The Use of Switching functions and Walsh Series to Calculate Waveform Distortion in Thyristor Controlled Compensated Power Circuits, *IEEE Transactions on Power Delivery*, Vol. 13, No. 4, pp. 1370–1377, October 1998.

Rico, J.J., Acha, E. and Miller, T.J.E., Harmonic Domain Modelling of Three Phase Thyristor-Controlled Reactors by Means of Switching Vectors and Discrete Convolutions, *IEEE Transactions on Power Delivery*, Vol. 11, No. 3, pp. 1678–1684, July 1996.

Rockot, J.H., Losses in High-Power Bipolar Transistors, *IEEE Transactions on Power Electronics*, Vol. PE-2, No. 1, pp. 72–80, January 1987.

Rohas, R., Ohnishi, T. and Suzuki, T., An Improved Voltage Vector Control Method for Neutral Point Clamped Inverters, *IEEE Transactions on Power Electronics*, Vol. 10, No. 6, pp. 666–672, November 1995.

Ruff, M., Schulze, H.J. and Kellner, U., Progress in the Development of an 8-kV Light-Triggered Thyristor with Integrated Protection Functions. *IEEE Transactions on Electron Devices*, Vol. 46, No. 8, pp. 1768–1774, 1999.

Schauder, C., Gernhardt, M., Stacey, E., Lemak, T., Gyugyi, L., Cease, T.W. and Edris, A. Development of a ±100 MVAR Static Condenser for Voltage Control of Transmission Systems, *IEEE Transactions on Power Delivery*, Vol. 10, No. 3, pp. 1486–1493, July 1995.

Schauder, C., Gyugyi, L., Lund, M.R., Hamai, D.M., Rietman, T.R., Torgerson, D.R. and Edris, A., Operation of the Unified Power Flow Controller (UPFC) under Practical Constraints, *IEEE Transactions on Power Delivery*, Vol. 13, pp. 630–639, April 1998.

Schibli, N.P., Nguyen, T. and Rufer, A.C., Three-Phase Multilevel Converter for High-Power Induction Motors. *IEEE Transactions on Power Electronics*, Vol. 13, No. 5, pp. 978–985, September 1998.

Schönung, A. and Stemmler, H., Static Frequency Changers with Subharmonic Control in Conjunction with reversible Variable-Speed AC-Drives. Brown Boveri Review, Vol. 51, 1964.

Schulting, L., A 100-kVA Resonant DC Link Inverter with GTO's – Design Consideration and First Practical Experience, *Record of IEEE Industry Applications Society Annual Meeting*, 729–736, 1992.

Schulze, H.J., Ruff, M., Baur, B., Pfirsch, F., Kabza, H. and Kellner, U., *Proceedings of International Symposium on Power Semiconductor Devices and Ics.*, pp. 197–200, 1996.

Schulze, H.J., Ruff, M., Baur, B., Pfirsch, F., Kabza, H., Kellner, U. and Voss, P., Light-Triggered 8-kV Thyristor with a New Integrated Breakover Diode. *Electronic Engineering* (London), Vol. 69, No. 848, pp. 24–28, August 1997.

Semlyen, A., Acha, E. and Arrillaga, J., Newton-Type Algorithms for the Harmonic Phasor Analysis of Non-Linear Power Circuits in Periodical Steady State with Special Reference to Magnetic Non-Linearities, *IEEE Transactions on Power Delivery*, Vol. 3, No. 3, pp. 1090–1098, July 1988.

Semlyen, A. and Rajakovic, N., Harmonic Domain Modelling of Laminated Iron Cores, *IEEE Transactions on Power Delivery*, Vol. 4, No. 1, pp. 382–390, January 1989.

Shipley, R.B., *Introduction to Matrices and Power Systems*, John Wiley & Sons, New York, 1976.

Singh, B., Al-Haddad, K. and Chandra, A., A Review of Active Filters for Power Quality Improvement. *IEEE Transactions on Industrial Electronics*, Vol. 46, No. 5, pp. 960–971, October, 1999.

Sinha, G. and Lipo, T.A., A Four-Level Rectifier Inverter System for Drive Applications, *Proceedings IEEE Industry Applications Society Annual Meeting*, pp. 980–987, 1996.

Sood, P. and Lipo, T.A., Power Conversion Distribution System using a Resonant High Frequency AC Link, *Record of IEEE Industry Applications Society Annual Meeting*, pp. 533–541, 1986.

Stagg, G.W. and El-Abiad, A.H., *Computer Methods in Power System Analysis*, McGraw-Hill Series in Electronic Systems, McGraw-Hill, 1968.

Stefanovic, V.R., Current Developments in AC Drives, *Record of International Power Electronics Conference (IPEC)*, 382–390, 1991.

Steinke, J.K., Switching Frequency Optimal PWM Control of a Three-Level Inverter, *IEEE Transactions on Power Electronics*, Vol. 7, No. 3, pp. 487–496, July 1992.

Stemmler, H. State of the Art and Future Trends in High Power Electronics, *Proceedings of International Power Electronics Conference (IPEC)*, Tokyo, Vol. 1, pp. 4–14, April 3–7, 2000.

Steyn, C.G., Analysis and Optimization of Regenerative Linear Snubbers, *IEEE Transactions on Power Electronics*, Vol. 4, No. 3, pp. 362–370, July 1989.

Stoll, H.G., *Least-Cost Electric Utility Planning*, John Wiley & Sons, New York, 1989.

Stott, B., Review of Load-Flow Calculations Methods, *IEEE Proceedings*, Vol. 62, pp. 916–929, July 1974.

Suh, B.S. and Hyun, D.S., A New N-Level High Voltage Inversion System, *IEEE Transactions on Industrial Electronics*, Vol. 44, No. 1, pp. 107–115, February 1997.

Tada, Akiharu, Kawakami, Akira, Miyazima, Tatsuo, Nakagawa, Tsutomu, Yamanaka, Kenichi, Ohtaki and Kaname, 4-kV, 1500-A Light Triggered Thyristor, *Proceedings, Solid State devices*, pp. 99–104, 1981.

Tadros, Y. and Salama, S., Three Level IGBT Inverter, *IEEE Transactions on Power Electronics*, No. 3, pp. 6–52, 1992.

Temple, V.A.K., Development of a 2.6-kV Light-Triggered Thyristor for Electric Power systems, *IEEE Transactions on Electron Devices*, ED-27, No. 3, pp. 583–591, March 1980.

Temple, V.A.K., Comparison of Light Triggered and Electrically Triggered Thyristor Turn-On. *IEEE Transactions on Electron Devices*, ED-28, No. 7, pp. 860–865, July 1981.

Teodorescu, R., Blaabjerg, F., Pedersen, J.K., Cengelci, E., Sulistijo, S.U., Woo, B.O. and Enjeti, P., Multilevel Converters – A Survey, *Proceedings of the European Power Electronics Conference*, pp. 2–11, 1999.

Tinney, W.F. and Hart, C.E., Power Flow Solutions by Newton's Method, *IEEE Transactions on Power Apparatus and Systems*, Vol. PAS-96, No. 11, pp. 1449–1460, November 1967.

Tolbert, L. Peng, F. and Habetler, T., Multilevel Converters for Large Electric Drives, *IEEE Transactions on Industry Applications*, Vol. 35, No. 1, pp. 36–44, January/February 1999.

Tolbert, L.M. and Habetler, T.G., Novel Multilevel Inverter Carrier-Based PWM Method, *IEEE Transactions on Industry Applications*, Vol. 35, No. 5, pp. 1098–1107, September–October 1999.

Tolbert, L.M. and Habetler, T.G., A Multilevel Converter-Based Universal Power Conditioner, *IEEE Power Electronics Specialists Conference 1999*, pp. 393–399.

Tolbert, L.M., Peng, F.Z. and Habetler, T.G., Multilevel Converters for Large Electric Drives, *IEEE Transactions on Industry Applications*, Vol. 35, No. 1, pp. 36–44, January–February 1999.

Tolbert, L.M., Peng, F.Z. and Habetler, T.G., Multilevel PWM Methods at Low Modulation Indices, *IEEE Applied Power Electronics Conference 1999*, pp. 1032–1038.

Trzynadlowski, A.M., Introduction to Modern Power Electronics, John Wiley & Sons, Inc., 1998.

Undeland, T.M., Switching Stress Reduction in Power Transistor Converters, *Record of IEEE Industry Applications Society Annual Meeting*, pp. 383–392, 1976.

Undeland, T.M., Snubbers for Pulse Width Modulated Bridge Converters with Power Transistors or GTOs, *Record of International Power Electronics Conference (IPEC)*, pp. 313–323, 1983.

Undeland, T.M., Jenset, F., Steinbakk, A., Rogne, T. and Hernes, M., A Snubber Configuration for both Power Transistors and GTO PWM Inverters, *Record of IEEE Power Electronics Specialists Conference (PESC)*, pp. 42–53, 1984.

Van Ligten, H. and Navon, D. Basic Turn-off of GTO Switches, *IRE Wescon Convention Record, Part 3 on Electron Devices*, pp. 49–52, August 1960.

Venkataramanan, G., and Divan, D.M., Pulse Width Modulation with Resonant DC Link Converters, *IEEE Transactions on Industry Applications*, Vol. 29, No. 1, pp. 113–120, January/February 1993.

Venkataramanan, G., Divan, D.M. and Jahns, T.M., Discrete Pulse Modulation Strategies for High-Frequency Inverter Systems, *IEEE Transactions on Power Electronics*, Vol. 8, No. 3, pp. 279–287, July 1993.

Walker, G. and Ledwich, G., Bandwidth Considerations for Multilevel Converters, *IEEE Transactions on Power Electronics*, Vol. 14, No. 1, pp. 74–81, January 1999.

Weedy, B.M., *Electric Power Systems*, 3rd edition, John Wiley & Sons, 1987.

Woo, B.O. and Cho, G.H., Soft Switching AC/DC/AC Converter with Current Freewheeling Circuit, *Record of IEEE Power Electronics Specialists Conference (PESC)*, pp. 31–38, 1991.

Wood, A.J. and Wollenberg, B.F., Power Generation Operation & Control, John Wiley & Sons, 1984.

Xu, L. and Agelidis, V.G., A Flying Capacitor Multilevel PWM Converter based UPFC, Paper presented at the *IEEE PESC '01*, Vancouver, Canada, June 2001.

Xu, L., Agelidis, V.G. and Acha, E., Development Considerations of a DSP-Controlled PWM VSC-Based STATCOM, *IEE Proceedings, Electric Power Applications*, September 2001.

Yacamini, R. and Resende, J.W., Thyristor Controlled Reactors as Harmonic Sources in HVDC Converters Stations and AC Systems, *IEE Proceedings*, Part B, Vol. 133, No. 4, pp. 263–269, July 1986.

Zach, F., Kaiser, K., Kolar, J. and Haselsteiner, F., New Lossless Turn-On and Turn-Off (Snubber) Networks for Inverters, Including Circuits for Blocking Voltage Limitation, *IEEE Transactions on Power Electronics*, Vol. PE-1, No. 2, April 1986.

Zhang, H., VonJouanne, A. and Wallace, A., Multilevel Inverter Modulation Schemes to Eliminate Common-Mode Voltages, *IEEE IAS Annual Meeting 1998*, pp. 752–758.

Zollenkopf, K., Bifactorization – Basic Computational Algorithm and Programming Techniques, *Conference on Large Sets of Sparse Linear Equations*, Oxford, pp. 75–96, 1970.

Index